MARINE MICROBIOME AND BIOGEOCHEMICAL CYCLES IN MARINE PRODUCTIVE AREAS

EDITED BY: Alejandro A. Murillo, Veronica Molina, Chris Harrod and Julio Salcedo-Castro

PUBLISHED IN: Frontiers in Marine Science and Frontiers in Microbiology

frontiers Research Topics

frontiers

Frontiers eBook Copyright Statement

The copyright in the text of individual articles in this eBook is the property of their respective authors or their respective institutions or funders. The copyright in graphics and images within each article may be subject to copyright of other parties. In both cases this is subject to a license granted to Frontiers.

The compilation of articles constituting this eBook is the property of Frontiers.

Each article within this eBook, and the eBook itself, are published under the most recent version of the Creative Commons CC-BY licence. The version current at the date of publication of this eBook is CC-BY 4.0. If the CC-BY licence is updated, the licence granted by Frontiers is automatically updated to the new version.

When exercising any right under the CC-BY licence, Frontiers must be attributed as the original publisher of the article or eBook, as applicable.

Authors have the responsibility of ensuring that any graphics or other materials which are the property of others may be included in the CC-BY licence, but this should be checked before relying on the CC-BY licence to reproduce those materials. Any copyright notices relating to those materials must be complied with.

Copyright and source acknowledgement notices may not be removed and must be displayed in any copy, derivative work or partial copy which includes the elements in question.

All copyright, and all rights therein, are protected by national and international copyright laws. The above represents a summary only. For further information please read Frontiers' Conditions for Website Use and Copyright Statement, and the applicable CC-BY licence.

ISSN 1664-8714
ISBN 978-2-88963-276-3
DOI 10.3389/978-2-88963-276-3

About Frontiers

Frontiers is more than just an open-access publisher of scholarly articles: it is a pioneering approach to the world of academia, radically improving the way scholarly research is managed. The grand vision of Frontiers is a world where all people have an equal opportunity to seek, share and generate knowledge. Frontiers provides immediate and permanent online open access to all its publications, but this alone is not enough to realize our grand goals.

Frontiers Journal Series

The Frontiers Journal Series is a multi-tier and interdisciplinary set of open-access, online journals, promising a paradigm shift from the current review, selection and dissemination processes in academic publishing. All Frontiers journals are driven by researchers for researchers; therefore, they constitute a service to the scholarly community. At the same time, the Frontiers Journal Series operates on a revolutionary invention, the tiered publishing system, initially addressing specific communities of scholars, and gradually climbing up to broader public understanding, thus serving the interests of the lay society, too.

Dedication to Quality

Each Frontiers article is a landmark of the highest quality, thanks to genuinely collaborative interactions between authors and review editors, who include some of the world's best academicians. Research must be certified by peers before entering a stream of knowledge that may eventually reach the public - and shape society; therefore, Frontiers only applies the most rigorous and unbiased reviews.
Frontiers revolutionizes research publishing by freely delivering the most outstanding research, evaluated with no bias from both the academic and social point of view. By applying the most advanced information technologies, Frontiers is catapulting scholarly publishing into a new generation.

What are Frontiers Research Topics?

Frontiers Research Topics are very popular trademarks of the Frontiers Journals Series: they are collections of at least ten articles, all centered on a particular subject. With their unique mix of varied contributions from Original Research to Review Articles, Frontiers Research Topics unify the most influential researchers, the latest key findings and historical advances in a hot research area! Find out more on how to host your own Frontiers Research Topic or contribute to one as an author by contacting the Frontiers Editorial Office: researchtopics@frontiersin.org

MARINE MICROBIOME AND BIOGEOCHEMICAL CYCLES IN MARINE PRODUCTIVE AREAS

Topic Editors:
Alejandro A. Murillo, European Molecular Biology Laboratory Heidelberg, Germany
Veronica Molina, Universidad de Playa Ancha, Chile
Chris Harrod, University of Antofagasta, Chile
Julio Salcedo-Castro, Universidad de Playa Ancha, Chile

Citation: Murillo, A. A., Molina, V., Harrod, C., Salcedo-Castro, J., eds. (2019). Marine Microbiome and Biogeochemical Cycles in Marine Productive Areas. Lausanne: Frontiers Media SA. doi: 10.3389/978-2-88963-276-3

Table of Contents

frontiers in Marine Science

EDITORIAL
published: 22 October 2019
doi: 10.3389/fmars.2019.00657

Editorial: Marine Microbiome and Biogeochemical Cycles in Marine Productive Areas

Alejandro A. Murillo[1]*, *Verónica Molina*[2], *Julio Salcedo-Castro*[2] and *Chris Harrod*[3,4]

[1] Structural and Computational Biology, European Molecular Biology Laboratory, Heidelberg, Germany, [2] Departamento de Biología, Universidad de Playa Ancha, Valparaíso, Chile, [3] Instituto de Ciencias Naturales Alexander von Humboldt, Universidad de Antofagasta, Antofagasta, Chile, [4] Núcleo Milenio INVASAL, Concepción, Chile

Keywords: coastal areas, upwelling systems, carbon cycle, nitrogen cycle, microbial oceanography, high nutrients, microbial diversity, coastal ecosystems

Editorial on the Research Topic

Marine Microbiome and Biogeochemical Cycles in Marine Productive Areas

The global ocean covers more than 70% of the Earth's surface and is remarkably heterogeneous. Marine productive areas, and coastal ecosystems comprise a minor fraction of the ocean in terms of surface area, yet have an enormous impact on global biogeochemical cycles carried out by microbial communities, which represent 90% of the ocean's biomass (Alexander et al., 2011). These marine productive areas also vary considerably in terms of primary and secondary production, and are classified as highly productive or class I (>300 gC m^{-2} yr^{-1}), moderately productive or class II (150–300 gC m^{-2} yr^{-1}), to low productive or class III (<150 gC m^{-2} yr^{-1}). Work to date has largely focused on cycling of carbon and macronutrients such as nitrogen, phosphorus, and silicate: other important elements such as sulfur or trace elements have been less studied, reflecting associated technical and logistical issues. Increasingly, these marine areas, and the taxa that form their ecosystems, are subject to significant anthropogenic pressure, impacting marine life and recycling of energy and nutrients (Galton, 1884; Hasler, 1969; Jickells et al., 2017). A key example is that of cultural eutrophication, where agricultural run-off leads to nitrogen and phosphorus enrichment of coastal ecosystems, greatly increasing productivity resulting in algal blooms, deoxygenation of the water column and seabed, and increased greenhouse gas emissions (Bouwman et al., 2005), with direct local and global impacts on nitrogen and carbon cycles. However, the runoff of organic matter from the mainland to coastal ecosystems is just one of a series of pressing threats stressing microbial communities due to global change. Climate change has also resulted in changes in the cryosphere, as glaciers and permafrost melt, resulting in intensified marine stratification, while shifts of the redox-state in different biomes are rapidly reshaping microbial assemblages at an unprecedented rate (Altieri and Gedan, 2015; Breitburg et al., 2018; Cavicchioli et al., 2019; Hutchins et al., 2019).

Global change is, therefore, affecting key processes including primary productivity, CO_2 and N_2 fixation, organic matter respiration/remineralization, and the sinking and burial deposition of fixed CO_2 (Hutchins et al., 2019). In addition to this, oceans are experiencing an acidification process, with a change of ∼0.1 pH units between the pre-industrial period and today, affecting carbonate/bicarbonate buffer chemistry. In turn, acidification has been reported to impact planktonic communities, principally through effects on calcifying taxa (Stillman and Paganini, 2015). There is also evidence for shifts in the production of key intermediary volatile products, some of which have marked greenhouse effects (e.g., N_2O and CH_4, reviewed by Breitburg et al., 2018), due to the increase in global temperature, ocean stratification and deoxygenation, driving

OPEN ACCESS

Edited and reviewed by:
François G. Schmitt, UMR8187 Laboratoire d'Océanologie et de Géosciences (LOG), France

***Correspondence:**
Alejandro A. Murillo
alejandro.murillo@embl.de

Specialty section:
This article was submitted to Coastal Ocean Processes, a section of the journal Frontiers in Marine Science

Received: *16 July 2019*
Accepted: *09 October 2019*
Published: *22 October 2019*

Citation:
Murillo AA, Molina V, Salcedo-Castro J and Harrod C (2019) Editorial: Marine Microbiome and Biogeochemical Cycles in Marine Productive Areas. Front. Mar. Sci. 6:657. doi: 10.3389/fmars.2019.00657

as much as ∼25–50% of nitrogen loss from the ocean to the atmosphere in the so-called oxygen minimum zones (Bertagnolli and Stewart, 2018) or anoxic marine zones (Ulloa et al., 2012), driven by microbial processes. Other products, that are typically toxic for the marine nekton, including reduced sulfur species such as H_2S, have a negative impact for marine resources like fisheries and coastal aquaculture. While global change has accelerated, there has been a parallel increase in awareness of the complexity of marine ecosystems, and especially the fundamental role of microbes as drivers of ecosystem functioning (Cavicchioli et al., 2019). At the same time, calls have intensified for the need for representative ecosystem-based models that can guide effective management of marine ecosystems. An example of this is the call made by the United Nations, proclaiming the Decade of Oceans Science for Sustainable Development 2012–2030 (https://en.unesco.org/ocean-decade).

This Research Topic is focused on studies characterizing the complexity of interactions seen in microbial communities, and their response to environmental variation across a comprehensive range of marine habitats. These extend from coral reefs stressors and microbialization (Meirelles et al.), through to coastal habitats including glaciers in a Norwegian archipelago (Garcia-Lopez et al.), to the deep-sea floor and the spatial heterogeneity of a submarine canyon system (Román et al.). Other authors examined the picoeukaryotic community dynamics in the Northwestern Pacific Ocean (Wang et al.), the influence of river discharges (Masotti et al.) and temporal variability of net primary production (Testa et al.) both in an upwelling system of the Eastern Subtropical South Pacific Ocean. The role of microbial communities in the carbon cycle is at the core of our Research Topic, including the fate of dissolved organic carbon in upwelling systems (Bif et al.), the utilization of one-carbon and methylated compounds in the coastal environment (Dinasquet et al.) and dissolved organic matter derived from permafrost thaw in Arctic fjords, influencing the microbial communities (Müller et al.). This diversity of environments and microbial processes provides a small glimpse of the multiple roles that microbial communities play in marine ecosystems. Other important aspects include the potential for biotechnological applications regarding the discovery of new bio-active compounds in a mangrove soil community (Chen et al.), the first sponge microbiome from the Persian Gulf (Najafi et al.) and the microbiome of the ecological engineer giant kelp *Macrocystis pyrifera*, including the utilization of alginate (Lin et al.).

As we face a climate crisis and other pressing threats to human life, such as the rise of antibiotic resistance (MacFadden et al., 2018) and the expansion of oxygen-deficient zones affecting fishing resources (Roman et al., 2019), marine microbial communities (including the microbiome of marine organisms) offer a plethora of potential sustainable and environmentally-friendly practices to reduce our impact on the environment and improve human lives. This includes the identification of novel bioactive compounds, development of green-blue energy, effective and efficient sewage treatments, and the mitigation of CO_2 production, as carbon burial, and other greenhouse gases. By increasing our understanding of the functioning of those natural processes that allow our planet to auto-regulate and respond to perturbations, we can apply such knowledge to surmount current and imminent environmental problems. Life is thought to have originated in the ocean and since then, to the actual state of the biosphere, marine habitats have been the support to an astonishing diversity of life forms and metabolic pathways. As such, increasing our understanding on how the largest biome on Earth functions is possibly the most important enterprise of the upcoming decades and can provide answers and solutions for many of the current challenges that humankind faces.

AUTHOR CONTRIBUTIONS

All authors listed have made a substantial, direct and intellectual contribution to the work, and approved it for publication.

ACKNOWLEDGMENTS

We thank all the contributors to this Research Topic.

REFERENCES

Alexander, V., Miloslavich, P., and Yarincik, K. (2011). The Census of Marine Life—evolution of worldwide marine biodiversity research. *Mar. Biodivers.* 41, 545–554. doi: 10.1007/s12526-011-0084-1

Altieri, A. H., and Gedan, K. B. (2015). Climate change and dead zones. *Glob. Chang. Biol.* 21, 1395–1406. doi: 10.1111/gcb.12754

Bertagnolli, A. D., and Stewart, F. J. (2018). Microbial niches in marine oxygen minimum zones. *Nat. Rev. Microbiol.* 16, 723–729. doi: 10.1038/s41579-018-0087-z

Bouwman, A. F., Van Drecht, G., Knoop, J. M., Beusen, A. H. W., and Meinardi, C. R. (2005). Exploring changes in river nitrogen export to the world's oceans. *Global Biogeochem. Cycles* 19:1002. doi: 10.1029/2004GB002314

Breitburg, D., Levin, L. A., Oschlies, A., Grégoire, M., Chavez, F. P., Conley, D. J., et al. (2018). Declining oxygen in the global ocean and coastal waters. *Science* 359:eaam7240. doi: 10.1126/science.aam7240

Cavicchioli, R., Ripple, W. J., Timmis, K. N., Azam, F., Bakken, L. R., Baylis, M., et al. (2019). Scientists' warning to humanity: microorganisms and climate change. *Nat. Rev. Microbiol.* 17, 569–586. doi: 10.1038/s41579-019-0222-5

Galton, D. (1884). 10th Meeting: report of the royal commission on metropolitan sewage. *J. Soc. Arts* 33, 290.

Hasler, A. D. (1969). Cultural eutrophication is reversible. *Bioscience* 19, 425–431. doi: 10.2307/1294478

Hutchins, D. A., Jansson, J. K., Remais, J. V., Rich, V. I., Singh, B. K., and Trivedi, P. (2019). Climate change microbiology — problems and perspectives. *Nat. Rev. Microbiol.* 17, 391–396. doi: 10.1038/s41579-019-0178-5.

Jickells, T. D., Buitenhuis, E., Altieri, K., Baker, A. R., Capone, D., Duce, R. A., et al. (2017). A reevaluation of the magnitude and impacts of anthropogenic atmospheric nitrogen inputs on the ocean. *Global Biogeochem. Cycles* 31, 289–305. doi: 10.1002/2016GB005586

MacFadden, D. R., McGough, S. F., Fisman, D., Santillana, M., and Brownstein, J. S. (2018). Antibiotic resistance increases with local temperature. *Nat. Clim. Change* 8, 510–514. doi: 10.1038/s41558-018-0161-6

Roman, M. R., Brandt, S. B., Houde, E. D., and Pierson, J. J. (2019). Interactive effects of hypoxia and temperature on coastal pelagic zooplankton and fish. *Front. Mar. Sci.* 6:139. doi: 10.3389/fmars.2019.00139

Stillman, J. H., and Paganini, A. W. (2015). Biochemical adaptation to ocean acidification. *J. Exp. Biol.* 218, 1946–1955. doi: 10.1242/jeb.115584

Ulloa, O., Canfield, D. E., DeLong, E. F., Letelier, R. M., and Stewart, F. J. (2012). Microbial oceanography of anoxic oxygen minimum zones. *Proc. Natl. Acad. Sci. U.S.A.* 109, 15996–16003. doi: 10.1073/pnas.1205009109

Conflict of Interest: The authors declare that the research was conducted in the absence of any commercial or financial relationships that could be construed as a potential conflict of interest.

Copyright © 2019 Murillo, Molina, Salcedo-Castro and Harrod. This is an open-access article distributed under the terms of the Creative Commons Attribution License (CC BY). The use, distribution or reproduction in other forums is permitted, provided the original author(s) and the copyright owner(s) are credited and that the original publication in this journal is cited, in accordance with accepted academic practice. No use, distribution or reproduction is permitted which does not comply with these terms.

frontiers in Marine Science

ORIGINAL RESEARCH
published: 29 May 2018
doi: 10.3389/fmars.2018.00179

Temporal Variability in Net Primary Production in an Upwelling Area off Central Chile (36°S)

Giovanni Testa[1,2,3], *Italo Masotti*[3,4] *and Laura Farías*[2,3]*

[1] Graduate Program in Oceanography, Department of Oceanography, University of Concepción, Concepción, Chile, [2] Department of Oceanography, Faculty of Natural and Oceanographic Sciences, University of Concepción, Concepción, Chile, [3] Center for Climate and Resilience Research, University of Chile, Santiago de Chile, Chile, [4] Facultad de Ciencias del Mar y de Recursos Naturales, Universidad de Valparaíso, Viña del Mar, Chile

The temporal variability of Net Primary Production (NPP) off central Chile (36°S, 73°W), an area subjected to seasonal coastal upwelling, was analyzed using monthly *in situ* ^{13}C incubations within the photic zone, along with bio-oceanographic variables from a fixed time series station; and satellite NPP estimations (NPPE) from the Vertically Generalized Production Model between 2006 and 2015. NPP and NPPE rates varied from 0.03 to 18.29 and from 0.45 to 9.07 g C m^{-2} d^{-1}, respectively. Both rates were fairly well correlated with each other ($r^2 = 0.61$), but when these data were separated into two periods, higher r^2 value was found during winter ($r^2 = 0.70$) with respect to the rest of the year ($r^2 = 0.24$); the latter correlation was partially due to increased weekly NPPE variability during active and relaxed upwelling events. NPP rates along with other biophysical variables allowed for a division of the annual cycle into three distinct periods: September to January (high productivity, mean integrated NPP rates of 4.0 g C m^{-2} d^{-1}), February to March (intermediate productivity, mean integrated NPP rates of 1.4 g C m^{-2} d^{-1}), and May to August (basal level, mean integrated NPP rates of 0.5 g C m^{-2} d^{-1}). NPP appeared to be partially controlled by nutrient inputs, either from upwelling (September-April) and river discharge (May-August), maintaining high NPP rates throughout the entire year, with an annual mean NPP rate of 1.1 kg C m^{-2} yr^{-1}. In this region, El Niño Southern Oscillation events did not appear to impact the NPP interannual variability.

Keywords: primary production rates, coastal upwelling, river discharge, El Niño Southern oscillation, central Chile

OPEN ACCESS

Edited by:
Alejandro A. Murillo, EMBL Heidelberg, Germany

Reviewed by:
X. Antón Álvarez-Salgado, Consejo Superior de Investigaciones Científicas (CSIC), Spain
Laura Lorenzoni, University of South Florida, United States

***Correspondence:**
Laura Farías
laura.farias@udec.cl

Specialty section:
This article was submitted to Coastal Ocean Processes, a section of the journal Frontiers in Marine Science

Received: *07 February 2018*
Accepted: *07 May 2018*
Published: *29 May 2018*

Citation:
Testa G, Masotti I and Farías L (2018) Temporal Variability in Net Primary Production in an Upwelling Area off Central Chile (36°S). Front. Mar. Sci. 5:179. doi: 10.3389/fmars.2018.00179

INTRODUCTION

The Eastern Boundary Upwelling Systems (EBUS) are considered the most productive regions in the world's oceans and sustain the greatest portion of global fishery production (Pauly and Christensen, 1995; Cubillos et al., 1998b). This high productivity is mainly the result of the coastal upwelling process by which subsurface, nutrient-rich waters ascend to the surface in response to wind stress on surface water, fertilizing waters in the photic zone and promoting phytoplankton blooms. Lachkar and Gruber (2012) identified equatorward alongshore wind, eddy activity, the width of the continental shelf and mixed layer depth as key physical and environmental factors controlling Net Primary Production (NPP) in the EBUS. On the other hand, Messié and Chavez (2015) detected wind-driven macronutrient supply, iron provision,

temperature, light and offshore export as main drivers of time-space NPP variability in the EBUS.

The coastal upwelling systems off Chile extend over a wide latitudinal range (∼19–40°S), along irregular coastline with diverse topographic features (including canyons and the continental shelf) and variable river runoff. NPP may therefore be temporally and spatially variable. Coastal upwelling off central Chile has been relatively well documented with regards to the hydrological properties and dynamics of upwelling waters (Montecino et al., 2006; Escribano and Schneider, 2007; Kämpf and Chapman, 2016). Additionally, biological properties (such as Chlorophyll-a distribution) and their roles in determining productivity have been investigated (Montero et al., 2007; Iriarte et al., 2012). However, a significant gap remains for understanding temporal NPP dynamics and rates, which in turn limits the knowledge of how NPP rates and their variability are maintained. Information on marine primary production has been centrally important in understanding the fluxes of energy and organic matter in the ocean and the major biogeochemical cycles (e.g., C, N, P).

NPP measurements off the Chilean coast have been performed using different techniques, including O_2, ^{14}C and ^{13}C methods (Montecino et al., 1998; Daneri et al., 2000; Farías et al., 2009; Iriarte et al., 2012). Volumetric primary production rates have been derived from different methods, each one with intrinsic assumptions and biases, which lead to differences in these measurements (Cullen, 2001; Regaudie-de-Gioux et al., 2014). The oxygen evolution (light and dark incubation) method was one of the first techniques capable of determining gross primary production (GPP) and has been widely applied due to its simplicity. However, the ^{14}C method (Steeman Nielsen, 1952) rapidly became the standard for the oceanographic community, and has been used to calibrate remote sensing algorithms (Behrenfeld and Falkowski, 1997a; Banse, 2002). This method was used to measure net primary production NPP, but has been gradually replaced by the use of stable isotope additions, including ^{13}C (Slawyk et al., 1977) and ^{18}O (Bender et al., 1987). The highest primary production estimates are derived using the ^{18}O addition method, while ^{13}C likely underestimates NPP rates, at least as compared to ^{14}C (Regaudie-de-Gioux et al., 2014).

In addition, advances in optical satellite technology over the last three decades have facilitated semi real-time estimations of global NPP (total and fractioned) using multiple models (e.g., Behrenfeld and Falkowski, 1997b; Behrenfeld et al., 2005; Hirata et al., 2009). Despite rich biological productivity (2.57 million tons in 2012 according to FAO, 2014), both measured and estimated NPP rates along Chile's continental shelf are few and discontinuous (i.e., see Table 1 in Thiel et al., 2007) and therefore warrant an effort to combine these approaches.

Different temporal variability in coastal upwelling affects NPP along Chile's coast. As upwelling process occurs, subsurface water of equatorial origin (Equatorial SubSurface Water, ESSW) is upwelled to the surface, delivering waters with low temperature and dissolved O_2 levels, but high salinity and nutrient content (Silva et al., 2009). Areas characterized by a semi-permanent upwelling (off Coquimbo, 30°S) show similar NPP rates throughout the year, while off central Chile (Concepción, 36°S) strong seasonal variability is observed (i.e., Table 1 in Thiel et al., 2007).

Off central Chile, upwelling events are mainly driven by South Pacific Subtropical Anticyclone seasonal fluctuations (Fuenzalida et al., 2008) that promote local southern winds concentrated in spring and summer (Sobarzo and Djurfeldt, 2004) and even synoptic variability with 3–12 day fluctuations leading active and relaxed upwelling events (Aguirre et al., 2014). In addition, upwelling events driven by the Biobío canyon (Sobarzo and Djurfeldt, 2004; Sobarzo et al., 2016) have been documented, as well as NPP enhancement due to the effect of geomorphological protection (Montecino et al., 2006; Henríquez et al., 2007).

The coastal area off Concepción is also influenced by river runoff, mainly from the Itata and Biobío rivers (Saldías et al., 2012; **Figure 1**). Seasonal freshwater discharge to the continental shelf (with a peak during the rainy June and July; Sobarzo et al., 2007) may affect the stability/stratification of the water column, as river runoff mainly affects salinity and coastal NPP with the input of substantial amounts of inorganic nutrients (Sánchez et al., 2008).

Furthermore, remote equatorial processes (i.e., El Niño Southern Oscillation, ENSO) affect the productivity and composition of the marine phytoplankton community in the northern Chile, resulting in a shift in thermocline depth and upwelling patterns (Ulloa et al., 2001; Escribano et al., 2004; Iriarte and González, 2004). The factors affecting NPP off central Chile and the effect of processes such as the ENSO cycle (El Niño (EN) and La Niña (LN) events) on the upwelling and the precipitation regime are poorly understood (Montecinos and Aceituno, 2003; Montecinos and Gomez, 2010), and information regarding biological productivity and phytoplankton phenology remains lacking (Corredor-Acosta et al., 2015).

This study investigates how upwelling events, river runoff, ENSO forcing, and other processes modulate NPP patterns in an upwelling region off Central Chile, using *in situ* NPP measurements and satellite estimated NPP rates. Bio-oceanographic data from the *Centro de Investigación Oceanográfica en el Pacífico Sur-Oriental* (COPAS) time series station, *in situ* NPP measurements from 2006 to 2013, and a decade's worth (2006–2015) of satellite NPP estimations (NPPE), were collected, calibrated and compared in order to infer the mechanisms that cause temporal variability in NPP off central Chile. In this way, this study represents one of the first temporal baselines registering mid-term NPP dynamics and will increase our understanding of how natural and anthropogenic changes in costal upwelling affect C, N and other biogeochemical cycles. Climate change is expected to contribute to a reduction in precipitation in central-south Chile with a concomitant decrease in freshwater discharge (Boiser et al., 2016), and to an increase of along coast winds, which will support upwelling off the coast of central Chile (Sydeman et al., 2014). These climate change scenarios and their impacts (some already observable) may affect NPP rates and timing. Consequently, we may observe alterations in the production of organic carbon and the trophic network, and therefore in heterotrophic organisms and fisheries (Neira and Arancibia, 2004), as well as changes to the magnitude of

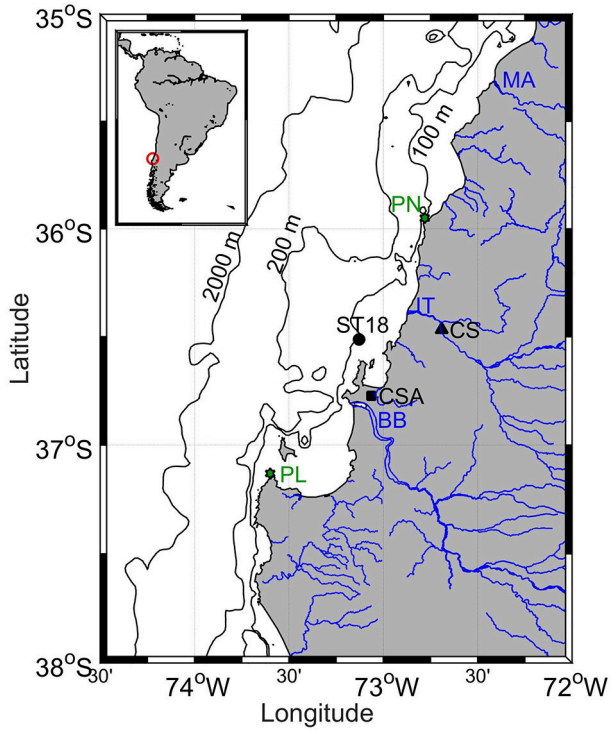

FIGURE 1 | Geographic location of Station 18 (ST18), Coelemu Station (CS), Carriel Sur Airport (CSA), Punta Nugurne (PN), Punta Lavapié (PL), Itata (IT), Biobío (BB), and Maule (MA) rivers. In addition 100, 200, and 2,000 m isobaths are shown.

greenhouse gas exchanges across the air-sea interface (Nevison et al., 2004; Cai et al., 2006).

MATERIALS AND METHODS

Study Zone and Sampling Strategy

The study area is located on the widest (approximately 60 km) continental shelf of Chile (excluding Patagonia) and framed by two submarine canyons (**Figure 1**), formed by the Itata and Biobío (Sobarzo and Djurfeldt, 2004). The area between 35 and 37°S is characterized by an upwelling front ∼25 km wide (Pizarro, 1999). The location of the upwelling front in relation to the coastline is dependent on the position of the major upwelling centers, Punta Nugurne (35°57′S) and Punta Lavapié (37°08′S; **Figure 1**), the width of the continental shelf, and the presence of eddies, filaments, meanders and coastal jet (Sobarzo and Djurfeldt, 2004; Letelier et al., 2009).

In situ observations from January 2006 to January 2016 were provided by the COPAS time series station (ST18), located at the center of the continental shelf, ∼18 nm from shore and a depth of 90 m (**Figure 1**). Monthly cruises (R/V Kay-Kay II) visited the site to collect continuous (temperature, salinity and Photosynthetically Active Radiation, PAR) profiles using a Conductivity Temperature Depth (CTD) probe (SeaBird 19 and SeaBird 25), along with discrete samples for O_2, nutrients, Chlorophyll-a (Chl-a) and NPP rates at depths of 2, 5, 10, 15, 20, 30, 40, 50, 65, and 80 m using 10 L Niskin bottles. In addition, estimations were computed for:

Upwelling Index

We computed the Upwelling Index (UI; m^{-3} s^{-1}) as Ekman zonal transport per 1,000 m of coastline (Bakun, 1973), from 2006 to 2015, using Equation (1):

$$UI = \left(\frac{\tau_y}{\rho f}\right) \cdot 1000m \quad (1)$$

where τ_y (Pa; kg m^{-1} s^{-2}) is the mean wind stress meridional component within the box 73–74°W, 36–39°S, ρ represents the mean density of the water column at ST18 (1026.21 kg m^{-3}), and f indicates the Coriolis parameter corresponding to the latitude of ST18 (8.67 $*10^{-5}$ s^{-1}). Daily τ_y data were obtained from the CoastWatch project (http://coastwatch.noaa.gov). In order to generate the 2006–2015 time series, Level 3 (L3) data were extracted from the Quik Scatterometer (QuikSCAT) mission (spatial resolution = 0.125°) for 1 January 2006 to18 November 2009, and L3 Metop Advanced Scatterometer (ASCAT) data (spatial resolution = 0.25°) was used for 19 November 2009 to 31 December 2015. We estimated a coefficient of determination (r^2) of 0.85, $p < 0.05$ (Fisher's p-value), observed during a period when two satellites overlapped (10 October 2009 until 18 November 2009; y-intercept: 0.0123 and slope: 0.8618).

Monthly standardized anomalies were calculated using Equation (2):

$$Anomaly = \frac{(xN - XN)}{\sigma N} \quad (2)$$

where xN is the discrete value at a certain time, XN is the mean climatological value and σN represents the climatological standard deviation.

Rivers Runoff and Precipitation Rates

Data for Itata River daily runoff were collected at the Coelemu Station (72°41′W, 36°28′S), and daily rainfall was recorded at a meteorological station at the Carriel Sur Airport (73°4′W, 36°46′S, **Figure 1**). Both datasets were provided by the Chilean *Dirección General de Aguas* (DGA; http://www.dga.cl/).

Oceanic Niño Index

ENSO was measured as the Oceanic Niño Index (ONI); data were obtained from the Climate Prediction Center (http://www.cpc.ncep.noaa.gov/). For cumulative analysis and considering that data did not cover the entire period of EN 2015-16, five EN and LN events were selected. We used Monte Carlo experiment (1,000 iterations) to assess statistical significance between cumulative NPPE during EN and LN events (Montecinos and Gomez, 2010).

Net Primary Production Estimations

NPPE were obtained using the standard Vertically Generalized Production Model (VGPM; Behrenfeld and Falkowski, 1997b) and extracted using 8-day average estimations at a spatial resolution of ∼9 km (Ocean Productivity Page, http://www.science.oregonstate.edu/ocean.productivity/). Among many

TABLE 1 | Summary of error statistics, i.e., Absolute Average Error (AAE), Root Mean Square Error (RMSE), Bias Mean Normalized Bias (P_{BIAS}), Mean Absolute Percentage Error (MPE) and r^2 coefficients for different satellite NPP areas.

Matrix dimensions (lon × lat)	Comments	*n*	AAE	RMSE	Bias	P_{BIAS} (%)	MPE (%)	r^2
1 × 1	*In situ* measurements	54	/	/	/	/	/	/
1 × 1	Pixel nearest to ST18	54	3.66	4.80	3.17	153.60	673.21	0.47
2 × 2	Avg of the 4 pixels nearest to ST18	54	3.35	4.40	2.73	132.15	619.00	0.51
3 × 3	Pixel nearest to ST18 in the center of the grid	54	3.33	4.27	2.75	133.22	620.52	0.56
5 × 5	″	54	3.07	3.95	2.45	118.69	594.08	0.57
7 × 7	″	54	2.85	3.62	2.20	106.41	578.06	0.58
9 × 9	″	54	2.66	3.37	1.98	95.80	561.85	0.58
11 × 11	″	54	2.47	3.14	1.73	83.63	546.15	0.58
13 × 13	″	54	2.33	2.97	1.48	71.80	531.21	0.59
15 × 13	74°-72°45′ W, 36°-37° S	54	2.02	2.75	0.89	43.31	462.99	0.61

NPP models, standard VGPM from SeaWiFS was considered as the model with higher correlation ($r^2 = 0.66$) with 610 *in situ* NPP measurements calculated for the California Current (Kahru et al., 2009).

In order to obtain representative satellite estimates, a NPPE time series was created with 8-day average estimations for a similar time period as used for *in situ* measurements. Next, basic statistics parameters were used to compare *in situ*-satellite data for different pixel boxes (Swirgon and Stramska, 2015). Comparison revealed higher correlation between NPP and NPPE, expressed as r^2, and lower error, within the boundaries of 72°45′-74°W, 36–37°S (**Table 1**), a zone with a total area of $13*10^3$ km^2 and approximately 55% located over the continental shelf. Analysis of variance (ANOVA) and linear regressions were performed using model II reduced major axis regression (Legendre and Legendre, 1998). Mean values for each pixel box were calculated, except in the case of the pixel box nearest to ST18, which used a single estimation. If a mean estimation described at least 33% of the pixels, it was considered valid.

NPPE Weekly Variability

The magnitude of week-to-week (WW) NPPE variability was calculated using Equation (3):

$$WW = w_t - w_{(t+1)} \quad (3)$$

where w_t represents the 8-day-average NPPE during time t and $w_{(t+1)}$ is the successive NPPE.

Wavelet analysis was used to establish dominant frequency bands and their recurrence in the time series, decomposing the signal and estimating its spectral characteristics as a function of time (Torrence and Compo, 1998). Continuous Morlet wavelet transform was applied using the MATLAB functions provided by Torrence and Compo (1998; http://paos.colorado.edu/research/wavelets).

Agglomerative hierarchical cluster analysis (single linkage technique) was used to evaluate the degree of dissimilarity in monthly bio-oceanographic features.

Photosynthetically Active Radiation

L3 satellite PAR data were obtained (using 8-day composites with a spatial resolution of ∼4 km) from the Aqua Moderate Resolution Imagining Spectroradiometer (MODIS) mission, within the limits 72–76°W and 35–39°S. Photic Layer Depth (PLD) was estimated using 62 *in situ* instant PAR profiles collected using a Biospherical QSP 2150 sensor deployed together with CTD profiler. PLD was identified as the depth where downwelling photosynthetic photon flux was equal to 1% of the surface value. Satellite-determined PLD was calculated as PLD = $\ln(0.01)*K_{490}^{-1}$ (Behrenfeld et al., 2005), using the 8-day composite Diffuse Attenuation Coefficient K_{490} (with a spatial resolution of 4 km) from the Aqua MODIS mission. The vertical attenuation coefficient for downward irradiance in the upper 20 m was calculated as described by Kirk (1983).

Phytoplankton Sizes Classes

Calculations from Hirata et al. (2011) were used to estimate the percentage contribution of micro-, nano- and picophytoplankton to total satellite Chl-a estimations. L3 MODIS Chl-a estimations (8-day average at a spatial resolution of 4 km) were analyzed for the area 72°45′-74°W, 36–37°S by setting the proportions of microphytoplankton >100% at 100%, and negative proportion of picophytoplankton at 0%.

Net Primary Production Measurements

A total of 54 *in situ* NPP monthly measurements were obtained from July 2006 to December 2013 at ST18 (**Figure 1**). At least four measurements for the photic layer are available for every month, with 5–9 monthly measurements available from 2008 to 2013. Light Carbon Assimilations Rates (LCAR) were calculated using the ^{13}C stable isotopic technique (Slawyk et al., 1977) on a mooring line. Samples were captured in polycarbonate 0.6 L bottles, starting at the surface and to a maximum depth of 50 m. The ^{13}C tracer concentration was 3.6456 mg ^{13}C mL^{-1}, equivalent to 0.5 mmol mL^{-1}, and 0.5 mL of tracer was added to each sample, to achieve approximately 10% enrichment. Immediately following tracer addition and prior to sunrise, bottles were deployed to sampling depths for *in situ* incubation.

Incubation periods of 10–12 h (counted from the time of sunrise) were used to average phytoplankton physiological activities along the day. Incubation was terminated at dusk using gentle vacuum filtration (<100 mm Hg) through precombusted grade GF/F glass filters. Filters were dried at 60°C for 24 h and then stored at constant temperature until laboratory analysis using continuous-flow isotope ratio mass spectrometry (Finnigan Delta Plus IRMS).

NPP rates were determined as LCAR (mg C m^{-3} t^{-1}) (Raimbault et al., 1999; Fernández et al., 2005) according to Equation (4):

$$\rho DI^{13}C = \left[\frac{(\%R_{POC} - R_n) * \left(\frac{POC}{12 * V_f} \right)}{\%R_{DIC}} \right] * 12 \quad (4)$$

$$\%R_{DIC} = \frac{\left(\frac{V^{13}C * {}^{13}DIC}{V_b} \right) + DIC_i * 0.01112}{DIC_i - \frac{V^{13}C * {}^{13}DIC}{V_b}} * 100 \quad (5)$$

where V_f represents filtered volume and *POC* is the amount of particulate organic carbon recovered in the filter after incubation and measured by mass spectrometry (μg). The excess enrichment of the tracer after inoculation (To) is indicated by $\%R_{DIC}$, calculated using Equation (5). $\%R_{POC}$ indicates ^{13}C enrichment in the filter after incubation, measured by the tracer mass. In Equation (5), $V^{13}C$ indicates the volume of ^{13}C added to the sample during the inoculation, while ^{13}DIC accounts for the tracer concentration added to the sample (3.6456 mg ^{13}C mL^{-1}). DIC_i represents the initial amount of dissolved inorganic carbon in the sample before inoculation. For this study, a constant value of 26 mg C L^{-1} was selected and applied based on previous measurements for the area (Paulmier, unpublished data). V_b is the volume in the incubation flask (0.6 L). Volumetric assimilation rates (LCAR) were integrated for the photic layer throughout the photoperiod in order to estimate integrated NPP rates (g C m^{-2} d^{-1}). In this way, our measurements do not include dark respiration, which may cause overestimation of NPP rates (Regaudie-de-Gioux et al., 2014).

Physico-chemical Variables

Brunt-Väisälä frequency (BVF) based on temperature and salinity data were obtained using the Ocean Data Viewer (version 4.7.4). Dissolved oxygen was analyzed in triplicate for a 125 mL sample by Winkler titration using a Dosimat 665 with automatic photometric end-point detector (detection limit ∼2 μmol L^{-1}). Fixed samples were analyzed between 12 and 24 h after collection and the percent saturation of dissolved oxygen was calculated based on Boyer et al. (1999).

Triplicate samples for nutrients were filtered onboard (using 0.7 μm, grade GF-F glass filters for NO_3^- and PO_4^{3-} and 0.45 μm membrane of cellulose acetate for $Si(OH)_4$, stored in 15 mL screw-capped centrifuge tubes, and frozen (at −20°C) until analysis. Until 2011, nutrient concentrations were determined using standard manual colorimetric techniques (Grasshoff et al., 1983) and *a posteriori* using the Seal AutoAnalyzer 3 (AA3). We only considered $Si(OH)_4$ data from 2010 to 2016 because of possible contamination due to sampling strategy during the period 2006–2009. Chl-a was measured for triplicate 250 mL water samples, filtered using 0.7 μm, grade GF/F glass fiber filters. Samples were frozen at −20°C and later analyzed using fluorometry (Turner Designs 10AU^{TM}) according to standard procedures (Parsons et al., 1984).

Upwelling-Driven Nutrient Flux

Upwelling-driven nutrient flux (kmol d^{-1}; with 1 kmol = 10^3 mol) from 2003 to 2016 was calculated according to Equation (6):

$$F = UI \cdot C \quad (6)$$

where *UI* is the mean upwelling index (m^3 s^{-1}) during the 3 days prior to field survey and C represents the mean concentration of subsurface nutrients (40–80 m; mmol m^{-3}) at ST18. *UI* was calculated as volumetric Ekman zonal transport per 1,000 m of coastline; explained by the width of the Itata River mouth (∼1,000 m) and our goal of comparing the two fluxes over an area of similar order of magnitude. This simple model assumes: (1) a constant wind field with no changes in magnitude and direction (i.e., without considering wind curl and Ekman pumping); (2) an ocean with no horizontal or vertical boundaries (i.e., ignoring upwelling events induced by topography and trapped waves); (3) the replacement of the zonal transport by vertical advection (i.e., without considering horizontal advection); (4) an absence of diapycnal mixing; and 5. downwelling-favorable winds produce nutrient loss from the photic layer.

Nutrient Export by River Discharge

Nutrient flux (kmol d^{-1}) from Itata River discharge between 2003 and 2016 was calculated using Equation (7):

$$F = Q \cdot C \quad (7)$$

where *Q* represents mean Itata runoff (m^3 s^{-1}) during the 3 days prior to field survey and *C* is the nutrient concentration (mol m^{-3}) at the Coelemu station (**Figure 1**). Approximately trimonthly NO_3^- and PO_4^{3-} concentrations were obtained from the DGA; NO_3^- was estimated using Kjeldahl methods; PO_4^{3-} was determined colorimetrically by spectrophotometry. In the absence of $Si(OH)_4$ measurements in the Coelemu station dataset, a well-established stoichiometric ratio, $Si(OH)_4$:NO_3^- = 7.745 (μM/μM; Yévenes, personal communication), was used to estimate $Si(OH)_4$ concentrations from existing NO_3^- data in the Itata River. Our simple approach attempted to compare nutrient input from wind-driven coastal upwelling (NO_3^-, PO_4^{3-} and $Si(OH)_4$) and from river discharge (freshwater source) in the study zone.

RESULTS

Annual Cycles and Their Interannual Variability

Meteorological and Hydrological Forcing Agents

From 2006 to 2015, the upwelling index (UI) oscillated between −3,324 and 4,369 m^3 s^{-1} 1,000 m^{-1} coastline (**Table 2**; Supplementary Figure 1).The annual cycle based on monthly

TABLE 2 | Summary of statistics values, i.e., number of samples (n), Minimum (Min), Maximum (Max), Mean and Standard Deviation (SD) for variables analyzed in annual cycles section. *In situ* mean values were calculated for the upper 10 m of the water column.

	n	Min	Max	Mean ± *SD*
METEOROLOGICAL AND HYDROLOGICAL FORCING AGENTS				
Upwelling Index [m^3 s^{-1} 1,000 m^{-1}]$^{\Phi}$	3,591	−3,324	4,369	646 ± 940
Itata Runoff [m^3 s^{-1}]	3,408	13.2	4,242	282.2 ± 347.8
Rain Rate [mm d^{-1}]	3,648	0	112.5	2.9 ± 8.8
Surface PAR [E m^{-2} d^{-1}]$^{\Phi}$	457	9.45	66.87	37.9 ± 16.6
OCEANOGRAPHIC VARIABLES				
Temperature [°C]	112	10.6	16.7	12.7 ± 1.2
Salinity	112	26.9	34.8	33.8 ± 1.2
Brunt-Vaisala Frecuency [cycl h^{-1}]	112	−17.9	57.7	8.0 ± 10.2
Oxygen [μM]	87	119.5	338.7	249.8 ± 43.5
Nitrate [μM]	107	0.3	28.1	11.3 ± 6.1
Upwelling Nitrate Flux [kmol d^{-1}]	140	−2152.2	6953.3	1470.6 ± 1769.9
Continental Nitrate Flux [kmol d^{-1}]	34	2.7	691.4	110.2 ± 153.1
Phosphate [μM]	107	0.1	2.8	1.4 ± 0.5
Upwelling Phosphate Flux [kmol d^{-1}]	140	−212.7	756.2	169.2 ± 193.3
Continental Phosphate Flux [kmol d^{-1}]	39	0.1	55.3	9.9 ± 11.0
Silicate [μM]	57	0.2	20.4	7.9 ± 5.3
Upwelling Silicate Flux [kmol d^{-1}]	59	−2927.8	6550.0	1352.0 ± 1753.6
Continental Silicate Flux [kmol d^{-1}]	34	20.9	5355.2	853.1 ± 1186.1
PHOTIC LAYER, CHLOROPHYLL-A AND PRIMARY PRODUCTION RATES				
Photic Layer depth [m]	58	7	49	23.8 ± 11.9
Photic Layer depth [m]$^{\Phi}$	440	6.7	61.6	32.3 ± 9.6
Chlorophyll-a [mg m^{-3}]	703	0.0	53.1	2.48 ± 5.83
Surface Chlorophyll [mg m^{-3}]	83	0.1	36.1	4.7 ± 7.2
Surface Chlorophyll [mg m^{-3}]$^{\Phi}$	450	0.4	18.6	4.1 ± 3.4
Microphytoplankton [% Chl-a]$^{\Phi}$	450	18.3	96.5	60.1 ± 13.6
Nanophytoplankton [% Chl-a]$^{\Phi}$	450	2.9	49.4	23.6 ± 7.9
Picophytoplankton [% Chl-a]$^{\Phi}$	450	0.5	32.3	16.3 ± 5.7
LCAR [g C m^{-3} d^{-1}]	216	0.2	1721.7	74.0 ± 207.7
NPP [g C m^{-2} d^{-1}]	54	0.03	18.23	2.06 ± 3.12
NPPE [g C m^{-2} d^{-1}]$^{\Phi}$	454	0.45	9.07	2.97 ± 1.69

$^{\Phi}$*indicates satellite estimation.*

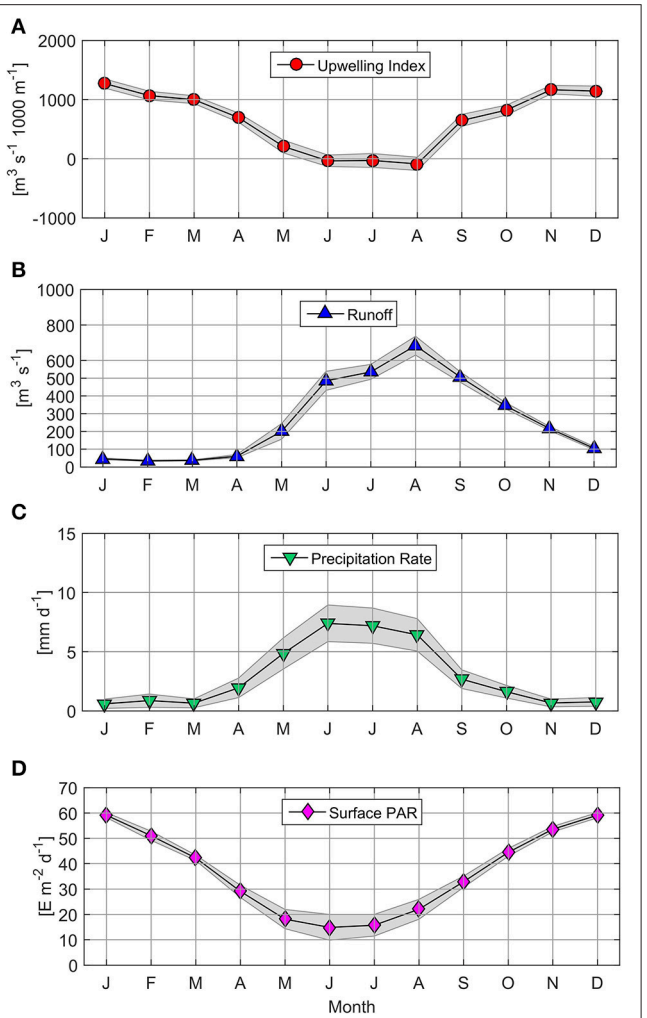

FIGURE 2 | Mean climatology for Upwelling Index **(A)**, Itata Runoff **(B)**, Precipitation Rate **(C)**, and Surface PAR **(D)**. Markers indicate monthly mean values; the shaded area represents monthly 95% confidence interval.

averages of UI time series revealed the predominance of upwelling favorable winds from September to April (66% of the year, with a maximum monthly mean of 1,271 m^3 s^{-1} 1,000 m^{-1} in January; see **Figure 2A**). By contrast, downwelling-favorable winds dominated between June and August and produced a negative UI value with a monthly mean of −87 m^3 s^{-1} 1,000 m^{-1} during August.

High Itata River runoff (>400 m^3 s^{-1}) was observed from June to September, with a maximum monthly mean of 683 m^3 s^{-1} during August (**Figure 2B**). River discharges of less than 60 m^3 s^{-1} were observed between January and April. The majority of Itata River runoff was explained by precipitation ($r^2 = 0.33$, $p < 0.05$, $n = 418$; **Figure 2C**).

Satellite surface PAR estimations (monthly means) were highest from November to February (>50 E m^{-2} d^{-1}; **Figure 2D**), and lowest (between 14.89 and 22.05 E m^{-2} d^{-1}) from May to August.

Oceanographic Variables

Temperature presented a clear seasonal variation (**Figure 3A**). From December to March, when a warming of the thin surface layer (with values higher than 13°C), caused by high levels of short wave radiation contrasted with the upwelling of cool subsurface water from the ESSW, created a marked thermal stratification. The intrusion of cold ESSW advected by coastal upwelling and demarked by an 11.2°C isotherm was clearly observed from September to March, due to a favorable upwelling process (**Figure 3A**). Between May and August the water column presented fairly homogeneous conditions, with higher temperatures with respect to upwelling periods mainly associated with Subantarctic Water (SAAW; Silva et al., 2009).

Seasonal variation in salinity was also observed (**Figure 3B**). Low salinity was detected in a thin surface layer each winter and spring and coincided with high precipitation and river runoff. From June to October, a low salinity area associated with the Itata River plume often extended as far as the zone around ST18, creating notable haline stratification (**Figure 3B**). During 2014 and 2015, the lowest salinities were also observed in the spring (i.e., 20.34 in November 2014 and 25.70 in October

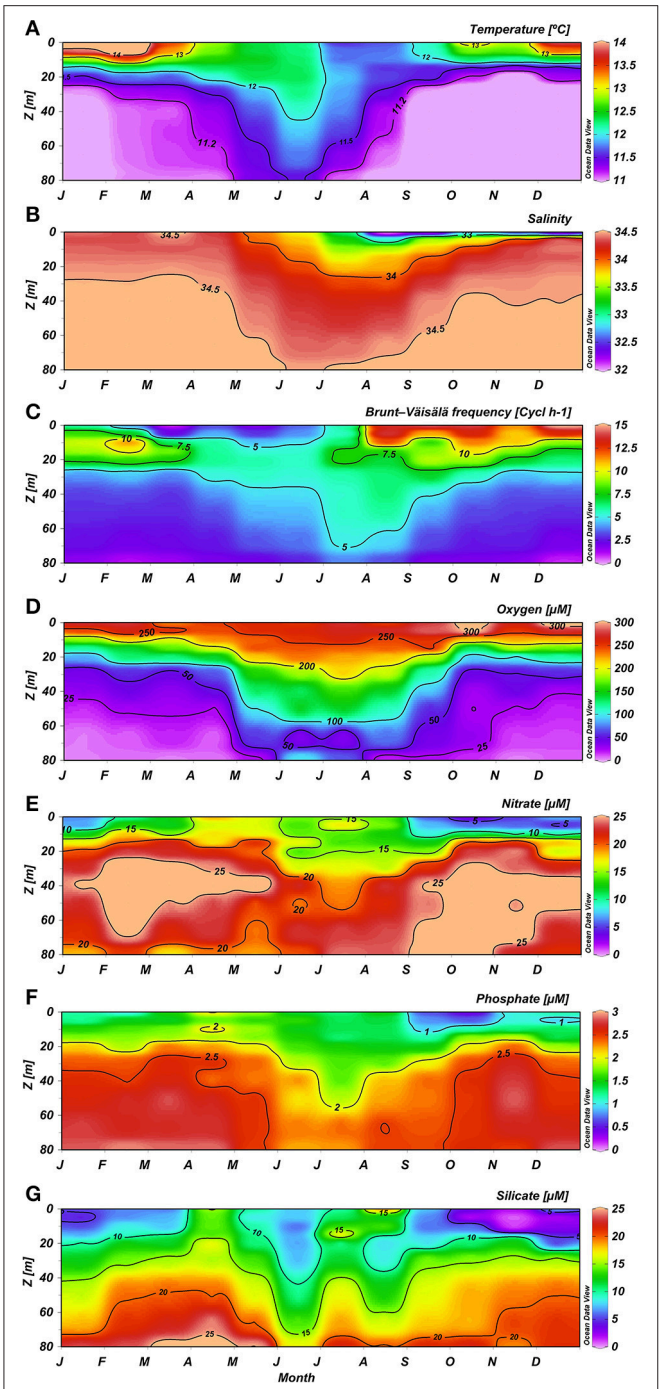

FIGURE 3 | Mean climatology for Temperature **(A)**, Salinity **(B)**, Brunt-Väisälä frequency **(C)**, Oxygen **(D)**, Nitrate **(E)**, Phosphate **(F)**, and Silicate **(G)** at ST18.

2015; Supplementary Figure 2). Salinity ≥34.0 was observed for the upper 20 m of the water column from June to September, with intermediate surface riverine influence between October and December, and sporadic events from January to April. Higher BVF values were observed between depths of 0 and 20 m, particularly from August to December (**Figure 3C**), and likely due to river discharge; subsurface BVF values appeared to be mainly associated with thermal stratification throughout the year, with the exception of late autumn (April and May). Upwelling of the nearly-homogenous ESSW between October and May caused high density homogeneity and lower BVF values between 30 and 80 m. During austral winter, however, elevated deep stability was observed.

Oxygen distribution in the water column (**Figure 3D**) presented higher O_2 concentrations (>200 µM) in the upper 15–20 m depth throughout the entire year, but subsurface water exhibited seasonal variation due to the intrusion of poorly-oxygenated ESSW from coastal upwelling. Subsurface hypoxic waters (with O_2 levels lower than 50 µM) were observable during the upwelling season from September to April; while between May and August this layer was deeper and more oxygenated (**Figure 3D**).

The surface layer showed reduced but not depleted nutrient concentrations, whereas the subsurface layer presented consistently higher nutrient concentrations (**Figures 3E–G**). Within the upper 10 m, NO_3^- and PO_4^{3-} showed minimum mean concentrations from September to January (with minimums of 6.66 and 0.75 µM in October, respectively), intermediate values in wintertime (at 13.74 and 1.41 µM in August, respectively) and higher values between February and May (with maximums of 17.46 and 1.96 µM, respectively, observed in April). These trends were consistent with the plankton temporal dynamics (see below). In contrast, $Si(OH)_4$ exhibited higher concentrations during late autumn and winter, and lower values (with a minimum mean value of 2.13 µM in November) during spring and summer (**Figure 3G**). This pattern reflects the high levels of $Si(OH)_4$ associated with river discharge and the development of diatom blooms in spring and summer.

Mean upwelling-driven NO_3^- and PO_4^{3-} fluxes were an order of magnitude higher than continental discharges from Itata River (**Table 2**). Conversely, mean oceanic $Si(OH)_4$ flux (1,352 kmol d^{-1}) was comparable to river input (853 kmol d^{-1}). High standard deviation was partially explained by seasonal variability (**Figure 4**). Indeed, wind-driver nutrient flux was higher from September to April (>1,086, 141, and 1,041 kmol d^{-1} for NO_3^-, PO_4^{3-} and $Si(OH)_4$, respectively), as compared with the rest of the year, whereas continental inputs reached maximum values between June and August (>226, 15, and 1,755 kmol d^{-1} for NO_3^-, PO_4^{3-} and $Si(OH)_4$, respectively).

Photic Layer, Chlorophyll-a and Primary Production Rates

Light penetration varied temporally, with a higher vertical attenuation coefficient (0.22 m^{-1}) from October to January, as compared with February to April (0.18 m^{-1}) and June to August (0.12 m^{-1}). In this way, PLD showed a distinctive seasonal pattern, with deepening in winter (to approximately 35 m) as compared to ∼15 m during spring-summer, and intermediate values during late summer-autumn (∼25 m, **Figure 5A**). Climatology for satellite-derived PLD revealed a similar temporal pattern (deeper values from April to August) as compared to *in situ* measurements (**Figure 5A**), although satellite estimations appeared to overestimate PLD, especially from September to February and in May.

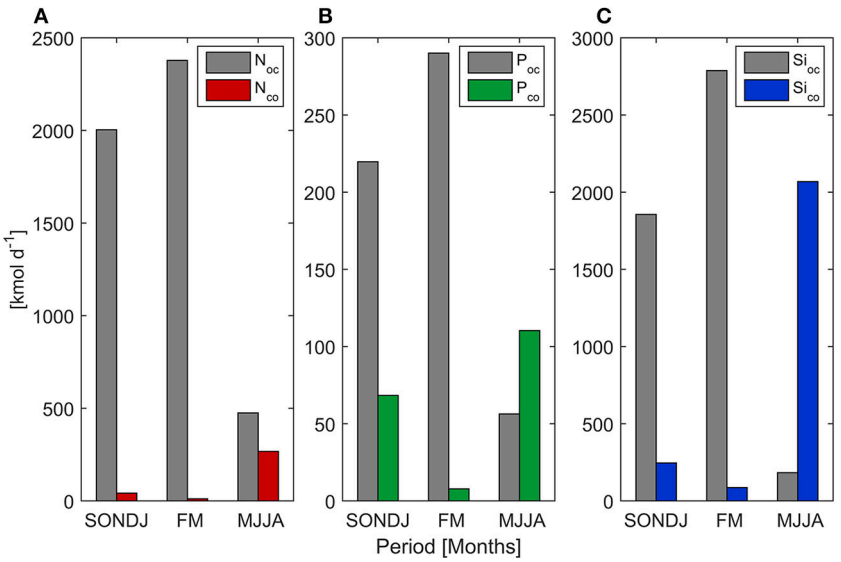

FIGURE 4 | Mean value of Nitrate **(A)**, Phosphate **(B)**, and Silicate **(C)** flux from upwelling ($_{oc}$) and river discharge ($_{co}$) during three periods of the year.

In situ Chl-a concentrations higher than 1 mg m^{-3} (with a marked subsurface peak through variable depths) were observed from September to May within the upper 20 m of the water column, while lower and more homogeneous values (ranging from 0.5 to 1 mg m^{-3}) were detected during winter (**Figure 5B**). Maximum monthly means of surface Chl-a were observed during October (12.0 mg m^{-3}), with minimum values (of 0.85 mg m^{-3}) recorded in July. The highest monthly mean of satellite Chl-a (7.7 mg m^{-3}) was registered during December (**Figure 5C**), while the lowest monthly mean (1.4 mg m^{-3}) was observed in July.

Microphytoplankton contributed between 18.3 and 96.5% of Chl-a, with the greatest overall contribution to total Chl-a observed during spring-summer (October–January), with monthly mean contributions from 65.5 to 69.2% (**Figure 5D**). The largest phytoplankton size class demonstrated elevated values from February to April (59.1–66.9% Chl-a), decreasing to below 50% in winter. Throughout the annual cycle, the nanophytoplankton community made greater contributions to Chl-a than picophytoplankton, with highest monthly means recorded in July (31.3 and 22.3% Chl-a, respectively).

Throughout the year, LCAR was greater than 20 mg C m^{-3} d^{-1} in the surface layer; LCAR greater than 100 mg C m^{-3} d^{-1} was observed during the entire upwelling season (**Figure 5E**). LCAR greater than 400 mg C m^{-3} d^{-1} was observed in surface waters (5–10 m depth) in spring and early summer (October 2006, December 2007, January, September and November 2009, and January 2011 and 2013; Supplementary Figure 3), and exceptionally high values of 1,721 and 1,536 mg C m^{-3} d^{-1} were recorded during November 2006 and 2013 at a 5 m depth, indicating NPP hotspots. Excluding the exceptionally high LCAR event in November 2006, LCAR:Chl-a mean values of 19.5 and 31.8 mg C mg Chl-a^{-1} d^{-1} were obtained for non-favorable and favorable upwelling periods, respectively, indicating that the wintertime phytoplankton community presents comparable photosynthetic efficiency with groups characterizing the upwelling season.

Daily integrated LCAR for the photic layer varied between 0.03 and 18.23 g C m^{-2} d^{-1}. NPP measurements showed a clear seasonal cycle, with lower monthly mean from February to August (from 0.22 to 1.81 g C m^{-2} d^{-1}, **Figure 5F**) as compared to September-January (1.81 to 6.43 g C m^{-2} d^{-1}). Monthly winter averages between 0.24 (July) and 0.84 g C m^{-2} d^{-1} (August) were observed.

Satellite NPPE fluctuated from 0.45 to 9.07 g C m^{-2} d^{-1} with the same seasonal variability as observed for Chl-a (**Figure 5F**). Between October and January, NPPE were higher than 3.9 g C m^{-2} d^{-1} (with a maximum monthly mean of 5.1 g C m^{-2} d^{-1} in December), while from February to June NPPE decreased to 1.1 g C m^{-2} d^{-1}. Basal productivity between 1.1 and 1.5 g C m^{-2} d^{-1} was observed using satellite estimations during the winter season. In September, mean NPPE rose to 2.9 g C m^{-2} d^{-1} with the activation of upwelling-favorable wind.

A linear regression calculated for *in situ* NPP and integrated Chl-a for the PLD and between satellite NPPE and Chl-a indicated significant determination coefficients of $r^2 = 0.50$ and $r^2 = 0.86$, respectively (**Table 3**). The regression for *in situ* NPP and satellite NPPE data within the limits of 72°45′-74°W and 36–37°S revealed a r^2 of 0.61 (**Table 3**), but when this data were separated into two periods, higher r^2 values were found during winter ($r^2 = 0.70$) with respect to the rest of the year ($r^2 = 0.24$).

The annual NPP cycle off central Chile has been traditionally divided in two oceanographic periods: a favorable and non-favorable upwelling season based on physical (Montecino et al., 2006; Sobarzo et al., 2007) and biological (Morales et al., 2007) criteria. However, when bio-oceanographic processes and variables, such as NPP, PLD and nutrients, are considered, a hierarchical cluster tree with a cophenetic correlation coefficient of 0.83 separates the annual NPP cycle into three

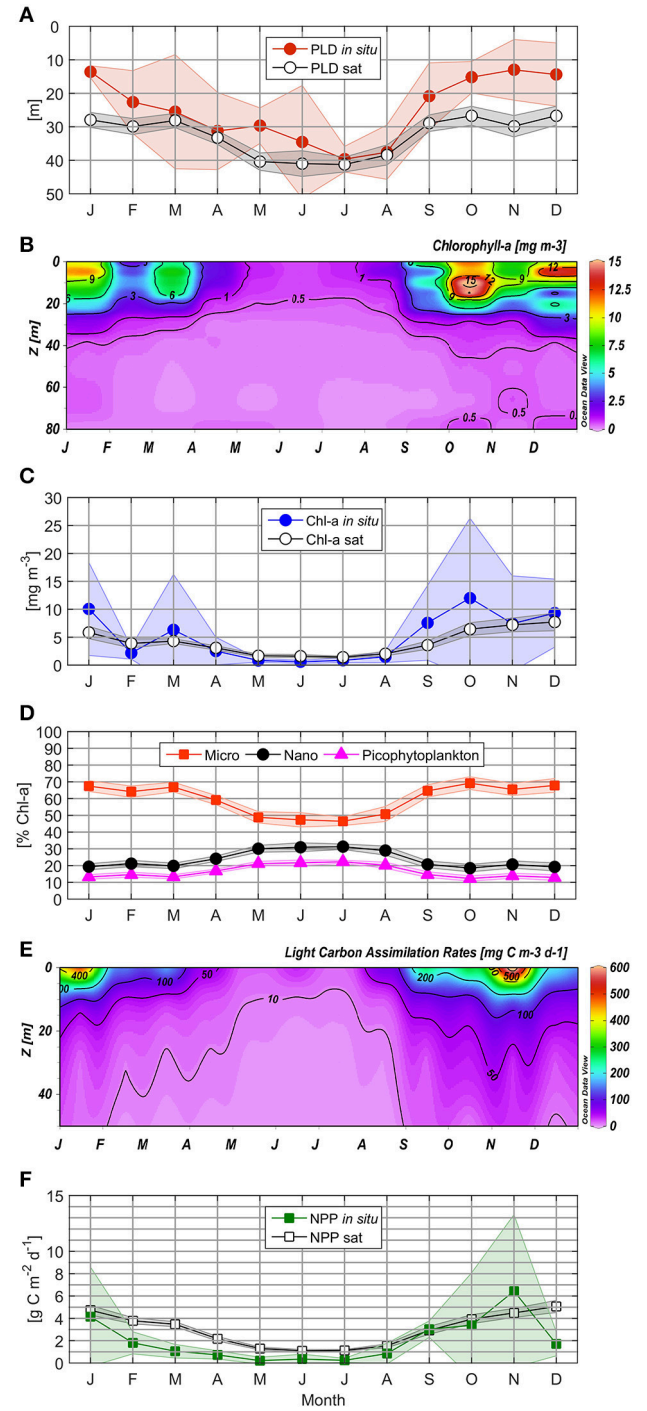

FIGURE 5 | Mean climatology for *in situ* and satellite Photic Layer Depth **(A)**, Chlorophyll-a **(B)**, *in situ* and satellite surface Chlorophyll-a **(C)**, Phytoplankton size classes **(D)**, Light Carbon Assimilation Rates **(E)**, and *in situ* and satellite Net Primary Production **(F)**. Markers indicate monthly mean values; the shaded area indicates monthly 95% confidence interval.

different periods (see **Figure 6**): a rising stage (high NPP), a falling stage (intermediate NPP) and a basal stage (low or basal NPP). The bio-oceanographic features observed for the study area during these periods are summarized in **Table 4**.

TABLE 3 | Summary of error statistics, i.e., number of observations (n), r^2 coefficient, and ANOVA F and *p*-values for biological variables (Chl-a, Chlorophyll-a; NPP, *in situ* Net Primary Production; NPPE, satellite-derived Net Primary Production Estimation).

				ANOVA	
		n	r^2	***F***	***p*-value**
Chl-a* vs. NPP		43	0.50	40.57	<0.001
Chl-a$^{\Phi}$ vs. NPPE		444	0.86	2799.40	<0.001
NPP vs. NPPE	All data	54	0.61	80.54	<0.001
	Upwelling	36	0.24	10.89	<0.001
	Winter	18	0.70	34.72	<0.001

**indicates Chlorophyll-a integrated within the photic layer; $^{\Phi}$indicates satellite estimation. Upwelling period: September to April. Winter: May to August.*

Interannual Variability of NPP and its Relationship With ENSO

We observed three EN (2006–07, 2009–10, 2015–16) and three LN (2007–08, 2010–11, 2011–12) events of varying magnitude and duration between 2006 and 2015 (**Figure 7**). Minimum ONI measurements (−1.4°C) were found during January 2008, October 2010 and December 2010, while maximum ONI indexes (+1.3°C) were observed during December 2009 and January 2010.

Interannual variability in NPPE was also observed, with higher cumulative NPPE during neutral year 2014–15, LN 2010–11, and LN 2011–12 (1.28, 1.21, and 1.15 kg C m^{-2} yr^{-1}, respectively; see **Figure 7C**). In contrast, the lowest values were observed during the neutral years 2012–13 and 2013–14 (0.98 and 1.01 kg C m^{-2} yr^{-1}, respectively). Cumulative NPPE during EN and LN years yielded mean values of 1.07 and 1.14 kg C m^{-2} yr^{-1}, respectively. Mean NPPE was 1.1 kg C m^{-2} yr^{-1}. No statistical significance (Monte Carlo simulations, 1,000 iterations) was determined for NPPE between EN and LN conditions. A NPP wavelet power spectrum and normalized global wavelet spectrum revealed low variance and no statistical significance in interannual variability (**Figure 8**), and identified annual variation as the dominant frequency band.

DISCUSSION

The continental shelf off Concepción is an important upwelling zone and has been described as one of the most productive areas within the Humboldt Current system (Montecino et al., 1998; Montero et al., 2007; Thiel et al., 2007; Daneri et al., 2012; Iriarte et al., 2012). However, no systematic measurements of NPP have been performed, and NPP rates showed a great variability (e.g., 0.1 and 25.8 g C m^{-2} d^{-1}). Understanding the wide variation in NPP rates, NPP dynamics and factors controlling NPP is vital to improve our knowledge of C, N, and P cycles in central Chile.

At 36°S, upwelling occurs over one of the widest continental shelves along the southern part (18–41°S) of Humboldt EBUS. This shelf accelerates benthic pelagic coupling and thus the

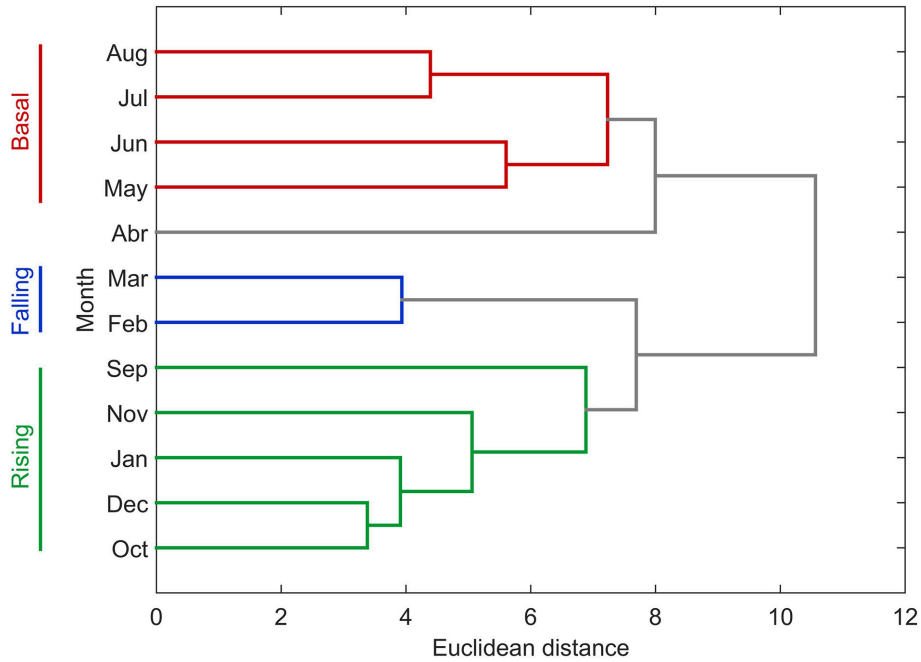

FIGURE 6 | Dendrogram presenting hierarchical clustering of the degree of similarity between monthly bio-oceanographic characteristics. We used monthly mean surface (0–10 m) values for temperature, salinity, nutrients (nitrate, phosphate and silicate) along with monthly means for satellite and *in situ* net primary production, satellite and *in situ* photic layer depth, satellite Chlorophyll-a and upwelling index.

TABLE 4 | Summary of bio-oceanographic conditions during three different periods of the year off central Chile (mean ± standard deviation).

Season	**Rising stage**	**Falling stage**	**Basal stage**
	(High productivity–upwelling activation)	**(Intermediate productivity–upwelling decay)**	**(Basal productivity–wet)**
Months	**September–January**	**February–March**	**May–August**
Upwelling index [m^3 s^{-1} 1,000 m^{-1}]$^{\Phi}$	1008.91 ± 772.75	1030.22 ± 609.94	13.46 ± 976.08
River runoff [m^3 s^{-1}]	249.36 ± 223.06	35.94 ± 25.74	482.04 ± 458.09
Temperature [°C]	12.91 ± 1.37	13.58 ± 1.33	12.02 ± 0.73
Salinity	33.71 ± 2.55	34.41 ± 0.33	33.47 ± 0.95
Brunt-Väisälä frequency [cycl h^{-1}]	10.86 ± 15.31	4.62 ± 8.57	6.83 ± 8.86
Oxygen [μM]	258.26 ± 67.19	236.79 ± 59.15	256.18 ± 30.06
Oxygen saturation (%)	126.25 ± 29.25	115.17 ± 28.75	120.90 ± 20.31
Nitrate [μM]	7.39 ± 7.04	12.91 ± 7.04	14.69 ± 4.95
Phosphate [μM]	1.05 ± 0.61	1.47 ± 0.56	1.48 ± 0.42
Silicate [μM]	4.66 ± 5.23	6.76 ± 3.49	10.52 ± 6.50
Surface PAR [E m^{-2} d^{-1}]$^{\Phi}$	46.55 ± 13.03	50.99 ± 6.44	18.57 ± 4.97
Diffuse attenuation coefficient [m^{-1}]$^{\Phi}$	0.46 ± 0.29	0.31 ± 0.12	0.14 ± 0.05
Photic Layer Depth [m]	15.65 ± 7.59	23.89 ± 9.58	35.82 ± 8.46
Photoperiod [h]	13.68 ± 0.94	12.45 ± 0.58	10.24 ± 0.58
Chlorophyll-a [mg m^{-3}]	9.58 ± 9.01	6.54 ± 12.38	0.90 ± 0.83
Microphytoplankton [% Chl-a]$^{\Phi}$	66.95 ± 11.41	65.71 ± 9.11	48.41 ± 11.37
NPP [g C m^{-2} d^{-1}]	3.98 ± 4.16	1.39 ± 0.69	0.46 ± 0.59

Based on cluster analysis, we considered April as transitional month with high variability. In situ mean values were calculated for the upper 10 m of the water column. $^{\Phi}$*indicates satellite estimations.*

supply of regenerated N, P and even Fe from sediment to bottom water (Farías et al., 1996; Graco et al., 2006; Fennel, 2010), which in turn controls NPP (Ryther and Dunstan, 1971). Thus, the Atlantic EBUS are also characterized by a wider continental shelf and higher NPP as compared to the Pacific, where the Humboldt EBUS presents higher productivity than the California

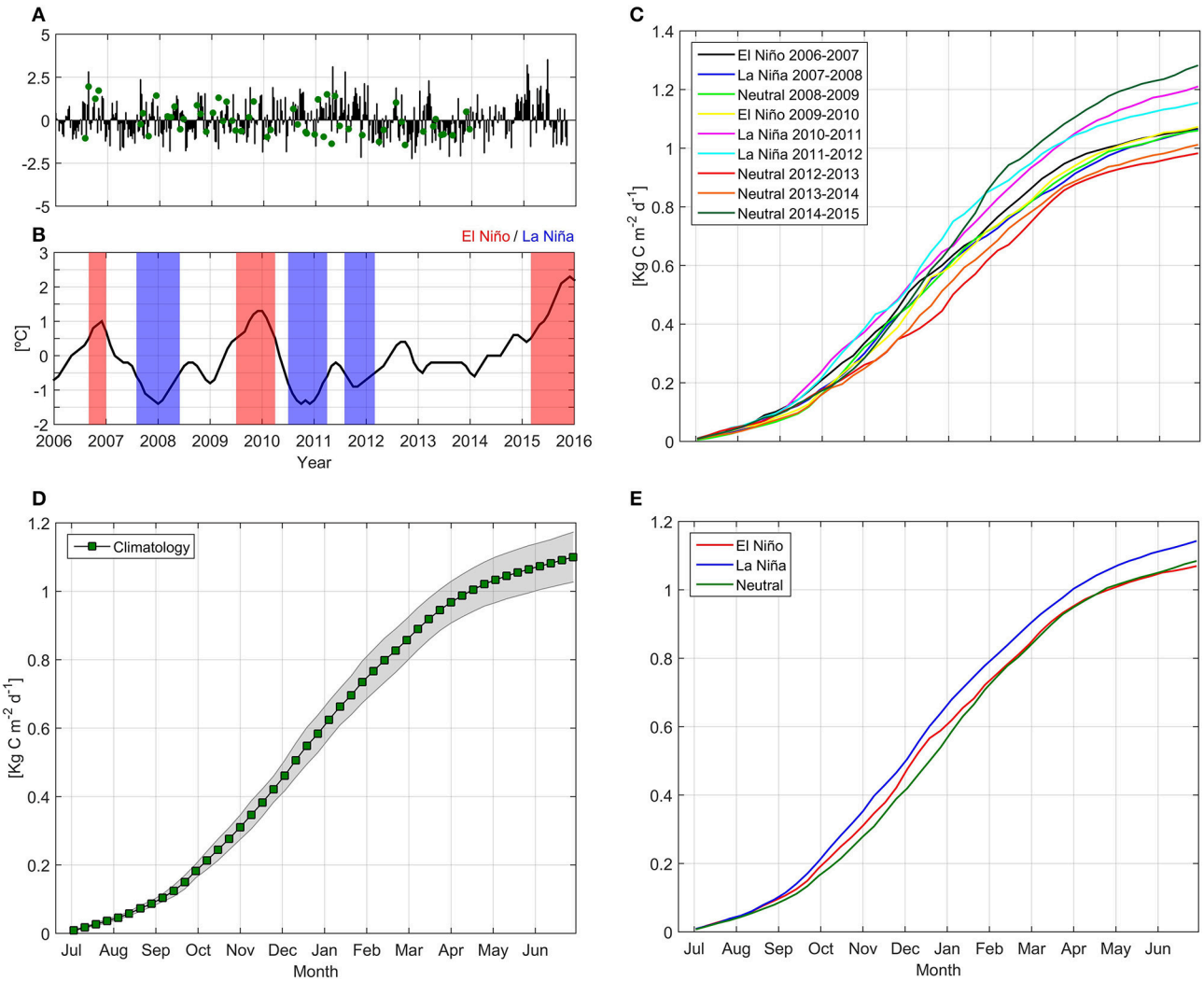

FIGURE 7 | Temporal evolution of standardized anomaly for *in situ* and satellite Net Primary Production (NPP, **A**), temporal evolution of the Oceanic Niño Index **(B)** and cumulative satellite NPP estimations by year **(C)**, climatological NPP mean with 95% confidence interval (markers and shaded area, respectively, **D**) and mean satellite-derived NPP values during El Niño, La Niña, and Neutral conditions **(E)**. Green points in NPP time series panel indicate *in situ* measurements.

EBUS (Lachkar and Gruber, 2012); this is partially explained by the presence of continental shelves in northern Peru and central Chile (Thiel et al., 2007). Nevertheless, central Chile is characterized by its intricate geometry, with gulfs, bays, islands and peninsulas generating high time-space NPP variability. A NPP spatial pattern was observed by Testa (2017) and found by Morales et al. (2013) to coincide with Chl-a distribution.

Each upwelling system is therefore considered unique in terms of its productivity. Off central Chile, the magnitude of fertilization in the photic layer appears to be significant and quasi-permanent throughout the year, not only due to the coastal upwelling present during 66% of the year, but also as a result of nutrient influx from rivers (see below). These nutrients can sustain a large population of photosynthetic organisms and in turn present a marked impact on subsequent trophic levels (Quiñones et al., 2010). We estimated mean annual NPP at 1.1 kg C m^{-2} yr^{-1} (**Figure 7D**), similar to the value determined by Daneri et al. (2000), who estimated an annual mean of ca. 1 kg C m^{-2} yr^{-1}, but lower than estimates for Benguela and Canary EBUS (Lachkar and Gruber, 2012). Cubillos et al. (1998b) estimated the primary production required to sustain central-southern Chile coastal pelagic fisheries at 0.65 kg C m^{-2} yr^{-1}, suggesting that no productive capacity limits the regional fisheries within this zone.

Seasonal Variability in NPP

The biological annual cycle has been statistically divided into three periods (**Figure 6**; **Table 4**):

Rising Period

From September to January, optimum conditions for the phytoplankton production are observed due to the

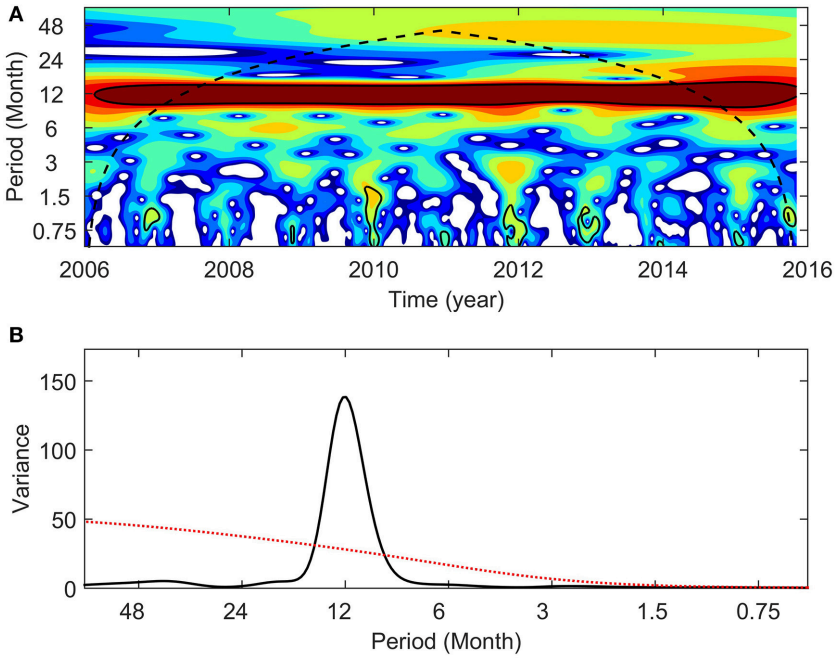

FIGURE 8 | Satellite Net Primary Production estimations wavelet power spectrum **(A)** and normalized global wavelet spectrum **(B)** with 95% confidence interval (black contours and red line, respectively). In wavelet power spectra the color scale indicates the strength of the periodicities over time (blue: weak variance; red: strong variance); the black dashed line represents the cone of influence.

synchronization of upwelling activation, optimal surface PAR values, thermal stratification and high subsurface nutrient input. During this period, NPP rates as high as 18.23 g C m^{-2} d^{-1} have been observed, with a mean integrated NPP of 4.0 g C m^{-2} d^{-1}. The strong light attenuation resulting in shallow PLD is likely to represent the main abiotic factor limiting NPP during the rising period. Nutrients, although occasionally reaching very low concentrations, were never depleted. Satellite estimations reveal a major proportion of Chl-a (and NPP) attributable to microphytoplankton (diatoms) during this period. *In situ* observations (Montero et al., 2007; Morales et al., 2007; Thiel et al., 2007; Iriarte et al., 2012; Anabalón et al., 2016) have revealed that chain-forming diatoms (*Skeletonema costatum*, *Thalassiosira* spp. and *Chaetoceros* spp.) dominate the phytoplankton community during periods of high NPP. A majority of NPP generated by diatoms is consumed by microheterotrophs (Thiel et al., 2007; Vargas et al., 2007), with only a small fraction (0–10%) of the C fixed by photosynthesis directly assimilated by copepods via the traditional herbivore food chain. Vargas et al. (2006) observed a negative relationship between egg hatching success, naupliar survival and diatom ingestion. Low direct herbivore zooplankton pressure on diatom communities may permit a proliferation of phytoplankton within this system. NPP rates of up to 18.3 (this study), 19.9 (Daneri et al., 2000) and 25.8 g C m^{-2} d^{-1} (Montero et al., 2007) have been observed, with the latter two determining the release of O_2 during photosynthesis based on changes in bulk O_2 concentration.

Falling Period

During February and March, PAR values remained adequate for supporting the phytoplankton community and the input of nutrients by coastal upwelling remained significant. Nevertheless, *in situ* NPP strongly decreased, with monthly mean values between 1.0 and 1.8 g C m^{-2} d^{-1}. Lower NPP rates and Chl-a values may result from a change in the physiological state of phytoplankton induced by biological (i.e., viral lysis; Brussaard, 2004) or physical components, such as decreases in ocean temperature and surface PAR and elevated turbulence (Garrison and Tang, 2014). The influence of top-down regulation by small ictiofauna species, particularly *Engraulis ringens*, should be considered. Cubillos et al. (1998a) observed that anchovy reached a maximum relative abundance between February and May, and stomach content analysis demonstrated that this specie is an omnivore and displays a preference for phytoplankton (Arrizaga et al., 1993).

Basal Period

In situ NPP revealed a mean basal productivity from May to August of 12% of spring-summer productivity, and a NPPE of approximately 24% of spring-summer values for the same period. Basal productivity (averaging 1.01 and 0.46 g C m^{-2} d^{-1} for NPPE and *in situ* measurements, respectively) may be supported by nutrient influx associated with continental runoff and river discharge. Maximum river discharge is correlated with precipitation in winter (Sobarzo et al., 2007). River discharge to the coastal zone produced a plume extending to the fixed station under study (Saldías et al., 2012). Northern wind patterns

observed during the study period are known to drive the downwelling of subantartic waters SAAW (Silva et al., 2009) and consequential mixing with fresh water inputs. In this way, SAAW water appears to maintain relatively lower, but continued productivity. Sobarzo et al. (2007) show that wind was too weak to disrupt the buoyancy stratification around the river mouth at any point during the year. Indeed, continental freshwater discharge increased water column stability and inhibited wind-driven vertical mixing. As a result, greater residence times in the water column were observed during winter (Montecino et al., 2006). More intense stratification, together with nutrients input from river discharge, may create favorable conditions for the growth of nano- and picophytoplankton communities (Iriarte et al., 2012).

During the wet season, higher stratification and a decrease in phytoplankton biomass (due to a reduced cell size) may create advantageous conditions for light penetration within the water column. In spite of lower surface PAR values, the 1% limit occurs at a greater depth. As a result, more homogenous Chl-a concentrations were observed within the upper 30 m during winter, with NPP resulting from the integration of a deeper layer. Comparable photosynthetic efficiency was found as compared to phytoplankton groups characterizing the upwelling season. *In situ* measurements of phytoplankton size classes (i.e., Collado-Fabbri et al., 2011; Iriarte et al., 2012; Velasco et al., in preparation) have shown that the empirical equations provided by Hirata et al. (2011) underestimate the nanophytoplankton community and overestimate microphytoplankton communities during the winter season, which can be attributed to elevated satellite Chl-a values within the area. Seasonal cycles of NO_3^-, PO_4^{3-} and $Si(OH)_4$ appear to be partially controlled by coastal upwelling, continental discharge, alterations in water masses (ESSW and SAAW) and nutrient uptake by phytoplankton groups.

Poor light attenuation near ST18 during winter suggests that particulate matter transported by the river plume may be predominantly deposited within the river terrace; therefore they do not affect the waters of the continental shelf (Saldías et al., 2012). However, inorganic nutrients from riverine sources seem to reach a greater area, as shown by high near-surface $Si(OH)_4$ concentrations observed at ST18 (located ∼27 km from the Itata River mouth). The study of seasonal continental and oceanic nutrient fluxes in this zone (**Figure 4**) reveals that during the wet season the Itata River is a primary source of $Si(OH)_4$ (11.4 times higher than the contribution of wind-driven costal upwelling). Hickey and Banas (2008) suggested that watershed-derived nutrients may help sustain productivity of the coastal ecosystem around the Columbia River during periods of weak upwelling-favorable winds and during periods of downwelling. These results indicate a smaller scale but similar dynamic within our study zone, and support an understanding of the zone off central Chile as one of the most productive in the world, even under non-upwelling conditions (Montecino et al., 2004). Hutchins et al. (2002) and Messié and Chavez (2015) identified an iron limitation on NPP in the northern zone of the Humboldt EBUS, particularly during austral winter. Itata River discharge may represent an important source of dissolved iron to our study zone (DGA, 2004; Salamanca and Pantoja, 2009), while helping to sustain high NPP near the river mouth during the non-upwelling season.

Surface salinity climatology (**Figure 3B**) differed from the results presented by Sobarzo et al. (2007), especially between September and December. We attributed this difference to surface salinity dynamics during 2014 and 2015 (e.g., surface salinity fluctuated between 20.34 and 32.96 from August to November 2014; Supplementary Figure 2). We recognized this period as anomalous, since 2014 and 2015 deviate from the observed trend of water column cooling and sea surface salinity increase at ST18, especially during the austral winter (Schneider et al., 2017). Cumulative Itata River runoff data from August to November 2014 reached decadal highs (Supplementary Figure 4). As a result, the cumulative NPPE value for November 2014 was one of the lowest of the decade (**Figure 7C**). Changes to river runoff timing may modify the division of the annual biological cycle as observed by cluster analysis. A potential variation in basal productivity magnitude and timing in river-influenced zones over the continental shelf plays a fundamental ecological role, as a greater abundance of *E. ringens* and *Strangomera bentincki* in early life stages (eggs and larvae) was observed during this season and at salinities between 32 and 34 (Soto-Mendoza et al., 2010). Additionally, increased stratification of the water column may favor a greater downward carbon flux (605 mg C m^{-2} d^{-1}) as compared to other periods of the year (between 152 and 268 mg C m^{-2} d^{-1}; Vargas et al., 2007).

NPP Hot Moments and Weekly Variability

This is the first study of NPP variability over an extended time period in this area, combining measurements and estimates to complement established understanding of coastal upwelling (Montero et al., 2007; Sobarzo et al., 2007). The continental shelf is also subjected to other kinds of variability, and one cause of misalignments between measurements and estimates of NPP are the high frequency variations in the relaxed and active phases of upwelling events, which cause variations in the microbiological community and production rates. *In situ* NPP measurements for ST18 reveal the occurrence of events where LCAR were highly increased (or "hot moments" as described by McClain et al., 2003). Peaks as high as 18.2 g C m^{-2} d^{-1} (October 2006) do not appear to be reflected by NPPE. This may be explained by the fact that NPP peaks lasted less than 8 days and/or covered an area of less than 81 km^2, and NPPE for the closest pixel to ST18 is unable to capture this level of variability; in general the hot moment's phenomenon is poorly documented. Farías et al. (2015) observed that nitrous oxide hot moments in central Chile are positively correlated with phytoplankton biomass, although these events do not specifically occur with high wind stress or with colder water. Effective Chl-a accumulation requires an optimal window of 3–7 days of reduced winds (Farías et al., 2015). It may be necessary to carry out daily, weekly and intra-seasonal investigations to identify NPP hot moments and avoid underestimations of NPP for this region during the upwelling season. Synoptic processes including active and relaxed coastal upwelling events and coastal waves may result in poor correlation between *in situ* and satellite-derived NPP during the upwelling season (**Table 3**). Monthly measurements are unable to

capture variability, and therefore generate a standard deviation that explains estimated and measured NPP rates. Week-to-week (WW) temporal variability presented in **Figure 9** varies between −5.33 and 3.15 g C m^{-2} d^{-1}, with a mean value ± SD of 0.72 ± 0.74 g C m^{-2} d^{-1} ($n = 454$). Absolute magnitude for maximum (>1.1 g C m^{-2} d^{-1}) WW monthly mean variability was observed from November to January, while lower (<0.32 g C m^{-2} d^{-1}) estimations were calculated between May and July (**Figure 9B**). Daneri et al. (2012) calculated up to a six-fold difference in WW gross primary production at a near-coast station within our study zone during the austral summer. We consider that a higher standard deviation in NPP and subsurface nutrients during spring-summer may also be caused by intense mesoscale activity (Morales et al., 2007), since a higher number of oceanic eddies were observed in the Peru-Chile current system for this period (Letelier, 2010). On the other hand, lower WW variability in NPP during the austral winter (**Figure 9**) may explain the higher coefficient of determination between *in situ* and satellite NPP (**Table 3**) for this period.

ENSO Effect on NPP Interannual Variability

Modest interannual variability was detected over the study period, with the highest NPPE variability observed during neutral years between 2006 and 2015 (**Figure 7**). The maximum cumulative PAR observed in 2014–15 (Supplementary Figure 4) may explain the highest observed NPPE values. On the other hand, minimum cumulative NPPE observed during 2012–2013 may be explained by a deficit in subsurface nutrient input (Supplementary Figure 2).

No statistical significance was found for NPPE between EN and LN conditions at 36°S. Iriarte and González (2004) suggested that the ENSO cycle affected NPP and water column properties in northern Chile (23°S) during the EN 1997–98, as compared with the non-EN period, driving a shift toward a major proportion of pico- and nanophytoplankton and decreasing NPP rates. Contrarily, Ulloa et al. (2001) and Pizarro et al. (2002) found no significant alteration in phytoplankton biomass in coastal waters close to this latitude during EN 1998. A similar ambiguity was observed at 36°S during the 2006–2015 ENSO cycles, which were less strong than previous events (i.e., EN 1997–98). *In situ* monthly surveys struggle to effectively capture the ENSO effect on bio-physicochemical properties in central Chile, while the use of remote sensing data may be a useful tool to increase the robustness of these observations. Corredor-Acosta et al. (2015) revealed that the effect of ENSO-related climate variability on Chl-a was relatively weak in the coastal zone, and this study observed no statistical significance for NPPE between EN and LN conditions, perhaps due to the distance from the equator. Nevertheless, a study over a longer time series and covering more intense EN and LN events is recommended in order to improve understanding of the ENSO effect on NPP off the coast of central Chile.

CONCLUSION

The analysis of a decade of bio-oceanographic information allowed for the identification of the main seasonal patterns modulating the annual biological cycle, which can be divided into three stages (i.e., rising, falling and basal).

The magnitude of fertilization in the photic layer appears to be significant and quasi-permanent throughout the year, not only due to the coastal upwelling present during 66% (from September to April) of the year, but also as a result of nutrient influx from rivers (from May to August). Specifically, the Itata River discharge during austral winter may partially support basal productivity around the river mouth, as a result of nutrient input and the influence of the fresh water plume on water column stratification.

Weekly and synoptic variability intensely influence the NPP annual cycle, especially during the upwelling season, which may explain the poor correlation between *in situ* and satellite-derived NPP for this season.

The ENSO cycle does not appear to impact annual NPP estimates for the study area, which was estimated at 1.1 kg C m^{-2} yr^{-1}.

This research presents relevant insights regarding NPP temporal variability in an upwelling area. The NPP baseline provided by this study may be useful in gaining improved understanding of how NPP responds to natural and human-induced changes in wind patterns and rivers runoff regimes. Changes in the NPP annual cycle, magnitude and timing may alter the carbon cycle and heterotrophic population dynamics and therefore present important implications for biogeochemical and ecological equilibriums.

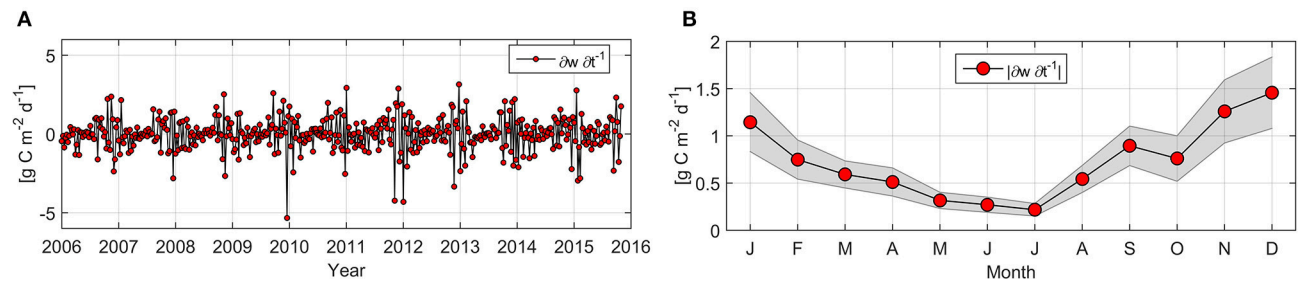

FIGURE 9 | Temporal evolution **(A)** and absolute climatology mean **(B)** for Net Primary Production week-to-week variability. Shaded area represents a 95% confidence interval.

AUTHOR CONTRIBUTIONS

LF provided in situ biogeochemical data from the fixed time series station; IM provided the VGPM estimations; GT supplied satellite data and the three authors wrote and analyzed data for the manuscript.

FUNDING

This research was funded by the Center of Excellence FONDAP-CONYCIT N° 15110009, FONDECYT N° 1161138 (LF) and GT was supported by CONICYT-PFCHA/Doctorado Nacional/2017-21170561.

ACKNOWLEDGMENTS

The authors thank the biogeochemistry group of the Universidad de Concepción for their help and support. We also thank F. Tapia, M. Sobarzo, C. Morales, R. Escribano, W. Schneider, and reviewers for their valuable comments and suggestions.

SUPPLEMENTARY MATERIAL

The Supplementary Material for this article can be found online at: https://www.frontiersin.org/articles/10.3389/fmars.2018.00179/full#supplementary-material

REFERENCES

Aguirre, C., Garreaud, R. D., and Rutllant, J. A. (2014). Surface ocean response to synoptic-scale variability in wind stress and heat fluxes off south-central Chile. *Dyn. Atmos. Oceans* 65, 64–85. doi: 10.1016/j.dynatmoce.2013.11.001

Anabalón, V., Morales, C. E., González, H. E., Menschel, E., Schneider, W., Hormazabal, S., et al. (2016). Micro-phytoplankton community structure in the coastal upwelling zone off Concepción (central Chile): annual and inter-annual fluctuations in a highly dynamic environment. *Prog. Oceanogr.* 149, 174–188. doi: 10.1016/j.pocean.2016.10.011

Arrizaga, A., Fuentealba, M., Espinoza, C., Chong, J., and Oyarzun, C. (1993). Hábitos tróficos de dos especies de peces pelágicos, la sardina *Strangomera bentincki* y la anchoveta *Engraulis ringens*, en el litoral de la Región del Bío-Bío, Chile. *Bol. Soc. Biol.* 64, 27–35.

Bakun, A. (1973). *Coastal Upwelling Indices, West Coast of North America, 1946-71*. Seattle, WA: National Oceanic and Atmospheric Administration.

Banse, K. (2002). Should we continue to measure ^{14}C-uptake by phytoplankton for another 50 years. *Limnol. Oceanogr Bull.* 11, 45–46.

Behrenfeld, M. J., Boss, E., Siegel, D. A., and Shea, D. M. (2005). Carbon-based ocean productivity and phytoplankton physiology from space. *Global Biogeochem. Cycles* 19:GB1006. doi: 10.1029/2004GB002299

Behrenfeld, M. J., and Falkowski, P. G. (1997a). A consumer's guide to phytoplankton primary productivity models. *Limnol. Oceanogr.* 42, 1479–1491.

Behrenfeld, M. J., and Falkowski, P. G. (1997b). Photosynthetic rates derived from satellite-based chlorophyll concentration. *Limnol. Oceanogr.* 42, 1–20. doi: 10.4319/lo.1997.42.1.0001

Bender, M. L., Grande, K., Johnson, K., Marra, J., Williams, P. J., Le, B., et al. (1987). A comparison of four methods for determining planktonic community production. *Limnol. Oceanogr.* 32, 1085–1098.

Boiser, J. P., Rondanelli, R., Garreaud, R. D., and Muñoz, F. (2016). Anthropogenic and natural contributions to the Southeast Pacific precipitation decline and recent megadrought in central Chile. *Geophys. Res. Lett.* 43, 413–421. doi: 10.1002/2015GL067265

Boyer, T., Conkright, M. E., and Levitus, S. (1999). Seasonal variability of dissolved oxygen, percent oxygen saturation, and apparent oxygen utilization in the Atlantic and Pacific Oceans. *Deep Sea Res. I* 46, 1593–1613. doi: 10.1016/S0967-0637(99)00021-7

Brussaard, C. P. (2004). Viral control of phytoplankton populations–a review. *J. Eukaryot. Microbiol.* 51, 125–138. doi: 10.1111/j.1550-7408.2004.tb00537.x

Cai, W. J., Dai, M., and Wang, Y. (2006). Air-sea exchange of carbon dioxide in ocean margins: a province-based synthesis. *Geophys. Res. Lett.* 33:L12603 doi: 10.1029/2006GL026219

Collado-Fabbri, S., Vaulot, D., and Ulloa, O. (2011). Structure and seasonal dynamics of the eukaryotic picophytoplankton community in a wind-driven coastal upwelling ecosystem. *Limnol. Oceanogr.* 56, 2334–2346. doi: 10.4319/lo.2011.56.6.2334

Corredor-Acosta, A., Morales, C. E., Hormazábal, S., Andrade, I., and Correa-Ramirez, M. A. (2015). Phytoplankton phenology in the coastal upwelling region off central-southern Chile (35°S–38°S): time-space variability, coupling to environmental factors, and sources of uncertainty in the estimates. *J. Geophys. Res. Ocean.* 120, 813–831. doi: 10.1002/2014JC010330

Cubillos, S. L., Canales, M., Hernández, R. A., Bucarey, S. D., Vilugrón, L., and Miranda, A. L. (1998b). Poder de pesca, esfuerzo de pesca y cambios estacionales e interanuales en la abundancia relativa de *Strangomera bentincki* y *Engraulis ringens* en el área frente a Talcahuano, Chile (1990-97). *Rev. Invest. Mar.* 26, 3–14.

Cubillos, S. L., Nuñez, S., and Arcos, D. (1998a). Producción primaria requerida para sustentar el desembarque de peces pelágicos en Chile. *Rev. Invest. Mar.* 26, 83–108. doi: 10.4067/S0717-71781998002600008

Cullen, J. J. (2001). "Primary production methods," in *Encyclopedia of Ocean Sciences*, ed J. H. Steele (Oxford: Academic Press), 578–584.

DGA (2004). *Diagnóstico y Clasificación de los Cursos y Cuerpos de Agua Según Objetivos de Calidad*. Cuenca del Rio Itata. Dirección General de Aguas.

Daneri, G., Dellarossa, V., Quiñones, R., Jacob, B., Montero, P., and Ulloa, O. (2000). Primary production and community respiration in the Humboldt Current System off Chile and associated oceanic areas. *Mar. Ecol. Prog. Ser.* 197, 41–49. doi: 10.3354/meps197041

Daneri, G., Lizárraga, L., Montero, P., González, H. E., and Tapia, F. J. (2012). Wind forcing and short-term variability of phytoplankton and heterotrophic bacterioplankton in the coastal zone of the Concepción upwelling system (Central Chile). *Prog. Oceanogr.* 92–95, 92–96. doi: 10.1016/j.pocean.2011.07.013

Escribano, R., Daneri, G., Farías, L., Gallardo, V. A., González, H. E., Gutiérrez, D., et al. (2004). Biological and chemical consequences of the 1997–1998 El Niño in the Chilean coastal upwelling system: a synthesis. *Deep Sea Res. II* 51, 2389–2411. doi: 10.1016/j.dsr2.2004.08.011

Escribano, R., and Schneider, W. (2007). The structure and functioning of the coastal upwelling system off central/southern Chile. *Prog. Oceanogr.* 75, 343–347. doi: 10.1016/j.pocean.2007.08.020

FAO (2014). *The State of World Fisheries and Aquaculture*. Opportunities and challenges. Rome: Food and Agriculture Organization of the United Nations.

Farías, L., Besoain, V., and García-Loyola, S. (2015). Presence of nitrous oxide hotspots in the coastal upwelling area off central Chile: an analysis of temporal variability based on ten years of a biogeochemical time series. *Environ. Res. Lett.* 10:44017. doi: 10.1088/1748-9326/10/4/044017

Farías, L., Chuecas, L. A., and Salamanca, M. A. (1996). Effect of coastal upwelling on nitrogen regeneration from sediments and ammonium supply to the water column in Concepción Bay, Chile. *Estuar. Coast. Shelf Sci.* 43, 137–155. doi: 10.1006/ecss.1996.0062

Farías, L., Fernández, C., Faúndez, J., Cornejo, M., and Alcaman, M. E. (2009). Chemolithoautotrophic production mediating the cycling of the greenhouse gases N2O and CH4 in an upwelling ecosystem. *Biogeosciences* 6, 3053–3069. doi: 10.5194/bg-6-3053-2009

Fennel, K. (2010). The role of continental shelves in nitrogen and carbon cycling: Northwestern North Atlantic case study. *Ocean Sci. J.* 6, 539–548. doi: 10.5194/os-6-539-2010

Fernández, C., Raimbault, P., Garcia, N., and Rimmelin, P. (2005). An estimation of annual new production and carbon fluxes in the northeast Atlantic Ocean during 2001. *J. Geophys. Res.* 110:C07S13. doi: 10.1029/2004JC002616

Fuenzalida, R., Schneider, W., Garcés-Vargas, J., and Bravo, L. (2008). Satellite altimetry data reveal jet-like dynamics of the humboldt current. *J. Geophys. Res.* 113:C07043. doi: 10.1029/2007JC004684

Garrison, H. S., and Tang, K. W. (2014). Effects of episodic turbulence on diatom mortality and physiology, with a protocol for the use of Evans Blue stain for live–dead determinations. *Hydrobiologia* 738, 155–170. doi: 10.1007/s10750-014-1927-0

Graco, M., Gutiérrez, D., and Farías, L. (2006). Inter-annual variability of the pelagic-benthic coupling in the upwelling system off central Chile. *Adv. Geosci.* 6, 127–132. doi: 10.5194/adgeo-6-127-2006

Grasshoff, K., Ehrhardt, M., and Kremling, K. (1983). *Methods of Seawater Analysis*. Basel: Springer-Verlag.

Henríquez, L. A., Daneri, G., Muñoz, C. A., Montero, P., Veas, R., and Palma, A. T. (2007). Primary production and phytoplanktonic biomass in shallow marine environments of central Chile: effect of coastal geomorphology. *Estuar. Coast. Shelf Sci.* 73, 137–147. doi: 10.1016/j.ecss.2006.12.013

Hickey, B. M., and Banas, N. S. (2008). Why is the northern end of the California current system so productive? *Oceanography* 21, 90–107. doi: 10.5670/oceanog.2008.07

Hirata, T., Hardman-Mountford, N. J., Barlow, R., Lamont, T., Brewin, R. J. W., Smyth, T., et al. (2009). An inherent optical property approach to the estimation of size-specific photosynthetic rates in eastern boundary upwelling zones from satellite ocean colour: an initial assessment. *Prog. Oceanogr.* 83, 393–397. doi: 10.1016/j.pocean.2009.07.019

Hirata, T., Hardman-Mountford, N. J., Brewin, R. J. W., Aiken, J., Barlow, R., Suzuki, K., et al. (2011). Synoptic relationships between surface Chlorophyll-a and diagnostic pigments specific to phytoplankton functional types. *Biogeosciences* 8, 311–327. doi: 10.5194/bg-8-311-2011

Hutchins, D. A., Hare, C. E., Weaver, R. S., Zhang, Y., Firme, G. F., DiTullio, G. R., et al. (2002). Phytoplankton iron limitation in the Humboldt Current and Peru upwelling. *Limnol. Oceanogr.* 47, 997–1011. doi: 10.4319/lo.2002.47.4.0997

Iriarte, J. L., and González, H. E. (2004). Phytoplankton size structure during and after the 1997/98 El Niño in a coastal upwelling area of the northern Humboldt current system. *Mar. Ecol. Prog. Ser.* 269, 83–90. doi: 10.3354/meps269083

Iriarte, J. L., Vargas, C. A., Tapia, F. J., Bermúdez, R., and Urrutia, R. E. (2012). Primary production and plankton carbon biomass in a river-influenced upwelling area off Concepción, Chile. *Prog. Oceanogr.* 92–95, 97–109. doi: 10.1016/j.pocean.2011.07.009

Kahru, M., Kudela, R., Manzano-Sarabia, M., and Mitchell, B. G. (2009). Trends in primary production in the California current detected with satellite data. *J. Geophy. Res.* 114:C02004. doi: 10.1029/2008JC004979

Kämpf, J., and Chapman, P. (2016). *Upwelling Systems of the World. A Scientific Journey to the Most Productive Marine Ecosystems*. Cham: Springer International Publishing.

Kirk, J. T. O. (1983). *Light & Photosynthesis in Aquatic Ecosystem*. New York, NY: Cambridge University Press.

Lachkar, Z., and Gruber, N. (2012). A comparative study of biological production in eastern boundary upwelling systems using an artificial neural network. *Biogeosciences* 9, 293–308. doi: 10.5194/bg-9-293-2012

Legendre, P., and Legendre, L. (1998). *Numerical Ecology*. Amsterdam: Elsevier Science.

Letelier, J. (2010). *Surgencia y estructuras de mesoescala frente a Chile (18°-42°S)*. [Ph.D. thesis]. [Concepción]: Universidad de Concepción

Letelier, J., Pizarro, O., and Nuñez, S. (2009). Seasonal variability of coastal upwelling and the upwelling front off central Chile. *J. Geophys. Res.* 114:C12009. doi: 10.1029/2008JC005171

McClain, M. E., Boyer, E. W., Dent, C. L., Gergel, S. E., Grimm, N. B., Groffman, P. M., et al. (2003). Biogeochemical hot spots and hot moments at the interface of terrestrial and aquatic ecosystems. *Ecosystems* 6, 301–312. doi: 10.1007/s10021-003-0161-9

Messié, M., and Chavez, F. P. (2015). Seasonal regulation of primary production in estern boundary upwelling systems. *Prog. Oceanog.* 134, 1–18. doi: 10.1016/j.pocean.2014.10.011

Montecino, V., Astoreca, R., Alarcón, G., Retamal, L., and Pizarro, G. (2004). Bio-optical characteristics and primary productivity during upwelling and non-upwelling conditions in a highly productive coastal ecosystem off central Chile (∼36°S). *Deep Sea Res. II* 51, 2413–2426. doi: 10.1016/j.dsr2.2004.08.012

Montecino, V., Pizarro, G., and Quiroz, D. (1998). "Primary production in the Chilean coast," in *Biotic Impact of Extratropical Climate Variability in the Pacific*, eds G. Holloway and D. Henderson (Honolulu, HI: SOEST), 69–76.

Montecino, V., Strub, T., Chavez, F., Thomas, A., Tarazona, J., and Baumgartner, T. (2006). Chapter 10 "Bio-physical interactions off Western South-America," in *The Sea. The Global Coastal Ocean: Interdisciplinary Regional Studies and Synthesis,* Vol. 14A, eds A. R. Robinson and K. H. Brink (Cambridge: Harvard Press).

Montecinos, A., and Aceituno, P. (2003). Seasonality of the ENSO-related rainfall variability in Central Chile and associated circulation anomalies. *J. Clim.* 16, 281–296. doi: 10.1175/1520-0442(2003)016<0281:SOTERR>2.0.CO;2

Montecinos, A., and Gomez, F. (2010). ENSO modulation of the upwelling season off southern-central Chile. *Geophys. Res. Lett.* 37:L02708. doi: 10.1029/2009GL041739

Montero, P., Daneri, G., Cuevas, A. L., González, H. E., Jacob, B., Lizárraga, L., et al. (2007). Productivity cycles in the coastal upwelling area off Concepcion: the importance of diatoms and bacterioplankton in the organic carbon flux. *Prog. Oceanogr.* 75, 518–530. doi: 10.1016/j.pocean.2007.08.013

Morales, C. E., González, H. E., Hormazábal, S. E., Yuras, G., Letelier, J., and Castro, L. R. (2007). The distribution of chlorophyll-a and dominant planktonic components in the coastal transition zone off Concepción, central Chile, during different oceanographic conditions. *Prog. Oceanogr.* 75, 452–469. doi: 10.1016/j.pocean.2007.08.026

Morales, C. E., Hormazabal, S., Andrade, I., and Correa-Ramirez, M. A. (2013). Time-space variability of Chlorophyll-a and associated physical variables within the region off central-southern Chile. *Remote Sens.* 5, 5550–5571. doi: 10.3390/rs5115550

Swirgon, M., and Stramska, M. (2015). Comparison of *in situ* and satellite ocean color determinations of particulate organic carbon concentration in the global ocean. *Oceanologia* 57, 25–31. doi: 10.1016/j.oceano.2014.09.002

Neira, S., and Arancibia, H. (2004). Trophic interactions and community structure in the upwelling system off Central Chile (33–39°S). *J. Exp. Mar. Biol. Ecol.* 312, 349–366. doi: 10.1016/j.jembe.2004.07.011

Nevison, C. D., Lueker, T. J., and Weiss, R. F. (2004). Quantifying the nitrous oxide source from coastal upwelling *Global Biogeochem. Cycles* 18:GB1018. doi: 10.1029/2003GB002110

Parsons, T., Maita, Y., and Lalli, C. (1984). *A Manual of Chemical and Biological Methods for Seawater Analysis*. Oxford: Pergamon Press.

Pauly, D., and Christensen, V. (1995). Primary production required to sustain global fisheries. *Nature* 374, 255–257. doi: 10.1038/374255a0

Pizarro, G., Iriarte, J., and Montecino, V. (2002). Mesoscale primary production and bio-optical variability off Antofagasta (23-24° S) during the transition to El Niño 1997–1998. *Rev. Chil. Hist. Nat.* 75, 201–215. doi: 10.4067/S0716-078X2002000100019

Pizarro, O. (1999). *Low Frequency fluctuations in the Eastern Boundary Current off South America: Remote and Local Forcing*. Ph.D. thesis, University of Göteborg, Göteborg.

Quiñones, R. A., Gutiérrez, M. H., Daneri, G., Gutierrez, D., González, H. E., and Chavez, F. (2010). "The humboldt current system," in *Carbon and Nutrient Fluxes in Continental Margins. A Global Synthesis*, eds K. K. Liu, L. Atkinson, R. Quiñones, and L. Talaue-McManus (Berlin: Springer), 44–64.

Raimbault, P., Diaz, F., Pouvesle, W., and Boudjellal, B. (1999). Simultaneous determinations of particulate organic carbon, nitrogen and phosphorus collected on filters, using a semiautomatic wet-oxidation method. *Mar. Ecol. Prog. Ser.* 180, 289–295. doi: 10.3354/meps180289

Regaudie-de-Gioux, A., Lasternas, S., Agustí, S., and Duarte, C. M. (2014). Comparing marine primary production estimates through different methods and development of conversion equations. *Front. Mar. Sci.* 1:19. doi: 10.3389/fmars.2014.00019

Ryther, J. H., and Dunstan, W. M. (1971). Nitrogen, phosphorus, and eutrophication in the coastal marine environment. *Science* 171, 1008–1013. doi: 10.1126/science.171.3975.1008

Salamanca, M. A., and Pantoja, S. (2009). "Caracterización química de la zona marina adyacente a la desembocadura del río Itata," in *La Cuenca Hidrográfica del río Itata. Aportes Científicos Para su Gestión Sustentable*, eds O. Parra, J. C. Castilla, H. Romero, R. Quiñones, and A. Comaño (Concepción: Editorial Universidad de Concepción), 177–191.

Saldías, G. S., Sobarzo, M., Largier, J., Moffat, C., and Letelier, R. M. (2012). Seasonal variability of turbid river plumes off central Chile base on high-resolution MODIS imagery. *Remote Sens. Environ.* 123, 220–233. doi: 10.1016/j.rse.2012.03.010

Sánchez, G. E., Pantoja, S., Lange, C. B., González, H. E., and Daneri, G. (2008). Seasonal changes in particulate biogenic and lithogenic silica in the upwelling system off Concepción (∼36°S), Chile, and their relationship to fluctuations in marine productivity and continental input. *Cont. Shelf Res.* 28, 2594–2600. doi: 10.1016/j.csr.2008.07.010

Schneider, W., Donoso, D., Garcés-Vargas, J., and Escribano, R. (2017). Water-column cooling and sea surface salinity increase in the upwelling region off central-south Chile driven by a poleward displacement of the South Pacific High. *Prog. Oceanogr.* 151, 38–48. doi: 10.1016/j.pocean.2016.11.004

Silva, N., Rojas, N., and Fedele, A. (2009). Water masses in the Humboldt Current System: properties, distribution, and the nitrate deficit as a chemical water mass tracer for Equatorial Subsurface Water off Chile. *Deep Sea Res. II* 56, 1004–1020. doi: 10.1016/j.dsr2.2008.12.013

Slawyk, G., Collos, Y., and Auclair, J. C. (1977). The use of the 13C and 15N isotopes for the simultaneous measurements of carbon and nitrogen turnover rates in marine phytoplankton. *Limnol. Oceanogr.* 22, 925–932. doi: 10.4319/lo.1977.22.5.0925

Sobarzo, M., Bravo, L., Donoso, D., Garcés-Vargas, J., and Schneider, W. (2007). Coastal upwelling and seasonal cycles that influence the water column over the continental shelf off central Chile. *Prog. Oceanogr.* 75, 363–382. doi: 10.1016/j.pocean.2007.08.022

Sobarzo, M., and Djurfeldt, L. (2004). Coastal upwelling process on a continental shelf limited by submarine canyons, Concepción, central Chile. *J. Geophys. Res.* 109:C12012. doi: 10.1029/2004JC002350

Sobarzo, M., Saldías, G. S., Tapia, F. J., Bravo, L., Moffat, C., and Largier, J. L. (2016). On subsurface cooling associated with the Biobío River Canyon (Chile). *J. Geophys. Res Ocean*. 121, 4568–4584. doi: 10.1002/2016JC011796

Soto-Mendoza, S., Castro, L. R., and Llanos-Rivera, A. (2010). Variabilidad espacial y temporal de huevos y larvas de *Strangomera bentincki* y *Engraulis ringens*, asociados a la desembocadura del río Itata, Chile. *Rev. Biol. Mar. Oceanogr.* 45, 471–487. doi: 10.4067/S0718-19572010000300012

Steeman Nielsen, E. (1952). The use of radioactive carbon (^{14}C) for measuring production in the sea. *J. Cons. Perm. Int. Explor. Mer*. 18, 117–140.

Sydeman, W. J., García-Reyes, M., Schoeman, D. S., Rykaczewski, R. R., Thompson, S. A., Black, B. A., et al. (2014). Climate change and wind intensification in coastal upwelling ecosystems. *Science* 345, 77–80. doi: 10.1126/science.1251635

Testa, G. (2017). *Variabilidad Espacio-Temporal de la Productividad Primaria Neta en la Plataforma Continental de Chile Central (73°W-36°S); Causas y Consecuencias*. Master's Thesis, Universidad de Concepción, Concepción.

Thiel, M., Macaya, E. C., Acuña, E., Arntz, W. E., Bastias, H., Brokordt, K., et al. (2007). The humboldt current system of Northern and Central Chile. *Oceanogr. Mar. Biol. Annu. Rev.* 45, 195–344. doi: 10.1201/9781420050943.ch6

Torrence, C., and Compo, G. P. (1998). A practical guide to wavelet analysis. *Bull. Am. Meteorol. Soc.* 79, 61–78. doi: 10.1175/1520-0477(1998)079<0061:APGTWA>2.0.CO;2

Ulloa, O., Escribano, R., Hormazábal, S., Quiñones, R. A., González, R. R., and Ramos, M. (2001). Evolution and biological effect of the 1997-98 El Niño in the upwelling ecosystem off northern Chile. *Geophys. Res. Lett.* 28, 1591–1594. doi: 10.1029/2000GL011548

Vargas, C. A., Escribano, R., and Poulet, S. (2006). Phytoplankton food quality determines time windows for successful zooplankton reproductive pulses. *Ecol.* 87, 2992–2999. doi: 10.1890/0012-9658(2006)87[2992:PFQDTW]2.0.CO;2

Vargas, C. A., Martínez, R. A., Cuevas, L. A., Pavez, M. A., Cartes, C., González, H. E., et al. (2007). The relative importance of microbial and classical food webs in a highly productive coastal upwelling area. *Limnol. Oceanogr.* 52, 1495–1510. doi: 10.4319/lo.2007.52.4.1495

Conflict of Interest Statement: The authors declare that the research was conducted in the absence of any commercial or financial relationships that could be construed as a potential conflict of interest.

Copyright © 2018 Testa, Masotti and Farías. This is an open-access article distributed under the terms of the Creative Commons Attribution License (CC BY). The use, distribution or reproduction in other forums is permitted, provided the original author(s) and the copyright owner are credited and that the original publication in this journal is cited, in accordance with accepted academic practice. No use, distribution or reproduction is permitted which does not comply with these terms.

frontiers in Microbiology

ORIGINAL RESEARCH
published: 06 July 2018
doi: 10.3389/fmicb.2018.01500

First Record of Microbiomes of Sponges Collected From the Persian Gulf, Using Tag Pyrosequencing

Akram Najafi[1], *Maryam Moradinasab*[2] *and Iraj Nabipour*[1]*

[1] The Persian Gulf Marine Biotechnology Research Center, The Persian Gulf Biomedical Sciences Research Institute, Bushehr University of Medical Sciences, Bushehr, Iran, [2] The Persian Gulf Tropical Medicine Research Center, The Persian Gulf Biomedical Sciences Research Institute, Bushehr University of Medical Sciences, Bushehr, Iran

The Persian Gulf is a special habitat of marine sponges whose bacterial communities are under-investigated. Recently, next-generation sequencing technology has comprehensively improved the knowledge of marine sponge-associated bacteria. For the first time, this study aimed to evaluate the diversity of the Persian Gulf sponge-associated bacteria using tag pyrosequencing in Iran. In this study, 10 sponge samples from 6 different taxonomic orders were collected from the Persian Gulf using SCUBA diving. The diversity of the bacteria associated with the marine sponges was investigated using the *16S rRNA* gene PCR-tagged pyrosequencing method. A total of 68,628 high-quality sequences were obtained and clustered at a 97% similarity into 724 unique operational taxonomic units (OTUs), representing 17 bacterial phyla. Cyanobacteria was the most abundant phylum in the sponges, followed by Proteobacteria, Chloroflexi, Acidobacteria, and Actinobacteria. Other phyla were detected as minor groups of bacteria. Bacterial community richness, Shannon, and Simpson indices revealed the highest diversity in sponge S11 (*Dictyoceratida* sp.) compared to other sponges. This study showed a diverse structure of bacterial communities associated with the Persian Gulf sponges. The dominance of Cyanobacteria may suggest an ecological importance of this phylum in the Persian Gulf sponges.

Keywords: sponge, symbionts, bacterial diversity, 454 pyrosequencing, the Persian Gulf

OPEN ACCESS

Edited by:
Alejandro A. Murillo, EMBL Heidelberg, Germany

Reviewed by:
David William Waite, University of Auckland, New Zealand
Fabiano Thompson, Instituto Alberto Luiz Coimbra de Pós-Graduação e Pesquisa de Engenharia (COPPE), Brazil

***Correspondence:**
Iraj Nabipour
nabipour@bpums.ac.ir

Specialty section:
This article was submitted to Aquatic Microbiology, a section of the journal Frontiers in Microbiology

Received: *05 February 2018*
Accepted: *18 June 2018*
Published: *06 July 2018*

Citation:
Najafi A, Moradinasab M and Nabipour I (2018) First Record of Microbiomes of Sponges Collected From the Persian Gulf, Using Tag Pyrosequencing. Front. Microbiol. 9:1500. doi: 10.3389/fmicb.2018.01500

INTRODUCTION

Marine sponges (phylum *Porifera*) are known as the oldest multicellular animals (metazoans) (found more than 600 million years ago) (Lee et al., 2011; Verhoeven et al., 2017) and represent ecologically important reef builders in benthic communities' worldwide (Bayer et al., 2014; Graça et al., 2015). In the last decade, sponges have attracted research interests because of their symbiotic relationships with a wide range of microbial communities including bacteria (Lee et al., 2011; Giles et al., 2013; Gao et al., 2014a), archaea (Zhang et al., 2014), Cyanobacteria (Gao et al., 2017; Regueiras et al., 2017), and fungi (Maldonado et al., 2005). The sponge-associated microorganisms can constitute up to 40–60% of the total sponge biomass (Gao et al., 2014a; Graça et al., 2015; Gaikwad et al., 2016). They may play crucial roles in sponge survival in the marine ecosystem including recycling of nutrients such as nitrogen and sulfur (Montalvo et al., 2014; Zhang et al., 2014), removing metabolic waste (Jackson et al., 2012), and producing bioactive secondary metabolites (Graça et al., 2015).

Extensive studies have been conducted to investigate the bacterial communities associated with different sponge species using both culture-dependent and culture-independent techniques (Giles et al., 2013; Jeong et al., 2014). As is common with most environments, <1% of bacteria present in sponge tissues can be successfully cultivated (Nam et al., 2011; Jackson et al., 2012). In the past two decades, culture-independent methods (mainly based on *16S rRNA* gene) have led to a deeper understanding of the microbial diversity in sponges (Alex and Antunes, 2015). Numerous sponge-associated bacteria have been identified using culture-independent techniques such as denaturing gradient gel electrophoresis (DGGE) (Li et al., 2006), fluorescent *in situ* hybridization (FISH) (Bayer et al., 2014), terminal restriction fragment length polymorphism (TRFLP) analyses (Zhang et al., 2006; Lee et al., 2011), PCR cloning and sequencing (Kennedy et al., 2008). The 454 tag pyrosequencing is a next-generation sequencing (NGS) technology that provides a faster and simpler way to analyze the microbial communities associated with marine sponges (Webster et al., 2010; Lee et al., 2011; Schmitt et al., 2012; Gao et al., 2014a; Gaikwad et al., 2016). This new method enables hundreds of thousands of nucleotide sequences from multiple samples to be examined in a single 10 h reaction (Lee et al., 2011; Nam et al., 2011; Jeong et al., 2013, 2014).

The next-generation sequencing techniques have revealed the presence of more than 25 different bacterial phyla and 2 archaeal lineages in marine sponges around the world (Moitinho-Silva et al., 2014; Rodríguez-Marconi et al., 2015; Verhoeven et al., 2017). Members of the phyla Actinobacteria, Acidobacteria, Cyanobacteria, Chloroflexi, Proteobacteria, Bacteroidetes, and Firmicutes have been described in association with different marine sponges (Jackson et al., 2012; Giles et al., 2013; Bayer et al., 2014). However, the marine bacterial communities can vary in different sponges with respect to both microbial richness and diversity.

The Persian Gulf, a small, shallow, semi-enclosed body of water bordered by the Arabian Peninsula and Iran, is a unique and greatly underexplored marine ecosystem. There are about 55 sponge genera recorded in the Persian Gulf (Najafi, 2012). However, next-generation sequencing technology has not been applied to identify the sponge-associated bacterial communities in Iran and the Middle East.

The present study was aimed at characterizing the bacterial community associated with the marine sponge species collected from the Persian Gulf, Iran using 454 pyrosequencing.

MATERIALS AND METHODS

Sponge Sampling

Sponge sampling was performed in May to September 2016 at a depth of 2–3 m offshore Bushehr, Persian Gulf, Iran by SCUBA diving. In this study, the sponges were living in an area where it was exposed to light. Sponge samples were placed in sterile plastic Ziploc bags containing seawater and immediately transported to the Persian Gulf of Marine Biotechnology Research Center. Sponge tissues were rinsed with 0.22-μm-membrane-filtered seawater (FSW) to remove exogenous materials and loosely attached microbes (Jackson et al., 2012). The samples were stored at −80°C until further processing.

Ethics Statement

In this study, the sponges collected did not involve endangered or protected sponge species. No specific scientific research permission was required to collect the sponges from the Persian Gulf.

Sponge Identification

Sponge taxonomic identifications were confirmed with a combination of multilocus DNA markers. The cytochrome oxidase subunit 1 (COI) and partial 28S rDNA fragments (ITS) were amplified using specific primers as previously reported (Becking et al., 2013). PCR amplifications were carried out on a thermal cycler PeQlab, peqSTAR 96X Universal Gradient, Germany under the following conditions: 94°C for 30 s; followed by 35 cycles of 94°C for 5 s; 50°C for 5 s; 72°C for 12 s; followed by 72°C for 1 min (Becking et al., 2013). PCR products were purified and sequenced by Macrogen Inc. (Seoul, Korea).

Also, morphological and spicule examination was carried out by Dr. Yusheng M. Huang (National Penghu University of Science and Technology, Taiwan). List of sponge species collected from different locations of the Persian Gulf is shown in **Table 1**.

Metagenomic DNA Extraction From Sponges

Frozen sponge tissues were defrosted and washed with sterilized and filtered seawater. Then, they were cut into small pieces (about 1 cm^3) and ground to fine powder under liquid N_2 using a sterile pestle and mortar (Jackson et al., 2012; Bayer et al., 2014). DNA was extracted using a hexadecyltrimethylammonium bromide (CTAB) method. Briefly, a subsample of approximately 100 mg of each sponge tissue was suspended in lysis buffer [100 mM Tris, 100 mM EDTA, 1.5 M NaCl (w/v), 1% CTAB (w/v), 2% SDS (w/v)]. Then they were disrupted in the presence of factors such as proteinase K and extraction buffer containing chloroform: isoamyl alcohol (24:1). Samples were washed with a solution of phenol-chloroform in a few steps for DNA purification. Finally, DNA was precipitated with sodium acetate (3 M, pH 5.2) and isopropanol, then washed in 70% ethanol, dried and re-dissolved in TE buffer (Jackson et al., 2012; Schmitt et al., 2012). Metagenomic DNA was qualified by agarose gel electrophoresis [1% *w/v* agarose in Tris-acetate-EDTA (TAE) buffer]. The quantitative assessment of the isolated DNA was carried out using a NanoDrop 1000 spectrophotometer (Thermo Scientific, Wilmington, DE, USA). The high-quality DNA was stored at −20°C until use (Schmitt et al., 2012; Jasmin et al., 2015).

Pyrosequencing of Barcoded *16S rRNA* Gene Amplicons

In this study, the universal primers 27F and 518R were used to amplify a ∼ 400 bp fragment of the bacterial *16S rRNA* gene targeting the V1 to V3 hyper-variable regions. These regions were amplified using primer sets (V1-27F: 5′-X-MID-GAGTTTGATCMTGGCTCAG-3′ and V3-518R: 5′-X-MID-WTTACCGCGGCTGCTGG-3′), in which X indicates the

TABLE 1 | List of sponge species collected from different locations of the Persian Gulf.

Site	Collection date	Coordinate	Depth (m)	Temp (C)	Sample ID	Sponge species	Taxonomy		
							Class	Order	Family
PG1	September 2016	27.8238 N, 51.8948 E	~2	32.0	S02	*Suberites diversicolor*	*Demospongiae*	*Suberitida*	*Suberitidae*
PG1	September 2016	27.8238 N, 51.8948 E	~2	32.0	S03	*Pseudoceratina arabica*	*Demospongiae*	*Verongida*	*Pseudoceratinidae*
PG2	July 2016	28.9817 N, 50.8243 E	3	29.6	S04	*Chondrilla* sp.	*Demospongiae*	*Chondrillida*	*Chondrillidae*
PG2	July 2016	28.9817 N, 50.8243 E	3	29.6	S05	*Cladocroce* sp.	*Demospongiae*	*Haplosclerida*	*Chalinidae*
PG2	July 2016	28.9817 N, 50.8243 E	3	29.6	S06	*Cladocroce* sp.	*Demospongiae*	*Haplosclerida*	*Chalinidae*
PG2	July 2016	28.9817 N, 50.8243 E	3	29.6	S07	*Halichondria* sp.	*Demospongiae*	*Halichondrida*	*Halichondriidae*
PG3	May 2016	28.9816 N, 50.8253 E	3	28.0	S09	*Chondrilla* sp.	*Demospongiae*	*Chondrillida*	*Chondrillidae*
PG3	May 2016	28.9816 N, 50.8253 E	3	28.0	S10	*Halichondria* sp.	*Demospongiae*	*Halichondrida*	*Halichondriidae*
PG3	May 2016	28.9816 N, 50.8253 E	3	28.0	S11	Dictyoceratida sp.	*Demospongiae*	*Dictyoceratida*	Unclassified Dictyoceratida
PG3	May 2016	28.9816 N, 50.8253 E	3	28.0	S13	*Ircinia ramose*	*Demospongiae*	*Dictyoceratida*	*Irciniidae*

adapter sequences and MID (multiplex identifier) shows the different oligomers comprised of 10 nucleotides to tag different samples for barcoded pyrosequencing (**Table 2**; Jeong et al., 2013, 2014). This approach allowed for the mixing of multiple samples in parallel and re-sorting the sequences into order (Nam et al., 2011; Jackson et al., 2012). PCR amplification was performed in a volume of 50 μL containing 3 mM of $MgCl_2$, 0.2 mM of dNTPs, 2.5 U of Pfu Turbo DNA polymerase (Stratagene, La Jolla, CA, USA), 1X Pfu reaction buffer, 0.1 μM of each pair of barcoded primers, and 20 ng of metagenomic DNA (Lee et al., 2011; Gao et al., 2014a). PCR was conducted in a Thermal Cycler (Applied Biosystems ABI Perkin Elmer 9600 GeneAmp) using the following conditions: an initial denaturation at 95°C for 5 min, followed by 35 cycles of denaturation at 95°C for 60 s, annealing at 55°C for 60 s, extension at 72°C for 60 s, and a final extension at 72°C for 5 min (White et al., 2012). The PCR amplicon libraries were purified using the NucleoSpin® Gel and PCR Clean-up (Macherey-Nagel, Germany) and quantified using NanoDrop 1000 spectrophotometer (Thermo Scientific, Wilmington, DE, USA). Pyrosequencing was performed through a GS FLX Titanium system (454 Life Sciences) according to the manufacturer's instructions (Roche, Germany) by a commercial sequencing provider (Macrogen, Seoul, Korea).

Processing of 454 Tag Sequences Data

In the present study, the sequences generated from pyrosequencing were analyzed as previously reported (Jeong et al., 2014). The low-quality sequences were filtered from the raw reads using Trimmomatic v0.30 (Gaikwad et al., 2016). Briefly, sequences with a read length of less than 172 bp or with mismatches on primer or barcode, a quality score of less than 25 with ambiguous bases N and homopolymers longer than 6 nucleotides were removed from further analysis (Gao et al., 2014a; Moitinho-Silva et al., 2014; Rodríguez-Marconi et al., 2015; Gaikwad et al., 2016). Final sequences that passed the quality checks were then assigned to respective samples based on the barcodes and subjected to Denoiser to increase the accuracy of the sequence processing (Gao et al., 2014a). The sequences were merged into one file and clustered into operational taxonomic units (OTUs) using the Quantitative Insights Into Microbial Ecology Toolkit (QIIME), version 1.8.0. (Caporaso et al., 2010). Chloroplast and mitochondria sequences and chimeric reads were excluded from downstream analyses. In this study, the chimeric reads were removed through the CD-HIT-OTU program (http://cd-hit.org). Taxonomic assignment of representative OTU sequences was performed using the UCLUST (version 1.2.22) taxonomy assigner method (Edgar, 2010) against the SILVA release 119 database as a reference. To have more information about the strains, each OTU was compared to the most closely related *16S rRNA* gene sequences from the NCBI nucleotide databases using BLAST search. Phylogenetic analysis was inferred by using the Maximum Likelihood method based on the Tamura-Nei model (Tamura and Nei, 1993). Also, the evolutionary analysis was conducted using MEGA version 7.0 (Kumar et al., 2016).

Analysis of Microbial Richness and Diversity

Taxonomic abundance was presented in the phylum, class, order, family, and genus. Alpha diversity metrics were computed

TABLE 2 | The MID barcodes for the amplification of *16S rRNA* genes.

Sample	S2	S3	S4	S5	S6	S7	S9	S10	S11	S13
MID	ACGAG TGCGT	ACGCT CGACA	CTCTA CGCTC	AGCAC TGTAG	ATCAG ACACG	ATATC GCGAG	CTGTA CATAC	CTCGC GTGTC	TAGAC TGCAC	TGATA CGTCT

(observed species, Chao1, Shannon and inverse Simpson) among sponge samples using the QIIME package with a step size of 100 and 100 repetitions per step. These indices were presented to evaluate the richness and evenness of the associated bacteria within each sponge sample (Caporaso et al., 2010). To show whether the number of reads used in the analysis was sufficient in identifying species/OTU, rarefaction curves were calculated using the QIIME script alpha_rarefaction.py. (Caporaso et al., 2010). Good's coverage index was calculated as C = 1-(s/n), where "s" is the number of unique OTUs and "n" is the number of individuals in the sample (Naim et al., 2014). The beta diversity among the microbial communities in different sponges was evaluated using UniFrac analysis and the QIIME package (Caporaso et al., 2010). The phylogenetic tree was constructed with the FastTree program to cluster the samples by an unweighted-pair group method with arithmetic mean (UPGMA) using average linkages (Nam et al., 2011; Giles et al., 2013). Also, principal coordinate analysis (PCoA) plots were provided using the QIIME to visualize the effect of the microbial community on structuring the diversity in different sponges (Caporaso et al., 2010).

RESULTS

Sponge Taxonomic Identification

In this study, 10 sponge samples were collected from three different sites in the Persian Gulf to evaluate their bacterial diversity (**Table 1**). Taxonomic identification of the sponges using a combination of multilocus DNA markers (28S rDNA and COI mtDNA) showed that the sponges belong to families Suberitidae, Pseudoceratinidae, Chondrillidae, Chalinidae, Halichondriidae, unclassified Dictyoceratida, and Irciniidae (**Table 1**).

Bacterial Richness and Diversity Analyses

A combined total of 134,495 raw pyrosequencing reads of the bacterial *16S rRNA* gene fragment comprising 52,835,851 bases were obtained from the sponge samples. Trimming and quality filtering of the raw reads derived 68,628 high-quality sequences. These denoised sequences were clustered at a 97% similarity into 724 unique OTUs. The highest number of OTUs was obtained from the sponge *Dictyoceratida* sp. (S11), representing 165 OTUs and minimum of 29 OTUs from the sponge *Suberites diversicolor* (S02).

In this study, 7.43% of *16S rRNA* gene fragments were unassigned OTUs at the phylum level. To have more detailed confirmation of the OTU representative sequences corresponding to unassigned, we extracted the sequences from each OTU and performed a BLAST search to check the sequences corresponding to the conserved region of the target region (*16S rDNA*). But the closest known sequences had less than 89% similarity rate (Supplementary Table 1) and the phylogenetic tree was not informative. Therefore, these OTUs were not included in subsequent analyses. The total number of reads retrieved and OTUs from each sponge are shown in **Table 3**.

Rarefaction plots were constructed based on OTUs at a 97% sequence similarity cut-off value by the QIIME package. Alpha rarefaction curve showed that a reasonable number of reads have been used in analysis and identifying species/OTU. The sequencing depth of the sponge samples indicated the microbial communities were very well sampled (**Figure 1**). However, additional reads may be required to discover more OTUs for the samples such as S02 to show their total bacterial diversity. OTU based alpha diversity measures and Chao1 estimation of species richness revealed the highest richness of bacterial species in the sponge S11 and lowest in the sponge S02 (**Table 3**). Microbial community diversity, Shannon and Simpson indices displayed the highest community diversity and obviously distinguished the sponge S11 when compared to other sponge species collected from the same location (**Table 3**). In this study, mean and s.d. Expected richness (Chao1) was 80.242 ± 37.647, non-parametric Shannon (H′) was 3.28 ± 1.070 and Simpson (D) was 0.774 ± 0.141. Also, the obtained average of the Good's coverage index was 99.8 % ± 0.001 for all the sponge species.

Taxonomic Composition of Bacterial Pyrosequencing Reads

Taxonomic assignment of the sequences of each OTU (68,628) was classified in the domains Bacteria (92.57% of the total dataset). Altogether, 17 bacterial phyla were recovered from the sponge samples. In the present study, 72.96% of the bacterial reads from the sponge samples were affiliated with two dominant phyla, Cyanobacteria (44.22%) and Proteobacteria (α-, β-, and γ- classes) (28.74%) (**Figure 2**). While the other reads belonging to Chloroflexi (8.67%), Acidobacteria (7.13%), Actinobacteria (4.72%), Bacteroidetes (2.04%), Gemmatimonadetes (2.04%), the candidate phylum TM7 (0.81%), Planctomycetes (0.69%), Deferribacteres (0.47%), Nitrospirae (0.19%), Firmicutes (0.10%), BD1-5 (0.07%), Tenericutes (0.06%), Armatimonadetes (0.02%), TM6 (0.02%), and Chlorobi (0.01%) were detected to be the minor groups in the sponge communities. Sponge S11 was obviously distinguished from the other sponges, in terms of containing taxa from 15 different bacterial phyla and candidate phyla. Other sponge samples contained 5 to 10 bacterial and candidate phyla. Also, the candidate phyla BD1-5 and TM6, and some phyla such as Firmicutes, Tenericutes, Armatimonadetes, and Chlorobi were only identified in sponge S11.

Diversity sponge-associated bacteria at the lower taxonomic levels showed that 45 classes and 87 orders were recovered from all datasets. *Cyanophyceae* (in Cyanobacteria),

TABLE 3 | The observed number of operational taxonomic units (OTUs) and estimations of richness (Chao1) and diversity index (Shannon, Simpson) for 16S rRNA libraries of the Persian Gulf sponge samples.

Sponge ID	Total reads	OTU richness		OTU diversity		Goods coverage (%)
		Observed OTUs	Chao1E	Shannon	Simpson	
S02	2,886	29.0	34.25	2.58	0.75	99.7
S03	3,433	67.0	76.33	4.62	0.92	99.8
S04	5,769	49.0	52.0	4.03	0.92	99.9
S05	6,083	47.0	50.27	2.57	0.75	99.8
S06	11,423	75.0	80.14	2.40	0.67	99.9
S07	7,358	67.0	81.25	2.45	0.73	99.7
S09	6,552	55.0	58.33	4.46	0.93	99.9
S10	10,910	95.0	114.25	1.94	0.48	99.8
S11	7,584	165.0	165.0	4.77	0.87	99.9
S13	6,630	75.0	90.6	2.98	0.72	99.8

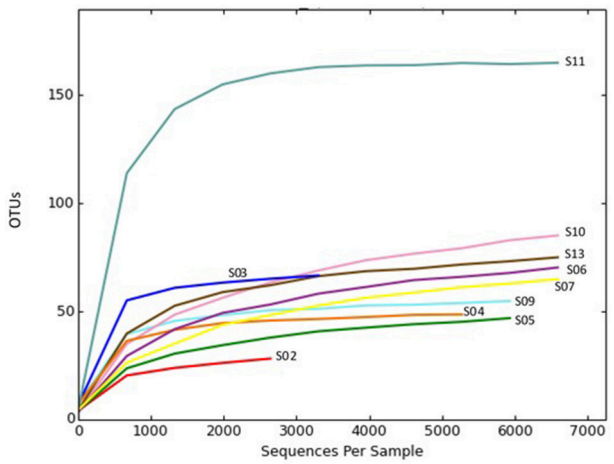

FIGURE 1 | Rarefaction plot of OTU diversity in sponge samples collected from the Persian Gulf. Rarefaction curves were constructed at a 97% sequence similarity cut-off value by the QIIME package.

Gammaproteobacteria, *Alphaproteobacteria* were the major classes in the sponges, making up 43.78, 15.82, and 7.79%, respectively. The bacterial communities in sponges at the order level were heavily loaded with *Synechococcales* (43.78%) in Cyanobacteria and *Rhodobacterales* (16.32%) and *Rhizobiales* (9.42%) in Proteobacteria. At all the three levels of taxonomic classification, the bacterial community in the sponge S11 was more diverse than those associated with other sponges. Interestingly, sponge S11 has contained more rare bacteria compared with other 9 sponges. In addition, the bacterial compositions in the same sponges (e.g., S05 and S06) from similar sites did vary substantially (**Figure 2**).

BLASTN and Phylogenetic Relationships of Highly Abundant OTUs

To have more information about the sponge-associated bacteria strains, the representative sequences of each OTU were compared against the nucleotide database in GenBank. In this study, the first 27 OTUs with average proportions of more than 0.5% among sponge samples are shown in **Figure 3**. The most predominant OTU was OTU_denovo0 in the phylum Cyanobacteria, which accounted for proportions of 16.60% in the sponge-associated bacteria and shared the highest similarity (99%) to *Synechococcus rubescens* (**Table 4**). The second most dominant OTU was OTU_denovo2 in the phylum Proteobacteria, which accounted for proportions of 5.30% and shared 93% identity with the closest relative Proteobacteria bacterium *Sinobacterium caligoides* (**Table 4**). The phylum Proteobacteria was divided into more than 100 OTUs mainly belonging to *Gammaproteobacteria*, *Alphaproteobacteria,* and *Betaproteobacteria*. Following these symbionts in terms of relative abundance were OTU_ denovo1 in the phylum Cyanobacteria, OTU_denovo4 in Acidobacteria (read count: 1614), and OTU_denovo9 in Chloroflexi (read count: 1472) (**Figure 3**). Another highly abundant OUT in the phylum Cyanobacteria was related to OTU_denovo11 that affiliated with *Prochlorococcus marinus* with an identity of 97%. Details of all cyanobacterial and proteobacterial sequences included in the study are summarized in **Table 4**. Also, the evolutionary analysis of these two dominant phyla involved 127 nucleotide sequences and are shown in **Figure 4**.

Clustering of Sponges According to Bacterial Diversity

Weighted UPGMA tree from the Unifrac analysis was constructed to show the relationships between different sponges according to their bacterial communities (**Figure 5**). In this study, sponge S11 was always distinct from the others in all trees. Also, sponges S4 and S9 exhibited the same topology and the closest distance to each other. The association among other sponges was not noticeable in the Unifrac UPGMA tree topologies. Because the bacterial profiles in each sponge were highly different from each other. Further, the difference in the bacterial community structure of the sponge samples was evaluated using Principal coordinate analysis (PCoA) plot based on the unweighted unifrac distance metrics (**Figure 6**). Sponge

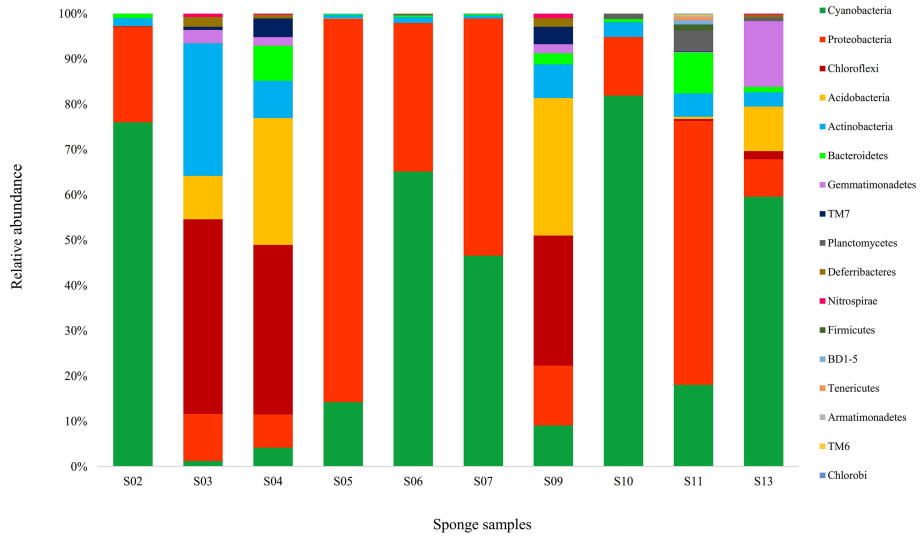

FIGURE 2 | Taxonomic classification of bacterial sequences retrieved from different sponge samples collected from the Persian Gulf at the phylum level. Refer to **Table 1** for sponge abbreviation.

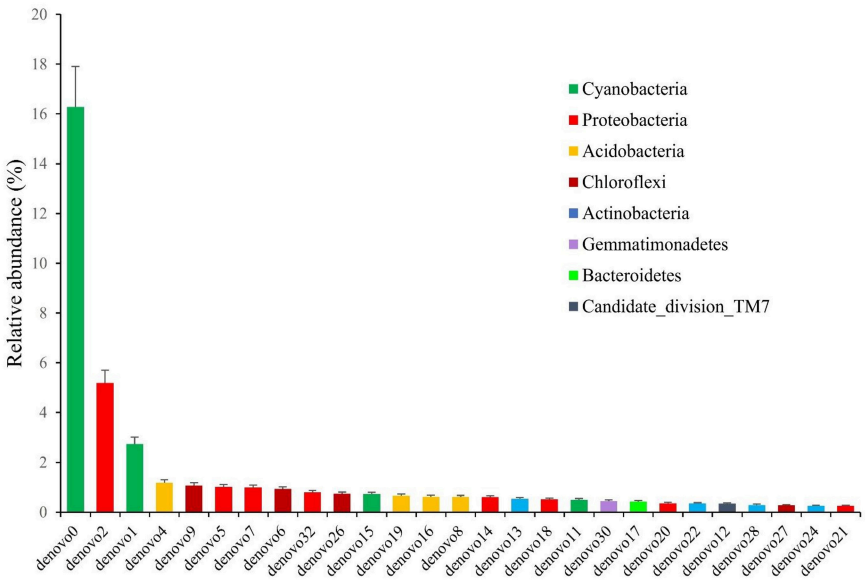

FIGURE 3 | The relative abundance of OTUs with average proportions of more than 0.5%. The Standard Deviations (SD) were shown with error bars.

S11 formed a distinct clade and showed notable differences from other sponges. Three pairs of sponges belonged to the same species (**Table 1**). But each pair was clustered in different clades except for the species *Chondrila* sp. (S04 and S09). Also, only the sponges S02, S10, and S13 contained Cyanobacteria as a major phylum.

DISCUSSION

Recently, marine sponges have been a major target of different studies due to their abundant and diverse microbial communities, ecological roles, production of novel bioactive natural compounds, and biotechnological significance (Menezes et al., 2010; Alex and Antunes, 2015). However, our understanding of bacteria-sponge interactions, nature, and diversity of bacteria associated with marine sponges is still incomplete. There are significant gaps in research on the bacterial composition, function, and maintenance of the symbiotic relationships (Menezes et al., 2010; Verhoeven et al., 2017). Deep sequencing approaches such as 454 tag pyrosequencing can be used to explore the microbial diversity of sponges with high efficiency rather than was possible by clone

library construction and Sanger sequencing methods (Gao et al., 2014a; Moitinho-Silva et al., 2014).

Taxonomic Richness and Bacterial Community Diversity

In this study, the number of unique OTUs (724) is in accordance with a study on 12 different marine sponge species from the Atlantic coast, where only 686 OTUs at 97% sequence similarity reported (Alex and Antunes, 2015). Here, the low diversity of OTUs in bacterial communities might be related to the bias of selected primers (V1–V3), in comparison to V3–V4 and V6 regions in other studies (Lee et al., 2011; Gaikwad et al., 2016; Souza et al., 2017). It will be led to inefficient amplification of the bacterial *16S rRNA* genes (Gao et al., 2017). On the other hand, differences in sampling depth and the water temperature may affect the number of OTUs in our sponge-associated bacterial communities than other studies (Jackson et al., 2012; Alex and Antunes, 2015; Souza et al., 2017). Another possibility may be because of the difference in using various bioinformatics patterns to analyze the sponge data. In CD-HIT-OTU program, when defining the OUT, there is a step to remove a cluster with fewer reads, such as a singleton or doubleton, as noise. This is not the same OTU picking method in MOTHUR or QIIME. It looks like the total number of OTU appears to be low when removing low size clusters. In the present study, the cutoff X value defined as the low size cluster was applied as 7, and the cluster consisting of less than 7 reads were removed without being picked by OTU. At this time, the total number of reads removed is 46,318.

In this study, alpha rarefaction curve showed that a reasonable number of reads have been used in analysis and identifying species/OTU. The bacterial richness estimation reported in the Persian Gulf sponges ranged from 29 to 165 OTUs. It is concordant with the range observed (29–370 OTUs) in a study targeting 12 marine sponge species sampled from the Atlantic coast (Alex and Antunes, 2015). In contrast, higher bacterial richness (570–3,013 OTUs) was found in the sponge-specific bacterial communities in Irish waters (Jackson et al., 2012) and also in the sponges from the Red Sea (251–444 OTUs) (Moitinho-Silva et al., 2014). Also, (Thomas et al., 2016) showed contributing marine sponges to the total bacterial diversity of the world's oceans, with a bacterial richness accounted for 50–3,820 OTUs in each sponge (Thomas et al., 2016). In the present study, diversity index and number of OTUs were higher in sponge S11 compared to other sponges. Sponge S11 was obviously distinguished from the other sponges, in terms of containing taxa from 15 different bacterial phyla and candidate phyla. At all the three levels of taxonomic classification, the bacterial community in the sponge S11 was more diverse than those associated with other studied sponges. Interestingly, sponge S11 has contained more rare bacteria compared with other sponges.

Taxonomic identification of sponge S11 using a combination of multilocus DNA markers showed that the sponge belongs to the genus of *Dictyoceratida* sp. Many studies have considered the order *Dictyoceratida* as the largest producer of new marine natural products, contributing more than 20% of all sponge-derived novel compounds (Mehbub et al., 2014, 2016). Different bacterial communities associated with the order *Dictyoceratida* are reported to produce a wide range of natural compounds with a variety of biological activities (Thakur et al., 2005; Mehbub et al., 2014, 2016). Also, Sponge S11 formed a distinct clade in the weighted UPGMA tree from Unifrac analysis and showed notable differences from other sponges.

Interestingly, in this study, the bacterial compositions in the same sponges (S05 and S06) from similar sites did vary substantially. There was a 100 m distance between the sampling sites of these two sponges. This finding confirms the previous studies, indicating that two cohabiting sponges may have different bacterial signatures (Jasmin et al., 2015; Jeong et al., 2015).

In the present study, a small number of OTUs (7.43%) were recorded as unassigned at the phylum level, after quality filtering and removal of chimera. When alignment is performed with UCLUST in the Reference DB, it means that there are no more than 90% references to match (OTU representative sequence). Unassigned OTUs may be a sequencing error element (Chimera, etc.) that could not be removed in the previous step (OTU picking step). Because there is no match result due to high cut off value, 90%. The frequency of unassigned OTUs was also maintained, after re-analysis of the OTU representative sequences corresponding to unassigned in a BLAST search for the conserved region of the target region (16S rDNA). These OTUs were not included in further analyses, but their presence is noteworthy. However, this number was much lower than those reported from Florida (White et al., 2012) and Indonesia (Cleary et al., 2013), where 36 and 34% of OTUs could not be assigned to any bacterial phylum, respectively.

Community Composition of Sponge-Associated Bacteria

One of the highlights of our study was the high frequency of Cyanobacteria in the Persian Gulf sponges, contributing 44.22% of the total phylum-level diversity. Also, the presence of Cyanobacteria was confirmed in all the sponges studied with various abundance. Cyanobacteria were also the dominant phylum in the sponge samples reported from other tropical and subtropical regions (Alex et al., 2012; Gao et al., 2014a, 2017; Regueiras et al., 2017).

Within this phylum, our sponge samples contained a high proportion (97.37%) of free-living *Synechococcus*. BLAST search further revealed the dominant OTU in sponge samples and showed a high similarity with previously reported freshwater-specific species "*Synechococcus rubescens*" isolated from the deep subalpine lakes (central Europe), Lake Biwa (Japan), Lake Balaton (Hungary), and the Baltic Sea (Ernst et al., 2003). The Cyanobacteria *Synechococcus* has considered as an autotrophic plankton community and a substantial fraction of marine primary production (Flombaum et al., 2013), as sponge feeding on Cyanobacteria has been extensively confirmed (Pile et al., 1996; Hadas et al., 2009). This genus of marine bacteria has widely distributed in many ocean regions, covering both polar and high-nutrient waters (Flombaum et al., 2013). Furthermore, the cyanobacterial *Synechococcus* lineage is believed to have several

TABLE 4 | Details of all cyanobacterial and proteobacterial sequences included in the study.

OTU	Read count	Phylum	Order	Family	Bacterial species	Strain	Accession no.	Similarity (%)	Habitat	Type source/place
denovo0	22,341	Cyanobacteria	Synechococcales	Synechococcaceae	*Synechococcus rubescens*	SAG 3.81	NR_125481.1	99	Freshwater	Deep subalpine lakes (central Europe), lake Biwa (Japan), lake Balaton (Hungary), the Baltic Sea
denovo1	3,758	Cyanobacteria	Synechococcales	Synechococcaceae	*Synechococcus rubescens*	SAG 3.81	NR_125481.1	99	Freshwater	Deep subalpine lakes (central Europe), lake Biwa (Japan), lake Balaton (Hungary), the Baltic Sea
denovo11	686	Cyanobacteria	Synechococcales	Prochloraceae	*Prochlorococcus marinus*	PCC 9511	NR_125480.1	97	Seawater	North Atlantic, Mediterranean Sea
denovo15	993	Cyanobacteria	Synechococcales	Synechococcaceae	*Synechococcus rubescens*	SAG 3.81	NR_125481.1	99	Freshwater	Deep subalpine lakes (central Europe), Lake Biwa (Japan), Lake Balaton (Hungary), the Baltic Sea
denovo105	38	Cyanobacteria	Synechococcales	Synechococcaceae	*Synechococcus rubescens*	SAG 3.81	NR_125481.1	97	Freshwater	Deep subalpine lakes (central Europe), lake Biwa (Japan), lake Balaton (Hungary), the Baltic Sea
denovo150	35	Cyanobacteria	Nostocales	Nostocaceae	*Cronbergia siamensis*	SAG 11.82	NR_153750.1	96	NA	Germany
denovo189	19	Cyanobacteria	Synechococcales	Synechococcaceae	*Synechococcus elongatus*	PCC 6301	NR_074309.1	98	Freshwater	California
denovo261	12	Cyanobacteria	Chroococcales	Aphanothecaceae	*Gloeothece membranacea*	PCC 6501	NR_119092.1	96	NA	USA
denovo2	7,122	γ-Proteobacteria	Chromatiales	Chromatiaceae	*Nitrosococcus halophilus*	Nc 4	NR_074790.1	93	Marine	USA
denovo5	1,382	γ-Proteobacteria	Legionellales	Coxiellaceae	*Coxiella burnetii*	ATCC VR-615	NR_104916.1	92	NA	USA
denovo7	1,364	γ-Proteobacteria	Chromatiales	Ectothiorhodospiraceae	*Thioalkalivibrio nitratireducens*	DSM 14787	NR_102486.1	96	NA	Russia
denovo10	1,565	α-Proteobacteria	Kordiimonadales	Kordiimonadaceae	*Kordiimonas lipolytica*	M41	NR_149297.1	92	Seawater	China
denovo14	822	α-Proteobacteria	Rhodobacterales	Rhodobacteraceae	*Boseongicola aestuarii*	BS-W15	NR_133983.1	99	Sediment	Tidal flat sediment, South Korea
denovo18	696	γ-Proteobacteria	Oceanospirillales	Halomonadaceae	*Halomonas flava*	YIM 94343	NR_109317.1	93	Soil	Soil from salt lake, Qijiaojing Lake, China
denovo20	499	α-Proteobacteria	Rhodobacterales	Rhodobacteraceae	*Oceanicola litoreus*	M-M22	NR_118461.1	96	Sediment	Seashore sediment, Geoje island, South Korea
denovo21	340	α-Proteobacteria	Rhizobiales	Hyphomicrobiaceae	*Methyloterrigena soli*	M48	NR_147729.1	92	Soil	Activated sludge, Republic of Korea
denovo29	276	γ-Proteobacteria	Oceanospirillales	Hahellaceae	*Kistimonas asteriae*	KMD 001	NR_116386.1	95	NA	Republic of Korea
denovo31	274	α-Proteobacteria	Pelagibacterales	Pelagibacteraceae	*Candidatus Pelagibacterubique*	HTCC1062	NR_074224.1	99	Seawater	USA
denovo32	1086	α-Proteobacteria	Pelagibacterales	Pelagibacteraceae	*Candidatus Pelagibacterubique*	HTCC1062	NR_074224.1	100	Seawater	USA
denovo33	244	γ-Proteobacteria	Chromatiales	Chromatiaceae	*Halochromatium glycolicum*	BN 3201	NR_044896.1	95	NA	Germany
denovo39	105	γ-Proteobacteria	Chromatiales	Woeseiaceae	*Woeseia oceani*	XK5	NR_147719.1	93	Sediment	Coastal sediment, Xiaoshi Island, Weihai, China
denovo42	152	α-Proteobacteria	Rhodobacterales	Rhodobacteraceae	*Amylibacter ulvae*	KMM 6515	NR_146351.1	99	NA	Republic of Korea
denovo44	99	α-Proteobacteria	Rhodospirillales	Rhodospirillaceae	*Tistrella mobilis*	NBRC 102134	NR_114036.1	95	NA	Japan

(Continued)

TABLE 4 | Continued

OTU	Read count	Phylum	Order	Family	Bacterial species	Strain	Accession no.	Similarity (%)	Habitat	Type source/place
denovo46	65	γ-Proteobacteria	Chromatiales	Woeseiaceae	*Woeseia oceani*	XK5	NR_147719.1	98	Sediment	Coastal sediment, Xiaoshi Island, Weihai, China
denovo50	142	α-Proteobacteria	Rhodobacterales	Rhodobacteraceae	*Pseudoruegeria aestuarii*	MME-001	NR_151932.1	96	Sediment	Tidal flat of Muui-do, Republic of Korea
denovo54	65	α-Proteobacteria	Kordiimonadales	Kordiimonadaceae	*Kordiimonas lipolytica*	M41	NR_149297.1	95	Seawater	China
denovo56	159	α-Proteobacteria	Rhodobacterales	Rhodobacteraceae	*Ruegeria conchae*	TW15	NR_109062.1	100	Ark clam	Strain: *Scapharca broughtonii*, South Korea
denovo59	79	α-Proteobacteria	Rhodobacterales	Rhodobacteraceae	*Rhodovulum strictum*	MB-G2	NR_025845.1	95	Seawater	Tidal and seawater pools, Japan
denovo62	73	α-Proteobacteria	Pelagibacterales	Pelagibacteraceae	*Candidatus Pelagibacterubique*	HTCC1062	NR_074224.1	94	Seawater	USA
denovo66	131	γ-Proteobacteria	Oceanospirillales	Oceanospirillaceae	*Neptunomonas qingdaonensis*	P10-2-4	NR_109382.1	94	Sand	Coastal area of Qingdao (Yellow Sea), China
denovo67	36	α-Proteobacteria	Rhodobacterales	Rhodobacteraceae	*Catellibacterium aquatile*	NBRC 104254	NR_114265.1	96	NA	Japan
denovo68	68	α-Proteobacteria	Kordiimonadales	Kordiimonadaceae	*Kordiimonas lipolytica*	M41	NR_149297.1	92	Seawater	China
denovo70	81	γ-Proteobacteria	Cellvibrionales	Halieaceae	*Haliea mediterranea*	7SM29	NR_116976.1	99	Seawater	Mediterranean sea water, Spain
denovo80	36	γ-Proteobacteria	Thiotrichales	Francisellaceae	*Francisella halioticida*	Shimane-1	NR_112804.1	99	Abalone	Strain: *Haliotis gigantean*, Japan
denovo82	41	γ-Proteobacteria	Oceanospirillales	Hahellaceae	*Endozoicomonas numazuensis*	HC50	NR_114318.1	99	Sponge	Strain: *Haliclona* sp., Coast of Numazu, Japan
denovo87	49	α-Proteobacteria	Sphingomonadales	Sphingomonadaceae	*Novosphingobium tardaugens*	NBRC 16725	NR_113869.1	99	NA	Japan
denovo90	31	γ-Proteobacteria	Oceanospirillales	Alteromonadaceae	*Marinobacterium marisflavi*	IMCC4074	NR_125520.1	93	Seawater	Atlantic Ocean, Yellow Sea, Incheon, Republic of Korea
denovo92	33	γ-Proteobacteria	Oceanospirillales	Alteromonadaceae	*Marinobacterium mangrovicola*	Gal22	NR_134077.1	97	Mangrove	Mangrove roots of *Rhizophora mangle*, Germany
denovo93	83	α-Proteobacteria	Rhodobacterales	Rhodobacteraceae	*Actibacterium atlanticum*	22II-S11-z10	NR_136418.1	96	NA	China
denovo94	56	γ-Proteobacteria	Pseudomonadales	Pseudomonadaceae	*Pseudomonas mucidolens*	NBRC 103159	NR_114225.1	100	NA	Japan
denovo95	35	γ-Proteobacteria	Chromatiales	Chromatiaceae	*Halochromatium salexigens*	6310: DSM 4395	NR_036810.1	94	Freshwater	Germany
denovo98	25	α-Proteobacteria	Rhodobacterales	Rhodobacteraceae	*Pelagibaca abyssi*	JLT2014	NR_148263.1	97	Seawater	China
denovo99	57	α-Proteobacteria	Rhizobiales	Methylocystaceae	*Terasakiella brassicae*	B3	NR_148851.1	93	Wastewater	Wastewater of a pickle-processing factory, China
denovo100	19	γ-Proteobacteria	Oceanospirillales	Hahellaceae	*Endozoicomonas euniceicola*	EF212	NR_109684.2	98	Octocoral	Strain: *Eunicea fusca* and *Plexaura* sp., coast of Florida, USA, and the coast of Bimini, Bahamas
denovo101	22	α-Proteobacteria	Rhodospirillales	Acetobacteraceae	*Craurococcus roseus*	NS130	NR_036877.1	92	Soil	Japan
denovo103	50	α-Proteobacteria	Rhodospirillales	Rhodospirillaceae	*Nisaea denitrificans*	DR41_21	NR_043923.1	95	Seawater	Coastal, surface waters of the north-western Mediterranean Sea, France

(Continued)

TABLE 4 | Continued

OTU	Read count	Phylum	Order	Family	Bacterial species	Strain	Accession no.	Similarity (%)	Habitat	Type source/place
denovo104	32	α-Proteobacteria	Rhodobacterales	Rhodobacteraceae	*Pelagibaca abyssi*	JLT2014	NR_148263.1	95	Seawater	China
denovo110	35	γ-Proteobacteria	Cellvibrionales	Halieaceae	*Haliea mediterranea*	7SM29	NR_116976.1	98	Seawater	Mediterranean sea water, Spain
denovo112	15	α-Proteobacteria	Sphingomonadales	Sphingomonadaceae	*Sphingopyxis italica*	SC13E-S71	NR_108877.1	93	Soil	Tuff, volcanic rock of the Roman catacombs, Rome, Italy
denovo116	29	γ-Proteobacteria	–	–	*Thiolapillus brandeum*	Hiromi 1	NR_148757.1	95	Hydrothermal vent	Hydrothermal vent chimney, Okinawa, Japan
denovo117	62	γ-Proteobacteria	Cellvibrionales	Halieaceae	*Luminiphilus syltensis*	Ivo14	NR_125526.1	98	Sediment	Tidal flat, island of Sylt, North Sea, Germany
denovo119	19	α-Proteobacteria	Rhizobiales	Rhodobiaceae	*Pyruvatibacter mobilis*	GYP-11	NR_147733.1	95	Microalga	Marine microalga, Strain: *Picochloruma* sp., China
denovo123	37	α-Proteobacteria	Rhodobacterales	Rhodobacteraceae	*Rhodovulum sulfidophilum*	KC2142	NR_115746.1	92	Clinical sample	USA
denovo125	39	α-Proteobacteria	Rhizobiales	Phyllobacteriaceae	*Hoeflea phototrophica*	NCIMB 14078	NR_118230.1	96	Seawater	Yellow Sea, Republic of Korea
denovo126	14	α-Proteobacteria	Rhodobacterales	Rhodobacteraceae	*Paenirhodobacter enshiensis*	DW2-9	NR_125604.1	98	Soil	Sewage outlet of the Bafeng pharmaceutical factory, Enshi, Hubei province, PR China
denovo130	16	α-Proteobacteria	Rhodobacterales	Rhodobacteraceae	*Labrenzia alba*	5OM6	NR_042378.1	99	Oyster	Mediterranean coast, Spain
denovo131	60	α-Proteobacteria	Rhodobacterales	Rhodobacteraceae	*Paracoccus cavernae*	0511ARD5E5	NR_149299.1	95	Air	Ardales Cave,Malaga, Spain
denovo135	35	γ-Proteobacteria	Cellvibrionales	Halieaceae	*Marimicrobium arenosum*	CAU1038	NR_148595.1	94	Sea sand	Modo, Republic of Korea
denovo136	42	γ-Proteobacteria	Cellvibrionales	Cellvibrionaceae	*Eionea nigra*	17X/A02/237	NR_115270.1	92	Water	Waters of the coastal north-western Mediterranean Sea, France
denovo137	14	γ-Proteobacteria	Oceanospirillales	Hahellaceae	*Endozoicomonas ascidiicola*	AVMART05	NR_146693.1	95	Ascidian	*Ascidiella* sp., Gullmarsfjord, Sweden
denovo139	36	α-Proteobacteria	Rhodobacterales	Rhodobacteraceae	*Roseibacterium elongatum*	DFL-43	NR_121734.1	98	Sand	Australia
denovo140	20	γ-Proteobacteria	Cellvibrionales	Microbulbiferaceae	*Microbulbifer chitinilyticus*	ABABA 212	NR_112918.1	97	Mangrove	Mangrove forests, Okinawa, Japan
denovo141	20	α-Proteobacteria	Rhodospirillales	Rhodospirillaceae	*Magnetospirillum marisnigri*	SP-1	NR_149242.1	93	Freshwater	Sediments, three distinct locations in European Russia
denovo143	12	γ-Proteobacteria	Legionellales	Coxiellaceae	*Coxiella burnetii*	ATCC VR-615	NR_104916.1	97	NA	USA
denovo146	23	α-Proteobacteria	Sphingomonadales	Sphingomonadaceae	Sphingopyxis fribergensis	Kp5.2	NR_137271.1	94	Soil	Saxony, Germany
denovo147	15	γ-Proteobacteria	Cellvibrionales	Halieaceae	Haliea atlantica	SM1351	NR_137377.1	94	Seawater	Surface seawater of the Atlantic Ocean
denovo148	24	γ-Proteobacteria	Oceanospirillales	Halomonadaceae	*Larsenimonas suaedae*	ST307	NR_151924.1	95	Seepweed	Euhalophyte Suaeda salsa, Dongying, China
denovo151	18	α-Proteobacteria	Rhodospirillales	Rhodospirillaceae	*Nisaea nitritireducens*	DR41_18	NR_043924.1	94	Water	Coastal, surface waters of the north-western Mediterranean Sea, France
denovo153	13	γ-Proteobacteria	Oceanospirillales	Oceanospirillaceae	*Neptunomonas japonica*	JAMM 0745	NR_041567.1	95	Sediment	Sediment adjacent to sperm whale carcasses off Kagoshima, Japan
denovo162	22	α-Proteobacteria	Rhizobiales	Bradyrhizobiaceae	*Bradyrhizobium lupini*	USDA 3051	NR_134836.1	100	Nodule	Spain

(Continued)

TABLE 4 | Continued

OTU	Read count	Phylum	Order	Family	Bacterial species	Strain	Accession no.	Similarity (%)	Habitat	Type source/place
denovo165	32	α-Proteobacteria	Rhodobacterales	Rhodobacteraceae	*Boseongicola aestuarii*	BS-W15	NR_133983.1	98	Sediment	Tidal flat sediment, South Korea
denovo169	24	α-Proteobacteria	Rhodobacterales	Rhodobacteraceae	*Phaeobacter caeruleus*	DSM 24564	NR_118542.1	99	Marine biofilm	Biofilm on stainless steel electrode, Genoa harbor, Italy
denovo173	10	α-Proteobacteria	Kiloniellales	Kiloniellaceae	*Kiloniella laminariae*	LD81	NR_042646.1	95	Marine macroalga	Strain: *Laminaria saccharina*,:Baltic Sea, Germany
denovo177	16	α-Proteobacteria	Sphingomonadales	Sphingomonadaceae	*Sphingorhabdus pacifica*	n34	NR_134813.1	99	Sediment	Sandy sediments of the Sea of Japan seashore
denovo181	16	γ-Proteobacteria	Chromatiales	Chromatiaceae	*Nitrosococcus halophilus*	Nc 4	NR_074790.1	93	Marine	USA
denovo186	11	γ-Proteobacteria	Chromatiales	Woeseiaceae	*Woeseia oceani*	XK5	NR_147719.1	98	Sediment	Coastal sediment, Xiaoshi Island, Weihai, China
denovo188	9	γ-Proteobacteria	Legionellales	Legionellaceae	*Legionella thermalis*	L-47	NR_146358.1	94	Water	Hot spring water, Tokyo, Japan
denovo192	16	γ-Proteobacteria	Chromatiales	Ectothiorhodospiraceae	*Ectothiorhodospira mobilis*	DSM 237	NR_125567.1	93	NA	NA
denovo193	9	α-Proteobacteria	Rhizobiales	Rhodobiaceae	*Anderseniella baltica*	BA141	NR_042626.1	98	Sediment	Surface of sediment in a deep basin of the central Baltic Sea, Germany
denovo194	37	α-Proteobacteria	Rhodobacterales	Rhodobacteraceae	*Agaricicola taiwanensis*	CC-SBABM117	NR_125534.1	96	Edible mushroom	Strain: *Agaricus blazei*, China
denovo199	10	α-Proteobacteria	Rickettsiales	Rickettsiaceae	*Rickettsia raoultii*	Khabarovsk	NR_043755.1	95	Tick	Strain: Dermacentor silvarum, Russia, France
denovo201	8	γ-Proteobacteria	Xanthomonadales	Xanthomonadaceae	*Stenotrophomonas maltophilia*	ATCC 19861	NR_040804.1	100	NA	Japan
denovo204	8	β-Proteobacteria	Nitrosomonadales	Methylophilaceae	*Methylobacillus glycogenes*	TK 0113	NR_104760.1	96	NA	NA
denovo206	8	γ-Proteobacteria	Cellvibrionales	Microbulbiferaceae	*Microbulbifer gwangyangensis*	GY2	NR_118158.1	98	Seawater	Tidal flat at Gwangyang Bay, Korea
denovo207	8	γ-Proteobacteria	Alteromonadales	Colwelliaceae	*Thalassomonas agarivorans*	TMA1	NR_043649.1	99	Water	Shallow coastal water of An-Ping Harbor, Taiwan
denovo208	14	α-Proteobacteria	Rhizobiales	Chelatococcaceae	*Chelatococcus reniformis*	B2974	NR_152704.1	96	Ice core	Muztagh Glacier, on the Tibetan Plateau, China
denovo210	15	α-Proteobacteria	Rhodobacterales	Rhodobacteraceae	*Silicimonas algicola*	KC90B	NR_152708.1	98	Diatom	Cell surface of the marine diatom, strain: *Thalassiosira delicatula*, France
denovo211	8	α-Proteobacteria	Rhizobiales	Hyphomicrobiaceae	*Devosia albogilva*	IPL15	NR_044212.1	99	Marine sediment	Yueqing Bay, Zhejiang Province, China
denovo212	28	γ-Proteobacteria	Cellvibrionales	Microbulbiferaceae	*Microbulbifer yueqingensis*	Y226	NR_108574.1	95	Dump	Hexachlorocyclohexane dump site, India
denovo213	7	α-Proteobacteria	Rhodobacterales	Rhodobacteraceae	*Oceanicola litoreus*	M-M22	NR_118461.1	99	Sediment	Seashore sediment, Geoje island, South Korea
denovo216	9	γ-Proteobacteria	Legionellales	Coxiellaceae	*Coxiella burnetii*	ATCC VR-615	NR_104916.1	97	NA	USA
denovo217	23	α-Proteobacteria	Rhodobacterales	Rhodobacteraceae	*Nautella italica*	LMG 24365	NR_042673.1	100	Marine biofilm	Marine electroactive biofilm, Genova harbor, Italy
denovo220	11	β-Proteobacteria	Nitrosomonadales	Methylophilaceae	*Methylobacillus flagellatus*	KT	NR_074178.1	96	NA	USA
denovo221	23	α-Proteobacteria	Rhodobacterales	Rhodobacteraceae	*Poseidonocella pacifica*	KMM 9010	NR_113209.1	99	Sediments	Shallow sandy sediments of the Sea of Japan

(Continued)

TABLE 4 | Continued

OTU	Read count	Phylum	Order	Family	Bacterial species	Strain	Accession no.	Similarity (%)	Habitat	Type source/place
denovo226	29	β-Proteobacteria	Burkholderiales	Burkholderiaceae	*Ralstonia pickettii*	NBRC 102503	NR_114126.1	100	NA	Japan
denovo228	14	α-Proteobacteria	Rhodobacterales	Rhodobacteraceae	*Pseudoruegeria marinistellae*	SF-16	NR_149190.1	99	Starfish	Sanya, China
denovo229	7	α-Proteobacteria	Rhizobiales	Rhizobiaceae	*Rhizobium gei*	ZFJT-2	NR_152093.1	97	Plant	Stem of Geum aleppicum, Taibai Mountain, Shaanxi Province, north-west China
denovo230	16	γ-Proteobacteria	Oceanospirillales	Kangiellaceae	*Kangiella chungangensis*	CAU 1040	NR_148305.1	92	Marine sand	Jeju Island, South Korea
denovo232	7	α-Proteobacteria	Rhizobiales	Rhizobiaceae	*Rhizobium rosettiformans*	W3	NR_116445.1	100	Ground water	Lucknow, India
denovo234	14	α-Proteobacteria	Caulobacterales	Caulobacteraceae	*Caulobacter mirabilis*	FWC 38	NR_041964.1	97	Freshwater	Germany
denovo235	10	α-Proteobacteria	Rhizobiales	-	*Methyloceanibacter caenitepidi*	Gela4	NR_125465.1	99	Marine sediment	Near a hydrothermal vent, Japan
denovo237	14	α-Proteobacteria	Kiloniellales	Kiloniellaceae	*Kiloniella litopenaei*	P1-1	NR_148331.1	92	Soil	Hoh Xil basin, China
denovo243	8	γ-Proteobacteria	Cellvibrionales	Halieaceae	*Marimicrobium arenosum*	CAU1038	NR_148595.1	95	Sea sand	Modo, Republic of Korea
denovo249	11	γ-Proteobacteria	-	-	*Thiolapillus brandeum*	Hiromi 1	NR_148757.1	93	Hydrothermal vent	Hydrothermal vent chimney, Okinawa, Japan
denovo253	14	α-Proteobacteria	Rhodobacterales	Rhodobacteraceae	*Roseovarius crassostreae*	CV919-312	NR_041731.1	99	Oyster	Damariscotta River, USA
denovo258	10	α-Proteobacteria	Rhizobiales	Hyphomicrobiaceae	*Devosia albogilva*	IPL15	NR_044212.1	98	Marine sediment	Yueqing Bay, Zhejiang Province, China
denovo264	8	γ-Proteobacteria	Oceanospirillales	-	*Oceanospirillum beijerinckii*	NBRC 15445	NR_113754.1	95	NA	Japan
denovo274	11	α-Proteobacteria	Rhizobiales	Rhodobiaceae	*Rhodobium gokarnense*	JA173	NR_042475.1	95	Salt pan	Saltern Gokarna, India
denovo275	7	α-Proteobacteria	Kordiimonadales	Kordiimonadaceae	*Kordiimonas sediminis*	N39	NR_149185.1	94	Sediment	Sample collected at a sea cucumber culture pond in Weihai, China
denovo276	9	α-Proteobacteria	Rhizobiales	Rhizobiaceae	*Rhizobium flavum*	YW14	NR_133843.1	100	Soil	China
denovo279	8	α-Proteobacteria	Rhodobacterales	Rhodobacteraceae	*Ahrensia kielensis*	NBRC 15762	NR_113807.1	96	NA	Japan
denovo280	7	α-Proteobacteria	Rhizobiales	Hyphomicrobiaceae	*Devosia crocina*	IPL20	NR_044213.1	92	Dump	hexachlorocyclohexane dump site, India
denovo281	8	α-Proteobacteria	Rhodobacterales	Rhodobacteraceae	*Aestuariivita boseongensis*	BS-B2	NR_133957.1	98	Sediment	Tidal flat sediment, Boseong, South Korea
denovo284	18	α-Proteobacteria	Pelagibacterales	Pelagibacteraceae	*Candidatus Pelagibacterubique*	HTCC1062	NR_074224.1	95	Seawater	USA
denovo287	11	α-Proteobacteria	Rhizobiales	Hyphomicrobiaceae	*Devosia chinhatensis*	IPL18	NR_044214.1	95	Dump	Hexachlorocyclohexane (HCH) dump site, India
denovo290	7	γ-Proteobacteria	Chromatiales	Woeseiaceae	*Woeseia oceani*	XK5	NR_147719.1	97	Sediment	Coastal sediment, Xiaoshi Island, Weihai, China
denovo292	8	α-Proteobacteria	Rhizobiales	Hyphomicrobiaceae	*Bauldia litoralis*	524-16	NR_117251.1	93	NA	NA

(Continued)

TABLE 4 | Continued

OTU	Read count	Phylum	Order	Family	Bacterial species	Strain	Accession no.	Similarity (%)	Habitat	Type source/place
denovo293	7	α-Proteobacteria	Rhodobacterales	Rhodobacteraceae	*Loktanella litorea*	DPG-5	NR_118329.1	100	Seawater	The South Sea, Republic of Korea
denovo295	8	γ-Proteobacteria	Pseudomonadales	Moraxellaceae	*Acinetobacter lwoffii*	JCM 6840	NR_113346.1	100	NA	Japan
denovo300	8	α-Proteobacteria	Rhodospirillales	Rhodospirillaceae	*Limibacillus halophilus*	CAU 1121	NR_137248.1	96	Soil	Reclaimed land in the Republic of Korea
denovo306	9	γ-Proteobacteria	Chromatiales	Granulosicoccaceae	*Granulosicoccus undariae*	W-BA3	NR_134740.1	94	Brown algae	Brown algae reservoir in Wando of South Korea
denovo319	9	γ-Proteobacteria	Chromatiales	Woeseiaceae	*Woeseia oceani*	XK5	NR_147719.1	95	Sediment	Coastal sediment, Xiaoshi Island, Weihai, China
denovo323	13	α-Proteobacteria	Rhodobacterales	Hyphomonadaceae	*Hellea balneolensis*	26III/A02/215	NR_042992.1	97	Freshwater	Surface water of the north-western Mediterranean Sea, France
denovo327	7	γ-Proteobacteria	–	–	*Thiohalobacter thiocyanaticus*	HRh1	NR_116699.1	93	Sediment	Mixed sediment from hypersaline chloride-sulfate lakes, Kulunda Steppe, Russia
denovo331	9	γ-Proteobacteria	Methylococcales	Methylococcaceae	*Methyloparacoccus murrellii*	R-49797	NR_133784.1	93	Pond water	South Africa
denovo333	7	α-Proteobacteria	Rhizobiales	Methylobacteriaceae	*Methylobacterium radiotolerans*	JCM 2831	NR_074244.1	100	NA	NA
denovo337	8	γ-Proteobacteria	Cellvibrionales	Halieaceae	*Halioglobus japonicus*	S1-36	NR_113277.1	100	Seawater	North-western Pacific Ocean near Japan

OTU was determined based on a 16S rRNA gene similarity of 90%.
NA, Not available.

ecotypes that are adapted to different environmental conditions including light, temperature, nutrients, and chlorophyll a concentration (Flombaum et al., 2013). It is possible that the core OTUs illustrate bacterial sponge ecotypes that are matched to the niche sponges and are probably environmentally transmitted (Schmitt et al., 2012). As Cyanobacteria are the center of carbon fixation and provide necessary nutrients to photosynthetic sponge hosts (Taylor et al., 2007), the high abundance of Cyanobacteria further indicated the specific roles of photosynthetic bacteria and their profitability in sponge biology (Lemloh et al., 2009; Alex et al., 2012).

The Persian Gulf sponges were recurrently exposed to light in low depth (<3 m) in this study. Therefore, the prominence of photosymbionts was predictable in these sponges. In spite of the important role of Cyanobacteria, they are typically absent in Antarctic sponges (Rodríguez-Marconi et al., 2015). It seems that environmental factors such as temperature, salinity or nutrient levels might impact the composition of bacterial community structures in different sponges (Giles et al., 2013; Cuvelier et al., 2014).

The co-evolution and functional aspects of sponge-cyanobacteria associations have not been revealed in details. Sponges may acquire their cyanobacterial symbionts by vertical, horizontal or combined transmission routes (Thacker and Freeman, 2012). The genome-level research on cyanobacterial symbionts of sponges showed that they have general and specific adaptations to life within the sponge host in comparison with free-living cyanobacteria (Gao et al., 2014b; Burgsdorf et al., 2015). Sponge symbionts have adapted mechanisms to actively seek out by their sponge hosts (Webster and Thomas, 2016). For example, cyanobacterial symbionts contains large number eukaryotic-like domains, such as ARs. These domains may be involved in avoiding digestion by the sponge host (Gao et al., 2017).

Lifestyle evolutionary and functional studies on other functions enriched and depleted in cyanobacterial symbionts of sponges compared to members of the closely related free-living strains reveled the precise and smart adaptation of cyanobacteria to live in full of challenge sponge's intercellular environment. Sponge amoebocytes may not actively distinguish between food bacteria and their cyanobacterial symbionts (Webster and Thomas, 2016). Hence, the depleted genes involved in biosynthesis of LPS O antigen in cyanobacterial symbionts of sponges produces a defense mechanism against sponge predation and phage attack (Burgsdorf et al., 2015; Webster and Thomas, 2016). In functional profile studies of bacterial symbionts with sponges, common functions in similar niches were found, indicating functionally convergence of symbionts in the divergent hosts (Fan et al., 2012; Rua et al., 2015). The biological and ecological roles of these functional equivalences may be of general importance for the adaptation of cyanobacterial symbiont to the sponge host environment and other symbiotic interactions.

In the present study, Proteobacteria was the second most abundant phylum in the microbiome of sponge-associated bacteria. Our study is in accordance with other studies showing

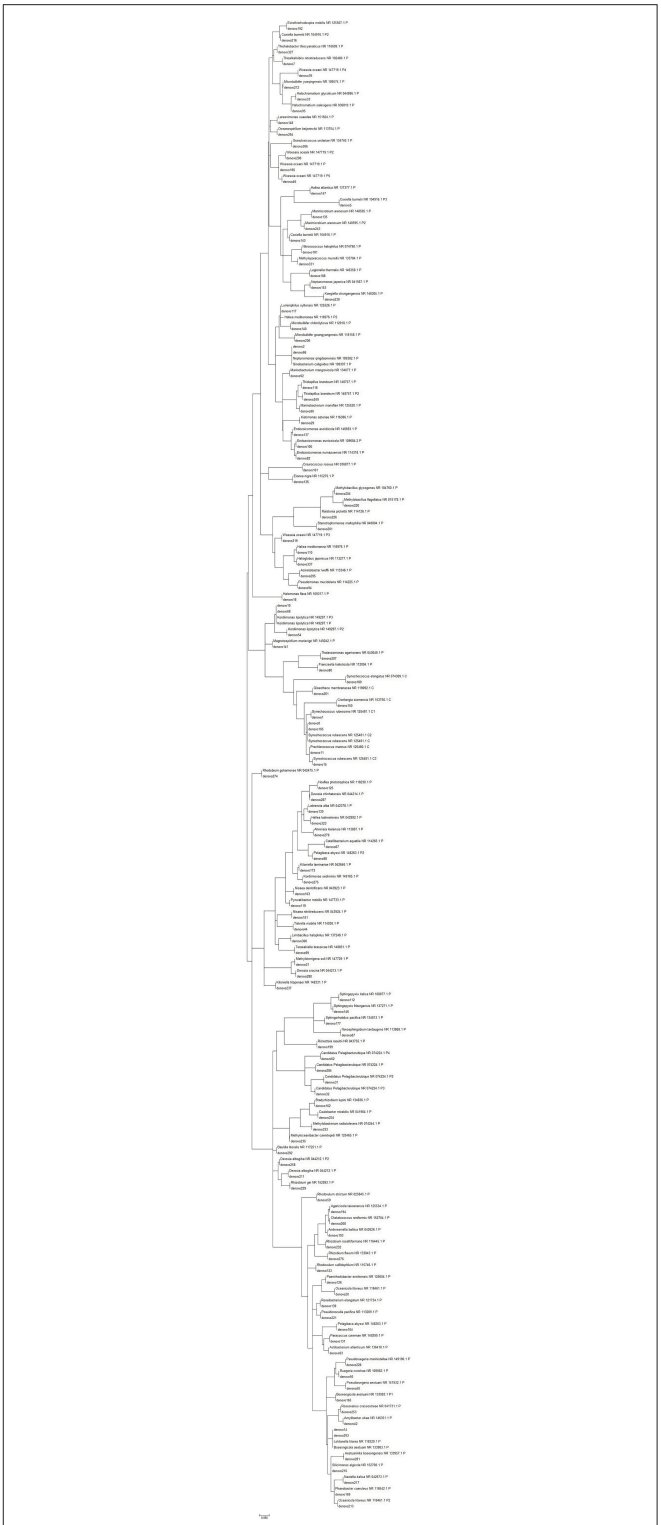

FIGURE 4 | Molecular phylogenetic analysis of Cyanobacteria (red color) and proteobacteria (blue color) phyla in sponge samples based on the bacterial *16S rRNA* gene in GenBank. Tree topology constructed using Maximum Likelihood method, with bootstrap values >90%. Scale bar: 0.06 substitutions per nucleotide position.

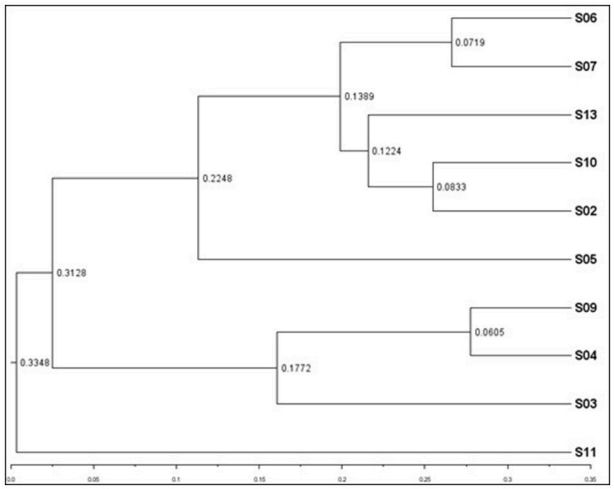

FIGURE 5 | Weighted UPGMA tree from Unifrac analysis showing relationships between different sponges according to bacterial communities. The figure was constructed on the basis of tag pyrosequencing data. The scale bar represents the distance between clusters in UniFrac units.

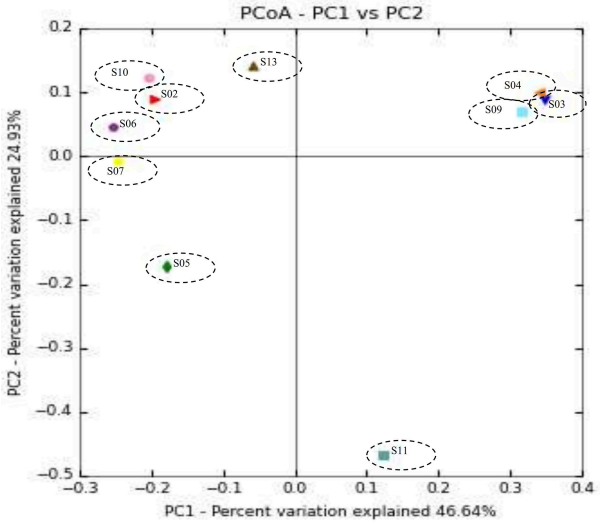

FIGURE 6 | Principal coordinate analysis (PCoA) plot of sponge samples obtained with the unweighted UniFrac distance metric.

proteobacteria as one of the most diverse phyla of sponge-isolated bacterial communities, irrespective of the habitat (Menezes et al., 2010; Schmitt et al., 2012; Jeong et al., 2014, 2015; Gao et al., 2017). In Proteobacteria phylum, OTUs were mainly affiliated with *Gammaproteobacteria*, *Alphaproteobacteria*, *Betaproteobacteria* classes, respectively. Multiple studies have highlighted the presence of *Gammaproteobacteria* in marine invertebrates, such as sponges (Menezes et al., 2010; Giles et al., 2013; Graça et al., 2015; Rodríguez-Marconi et al., 2015), corals (Sun et al., 2014), and oysters (Garnier et al., 2007). In this study, *Gammaproteobacteria* accounted for 15.82% of the total bacterial community, including mainly isolates belonging to genus *Nitrosococcus*. Different species of the genus *Nitrosococcus* are well known as ammonia-oxidizing bacteria (AOB), inducing the process of nitrification in different sponges and removing the ammonia excreted by the sponge host (Hentschel et al., 2006; Gao et al., 2017). The combined action between AOB and nitrite-oxidizing bacteria (NOB), such as members of the phylum Nitrospirae might then be responsible for the conversion of ammonia to nitrate in sponges (Bayer et al., 2007; Han et al., 2013). In the present study, nitrite-oxidizing phylum Nitrospirae (0.19%) was identified as one of the minor phyla in the Persian Gulf sponges. Our study is in accordance to other pyrosequencing studies in which Nitrospirae constituted a small portion of reads, accounted for 0.01–3% among several sponge species (Webster et al., 2010; Lee et al., 2011; Bayer et al., 2014; Gaikwad et al., 2016).

Chloroflexi was ranked as the third most abundant group (8.67%) using our sequencing approach. In this study, sponge 04 (*Chondrilla* sp.) harbored the largest proportion of Chloroflexi in comparison to other sponges. The presence of this phylum was previously reported in the Mediterranean sponge *Chondrilla nucula* using a clone library of *16S rRNA* gene sequences (Thiel et al., 2007). The Chloroflexi is one of the most common and diverse bacterial phyla associated with a wide range of sponges, with many sponge-specific lineages detected (Schmitt et al., 2011; Hardoim et al., 2012; Jeong et al., 2013; Gao et al., 2017). Different studies have revealed the important role of Chloroflexi in nutrition, defense (Hardoim et al., 2012) and carbon fixation through photosynthesis in marine sponges (Brück et al., 2010), indicating its autotrophic lifestyle. In the present study, the Chloroflexi OTUs were closer to the autotrophic lineages.

Actinobacteria was another phylum inhabiting the Persian Gulf sponges. This phylum has been widely reported in marine sponges (Schmitt et al., 2012; Giles et al., 2013; Bayer et al., 2014; Cuvelier et al., 2014; Naim et al., 2014). Different studies have been considered Actinobacteria as an important source of bioactive natural products (Izumikawa et al., 2010; Pimentel-Elardo et al., 2010; Abdelmohsen et al., 2012), protecting the sponge hosts against pathogens (O'Connor-Sánchez et al., 2014). There is a possibility that this phylum may provide new opportunities for novel marine drug discovery.

The candidate division TM7, also known as phylum candidatus Saccharibacteria, is a highly ubiquitous and uncultured phylum of bacteria, described through environmental *16S rRNA* gene sequence and genome data only (Ferrari et al., 2014). The existence of this phylum has widely been reported from different sponges (Webster et al., 2010; Lee et al., 2011; Schmitt et al., 2012; Gao et al., 2014a; Montalvo et al., 2014; Alex and Antunes, 2015; Gaikwad et al., 2016). In the present study, TM7 was found at very low abundance in some sponge species. It highlights the importance of deep sequencing technology for detection of the sponge-associated uncultivated bacteria and rare microbial groups in sponges. Otherwise, they might have been not discovered by other routine molecular methods (Lee et al., 2011). However, because of the lack of cultivated representatives and minimal genomic sampling knowledge on the metabolism and biological activities of this enigmatic group has been remained unclear (Ferrari et al., 2014).

The candidate phylum Poribacteria is a sponge-specific phylum that has been widely detected and described in a variety of sponge species (Lafi et al., 2009; Cleary et al., 2013). This candidate phylum has typically been reported in high microbial abundance (HMA) sponge microbiomes (Hochmuth et al., 2010) and considered as "indicator species" for these group of sponges (Bayer et al., 2014). However, unexpectedly, no Poribacteria was found in sponges of the present study.

One reason for the lack of Poribacteria in the Persian Gulf sponges could be related to the use of different primers and bioinformatics pipelines (Souza et al., 2017). Also, some studies have shown that Poribacteria has not been associated with the orders such as *Halichondrida*, *Dictyoceratida*, and *Haplosclerida* (Lafi et al., 2009; Jeong et al., 2013). Noteworthy, these orders have been among the six orders found in this study. In addition, in contrast to other studies conducted on sponges (Kennedy et al., 2008; Montalvo et al., 2014; Alex and Antunes, 2015), the Verrucomicrobia and Spirochaetes phyla were not observed in the bacterial community of the Persian Gulf sponges.

Our study showed that more than 90% of the microbial groups observed in the Persian Gulf sponges were also represented in other studies conducted on the seawater samples (Lee et al., 2011; Schmitt et al., 2011; Gao et al., 2014a; Alex and Antunes, 2015). Nitrospirae, Tenericutes, Armatimonadetes, and the two candidate phyla BD1-5 and TM6 were the only bacterial communities reported exclusively in association with the marine sponges.

Our results showed that the representative OTUs sequences were related to sequences mainly from marine environments such as seawater and marine sediments. Interestingly, sponges had a very low proportion of the isolation source in the closest relative bacteria. Also, some sequences were related to other marine invertebrates such as abalone, octocoral, sea cucumber, oyster, ascidian, starfish, etc. This finding supports the hypothesis of possible environmental acquisition and/or horizontal transmission of bacteria (Moitinho-Silva et al., 2014; Alex and Antunes, 2015). It seems that innate immune system in sponges is responsible for differentiation between symbionts and food microbes (Müller and Müller, 2003). As a result, some overlap between the bacteria in the surrounding seawater and marine sponges would occur. A further deep-sequencing approach is needed to improve our knowledge about the nature of the bacterial specificity among the marine sponges (Alex and Antunes, 2015).

CONCLUSION

In this study, evaluation of 16S rRNA gene amplicon tag pyrosequencing data showed a complex structure of the previously uncharacterized bacterial communities associated with the Persian Gulf sponges (class *Demospongiae*). OTU-based description of the bacterial communities exhibited altogether 17 different bacterial phyla, containing 14 formally described phyla and three candidate phyla. The dominance of Cyanobacteria may suggest an ecological importance of this phylum in the Persian Gulf sponges. More specifically, most of the bacterial symbionts were previously described as significant participants in the carbon, nitrogen cycle, and chemical defense of the studied sponges. Sponge S11 was highly diverse in comparison to other studied sponges and contained more rare bacteria. More research is needed to fully understand the composition of the Persian Gulf sponge-associated prokaryotic communities, specifically the functionality of these specific microbiomes as an important part of the marine ecosystem.

AUTHOR CONTRIBUTIONS

IN and AN designed the research. AN and MM performed the experiments. AN analyzed the data. AN and IN wrote the manuscript with contributions from all authors.

ACKNOWLEDGMENTS

This work was partly supported by the Persian Gulf Marine Biotechnology Research Center, Bushehr University of Medical Sciences under grant number 1667 and the Iran National Science Foundation (Research Chair Award No. 95/INSF/44913). The authors are grateful to Dr. Yusheng Huang for morphological identification of the sponge samples and also, Dr. Stephen A. Jackson for advice and critical reading of the manuscript.

SUPPLEMENTARY MATERIAL

The Supplementary Material for this article can be found online at: https://www.frontiersin.org/articles/10.3389/fmicb.2018.01500/full#supplementary-material

REFERENCES

Abdelmohsen, U. R., Szesny, M., Othman, E. M., Schirmeister, T., Grond, S., Stopper, H., et al. (2012). Antioxidant and anti-protease activities of diazepinomicin from the sponge-associated Micromonospora strain RV115. *Mar. Drugs* 10, 2208–2221. doi: 10.3390/md10102208

Alex, A., and Antunes, A. (2015). Pyrosequencing characterization of the microbiota from Atlantic intertidal marine sponges reveals high microbial diversity and the lack of co-occurrence patterns. *PLoS ONE* 10:e0127455. doi: 10.1371/journal.pone.0127455

Alex, A., Vasconcelos, V., Tamagnini, P., Santos, A., and Antunes, A. (2012). Unusual symbiotic Cyanobacteria association in the genetically diverse intertidal marine sponge *Hymeniacidon perlevis* (Demospongiae, Halichondrida). *PLoS ONE* 7:e51834. doi: 10.1371/journal.pone.0051834

Bayer, K., Kamke, J., and Hentschel, U. (2014). Quantification of bacterial and archaeal symbionts in high and low microbial abundance sponges using real-time PCR. *FEMS Microbiol. Ecol.* 89, 679–690. doi: 10.1111/1574-6941.12369

Bayer, K., Schmitt, S., and Hentsche, U. (2007). "Microbial nitrification in Mediterranean sponges: possible involvement of ammonia-oxidizing Betaproteobacteria," in *Porifera Research: Biodiversity, Innovation and Sustainability*, eds M. C. Custo dio, G. Lobo- Hajdu, E. Hajdu, and G. Muricy

(Rio de Janeiro: Série Livros, Museu Naciona; Universidade Federal do Rio de Janeiro), 165–171.

Becking, L. E., Erpenbeck, D., Peijnenburg, K. T. C. A., and de Voogd, N. J. (2013). Phylogeography of the sponge *Suberites diversicolor* in Indonesia: insights into the evolution of marine lake populations. *PLoS ONE* 8:e75996. doi: 10.1371/journal.pone.0075996

Brück, W. M., Brück, T. B., Self, W. T., Reed, J. K., Nitecki, S. S., and McCarthy, P. J. (2010). Comparison of the anaerobic microbiota of deep-water *Geodia* spp. and sandy sediments in the Straits of Florida. *ISME J.* 4, 686–699. doi: 10.1038/ismej.2009.149

Burgsdorf, I., Slaby, B. M., Handley, K. M., Haber, M., Blom, J., Marshall, C. W., et al. (2015). Lifestyle evolution in cyanobacterial symbionts of sponges. *MBio* 6:e00391-15. doi: 10.1128/mBio.00391-15

Caporaso, J. G., Kuczynski, J., Stombaugh, J., Bittinger, K., Bushman, F. D., Costello, E. K., et al. (2010). QIIME allows analysis of high-throughput community sequencing data. *Nat. Methods*. 7, 335–336. doi: 10.1038/nmeth.f.303

Cleary, D. F., Becking, L. E., de Voogd, N. J., Pires, A. C., Polónia, A. R., Egas, C., et al. (2013). Habitat- and host-related variation in sponge bacterial symbiont communities in Indonesian waters. *FEMS Microbiol. Ecol.* 85, 465–482. doi: 10.1111/1574-6941.12135

Cuvelier, M. L., Blake, E., Mulheron, R., McCarthy, P. J., Blackwelder, P., Thurber, R. L., et al. (2014). Two distinct microbial communities revealed in the sponge Cinachyrella. *Front. Microbiol*. 5:581. doi: 10.3389/fmicb.2014.00581

Edgar, R. C. (2010). Search and clustering orders of magnitude faster than BLAST. *Bioinformatics* 26, 2460–2461. doi: 10.1093/bioinformatics/btq461

Ernst, A., Becker, S., Wollenzien, U. I., and Postius, C. (2003). Ecosystem-dependent adaptive radiations of picocyanobacteria inferred from 16S rRNA and ITS-1 sequence analysis. *Microbiology* 149, 217–228. doi: 10.1099/mic.0.25475-0

Fan, L., Reynolds, D., Liu, M., Stark, M., Kjelleberg, S., Webster, N. S., et al. (2012). Functional equivalence and evolutionary convergence in complex communities of microbial sponge symbionts. *Proc. Natl. Acad. Sci. U.S.A*. 109, E1878–E1887. doi: 10.1073/pnas.1203287109

Ferrari, B., Winsley, T., Ji, M., and Neilan, B. (2014). Insights into the distribution and abundance of the ubiquitous Candidatus Saccharibacteria phylum following tag pyrosequencing. *Sci. Rep*. 4:3957. doi: 10.1038/srep03957

Flombaum, P., Gallegos, J. L., Gordillo, R. A., Rincón, J., Zabala, L. L., Jiao, N., et al. (2013). Present and future global distributions of the marine *Cyanobacteria Prochlorococcus* and *Synechococcus*. *Proc. Natl. Acad. Sci. U.S.A*. 110, 9824–9829. doi: 10.1073/pnas.1307701110

Gaikwad, S., Shouche, Y. S., and Gade, W. N. (2016). Microbial community structure of two freshwater sponges using Illumina MiSeq sequencing revealed high microbial diversity. *AMB Express* 6:40. doi: 10.1186/s13568-016-0211-2

Gao, Z. M., Wang, Y., Lee, O. O., Tian, R. M., Wong, Y. H., Bougouffa, S., et al. (2014a). Pyrosequencing reveals the microbial communities in the Red Sea sponge *Carteriospongia foliascens* and their impressive shifts in abnormal tissues. *Microb. Ecol.* 68, 621–632. doi: 10.1007/s00248-014-0419-0

Gao, Z. M., Wang, Y., Tian, R. M., Wong, Y. H., Batang, Z. B., Al-Suwailem, A. M., et al. (2014b). Symbiotic adaptation drives genome streamlining of the cyanobacterial sponge symbiont "Candidatus Synechococcus spongiarum". *MBio* 5, e00079–e00014. doi: 10.1128/mBio.00079-14

Gao, Z. M., Zhou, G. W., Huang, H., and Wang, Y. (2017). The cyanobacteria-dominated sponge *Dactylospongia elegans* in the South China Sea: prokaryotic community and metagenomic insights. *Front. Microbiol.* 8:1387. doi: 10.3389/fmicb.2017.01387

Garnier, M., Labreuche, Y., Garcia, C., Robert, M., and Nicolas, J. L. (2007). Evidence for the involvement of pathogenic bacteria in summer mortalities of the Pacific oyster *Crassostrea gigas*. *Microb. Ecol*. 53, 187–196. doi: 10.1007/s00248-006-9061-9

Giles, E. C., Kamke, J., Moitinho-Silva, L., Taylor, M. W., Hentschel, U., Ravasi, T., et al. (2013). Bacterial community profiles in low microbial abundance sponges. *FEMS Microbiol. Ecol*. 83, 232–241. doi: 10.1111/j.1574-6941.2012.01467.x

Graça, A. P., Viana, F., Bondoso, J., Correia, M. I., Gomes, L., Humanes, M., et al. (2015). The antimicrobial activity of heterotrophic bacteria isolated from the marine sponge *Erylus deficiens* (Astrophorida, Geodiidae). *Front. Microbiol*. 6:389. doi: 10.3389/fmicb.2015.00389

Hadas, E., Shpigel, M., and Ilan, M. (2009). Particulate organic matter as a food source for a coral reef sponge. *J. Exp. Biol.* 212, 3643–3650. doi: 10.1242/jeb.027953

Han, M., Li, Z., and Zhang, F. (2013). The ammonia oxidizing and denitrifying prokaryotes associated with sponges from different sea areas. *Microb. Ecol.* 66, 427–436. doi: 10.1007/s00248-013-0197-0

Hardoim, C. C., Esteves, A. I., Pires, F. R., Gonçalves, J. M., Cox, C. J., Xavier, J. R., et al. (2012). Phylogenetically and spatially close marine sponges harbour divergent bacterial communities. *PLoS ONE* 7:e53029. doi: 10.1371/journal.pone.0053029

Hentschel, U., Usher, K. M., and Taylor, M. W. (2006). Marine sponges as microbial fermenters. *FEMS Microbiol. Ecol.* 55, 167–177. doi: 10.1111/j.1574-6941.2005.00046.x

Hochmuth, T., Niederkrüger, H., Gernert, C., Siegl, A., Taudien, S., Platzer, M., et al. (2010). Linking chemical and microbial diversity in marine sponges: possible role for poribacteria as producers of methyl-branched fatty acids. *Chembiochem* 11, 2572–2578. doi: 10.1002/cbic.201000510

Izumikawa, M., Khan, S. T., Takagi, M., and Shin-ya, K. (2010). Sponge-derived streptomyces producing isoprenoids via the mevalonate pathway. *J. Nat. Prod*. 73, 208–212. doi: 10.1021/np900747t

Jackson, S. A., Kennedy, J., Morrissey, J. P., O'Gara, F., and Dobson, A. D. (2012). Pyrosequencing reveals diverse and distinct sponge-specific microbial communities in sponges from a single geographical location in Irish waters. *Microb. Ecol*. 64, 105–116. doi: 10.1007/s00248-011-0002-x

Jasmin, C., Anas, A., and Nair, S. (2015). Bacterial diversity associated with *Cinachyra cavernosa* and *Haliclona pigmentifera*, cohabiting sponges in the coral reef ecosystem of Gulf of Mannar, Southeast coast of India. *PLoS ONE* 10:e0123222. doi: 10.1371/journal.pone.0123222

Jeong, I. H., Kim, K. H., and Park, J. S. (2013). Analysis of bacterial diversity in sponges collected off Chujado, an Island in Korea, using barcoded 454 pyrosequencing: analysis of a distinctive sponge group containing Chloroflexi. *J. Microbiol.* 51, 570–577. doi: 10.1007/s12275-013-3426-9

Jeong, I. H., Kim, K. H., Lee, H. S., and Park, J. S. (2014). Analysis of bacterial diversity in sponges collected from Chuuk and Kosrae Islands in Micronesia. *J. Microbiol*. 52, 20–26. doi: 10.1007/s12275-014-3619-x

Jeong, J. B., Kim, K. H., and Park, J. S. (2015). Sponge-specific unknown bacterial groups detected in marine sponges collected from Korea through barcoded pyrosequencing. *J. Microbiol. Biotechnol.* 25, 1–10. doi: 10.4014/jmb.1406.06041

Kennedy, J., Codling, C. E., Jones, B. V., Dobson, A. D., and Marchesi, J. R. (2008). Diversity of microbes associated with the marine sponge, *Haliclona simulans*, isolated from Irish waters and identification of polyketide synthase genes from the sponge metagenome. *Environ. Microbiol.* 10, 1888–1902. doi: 10.1111/j.1462-2920.2008.01614.x

Kumar, S., Stecher, G., and Tamura, K. (2016). MEGA7: molecular evolutionary genetics analysis version 7.0 for bigger datasets. *Mol. Biol. Evol.* 33, 1870–1874. doi: 10.1093/molbev/msw054

Lafi, F. F., Fuerst, J. A., Fieseler, L., Engels, C., Goh, W. W., and Hentschel, U. (2009). Widespread distribution of poribacteria in demospongiae. *Appl. Environ. Microbiol*. 75, 5695–5699. doi: 10.1128/AEM.00035-09

Lee, O. O., Wang, Y., Yang, J., Lafi, F. F., Al-Suwailem, A., and Qian, P. Y. (2011). Pyrosequencing reveals highly diverse and species-specific microbial communities in sponges from the Red Sea. *Int. Soc. Microb. Ecol. J*. 5, 650–664. doi: 10.1038/ismej.2010.165

Lemloh, M. L., Fromont, J., Brümmer, F., and Usher, K. M. (2009). Diversity and abundance of photosynthetic sponges in temperate Western Australia. *BMC Ecol*. 9:4. doi: 10.1186/1472-6785-9-4

Li, Z. Y., He, L. M., Wu, J., and Jiang, Q. (2006). Bacterial community diversity associated with four marine sponges from the South China Sea based on 16S rDNA-DGGE fingerprinting. *J. Exp. Mar. Biol. Ecol*. 329, 75–85. doi: 10.1016/j.jembe.2005.08.014

Maldonado, M., Cortadellas, N., Trillas, M. I., and Rützler, K. (2005). Endosymbiotic yeast maternally transmitted in a marine sponge. *Biol. Bull*. 209, 94–106. doi: 10.2307/3593127

Mehbub, M. F., Perkins, M. V., Zhang, W., and Franco, C. M. M. (2016). New marine natural products from sponges (Porifera) of the order Dictyoceratida (2001 to 2012); a promising source for drug discovery, exploration and future prospects. *Biotechnol. Adv*. 34, 473–491. doi: 10.1016/j.biotechadv.2015.12.008

Mehbub, M., Lei, J., Franco, C., and Zhang, W. (2014). Marine sponge derived natural products between 2001 and 2010: trends and opportunities for discovery of bioactives. *Mar. Drugs* 12, 4539–4577. doi: 10.3390/md12084539

Menezes, C. B., Bonugli-Santos, R. C., Miqueletto, P. B., Passarini, M. R., Silva, C. H., Justo, M. R., et al. (2010). Microbial diversity associated with algae, ascidians and sponges from the north coast of São Paulo state, Brazil. *Microbiol. Res*. 165, 466–482. doi: 10.1016/j.micres.2009.09.005

Moitinho-Silva, L., Bayer, K., Cannistraci, C. V., Giles, E. C., Ryu, T., Seridi, L., et al. (2014). Specificity and transcriptional activity of microbiota associated with low and high microbial abundance sponges from the Red Sea. *Mol. Ecol*. 23, 1348–1363. doi: 10.1111/mec.12365

Montalvo, N. F., Davis, J., Vicente, J., Pittiglio, R., Ravel, J., and Hill, R. T. (2014). Integration of culture-based and molecular analysis of a complex sponge-associated bacterial community. *PLoS ONE* 9:e90517. doi: 10.1371/journal.pone.0090517

Müller, W. E., and Müller, I. M. (2003). Origin of the metazoan immune system: identification of the molecules and their functions in sponges. *Integr. Comp. Biol.* 43, 281–292. doi: 10.1093/icb/43.2.281

Naim, M. A., Morillo, J. A., Sørensen, S. J., Waleed, A. A., Smidt, H., and Sipkema, D. (2014). Host-specific microbial communities in three sympatric North Sea sponges. *FEMS Microbiol. Ecol*. 90, 390–403. doi: 10.1111/1574-6941.12400

Najafi, A. (2012). Book review: medicinal sponges of the Persian Gulf. *Iran South Med. J.* 15, 81–83. [In Persian] Available online at: http://ismj.bpums.ac.ir/article-1-316-en.html

Nam, Y. D., Jung, M. J., Roh, S. W., Kim, M. S., and Bae, J. W. (2011). Comparative analysis of Korean human gut microbiota by barcoded pyrosequencing. *PLoS ONE* 6:e22109. doi: 10.1371/journal.pone.0022109

O'Connor-Sánchez, A., Rivera-Domínguez, A. J., Santos-Briones, C. L., López-Aguiar, L. K., Peña-Ramírez, Y. J., and Prieto-Davo, A. (2014). Acidobacteria appear to dominate the microbiome of two sympatric Caribbean Sponges and one Zoanthid. *Biol. Res*. 47:67. doi: 10.1186/0717-6287-47-67

Pile, A. J., Patterson, M. R., and Witman, J. D. (1996). *In situ* grazing on plankton <10 lm by the boreal sponge Mycale lingua. *Mar. Ecol. Prog. Ser.* 141, 95–102.

Pimentel-Elardo, S. M., Kozytska, S., Bugni, T. S., Ireland, C. M., Moll, H., and Hentschel, U. (2010). Anti-parasitic compounds from *Streptomyces* sp. strains isolated from Mediterranean sponges. *Mar. Drugs* 8, 373–380. doi: 10.3390/md8020373

Regueiras, A., Alex, A., Pereira, S., Costa, M. S., Antunes, A., and Vasconcelos, V. (2017). Cyanobacterial diversity in the marine sponge *Hymeniacidon perlevis* from a temperate region (Portuguese coast, Northeast Atlantic). *Aquat. Microb. Ecol*. 79, 259–272. doi: 10.3354/ame01830

Rodríguez-Marconi, S., De la Iglesia, R., Díez, B., Fonseca, C. A., Hajdu, E., and Trefault, N. (2015). Characterization of bacterial, archaeal and eukaryote symbionts from Antarctic sponges reveals a high diversity at a three-domain level and a particular signature for this ecosystem. *PLoS ONE* 10:e0138837. doi: 10.1371/journal.pone.0138837

Rua, C. P., Gregoracci, G. B., Santos, E. O., Soares, A. C., Francini-Filho, R. B., and Thompson, F. (2015). Potential metabolic strategies of widely distributed holobionts in the oceanic archipelago of St Peter and St Paul (Brazil). *FEMS Microbiol. Ecol*. 91:fiv043. doi: 10.1093/femsec/fiv043

Schmitt, S., Deines, P., Behnam, F., Wagner, M., and Taylor, M. W. (2011). Chloroflexi bacteria are more diverse, abundant, and similar in high than in low microbial abundance sponges. *FEMS Microbiol. Ecol*. 78, 497–510. doi: 10.1111/j.1574-6941.2011.01179.x

Schmitt, S., Tsai, P., Bell, J., Fromont, J., Ilan, M., Lindquist, N., et al. (2012). Assessing the complex sponge microbiota: core, variable and species-specific bacterial communities in marine sponges. *ISME J*. 6, 564–576. doi: 10.1038/ismej.2011.116

Souza, D. T., Genuário, D. B., Silva, F. S., Pansa, C. C., Kavamura, V. N., Moraes, F. C., et al. (2017). Analysis of bacterial composition in marine sponges reveals the influence of host phylogeny and environment. *FEMS Microbiol. Ecol.* 93: fiw204. doi: 10.1093/femsec/fiw204

Sun, W., Zhang, F., He, L., and Li, Z. (2014). Pyrosequencing reveals diverse microbial community associated with the zoanthid *Palythoa australiae* from the South China Sea. *Microb. Ecol*. 67, 942–950. doi: 10.1007/s00248-014-0395-4

Tamura, K., and Nei, M. (1993). Estimation of the number of nucleotide substitutions in the control region of mitochondrial DNA in humans and chimpanzees. *Mol. Biol. Evol*. 10, 512–526.

Taylor, M. W., Radax, R., Steger, D., and Wagner, M. (2007). Sponge-associated microorganisms: evolution, ecology, and biotechnological potential. *Microbiol. Mol. Biol. R.* 71, 295–347. doi: 10.1128/MMBR.00040-06

Thacker, R. W., and Freeman, C. J. (2012). Sponge-microbe symbioses: recent advances and new directions. *Adv. Mar. Biol*. 62, 57–111. doi: 10.1016/B978-0-12-394283-8.00002-3

Thakur, A. N., Thakur, N. L., Indap, M. M., Pandit, R. A., Datar, V. V., and Müller, W. E. (2005). Antiangiogenic, antimicrobial, and cytotoxic potential of sponge-associated bacteria. *Mar. Biotechnol*. 7, 245–252. doi: 10.1007/s10126-004-4085-y

Thiel, V., Leininger, S., Schmaljohann, R., Brümmer, F., and Imhoff, J. F. (2007). Sponge-specific bacterial associations of the Mediterranean sponge *Chondrilla nucula* (Demospongiae, Tetractinomorpha). *Microb. Ecol*. 54, 101–111. doi: 10.1007/s00248-006-9177-y

Thomas, T., Moitinho-Silva, L., Lurgi, M., Björk, J. R., Easson, C., Astudillo-García, C., et al. (2016). Diversity, structure and convergent evolution of the global sponge microbiome. *Nat. Commun*. 7:11870. doi: 10.1038/ncomms11870

Verhoeven, J. T., Kavanagh, A. N., and Dufour, S. C. (2017). Microbiome analysis shows enrichment for specific bacteria in separate anatomical regions of the deep-sea carnivorous sponge *Chondrocladia grandis*. *FEMS Microbiol. Ecol*. 93:fiw214. doi: 10.1093/femsec/fiw214

Webster, N. S., and Thomas, T. (2016). The sponge hologenome. *MBio* 7:e00135–16. doi: 10.1128/mBio.00135-16

Webster, N. S., Taylor, M. W., Behnam, F., Lücker, S., Rattei, T., Whalan, S., et al. (2010). Deep sequencing reveals exceptional diversity and modes of transmission for bacterial sponge symbionts. *Environ. Microbiol.* 12, 2070–2082. doi: 10.1111/j.1462-2920.2009.02065.x

White, J. R., Patel, J., Ottesen, A., Arce, G., Blackwelder, P., and Lopez, J. V. (2012). Pyrosequencing of bacterial symbionts within *Axinella corrugata* sponges: diversity and seasonal variability. *PLoS ONE* 7:e38204. doi: 10.1371/journal.pone.0038204

Zhang, F., Pita, L., Erwin, P. M., Abaid, S., López-Legentil, S., and Hill, R. T. (2014). Symbiotic archaea in marine sponges show stability and host specificity in community structure and ammonia oxidation functionality. *FEMS Microbiol. Ecol.* 90, 699–707. doi: 10.1111/1574-6941.12427

Zhang, H., Lee, Y. W., Zhang, W., and Lee, H. K. (2006). Culturable actinobacteria from the marine sponge *Hymeniacidon perleve*: isolation and phylogenetic diversity by *16S rRNA* gene-RFLP analysis. *Antonie Van Leeuwenhoek* 90, 159–169. doi: 10.1007/s10482-006-9070-1

Conflict of Interest Statement: The authors declare that the research was conducted in the absence of any commercial or financial relationships that could be construed as a potential conflict of interest.

Copyright © 2018 Najafi, Moradinasab and Nabipour. This is an open-access article distributed under the terms of the Creative Commons Attribution License (CC BY). The use, distribution or reproduction in other forums is permitted, provided the original author(s) and the copyright owner(s) are credited and that the original publication in this journal is cited, in accordance with accepted academic practice. No use, distribution or reproduction is permitted which does not comply with these terms.

frontiers in Microbiology

ORIGINAL RESEARCH
published: 18 July 2018
doi: 10.3389/fmicb.2018.01587

Streptomyces nigra sp. nov. Is a Novel Actinobacterium Isolated From Mangrove Soil and Exerts a Potent Antitumor Activity *in Vitro*

Can Chen[1], Yanghui Ye[1], Ruijun Wang[1], Yinglao Zhang[2], Chen Wu[3], Sanjit C. Debnath[1], Zhongjun Ma[1], Jidong Wang[4] and Min Wu[1]**

[1] *Laboratory of Marine Microbial Resources Utilization, Ocean College, Institute of Marine Biology, Zhejiang University, Hangzhou, China,* [2] *Biomedical Research Program, School of Life Sciences, Anhui Agricultural University, Hefei, China,* [3] *Institute of Hydraulic and Marine Engineering, School of Hydraulic and Environmental Engineering, Zhejiang University of Water Resources and Electric Power, Hangzhou, China,* [4] *Department of New Drug Screening, Zhejiang Hisun Pharmaceutical Co., Ltd., Taizhou, China*

OPEN ACCESS

Edited by:
Alejandro A. Murillo, EMBL Heidelberg, Germany

Reviewed by:
Joachim Wink, Helmholtz-Zentrum für Infektionsforschung, Germany
Polpass Arul Jose, Hebrew University of Jerusalem, Israel

***Correspondence:**
Jidong Wang
jdwang@hisunpharm.com
Min Wu
wumin@zju.edu.cn

Specialty section:
This article was submitted to Aquatic Microbiology, a section of the journal Frontiers in Microbiology

Received: *07 December 2017*
Accepted: *26 June 2018*
Published: *18 July 2018*

Citation:
Chen C, Ye Y, Wang R, Zhang Y, Wu C, Debnath SC, Ma Z, Wang J and Wu M (2018) Streptomyces nigra sp. nov. Is a Novel Actinobacterium Isolated From Mangrove Soil and Exerts a Potent Antitumor Activity in Vitro. Front. Microbiol. 9:1587. doi: 10.3389/fmicb.2018.01587

A new bacterial strain, designated 452^T, was isolated from the rhizosphere soil of the mangrove *Avicennia marina* in China. As determined, its cell wall peptidoglycan contained LL-diaminopimelic acid; MK-9(H8) and MK-9(H6) were the major isoprenoid quinones; and iso-$C_{16:0}$ (31.3%), anteiso-$C_{15:0}$ (16.9%), and iso-$C_{15:0}$ (12.5%) were the major cellular fatty acids (>10.0%). Phylogenetic analysis based on the 16S rRNA gene sequence revealed that strain 452^T formed a distinct lineage in the clade of the genus *Streptomyces*, and was closely related to *S. coerulescens* DSM 40146^T (99.6% sequence identity), *S. bellus* DSM 40185^T (99.5%), and *S. coeruleorubidus* DSM 41172^T (99.3%). The DNA-DNA relatedness between strain 452^T and these type strains ranged between 29.3 and 42.3%. Based on the phenotypic, chemotaxonomic, and phylogenetic features, the strain 452^T is considered to represent a novel species of the genus *Streptomyces*, for which the name *Streptomyces nigra* sp. nov. is proposed. The type strain is 452^T (=KCTC 39960^T = MCCC 1K03346^T). Further, strain 452^T extracts exhibited a pronounced antitumor activity against human cancer cell lines A549, HCT-116, and HepG2, but not against normal human colon cells CCD-18Co. Active substances in the fermentation broth of strain 452^T were isolated by bioassay-guided analysis, and then purified using a macroporous resin, silica gel, sephadex LX-20 column, and semi-preparative high-performance liquid chromatography (HPLC). Eight proline-containing diketopiperazines, namely, cyclo(Pro-Ala), cyclo(Pro-Gly), cyclo(Pro-Phe), cyclo(Pro-Met), cyclo(Pro-Val), cyclo(Pro-Leu), cyclo(Pro-Tyr), and cyclo(L-Leu-trans-4-hydroxy-L-Pro), were identified by electrospray ionization mass spectrometry (MS) and nuclear magnetic resonance (NMR). The compounds displayed different levels of cytotoxicity. The highest cytotoxicity was exhibited by cyclo(Pro-Ala) and cyclo(Pro-Met) against A549 cells, and cyclo(Phe-Pro) and cyclo(Pro-Ala) against HCT-116 cells, with average IC_{50} values equal to 18.5, 27.3, 32.3, and 47.6 μg/mL, respectively. The diversity of diketopiperazines and other chemicals produced by 452^T

was further investigated using gas chromatography (GC)-MS and liquid chromatography (LC)-MS. The analysis revealed 16 types of metabolites with antitumor activity and 16 other types of diketopiperazines. Hence, extracts of the newly identified strain may be used a starting material for the development of antitumor agents.

Keywords: *Streptomyces nigra* sp. nov., polyphasic taxonomy, antitumor, bioactive metabolites, diketopiperazine

INTRODUCTION

The genus *Streptomyces* contains over 770 species with valid published names at the time of writing[1]. Numerous species from this genus produce antibiotics and several other biologically important compounds, including herbicides, antiparasitic agents, immunosuppressants, and other compounds of industrial interest (Běhal, 2000; Chater, 2006; Bull and Stach, 2007; Schinke et al., 2017; Ser et al., 2017). *Streptomyces* are widely distributed in terrestrial ecosystems, especially in the soil. Specific marine environments are pronouncedly different from the terrene environments, and stimulate the production of novel metabolites by marine microorganisms and the evolution of countless new microbes (Simister et al., 2016; Dudek et al., 2017; Kamjam et al., 2017; Petro et al., 2017; Picard, 2017). Marine environments are considered to be a potential source for the discovery of novel *Streptomyces* that produce bioactive compounds (Sunagawa et al., 2015; Christensen and Martin, 2017; Wei et al., 2018). In recent years, over 20 novel species of the genus *Streptomyces* have been identified in marine and mangrove environments[2]. The mangrove occupies millions of hectares of coastal areas; it is one of the most dynamic environments in the world, and the habitat of various flora and fauna of terrestrial, freshwater, and marine species (Law et al., 2017). Recently, utilization of the mangrove microorganism resource has received a lot of attention, subsequently leading to the discovery of novel *Streptomyces* species (Hong et al., 2009; Lee et al., 2014).

The genus *Streptomyces* is an important biological resource for the exploration and discovery of antitumor substances. Anthracycline-based drugs, e.g., erythromycin, doxorubicin, and epirubicin, are widely used in the clinic to treat various types of cancer, including breast cancer, small cell lung cancer, cervical cancer, and head and neck cancer. These drugs are produced by *S. peucetius* and *S. nogalater* (Nobili et al., 2009; Zhang Z.G. et al., 2015; Lu et al., 2017). The polypeptide metabolite dactinomycin is an antibiotic with antibacterial and antifungal activity. Its antitumor activity was confirmed by Juliano and Stamp (1978). Similarly, bleomycin, a natural hybrid peptide-polyketide metabolite and an antitumor drug, is produced by *S. plicatus*, *S. chrysomallus*, and *S. verticillus* (Katz et al., 1961; Juliano and Stamp, 1978; Du et al., 2000; Lam et al., 2002; Cai et al., 2016; Lee J.H. et al., 2016). Mithramycin is an aromatic polyketide that contains two deoxysugar chains (a disaccharide of two D-olivoses, and a trisaccharide consisting of D-olivose), a D-oliose, and a D-mycarose, which inhibits testicular cancer and is produced by *S. argillaceus* (Fernandez et al., 1998; Bilyk and Luzhetskyy, 2016; Novakova et al., 2018). *Streptomyces* also produce 2,5-diketopiperazines (also known as 2,5-dioxopiperazines or cyclic dipeptides), a class of organic molecules, in which the two nitrogen atoms of the 6-membered ring of piperazine form amide linkages (Huang et al., 2014). They are the minimum natural cyclopeptides and possess important biological activities, such as antitumor, antiviral, antifungal, antibacterial, and antihyperglycemic activities (Martins and Carvalho, 2007; Borthwick and Da Costa, 2017). Remarkably, these bacteria also produce mitomycin C and enediyne compounds (including calicheamicins, neocarzinostatin, and lidamycin), which have unique structural characteristics and display pronounced antitumor-activity (Hata et al., 1956; Mao et al., 1999; Liu et al., 2005; Lee, 2009).

In the current study, we isolated a novel member of the genus *Streptomyces* from the rhizosphere soil of the mangrove *Avicennia marina* in China, evaluated its antitumor activity *in vitro*, and characterized the active compounds in its extract.

MATERIALS AND METHODS

Sample Collection and Strain Isolation

Strain 452^T was isolated from a sample of a rhizosphere soil collected during the spring of 2016 in the mangrove *Avicennia marina* forest of Zhangzhou (24°20', 117°45'), Fujian Province (China), and stored at 4°C until use. The soil sample were suspended in sterile water and diluted in a tenfold series. The dilutions were then spread onto modified ZoBell 2216E agar plates and incubated at 28°C for 5 days. After incubation, a brown colony that secreted dark brown pigment was selected and purified by repeated streaking onto marine agar 2216 (MA; Difco). The strain was named 452^T. It was routinely cultured on MA and preserved at −80°C in marine broth 2,216 (MB; Difco) supplemented with 20% (v/v) glycerol.

Genomic and Phylogenetic Analyses

Genomic DNA was extracted for amplification in a polymerase chain reaction as described by Hong et al. (2009). The DNA G + C content was determined by reversed-phase high-performance liquid chromatography (HPLC) (Mesbah et al., 1989) using the genomic DNA of *Escherichia coli* K-12 and salmon sperm DNA (Sigma) as calibration standards. The 16S rRNA gene of strain 452^T was amplified using the universal primers 27F (5'-AGAGTTTGATCMTGGCTCAG-3') and 1492R (5'-TACGGYTACCTTGTTACGACTT-3') (Weisburg et al., 1991). The amplification products were cloned into the pMD19-T vector (TaKaRa) and sequenced. The determined 16S rRNA gene sequence (1,490 bases) was analyzed in pairwise sequence

[1]http://www.bacterio.net/streptomyces.html

[2]http://ijs.microbiologyresearch.org

alignments using the BLASTN program[3] and the EzTaxon-e server[4] (Yoon et al., 2017). Multiple sequence alignments based on the 16S rRNA gene sequences of strain 452^T and related taxa were done as described by Zhang X.Q. et al. (2015) and Zhang Z.G. et al. (2015) using MEGA program version 5 (Tamura et al., 2011). Phylogenetic trees were reconstructed by using the neighbor-joining, maximum-likelihood, and maximum-parsimony methods based on 1,000 replications, and bootstrap analysis was performed.

Genomic DNA extraction for DNA-DNA hybridization of strain 452^T, *S. coerulescens* DSM 40146^T, *S. bellus* DSM 40185^T, and *S. coeruleorubidus* DSM 41172^T (obtained from the DSMZ; unless otherwise stated, all strains were incubated in MA or MB at 28°C) were performed following a protocol of Cashion et al. (1977). DNA-DNA hybridization values of strain 452^T and type strains were determined by using a Beckman DU800 spectrophotometer according to the method of Zhang et al. (2010). The hybridization temperature was set at 57°C. The complete genome of strain 452^T was sequenced and assembled by Beijing Genomics Institute (BGI, Beijing, China), and the genome sequences of reference strains were retrieved from the GenBank database. The average nucleotide identity (ANI) was calculated using the OrthoANIu algorithm of the Chun lab's online Average Nucleotide Identity calculator (Lee I. et al., 2016). *In silico* DNA-DNA hybridization (DDH) values were calculated by genome-to-genome distance calculator (GGDC) (Meier-Kolthoff et al., 2013).

Phenotypic Characterization

Growth of strain 452^T was tested in the presence of various NaCl concentrations (0–15.0%, w/v, at 0.5% increments) in MB (pH 7.0). The growth temperature range was tested at 4, 10, 15, 20, 25, 28, 30, 35, 40, 45, and 50°C in MB (pH 7.0). The growth pH range was determined at 0.5-pH unit intervals by supplementing MB with 30 mM buffering agents at 28°C: 2-(*N*-morpholino)ethanesulfonic acid (pH 5.5–6.4), 3-(*N*-morpholino)propanesulfonic acid (pH 6.5–7.9), tricine (pH 8.0–8.9), and bis-Tris propane (pH 9.0–9.5) (Zhong et al., 2014). The optimal growth was determined after 5 days of incubation, and the growth limits were assessed after 14 days of incubation (Zhang X.Q. et al., 2015). Strain 452^T was incubated at 28°C for 5 days on MA medium, and cell morphology was examined and observed by transmission electron microscopy (80 kV, JEM-1230; Jeol) after uranyl acetate (0.5%, w/v) staining, scanning electron microscope (3.0 kV, SU8010, Hitachi) fixation by osmium tetroxide vapor (4%, w/v), and optical microscopy (BX40; Olympus) after gram staining. The culture characteristics were determined following growth on ISP 2, ISP 3, ISP 4, ISP 5, ISP 6, and ISP 7 agars (Shirling and Gottlieb, 1966); *Streptomyces* agar (Atlas, 2010), starch casein nitrate agar (Ser et al., 2016b), nutrient agar (Odds, 1981), potato-glucose agar (Wang et al., 2017), tryptone soya agar (Williams et al., 1983), and MA 2216 (Difco) for 14 days at 28°C. The colors of substrate, aerial mycelium and any soluble pigments produced were determined by comparison with chips from the ISCC-NBS color charts (Kelly and Judd, 1964).

Degradation of starch; oxidase and catalase activities; hydrolysis of Tweens 20, 40, 60, 80, hypoxanthine, and xanthine; nitrate reduction and urease activity; the ability to hydrolyze casein, chitin, carboxymethyl (CM) cellulose, filter paper, and gelatin; H_2S production; and methyl red and Voges-Proskauer reactions were all evaluated as described previously (Chen et al., 2017). Degradation of tyrosine was determined on MA supplemented with 5 g/L tyrosine. The presence of flexirubin-type pigments was investigated using 20% (w/v) KOH solution. Anaerobic growth was determined in an anaerobic system (AnaeroPack-MicroAero, 2.5-L, MGC, Japan) on MA supplemented with 20 mM sodium thiosulfate, 5 mM sodium sulfite, 20 mM sodium sulfate, 5 mM sodium nitrite, or 20 mM sodium nitrate as electron acceptors (Zhong et al., 2016). Utilization of carbon substrates (0.5%, w/v) was tested according to the protocol of Dong and Cai (2001) using whole components of the inorganic salts of MB with yeast extract (0.01%, w/v) as growth factors. Acid production was evaluated using the marine oxidation-fermentation medium supplemented with 1% (w/v) sugars (Wu et al., 2017). Enzyme activities, and other physiological and biochemical traits were analyzed using API ZYM and API 20NE stripes (bioMérieux) according to the manufacturer's instructions. The three reference strains were used as controls in the above tests.

Chemotaxonomic Characterization

Strain 452^T, *S. coerulescens* DSM 40146^T, *S. bellus* DSM 40185^T, and *S. coeruleorubidus* DSM 41172^T cells were harvested during the third quadrants on MA (28°C, 3 days) for cellular fatty acid analysis. Whole-cell fatty acids were analyzed according to the instructions of the Microbial Identification System (MIDI; Microbial ID) using the standard MIS library generation software version 4.5. Isoprenoid quinones were extracted with a chloroform/methanol mixture (2:1, v/v) from freeze-dried cells (500 mg) and analyzed by LC-MS (Agilent) (Komagata and Suzuki, 1987). Polar lipids were extracted with a chloroform/methanol mixture (1:2, v/v) and identified by two-dimensional thin-layer chromatography on silica gel 60 F_{254} plates (Merck). Molybdophosphoric acid, ninhydrin reagent, molybdenum blue, and α-naphthol/H_2SO_4 reagents were sprayed onto the plates to detect total lipids, lipids containing free aminolipids, phosphorus-containing lipids, and glycolipids, respectively (Tindall, 1990).

Preparation of the 452^T Fermented Broth and Extract

Strain 452^T was inoculated into a 500 mL Erlenmeyer flask containing 200 mL of tryptone soya liquid medium and incubated at 28°C for 7 days on a rotary shaker at 150 rpm, as seed medium prior to the fermentation process. Then, 1% (v/v) of the starting inoculum was transferred into 1-L Erlenmeyer flasks containing 600 mL of MB, and the incubation was continued on a rotary shaker at 180 rpm at 30°C for 10 days. The cell-free supernatant was collected after centrifugation at 13,000 × *g* for

[3]http://www.ncbi.nlm.nih.gov

[4]https://www.ezbiocloud.net

10 min, freeze-dried, and extracted repeatedly with methanol. The organic phase was separated and evaporated to dryness using a rotary evaporator at 40°C (Ahmad et al., 2017). The extracted residues were suspended in dimethyl sulfoxide for bioactivity, gas chromatography-mass spectrometry (GC-MS), and liquid chromatography (LC)-MS assays.

In Vitro Antitumor Cytotoxicity Testing

HCT-116 (human colorectal carcinoma), A549 (human lung carcinoma), SF-268 (human central nervous system cancer), HepG2 (human hepatocellular carcinoma), and CCD-18Co (human normal colon cells) cell lines were obtained from the Department of New Drug Screening, Zhejiang Hisun Pharmaceutical Co., Ltd. (Taizhou, China). U87 (human glioblastoma cell) and MCF-7 (human breast adenocarcinoma cell) cells were provided by the School of Pharmacy of the China Pharmaceutical University (Nanjing, China). All cell lines used in this study were maintained in Dulbecco's modified Eagle's medium supplemented with 10% (w/v) fetal bovine serum in a humidified incubator (5% CO_2 in air at 37°C). The antitumor activity of 452^T extracts with different concentrations (20, 100, or 200 μg/mL) were investigated by the 3-(4,5-dimethylthiazol-2yl)-2,5-diphenyltetrazolium-bromide assay, doxorubicin was tested as positive control, and MB with same preparation method of 452^T extract was tested as negative control. Briefly, confluent cells were harvested and seeded at a density of 6×10^4 cells/well into a sterile flat bottom 96-well plate overnight, the cells were treated with different concentrations of the extracts for 48 h and growth inhibition was measured by determining the optical density at 570 nm, and the assay was performed according to an established method (Skehan et al., 1990). The cell morphology was observed by inverted microscope (Nikon TS100).

GC-MS and LC-MS Analyses

GC-MS analysis was performed using an Agilent 7890 gas chromatograph system coupled with an Agilent 5975C mass spectrometer. The system utilized DB-Wax (30 m × 250 μm inner diameter, 0.25 μm film thickness). For the analysis, a 1 μL aliquot of the analyte was injected in the splitless mode. Helium was used as the carrier gas, the front inlet purge flow was 3 mL/min, and the gas flow rate through the column was 1 mL/min. The initial temperature was kept at 40°C for 5 min, then raised to 250°C at a rate of 5°C/min, and finally maintained at 250°C for 5 min. The energy was -70 eV in the electron impact mode. The MS data were acquired in a full-scan mode over 20–400 m/*z*. The extracted constituents were identified by comparing the MS data with data from the NIST 05 Spectral Library.

LC-MS/MS analyses were performed at the Zhejiang Hisun Pharmaceutical Co., Ltd. The MS spectra were acquired using an LC-MS/MS ion trap time-of-flight (IT-TOF) spectrometer (Shimadzu, Japan) equipped with an electro-spray ionization source (Abe et al., 2005) operated in the positive and negative ion modes. HPLC was performed according to Zhou et al. (2015). Briefly, the sample (2 μL) was injected onto a column (Waters ACQUITY UPLC BEH Amide, 2.1 × 100 mm, 1.7 μm) and resolved at a flow rate of 0.2 mL/min. Mobile phases used were: A (0.1%, v/v, formic acid/water) and B (0.1%, v/v, formic acid/acetonitrile). The separation gradient was as follows: 0–30 min: 10–100% B.

Isolation and Characterization of Bioactive Metabolites

The procedure of cultivation in method 2.5 was repeated, filtrate (15 L) of the culture broth was collected. The filtrate was separated and purified on an HP-20 macroporous resin (Mitsubishi, Japan) column, and eluted with absolute ethyl alcohol. After evaporation of the menstruum *in vacuo*, the residue (5.2 g) was resolved by chromatography on a silica gel column eluted with $CHCl_3$/MeOH mixtures with a growing polarity (100:0–30:70, v/v) to obtain six fractions (F1–6). Bioactivity assays (*in vitro* antitumor toxicity) indicated that F4 ($CHCl_3$/MeOH, 50:50) and F5 ($CHCl_3$/MeOH, 40:60) fractions were cytotoxic *in vitro*. The active fractions (F4 and 5) were repeatedly purified, and separated on Sephadex LH-20 (MeOH) and using semi-preparative HPLC (Agilent 1100, Zorbax SB-C18, 5 μm, 250 × 9.4 mm inner diameter; Agilent, Palo Alto, CA, United States) to obtain compounds **1–8** (5.1–10.7 mg of each).

Structural identification of the bioactive metabolites was based on spectroscopic analysis. ^{1}H nuclear magnetic resonance (NMR) and ^{13}C NMR spectra were acquired with a Bruker DRX-400 spectrometer (400 MHz for ^{1}H and 100 MHz for ^{13}C) (Bruker, Rheinstetten, Germany). Chemical shifts are reported in ppm. (δ), using residual $CHCl_3$ (δ_H 7.26 ppm; δ_C 77.0) as an internal standard, with coupling constants (J) in Hz.^{1}H and ^{13}C NMR assignments were supported by ^{1}H-1H COSY, HMQC, and HMBC experiments. The electrospray ionization MS data were recorded using the Bruker APEX III 7.0T spectrometer.

RESULTS AND DISCUSSION

Genomic and Phylogenetic Analyses

The 16S rRNA gene sequence of strain 452^T comprised 1490 bases. According to the information in the EzTaxon server, it was most closely related to *S. coerulescens* DSM 40146^T (99.6%), and shared 99.6–98.5% sequence similarity with the type strains of other species of the genus *Streptomyces*. The 16S rRNA gene sequences of strain 452^T and the type strains of other genera shared <90% similarity. Phylogenetic trees were reconstructed from 1000 replicates each for bootstrap analysis using the neighbor-joining (**Figure 1**), maximum-parsimony (Supplementary Figure S1), and maximum-likelihood (Supplementary Figure S2) methods. These analyses revealed that strain 452^T belonged to a clade of the genus *Streptomyces* and formed a distinct lineage among the most closely related species: *S. coerulescens* DSM 40146^T (99.6%), *S. bellus* DSM 40185^T (99.5%), and *S. coeruleorubidus* DSM 41172^T (99.3%). Hence, these three type strains were obtained from DSMZ (Germany), and selected as reference strains in the current study, unless otherwise stated, all strains were incubated in MB at 28°C. Twenty-five additional strains were chosen as reference strains which were representatives of adjacent clusters from the NJ, MP, and ML trees. Data of these strains were collected

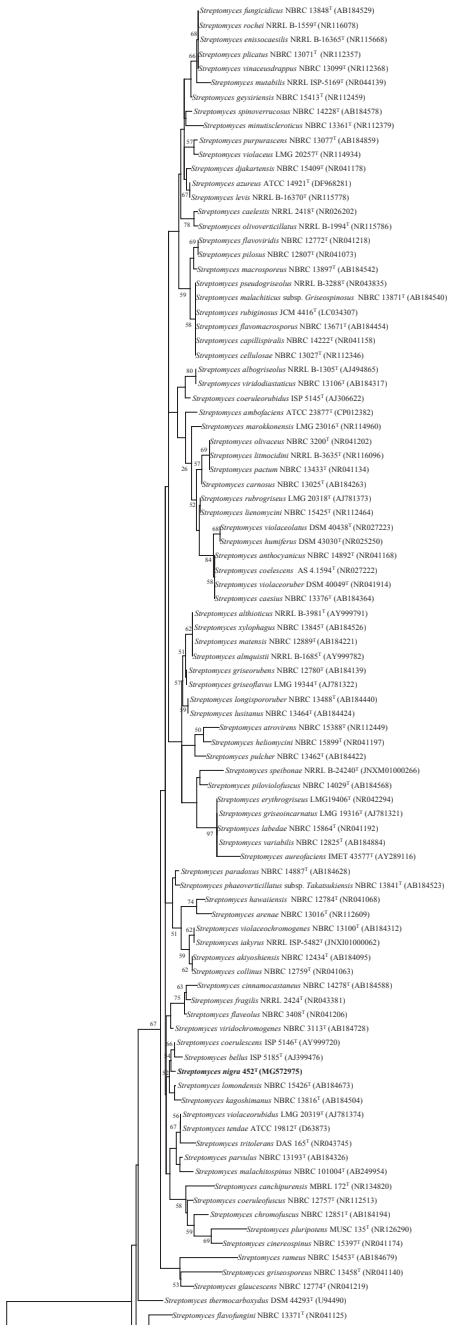

FIGURE 1 | Neighbor-joining phylogenetic tree based on the 16S rRNA gene sequences of strain 452^T and representatives of related taxa. Bootstrap values were expressed as a percentage of 1,000 replicates and only values >50% are shown at the branch points. Bar, 0.005 substitutions per nucleotide position.

from literatures and compared with strain 452^T (Supplementary Table S1). The DNA G + C content of strain 452^T was 71.7 mol%, which is similar to other strains from the *Streptomyces* genus.

The DNA-DNA relatedness values between strain 452^T and *S. coerulescens* DSM 40146^T (42.3 ± 1.0%), *S. bellus* DSM 40185^T (29.3 ± 0.4%), and *S. coeruleorubidus* DSM 41172^T (37.8 ± 0.7%) were well below the threshold value (70%) for determining a bacterial species (Wayne et al., 1987). The whole Genome Shotgun project of strain 452^T has been deposited at DDBJ/ENA/GenBank under the accession CP029043. The ANI values and *in silico* DDH values between strain 452^T and reference strains were 71.16–84.86% and 15.27–22.18%, respectively (**Table 1**). Which were below the 95% threshold value for ANI, 70% for GGDC proposed for the delineation of bacterial species, indicating that strain 452^T belongs to a novel species of the genus *Streptomyces* (Richter and Rossello-Mora, 2009; Auch et al., 2010).

Phenotypic Characterization of Strain 452^T

Strain 452^T grew well on ISP 2, ISP 3, ISP 4, ISP 5, ISP 7, MA, and tryptone soya agars after 7–14 days at 28°C; it grew moderately well on ISP 6 agar, *Streptomyces* agar, starch casein nitrate agar, nutrient agar, and potato-glucose agar, which was distinct from reference strains (Supplementary Table S2). As shown in Supplementary Figure S3, the strain formed a branched substrate mycelium, sparse aerial hyphae that differentiated into straight to flexuous chains and smooth bud-shaped spores on the ends of the aerial mycelium were formed on MA. The colors of the aerial, substrate mycelium, diffused pigment, and spore surface were media-dependent and are shown in **Table 2** and Supplementary Table S2; these characteristics distinguished this strain from the type strains. Strain 452^T was positive for catalase activity; hydrolysis of casein, starch, nitrate, and gelatin; and production of H_2S. In contrast to the reference strains, for examples, *S. bellus* DSM 40185^T and *S. coeruleorubidus* DSM 41172^T were negative for catalase; *S. coerulescens* DSM 40146^T was positive for oxidase, *S. bellus* DSM 40185^T was positive for anaerobic, which were unique characteristics distinct from other reference strains and 452^T. All reference strains were negative for production of H_2S, degradation of casein and gelatin, utilization of D-fructose as sole carbon, which were positive for strain 452^T. All reference strains were positive for α-chymotrypsin and able to utilized xylitol as sole energy source which were not shown in strain 452^T. Additionally, large numbers of differential features existed between strain 452^T and reference strains which shown in Supplementary Table S1, indicating that strain 452^T cannot be affiliated with any related species. In general, based on its phenotypic characteristics, strain 452^T could be differentiated from the closely related type strains; these properties were consistent with the assignment of the strain to the genus *Streptomyces*.

Chemotaxonomic Characterization of Strain 452^T

The results of chemotaxonomic analysis revealed that MK-9(H8) (74.1%) and MK-9(H6) (22.2%) were the major respiratory quinones of strain 452^T. The cell wall of strain 452^T contained LL-diaminopimelic acid as the diamino acid, and was hence

type-I cell wall (Lechevalier et al., 1970). Glutamic acid, alanine, and aspartic acid were the major amino acids of the cell wall. Whole-cell hydrolysates predominantly contained glucose, and small traces of ribose and mannose. The detailed fatty acid and polar lipid profiles of strain 452^T and the reference strains are shown in Supplementary Table S3 and Supplementary Figure S4, respectively. The major fatty acids (>5%) detected in strain 452^T included iso-$C_{16:0}$ (31.3%), anteiso-$C_{15:0}$ (16.9%), iso-$C_{15:0}$ (12.5%), $C_{16:0}$ (6.5%), iso-$C_{16:0}$ H (6.1%), anteiso-$C_{17:0}$

TABLE 1 | Average nucleotide identity (ANI) and *in silico* DNA-DNA hybridization (DDH) values between strain 452^T and the reference type strains of related species of genus *Streptomyces*.

Strains	Strain 452^T	
	ANI(%)	DDH(%)
Strain 452^T	100	0.00
Streptomyces almquistii NRRL B-1685^T (LIPO00000000)	72.81	19.84
Streptomyces azureus ATCC 14921^T (BBYS00000000)	83.86	14.72
Streptomyces caelestis NRRL 2418^T (LGCN00000000)	83.37	16.32
Streptomyces cellulosae NBRC 13027^T (JOEV00000000)	79.00	16.17
Streptomyces flaveolus NBRC 3408^T (JNWV00000000)	84.25	16.62
Streptomyces glaucescens NBRC 12774^T (MUND00000000)	82.80	16.53
Streptomyces minutiscleroticus NBRC 13361^T (MAZZ00000000)	84.86	15.73
Streptomyces olivaceus NBRC 3200^T (JOFH00000000)	79.37	18.12
Streptomyces pactum NBRC 13433^T (LIQD00000000)	83.62	16.51
Streptomyces parvulus NBRC 13193^T (NZ CP015866)	82.92	17.32
Streptomyces pluripotens MUSC 135^T (NZ CP021080)	81.37	18.66
Streptomyces speibonae NRRL B-24240^T (JNXM00000000)	84.05	15.27
Streptomyces violaceoruber DSM 40049^T (JOCE00000000)	75.35	19.31
Streptomyces viridochromogenes NBRC 3113^T (ACEZ00000000)	83.37	16.55
Streptomyces violaceorubidus LMG 20319^T (JODM00000000)	84.30	16.83
Streptomyces rochei NRRL B-1559^T (MUMD00000000)	71.16	22.18
Streptomyces ambofaciens ATCC 23877^T (NZ CP012382)	83.05	16.45
Streptomyces collinus NBRC 12759^T (NC CP021985)	82.95	17.26
Streptomyces griseoflavus LMG 19344^T (LGUW00000000)	74.15	21.07
Streptomyces griseorubens NBRC 12780^T (JJMG00000000)	82.79	16.40
Streptomyces iakyrus NRRL ISP-5482^T (JNXI00000000)	80.17	18.56
Streptomyces misionensis NBRC 13063^T (FNTD00000000)	82.27	17.26
Streptomyces pseudogriseolus NRRL B-3288^T (MUNG00000000)	79.50	15.71
Streptomyces violaceus LMG 20257^T (JNXN00000000)	72.89	17.45
Streptomyces xylophagus NBRC 13845^T (JNWO00000000)	79.33	16.83

TABLE 2 | Differential phenotypic characteristics of strain 452^T and its most closely related species.

Characteristic	1	2	3	4
ACTIVE OF				
Catalase	+	−	w	−
Oxidase	−	−	+	−
Anaerobic	−	+	−	−
H_2S production	+	−	−	−
Degradation of:				
Tween 20	−	+	+	−
Tween 80	−	+	−	+
Casein	+	−	−	−
Gelatin	+	−	−	−
Tests of API ZYM				
Esterase lipase (C8)	−	+	−	+
α-chymotrypsin	−	+	+	+
α-galactosidase	−	w	w	+
N-acetyl-β-glucosaminidase	+	−	w	−
α-mannosidase	+	−	w	w
CARBON UTILIZATION				
Succinic acid	+	−	+	+
D-maltose	+	−	+	+
Sodium citrate	+	−	−	+
D-lactose	+	−	+	+
Iinositol	+	−	+	+
Sucrose	+	−	+	+
D-mannose	+	+	+	−
D-fructose	+	−	−	−
D-galactose	+	+	−	−
L-arginine	+	+	+	−
Xylitol	−	+	+	+
D-melibiose	−	−	+	+
MAJOR FATTY ACIDS (%)				
$C_{16:0}$	6.5	12.1	6.5	8.5
$C_{18:0}$	tr	5.5	1.8	tr
iso-$C_{15:0}$	12.5	15.5	12.4	20.1
iso-$C_{16:0}$	31.3	21.0	14.3	14.1
iso-$C_{17:0}$	2.9	8.6	6.8	5.2
iso-$C_{16:0}$ H	6.1	2.3	5.6	1.9
anteiso-$C_{15:0}$	16.9	9.4	8.2	8.5
Summed feature 9*	3.2	7.8	8.1	11.2
MORPHOLOGY (ON ISP4)				
Color of aerial	Grayish blue	Gray	White	White
MORPHOLOGY (ON ISP5)				
Color of aerial	White	White	–	Pink
Color of substrate	Yellow	Orange	–	Pink

(Continued)

TABLE 2 | Continued

Characteristic	1	2	3	4
MORPHOLOGY (ON ISP7)				
Color of aerial	Gray	Yellowish white	White	Gray
Color of substrate	Gray	Yellow	White	Gray
Colony surface	Smooth	Rough	Hairy	Hairy
MORPHOLOGY (ON NA)				
Color of aerial	White	Gray	Yellowish white	Gray
Color of substrate	Yellowish brown	White	Yellowish brown	Yellowish brown
MORPHOLOGY (ON MA)				
Color of aerial	Gray	White	Gray	Brown
Color of substrate	Gray	Reddish brown	Gray	Brown
Colony surface	Rough	Hairy	Rough	Smooth

Taxa: 1, strain 452^T; 2, Streptomyces bellus DSM 40185^T; 3, Streptomyces coerulescens DSM 40146^T; 4, Streptomyces coeruleorubidus DSM 41172^T. All strains were positive for alkaline phosphatase, esterase (C4), leucine arylamidase, valine arylamidase, trypsin, acid phosphatase, naphthol-AS-BI-phosphohydrolase, β-galactosidase, β-glucosidase, and nitrate reduction; degradation of starch; and utilization as a sole carbon: erythritol, D-*ribose,* D-*sorbitol, trehalose, salicylic acid,* D-*glucose,* D-*mannitol,* L-*alanine, glycerine, sodium gluconate, sodium malonate,* DL-*methionine, and* L-*tryptophan. All strains were negative for lipase (C14), cysteine arylamidase, β-glucuronidase, α-fucosidase, nitrite reduction; degradation of CM-cellulose, tyrosine, Tween 40, Tween 60, and filter paper; flexirubin-type pigment, motility, methyl red testing, Voges-Proskauer reaction; and utilization of* D-*arabinose,* D-*xylose, and* L-*sorbose as sole carbon sources. –, not detected or no growth; tr, trace amount (<1%). *Summed feature 9 (ECL 16.443) is composed of C16:0 10-methyl and/or ios-$C_{17:1}\omega9c$.*

(5.7%), iso-$C_{14:0}$ (5.4%), and summed feature 3 ($C_{16:1}\omega7c$ and/or $C_{16:1}\omega6c$, 5.2%). The polar lipid profile of strain 452^T was comprised of diphosphatidylglycerol, phosphatidylethanolamine, phosphatidylglycerol, phosphatidylinositol, phosphatidylinositol mannoside, three unidentified phospholipids, an unidentified aminolipid, an unidentified phosphoaminolipid and an unidentified lipid. The fatty acid and polar lipid profiles of strain 452^T were similar to those of the reference strains (Supplementary Table S3), despite some differences in their proportions and minor constituents, respectively. Chemotaxonomic features of strain 452^T were also similar to the features of other species from the genus *Streptomyces* (Lee and Whang, 2016; Ser et al., 2016a; Law et al., 2017; Röttig et al., 2017; Wang et al., 2017).

Cytotoxic Activity of the Extract From Strain 452^T

The potential anti-proliferative effect of extract of strain 452^T was evaluated using several human-derived cancer cell lines (U87, MCF-7, HCT-116, HepG2, A549, and SF-268) and normal human colon cells (CCD-18Co), which were tested *in vitro* using growth-inhibition assays. The results are summarized in Supplementary Figure S5. All cancer cell lines showed susceptibility to the extract of strain 452^T with inhibition ratio of 90.8–60.0% (100 μg/mL of the extract was tested). As indicated, HCT-116 cells were most sensitive to the extract, with the inhibition ratio of 90.8 ± 4.2% and 72.1 ± 2.7% at concentration of 100 μg/mL and 20 μg/mL, respectively. HepG2 and A549 cells were more sensitive (inhibition ratio >80% at 100 μg/mL and >60% at 20 μg/mL) to the extract than the U87, MCF-7 and SF268 cells. The inhibition ratios of U87, MCF-7 and SF268 cells were 80.0–55.0% (100 μg/mL of the extract was tested), and 55.0–40.0% (20 μg/mL of the extract was tested). In contrast, the normal human colon cells CCD-18Co were resistant to the extract, with the inhibition ratio lower than 15%. Morphological changes of all tested cell lines in response to extract of 452^T after 48 h treatment were showed in Supplementary Figure S6. All morphologies of cancer cell lines exhibited varying degrees of alterations, including shrunken cell, arranged loosely and detached from the surface. Ratios of normal morphological cells decreased as the concentration of the extract increased. However, only a few normal colorectal CCD-18Co cells shrank after treatment with the extract. Overall, the extract showed a broad-spectrum antitumor potential against human colon, breast, lung, liver, glioma cancer cells and had no cytotoxicity toward normal human colon cells. Based on the cytotoxicity results, we elected to further characterize signaling events affected by the metabolites of strain 452^T in HCT-116, HePG2, and A549 cells.

Structure and Cytotoxicity of Bioactive Metabolites From Strain 452^T

Bioassay-guided isolation of the active components of 452^T in the ethyl alcohol eluent after a macroporous resin separation yielded eight main bioactive metabolites, which were then characterized by spectroscopic analyses (Supplementary Data Sheet 1) and by comparison with the literature data. As shown in **Figure 2**, the constituents (compounds **1–8**) were identified as cyclo(Pro-Ala) (**1**) (Trigos et al., 1997), cyclo(Pro-Gly) (**2**) (Chen et al., 2012), cyclo(Pro-Phe) (**3**) (Sansinenea et al., 2016), cyclo(Pro-Met) (**4**) (Kumar et al., 2013), cyclo(Pro-Val) (**5**) (Furtado et al., 2005), cyclo(Pro-Leu) (**6**) (Sansinenea et al., 2016), cyclo(Pro-Tyr) (**7**) (Sansinenea et al., 2016), and cyclo(L-Leu-trans-4-hydroxy-L-Pro) (**8**) (Cronan et al., 1998).

The cytotoxic activities of compounds **1–8** against HCT-116, HepG2, and A549 cancer cell lines are shown in **Table 3**. Both compounds **1** and **5** suppressed the proliferation of all tested cells, but compound **1** showed stronger cytotoxic activities than compound **5**. Compounds **1** and **4** exhibited good cytotoxicity against A549 with IC_{50} values of 18.5 and 27.3 μg/mL, compounds **1** and **5** showed cytotoxicity against HCT-116 cells with IC_{50} values of 47.6 and 32.3 μg/mL, which the average IC_{50} values were lower 50.0 μg/mL. The compounds exhibited different degrees of cytotoxicity, compounds **2** and **5–8**, weakly inhibited the growth of some cells (average IC_{50} of 50.0–100.0 μg/mL) or showed no cytotoxicity against some cells (average IC_{50} > 100.0 μg/mL). It is noteworthy that the compounds **1–8** were diketopiperazines which were isolated under guidance of cytotoxic activities. Comparison of the results of the compounds **1–8**, suggested that the proline was probably critical for the cytotoxic activity of diketopiperazine.

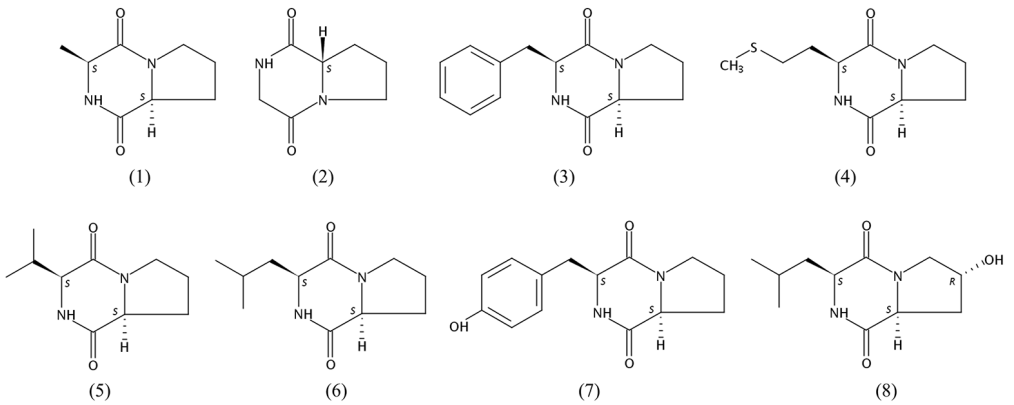

FIGURE 2 | Chemical structures of compounds **1–8**.

GC-MS Analysis of the Extract From Strain 452^T

Streptomyces produce various secondary metabolites with diverse biological activity, and GC-MS analysis is used to facilitate chemical profiling and to identify such active compounds (Ser et al., 2015; Law et al., 2017). GC-MS analysis conducted in the current study revealed the presence of more than 500 compounds in the strain 452^T extract, including sinapyl alcohol (**9**), phloroglucinol (**10**), azelaic acid (**11**), hydroxyurea (**12**), androsterone (**13**), shikimic acid (**14**), spermidine (**15**), 2-deoxy-D-glucose (**16**), and dehydroepiandrosterone (**17**) (**Figure 3**). Zhao et al. (2002) isolated seven sinapyl alcohol analogs from *Ligularia nelumbifolia*, and verified their cytotoxic activities against cancer cell lines A549, HL-60, and KB. Phloroglucinol significantly inhibits the growth of a lung carcinoma tumor in the mouse model, and potentially inhibits the bioactivity of endothelial progenitor cells, thereby attenuating tumor growth and angiogenesis (Kwon et al., 2012). Azelaic acid is a natural dicarboxylic acid and an antiproliferative agent that is cytotoxic to a variety of tumor cell lines, including human melanoma cells; because of its inhibition of mitochondrial oxidoreductases of the respiratory chain and of enzymes involved in DNA synthesis, normal cells are unaffected at dosages and times of exposure similar to used for tumor cell treatment (Zaffaroni et al., 1990; Breathnach, 1999). Hydroxyurea is a widely used drug in the therapy for several human cancers; it inhibits deoxynucleotide synthesis and, consequently, DNA synthesis by blocking the cellular enzyme ribonucleotide reductase (Stearns et al., 1963; Lori et al., 1994). Androsterone is an androgen and a steroid hormone drug. Several studies reported that androsterone is cytotoxic to MCF-7 breast cancer cells and HT-29 cancer cells *in vitro* (Carroll et al., 1972; Gao et al., 2010). Dehydroepiandrosterone is a derivative of androsterone, a potent inhibitor of glucose-6-phosphate dehydrogenase, which has been shown to inhibit the growth of neoplasms from the human skin, lung, colon, and mammary tissue (Melvin et al., 1997). Shikimic acid is highly cytotoxic and inhibits the spread of cancer cells in mouse (Hirono et al., 1977; Ganem, 1978). Spermidine is an organic cation required for cell proliferation but its accumulation can induce apoptosis. Spermine triggers the cell death program, characterized by cytochrome c exit from the mitochondria, dATP-dependent processing of pro-caspase-3, and caspase activation (Stefanelli et al., 1999; Zahedi et al., 2007). Finally, 2-deoxy-D-glucose is a glycolysis inhibitor that differentially enhances the radiation and chemotherapeutic drug-induced cell death in cancer cells *in vitro*. Its potential as an immunomodulator, in addition to a direct effect on the tumor, is specifically employed in a combination treatment of Lewis lung carcinoma (Farooque et al., 2014; Pyaskovskaya et al., 2016). The antitumor activity and low toxicity of the above compounds have been documented in numerous studies, supporting the notion that they at least partially, account for the cytotoxic activity of the strain 452^T extract.

TABLE 3 | IC_{50} values (μg/mL) of compounds **1–8** against human cancer cell lines.

Metabolite	HCT-116	HepG2	A549
Cyclo(Pro-Ala) (**1**)	47.6 + 2.9	88.3 + 5.6	18.5 + 0.9
Cyclo(Pro-Gly) (**2**)	–	94.5 + 7.3	–
Cyclo(Pro-Phe) (**3**)	32.3 + 1.5	57.0 + 2.1	–
Cyclo(Pro-Met) (**4**)	–	105.5 + 3.2	27.3 + 1.1
Cyclo(Pro-Val) (**5**)	67.2 + 4.9	102.9 + 5.2	111.7 + 2.3
Cyclo(Pro-Leu) (**6**)	92.6 + 7.8	–	120.3 + 6.7
Cyclo(Pro-Tyr) (**7**)	–	84.2 + 8.6	–
Cyclo(L-Leu-trans-4-hydroxy-L-Pro) (**8**)	–	–	92.8 + 2.3
Doxorubicin	1.3 + 0.2	2.9 + 0.3	2.1 + 0.3

Doxorubicin was tested as a positive control. Values represent the mean of three replications ± standard deviation. –, not tested or average IC_{50} > 150.0 μg/mL.

LC-MS/MS Analysis of the Extract From Strain 452^T

LC-MS/MS combined with UV data and database analyses are used to confirm the structure of compounds of interest (Ferreira et al., 2016). A variety of diketopiperazines from strain 452^T were detected using LC-MS/MS and analyzed by comparing

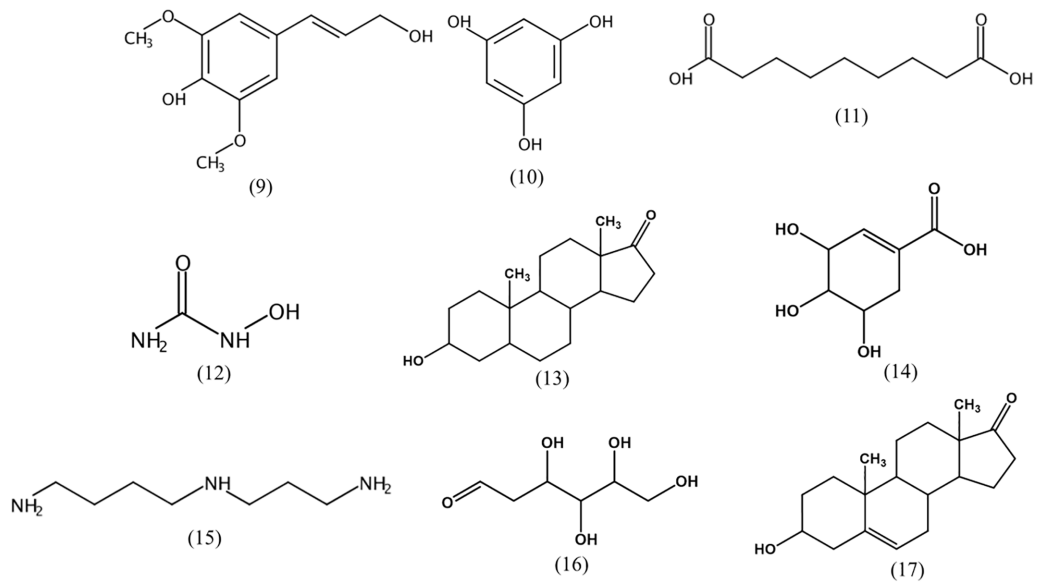

FIGURE 3 | Chemical structures of cytotoxic compounds identified by GC-MS.

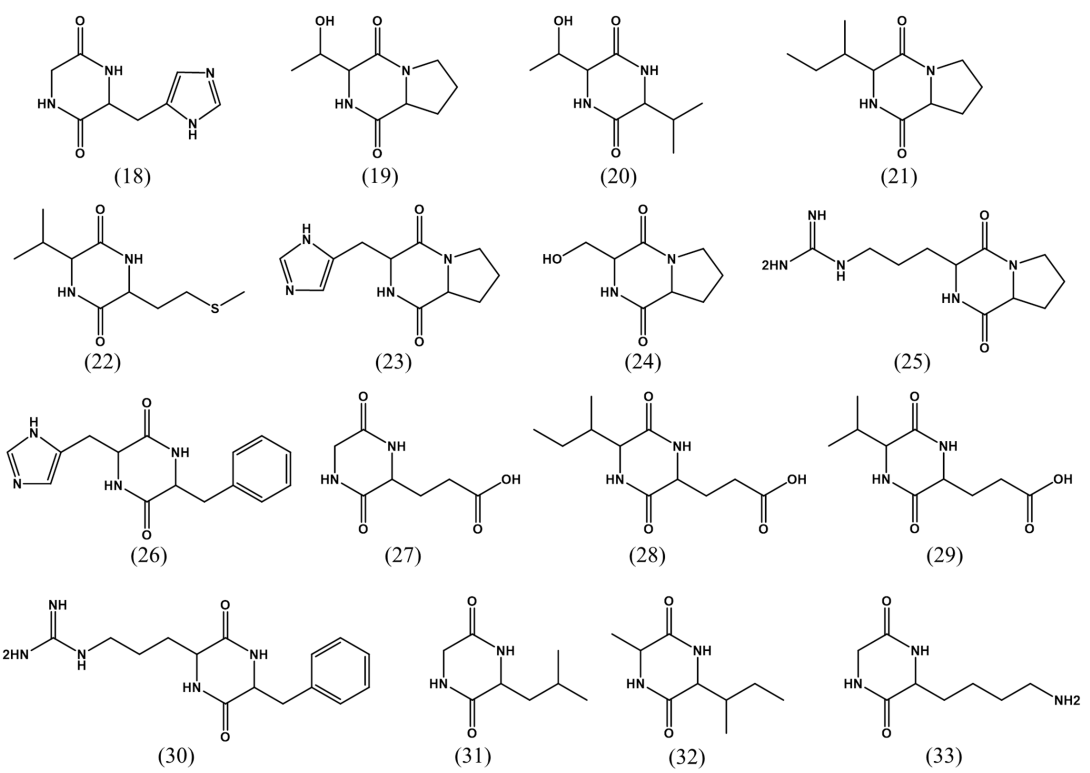

FIGURE 4 | Chemical structures of diketopiperazines indicated by LC-MS/MS.

with data in the Human Metabolome Database[5]. Excluding 8 types of diketopiperazine (compounds **1–8**), another 16 types of diketopiperazine were tentatively identified. As shown in **Figure 4**, these were cyclo(Gly-His) (**18**), cyclo(Pro-Thr) (**19**), cyclo(Thr-Val) (**20**), cyclo(Ile-Pro) (**21**), cyclo(Met-Val) (**22**), cyclo(His-Pro) (**23**), cyclo(Pro-Ser) (**24**), cyclo(Pro-Arg) (**25**), cyclo(His-Phe) (**26**), cyclo(Gly-Glu) (**27**), cyclo(Ile-Glu) (**28**), cyclo(Val-Glu) (**29**), cyclo(Arg-Phe) (**30**), cyclo(Gly-Leu) (**31**),

[5]http://www.hmdb.ca

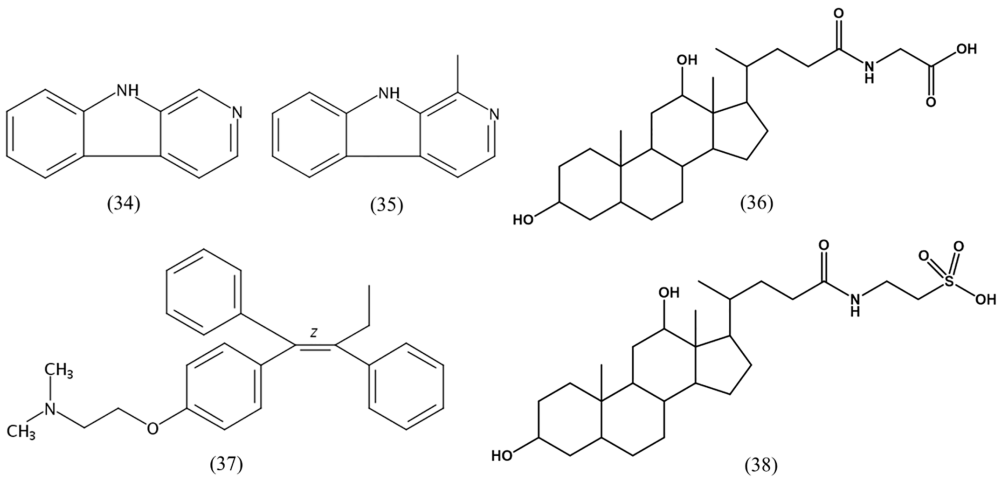

FIGURE 5 | Chemical structures of cytotoxic compounds indicated by LC-MS/MS.

cyclo(Ile-Ala) (**32**), and cyclo(Gly-Lys) (**33**). These compounds have been also identified in other microbes.

The other detected compounds were β-carboline (**34**), harman (**35**), glycodeoxycholic acid (**36**), tamoxifen (**37**), and taurodeoxycholic acid (**38**) (**Figure 5**). β-Carboline is a natural indole alkaloid, and widely occurs in plants and microbes. Previous studies reported that β-carboline and a series of its derivatives (including harman alkaloids) inhibit DNA topoisomerases and interfere with DNA synthesis; They interact with DNA by groove binding and intercalation, which may lead to major structural changes in the DNA (Nafisi et al., 2010). Further, they exert a pronounced antitumor activity against human tumor cells, including KB, DLD, NCI-H661, Hepa, and HepG2/A2 cell lines (Prinsep et al., 1991; Shen et al., 2011; Silva et al., 2016). Glycodeoxycholic acid and taurodeoxycholic acid are important components of bile acid, and cause liver injury during cholestasis by inducing hepatocyte apoptosis via Fas-dependent and -independent mechanisms (Higuchi et al., 2001). The *p53* gene expression induced telomerase activity and *hTERT* expression was obviously reduced after the human liver cancer cells SMMC7721 were treated by glycodeoxycholic acid, with a subsequent induction of apoptosis of the liver cancer cells (Patel et al., 1994; Toledo et al., 2004). Tamoxifen is an antagonist of the estrogen receptor, able to competitively bind to the estrogen receptor and prevent estrogen activity. It is widely used for breast cancer prevention and treatment, ovarian cancer treatment, and also for the pancreatic cancer and polycystic ovarian syndrome treatment (Abe et al., 2005).

Description of *Streptomyces nigra* sp. nov.

(*ni'gra*. L. fem. adj. *nigra* black, referring to the color of melanin produced by mature colonies on MA and MB).

Cells are gram-positive, non-motile, and form gray aerial and dark-substrate mycelia on MA. On the ends of the aerial mycelium bud-shaped spores are formed, the spore surface is smooth and there are no spore-chains on aerial mycelium. The colors of the aerial and substrate mycelia are media-dependent. Cells secrete melanin on MA and MB at 28°C, grow well on ISP 2, ISP 3, ISP 4, ISP 5, and ISP 7 agars, and on MA and tryptone soya agar for 7–14 days at 28°C; they grow moderately well on ISP 6 agar, *Streptomyces* agar, starch casein nitrate agar, nutrient agar, and potato-glucose agar. Growth occurs at 15–45°C (25°C optimum), pH 5.0–9.0 (pH 7.0 optimum), and 0–8.0% (w/v) NaCl (1.5% optimum). The cells are positive for catalase, alkaline phosphatase, esterase (C4), esterase lipase (C8), leucine arylamidase, valine arylamidase, trypsin, acid phosphatase, naphthol-AS-BI-phosphohydrolase, β-galactosidase, α-glucosidase, β-glucosidase, *N*-acetyl-β-glucosaminidase, and α-mannosidase activities; they hydrolyze casein, starch, nitrate, and gelatin; and produce H_2S. The cells are negative for oxidase, and in methyl red test and Voges-Proskauer test; hydrolysis of L-tyrosine, CM-cellulose, and crystalline cellulose (filter paper); and degradation of Tween 20, 40, 60, and 80. The following compounds are utilized as the sole carbon and energy sources: succinic acid, D-maltose, citric acid, α-D-lactose, *myo*-inositol, erythritol, adonitol, D-sorbitol, sucrose, trehalose, saligenin, D-mannose, D-fructose, D-galactose, D-glucose, mannitol, glycerol, L-alanine, L-methionine, L-tryptophan, and L-arginine. The major fatty acids (>5%) are iso-$C_{16:0}$ (31.3%), anteiso-$C_{15:0}$ (16.9%), iso-$C_{15:0}$ (12.5%), $C_{16:0}$ (6.5%), iso-$C_{16:0}$ H (6.1%), anteiso-$C_{17:0}$ (5.7%), iso-$C_{14:0}$ (5.4%), and summed feature 3 ($C_{16:1}\omega7c$ and/or $C_{16:1}\omega6c$, 5.2%). The polar lipid profile of strain 452^T contains diphosphatidylglycerol, phosphatidylethanolamine, phosphatidylglycerol, phosphatidylinositol, phosphatidylinositol mannoside, three unidentified phospholipids, an unidentified aminolipid, an unidentified phosphoaminolipid, and an unidentified lipid. The DNA G + C content of the type strain is 71.7% mol.

The type strain is 452^T (=KCTC 39960^T = MCCC $1K03346^T$), which was isolated from the rhizosphere soil of the mangrove *A. marina* forest of Zhangzhou (24°20′, 117°45′) in Fujian

Province, China. The GenBank/EMBL/DDBJ accession number for the 16S rRNA gene sequence of strain 452^T is MG572975.

CONCLUSION

Phylogenetic, genomic, phenotypic, and chemotaxonomic analyses revealed that strain 452^T was localized in the clade of the genus *Streptomyces*, but was pronouncedly different from the most closely related type strains. Strain 452^T is therefore considered to represent a novel species, for which the name *S. nigra* sp. nov. is proposed. The type strain is 452^T (=KCTC 39960^T = MCCC 1K03346^T). Treatment with the extract from strain 452^T resulted in a 58.5–90.8% inhibition ratio against six types of cancer cell lines when tested at a concentration at 100 μg/mL, indicating a broad-spectrum cytotoxic activity against cancer cells and inactivity toward normal human cells. Hence, strain 452^T is potentially a rich reservoir of natural products with antitumor activity.

Bioassay-guided separation and purification on a macroporous resin, silica gel, sephadex LX-20 column, and semi-preparative HPLC were successfully used to identify the active fractions. Further identification by electrospray ionizing-MS and NMR revealed that the active compounds were related to the diketopiperazine family, with different cytotoxic activities against cancer cells, as previously reported and confirmed in the current study (Yang et al., 2002; Tan et al., 2004; Kanoh et al., 2005; Capon et al., 2007). Interestingly, all eight diketopiperazines isolated in the current study contain proline. According to the literature, more than 12 proline-containing diketopiperazines show widespread biological activity, including antitumor activity (Ortiz and Sansinenea, 2017). The array of diketopiperazines produced by strain 452^T was investigated by LC-MS/MS, and additional 16 diketopiperazines were detected, and known to possess antitumor activity (Yang et al., 2002; Tan et al., 2004; Kanoh et al., 2005; Capon et al., 2007). Overall, 24 diketopiperazines produced by strain 452^T were identified. Chemical analysis via GC-MS and LC-MS/MS further confirmed that the strain produces metabolites with antitumor activity; 14 metabolites previously shown to possess antitumor activity were identified in strain 452^T in the current study. In general, compounds **1–8** (eight diketopiperazines) were produced in high enough quantities when the bacterium was grown on MB medium to allow their isolation and identification. Cytotoxicity of these main bioactive metabolites greatly contributed to the observed bioactivity of strain 452^T, with other metabolites detected in the current study adding to the suppressive effect on tumor cells. This demonstrated the biopharmaceutical potential of the novel *S. nigra* strain to produce bioactive compounds with cytotoxic activity. Future studies should focus on strain 452^T as a potentially high-quality and valuable resource for anticancer or chemo-preventive drug discovery.

AUTHOR CONTRIBUTIONS

CC designed, carried out the experiments, and wrote the manuscript. YY and RW carried out the experiments. YZ and MW designed the experiments. JW and ZM analyzed experimental results. SCD and CW revised the manuscript.

FUNDING

This work was supported by Si Yuan Foundation (Research on anti-tumor compounds from marine microorganisms) and the National Natural Science Foundation of China (Grant No. 31770007).

SUPPLEMENTARY MATERIAL

The Supplementary Material for this article can be found online at: https://www.frontiersin.org/articles/10.3389/fmicb.2018.01587/full#supplementary-material

REFERENCES

Abe, O., Abe, R., Enomoto, K., Kikuchi, K., Koyama, H., Masuda, H., et al. (2005). Effects of chemotherapy and hormonal therapy for early breast cancer on recurrence and 15-year survival: an overview of the randomised trials. *Lancet* 365, 1687–1717. doi: 10.1016/s0140-6736(05)66544-0

Ahmad, M. S., Elgendy, A. O., Ahmed, R. R., Hassan, H. M., Elkabbany, H. M., and Merdash, A. G. (2017). Exploring the antimicrobial and antitumor potentials of *Streptomyces* sp. AGM12-1 isolated from egyptian soil. *Front. Microbiol.* 8:438. doi: 10.3389/fmicb.2017.00438

Atlas, R. M. (2010). *Handbook of Microbiological Media*. Boca Raton, FL: CRC Press.

Auch, A. F., von Jan, M., Klenk, H. P., and Goker, M. (2010). Digital DNA-DNA hybridization for microbial species delineation by means of genome-to-genome sequence comparison. *Stand. Genomic Sci.* 2, 117–134. doi: 10.4056/sigs.531120

Běhal, V. (2000). Bioactive products from *Streptomyces*. *Adv. Appl. Microbiol.* 47, 113–156. doi: 10.1016/s0065-2164(00)47003-6

Bilyk, O., and Luzhetskyy, A. (2016). Metabolic engineering of natural product biosynthesis in actinobacteria. *Curr. Opin. Biotechnol.* 42, 98–107. doi: 10.1016/j.copbio.2016.03.008

Borthwick, A. D., and Da Costa, N. C. (2017). 2,5-diketopiperazines in food and beverages: taste and bioactivity. *Crit. Rev. Food Sci.* 57, 718–742. doi: 10.1080/10408398.2014.911142

Breathnach, A. S. (1999). Azelaic acid: potential as a general antitumoural agent. *Med. Hypotheses* 52, 221–226. doi: 10.1054/mehy.1997.0647

Bull, A. T., and Stach, J. E. M. (2007). Marine actinobacteria: new opportunities for natural product search and discovery. *Trends Microbiol.* 15, 491–499. doi: 10.1016/j.tim.2007.10.004

Cai, W. L., Wang, X. C., Elshahawi, S. I., Ponomareva, L. V., Liu, X. D., McErlean, M. R., et al. (2016). Antibacterial and cytotoxic actinomycins Y_6–Y_9 and Zp from *Streptomyces* sp strain go-GS12. *J. Nat. Prod.* 79, 2731–2739. doi: 10.1021/acs.jnatprod.6b00742

Capon, R. J., Stewart, M., Ratnayake, R., Lacey, E., and Gill, J. H. (2007). Citromycetins and bilains A-C: new aromatic polyketides and diketopiperazines from Australian marine-derived and terrestrial *Penicillium* spp. *J. Nat. Prod.* 70, 1746–1752. doi: 10.1021/np0702483

Carroll, F. I., Blackwell, J. T., Wall, M. E., Taylor, D. J., and Philip, A. (1972). Antitumor and antileukemic effects of some steroids and other biologically interesting compounds containing an alkylating agent. *J. Med. Chem.* 15, 1158–1161. doi: 10.1021/jm00281a016

Cashion, P., Holder-Franklin, M. A., and Mccully, J. (1977). A rapid method for the base ratio determination of bacterial DNA. *Anal. Biochem.* 81, 461–466. doi: 10.1016/0003-2697(77)90720-5

Chater, K. F. (2006). *Streptomyces* inside-out: a new perspective on the bacteria that provide us with antibiotics. *Philos. Trans. R. Soc. Lond. B Biol. Sci.* 361, 761–768. doi: 10.1098/rstb.2005.1758

Chen, C., Su, Y., Tao, T. Y., Fu, G. Y., Zhang, C. Y., Sun, C., et al. (2017). *Maripseudobacter aurantiacus* gen. nov., sp nov., a novel member of the family *Flavobacteriaceae* isolated from a sedimentation basin. *Int. J. Syst. Evol. Microbiol.* 67, 778–783. doi: 10.1099/ijsem.0.001580

Chen, J. H., Lan, X. P., Liu, Y. H., and Jia, A. Q. (2012). The effects of diketopiperazines from *Callyspongia* sp on release of cytokines and chemokines in cultured J774A.1 macrophages. *Bioorg. Med. Chem. Lett.* 22, 3177–3180. doi: 10.1016/j.bmcl.2012.03.045

Christensen, A., and Martin, G. D. A. (2017). Identification and bioactive potential of marine microorganisms from selected Florida coastal areas. *Microbiologyopen* 6:e00448. doi: 10.1002/mbo3.448

Cronan, J. M. Jr., Davidson, T. R., Singleton, F., Colwell, R. R., and Cardellina, J. H. (1998). Plant growth promoters isolated from a marine bacterium associated with *Palythoa* sp. *Nat. Prod. Lett.* 11, 271–278. doi: 10.1080/10575639808044959

Dong, X. Z., and Cai, M. (2001). *Determinative Manual for Routine Bacteriology*. Beijing: Scientific Press.

Du, L. C., Sanchez, C., Chen, M., Edwards, D. J., and Shen, B. (2000). The biosynthetic gene cluster for the antitumor drug bleomycin from *Streptomyces verticillus* ATCC15003 supporting functional interactions between nonribosomal peptide synthetases and a polyketide synthase. *Chem. Biol.* 7, 623–642. doi: 10.1016/s1074-5521(00)00011-9

Dudek, N. K., Sun, C. L., Burstein, D., Kantor, R. S., Goltsman, D. S. A., Bik, E. M., et al. (2017). Novel microbial diversity and functional potential in the marine mammal oral microbiome. *Curr. Biol.* 27, 3752–3762. doi: 10.1016/j.cub.2017.10.040

Farooque, A., Singh, N., Adhikari, J. S., Afrin, F., and Dwarakanath, B. S. R. (2014). Enhanced antitumor immunity contributes to the radio-sensitization of ehrlich ascites tumor by the glycolytic inhibitor 2-Deoxy-D-Glucose in mice. *PLOS One* 9:e108131. doi: 10.1371/journal.pone.0108131

Fernandez, E., Weissbach, U., Reillo, C. S., Brana, A. F., Mendez, C., Rohr, J., et al. (1998). Identification of two genes from *Streptomyces argillaceus* encoding glycosyltransferases involved in transfer of a disaccharide during biosynthesis of the antitumor drug mithramycin. *J. Bacteriol.* 180, 4929–4937.

Ferreira, E. G., Torres, M. D., da Silva, A. B., Colares, L. L. F., Pires, K., Lotufo, T. M. C., et al. (2016). Prospecting anticancer compounds in actinomycetes recovered from the sediments of saint peter and saint paul's archipelago, Brazil. *Chem. Biodivers.* 13, 1149–1157. doi: 10.1002/cbdv.201500514

Furtado, N. A. J. C., Pupo, M. T., Carvalho, I., Campo, V. L., Duarte, M. C. T., and Bastos J. K. (2005). Diketopiperazines produced by an *Aspergillus fumigatus* Brazilian strain. *J. Braz. Chem. Soc.* 16, 1448–1453. doi: 10.1590/S0103-50532005000800026

Ganem, B. (1978). From glucose to aromatics: recent developments in natural products of the shikimic acid pathway. *Tetrahedron* 34, 3353–3383. doi: 10.1016/0040-4020(78)80222-1

Gao, L. M., Vera, J. L., Matta, J., and Melendez, E. (2010). Synthesis and cytotoxicity studies of steroid-functionalized titanocenes as potential anticancer drugs: sex steroids as potential vectors for titanocenes. *J. Biol. Inorg. Chem.* 15, 851–859. doi: 10.1007/s00775-010-0649-7

Hata, T., Sano, Y., Sugawara, R., Matsumae, A., Kanamori, K., Shima, T., et al. (1956). Mitomycin, a new antibiotic from Streptomyces I. *J. Antibiot.* 9, 141–146. doi: 10.1038/176646a0

Higuchi, H., Miyoshi, H., Bronk, S. F., Zhang, H., Dean, N., and Gores, G. J. (2001). Bid antisense attenuates bile acid-induced apoptosis and cholestatic liver injury. *J. Pharmacol. Exp. Ther.* 299, 866–873.

Hirono, I., Fushimi, K., and Matsubara, N. (1977). Carcinogenicity test of shikimic acid in rats. *Toxicol. Lett.* 1, 9–10. doi: 10.1016/0378-4274(77)90013-3

Hong, K., Gao, A. H., Xie, Q. Y., Gao, H., Zhuang, L., Lin, H. P., et al. (2009). Actinomycetes for marine drug discovery isolated from mangrove soils and plants in China. *Mar. Drugs* 7, 24–44. doi: 10.3390/md7010024

Huang, R. M., Yi, X. X., Zhou, Y. Y., Su, X. D., Peng, Y., and Gao, C. H. (2014). An update on 2,5-diketopiperazines from marine organisms. *Mar. Drugs* 12, 6213–6235. doi: 10.3390/md12126213

Juliano, R. L., and Stamp, D. (1978). Pharmacokinetics of liposome-encapsulated anti-tumor drugs-studies with vinmlastine, actinomycin D, cytosine-arabinoside, and daunomycin. *Biochem. Pharmacol.* 27, 21–27. doi: 10.1016/0006-2952(78)90252-6

Kamjam, M., Sivalingam, P., Deng, Z. X., and Hong, K. (2017). Deep sea actinomycetes and their secondary metabolites. *Front. Microbiol.* 8:760. doi: 10.3389/fmicb.2017.00760

Kanoh, K., Matsuo, Y., Adachi, K., Imagawa, H., Nishizawa, M., and Shizuri, Y. (2005). Mechercharmycins A and B, cytotoxic substances from marine-derived *Thermoactinomyces* sp YM3-251. *J. Antibiot.* 58, 289–292. doi: 10.1002/chin.200543201

Katz, E., Waldron, C. R., and Meloni, M. L. (1961). Role of valine and isoleucine as regulators of actinomycin peptide formation by *Streptomyces chrysomallus*. *J. Bacteriol.* 82, 600–608.

Kelly, K. L., and Judd, D. B. (1964). *ISCC-NBS Color(-)Name Charts Illustrated with Centroid Colors*. Washington, DC: National Bureau of Standards.

Komagata, K., and Suzuki, K. (1987). Lipid and cell-wall analysis in bacterial systematics. *Methods Mircrobiol.* 19, 161–207. doi: 10.1016/s0580-9517(08)70410-0

Kumar, N., Mohandas, C., Nambisan, B., Kumar, D. R., and Lankalapalli, R. S. (2013). Isolation of proline-based cyclic dipeptides from *Bacillus* sp. N strain associated with rhabditid [corrected] entomopathogenic nematode and its antimicrobial properties. *World J. Microbiol. Biotechnol.* 29, 355–364. doi: 10.1007/s11274-012-1189-9

Kwon, Y. H., Jung, S. Y., Kim, J. W., Lee, S. H., Lee, J. H., Lee, B. Y., et al. (2012). Phloroglucinol inhibits the bioactivities of endothelial progenitor cells and suppresses tumor angiogenesis in LLC-tumor-bearing mice. *PLOS One* 7:e33618. doi: 10.1371/journal.pone.0033618

Lam, K., Gustavson, D. R., Pirnik, D. L., Pack, E., Bulanhagui, C., Mamber, S. W., et al. (2002). The effect of space flight on the production of actinomycin D by *Streptomyces plicatus*. *J. Ind. Microbiol. Biotechnol.* 29, 299–302. doi: 10.1038/sj.jim.7000312

Law, W. F., Ser, H. L., Duangjai, A., Saokaew, S., Bukhari, S. I., Khan, T. M., et al. (2017). *Streptomyces colonosanans* sp. nov., a novel actinobacterium isolated from Malaysia mangrove soil exhibiting antioxidative activity and cytotoxic potential against human colon cancer cell lines. *Front. Microbiol.* 8:877. doi: 10.3389/fmicb.2017.00877

Lechevalier, H. A., Lechevalier, M. P., and Gerber, N. N. (1970). Chemical composition as a criterion in the classification of actinomycetes. *Adv. Appl. Microbiol.* 14, 47–72. doi: 10.1016/s0065-2164(08)70539-2

Lee, H. J., and Whang, K. S. (2016). *Streptomyces rhizosphaerihabitans* sp. nov., and *Streptomyces adustus* sp. nov., isolated from bamboo forest soil. *Int. J. Syst. Evol. Microbiol.* 66, 3573–3578. doi: 10.1099/ijsem.0.001236

Lee, J. H., Kim, Y. G., Lee, K., Kim, C. J., Park, D. J., Ju, Y., et al. (2016). *Streptomyces*-derived actinomycin D inhibits biofilm formation by *Staphylococcus aureus* and its hemolytic activity. *Biofouling* 32, 45–56. doi: 10.1080/08927014.2015.1125888

Lee, I., Kim, Y. O., Park, S. C., and Chun, J. (2016). OrthoANI: an improved algorithm and software for calculating average nucleotide identity. *Int. J. Syst. Evol. Microbiol.* 66, 1100–1103. doi: 10.1099/ijsem.0.000760

Lee, L. H., Zainal, N., Azman, A. S., Eng, S. K., Goh, B. H., Yin, W. F., et al. (2014). Diversity and antimicrobial activities of actinobacteria isolated from tropical mangrove sediments in malaysia. *Sci. World J.* 2014:698178. doi: 10.1155/2014/698178

Lee, S. H. (2009). Disulfide and multisulfide antitumor agents and their modes of action. *Arch. Pharm. Res.* 32, 299–315. doi: 10.1007/s12272-009-1300-4

Liu, W., Nonaka, K., Nie, L. P., Zhang, J., Christenson, S. D., Bae, J., et al. (2005). The neocarzinostatin biosynthetic gene cluster from *Streptomyces carzinostaticus* ATCC 15944 involving two iterative type I polyketide synthases. *Chem. Biol.* 12, 293–302. doi: 10.1016/j.chembiol.2004.12.013

Lori, F., Malykh, A., Cara, A., Sun, D., Weinstein, J. N., Lisziewicz, J., et al. (1994). Hydroxyurea as an inhibitor of human immunodeficiency virus-type-1 replication. *Science* 266, 801–805. doi: 10.1126/science.7973634

Lu, C., Zhao, Y., Jia, W. Q., Zhang, H., Qi, H., Xiang, W. S., et al. (2017). A new anthracycline-type metabolite from *Streptomyces* sp NEAU-L3. *J. Antibiot.* 70, 1026–1028. doi: 10.1038/ja.2017.95

Mao, Y. Q., Varoglu, M., and Sherman, D. H. (1999). Molecular characterization and analysis of the biosynthetic gene cluster for the antitumor antibiotic

mitomycin C from *Streptomyces lavendulae* NRRL 2564. *Chem. Biol.* 6, 251–263. doi: 10.1016/s1074-5521(99)80040-4

Martins, M. B., and Carvalho, I. (2007). Diketopiperazines: biological activity and synthesis. *Tetrahedron* 63, 9923–9932. doi: 10.1002/chin.200751231

Meier-Kolthoff, J. P., Auch, A. F., Klenk, H. P., and Goker, M. (2013). Genome sequence-based species delimitation with confidence intervals and improved distance functions. *BMC Bioinformatics* 14:60. doi: 10.1186/1471-2105-14-60

Melvin, W. S., Boros, L. G., Muscarella, P., Brandes, J. L., Johnson, J. A., Fisher, W. E., et al. (1997). Dehydroepiandrosterone-sulfate inhibits pancreatic carcinoma cell proliferation in vitro and in vivo. *Surgery* 121, 392–397. doi: 10.1016/s0039-6060(97)90308-1

Mesbah, M., Premachandran, U., and Whitman, W. B. (1989). Precise measurement of the G+C content of deoxyribonucleic acid by high-performance liquid chromatography. *Int. J. Syst. Bacteriol.* 39, 159–167. doi: 10.1099/00207713-39-2-159

Nafisi, S., Bonsaii, M., Maali, P., Khalilzadeh, M. A., and Manouchehri, F. (2010). Beta-carboline alkaloids bind DNA. *J. Photochem. Photobiol. B* 100, 84–91. doi: 10.1016/j.jphotobiol.2010.05.005

Nobili, S., Lippi, D., Witort, E., Donnini, M., Bausi, L., Mini, E., et al. (2009). Natural compounds for cancer treatment and prevention. *Pharmacol. Res.* 59, 365–378. doi: 10.1016/j.phrs.2009.01.017

Novakova, R., Nunez, L. E., Homerova, D., Knirschova, R., Feckova, L., Rezuchova, B., et al. (2018). Increased heterologous production of the antitumoral polyketide mithramycin A by engineered *Streptomyces lividans* TK24 strains. *Appl. Microbiol. Biotechnol.* 102, 857–869. doi: 10.1007/s00253-017-8642-5

Odds, F. (1981). Biochemical tests for identification of medical bacteria. *J. Clin. Pathol.* 34:572. doi: 10.1128/9781555817435.ch3.17

Ortiz, A., and Sansinenea, E. (2017). Cyclic dipeptides: secondary metabolites isolated from different microorganisms with diverse biological activities. *Curr. Med. Chem.* 24, 2773–2780. doi: 10.2174/0929867324666170623092818

Patel, T., Bronk, S. F., and Gores, G. J. (1994). Increases of intracellular magnesium promote glycodeoxycholate-induced apoptosis in rat hepatocytes. *J. Clin. Invest.* 94, 2183–2192. doi: 10.1172/jci117579

Petro, C., Starnawski, P., Schramm, A., and Kjeldsen, K. U. (2017). Microbial community assembly in marine sediments. *Aquat. Microb. Ecol.* 79, 177–195. doi: 10.3354/ame01826

Picard, K. T. (2017). Coastal marine habitats harbor novel early-diverging fungal diversity. *Fungal Ecol.* 25, 1–13. doi: 10.1016/j.funeco.2016.10.006

Prinsep, M. R., Blunt, J. W., and Munro, M. H. G. (1991). New cytotoxic beta-carboline alkaloids from the marine bryozoan, cribricellina-cribricellina. *J. Nat. Prod.* 54, 1068–1076. doi: 10.1021/np50076a023

Pyaskovskaya, O. N., Kolesnik, D. L., Fedorchuk, A. G., Prochorova, I. V., and Solyanik, G. I. (2016). 2-Deoxy-D-Glucose enhances dichloroacetate antitumor action against lewis lung carcinoma. *Exp. Oncol.* 38, 176–180.

Röttig, A., Atasayar, E., Meierkolthoff, J. P., Spröer, C., Schumann, P., Schauer, J., et al. (2017). *Streptomyces jeddahensis* sp. nov., an oleaginous bacterium isolated from desert soil. *Int. J. Syst. Evol. Microbiol.* 67, 1676–1682. doi: 10.1099/ijsem.0.001839

Richter, M., and Rossello-Mora, R. (2009). Shifting the genomic gold standard for the prokaryotic species definition. *Proc. Natl. Acad. Sci. U.S.A.* 106, 19126–19131. doi: 10.1073/pnas.0906412106

Sansinenea, E., Salazar, F., Jimenez, J., Mendoza, A., and Ortiz, A. (2016). ChemInform abstract: diketopiperazines derivatives isolated from *Bacillus thuringiensis* and *Bacillus endophyticus*, establishment of their configuration by X-Ray and their synthesis. *Tetrahedron Lett.* 57, 2604–2607. doi: 10.1002/chin.201641222

Schinke, C., Martins, T., Queiroz, S. C. N., Melo, I. S., and Reyes, F. G. R. (2017). Antibacterial compounds from marine bacteria, 2010-2015. *J. Nat. Prod.* 80, 1215–1228. doi: 10.1021/acs.jnatprod.6b00235

Ser, H. L., Palanisamy, U. D., Yin, W. F., Chan, K. G., Goh, B. H., and Lee, L. H. (2016a). *Streptomyces malaysiense* sp. nov.: a novel Malaysian mangrove soil actinobacterium with antioxidative activity and cytotoxic potential against human cancer cell lines. *Sci. Rep.* 6:24247. doi: 10.1038/srep24247

Ser, H. L., Palanisamy, U. D., Yin, W. F., Malek, N. A., Chan, K. G., Goh, B. H., et al. (2015). Presence of antioxidative agent, Pyrrolo 1,2-a pyrazine-1,4-dione, hexahydro- in newly isolated *Streptomyces mangrovisoli* sp nov. *Front. Microbiol.* 6:354. doi: 10.3389/fmicb.2015.00354

Ser, H. L., Tan, L. T., Law, J. W. F., Chan, K. G., Duangjai, A., Saokaew, S., et al. (2017). Focused review: cytotoxic and antioxidant potentials of mangrove-derived *Streptomyces*. *Front. Microbiol.* 8:2065. doi: 10.3389/fmicb.2017.02065

Ser, H. L., Tan, T. H., Palanisamy, U. D., Malek, S. N. A., Yin, W. F., Chan, K. G., et al. (2016b). *Streptomyces antioxidans* sp. nov., a novel mangrove soil actinobacterium with antioxidative and neuroprotective potentials. *Front. Microbiol.* 7:899. doi: 10.3389/fmicb.2016.00899

Shen, Y. C., Chang, Y. T., Lin, C. L., Liaw, C. C., Kuo, Y. H., Tu, L. C., et al. (2011). Synthesis of 1-substituted carbazolyl-1,2,3,4-tetrahydro- and carbazolyl-3,4-dihydro-beta-carboline analogs as potential antitumor agents. *Mar. Drugs* 9, 256–277. doi: 10.3390/md9020256

Shirling, E. B., and Gottlieb, D. (1966). Methods for characterization of *Streptomyces species*. *Int. J. Syst. Bacteriol.* 16, 313–340. doi: 10.1099/00207713-16-3-313

Silva, M. M., Savariz, F. C., Silva, E. F., de Aquino, T. M., Sarragiotto, M. H., Santos, J. C. C., et al. (2016). Interaction of beta-carbolines with DNA: spectroscopic studies, correlation with biological activity and molecular docking. *J. Braz. Chem. Soc.* 279, 1558–1568. doi: 10.5935/0103-5053.20160035

Simister, R. L., Antzis, E. W., and White, H. K. (2016). Examining the diversity of microbes in a deep-sea coral community impacted by the Deepwater Horizon oil spill. *Deep Sea Res. Part II Top. Stud. Oceanogr.* 129, 157–166. doi: 10.1016/j.dsr2.2015.01.010

Skehan, P., Storeng, R., Scudiero, D., Monks, A., McMahon, J., Vistica, D., et al. (1990). New colorimetric cytotoxicity assayfor anticancer-drug screeing. *J. Natl. Cancer Inst.* 82, 1107–1112. doi: 10.1093/jnci/82.13.1107

Stearns, B., Losee, K. A., and Bernstein, J. (1963). Hydroxyurea. A new type of potential antitumor agent. *J. Med. Chem.* 6:201. doi: 10.1021/jm00338a026

Stefanelli, C., Bonavita, F., Stanic, I., Pignatti, C., Flamigni, F., Guarnieri, C., et al. (1999). Spermine triggers the activation of caspase-3 in a cell-free model of apoptosis. *FEBS Lett.* 451, 95–98. doi: 10.1016/s0014-5793(99)00549-9

Sunagawa, S., Coelho, L. P., Chaffron, S., Kultima, J. R., Labadie, K., Salazar, G., et al. (2015). Structure and function of the global ocean microbiome. *Science* 348:1261359. doi: 10.1126/science.1261359

Tamura, K., Peterson, D., Peterson, N., Stecher, G., Nei, M., and Kumar, S. (2011). MEGA5: molecular evolutionary genetics analysis using maximum likelihood, evolutionary distance, and maximum parsimony methods. *Mol. Biol. Evol.* 28, 2731–2739. doi: 10.1093/molbev/msr121

Tan, R. X., Jensen, P. R., Williams, P. G., and Fenical, W. (2004). Isolation and structure assignments of rostratins A-D, cytotoxic disulfides produced by the marine-derived fungus *Exserohilum rostratum*. *J. Nat. Prod.* 67, 1374–1382. doi: 10.1021/np049920b

Tindall, B. J. (1990). Lipid-composition of *Halobacterium lacusprofundi*. *FEMS Microbiol. Lett.* 66, 199–202. doi: 10.1016/0378-1097(90)90282-u

Toledo, A., Yamaguchi, J., Wang, J. Y., Bass, B. L., Turner, D. J., and Strauch, E. D. (2004). Taurodeoxycholate stimulates intestinal cell proliferation and protects against apoptotic cell death through activation of NF-kappa B. *Dig. Dis. Sci.* 49, 1664–1671. doi: 10.1023/b:ddas.0000043383.96077.99

Trigos, A., Reyna, S., Gutierrez, M. L., and Sanchez, M. (1997). Diketopiperazines from cultures of the fungus *Colletotrichum gloesporoides*. *Nat. Prod. Lett.* 11, 13–16. doi: 10.1080/10575639708043751

Wang, H. F., Li, Q. L., Xiao, M., Zhang, Y. G., Zhou, X. K., Rao, M. P. N., et al. (2017). *Streptomyces capparidis* sp. nov., a novel endophytic actinobacterium isolated from fruits of *Capparis spinosa* L. *Int. J. Syst. Evol. Microbiol.* 67, 133–137. doi: 10.1099/ijsem.0.001586

Wayne, L. G., Brenner, D. J., Colwell, R. R., Grimont, P. A. D., Kandler, O., Krichevsky, M. I., et al. (1987). Report of the ad-hoc-committee on reconciliation of approaches to bacterial systematics. *Int. J. Syst. Bacteriol.* 37, 463–464. doi: 10.1099/00207713-37-4-463

Wei, Y. J., Zhang, L., Zhou, Z. H., and Yan, X. (2018). Diversity of gene clusters for polyketide and nonribosomal peptide biosynthesis revealed by metagenomic analysis of the yellow sea sediment. *Front. Microbiol.* 9:295. doi: 10.3389/fmicb.2018.00295

Weisburg, W. G., Barns, S. M., Pelletier, D. A., and Lane, D. J. (1991). 16S ribosomal DNA amplification for phylogenetic study. *J. Bacteriol.* 173, 697–703. doi: 10.1128/jb.173.2.697-703.1991

Williams, S. T., Goodfellow, M., Alderson, G., Wellington, E. M. H., Sneath, P. H. A., and Sackin, M. J. (1983). Numerical classification of Streptomyces and related genera. *J. Gen. Microbiol.* 129, 1743–1813. doi: 10.1099/00221287-129-6-1743

Wu, Y. H., Cheng, H., Huo, Y. Y., Jin, X. B., Wang, C. S., and Xu, X. W. (2017). *Henriciella pelagia* sp. nov., isolated from seawater. *Int. J. Syst. Evol. Microbiol.* 67, 3020–3025. doi: 10.1099/ijsem.0.002066

Yang, L., Tan, R. X., Wang, Q., Huang, W. Y., and Yin, Y. X. (2002). Antifungal cyclopeptides from *Halobacillus litoralis* YS3106 of marine origin. *Tetrahedron Lett.* 43, 6545–6548. doi: 10.1016/s0040-4039(02)01458-2

Yoon, S. H., Ha, S. M., Kwon, S., Lim, J., Kim, Y., Seo, H., et al. (2017). Introducing EzBioCloud: a taxonomically united database of 16S rRNA gene sequences and whole-genome assemblies. *Int. J. Syst. Evol. Microbiol.* 67, 1613–1617. doi: 10.1099/ijsem.0.001755

Zaffaroni, N., Villa, R., Silvestro, L., Sanfilippo, O., and Silvestrini, R. (1990). Cytotoxic activity of azelaic acid against huamn-melanoma primary cultures and established cell-lines. *Anticancer Res.* 10, 1599–1602.

Zahedi, K., Bissler, J. J., Wang, Z. H., Josyula, A., Lu, L., Diegelman, P., et al. (2007). Spermidine/spermine N^1-acetyltransferase overexpression in kidney epithelial cells disrupts polyamine homeostasis, leads to DNA damage, and causes G(2) arrest. *Am. J. Physiol. Cell Physiol.* 292, C1204–C1215. doi: 10.1152/ajpcell.00451.2006

Zhang, X.-Q., Zhang, W.-J., and Wei, B.-P. (2010). *Meiothermus cateniformans* sp. nov., a slightly thermophilic species from north-eastern China. *Int. J. Syst. Evol. Microbiol.* 60, 840–844. doi: 10.1099/ijs.0.007914-0

Zhang, Z. G., Yu, X. Y., Wang, Z., Wu, P., and Huang, J. (2015). Anthracyclines potentiate anti-tumor immunity: a new opportunity for chemoimmunotherapy. *Cancer Lett.* 369, 331–335. doi: 10.1016/j.canlet.2015.10.002

Zhang, X. Q., Sun, C., Wang, C. S., Zhang, X., Zhou, X., Wu, Y. H., et al. (2015). *Sinimarinibacterium flocculans* gen. nov., sp nov., a gammaproteobacterium from offshore surface seawater. *Int. J. Syst. Evol. Microbiol.* 65, 3541–3546. doi: 10.1099/ijsem.0.000452

Zhao, Y., Hao, X. J., Lu, W., Cai, J. C., Yu, H., Sevenet, T., et al. (2002). Syntheses of two cytotoxic sinapyl alcohol derivatives and isolation of four new related compounds from *Ligularia nelumbifolia*. *J. Nat. Prod.* 65, 902–908. doi: 10.1021/np0200257

Zhong, Z. P., Liu, Y., Liu, H. C., Wang, F., Zhou, Y. G., and Liu, Z. P. (2014). *Roseibium aquae* sp nov., isolated from a saline lake. *Int. J. Syst. Evol. Microbiol.* 64, 2812–2818. doi: 10.1099/ijs.0.065508-0

Zhong, Z. P., Liu, Y., Wang, F., Zhou, Y. G., Liu, H. C., Liu, Q., et al. (2016). *Planktosalinus lacus* gen. nov., sp nov., a member of the family *Flavobacteriaceae* isolated from a salt lake. *Int. J. Syst. Evol. Microbiol.* 66, 2084–2089. doi: 10.1099/ijsem.0.000997

Zhou, Z. F., Wang, X., Zhang, H., Sun, J. Y., Zheng, L. H., Liu, H. C., et al. (2015). Chromopeptide A, a highly cytotoxic depsipeptide from the marine sediment-derived bacterium *Chromobacterium* sp. HS-13-94. *Acta Pharm. Sin. B* 5, 62–66. doi: 10.1016/j.apsb.2014.11.001

Conflict of Interest Statement: The authors declare that the research was conducted in the absence of any commercial or financial relationships that could be construed as a potential conflict of interest.

Copyright © 2018 Chen, Ye, Wang, Zhang, Wu, Debnath, Ma, Wang and Wu. This is an open-access article distributed under the terms of the Creative Commons Attribution License (CC BY). The use, distribution or reproduction in other forums is permitted, provided the original author(s) and the copyright owner(s) are credited and that the original publication in this journal is cited, in accordance with accepted academic practice. No use, distribution or reproduction is permitted which does not comply with these terms.

frontiers in Marine Science

ORIGINAL RESEARCH
published: 06 August 2018
doi: 10.3389/fmars.2018.00263

Bacterial Response to Permafrost Derived Organic Matter Input in an Arctic Fjord

Oliver Müller[1]*, *Lena Seuthe*[2], *Gunnar Bratbak*[1] and *Maria L. Paulsen*[1]

[1] Department of Microbiology, University of Bergen, Bergen, Norway, [2] Department of Arctic and Marine Biology, UiT – The Arctic University of Tromsø, Tromsø, Norway

The warming of the Arctic causes increased riverine discharge, coastal erosion, and the thawing of permafrost. Together, this is leading to an increased wash out of terrestrial dissolved organic matter (tDOM) into the coastal Arctic ecosystems. This tDOM may be anticipated to affect both carbon and nutrient flow in the microbial food web and microbial community composition, but there are few studies detailing this in Arctic marine ecosystems. We tested the effects of tDOM on the bacterial community composition and net-growth by extracting DOM from the active layer of permafrost soil and adding the aged tDOM concentrate to a natural microbial fjord community (Kongsfjorden, NW Svalbard). This resulted in an increased carbon load of 128 μM DOC in the tDOM treatment relative to the control of 83 μM DOC. We observed changes in community composition and activity in incubations already within 12 h where tDOM was added. Flow cytometry revealed that predominantly large bacteria increased in the tDOM treated incubations. The increase of this group correlated with the increase in relative abundance of the genus *Glaciecola* (Gammaproteobacteria). *Glaciecola* were initially not abundant in the bacterial community (0.6%), but their subsequent increase up to 47% after 4 days upon tDOM addition compared to 8% in control incubations indicates that they are likely capable of degrading permafrost derived DOM. Further, according to our experimental results we hypothesize that the tDOM addition increased bacterivorous grazing by small protists and thus tDOM might indirectly also effect higher trophic levels of the microbial food web.

Keywords: dissolved organic matter, Arctic, terrestrial run-off, permafrost, tDOM, Kongsfjorden, microbial community composition, Glaciecola

OPEN ACCESS

Edited by:
Veronica Molina, Universidad de Playa Ancha, Chile

Reviewed by:
Eva Ortega-Retuerta, UMR7621 Laboratoire d'Océanographie Microbienne (LOMIC), France
Claudia Piccini, Instituto de Investigaciones Biológicas Clemente Estable (IIBCE), Uruguay

***Correspondence:**
Oliver Müller
oliver.muller@uib.no

Specialty section:
This article was submitted to Aquatic Microbiology, a section of the journal Frontiers in Marine Science

Received: *28 February 2018*
Accepted: *16 July 2018*
Published: *06 August 2018*

Citation:
Müller O, Seuthe L, Bratbak G and Paulsen ML (2018) Bacterial Response to Permafrost Derived Organic Matter Input in an Arctic Fjord. Front. Mar. Sci. 5:263. doi: 10.3389/fmars.2018.00263

INTRODUCTION

The Arctic is experiencing a warming at nearly twice the global rate, with drastic changes for the ecosystem (Trenberth and Josey, 2007; Screen and Simmonds, 2010; Vincent, 2010). Higher sea surface temperatures, melting sea ice, and increased freshwater input from large Arctic rivers, transporting nutrients, and terrestrial organic matter into the ocean, have multiple implications for the marine carbon cycle (Li et al., 2009; Doney et al., 2012; Fichot et al., 2013; Holmes et al., 2013; El-Swais et al., 2015). Higher temperatures are on the one hand responsible for a decreasing sea ice cover, which in turn may enhance primary production and thus the biological carbon pump (CO_2 burial), but on the other hand could also increase the rate of bacterial degradation of phytoplankton derived dissolved organic matter (DOM) (CO_2 production) (Wohlers et al., 2009). This bacterial

transformation of phytoplankton derived DOM might lead to the accumulation of more complex humic-like organic matter via the microbial carbon pump (Jiao et al., 2010).

In the Arctic, another source of DOM comes from permafrost soil organic matter and enters the Arctic Ocean via rivers (Feng et al., 2013; Holmes et al., 2013). Estimations show that mobilization of DOM has increased up to 6% from 1985 to 2004 (Feng et al., 2013) and will further increase under the current warming climate (Amon et al., 2012).Yearly, about 3,300 km^3 of freshwater stream into the Arctic Ocean and influence stratification, light absorption, surface temperature, gas exchange, productivity, and carbon sequestration (Rachold et al., 2004). This input is often characterized by a high dissolved organic carbon (DOC) concentration, reaching more than 1,000 $\mu mol\ kg^{-1}$, compared to open ocean concentrations of around 80 $\mu mol\ kg^{-1}$ (Dittmar and Kattner, 2003; Hansell et al., 2009; Stedmon et al., 2011). The quality of the DOC has in some studies been described to be mainly refractory (Opsahl et al., 1999; Dittmar and Kattner, 2003; Xie et al., 2012), while other studies showed that up to 40% can be degraded within weeks up to months (Hansell, 2004; Holmes et al., 2008; Vonk et al., 2013; Sipler et al., 2017a). Thus, it is still disputed whether Arctic tDOM can represent an important carbon source for marine bacteria, leading to increased CO_2 production and how this may affect the marine trophic network via the microbial loop.

Several studies have examined the ability of bacteria to degrade the seasonally available phytoplankton derived DOM and found that an increase of such carbon sources influences both the structure and the activity of the bacterial community (Pinhassi et al., 2004; Sapp et al., 2007; Teeling et al., 2012). Especially a versatile group of Gammaproteobacteria, belonging to the order *Alteromonadales,* responds immediately both in abundance and activity, when phytoplankton derived DOM becomes available (Eilers et al., 2000; McCarren et al., 2010; Pedler et al., 2014; Beier et al., 2015; von Scheibner et al., 2017). Only few studies have investigated the effects of terrestrial derived DOM on marine microbial community structure and activity (Herlemann et al., 2014, 2017; Blanchet et al., 2017; Traving et al., 2017), of which even less have been conducted in the coastal Arctic (Sipler et al., 2017a). Common for all studies is an observed shift in bacterial community structure due to the addition of tDOM. There is a need to understand how this community shift might affect higher trophic levels in order to better understand climate change impacts on the marine Arctic ecosystem. A higher bacterial activity due to the degradation of tDOM might cause a higher turnover within the microbial loop and therewith increased CO_2 production, but ultimately depends on the bacterial growth efficiency. Increased carbon availability might also enhance the competition between bacteria and phytoplankton for inorganic nutrients and indirectly disadvantage larger phytoplankton (Thingstad et al., 2008; Sipler et al., 2017b). Thus, high tDOM input may decrease primary production in coastal Arctic areas.

We here studied the impact of permafrost-derived DOM on an Arctic fjord microbial community using 16S rRNA amplicon sequencing and followed the changes over the course of a nine-day incubation experiment. We hypothesized that the increased organic matter input, as a consequence of increased run-off from land, would provide a potential source of organic matter for fjord microbial communities. If bioavailable, this tDOM will stimulate the growth of some fast-responding bacterial groups that were initially underrepresented and increase in abundance over time. In particular, we were interested in answering two questions (1) how tDOM might alter the fjord bacterial community composition and (2) how tDOM might affect the growth and size of bacteria and subsequently protist grazers. This study thus aims to improve our understanding of the implications of a warmer Arctic, influenced by increased run-off from land, on coastal microbial communities.

MATERIALS AND METHODS

Preparation of Aged Permafrost-Derived tDOM Stock Solution

Active layer permafrost soil from 50 cm depth, just above the frozen permafrost table, was sampled in Adventdalen, Svalbard (78.19 N, 15.89 E), and mixed with unfiltered water from the nearby Adventfjorden (1 m depth) in the ratio 600 g soil to 1 L water. The mix was stored in the dark for 30 days at 4°C to degrade the predominantly labile compounds, thus producing "aged tDOM" as has been done in similar studies (Eiler et al., 2003). The rationale behind using an aged tDOM stock was to increase resemblance to the organic matter that reaches the coastal systems, as the most labile compounds will be degraded during its transportation from soil to coastal waters (Lobbes et al., 2000). Before being added to tDOM incubations, the stock solution was filtered through 0.2 µm polycarbonate filters, ensuring that only dissolved organic matter was present in the tDOM stock solution. To test the character of DOM in the tDOM-solution relative to the control, the fluorescent properties were examined during an earlier analysis, performed in 2014. Here five fluorescence components (two humic-like and three amino-like) were described following the method explained in Stedmon and Markager (2005). The averaged intensity (given in Raman units) of these components are given in **Table S1**. The intensity of the humic-like substances was two-fold higher in the tDOM-stock relative to the control (0.2 µm filtered Atlantic water) and further one of the amino-like components was 100 times higher in the tDOM stock solution. Since we did not characterize the DOM composition at the end of the experiment, we cannot say what exact compounds were consumed or produced throughout our incubations. The rationale behind measuring the DOM components in the beginning was to ensure that more complex compounds were enriched in the tDOM-solution. The results strongly indicate that the character of the DOM was significantly different in the tDOM treatment compared to the control.

Study Site and Experimental Set-Up

Kongsfjorden is a 26 km long fjord, 6 to 14 km wide and includes two tidewater-glaciers, Kronebreen and Kongsvegen (**Figure 1A**). Water samples for incubations were collected on the 29th of June in 2015 from the center of the fjord near Kings Bay (78.95°N, 11.93°E) at 40 m depth (**Figure 1A**). The water was

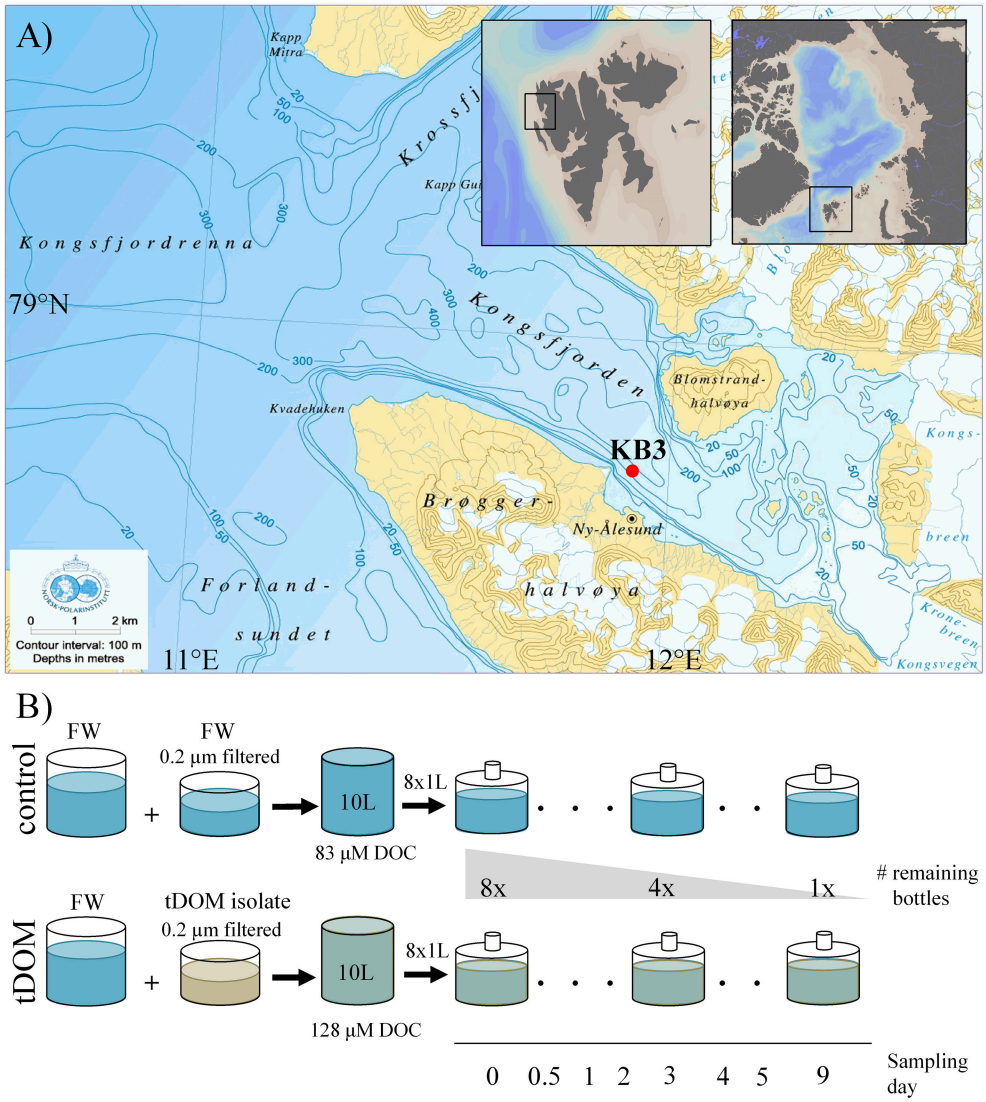

FIGURE 1 | (A) Study area in northwest Svalbard (78.95°N, 11.93°E) showing the sampling location in Kongsfjorden (red circle). © Norwegian Polar Institute and small maps were created using Ocean Data View (Schlitzer, 2011). **(B)** Illustration of the experimental design showing that for both tDOM treatment and control eight bottles with the same starting condition were incubated for different periods (from 12 h up to 9 days). One bottle was harvested at each sampling point to analyse the bacterial community composition. Bacterial abundance was measured using flow cytometry for samples at the beginning of the experiment, including the fjord water (8.1×10^5 mL^{-1}), the 0.2 µm filtered fjord water (2.8×10^4 mL^{-1}), and the tDOM isolate (3.2×10^4 mL^{-1}) and over the course of the incubation in both treatment and control bottles (number of replicates was dependent on the number of remaining bottles). FW, fjord water; tDOM, solution of terrigenous dissolved organic matter from permafrost; DOC, dissolved organic carbon.

filtered through pre-combusted GFC filters (1.2 µm) to reduce the presence of protists. The tDOM-stock solution had a carbon concentration of 190 µM DOC and was mixed in the ratio of 1:2.5 with fjord water (83 µM DOC) and aliquoted into eight 1 L air-tight glass bottles (**Figure 1B**). Filtered (0.2 µm) fjord water was added in the same ratio to the eight control bottles. The final DOC concentration was 1.5 times higher in the tDOM treatment incubations (128 µM) than in the control incubations (83 µM). The elevated DOC concentration in the tDOM treatment reflects ranges of natural, elevated concentrations near the sample site in Kongsfjorden (Zhu et al., 2016). The 16 bottles, 8 treatment and 8 controls were incubated in the dark at 2°C. Samples for bacterial community composition were obtained after 0, 0.5, 1, 2, 3, 4, 5, and 9 days of incubation by harvesting one treatment and one control bottle, each representing an independent incubation, as described below. The rationale behind the experimental design and the statistical power of such an un-replicated time series sampling strategy are evaluated in the Supplementary Material (**Figures S3**, **S4**). Samples (6 mL) for measurements of bacterial abundance via flow-cytometry were collected as replicates according to the number of bottles remaining at each respective sampling point (e.g., 8 replicates at t0, 4 at d4 and 1 at

d9). Both bacterial abundance and community composition were also analyzed for the untreated 40 m fjord sample and 0.2 μm filtered tDOM-stock solution.

Bacterial Enumeration Using Flow Cytometry

The abundance of bacteria, virus and heterotrophic nanoflagellates (HNF) were determined on an Attune® Acoustic Focusing Flow Cytometer (Applied Biosystems by Life technologies) with a syringe-based fluidic system and a 20 mW 488 nm (blue) laser. Triplicate samples of 2 mL were fixed with glutaraldehyde (0.5% final conc.) at 4°C for a minimum of 30 min, flash frozen in liquid nitrogen and stored at −80°C. Samples were first thawed and diluted x10 with 0.2 μm filtered TE buffer (Tris 10 mM, EDTA 1 mM, pH 8), stained with a green fluorescent nucleic acid dye (SYBR Green I; Molecular Probes, Eugene, Oregon, USA) and then incubated for 10 min at 80°C in a water bath (Marie et al., 1999). Samples were counted at a low flow rate of 25 μL min^{-1} and a minimum volume of 100 μL. Bacteria were discriminated on a biparametric plot of green florescence (BL1) vs. red florescence (BL3).

Additionally, these plots allowed to distinguish between low nuclear acid (LNA) and high nuclear acid (HNA) bacteria, virus, and a subgroup we here term "large bacteria." Heterotrophic nanoflagellates (HNF) were measured at a high flow rate (500 μL min^{-1}) according to Zubkov et al. (2007). Pico-and nano-sized phytoplankton were counted directly after thawing and the various groups discriminated based on their red fluorescence (BL3) vs. orange fluorescence (BL2) (Paulsen et al., 2016).

DNA Extraction, PCR Amplification, and Amplicon Sequencing

The bacterial biomass for molecular analysis was collected by filtering ca. 1 L onto 0.22 μm Millipore® Sterivex filters (Merck-Millipore), which were flash frozen in liquid nitrogen and stored at −80°C. DNA and RNA were simultaneously extracted from the Sterivex filters using the AllPrep DNA/RNA Mini Kit (Qiagen, Hilden, Germany) according to the manufacturer's instructions. In this study, only RNA was used in order to investigate changes in the active community. Before PCR amplification, RNA was treated with the DNA-free DNA Removal kit (Invitrogen, CA, USA). Subsequently, 10 ng of DNA-free RNA was reverse transcribed using the SuperScript III First-Strand Synthesis System for RT-PCR (Invitrogen), according to the manufacturer's instructions. Amplification of cDNA (reverse transcribed RNA), targeting the bacterial/archaeal 16S rRNA gene V4 hypervariable region, was performed using a two-step nested PCR approach with primers 519F (CAGCMGCCGCGGTAA; Øvreås et al., 1997) and 806R (GGA CTACHVGGGTWTCTAAT; Caporaso et al., 2011b). In brief, the first PCR step was performed in triplicates. Samples were amplified, comprising 10 ng cDNA, 10 μL HotStarTaq Master Mix (Qiagen), 0.5 μM of each primer and nuclease-free water. PCR reaction conditions were as follows: initial denaturation of 15 min at 95°C, followed by 25 cycles of 95°C for 20 s, 55°C for 30 s, and 72°C for 30 s and a final extension step of 72°C for 7 min. After triplicate PCR products were pooled, the DNA Clean & Concentrator-5 kit (Zymo Research Corporation, CA, USA) was used for purification. During the second PCR step, 10 ng of pooled PCR product, 25 μL HotStarTaq Master Mix, 0.5 μM of each nested primer (containing a unique eight-nucleotide barcode) were mixed with nuclease-free water to a reaction volume of 50 μL. PCR reaction conditions were as follows: initial denaturation of 15 min at 95°C, followed by 15 cycles of 95°C for 20 s, 62°C for 30 s, 72°C for 30 s, and a final extension step of 72°C for 7 min. Final PCR products were purified using Agencourt AMPure XP Beads (Beckman Coulter Inc., CA, USA) and pooled in equimolar amounts. Before sequencing, the quality, and concentration of the amplicon pool were assessed by agarose gel electrophoresis and a Qubit 3.0 Fluorometer, respectively. The final amplicon library was sequenced at the Norwegian Sequencing Centre (Oslo, Norway) using their MiSeq platform (MiSeq Reagent Kit v2, Illumina, CA, USA). All Illumina sequencing data is available at the European Nucleotide Archive (ENA) under study accession number PRJEB25031.

16S rRNA Gene Sequence Analysis

Illumina Paired-end sequence data was processed using different bioinformatic tools incorporated on a QIIME-processing platform (Caporaso et al., 2011a). In short, FASTQ files were quality end-trimmed at a phred quality score $\geq$ 24 using Trimmomatic (Bolger et al., 2014) and merged using PANDAseq (Masella et al., 2012), while all reads <200 bp were removed. A total of 1,916,574 sequences were retrieved across 18 samples and two sequencing controls. Those sequences were used to select prokaryotic OTUs at a sequence similarity threshold of 97%, using a de novo uclust (Edgar, 2010) OTU clustering method and taxonomy assigned using the Silva 111 reference database (Quast et al., 2013). After removal of singletons and unassigned OTUs, sequences were rarefied to 10,000 reads per sample, with a total of 15,513 unique OTUs at 97% sequence identity. Rarefaction curves were calculated using QIIME's alpha rarefaction script and showed that sequencing coverage was sufficiently high, as samples approached an asymptote. The phylogenetic data was then used to calculate relative abundance at different taxonomical levels. When combined with absolute bacterial abundance data from flow cytometer measurements, the absolute abundance of taxa can be calculated. For this the bacterial abundance in cells per mL is multiplied with the relative abundance of the taxa of interest.

Indicator OTU Analysis

Calculations to identify indicator OTUs associated with the treatment of tDOM addition were performed using the "indicspecies" package (De Cáceres and Legendre, 2009) included in the statistical software R 3.2.3 (R Development Core Team, 2012) and the script "otu_category_significance.py" within the QIIME-processing platform (Caporaso et al., 2011a). Both tools can be used to assess statistically significant differences between OTU abundances and defined groups. We defined groups according to the experimental strategy in tDOM treatment and control. The analysis included only samples after 2 days of the

experiment when abundances of *Pseudoalteromonas* sequences, an artifact of the experimental set-up, were greatly reduced.

Statistical Analysis

The statistical power of the experimental design is evaluated in detail in the **Supplementary Material**. The significance of changes in relative abundance of certain taxa can be calculated by comparing the slopes of regression analysis of treatment and control incubations. Correlations between bacterial abundance and community composition were calculated using the Pearson correlation coefficient (Pearson's r) and were carried out using GraphPad Prism v 6.01 for Windows (GraphPad Software, CA, USA).

Calculations to Estimate Bacterial and HNF Carbon Turnover

Calculations of carbon turnover are based on measurements of abundance and growth efficiency values for bacteria ($_B$) and HNF ($_{HNF}$) from literature. First carbon accumulation (CA) was calculated from the difference in cell abundance over time (ΔA) and values of fixed carbon content per cell for bacteria (0.02 pg C per cell; Lee and Fuhrman, 1987) and HNF (3.8 pg C per cell; Børsheim and Bratbak, 1987) from literature (1). The release of carbon as CO_2 via respiration (R) is further calculated from the estimated CA values and expected growth efficiency of bacteria (10%; Kritzberg et al., 2010; Middelboe et al., 2012; Paulsen et al., 2017) and HNF (30%; Fenchel, 1982) (2).

$$\begin{aligned} \mathrm{CA}_B\left[\mu\mathrm{g\ C}\right] &= \Delta\mathrm{A}_B{*}2{*}10^{-8}\mu g\ \mathrm{C} \\ \mathrm{CA}_{HNF}\left[\mu\mathrm{g\ C}\right] &= \Delta\mathrm{A}_{HNF}{*}3.8{*}10^{-6}\mu\mathrm{g\ C} \end{aligned} \quad (1)$$

$$\begin{aligned} \mathrm{R}_B\left[\mu\mathrm{g\ C}_{CO_2}\right] &= \left(\frac{\mathrm{CA}_B}{0.1}\right){*}0.9 \\ \mathrm{R}_{HNF}\left[\mu\mathrm{g\ C}_{CO_2}\right] &= \left(\frac{\mathrm{CA}_{HNF}}{0.3}\right){*}0.7 \end{aligned} \quad (2)$$

RESULTS

tDOM Effect on Bacterial Growth

During the 9-day incubation period the bacterial net-growth was documented (**Figure 2**). The initial fjord water contained 8.13×10^5 bacteria mL^{-1} and when mixed with either the aged tDOM-solution (tDOM treatment) or 0.22 µm filtered fjord water (control), this concentration was diluted to an average abundance of 4.32×10^5 or 4.19×10^5 mL^{-1}, respectively (**Figure 2A**). After a lag phase during the first 24 h, we observed net-growth in both treatment and control. The bacterial abundance (BA) increased at twice the rate in the tDOM treatment between day 1 and 4 and the BA was on average 24% higher in the tDOM treatment than in the control during the first 4 days. After day 5, a different pattern emerged. While bacteria continued to grow in the control incubations reaching 4.32×10^6 mL^{-1} by day 9, we observed a significant decline of 63% in BA from 1.76×10^6 mL^{-1} (5 d) to 6.51×10^5 mL^{-1} (9 d) in the incubations with tDOM addition (**Figure 2A**).

The group of total bacteria was divided into three subgroups, "LNA," "HNA," and "large bacteria" within the HNA group, to investigate whether a specific group is connected to the increase or decrease in BA (**Figures 2B–D**). The LNA group showed no differences in abundance between treatment and control over the 9 days and stayed overall stable, ranging between 1.78×10^5 and 4.04×10^5 mL^{-1} (**Figure 2B**). In contrary, the HNA group showed significant correlations ($r = 0.99$; $p < 0.0001$) with the increase in BA, including the same differences between treatment and control described earlier (**Figure 2C**). At day 3 we observed a new group on the flow cytometer plots within the HNA group, which we here term "large bacteria" (**Figure 3**). This group was well-defined in tDOM treatments where it started with low values of 1.5×10^4 mL^{-1} (day 2) and reached up to 1.36×10^6 mL^{-1} at day 5, thereby contributing to more than 77% of the BA (**Figure 2D**).

Virus abundance was on average one order of magnitude higher than bacteria ranging from 2.58×10^6 mL^{-1} to 1.56×10^7 mL^{-1} and followed the changes observed for BA in both treatment and control (**Figure 2E**). Due to the pre-filtration of the fjord water through 1.2 µm GFC filters, the abundance of small protists was substantially reduced from 600 mL^{-1} in the fjord water to 16 ± 2 mL^{-1} in both treatment and control until day 6 (**Figure 2F**). At day 9, the abundance of HNF reached 651 mL^{-1} in the incubation where tDOM was added, while it remained low in the control (47 mL^{-1}). Picophytoplankton were additionally enumerated throughout the incubation period to confirm that autotrophic production did not contribute to the carbon pool. Abundances were reduced from 2,056 mL^{-1} in fjord water to <100 mL^{-1} at the beginning of the experiment and remained low (<150 mL^{-1}).

tDOM Effect on Community Composition

The fjord water used to set up the incubations was taken from 40 m depth and was characterized as Atlantic water with a salinity of 34.6 and temperature of 4°C. The analysis of the untreated Atlantic water showed a high abundance of the phylum Proteobacteria (96.5%) (**Figure 4A**). Gammaproteopbacteria were dominating (±76.2%), followed by Alphaproteobacteria (±14.9%) and Betaproteobacteria (±3.0%). Due to the high diversity within the different Proteobacteria classes, 40% of all sequences at genus level were categorized as "Other" (**Figure 4A**).

Community composition at the beginning of the experiment was similar in the control and the tDOM treatment, with around 30–50% of the sequences resembling the *in situ* fjord community and all other sequences belonging to the genus *Pseudoalteromonas*. Sequences belonging to this genus, possibly introduced with the addition of 0.22 µm filtered tDOM solution and 0.22 µm filtered fjord water, decreased within 4 days from up to 70 to 4% in the treatment and from 30 to 3% in the control incubations. With increasing incubation time, changes could be attributed to the increase of certain genera. We observed a substantial increase in relative abundance of *Glaciecola, Marinomonas,* and *Colwellia* in the treatment experiments. In the control incubations, it was predominantly *Colwellia* that increased in relative abundance and to a lesser extend *Glaciecola*, *Marinomonas,* and *Psychromonas*. *Glaciecola* increased from 1.5 to 47.1% on day 5 in the incubations where tDOM was added, while the abundance in the controls increased only up to 7.9%. A Simper analysis showed in agreement, that predominantly the changes in *Glaciecola* relative abundance contributed, with up to 40% (at day 4), for the differences caused by the tDOM addition.

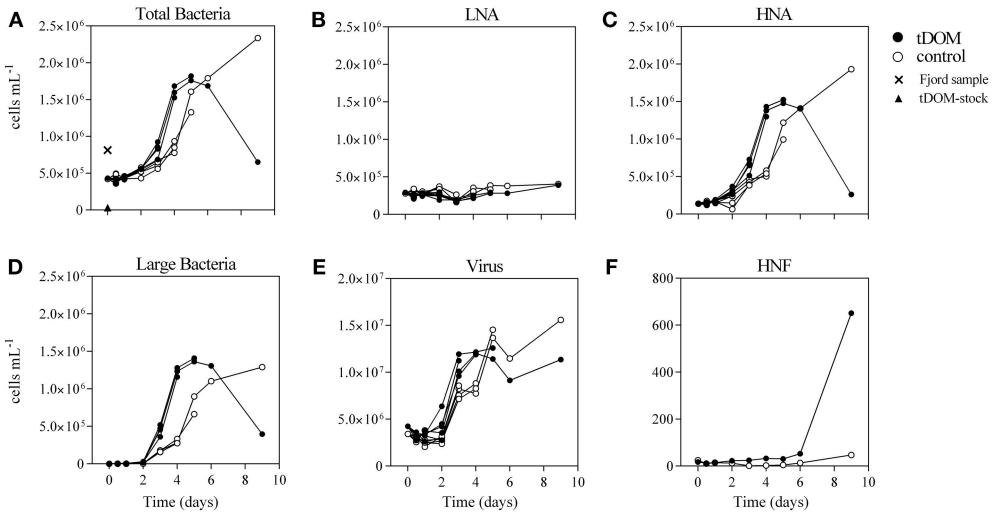

FIGURE 2 | Flow cytometer counts over the course of the experiment in cells mL^{-1} of **(A)** Total bacteria; **(B)** low nucleic acid (LNA) containing bacteria; **(C)** high nucleic acid (HNA) containing bacteria; **(D)** a group of large bacteria; **(E)** Virus; **(F)** and heterotrophic nanoflagellates (HNF). Treatment incubations with added tDOM are illustrated as black circles and control incubations as open circles. The bacterial abundance of the untreated fjord sample and of the 0.2 µm filtered tDOM-stock solution is indicated as cross and triangle, respectively. The different lines represent the sample replicates, which declined over the course of the experiment depending on the number of remaining bottles (e.g., eight at t0, four at day 3 and one at day 9).

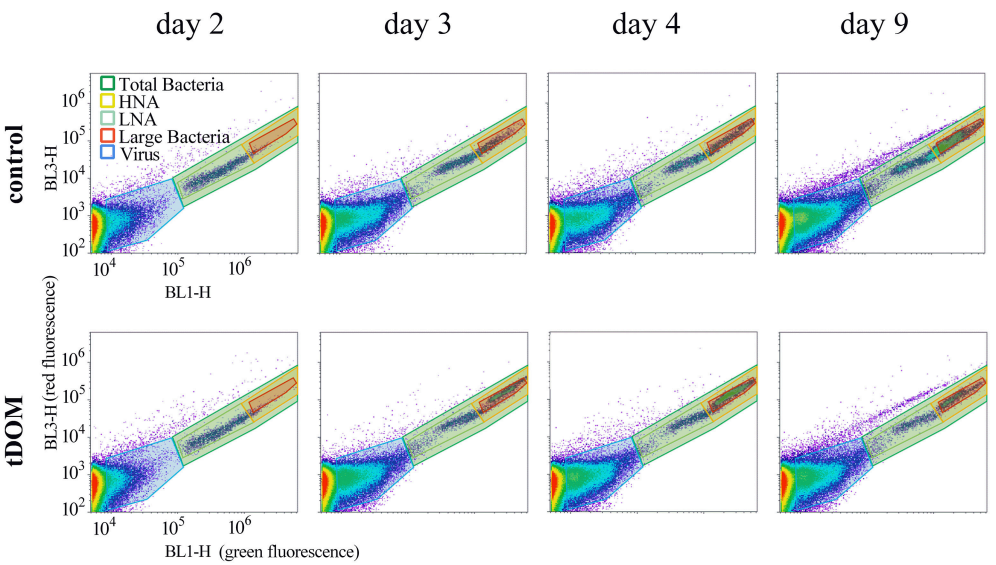

FIGURE 3 | Flow cytometer plots of measurements from day 2 to 9 showing the changes in bacterial abundance and the subgroups within, illustrating the increase in large bacteria in the tDOM treatment. HNA, High nucleic acid containing bacteria; LNA, Low nucleic acid containing bacteria.

We analyzed the effect of tDOM addition on the community structure by combining the relative abundance of bacterial community composition and absolute abundance of bacterial counts obtained from sequencing data and flow cytometer counts, respectively (**Figure 4B**). Using this estimation of absolute species abundance, the *Glaciecola* abundance increased two-fold within the first 12 h and 138-fold after 4 days relative to the beginning (**Figure 4B**). At day 4, *Glaciecola* abundance was 90.6% higher in tDOM treatment incubations than in control incubations. The abundance of *Marinomonas* increased 92-fold after 5 days and was up to 93.8% higher in incubations with added tDOM than in controls (**Figure 4B**). Both genera, *Glaciecola* and *Marinomonas*, showed significant ($p = 0.006$ and $p = 0.018$) responses due to the addition of tDOM. Only in the tDOM treatment incubations *Glaciecola* abundance significantly correlated (r=0.77; p=0.03) with the abundance of large bacteria (**Figure S1**). In the control incubations it was only *Colwellia* abundance that correlated significantly ($r = 0.83$; $p = 0.01$) with

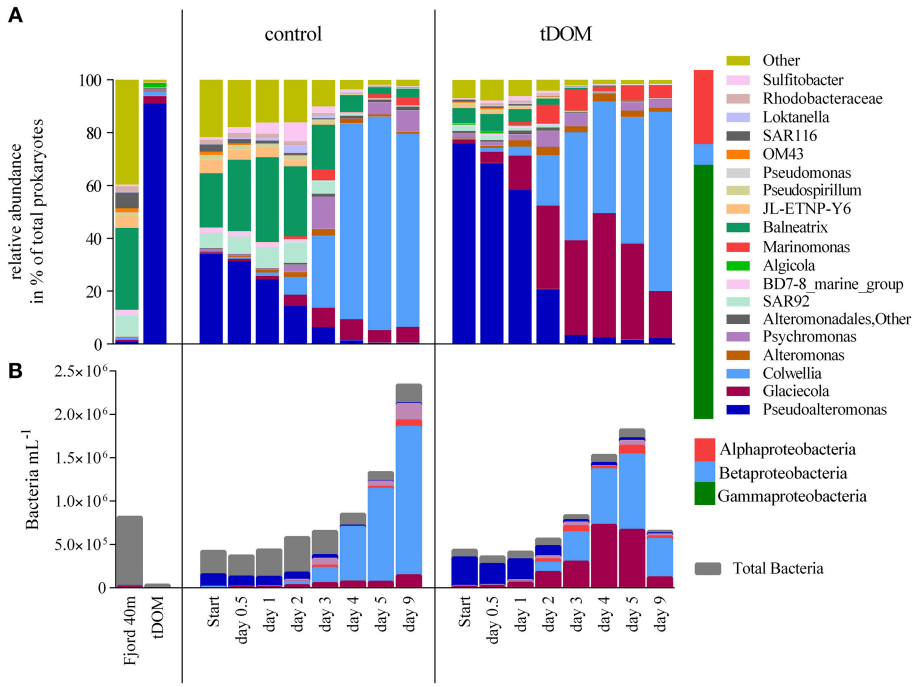

FIGURE 4 | (A) Bacterial community composition derived from 16S rRNA sequencing data showing the relative abundance of the 20 most abundant taxa at genus level in the fjord sample from 40 m depth and during the 9 days of incubation in the control and treatment incubations where tDOM was added. Taxa comprising <1% of the total number of sequences within a sample were summarized as "Other." **(B)** Calculated absolute abundance of the most abundant genera in control and treatment incubations, based on absolute bacterial abundance measured on the flow cytometer and phylogenetic relative abundance.

the abundance of large bacteria. This genus however showed no significant difference in abundance between treatment and control. In the first days until day 3, the abundance was up to three times higher in the tDOM treatment than the control. This changed on day 4, when abundance in the control incubation was twice as high as in the treatment.

The observed changes for the different genera are based on cumulative abundances of several OTUs which were taxonomically assigned to these genera and grouped accordingly. In order to identify whether all or just some OTUs within each genus are causing the observed changes between treatment and controls, we performed an indicator OTU analysis (**Figure 5**). This analysis identified the OTUs that significantly contributed to the differences between tDOM treatment and control. Out of the 20 most significant OTUs, seven were significantly more abundant in incubations with tDOM addition and 13 OTUs had a significant higher abundance in control incubations. Taxonomically, the great majority of OTUs (19/20) belonged to the class of Gammaproteobacteria and within that class to genera including *Glaciecola*, *Marinomonas*, *Colwellia*, *Balneatrix*, *SAR92,* and *Psychromonas*. The overall most abundant OTU (33%) belonged to the genus *Glaciecola* and was at day 3 seven times more abundant in the tDOM treatment than the control incubations. Of all genera, *Glaciecola* was the genus with the highest number of OTUs (85%) that were positively associated with incubations where tDOM was added. Other genera, like *Colwellia*, with an overall high abundance had a more equal distribution of OTUs, which were higher in abundance in either treatment or control. 66% of *Colwellia* OTUs were significantly more abundant in control incubations and 33% more abundant in treatment incubations.

The results in this study are based on an experimental setup using an un-replicated sampling strategy. Using this strategy improves the probability of identifying trends in community composition change, and reduces the chance of making a type-2-error (finding a pattern that is not there) compared to a replicate sampling strategy. The statistical power of the results obtained from the incubation experiments is evaluated in the Supplementary Material (**Figures S3**, **S4**).

DISCUSSION

Climate model predictions suggest a 30% increase of terrestrial run-off into the Arctic Ocean by the end of the century (Lehner et al., 2012). The tDOM in this run-off is originating from thawing Arctic soil and is modified during the transport into the Arctic Ocean (Lobbes et al., 2000; Serreze et al., 2000; Feng et al., 2013; Fichot et al., 2013; Holmes et al., 2013). It is uncertain how this will affect the marine microbial life and in particular the coastal communities. Our results indicated increased bacterial abundance (**Figure 2**), enlarged cell sizes (**Figure 3**) and changes in the community composition (**Figure 4**) as an immediate (within 3 days) response to tDOM addition. Together, this

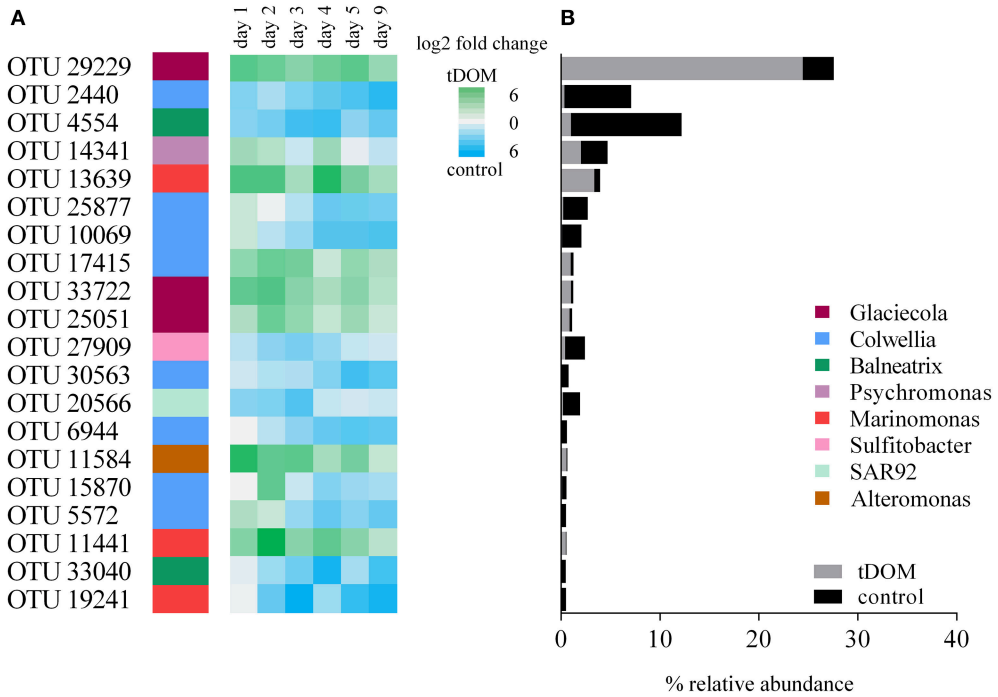

FIGURE 5 | (A) The 20 most significant OTUs, identified by an indicator OTU analysis, contributing to the differences in community composition between control and treatment incubations. Relative abundance differences are visualized as 2-fold change from day1 until day 9. **(B)** Relative abundance (average values from d1 to d9) of the 20 most significant indicator OTUs visualized in the same order as in **(A)**.

suggests that in the future the activity, the physiology and the structure of the fjord microbial community might be affected by increased tDOM rich run-off.

In Situ Microbial Community Composition

Environmental conditions in the Arctic are highly affected by seasonality. In accordance, seasonal changes in microbial community composition have been reported for different parts of the Arctic Oceans, i.e., the increase of *Gammaproteobacteria*, in association to phytoplankton bloom dynamics and increased concentrations of dissolved organic matter in the summer months (Alonso-Sáez et al., 2008; Buchan et al., 2014; El-Swais et al., 2015; Wilson et al., 2017). The fjord water used for our incubation experiments, taken in June, was indicative for a post-bloom situation, with high relative abundance of the phylum Proteobacteria (96.5%) and in particular the class *Gammaproteobacteria*, with up to 76.1% of all proteobacterial reads (**Figure 4**), similar to reports from other studies (Piquet et al., 2010; Zeng et al., 2013). The largest contributor was the genus *Balneatrix* (30.9%), known to be associated with phytoplankton blooms and observed in other Arctic fjords (Nikrad et al., 2014; Paulsen et al., 2017). Other dominant taxa within the *Gammaproteobacteria,* such as *SAR92* (10%) and *OM182* (13%), are commonly associated with rather oligotrophic conditions (Cho and Giovannoni, 2004). Surprisingly, Bacteroidetes, commonly found in summer coastal Arctic communities, comprised only 0.3% in our samples (Nikrad et al., 2012; Sipler et al., 2017a). The low abundance of Betaproteobacteria, which comprised, with up to 3%, only a small proportion of all proteobacterial reads is characteristic for Atlantic water masses (Cottrell and Kirchman, 2003; Garneau et al., 2006).

tDOM Addition Induced Changes in Bacterial Community Composition

The large initial relative abundance of *Pseudoalteromonas* was likely an experimental artifact and rapidly decreased in abundance under both experimental conditions. Changes in community composition due to tDOM addition were already measurable after 12 h of incubation, for example the doubling of *Glaciecola* relative abundance (**Figure 4**). *Glaciecola* also increased in abundance in control incubations (4171% increase from t0 until d4), confirming both that this taxa is part of the *in situ* microbial community and able to grow using *in situ* carbon sources. The fact that *Glaciecola* grew faster and to a higher abundance in the treatment incubations (10781% increase from t0 until d4) indicates that this genus has the potential to degrade the introduced complex tDOM compounds. Other growth experiments with *Glaciecola* revealed both general phylotypes, capable of degrading a broad range of carbon compounds and specialized phylotypes, capable of degrading only specific carbon sources (Gómez-Consarnau et al., 2012).

Besides *Glaciecola*, *Marinomonas,* and *Colwellia*, two taxa known to degrade complex organic matter, also increased in

abundance in the tDOM treatment incubations. *Marinomonas* and *Colwellia* had, similar to *Glaciecola*, low starting abundances and increased in both treatment and control incubations, with a stronger response under tDOM addition. It has been shown that a member of the genus *Marinomonas* is capable of catalyzing ring cleavage of aromatic compounds and correlates with lignocellulosic carbon uptake (Chandra and Chowdhary, 2015; Gontikaki et al., 2015). Also *Colwellia* has been considered to produce extracellular enzymes for the breakdown of high molecular-weight organic compounds (Huston et al., 2004; Methé et al., 2005). *Glaciecola* and *Colwellia* have also recently been shown to increase in abundance under the presence of tDOM derived from Arctic rivers (Sipler et al., 2017a). Interestingly, it was a different *Glaciecola* OTU that was dominating in their dataset. This OTU was also found in our data set, but is only one of the least abundant *Glaciecola* OTUs. It remains unclear whether this difference is caused by substrate specificity or simply which OTU is most abundant at *in situ* conditions. Sipler and colleagues used seven times higher DOC concentrations (400–500 μM) than in their control to stimulate a community response, while the DOC concentrations (128 μM) in our study were only 1.5 times higher than in the control incubations. Pulses of tDOM released via Arctic rivers can reach the DOC concentrations used by Sipler and colleagues (Benner et al., 2005), but at our sampling site in Kongsfjorden the DOC concentration is on average 109 μM (Zhu et al., 2016). Despite the relatively small increase in tDOM concentration in our study, we here stimulated faster growth of certain taxa than the change reported by Sipler and colleagues. This might be due to the fact that our incubations were conducted in the dark and therefore inhibited phototrophic processes.

OTU Specific Response to tDOM Addition and "the Bottle Effect"

We detected a significantly stronger increase of the genera *Glaciecola* and *Marinomonas* in incubations where we added tDOM compared to control incubations. The other genus found to increase, *Colwellia*, showed no significant difference between treatment and control. This is reflected in the differential response we observed at the taxonomic level of OTUs (**Figure 5**). Several OTUs were positively affected by tDOM addition and became more abundant during incubation, whereas other OTUs of the same genus decreased upon tDOM addition (**Figure 5**). This non-coherent tendency was found for all genera and indicates that strains within the same genus might have different functional roles. This was also observed by Sipler and colleagues, where they identified so called sentinels of increasing tDOM, OTUs that increased in abundance due to tDOM addition, while they did not identified genera where all OTUs were affected by the tDOM addition.

We compared changes in relative OTU abundance between treatment and control to differentiate between potential effects due to the tDOM input and effects caused by the experimental set-up, the so called "bottle effects." The increase of a number of Colwellia OTUs was similar in both control and treatment incubations and is therefore likely to be attributed to the bottle effect, which is a well-known inherent concern in incubations studies (Lee and Fuhrman, 1991; Massana et al., 2001; Stewart et al., 2012). Several studies have suggested a combination of factors, including biofilm formation and the binding of nutrients, cells or carbon to the surface of the incubation container, as potential cause of bottle effects (Fogg and Calvario-Martinez, 1989; Fletcher, 1996; Eilers et al., 2000). It appears that the bottle effect predominantly leads to an increase in Gammaproteobacteria taxa, as documented in our and other studies (Eilers et al., 2000; Stewart et al., 2012; Dinasquet et al., 2013; Herlemann et al., 2014). While the bottle effect in the study from Stewart and colleagues and in our study can be attributed to an increase in *Colwelliaceae*, different families, such as *Moraxellaceae* (Herlemann et al., 2014), *Pseudoalteromonadaceae* (Dinasquet et al., 2013), or *Oceanospirillaceae* (Sipler et al., 2017a) were affected in other studies. This suggests that several different types of Gammaproteobacteria can benefit from a bottle effect and that the starting community composition might be the determining factor.

tDOM Effects on the Coastal Microbial Food Web

The increase of Gammaproteobacteria, in particular of taxa belonging to the order Alteromonadales including *Glaciecola* and *Colwellia*, has also been observed during marine phytoplankton spring blooms in lower latitudes (Tada et al., 2011; Teeling et al., 2012) and in the Arctic Ocean (Bano and Hollibaugh, 2002; Wilson et al., 2017). This suggests that they can rapidly proliferate in response to new carbon sources, including phytoplankton-derived organic carbon or tDOM as indicated in our study. A strong grazing pressure by bacterivorous protists has been shown to particularly affect Gammaproteobacteria of the order Alteromonadales (Beardsley et al., 2003; Allers et al., 2007). These studies demonstrated selective grazing on large metabolically active bacteria by heterotrophic flagellate grazers. Size-selective predator-prey interactions have also been shown for *Glaciecola*, that first became abundant upon rapid utilization of phytoplankton derived DOM and subsequently declined in their abundance due to grazing (von Scheibner et al., 2017). It was suggested that once abundant, *Glaciecola* became a target for size selective predation by protists, including heterotrophic nanoflagellates (HNF) due to their above-average cell size.

We also observed an increase in *Glaciecola* abundance upon tDOM addition, which correlated with the appearance of above-average large bacteria measured via flow cytometry (**Figure 3** and **Figure S1**). Toward the end of the experiment, *Glaciecola* abundance declined by 84%, while at the same time the abundance of HNF increased substantially (from 32 to 651 cells mL^{-1}). Interestingly, in the control incubations where *Glaciecola* abundance stayed low, HNF abundance remained unchanged at a low level and did not increase toward the end. This suggests that after *Glaciecola*, fueled by the tDOM addition, increased in abundance, size-selective

HNF caused the decline in *Glaciecola* abundance. The specific predator-prey relation between *Glaciecola* and HNF might be an important link in the microbial food web of Arctic fjord systems, with cascading effects on higher trophic levels, including ciliates, copepods and up to the top level predators.

This link has also consequences for the coastal carbon budget. We calculated carbon turnover assuming a bacterial biomass of 0.02 pg per cell (Lee and Fuhrman, 1987) and a 10% growth efficiency for bacteria (Kritzberg et al., 2010; Middelboe et al., 2012; Paulsen et al., 2017). From day 2 to 4, bacterial growth resulted in the release of 188 μg C-CO_2 L^{-1} in the tDOM treatment compared to 41 μg C-CO_2 L^{-1} in the control. Based on these calculations, 30% of the added tDOM was already processed by the bacteria within 4 days. Since the increase in bacterial abundance after day 4 in the control incubations most likely was caused by the bottle effect, carbon turnover for the later period was not considered as representative for an *in situ* fjord community carbon turnover. The grazing and subsequent growth of HNF in the tDOM treatment caused a further transition of the bacterial biomass. The carbon turnover by HNF was calculated assuming a biomass of 3.8 pg (Børsheim and Bratbak, 1987) and 30% growth efficiency for HNF (Fenchel, 1982). The increase of HNF from day 5 to day 9 resulted in the incorporation of 2 μg C L^{-1} as biomass and an additional release of 6 μg C-CO_2 L^{-1}. Both the initial growth of *Glaciecola* and the subsequent grazing by HNF will thus affect the carbon turnover in Arctic coastal ecosystems with increased tDOM inputs. Based on our study design, we cannot fully predict such effects, but we can document that the addition of tDOM affected not only bacteria, but indirectly also the organisms grazing on bacteria. To our knowledge we here provide the first results on the effects of permafrost-derived tDOM input on fjord microbial communities and to understand the interactions at higher trophic levels, it is necessary to conduct further experiments with tDOM additions at larger scales, including more members of the marine food web.

AUTHOR CONTRIBUTIONS

MP and OM led the planning of the study. LS collected and OM processed samples. MP did flow cytometric analysis. OM, GB, LS, and MP analyzed data, OM prepared figures and tables and led the writing of the paper. All authors contributed to discussing and interpreting data and writing the paper.

FUNDING

This study is part of the project MicroPolar (RCN 225956) funded by the Norwegian Research Council. LS participated as member of the Carbon Bridge project (RCN 226415). Parts of the study was funded by the project Microorganisms in the Arctic: Major drivers of biogeochemical cycles and climate change (RCN 227062).

ACKNOWLEDGMENTS

We would like to thank all colleagues in the UiB Marine Microbiology group and collaborators abroad who contributed to the research effort. We would like to thank Lise Øvreås for her assistance throughout the sampling. Also thank you Aud Larsen for facilitating the transport of samples and Colin Stedmon for performing the Parafac analysis.

SUPPLEMENTARY MATERIAL

The Supplementary Material for this article can be found online at: https://www.frontiersin.org/articles/10.3389/fmars.2018.00263/full#supplementary-material

REFERENCES

Allers, E., Gómez-Consarnau, L., Pinhassi, J., Gasol, J. M., Simek, K., and Pernthaler, J. (2007). Response of Alteromonadaceae and Rhodobacteriaceae to glucose and phosphorus manipulation in marine mesocosms. *Environ. Microbiol.* 9, 2417–2429. doi: 10.1111/j.1462-2920.2007.01360.x

Alonso-Sáez, L., Sánchez, O., Gasol, J. M., Balagué, V., and Pedrós-Alio, C. (2008). Winter-to-summer changes in the composition and single-cell activity of near-surface Arctic prokaryotes. *Environ. Microbiol.* 10, 2444–2454. doi: 10.1111/j.1462-2920.2008.01674.x

Amon, R. M. W., Rinehart, A. J., Duan, S., Louchouarn, P., Prokushkin, A., Guggenberger, G., et al. (2012). Dissolved organic matter sources in large Arctic rivers. *Geochim. Cosmochim. Acta* 94, 217–237. doi: 10.1016/j.gca.2012.07.015

Bano, N., and Hollibaugh, J. T. (2002). Phylogenetic composition of bacterioplankton assemblages from the Arctic Ocean. *Appl. Environ. Microbiol.* 68, 505–518. doi: 10.1128/AEM.68.2.505-518.2002

Beardsley, C., Pernthaler, J., Wosniok, W., and Amann, R. (2003). Are readily culturable bacteria in coastal North Sea waters suppressed by selective grazing mortality? *Appl. Environ. Microbiol.* 69, 2624–2630. doi: 10.1128/AEM.69.5.2624-2630.2003

Beier, S., Rivers, A. R., Moran, M. A., and Obernosterer, I. (2015). The transcriptional response of prokaryotes to phytoplankton-derived dissolved organic matter in seawater. *Environ. Microbiol.* 17, 3466–3480. doi: 10.1111/1462-2920.12434

Benner, R., Louchouarn, P., and Amon, R. M. W. (2005). Terrigenous dissolved organic matter in the Arctic Ocean and its transport to surface and deep waters of the North Atlantic. *Glob. Biogeochem. Cycles* 19:GB2025. doi: 10.1029/2004GB002398

Blanchet, M., Pringault, O., Panagiotopoulos, C., Lefèvre, D., Charrière, B., Ghiglione, J. F., et al. (2017). When riverine dissolved organic matter (DOM) meets labile DOM in coastal waters: changes in bacterial community activity and composition. *Aquat. Sci.* 79, 27–43. doi: 10.1007/s00027-016-0477-0

Bolger, A. M., Lohse, M., and Usadel, B. (2014). Trimmomatic: a flexible trimmer for Illumina sequence data. *Bioinformatics* 30, 2114–2120. doi: 10.1093/bioinformatics/btu170

Børsheim, K., and Bratbak, G. (1987). Cell volume to cell carbon conversion factors for a bacterivorous Monas sp. enriched from seawater. *Mar. Ecol. Prog. Ser.* 36, 171–175. doi: 10.3354/meps036171

Buchan, A., LeCleir, G. R., Gulvik, C. A., and González, J. M. (2014). Master recyclers: features and functions of bacteria associated with phytoplankton blooms. *Nat. Rev. Microbiol.* 12, 686–698. doi: 10.1038/nrmicro3326

Caporaso, J. G., Kuczynski, J., Stombaugh, J., Bittinger, K., Bushman, F. D., Costello, E. K., et al. (2011a). QIIME allows analysis of high-throughput community sequencing data. *Nat. Methods* 7, 335–336. doi: 10.1038/nmeth.f.303

Caporaso, J. G., Lauber, C. L., Walters, W. A., Berg-Lyons, D., Lozupone, C. A., Turnbaugh, P. J., et al. (2011b). Global patterns of 16S rRNA diversity at a depth of millions of sequences per sample. *Proc. Natl. Acad. Sci. U.S.A.* 108, 4516–4522. doi: 10.1073/pnas.1000080107

Chandra, R., Chowdhary, P. (2015). Properties of bacterial laccases and their application in bioremediation of industrial wastes. *Environ. Sci. Process. Impacts* 17, 326–342. doi: 10.1039/C4EM00627E

Cho, J. C., and Giovannoni, S. J. (2004). Cultivation and growth characteristics of a diverse group of oligotrophic marine *Gammaproteobacteria*. *Appl. Environ. Microbiol.* 70, 432–440. doi: 10.1128/AEM.70.1.432-440.2004

Cottrell, M. T., and Kirchman, D. L. (2003). Contribution of major bacterial groups to bacterial biomass production (thymidine and leucine incorporation) in the Delaware estuary. *Limnol. Oceanogr.* 48, 168–178. doi: 10.4319/lo.2003.48.1.0168

De Cáceres, M., and Legendre, P. (2009). Associations between species and groups of sites: indices and statistical inference. *Ecology* 90, 3566–3574. doi: 10.1890/08-1823.1

Dinasquet, J., Kragh, T., Schrøter, M. L., Søndergaard, M., and Riemann, L. (2013). Functional and compositional succession of bacterioplankton in response to a gradient in bioavailable dissolved organic carbon. *Environ. Microbiol.* 15, 2616–2628. doi: 10.1111/1462-2920.12178

Dittmar, T., and Kattner, G. (2003). The biogeochemistry of the river and shelf ecosystem of the Arctic Ocean: a review. *Mar. Chem.* 83, 103–120. doi: 10.1016/S0304-4203(03)00105-1

Doney, S. C., Ruckelshaus, M., Emmett Duffy, J., Barry, J. P., Chan, F., English, C. A., et al. (2012). Climate change impacts on marine ecosystems. Annu. *Rev. Mar. Sci.* 4, 11–37. doi: 10.1146/annurev-marine-041911-111611

Edgar, R. C. (2010). Search and clustering orders of magnitude faster than BLAST. *Bioinformatics* 26, 2460–2461. doi: 10.1093/bioinformatics/btq461

Eiler, A., Langenheder, S., Bertilsson, S., and Tranvik, L. J. (2003). Heterotrophic bacterial growth efficiency and community structure at different natural organic carbon concentrations. *Appl. Environ. Microbiol.* 69, 3701–3709. doi: 10.1128/AEM.69.7.3701-3709.2003

Eilers, H., Pernthaler, J., and Amann, R. (2000). Succession of pelagic marine bacteria during enrichment: a close look at cultivation-induced shifts. *Appl. Environ. Microbiol.* 66, 4634–4640. doi: 10.1128/AEM.66.11.4634-4640.2000

El-Swais, H., Dunn, K. A., Bielawski, J. P., Li, W. K., and Walsh, D. A. (2015). Seasonal assemblages and short-lived blooms in coastal north-west Atlantic Ocean bacterioplankton. *Environ. Microbiol.* 17, 3642–3661. doi: 10.1111/1462-2920.12629

Fenchel, T. (1982). Ecology of heterotrophic microflagellates. IV quantitative occurrence and importance as bacterial consumers. *Mar. Ecol. Prog. Ser.* 9, 35–42. doi: 10.3354/meps009035

Feng, X., Vonk, J. E., van Dongen, B. E., Gustafsson, Ö., Semiletov, I. P., Dudarev, O. V., et al. (2013). Differential mobilization of terrestrial carbon pools in Eurasian Arctic river basins. *Proc. Natl. Acad. Sci. U.S.A.* 110, 14168–14173. doi: 10.1073/pnas.1307031110

Fichot, C. G., Kaiser, K., Hooker, S. B., Amon, R. M., Babin, M., Bélanger, S., et al. (2013). Pan-Arctic distributions of continental runoff in the Arctic Ocean. *Sci. Rep.* 3:1053. doi: 10.1038/srep01053

Fletcher, M. (1996). *Bacterial Adhesion: Molecular and Ecological Diversity*. Wiley. Available online at: https://books.google.com/books?hl=en&lr=&id=bYmsjh4ppZYC&pgis=1 (Accessed December 6, 2017).

Fogg, G. E., and Calvario-Martinez, O. (1989). Effects of bottle size in determinations of primary productivity by phytoplankton. *Hydrobiologia* 173, 89–94. doi: 10.1007/BF00015518

Garneau, M., Vincent, W., Alonso-Sáez, L., Gratton, Y., and Lovejoy, C. (2006). Prokaryotic community structure and heterotrophic production in a river-influenced coastal arctic ecosystem. *Aquat. Microb. Ecol.* 42, 27–40. doi: 10.3354/ame042027

Gómez-Consarnau, L., Lindh, M. V., Gasol, J. M., and Pinhassi, J. (2012). Structuring of bacterioplankton communities by specific dissolved organic carbon compounds. *Environ. Microbiol.* 14, 2361–2378. doi: 10.1111/j.1462-2920.2012.02804.x

Gontikaki, E., Thornton, B., Cornulier, T., Witte, U. (2015). Occurrence of priming in the degradation of lignocellulose in marine sediments. *PLoS ONE* 10:e0143917. doi: 10.1371/journal.pone.0143917

Hansell, D. A. (2004). Degradation of terrigenous dissolved organic carbon in the Western Arctic Ocean. *Science* 304, 858–861. doi: 10.1126/science.1096175

Hansell, D. A., Carlson, C. A., Repeta, D. J., and Schlitzer, R. (2009). Dissolved organic matter in the ocean - a controversy stimulates new insights. *Oceanography* 22, 202–211. doi: 10.5670/oceanog.2009.109

Herlemann, D. P. R., Manecki, M., Dittmar, T., and Jürgens, K. (2017). Differential responses of marine, mesohaline and oligohaline bacterial communities to the addition of terrigenous carbon. *Environ. Microbiol.* 19, 3098–3117. doi: 10.1111/1462-2920.13784

Herlemann, D. P., Manecki, M., Meeske, C., Pollehne, F., Labrenz, M., Schulz-Bull, D., (2014). Uncoupling of bacterial and terrigenous dissolved organic matter dynamics in decomposition experiments. *PLoS ONE* 9:e93945. doi: 10.1371/journal.pone.0093945

Holmes, R. M., Coe, M. T., Fiske, G. J., Gurtovaya, T., McClelland, J. W., Shiklomanov, A. I., et al. (2013). "Climate change impacts on the hydrology and biogeochemistry of Arctic rivers," in *Climatic Change and Global Warming of Inland Waters: Impacts and Mitigation for Ecosystems and Societies*, eds C. R. Goldman, M. Kumagai, and R. D. Robarts (Oxford UK: John Wiley), 1–26.

Holmes, R. M., McClelland, J. W., Raymond, P. A., Frazer, B. B., Peterson, B. J., and Stieglitz, M. (2008). Lability of DOC transported by Alaskan rivers to the Arctic Ocean. *Geophys. Res. Lett.* 35:L03402. doi: 10.1029/2007GL032837

Huston, A. L., Methe, B., and Deming, J. W. (2004). Purification, characterization, and sequencing of an extracellular cold-active aminopeptidase produced by marine psychrophile *Colwellia psychrerythraea* strain 34H. *Appl. Environ. Microbiol.* 70, 3321–3328. doi: 10.1128/AEM.70.6.3321-3328.2004

Jiao, N., Herndl, G. J., Hansell, D. A., Benner, R., Kattner, G., Wilhelm, S. W., et al. (2010). Microbial production of recalcitrant dissolved organic matter: long-term carbon storage in the global ocean. *Nat. Rev. Microbiol.* 8, 593–599. doi: 10.1038/nrmicro2386

Kritzberg, E. S., Duarte, C. M., and Wassmann, P. (2010). Changes in Arctic marine bacterial carbon metabolism in response to increasing temperature. *Polar Biol.* 33, 1673–1682. doi: 10.1007/s00300-010-0799-7

Lee, S., and Fuhrman, J. A. (1987). Relationships between biovolume and biomass of naturally derived marine bacterioplankton. *Appl. Environ. Microbiol.* 53, 1298–1303.

Lee, S., and Fuhrman, J. A. (1991). Species composition shift of confined bacterioplankton studies at the level of community DNA. *Mar. Ecol. Prog. Ser.* 79, 195–201. doi: 10.3354/meps079195

Lehner, F., Raible, C. C., Hofer, D., and Stocker, T. F. (2012). The freshwater balance of polar regions in transient simulations from 1500 to 2100 AD using a comprehensive coupled climate model. *Clim. Dyn.* 39, 347–363. doi: 10.1007/s00382-011-1199-6

Li, W. K. W., McLaughlin, F. A., Lovejoy, C., and Carmack, E. C. (2009). Smallest algae thrive as the arctic ocean freshens. *Science* 326:539. doi: 10.1126/science.1179798

Lobbes, J. M., Fitznar, H. P., and Kattner, G. (2000). Biogeochemical characteristics of dissolved and particulate organic matter in Russian rivers entering the Arctic Ocean. *Geochim. Cosmochim. Acta* 64, 2973–2983. doi: 10.1016/S0016-7037(00)00409-9

Marie, D., Brussaard, C. P. D., Thyrhaug, R., Bratbak, G., and Vaulot, D. (1999). Enumeration of marine viruses in culture and natural samples by flow cytometry. *Appl. Environ. Microbiol.* 65, 45–52.

Masella, A. P., Bartram, A. K., Truszkowski, J. M., Brown, D. G., and Neufeld, J. D. (2012). PANDAseq : PAired-eND Assembler for Illumina sequences. *BMC Bioinformatics* 13:31. doi: 10.1186/1471-2105-13-31

Massana, R., Pedros-Alio, C., Casamayor, E. O., and Gasol, J. M. (2001). Changes in marine bacterioplankton phylogenetic composition during incubations designed to measure biogeochemically significant parameters. *Limnol. Oceanogr.* 46, 1181–1188. doi: 10.4319/lo.2001.46.5.1181

McCarren, J., Becker, J. W., Repeta, D. J., Shi, Y., Young, C. R., Malmstrom, R. R., et al. (2010). Microbial community transcriptomes reveal microbes and metabolic pathways associated with dissolved organic matter turnover in the sea. *Proc. Natl. Acad. Sci. U.S.A.* 107, 16420–16427. doi: 10.1073/pnas.1010732107

Methé, B. A., Nelson, K. E., Deming, J. W., Momen, B., Melamud, E., Zhang, X., et al. (2005). The psychrophilic lifestyle as revealed by the genome sequence of

Colwellia psychrerythraea 34H through genomic and proteomic analyses. *Proc. Natl. Acad. Sci. U.S.A.* 102, 10913–10918. doi: 10.1073/pnas.0504766102

Middelboe, M., Glud, R. N., and Sejr, M. K. (2012). Bacterial carbon cycling in a subarctic fjord: a seasonal study on microbial activity, growth efficiency, and virus-induced mortality in Kobbefjord, Greenland. *Limnol. Oceanogr.* 57, 1732–1742. doi: 10.4319/lo.2012.57.6.1732

Nikrad, M. P., Cottrell, M. T., and Kirchman, D. L. (2012). Abundance and single-cell activity of heterotrophic bacterial groups in the western Arctic Ocean in summer and winter. *Appl. Environ. Microbiol.* 78, 2402–2409. doi: 10.1128/AEM.07130-11

Nikrad, M. P., Cottrell, M. T., and Kirchman, D. L. (2014). Growth activity of gammaproteobacterial subgroups in waters off the west Antarctic Peninsula in summer and fall. *Environ. Microbiol.* 16, 1513–1523. doi: 10.1111/1462-2920.12258

Opsahl, S., Benner, R., and Amon, R. M. W. (1999). Major flux of terrigenous dissolved organic matter through the Arctic Ocean. *Limnol. Oceanogr.* 44, 2017–2023. doi: 10.4319/lo.1999.44.8.2017

Ovreås, L., Forney, L., Daae, F. L. Torsvik, V. (1997). Distribution of bacterioplankton in meromictic lake sælenvannet, as determined by denaturing gradient gel electrophoresis of PCR-amplified gene fragments coding for 16S rRNA. *Appl. Environ. Microbiol.* 63, 3367–3373.

Paulsen, M. L., Doré, H., Garczarek, L., Seuthe, L., Müller, O., Sandaa, R.-A., et al. (2016). Synechococcus in the Atlantic gateway to the Arctic Ocean. *Front. Mar. Sci.* 3:191. doi: 10.3389/fmars.2016.00191

Paulsen, M. L., Nielsen, S. E. B., Müller, O., Møller, E. F., Stedmon, C. A., Juul-Pedersen, T., et al. (2017). Carbon bioavailability in a high arctic fjord influenced by glacial meltwater, NE Greenland. *Front. Mar. Sci.* 4:176. doi: 10.3389/fmars.2017.00176

Pedler, B. E., Aluwihare, L. I., and Azam, F. (2014). Single bacterial strain capable of significant contribution to carbon cycling in the surface ocean. *Proc. Natl. Acad. Sci. U.S.A.* 111, 7202–7207. doi: 10.1073/pnas.1401887111

Pinhassi, J., Sala, M. M., Havskum, H., Peters, F., Guadayol, O., Malits, A., et al. (2004). Changes in bacterioplankton composition under different phytoplankton regimens. *Appl. Environ. Microbiol.* 70, 6753–6766. doi: 10.1128/AEM.70.11.6753-6766.2004

Piquet, A. M.-T., Scheepens, J. F., Bolhuis, H., Wiencke, C., and Buma, A. G. J. (2010). Variability of protistan and bacterial communities in two Arctic fjords (Spitsbergen). *Polar Biol.* 33, 1521–1536. doi: 10.1007/s00300-010-0841-9

Quast, C., Pruesse, E., Yilmaz, P., Gerken, J., Schweer, T., Yarza, P., et al. (2013). The SILVA ribosomal RNA gene database project : improved data processing and web-based tools. *Nucleic Acid Res.* 41, 590–596. doi: 10.1093/nar/gks1219

R Development Core Team (2012). *R: A Language and Environment for Statistical Computing*.

Rachold, V., Eicken, H., Gordeev, V. V., Grigoriev, M. N., Hubberten, H.-W., Lisitzin, A. P., et al. (2004). *The Organic Carbon Cycle in the Arctic Ocean*. Heidelberg: Springer, 33–55.

Sapp, M., Wichels, A., Wiltshire, K. H., and Gerdts, G. (2007). Bacterial community dynamics during the winter-spring transition in the North Sea. *FEMS Microbiol. Ecol.* 59, 622–637. doi: 10.1111/j.1574-6941.2006.00238.x

Schlitzer, R. (2011). *Ocean Data View User's Guide*, 1–156. Available online at: http://odv.awi.de

Screen, J. A., and Simmonds, I. (2010). The central role of diminishing sea ice in recent Arctic temperature amplification. *Nature* 464, 1334–1337. doi: 10.1038/nature09051

Serreze, M., Walsh, J., and Iii, F. C. (2000). Observational evidence of recent change in the northern high-latitude environment. *Clim. Change* 46, 159–207. doi: 10.1023/A:1005504031923

Sipler, R. E., Kellogg, C. T. E., Connelly, T. L., Roberts, Q. N., Yager, P. L., and Bronk, D. A. (2017a). Microbial community response to terrestrially derived dissolved organic matter in the coastal Arctic. *Front. Microbiol.* 8:1018. doi: 10.3389/fmicb.2017.01018

Sipler, R. E., Baer, S. E., Connelly, T. L., Frischer, M. E., Roberts, Q. N., Yager, P. L., et al. (2017b). Chemical and photophysiological impact of terrestrially-derived dissolved organic matter on nitrate uptake in the coastal western Arctic. *Limnol. Oceanogr.* 62, 1881–1894. doi: 10.1002/lno.10541

Stedmon, C. A., and Markager, S. (2005). Resolving the variability in dissolved organic matter fluorescence in a temperate estuary and its catchment using PARAFAC analysis. *Limnol. Oceanogr.* 50, 686–697. doi: 10.4319/lo.2005.50.2.0686

Stedmon, C. A., Amon, R. M. W., Rinehart, A. J., and Walker, S. A. (2011). The supply and characteristics of colored dissolved organic matter (CDOM) in the Arctic ocean: pan Arctic trends and differences. *Mar. Chem.* 124, 108–118. doi: 10.1016/j.marchem.2010.12.007

Stewart, F. J., Dalsgaard, T., Young, C. R., Thamdrup, B., Revsbech, N. P., Ulloa, O., et al. (2012). Experimental incubations elicit profound changes in community transcription in OMZ bacterioplankton. *PLoS ONE* 7:e37118. doi: 10.1371/journal.pone.0037118

Tada, Y., Taniguchi, A., Nagao, I., Miki, T., Uematsu, M., Tsuda, A., et al. (2011). Differing growth responses of major phylogenetic groups of marine bacteria to natural phytoplankton blooms in the western North Pacific Ocean. *Appl. Environ. Microbiol.* 77, 4055–4065. doi: 10.1128/AEM.02952-10

Teeling, H., Fuchs, B. M., Becher, D., Klockow, C., Gardebrecht, A., Bennke, C. M., et al. (2012). Induced by a phytoplankton bloom. *Science* 336, 608–611. doi: 10.1126/science.1218344

Thingstad, T. F., Bellerby, R. G., Bratbak, G., Børsheim, K. Y., Egge, J. K., Heldal, M., et al. (2008). Counterintuitive carbon-to-nutrient coupling in an Arctic pelagic ecosystem. *Nature* 455, 387–390. doi: 10.1038/nature07235

Traving, S. J., Rowe, O., Jakobsen, N. M., Sørensen, H., Dinasquet, J., Stedmon, C. A., et al. (2017). The effect of increased loads of dissolved organic matter on estuarine microbial community composition and function. *Front. Microbiol.* 8:351. doi: 10.3389/fmicb.2017.00351

Trenberth, K. E., and Josey, S. A. (2007). Observations: surface and atmospheric climate change. *Changes* 164, 235–336. doi: 10.5194/cp-6-379-2010

Vincent, W. F. (2010). Microbial ecosystem responses to rapid climate change in the Arctic. *ISME J.* 4, 1087–1090. doi: 10.1038/ismej.2010.108

Vonk, J. E., Mann, P. J., Davydov, S., Davydova, A., Spencer, R. G. M., Schade, J., et al. (2013). High biolability of ancient permafrost carbon upon thaw. *Geophys. Res. Lett.* 40, 2689–2693. doi: 10.1002/grl.50348

von Scheibner, M., Sommer, U., and Jürgens, K. (2017). Tight coupling of Glaciecola spp. and diatoms during cold-water phytoplankton spring blooms. *Front. Microbiol.* 8:27. doi: 10.3389/fmicb.2017.00027

Wilson, B., Müller, O., Nordmann, E.-L., Seuthe, L., Bratbak, G., and Øvreås, L. (2017). Changes in marine prokaryote composition with season and depth over an arctic polar year. *Front. Mar. Sci.* 4:95. doi: 10.3389/fmars.2017.00095

Wohlers, J., Engel, A., Zöllner, E., Breithaupt, P., Jürgens, K., Hoppe, H. G., et al. (2009). Changes in biogenic carbon flow in response to sea surface warming. *Proc. Natl. Acad. Sci. U.S.A.* 106, 7067–7072. doi: 10.1073/pnas.0812743106

Xie, H., Bélanger, S., Song, G., Benner, R., Taalba, A., Blais, M., et al. (2012). Photoproduction of ammonium in the southeastern Beaufort Sea and its biogeochemical implications. *Biogeosciences* 9, 3047–3061. doi: 10.5194/bg-9-3047-2012

Zeng, Y. X., Zhang, F., He, J. F., Lee, S. H., Qiao, Z. Y., Yu, Y., et al. (2013). Bacterioplankton community structure in the Arctic waters as revealed by pyrosequencing of 16S rRNA genes. *Antonie Van Leeuwenhoek* 103, 1309–1319. doi: 10.1007/s10482-013-9912-6

Zhu, Z. Y., Wu, Y., Liu, S. M., Wenger, F., Hu, J., Zhang, J., et al. (2016). Organic carbon flux and particulate organic matter composition in Arctic valley glaciers: examples from the Bayelva River and adjacent Kongsfjorden. *Biogeosciences* 13, 975–987. doi: 10.5194/bg-13-975-2016

Zubkov, M. V., Burkill, P. H., and Topping, J. N. (2007). Flow cytometric enumeration of DNA-stained oceanic planktonic protists. *J. Plankton Res.* 29, 79–86. doi: 10.1093/plankt/fbl059

Conflict of Interest Statement: The authors declare that the research was conducted in the absence of any commercial or financial relationships that could be construed as a potential conflict of interest.

Copyright © 2018 Müller, Seuthe, Bratbak and Paulsen. This is an open-access article distributed under the terms of the Creative Commons Attribution License (CC BY). The use, distribution or reproduction in other forums is permitted, provided the original author(s) and the copyright owner(s) are credited and that the original publication in this journal is cited, in accordance with accepted academic practice. No use, distribution or reproduction is permitted which does not comply with these terms.

frontiers in Microbiology

ORIGINAL RESEARCH
published: 20 August 2018
doi: 10.3389/fmicb.2018.01914

Diverse Bacteria Utilize Alginate Within the Microbiome of the Giant Kelp *Macrocystis pyrifera*

Jordan D. Lin[1†], Matthew A. Lemay[1,2] and Laura W. Parfrey[1,2,3*]*

[1] Department of Botany, Biodiversity Research Centre, The University of British Columbia, Vancouver, BC, Canada, [2] Hakai Institute, Heriot Bay, BC, Canada, [3] Department of Zoology, University of British Columbia, Vancouver, BC, Canada

Bacteria are integral to marine carbon cycling. They transfer organic carbon to higher trophic levels and remineralise it into inorganic forms. Kelp forests are among the most productive ecosystems within the global oceans, yet the diversity and metabolic capacity of bacteria that transform kelp carbon is poorly understood. Here, we use 16S amplicon and metagenomic shotgun sequencing to survey bacterial communities associated with the surfaces of the giant kelp *Macrocystis pyrifera* and assess the capacity of these bacteria for carbohydrate metabolism. We find that *Macrocystis*-associated communities are distinct from the water column, and that they become more diverse and shift in composition with blade depth, which is a proxy for tissue age. These patterns are also observed in metagenomic functional profiles, though the broader functional groups—carbohydrate active enzyme families—are largely consistent across samples and depths. Additionally, we assayed more than 250 isolates cultured from *Macrocystis* blades and the surrounding water column for the ability to utilize alginate, the primary polysaccharide in *Macrocystis* tissue. The majority of cultured bacteria (66%) demonstrated this capacity; we find that alginate utilization is patchily distributed across diverse genera in the Bacteroidetes and Proteobacteria, yet can also vary between isolates with identical 16S rRNA sequences. The genes encoding enzymes involved in alginate metabolism were detected in metagenomic data across taxonomically diverse bacterial communities, further indicating this capacity is likely widespread amongst bacteria in kelp forests. Overall, the *M. pyrifera* epibiota shifts across a depth gradient, demonstrating a connection between bacterial assemblage and host tissue state.

Keywords: kelp, microbiome, metagenomics, *Macrocystis*, alginate, epibiota

OPEN ACCESS

Edited by:
Veronica Molina, Universidad de Playa Ancha, Chile

Reviewed by:
François Thomas, UMR8227 Laboratoire de Biologie Intégrative des Modèles Marins, France
Rodrigo De La Iglesia, Pontificia Universidad Católica de Chile, Chile

****Correspondence:***
Jordan D. Lin
jordand.lin@mail.utoronto.ca
Laura W. Parfrey
lwparfrey@botany.ubc.ca

†Present address:
Jordan D. Lin, Department of Molecular Genetics, University of Toronto, Toronto, ON, Canada

Specialty section:
This article was submitted to Aquatic Microbiology, a section of the journal Frontiers in Microbiology

Received: *10 March 2018*
Accepted: *30 July 2018*
Published: *20 August 2018*

Citation:
Lin JD, Lemay MA and Parfrey LW (2018) Diverse Bacteria Utilize Alginate Within the Microbiome of the Giant Kelp Macrocystis pyrifera. Front. Microbiol. 9:1914. doi: 10.3389/fmicb.2018.01914

INTRODUCTION

Heterotrophic bacteria play an essential role in the world's oceans by metabolizing and remineralising dissolved and particulate organic carbon that would otherwise be unavailable to higher trophic levels (Azam and Malfatti, 2007). These interactions provide a key contribution to biogeochemical cycling by liberating refractory carbon, shuttling carbon between coastal systems (Säwström et al., 2016), and reducing the sequestration of carbon to the deep ocean (Jiao et al., 2010).

Within the global oceans, kelp forests are one of the most productive ecosystems and a large reservoir of organic carbon (Reed et al., 2008), contributing an estimated 5662 g C m^{-2} yr^{-1} to global net primary production (Krumhansl and Scheibling, 2012). The majority

of kelp carbon is released to the environment as detritus (i.e., particulate organic carbon; Krumhansl and Scheibling, 2012), while a smaller portion is exuded as dissolved organic matter (Reed et al., 2015). Both of these substrates represent substantial pools of organic carbon for bacterial utilization. Given the abundance of carbon within kelp forest ecosystems and the interdependence between bacterial metabolism and marine productivity, the kelp forest is an important system in which to study microbial carbon cycling and oceanic nutrient fluxes.

The giant kelp *Macrocystis pyrifera* is the largest, fastest growing macroalgal species (Ravanal et al., 2017) and serves as the structural foundation in Pacific kelp forests (Steneck et al., 2002), yet the diversity and metabolic capacity of bacteria that cycle *Macrocystis* carbon is poorly known. The epibiota of *Macrocystis* (Michelou et al., 2013), and kelp generally (Lemay et al., 2018), are distinct from that of the water column. Yet, kelp influence the water column microbiota (Lam and Harder, 2007; Chen and Parfrey, 2018) and their carbohydrate degradation capacity (Clasen and Shurin, 2015). Studies comparing across seaweeds find species-specificity of associated bacteria in taxonomic profiles (Lachnit et al., 2009; Lemay et al., 2018) and functional profiles, with functional differences in part reflecting metabolism of host polysaccharides (Roth-Schulze et al., 2016). Across kelps, host tissue age (Bengtsson et al., 2012) and condition (Marzinelli et al., 2015) shape epibiota diversity and composition. For example, Bengtsson et al. (2012) documented seasonal microbiota succession on blades of *Laminaria hyperborea,* and Lemay et al. (2018) show an analogous pattern in which perennial and annual kelp species harbor different epibiotic communities.

Bacteria transform algal-derived carbon by utilizing a diverse suite of degradative enzymes (Wang et al., 2016) that target numerous host polysaccharides (Dong et al., 2012; Martin et al., 2015). Brown algae, including kelp, produce an extracellular matrix primarily composed of the polysaccharides alginate, cellulose, and fucoidan (Michel et al., 2010), with the relative abundance of these polysaccharides varying across species and seasons. Alginate is the dominant polysaccharide in several kelp species, including *M. pyrifera*, where it comprises roughly 15–25% of dry weight, with highest concentrations observed in the fall (Whyte and Englar, 1978) and in young blades (McKee et al., 1992). Polymeric alginate is metabolized via alginate and oligoalginate lyase enzymes that are typically found within bacterial operons (Thomas et al., 2012). Alginate assimilation is initiated by the depolymerization of polymeric alginate, which is typically catalyzed by extracellular alginate lyases, although direct uptake of the polymer has been reported (Hisano et al., 1995). Oligomeric products are then imported into the bacterial periplasm, where they are further degraded into monosaccharides by oligoalginate lyases (Thomas et al., 2012) prior to transport into the bacterial cytosol. Because alginate is one of the primary organic carbon sources in kelp forests and a known substrate of bacterial metabolism, its utilization by bacteria is likely an important process in coastal carbon turnover.

The objective of this study is to determine the distribution and variability of alginate utilization among bacteria in Pacific *Macrocystis* forests, and to reconstruct the broader communities in which this activity occurs. We perform amplicon and shotgun metagenomic sequencing on epibiotic and water column communities to reconstruct their taxonomic and carbohydrate metabolic profiles, and provide the first metagenomic survey of alginate metabolic genes in kelp forests. We also assay cultured bacteria isolated from the kelp forest to determine their ability to degrade polymeric alginate and metabolize it for growth (referred to together as alginate utilization). These data provide a better understanding of the relationship between taxonomic and functional diversity in marine bacterial communities.

MATERIALS AND METHODS

Surface-Associated Microbial Communities

Macrocystis pyrifera blades were sampled by scuba in August, 2015 from three subtidal kelp beds adjacent to Calvert Island, British Columbia (Site 1 (Stryker): 52 04.962 N, 128 21.883 W; Site 2 (Triquet): 51 48.343 N, 128 15.479 W; Site 3 (Goose South): 51 55.226 N, 128 27.571 W; **Supplementary Data Sheet S2**). These sites were chosen due to their similar oceanographic properties, depths (Site 1 – 5 m; Site 2 – 5 m; Site 3 – 7 m), and inclusion in long term monitoring projects. At each site, five kelp blade replicates were sampled at the bottom (1 m above sediment), middle (1 m below surface), and top (surface) of the water column. Each blade was removed and brought to the surface in a sterile Ziploc® bag. On the surface, each blade ($n = 45$) was rinsed with sterile seawater for 10 s to remove transient microbes, and then a 10 cm^2 area in the center of the blade was swabbed with a sterile Puritan® cotton swab for 10 s. Swabs were immediately transferred into sterile cryovials (VWR) and placed on ice for transport back to the lab, where they were stored at −80°C. Water samples from each site were collected from the same depths as kelp blades and were stored in sterile 500 ml Nalgene® bottles ($n = 12$). Water was pre-filtered at 150 μm to remove larger organisms and bacteria were subsequently filtered from the water samples using a Cole-Parmer MasterFlex L/S peristaltic pump with a 0.22 μm Durapore® membrane filter (Merck Millipore Ltd.). Filters from each water sample were immediately stored at −80°C in individual Whirl-Pak® bags.

Bacterial DNA from the kelp blade swabs and water column filters was extracted with the MoBio PowerSoil®-htp 96 well DNA extraction kit using standard protocols (Mo Bio Laboratories, United States). The V4 region of the 16S rRNA gene was amplified by PCR using redesigned versions of the primers *515f/806r* (Caporaso et al., 2012): *515f*: 5′–GTGYCAGCMGCCGCGGTAA–3′, *806r*: 5′–GGACT ACNVGGGTWTCTAAT–3′. These primers have been modified to include a 12 bp Golay barcode on the forward primer and degeneracies were added to improve taxonomic coverage[1]. Each PCR consisted of 10 μl of 5-Prime Master Mix, 1 μl of each primer (final concentration = 0.2 μM), 2 μl of DNA, and PCR grade water to a final volume of 25 μl. The PCR protocol consisted of an initial denaturation step at 94°C for 3 min,

[1]http://www.earthmicrobiome.org/protocols-and-standards/16s/

followed by 25 cycles of denaturation at 94°C for 45 s, primer annealing at 50°C for 60 s, and extension at 72°C for 90 s, with a final extension step of 72°C for 10 min. PCR products were quantified using Quant-IT Pico Green® ds DNA Assay Kit (Life Technologies). Sample DNA was then pooled in equal amounts (25 ng) and purified using the MoBio UltraClean® PCR clean-up kit. Quantitation of the pooled library and paired-end Illumina MiSeq sequencing (2 × 300 bp) were performed at the Integrated Microbiome Resource facility at Dalhousie University (Halifax, Canada).

The resulting raw sequencing reads were demultiplexed in QIIME v1.9.1 (Caporaso et al., 2010b) using split_libraries_fastq.py, which yielded an average of 86,857 reads/sample. Demultiplexed reads were trimmed to 250 bp using the FastX Toolkit[2] and clustered using Minimum Entropy Decomposition (MED; Eren et al., 2015) into nodes analogous to operational taxonomic units (OTUs). This clustering was performed as implemented in the Oligotyping microbial analysis software package (Eren et al., 2013) and carried out with the minimum substantive abundance parameter (−M) set at 250 reads. All other parameters retained the default settings. MED OTUs were taxonomically identified using UCLUST (Edgar, 2010) and assign_taxonomy.py in QIIME by querying the SILVA SSU Ref NR 128 database (**Supplementary Data Sheet S4**). OTUs were subsequently filtered for host contamination by removing chloroplast and mitochondrial annotations, and by sample occurrence (≥2 samples) and read count (≥100 reads per OTU). The remaining OTU representative sequences were aligned with PyNAST v.1.2.2 (Caporaso et al., 2010a) using the SILVA SSU Ref NR 128 alignment as a template and a tree was constructed in QIIME using FastTree (Price et al., 2010). An OTU heatmap was constructed in the R statistical environment (all analyses in R performed with v3.4.0; R Core Team, 2017).

Bacterial Community Comparisons

To quantify the richness of culture-independent bacterial communities, the Chao1 metric (Chao, 1984) was calculated for each sample in QIIME using alpha_diversity.py. Samples were first rarefied at a depth of 30,000 sequences. Richness was compared using mixed effect analysis of variance (ANOVA) with the lmerTest package (Kuznetsova et al., 2015) in R. Briefly, when comparing *Macrocystis* and water samples, site was set as a random effect while depth (bottom, middle, surface) and sample type (seawater, macroalgae) were both set as fixed effects. When comparing only kelp blades, site was again set as a random effect and depth was set as a fixed effect. Pairwise comparisons of kelp communities across depths were performed within lmerTest as Student's *t*-tests.

We compared bacterial community composition using the weighted UniFrac metric, which takes abundance into account (Lozupone et al., 2007). Beta diversity distance matrices were generated in QIIME at a rarefaction depth of 30,000 sequences/sample and visualized as Principal Coordinates plots in R. Communities were compared using a permutational multivariate analysis of variance (PERMANOVA; Anderson et al., 2005) and a permutational analysis of within group multivariate dispersion (PERMDISP; Anderson, 2004), both with 9999 permutations and implemented in Primer (v.6; Clarke and Gorley, 2006). When comparing all bacterial communities, both depth and sample type were set as fixed effects while site was set as a random effect. For comparisons of *Macrocystis* samples only, depth was once again a fixed effect and site a random effect. Pairwise PERMANOVA analyses conducted within Primer were used to compare *Macrocystis* communities across depths.

Testing for the differential abundance of bacterial genera across *Macrocystis* blade depths was performed in R using the two-tailed Welch's *t*-test (t.test). Benjamini–Hochberg adjusted *p*-values were used to account for multiple hypothesis testing (Benjamini and Hochberg, 1995). Read counts were normalized to total sample counts prior to analysis. Genera were considered differentially abundant if their FDR corrected p-value < 0.1 and log2 fold change across depths was $\geq |2|$.

Carbohydrate Metabolic Profile Reconstruction

To assess the capacity for alginate utilization in kelp forest bacterial communities, a subset of samples were sent for shotgun metagenomic sequencing using the same DNA as 16S rRNA gene sequencing. These samples consisted of 10 kelp (5 bottom depth, 5 middle depth) and 5 water samples (4 bottom depth, 1 surface depth) from one kelp bed (Site 3). Metagenomic libraries were prepared using the Illumina Nextera XT kit and 150-bp fragments and sequenced on an Illumina NextSeq 550 at the Integrated Microbiome Resource facility at Dalhousie University. Quality statistic generation, paired-end read merging, and quality filtering were performed with VSEARCH (Rognes et al., 2016) on the resulting raw sequencing reads. Merging was performed with default parameters (except maximum mismatch was reduced to 2 nucleotides) and non-merged forward reads were added to the merged reads to increase coverage. Reads were trimmed at the beginning to remove low quality bases, quality filtered (minimum length: 100-bp; maximum error rate: 0.005), and truncated once base quality dropped below 30. This yielded 7,924,598 reads with an average length of 147-bp. The mean sequences per sample was 528,307, and one kelp sample with 1169 reads was removed prior to analysis due to low sequence count.

Open reading frames (ORFs) were predicted in MetaPathways v2.5.1 (Konwar et al., 2015) using the prodigal algorithm and a minimum peptide length of 33. Predicted ORFs were annotated in MetaPathways with the LAST algorithm and default run parameters against the Carbohydrate Active Enzymes database (CAZy; release 2014.09.04; Lombard et al., 2014). This resulted in 6,799,723 ORFs, of which 138,785 were annotated to the CAZy database (**Supplementary Data Sheets S5, S6**). Subsequent filtering to remove eukaryotic, viral, archaeal, and unclassified proteins resulted in 126,084 ORFs corresponding to 26,509 CAZy annotations (**Supplementary Data Sheets S7, S8**).

Carbohydrate Active Enzymes functional profiles were rarefied at a depth of 1000 sequences/sample prior to comparisons of composition and richness. Profile dissimilarity matrices were generated using the Bray-Curtis metric (Bray

[2]http://hannonlab.cshl.edu/fastx_toolkit/

and Curtis, 1957) and differences in composition were tested using PERMANOVA and PERMDISP in Primer v.6 (9999 permutations each; $p < 0.05$), and visualized with principle coordinate plots. Functional richness was determined by the observed number of enzyme annotations and families within each sample and compared using the two-tailed Welch's *t*-test in *R* (t.test). Communities were compared across sample type and depth separately, instead of a mixed effect design, as the water samples did not sufficiently represent multiple depths. Testing for an association between functional and taxonomic richness was performed using the two-tailed Spearman's rank correlation test in *R* (cor.test).

Differential abundance analysis for CAZy families and individual gene annotations was performed using the two-tailed Welch's *t*-test in *R*. Genes with <100 total reads and families with <1000 total reads were excluded from the analysis in order to compare only high abundance groups. Read counts were normalized to sample counts and p-values were adjusted for multiple hypothesis testing using the Benjamini–Hochberg method (Benjamini and Hochberg, 1995). Genes and families were considered differentially abundant if their FDR corrected *p*-value < 0.1 and log2 fold change $\sim|1|$ or greater. The log2 fold change threshold was relaxed relative to genus enrichment due to low sequence coverage in the metagenomic dataset.

To determine how well the metagenomic dataset corresponded to the 16S amplicon data, and to better link the two bacterial community profiles, we performed closed reference OTU picking in QIIME (pick_closed_reference_otus.py) on the quality filtered metagenomic sequences against the SILVA SSU Ref NR 128 database. OTUs were taxonomically assigned using UCLUST (Edgar, 2010) and assign_taxonomy.py, and OTUs assigned to chloroplast or mitochondria were removed. Taxa summary plots were then constructed for comparison with the 16S rRNA gene amplicon dataset.

Cultured Bacterial Isolates and Detection of Alginate Utilizing Bacteria

Bacteria were cultured from a subset of the macroalgal blades and water column samples used for amplicon sequencing (**Supplementary Data Sheet S3**). *Macrocystis* blades from the bottom and middle depth at each site that were swabbed for sequencing were immediately swabbed again for culturing. These swabs were plated directly onto both alginate and tryptone marine agar media ($n = 30$ for each media type). Alginate marine agar media was made using a previously published protocol (Clasen and Shurin, 2015) and consisted of distilled water, Instant Ocean® (to salinity$\sim$31 ppt), 1.5% agar, and 0.3% sodium alginate (Sigma-Aldrich A0682). Tryptone marine agar media was made using distilled water, Instant Ocean® (to salinity$\sim$31 ppt), 1.5% agar, and 1% tryptone (BD REF211705). Liquid versions of both media types were prepared in identical fashion with agar excluded. One water sample from mid and bottom depths at each site was also plated on each media type ($n = 12$). Plates were sealed with parafilm and stored at 4°C for 2 weeks to facilitate transport from the remote field site to the lab. Once in the lab cultures were incubated at 12°C, as this was approximately the *in situ* water temperature when sampling. After plates had been incubated for several days, 5–10 colonies displaying morphological variation were isolated using standard microbiological techniques. Subsequent assays and maintenance of cultures all occurred at 12°C.

Growth With Alginate as the Sole Carbon Source

Isolated bacteria were inoculated in triplicate into 96 well microplates containing alginate marine media to determine if any were capable of utilizing alginate as a sole carbon source. Growth was measured daily using turbidimetry over 4 days. Isolates were considered to be growing if absorbance readings at the first and final time point were significantly different (two-tailed paired *t*-test; $p < 0.05$), a minimum increase of 0.1 OD_{492} was detected, and mean absorbance increased by $\geq$50%.

Alginate Utilization Assays

We aimed to broadly detect alginate utilization by bacteria and performed two distinct assays on each isolate to better capture the different stages of the alginate metabolic pathway. The use of two assays allowed us to partially account for the complex metabolic interactions and substrate partitioning that have been reported for alginate (Wong et al., 2000; Kita et al., 2016). For example, some bacteria that do not degrade polymeric alginate can metabolize alginate oligosaccharides (Hehemann et al., 2016) and some taxa can directly uptake the polymer (Hisano et al., 1995). One assay employed here assessed extracellular degradation of polymeric alginate and another tested for enhanced growth yielded by alginate metabolism within the cell. It should be noted these assays were chosen to detect possible interactions with extracellular, kelp-derived alginate, but they do not distinguish this from the biosynthesis of alginate, of which some bacteria are capable and similar enzymes are involved (Kim et al., 2011). Furthermore, quantitative assays were chosen over traditional plate staining methods to minimize subjectivity, due to the lack of substrate specificity reported in analogous assays of polysaccharide degradation (Meddeb-Mouelhi et al., 2014), and to provide consistent and conservative thresholds for detecting alginate utilization.

Metabolism of alginate for growth was assessed by comparing the growth of liquid cultures with and without alginate supplemented to the medium. The alginate supplemented media consisted of tryptone marine media (see above) with 0.3% sodium alginate added. Each isolate was grown for 3 days prior to the experiment. This likely corresponded to post-exponential phase for most isolates, but we did not construct individual growth curves. Cultures were then inoculated in triplicate into a 96 well plate containing tryptone media and a plate containing alginate supplemented media. Growth was then measured daily using turbidimetry over 4 days. Isolates were considered to be metabolizing alginate if they grew in alginate supplemented media (according to the criteria listed above for the alginate only media) and net growth in alginate supplemented media was 50% greater than in un-supplemented media. It should be noted that while this assay was used to detect increased growth in alginate supplemented media, it is unable to identify organisms

who utilize alginate but achieve the same maximal growth in culture, or taxa whose metabolism of tryptone is inhibitory to the metabolism of alginate.

The second aspect of alginate utilization, degradation of polymeric alginate, was assessed by measuring the strong absorption of UV light characteristic of de-polymerized alginate, due to the formation of C-4 = C-5 double bonds within alginate oligosaccharides (Wong et al., 2000; Han et al., 2016). As above, each isolate was grown for 3 days prior to the experiment and inoculated in triplicate into a 96 well plate containing alginate marine media. UV absorbance was measured daily over a 4 days time period. Isolates were considered to degrade alginate if the absorbance readings at the first and final time point were significantly different (paired *t*-test, $p < 0.05$), a minimum change of 0.1 OD_{230} was detected, and absorbance increased by $\geq$50%. This assay was used to detect the increase in UV absorbance over the course of the growth period, however, it was not used to detect an initial increase in absorbance followed by a reduction (owing to the uptake of alginate oligosaccharides). Thus, bacterial isolates that rapidly imported the cleaved alginate oligosaccharides at a rate greater than depolymerization were not detected using this technique. Negative controls for all assays consisted of media without bacterial inoculum.

Isolate Sequencing and Taxonomy Assignment

Isolates assayed for alginate utilization were sequenced at the V4–V9 region of the 16S rRNA gene. DNA was extracted using Prepman Ultra® and amplified with primers *515f/1492r*: *515f*: 5′–GTGYCAGCMGCCGCGGTAA–3′, *1492r*: 5′–CGGTTACC TTGTTACGACTT–3′. Each PCR contained 12.5 μl of 2X Phusion Flash Master Mix®, 1.25 μl of each primer (final concentration: 0.5 μM), 1 μl of DNA, and PCR grade water to final volume of 25 μl. PCR was performed with an initial denaturation temperature of 98°C for 10 s, followed by 30 cycles of denaturation at 98°C for 1 s, annealing at 52.3°C for 5 s, and extension at 72°C for 15 s, with final extension at 72°C for 1 min. PCR products were Sanger sequenced at the Genome Quebec Innovation Centre at McGill University (Montreal, Canada).

Isolate sequence data was initially trimmed in Geneious (v.9.1; Biomatters) to remove low quality ends and ambiguities. The resulting sequences were then aligned using the SILVA Incremental Aligner (SINA v1.2.11; Pruesse et al., 2012), queried against the SILVA SSU Ref 128 database (minimum identity 95%; Quast et al., 2012), and the highest matching taxon was recorded. Sequences were subsequently queried against the SILVA SSU Ref 128 database locally using BLAST+ (blastn; Camacho et al., 2009) to confirm taxonomy and retrieve additional quality scoring metrics. Isolate sequences were then collapsed into OTUs in QIIME by clustering at 100% sequence identity using UCLUST (Edgar, 2010) and a representative sequence was picked for each OTU. For each 100% OTU, we then aligned all sequences that were collapsed into the OTU with MUSCLE (Edgar, 2004) to confirm that sequences were 99.8–100% identical; they were.

Phylogenetic trees of isolate OTUs and reference sequences were constructed using RAxML v.8.2.9 (Stamatakis, 2014) for the three major bacterial clades detected. Briefly, OTU representative sequences were aligned to the SILVA SSU Ref NR 128 alignment using PyNAST within QIIME. Aligned sequences, along with a filtered SILVA SSU Ref NR 128 alignment and tree, were then used to construct a Maximum Likelihood tree using the GAMMA model of rate heterogeneity and the evolutionary placement algorithm (Berger et al., 2011). The SILVA alignment and tree were filtered to retain only genera detected in either the culture-independent or cultured communities of *Macrocystis* and the water column for each clade. Reference sequences for each genus were selected because they were either the type species or a common marine taxon. The number of reference sequences to include for each genus was chosen relative to the number of OTUs falling within that genus. Annotation of phylogenetic trees was performed using the ggtree package (Yu et al., 2017) in R.

We assessed the taxonomic composition of the cultured community with high-throughput 16S rRNA gene sequencing by scraping all colonies off of a subset of culture plates with a sterile cell scraper following isolation of individual colonies; 1 sample per plate. These pooled bacterial colonies were then processed with the same DNA extraction, PCR, and amplicon sequencing procedures as the uncultured communities (above). The plates used here were from one water and three kelp samples from each site, and both media types were included ($n = 24$ total; water = 6, middle depth kelp blades = 18).

Figure Generation

All figures were generated and exported in the R statistical environment (v3.4.0; R Core Team, 2017). Minor modifications, when needed, were performed using Inkscape v0.91.

Accession Numbers

Raw Illumina MiSeq and NextSeq reads, along with associated MiMARKS compliant metadata, have been accessioned in the European Bioinformatics Institute[3] (Study Accession Number: PRJEB21672). Raw Sanger sequencing reads have been accessioned in GenBank[4] (Accession Numbers: MF443456 – MF443740).

RESULTS

Bacterial Communities on *Macrocystis pyrifera* and in the Surrounding Water Column

We sampled the cultured and uncultured epibiota on *M. pyrifera* blades from three depths, along with 11 nearby water column communities, within three kelp beds adjacent to Calvert Island, British Columbia. Overall, these bacterial assemblages are composed of 1001 OTUs assigned to 198 genera. Unsurprisingly, there are substantial differences between cultured and uncultured communities and fewer OTUs detected in cultured communities (**Figure 1A**). At broad taxonomic

[3]www.ebi.ac.uk

[4]www.ncbi.nlm.nih.gov/genbank/

levels, uncultured communities are primarily composed of Gammaproteobacteria, Alphaproteobacteria, Verrucomicrobia, Planctomycetes, and Bacteroidetes (**Figures 1A,B**), while Gammaproteobacteria and Bacteroidetes dominate cultured communities (**Figure 1A** and **Supplementary Figure S1**). The uncultured *M. pyrifera* epibiota differs strongly from the uncultured bacterial community found in the water column; while many OTUs are shared across these sample types their relative abundance differs markedly (**Figure 1A**). Differences between water and *M. pyrifera* are driven in part by high abundance of Cyanobacteria (mostly *Synechococcus*) in the water, but near absence on *M. pyrifera*, and abundant Verrucomicrobia (*Persicirhabdus*) and Planctomycetes (*Blastopirellula*) on *M. pyrifera* blades from middle and top depths (**Figures 1A,B**). Within shared phyla we also observe turnover at the genus level across Proteobacteria and Bacteroidetes (**Figure 1C**). The cultured community is quite similar between the water column and *M. pyrifera*, likely due to the selectivity of culturing (**Figure 1A** and **Supplementary Figure S1**).

At higher resolution, bacterial diversity again differs between the *M. pyrifera* epibiota and surrounding water column across uncultured communities, and also across blade depth for *M. pyrifera*. Unless otherwise specified we focus on the uncultured bacterial communities from this point on. We used a mixed effect ANOVA implemented in lmer to test for differences in richness, as measured by the Chao1 index, between sample types (water versus *Macrocystis* blades; fixed effect) and across *Macrocystis* blade depth (top, middle, bottom; fixed effect), while accounting for site, which was included as a random effect. Richness differs significantly across sample type (Chao1; $F = 18.2$, df = 1, $p = 0.0001$) and blade depth ($F = 9.7$, df = 2, $p = 0.0003$), but not across site ($p = 0.87$). Pairwise comparisons of richness across depth revealed that *M. pyrifera* communities are significantly richer on blades from bottom depths ($p < 0.001$), while richness is similar on middle and top blades ($p = 0.64$; **Figure 1D**).

We visualized similarity in bacterial community composition with a principle coordinate plot generated from a weighted UniFrac distance matrix, which clearly shows that water column communities are distinct from those on *Macrocystis* (**Figure 1E**). We then tested for differences in community composition between sample types and across *Macrocystis* blades of differing depth with multifactor PERMANOVA that included fixed terms for sample type (*Macrocystis* versus water) and depth (top, middle, and bottom), and site as a random effect ($N = 55$ total). In this full model sample type was highly significant (Pseudo-$F = 3.33$, df = 1, $p = 0.0001$), but depth and site were not (depth: Pseudo-$F = 2.59$, df = 2, $p = 0.11$; site: Pseudo-$F = 0.73$, df = 2, $p = 0.7$) and dispersion differed across all three factors (PERMDISP $p < 0.05$). The substantial differences in community composition between water and *Macrocystis* are apparent in the OTU heatmap and taxa summaries (**Figure 1**). In order to assess differences in community structure within *Macrocystis* epibiota, we conducted a separate PERMANOVA on only *Macrocystis* samples ($N = 44$), again with depth as a fixed factor and site random. Here, depth is a significant determinant of community structure (Pseudo-$F = 4.31$, df = 2, $p = 0.015$), but site is not (Pseudo-$F = 1.63$, df = 2, $p = 0.09$). Pairwise comparisons across depth again show that the epibiota on bottom blades are distinct (p = 0.001), but epibiota on top and middle blades do not differ ($p = 0.48$). Differences across depth are driven by changes in the relative abundance of several phyla — Verrucomicrobia and Alphaproteobacteria are more abundant on upper and middle blades, while Gammaproteobacteria are more abundant on deeper blades (**Figure 1B** and **Supplementary Figure S2**) — and particularly by the turnover of dominant genera within major clades (**Figure 1C**). For instance, *Persicirhabdus* (Verrucomicrobia) is highly enriched in the upper depths, while a shift from Saprospiraceae to *Dokdonia* occurs within Bacteroidetes from deep to shallow. Overall, 21 genera are differentially abundant between bottom and upper depths (FDR adjusted $p < 0.1$; **Supplementary Table S2**). Genera enriched on blades from the bottom depth predominantly fall in the Gammaproteobacteria, including *Psychromonas,* a genus with demonstrated capacity for alginate utilization (**Table 1**). Blades from upper depths were enriched for Sphingomonadales (Alphaproteobacteria), *Dokdonia,* and *Persicirhabdus* (**Figure 1C** and **Supplementary Table S2**).

Carbohydrate Metabolic Profiles

We reconstructed carbohydrate metabolic profiles for *M. pyrifera* and water column samples from one kelp bed (Site 3), using shotgun metagenomic sequencing, to assess the capacity for alginate utilization in these bacterial communities (**Figure 2**). Metagenomic reads were annotated using the Carbohydrate Active Enzymes database (CAZy; release 2014.09.04; Lombard et al., 2014). The majority of CAZy annotations detected on *M. pyrifera* and in water column bacterial communities fall within Glycoside Hydrolase and Glycosyl Transferase enzymes (**Figure 2C**). Overall, metagenomic reads mapping to CAZy genes were assigned to enzyme families associated with the metabolism of diverse algal carbohydrates, in addition to the metabolism of substrates related to fundamental bacterial processes (e.g., peptidoglycan, lipopolysaccharide; CAZypedia Consortium, 2017; **Supplementary Table S3**).

Most CAZy families are found in similar proportions across kelp and water column bacterial communities (**Figure 2C**), despite the substantial taxonomic differences observed (**Figures 1**, **2A,B**). The Polysaccharide Lyase (PL) enzyme class, which includes alginate and oligoalginate lyases, represents a small portion of the carbohydrate functional profiles, 5–10% overall (**Figure 2C**). However, the majority of PL genes belong to the PL6, 7, 15, and 17 families (**Figure 2D**) within both kelp and water column communities. The only known activities in these families are alginate and oligoalginate lyases, with the exception of PL6 which also contains chondroitinase B. Notably, three of these families (PL6, 7, 17) are among the most abundant CAZy families in the *Macrocystis* epibiota and together represent ∼5% of the total carbohydrate metabolic profile (**Figure 2** and **Supplementary Table S3**). The same polysaccharide lyase families are found in the water column, though they make up less of the relative abundance of the overall CAZy profile (**Figure 2**). Indeed, we found 4 CAZy families to be differentially enriched between *Macrocystis* communities

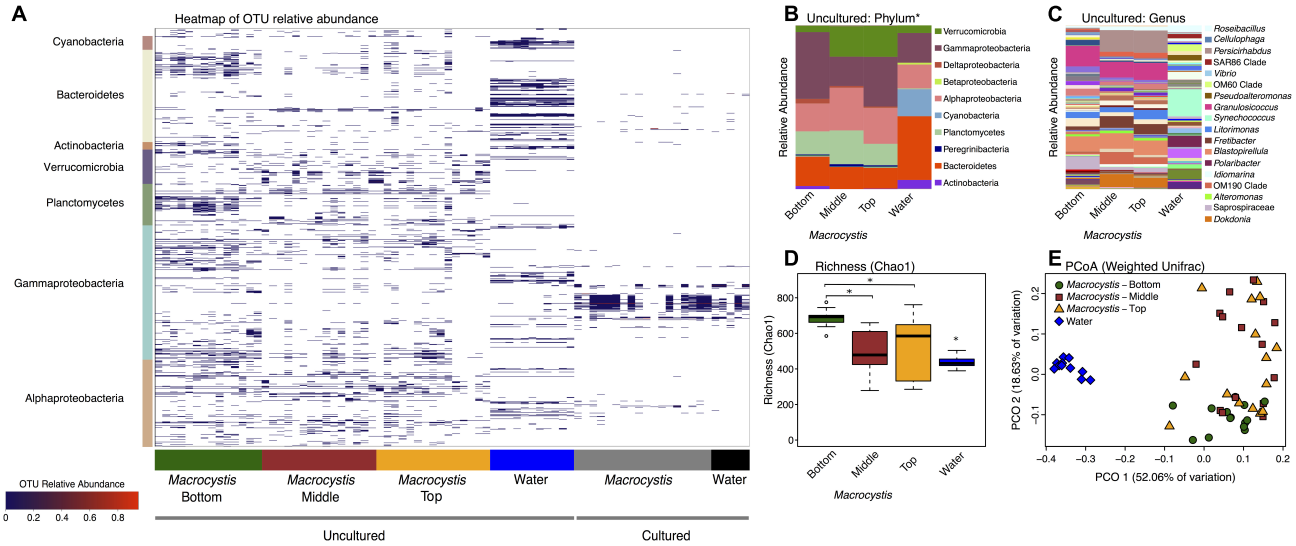

FIGURE 1 | Bacterial diversity associated with *Macrocystis* blades and the nearby water column. **(A)** Heatmap of the relative abundance of operational taxonomic units (OTUs) detected on *Macrocystis* blades from different depths and in the water column from cultured and uncultured samples. OTUs are ordered by taxonomy and the major bacterial clades detected are indicated on the *y*-axis. **(B–E)** Uncultured samples only. **(B)** Taxa summaries of uncultured communities on *Macrocystis* and in the water column at the Phylum level (*Class for Proteobacteria). All samples within a sample type merged. **(C)** Genus level plot of **(B)**. **(D)** Bacterial species richness (Chao1 index) is higher on the *Macrocystis* surface compared to the water column ($N = 11$), and greater on blades at bottom depth ($N = 14$) compared to middle ($N = 15$) and top ($N = 15$) depths. Statistical tests summarized in text; $^*p < 0.01$. **(E)** Principle coordinate plot of Weighted UniFrac distance for kelp and water bacterial communities.

and the water column (**Supplementary Table S2**), with all four families enriched on the *Macrocystis* surface. Notably, two of these families contain alginate lyase enzymes (PL7 and PL17), while a third (CBM32) has been shown to be involved in the binding of alginate by polysaccharide lyases (Sim et al., 2017; Lyu et al., 2018).

Functional profiles of CAZy genes differ in composition between *M. pyrifera* and the water column, and across blade depths, consistent with the observed patterns of taxonomic composition. We compared functional composition across sample types with PERMANOVA analysis of Bray–Curtis distance matrices and visualized differences with PCoA plots (**Figure 2E**). The profiles of carbohydrate metabolic potential differ significantly between the water column and *Macrocystis* epibiota (PERMANOVA: Pseudo-$F = 1.92$, df = 1, $p = 0.0006$) and the *Macrocystis* communities are significantly more dispersed (PERMDISP: $p = 0.0005$) (**Table 2**). Comparing *Macrocystis* samples between middle and bottom depth reveals significant differences in functional composition (PERMANOVA: Pseudo-$F = 1.3$, df = 1, $p = 0.0066$), while dispersion does not differ (**Table 2**). In contrast, we see no difference in functional richness between *Macrocystis* and water column communities at the gene (Welch's *t*-test for observed genes: $p = 0.18$) or family level (Welch's *t*-test for observed families: $p = 0.33$; **Table 2**). *Macrocystis*-associated communities from bottom depths do harbor greater CAZy richness at the family level (Welch's *t*-test $p = 0.0023$; **Table 2**), while depths do not differ in CAZy gene richness (Welch's *t*-test $p = 0.23$; **Table 2**). *Macrocystis* blade communities at the bottom depth were also taxonomically richer, and we find that *Macrocystis*-associated community functional richness (CAZy families) is positively correlated with taxonomic richness (Spearman's rank correlation test: $p = 0.0045$, $r_s = 0.87$; **Figure 2F**).

We hypothesized that alginate metabolic capacity might differ with depth in the *Macrocystis* epibiota, given the significant difference in functional community structure across depth and the prevalence of several alginate lyase families within carbohydrate metabolic profiles. However, no genes encoding alginate degrading enzymes or PL families are differentially enriched across blade depths. We next looked at the total metabolic profiles to identify metabolic processes that might be associated with the observed depth patterning. While no CAZy genes were differentially enriched, we identified three CAZy families (GH16, CBM6, and CBM13) that were enriched in the bottom depth (adjusted $p < 0.1$; **Supplementary Table S2**). These families contain enzymes involved in the hydrolysis of diverse algal polymers (GH16), in particular cellulose (CBM6, CBM13; Adams et al., 2011).

Alginate Utilizing Bacteria

We cultured bacteria from a subset of the kelp blades and water samples using tryptone and alginate marine media. A total of 338 isolates were assayed for the utilization of alginate, and 255 of these were successfully identified by Sanger sequencing the V4–V9 region of the 16S rRNA. Of these 255 isolates (**Table 1**), 91 were capable of depolymerizing alginate (36%), 33 were capable of metabolizing it for growth (13%), and 44 could do both (17%). A larger proportion of bacteria isolated on alginate media (76%) demonstrated alginate utilization compared to bacteria isolated on tryptone media (55%). Bacterial isolates were predominantly

TABLE 1 | Diverse bacterial genera from isolates cultured in the *Macrocystis pyrifera* forest demonstrate alginate utilization.

Genus	Isolates	Observed activity					OTUs*	Reported alginate utilization
		Growth (obligate)	Growth (supplemented)	Degrade	Both	None		
Alteromonas	35	–	9%	34%	11%	46%	16	Sawabe et al., 1995; Iwamoto et al., 2001
Cellulophaga	9	–	0%	11%	67%	22%	7	Martin et al., 2015; Zhu et al., 2016
Cobetia	9	–	44%	22%	11%	22%	6	Martin et al., 2015; Gong et al., 2016
Colwellia	3	–	33%	33%	33%	0%	3	^This study
Formosa	1	–	0%	100%	0%	0%	1	Mann et al., 2013; Tanaka et al., 2015
Glaciecola	2	–	50%	50%	0%	0%	2	Xu et al., 2017
Halomonas	10	–	10%	10%	20%	60%	8	Wong et al., 2000
Idiomarina	5	–	20%	0%	20%	60%	3	^This study
Litoreibacter	1	–	0%	0%	0%	100%	1	
Maribacter	5	–	0%	80%	0%	20%	5	Nedashkovskaya et al., 2004; Zhan et al., 2017
Marinobacter	2	–	0%	0%	0%	100%	1	
Paraglaciecola	13	–	8%	38%	31%	23%	9	Schultz-Johansen et al., 2016
Photobacterium	2	–	50%	50%	0%	0%	1	Wong et al., 2000
Polaribacter	1	–	100%	0%	0%	0%	1	Dong et al., 2012; Tanaka et al., 2015
Pseudoalteromonas	94	–	14%	46%	18%	22%	44	Matsushima et al., 2010; Li et al., 2011
Pseudomonas	4	–	0%	0%	0%	100%	2	Boyd et al., 1993
Psychrobacter	2	–	50%	0%	0%	50%	2	Dong et al., 2012
Psychromonas	3	–	33%	33%	33%	0%	1	Dong et al., 2012
Rheinheimera	2	–	0%	0%	100%	0%	1	^This study
Rhodococcus	1	–	0%	0%	0%	100%	1	
Shewanella	2	–	50%	50%	0%	0%	2	Martin et al., 2015; Tanaka et al., 2015
Sulfitobacter	26	–	8%	19%	4%	69%	8	Ivanova et al., 2004
Tamlana	1	+	0%	0%	100%	0%	1	Tanaka et al., 2015
Vibrio	22	+	5%	50%	18%	27%	12	Han et al., 2004; Martin et al., 2015
Total	255		13%	36%	17%	34%	138	

**OTUs represent isolates within each genus clustered at 99.8–100% similarity in 16S rRNA sequences. ^We identified three bacterial genera that were not previously known to use alginate (Colwellia, Idiomarina, and Rheinheimera).*

from the Gammaproteobacteria (**Figure 3** and **Table 1**), with *Pseudoalteromonas* being the most abundant cultured genus (94/255 isolates) and containing the most active isolates ($n = 73$), followed by *Alteromonas* and *Vibrio*. Two isolates were capable of obligate growth on alginate; these were assigned to *Tamlana* (Flavobacteriaceae) and *Vibrio* (Gammaproteobacteria). Finally, while alginate utilization has been reported for most assayed genera previously (**Table 1**), we observed this capacity for the first time in three genera: *Colwellia, Idiomarina,* and *Rheinheimera*.

To further understand how alginate utilization varies across closely related taxa, Sanger sequences from the 255 isolates were clustered at 100% similarity into OTUs. The resulting 138 OTUs fall in 24 genera within the Gammaproteobacteria, Alphaproteobacteria, and Flavobacteriaceae (**Table 1**). OTU representative sequences were aligned to the SILVA 128 reference database and placed into phylogenetic trees for each of these clades (**Figure 3** and **Supplementary Figures S3–S5**). In total, 104 OTUs (representing 20 genera) demonstrated alginate utilization (**Supplementary Table S1**). Importantly, 17 OTUs were composed of isolates with and without this capacity; these taxa were thus discordant for alginate utilization despite identical 16S sequences. Discordance was also observed for type of activity (metabolism, degradation, both; **Supplementary Table S1**).

To deeply survey the total cultured bacteria from *M. pyrifera* and the water column, and to investigate how representative the isolated taxa were, we sequenced bacterial colonies from 24 culture plates (18 kelp; 6 water). Plates were scraped for all colonies and sequenced at the V4 region of the 16S rRNA gene on the Illumina MiSeq platform. Sequences were clustered into 150 OTUs that fall within 62 genera. Cultured taxa belong almost

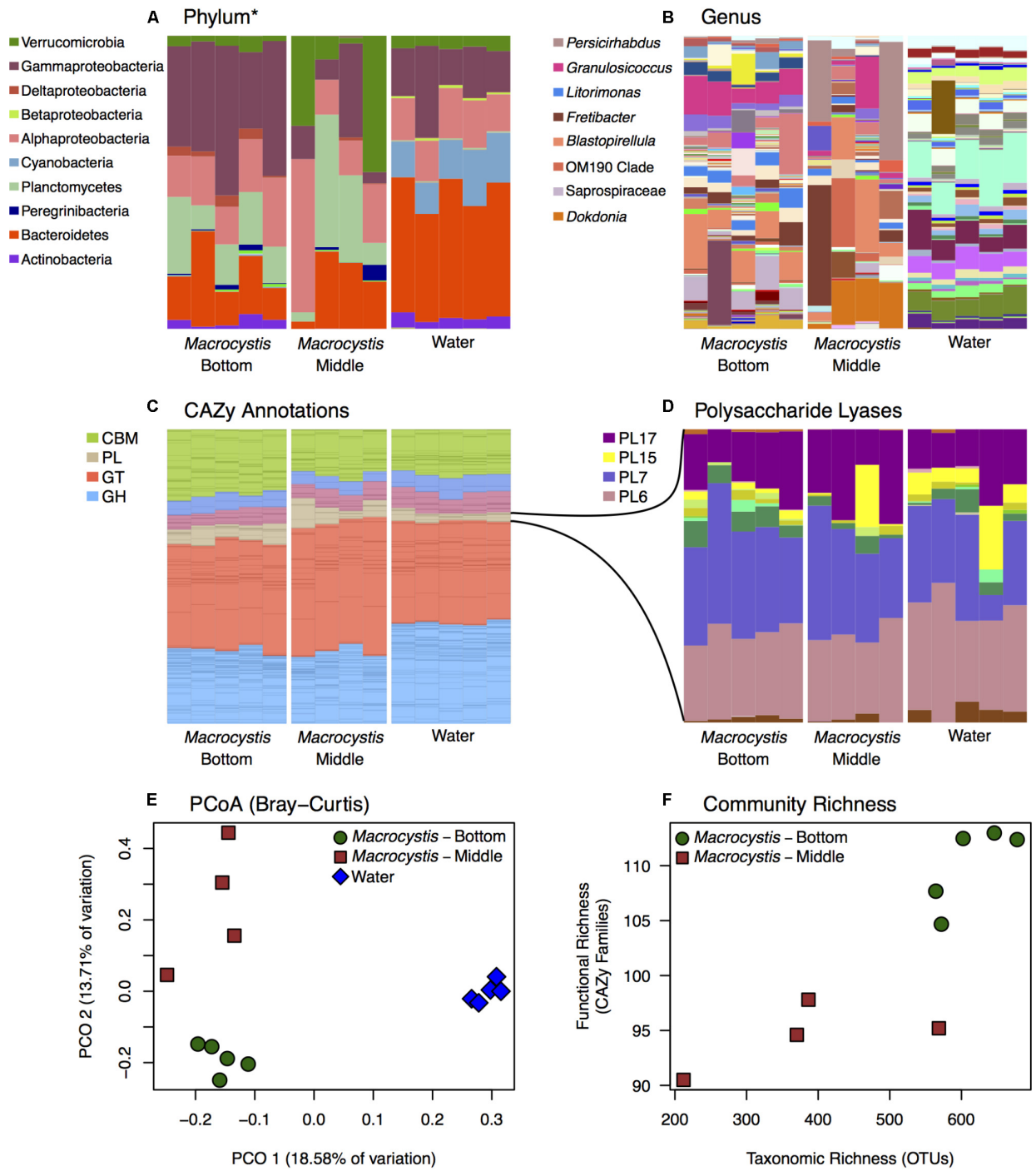

FIGURE 2 | Bacterial taxonomic and functional profiles within a single kelp bed. Bacterial communities from kelp blades at middle (n = 4) and bottom (n = 5) depths, and in the surrounding water column (n = 5), in one kelp bed (Site 3). **(A,B)** Taxonomic profiles from 16S rRNA gene amplicon sequencing are variable between water and *Macrocystis*, and across depth. See **Supplementary Figure S6** for corresponding taxonomic profiles derived from metagenomic data. **(A)** Phylum (*Class for Proteobacteria) level. **(B)** Genus level (most abundant genera shown in legend). **(C,D)** Relative abundance of Carbohydrate Active Enzyme (CAZy) annotations from these communities is largely consistent across sample types. **(C)** CAZy annotations largely fall within Carbohydrate Binding Modules (CBM), Glycosyl Transferases (GT), Glycoside Hydrolases (GH), and Polysaccharide Lyase classes (PL). Enzyme families within these broader groups are represented by stacked bars of the same color. **(D)** Relative abundance of CAZy families within the Polysaccharide Lyase class. Families PL6, 7, 15, and 17 are the most abundant and almost exclusively contain alginate and oligoalginate lyases. **(E)** Principle coordinate plot of CAZy annotations constructed from Bray–Curtis dissimilarity matrix shows differences between *Macrocystis* bottom and middle blades, and the water column, similar to taxonomic composition (statistical tests summarized in **Table 2**). **(F)** Functional richness (number of CAZy families) is correlated with taxonomic richness of OTUs in *Macrocystis* communities (r_s = 0.87).

TABLE 2 | Summary of statistical tests comparing bacterial carbohydrate metabolic profiles.

Data	Comparison		Welch's *t*-test Observed genes			Welch's *t*-test Observed families		
	Group 1	Group 2	df	*t*	*p*	df	*t*	*p*
(A) CAZy functional profile richness								
All samples	Blade (n = 9)	Water (n = 5)	11.61	−1.43	0.18	4.78	1.07	0.33
Macrocystis	Bottom (n = 5)	Middle (n = 4)	9.86	−1.27	0.23	6.98	6.95	0.0023
(B) CAZy functional profile dissimilarity								
All samples	Blade (n = 9)	Water (n = 5)	1	1.92	0.0006	1,12	67.65	0.0005
Macrocystis	Bottom (n = 5)	Middle (n = 4)	1	1.3	0.0066	1,7	4.78	0.087

entirely to the Gammaproteobacteria, Alphaproteobacteria, and Flavobacteriaceae (**Figure 1A** and **Supplementary Figure S1**). Planctomycetes and Verrucomicrobia, which were abundant in the culture-independent dataset, were absent among cultured taxa. Notably, the three genera (*Alteromonas, Pseudoalteromonas,* and *Vibrio*) comprising the majority of cultured taxa occur at very low abundance in the *M. pyrifera* epibiota (**Supplementary Figure S1**). Overall, there is little overlap between the cultured and uncultured bacterial communities (**Figure 1A**).

DISCUSSION

Structure and Diversity of the *Macrocystis pyrifera* Epibiota

The epibiota of *M. pyrifera* (**Figure 1** and **Supplementary Figure S2**) is composed of bacteria known to be prevalent in the marine environment (Wahl et al., 2012; Singh and Reddy, 2014) and on algal surfaces (Staufenberger et al., 2008; Burke et al., 2011; Michelou et al., 2013). We find distinct bacterial communities on *Macrocystis* compared to the water column, though large numbers of OTUs are shared across both, consistent with other kelps (Lemay et al., 2018). The Planctomycetes phylum in particular was highly enriched relative to the water column (**Figure 1B**), and is commonly found on kelp (Vollmers et al., 2017; Lemay et al., 2018). Planctomycetes are often underrepresented in amplicon sequencing studies, but were found to dominate biofilms on *Laminaria* (Bengtsson and Øvreås, 2010). *Persicirhabdus* and *Rubritalea* (Verrucomicrobia) are also emerging as common associates of *Macrocystis* (**Figure 1C**) and kelp more generally (Vollmers et al., 2017).

We observed that epibiotic communities differ in composition and richness across blade depths (**Figure 1** and **Supplementary Figure S2**), with richer communities being found at the bottom depth (**Figure 1D**). This depth associated structuring of bacterial communities represents a novel axis of community variation in *Macrocystis* forests. Blades at lower depths are older (Wheeler and North, 1981; Reed et al., 2015), and while this age difference may only correspond to several months (Druehl and Wheeler, 1986; Van Tussenbroek, 1989), this pattern is consistent with work in other kelp documenting microbial succession and increasing richness as blades age (Bengtsson et al., 2012), as well as microbiota changes with tissue degradation and disease state (Marzinelli et al., 2015). Additionally, we did not observe such differences between water column communities across depths, which would indicate that abiotic factors are not driving community variation. However, due to an unbalanced distribution of water samples across sites, these observations were not statistically validated. Regardless, the increasing diversity of bacteria and functional genes involved in carbohydrate metabolism observed on deeper blades is likely a consequence of reduced production of anti-fouling metabolites, and other processes during senescence, that make the host surface increasingly permissive to colonization and degradation (Egan et al., 2013).

The taxa that are enriched at lower depths (**Figure 1** and **Supplementary Table S2**) may be opportunistic metabolisers of kelp tissue. Interestingly, several Gammaproteobacteria genera were enriched in deeper communities and this may be explained by their capacity for degrading diverse algal polysaccharides (Michel et al., 2006), making them well suited as generalists on older tissue. Further, the substantial enrichment of Saprospiraceae on lower depth blades may reflect a similar role for this group in tissue degradation, as this family includes known degraders of algal polysaccharides (McIlroy and Nielsen, 2014). Younger tissue may be more likely to host taxa specifically associated with kelps, and we find several abundant taxa that are detected on kelps in other studies, such as *Persicirhabdus* (Vollmers et al., 2017; Chen and Parfrey, 2018) and *Dokdonia* (**Figure 1C**), which is often found on seaweeds generally. Taken together, these patterns are consistent with succession on *M. pyrifera* blades with increasing depth. However, as depth is additionally associated with light reduction and variations in *Macrocystis* tissue physiology (Konotchick et al., 2013), the exact cause of this patterning remains unclear. Furthermore, the tidal range at these kelp beds was high during the period of collection (>3 m) and blades at the middle depth were likely at the surface at some points during the day. Thus the exposure to similar abiotic factors, such as air temperature, sunlight, and oxygen, maybe have also contributed to the similarity observed between shallower communities relative to those at depth.

Epibiotic Functional Profiles Change With Depth

Carbohydrate metabolism in the *Macrocystis* forest appears to be structured around the major constituents of kelp tissue. Of the most abundant CAZy families that we detected, many represent activities related to carbohydrate substrates in *Macrocystis* (**Supplementary Table S3**; Ravanal et al., 2016), in particular alginate and cellulose. Despite their taxonomic

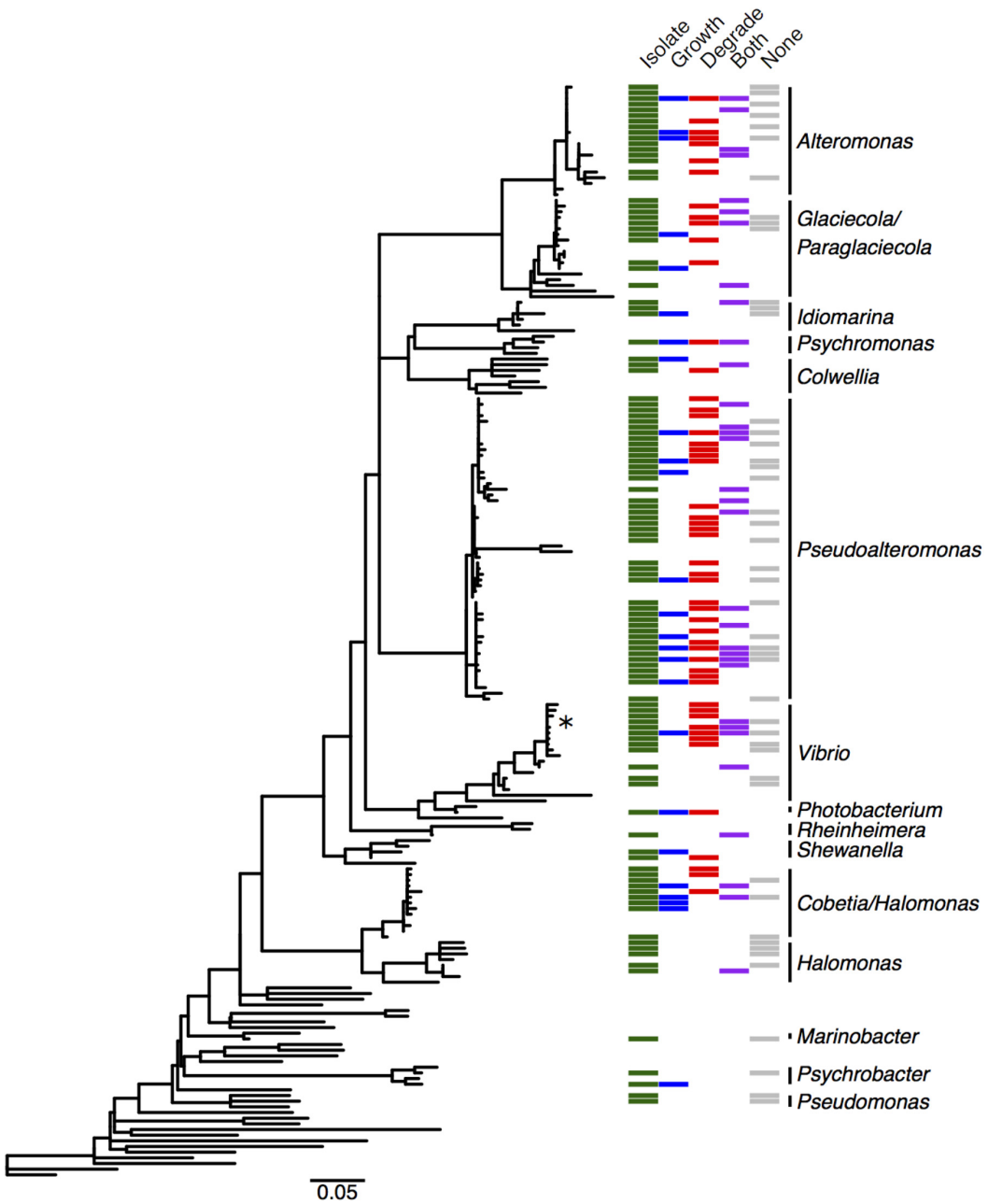

FIGURE 3 | Distribution of alginate utilizing taxa within the Gammaproteobacteria. Phylogenetic tree of Gammaproteobacteria genera detected in the *M. pyrifera* epibiota and surrounding water column in this study, constructed from 16S rRNA gene sequences by placing cultured bacterial isolates into a tree of reference sequences with RAxML EPA. See **Supplementary Figure S3** for labeled tree with isolate identities, reference taxa, and accession numbers. Green: cultured bacterial isolates in this study; sequences from isolated bacteria with 99.8–100% 16S similarity were collapsed into operational taxonomic units (OTUs). Blue: cultured isolates from this study whose growth was enriched by at least 50% in the presence of alginate, or that grew with alginate as the sole carbon source (marked with *). Red: cultured isolates in this study that degrade alginate. Purple: cultured isolates whose growth was enhanced and that degrade alginate. Gray: cultured isolates demonstrating neither enhanced growth nor degradation. Detailed information on cultured isolates in **Supplementary Table S1**.

differences, kelp and water column metabolic profiles appear compositionally similar at the level of CAZy families (**Figure 2C** and **Supplementary Table S3**). Yet, we did observe differences between carbohydrate metabolic profiles with regard to alginate metabolism. Interestingly, two CAZy families containing alginate lyase enzymes, and one family shown to be involved in binding alginate, were enriched on the *Macrocystis* surface relative to the water column (**Supplementary Table S2**). This may reflect an abundance of alginate on the kelp surface relative to the water column and could underlie some of the

taxonomic differences observed between kelp and water bacterial communities. However, the pre-filtering of water column samples prior to processing (thereby removing larger detrital material), in addition to the highly disparate sequencing coverage of the metagenomic samples and unbalanced distribution of water samples across depths, necessitate further validation of these observations.

The capacity for alginate utilization was observed across all bacterial communities (**Figure 2D**) and the majority of all PL genes fall within four families that almost exclusively contain alginate and oligoalginate lyases (Jagtap et al., 2014). Interestingly, these same families were shown by Hehemann et al. (2016) to contain sufficient metabolic diversity to partition alginate within bacterial populations. Furthermore, the abundance of three of these families (PL7, 6, 17) in epibiotic functional profiles indicates the importance of alginate as a carbon source in this system. Finally, the presence of these families across taxonomically diverse bacterial communities (**Figures 2A,B**) indicates a broad capacity for alginate utilization, particularly as the cultured taxa we assayed are underrepresented in these communities. While inferences drawn by comparing across these different datasets are understandably limited, the correspondence observed between taxa summaries generated from both metagenomic and amplicon sequences (**Supplementary Figure S6**) supports the observation of taxonomic variability across these samples. Interestingly, many of the genes within these PL families are annotated to taxa that were also cultured and demonstrated the capacity for alginate utilization, though conversely, alginolytic genes assigned to numerous uncultured genera were also present in the functional profiles. The annotation of alginate lyase genes from diverse taxa may also indicate the potential for broad distribution of this capacity, however, these results alone do not conclusively demonstrate the presence of alginate utilization in genera other than those that were assayed. While bacteria that utilize alginate may persist on the algal surface at lower abundances or as opportunists, further work is required to conclusively determine how prevalent this metabolic capacity is.

We report a depth associated structuring of epibiotic functional profiles consistent with the observed taxonomic structuring. Communities on deeper blades are compositionally different (**Figures 2C–E**) and host functionally and taxonomically richer assemblages (**Figure 2F**). These observations are consistent with dynamics of bacterial succession, whereby poorly defended tissue is increasingly colonized by generalist taxa. Despite these differences, no CAZy genes or families related to alginate metabolism were differentially abundant across blade depths. Given the magnitude of alginate in this system, this may indicate the occurrence of constitutive, rather than variable alginate turnover. Possibly, only a subset of bacteria on the *Macrocystis* surface metabolize alginate, regardless of tissue state and community composition, and this activity is sufficient to liberate alginate carbon. It should be noted that the lack of differentially abundant CAZy genes observed attests only to the gene content of these communities and does not reflect variation in gene expression that may be present across depths. Thus the capacity for alginate utilization may be present within all functional profiles, while a depth associated patterning of activity may only be apparent from gene expression data. While it remains unclear whether alginate metabolism underlies the differences between epibiotic communities, it may be integral to structuring assemblages on detrital material, particularly as detritus accounts for the majority of kelp carbon export (Krumhansl and Scheibling, 2012). As stated previously, the filtering of water samples in this work precludes a robust characterization of detrital-associated assemblages. Future work should aim to determine whether these bacterial communities are in fact structured around the utilization of kelp derived alginate.

We did detect the enrichment of three CAZy families (GH16, CBM6, CBM13; **Supplementary Table S2**) in communities on deeper blades and these contain enzymes targeting several algal carbohydrates, particularly cellulose (Adams et al., 2011). As cellulose is the second most abundant carbohydrate in *Macrocystis* (Ravanal et al., 2016), this may reflect a more complete degradation of algal tissue occurring on deeper blades, supporting a successional role for these communities. Interestingly, alginate degradation prior to cellulose saccharification improves carbohydrate liberation in *Macrocystis* tissue (Ravanal et al., 2016). Constitutive alginate turnover may therefore be advantageous, as it would increase access to other carbon substrates once host defenses are reduced. In this case, successional bacterial communities would be structured around the availability of other carbon substrates, as opposed to alginate.

Diverse Cultured Bacteria in *Macrocystis* Forests Are Capable of Utilizing Alginate

A large proportion of isolates cultured from the epibiota of *M. pyrifera* and surrounding water column are capable of degrading and/or metabolizing alginate (66%; **Table 1**). The majority of isolates cultured on both selective (containing alginate) and non-selective media demonstrated this activity, indicating that this pattern is not simply the product of media bias. The capacity for alginate utilization is broadly, but unevenly, distributed across the major taxonomic groups cultured here (Gammaproteobacteria: **Figure 3** and **Supplementary Figure S3**, Alphaproteobacteria: **Supplementary Figure S4**, and Flavobacteriaceae: **Supplementary Figure S5**), all of which are important marine carbon metabolisers (Edwards et al., 2010; Teeling et al., 2016). Most of the taxa capable of utilizing alginate have been reported in previous studies, however, we extend this catalog of genera by three, all within the Gammaproteobacteria (**Table 1**).

The capacity for alginate utilization, and polysaccharide degradation more generally, is likely more widespread than estimated by culturing alone (Bengtsson et al., 2011; Martin et al., 2015). The poor representation of cultured genera in *M. pyrifera* epibiotic communities (**Figure 1A**) is consistent with previous studies, and this culturing inefficiency evidently biases characterizing metabolic activity, such as alginate utilization, toward underestimation. Indeed, the vast majority of taxa detected by sequencing uncultured communities were not isolated and assayed, though genes involved in alginate

metabolism (PL families 6, 7, 15, 17 in **Figure 2D**) are consistently present and reasonably abundant across all communities. Specifically, the Planctomycetes and Verrucomicrobia are well represented in epibiotic communities but are entirely absent among cultured taxa (**Supplementary Figure S1**). These groups may participate in important interactions with the algal host (Lage and Bondoso, 2011; Vollmers et al., 2017), including carbon metabolism (Bengtsson and Øvreås, 2010), yet are historically difficult to culture (Op den Camp et al., 2009; Fuerst and Sagulenko, 2011).

The patchy phylogenetic distribution of observed alginate utilization may result from horizontal gene transfer (HGT), which would further support the potential for diverse taxa to possess this capacity. Marine bacteria are capable of highly frequent HGT (McDaniel et al., 2010) and the transfer of alginate lyase genes has been reported previously (Wargacki et al., 2012; Hehemann et al., 2016; Zhu et al., 2017). Simple carbohydrate metabolism is also often shallowly conserved within bacterial phylogenies (Martiny et al., 2013), likely owing to the relative ease of transferring genes required for low complexity metabolic pathways. The abundance of alginate in kelp forests coupled with its relatively simple metabolic requirements could therefore produce a broad incorporation of alginate lyase genes. Interestingly, many of the genera that demonstrate alginate utilization in this study also metabolize numerous other algal polysaccharides (Michel et al., 2006; Alderkamp et al., 2007; Mann et al., 2013; Schultz-Johansen et al., 2016). This metabolic heterogeneity and the diversity of observed alginate utilizing taxa both support a disconnect between 16S identity and simple carbohydrate metabolism that is consistent with HGT.

We demonstrate here that the *M. pyrifera* epibiota and surrounding water column harbor diverse culturable bacteria capable of degrading and metabolizing alginate, a function that is integral to the cycling of kelp carbon in the coastal ocean. The capacity for alginate utilization appears to have a broad, but patchy distribution in bacterial phylogenies; it is not always present within a given genus and is variable even across isolates with identical 16S rRNA sequences. This indicates a weak association between functional capacity and taxonomy at high resolution. While the prevalence and distribution of alginate utilization across taxa within the *M. pyrifera* epibiota remains unclear, the pervasiveness of this trait within cultured bacteria, abundance of alginate metabolic genes assigned to diverse genera, and presence of these genes across taxonomically variable bacterial communities, suggests that it may be common and the cycling of algal carbon is performed by diverse groups of marine bacteria.

AUTHOR CONTRIBUTIONS

ML, LP, and JL designed the project. JL conducted the assays of cultured samples, generated the sequencing data for cultured and uncultured samples, and analyzed the data with input from ML and LP. JL wrote the first draft of the manuscript. All authors contributed to the revisions.

FUNDING

This work was supported by a Hakai Postdoctoral Fellowship to ML, a Tula Foundation grant to LP, and an NSERC-DG to LP.

ACKNOWLEDGMENTS

We thank M. Chen and R. Sanders-Smith for field assistance. Many thanks to the staff of the Hakai Institute Calvert Island Field Station for logistical support. We also thank M. Campbell for statistical help, K. Chan and E. Morien for data management, C. Foley for culturing assistance, H. Lim for sample preparation, and N. Firmino and S. Louca for critical feedback. Thanks to members of the LP's lab for providing feedback on an earlier version of this manuscript.

SUPPLEMENTARY MATERIAL

The Supplementary Material for this article can be found online at: https://www.frontiersin.org/articles/10.3389/fmicb.2018.01914/full#supplementary-material

REFERENCES

Adams, A. S., Jordan, M. S., Adams, S. M., Suen, G., Goodwin, L. A., Davenport, K. W., et al. (2011). Cellulose-degrading bacteria associated with the invasive woodwasp *Sirex noctilio*. *ISME J.* 5, 1323–1331. doi: 10.1038/ismej.2011.14

Alderkamp, A. C., Van Rijssel, M., and Bolhuis, H. (2007). Characterization of marine bacteria and the activity of their enzyme systems involved in degradation of the algal storage glucan laminarin. *FEMS Microbiol. Ecol.* 59, 108–117. doi: 10.1111/j.1574-6941.2006.00219.x

Anderson, M. J. (2004). *PERMDISP: a FORTRAN Computer Program for Permutational Analysis of Multivariate Dispersions (for Any Two-Factor ANOVA Design) Using Permutation Tests*. Auckland: Department of Statistics, University of Auckland.

Anderson, M. J., Gorley, R. N., and Clarke, R. K. (2005). *Permanova. Permutational Multivariate Analysis of Variance, a Computer Program*. Auckland: Department of Statistics, University of Auckland, 24.

Azam, F., and Malfatti, F. (2007). Microbial structuring of marine ecosystems. *Nat. Rev. Microbiol.* 5, 782–791. doi: 10.1038/nrmicro1747

Bengtsson, M. M., and Øvreås, L. (2010). Planctomycetes dominate biofilms on surfaces of the kelp *Laminaria hyperborea*. *BMC Microbiol.* 10:261. doi: 10.1186/1471-2180-10-261

Bengtsson, M. M., Sjøtun, K., Lanzén, A., and Øvreås, L. (2012). Bacterial diversity in relation to secondary production and succession on surfaces of the kelp *Laminaria hyperborea*. *ISME J.* 6, 2188–2198. doi: 10.1038/ismej.2012.67

Bengtsson, M. M., Sjøtun, K., Storesund, J. E., and Øvreås, L. (2011). Utilization of kelp-derived carbon sources by kelp surface-associated bacteria. *Aquat. Microb. Ecol.* 62, 191–199. doi: 10.3354/ame01477

Benjamini, Y., and Hochberg, Y. (1995). Controlling the false discovery rate: a practical and powerful approach to multiple testing. *J. R. Stat. Soc. B* 57, 289–300.

Berger, S. A., Krompass, D., and Stamatakis, A. (2011). Performance, accuracy, and web server for evolutionary placement of short sequence reads under maximum likelihood. *Syst. Biol.* 60, 291–302. doi: 10.1093/sysbio/syr010

Boyd, A., Ghosh, M., May, T. B., Shinabarger, D., Keogh, R., and Chakrabarty, A. M. (1993). Sequence of the algL gene of *Pseudomonas aeruginosa* and purification of its alginate lyase product. *Gene* 131, 1–8. doi: 10.1016/0378-1119(93)90662-M

Bray, J. R., and Curtis, J. T. (1957). An ordination of the upland forest communities of southern Wisconsin. *Ecol. Monogr.* 27, 325–349. doi: 10.2307/1942268

Burke, C., Thomas, T., Lewis, M., Steinberg, P., and Kjelleberg, S. (2011). Composition, uniqueness and variability of the epiphytic bacterial community of the green alga Ulva australis. *ISME J.* 5, 590–600. doi: 10.1038/ismej.2010.164

Camacho, C., Coulouris, G., Avagyan, V., Ma, N., Papadopoulos, J., Bealer, K., et al. (2009). BLAST+: architecture and applications. *BMC Bioinformatics* 10:421. doi: 10.1186/1471-2105-10-421

Caporaso, J. G., Bittinger, K., Bushman, F. D., DeSantis, T. Z., Andersen, G. L., and Knight, R. (2010a). PyNAST: a flexible tool for aligning sequences to a template alignment. *Bioinformatics* 26, 266–267. doi: 10.1093/bioinformatics/btp636

Caporaso, J. G., Kuczynski, J., Stombaugh, J., Bittinger, K., Bushman, F. D., Costello, E. K., et al. (2010b). QIIME allows analysis of high-throughput community sequencing data. *Nat. Methods* 7, 335–336. doi: 10.1038/nmeth.f.303

Caporaso, J. G., Lauber, C. L., Walters, W. A., Berg-Lyons, D., Huntley, J., Fierer, N., et al. (2012). Ultra-high-throughput microbial community analysis on the Illumina HiSeq and MiSeq platforms. *ISME J.* 6, 1621–1624. doi: 10.1038/ismej.2012.8

CAZypedia Consortium (2017). Ten years of CAZypedia: a living encyclopedia of carbohydrate-active enzymes. *Glycobiology* 28, 3–8.

Chao, A. (1984). Nonparametric estimation of the number of classes in a population. *Scand. J. Stat.* 11, 265–270.

Chen, M. Y., and Parfrey, L. W. (2018). Incubation with macroalgae induces large shifts in water column microbiota, but minor changes to the epibiota of co-occurring macroalgae. *Mol. Ecol.* 27, 1966–1979. doi: 10.1111/mec.14548

Clarke, K. R., and Gorley, R. N. (2006). *PRIMER v6: User Manual/Tutorial*. Plymouth: PRIMER-E.

Clasen, J. L., and Shurin, J. B. (2015). Kelp forest size alters microbial community structure and function on Vancouver Island, Canada. *Ecology* 96, 862–872. doi: 10.1890/13-2147.1

Dong, S., Yang, J., Zhang, X. Y., Shi, M., Song, X. Y., Chen, X. L., et al. (2012). Cultivable alginate lyase-excreting bacteria associated with the arctic brown alga Laminaria. *Mar. Drugs* 10, 2481–2491. doi: 10.3390/md10112481

Druehl, L. D., and Wheeler, W. N. (1986). Population biology of *Macrocystis integrifolia* from British Columbia, Canada. *Mar. Biol.* 90, 173–179. doi: 10.1007/BF00569124

Edgar, R. C. (2004). MUSCLE: multiple sequence alignment with high accuracy and high throughput. *Nucleic Acids Res.* 32, 1792–1797. doi: 10.1093/nar/gkh340

Edgar, R. C. (2010). Search and clustering orders of magnitude faster than BLAST. *Bioinformatics* 26, 2460–2461. doi: 10.1093/bioinformatics/btq461

Edwards, J. L., Smith, D. L., Connolly, J., McDonald, J. E., Cox, M. J., Joint, I., et al. (2010). Identification of carbohydrate metabolism genes in the metagenome of a marine biofilm community shown to be dominated by Gammaproteobacteria and Bacteroidetes. *Genes* 1, 371–384. doi: 10.3390/genes1030371

Egan, S., Harder, T., Burke, C., Steinberg, P., Kjelleberg, S., and Thomas, T. (2013). The seaweed holobiont: understanding seaweed–bacteria interactions. *FEMS Microbiol. Rev.* 37, 462–476. doi: 10.1111/1574-6976.12011

Eren, A. M., Maignien, L., Sul, W. J., Murphy, L. G., Grim, S. L., Morrison, H. G., et al. (2013). Oligotyping: differentiating between closely related microbial taxa using 16S rRNA gene data. *Methods Ecol. Evol.* 4, 1111–1119. doi: 10.1111/2041-210X.12114

Eren, A. M., Morrison, H. G., Lescault, P. J., Reveillaud, J., Vineis, J. H., and Sogin, M. L. (2015). Minimum entropy decomposition: unsupervised oligotyping for sensitive partitioning of high-throughput marker gene sequences. *ISME J.* 9, 968–979. doi: 10.1038/ismej.2014.195

Fuerst, J. A., and Sagulenko, E. (2011). Beyond the bacterium: planctomycetes challenge our concepts of microbial structure and function. *Nat. Rev. Microbiol.* 9, 403–413. doi: 10.1038/nrmicro2578

Gong, J. S., Liu, X. M., Zhang, M. J., Li, H., Geng, Y., Li, H., et al. (2016). Purification and characterization of a high salt-tolerant alginate lyase from *Cobetia* sp. WG-007. *Biotechnol. Appl. Biochem.* 64, 519–524. doi: 10.1002/bab.1506

Han, F., Gong, Q. H., Song, K., Li, J. B., and Yu, W. G. (2004). Cloning, sequence analysis and expression of gene alyVI encoding alginate lyase from marine bacterium *Vibrio* sp. QY101. *DNA Seq.* 15, 344–350. doi: 10.1080/10425170400019300

Han, W., Gu, J., Cheng, Y., Liu, H., Li, Y., and Li, F. (2016). Novel alginate lyase (Aly5) from a polysaccharide-degrading marine bacterium, Flammeovirga strain MY04: effects of module truncation on biochemical characteristics, alginate degradation patterns, and oligosaccharide-yielding properties. *Appl. Environ. Microbiol.* 82, 364–374. doi: 10.1128/AEM.03022-15

Hehemann, J. H., Arevalo, P., Datta, M. S., Yu, X., Corzett, C. H., Henschel, A., et al. (2016). Adaptive radiation by waves of gene transfer leads to fine-scale resource partitioning in marine microbes. *Nat. Commun.* 7:12860. doi: 10.1038/ncomms12860

Hisano, T., Yonemoto, Y., Yamashita, T., Fukuda, Y., Kimura, A., and Murata, K. (1995). Direct uptake of alginate molecules through a pit on the bacterial cell surface: a novel mechanism for the uptake of macromolecules. *J. Ferment. Bioeng.* 79, 538–544. doi: 10.1016/0922-338X(95)94744-C

Ivanova, E. P., Gorshkova, N. M., Sawabe, T., Zhukova, N. V., Hayashi, K., Kurilenko, V. V., et al. (2004). *Sulfitobacter delicatus* sp. nov. and *Sulfitobacter dubius* sp. nov., respectively from a starfish (*Stellaster equestris*) and sea grass (*Zostera marina*). *Int. J. Syst. Evol. Microbiol.* 54, 475–480. doi: 10.1099/ijs.0.02654-0

Iwamoto, Y., Araki, R., Iriyama, K. I., Oda, T., Fukuda, H., Hayashida, S., et al. (2001). Purification and characterization of bifunctional alginate lyase from *Alteromonas* sp. strain no. 272 and its action on saturated oligomeric substrates. *Biosci. Biotechnol. Biochem.* 65, 133–142. doi: 10.1271/bbb.65.133

Jagtap, S. S., Hehemann, J. H., Polz, M. F., Lee, J. K., and Zhao, H. (2014). Comparative biochemical characterization of three exolytic oligoalginate lyases from *Vibrio splendidus* reveals complementary substrate scope, temperature, and pH adaptations. *Appl. Environ. Microbiol.* 80, 4207–4214. doi: 10.1128/AEM.01285-14

Jiao, N., Herndl, G. J., Hansell, D. A., Benner, R., Kattner, G., Wilhelm, S. W., et al. (2010). Microbial production of recalcitrant dissolved organic matter: long-term carbon storage in the global ocean. *Nat. Rev. Microbiol.* 8, 593–599. doi: 10.1038/nrmicro2386

Kim, H. S., Lee, C.-G., and Lee, E. Y. (2011). Alginate lyase: structure, property, and application. *Biotechnol. Bioproc. Eng.* 16:843. doi: 10.1007/s12257-011-0352-8

Kita, A., Miura, T., Kawata, S., Yamaguchi, T., Okamura, Y., Aki, T., et al. (2016). Bacterial community structure and predicted alginate metabolic pathway in an alginate-degrading bacterial consortium. *J. Biosci. Bioeng.* 121, 286–292. doi: 10.1016/j.jbiosc.2015.06.014

Konotchick, T., Dupont, C. L., Valas, R. E., Badger, J. H., and Allen, A. E. (2013). Transcriptomic analysis of metabolic function in the giant kelp, *Macrocystis pyrifera*, across depth and season. *New Phytol.* 198, 398–407. doi: 10.1111/nph.12160

Konwar, K. M., Hanson, N. W., Bhatia, M. P., Kim, D., Wu, S. J., Hahn, A. S., et al. (2015). MetaPathways v2. 5: quantitative functional, taxonomic and usability improvements. *Bioinformatics* 31, 3345–3347. doi: 10.1093/bioinformatics/btv361

Krumhansl, K. A., and Scheibling, R. E. (2012). Production and fate of kelp detritus. *Mar. Ecol. Prog. Ser.* 467, 281–302. doi: 10.3354/meps09940

Kuznetsova, A., Brockhoff, P. B., and Christensen, R. H. B. (2015). *Package 'lmerTest'. R Package Version, 2*. Available at: https://cran.r-project.org/web/packages/lmerTest/lmerTest.pdf

Lachnit, T., Blümel, M., Imhoff, J. F., and Wahl, M. (2009). Specific epibacterial communities on macroalgae: phylogeny matters more than habitat. *Aquat. Biol.* 5, 181–186. doi: 10.3354/ab00149

Lage, O. M., and Bondoso, J. (2011). Planctomycetes diversity associated with macroalgae. *FEMS Microbiol. Ecol.* 78, 366–375. doi: 10.1111/j.1574-6941.2011.01168.x

Lam, C., and Harder, T. (2007). Marine macroalgae affect abundance and community richness of bacterioplankton in close proximity. *J. Phycol.* 43, 874–881. doi: 10.1111/j.1529-8817.2007.00385.x

Lemay, M. A., Martone, P. T., Keeling, P. J., Burt, J. M., Krumhansl, K. A., Sanders, R. D., et al. (2018). Sympatric kelp species share a large portion of their surface

bacterial communities. *Environ. Microbiol.* 20, 658–670. doi: 10.1111/1462-2920.13993

Li, J.-W., Dong, S., Song, J., Li, C.-B., Chen, X.-L., Xie, B.-B., et al. (2011). Purification and characterization of a bifunctional alginate lyase from *Pseudoalteromonas* sp. SM0524. *Mar. Drugs* 9, 109–123. doi: 10.3390/md9010109.

Lombard, V., Ramulu, H. G., Drula, E., Coutinho, P. M., and Henrissat, B. (2014). The carbohydrate-active enzymes database (CAZy) in 2013. *Nucleic Acids Res.* 42, D490–D495. doi: 10.1093/nar/gkt1178

Lozupone, C. A., Hamady, M., Kelley, S. T., and Knight, R. (2007). Quantitative and qualitative beta diversity measures lead to different insights into factors that structure microbial communities. *Appl. Environ. Microbiol.* 73, 1576–1585. doi: 10.1128/aem.01996-06

Lyu, Q., Zhang, K., Zhu, Q., Li, Z., Liu, Y., Fitzek, E., et al. (2018). Structural and biochemical characterization of a multidomain alginate lyase reveals a novel role of CBM32 in CAZymes. *Biochim. Biophys. Acta* 1862, 1862–1869. doi: 10.1016/j.bbagen.2018.05.024

Mann, A. J., Hahnke, R. L., Huang, S., Werner, J., Xing, P., Barbeyron, T., et al. (2013). The genome of the alga-associated marine flavobacterium *Formosa agariphila* KMM 3901T reveals a broad potential for degradation of algal polysaccharides. *Appl. Environ. Microbiol.* 79, 6813–6822. doi: 10.1128/AEM.01937-13

Martin, M., Barbeyron, T., Martin, R., Portetelle, D., Michel, G., and Vandenbol, M. (2015). The cultivable surface microbiota of the brown alga *Ascophyllum nodosum* is enriched in macroalgal-polysaccharide-degrading bacteria. *Front. Microbiol.* 6:1487. doi: 10.3389/fmicb.2015.01487

Martiny, A. C., Treseder, K., and Pusch, G. (2013). Phylogenetic conservatism of functional traits in microorganisms. *ISME J.* 7, 830–838. doi: 10.1038/ismej.2012.160

Marzinelli, E. M., Campbell, A. H., Zozaya Valdes, E., Vergés, A., Nielsen, S., Wernberg, T., et al. (2015). Continental-scale variation in seaweed host-associated bacterial communities is a function of host condition, not geography. *Environ. Microbiol.* 17, 4078–4088. doi: 10.1111/1462-2920.12972

Matsushima, R., Danno, H., Uchida, M., Ishihara, K., Suzuki, T., Kaneniwa, M., et al. (2010). Analysis of extracellular alginate lyase and its gene from a marine bacterial strain, *Pseudoalteromonas atlantica* AR06. *Appl. Microbiol. Biotechnol.* 86, 567–576. doi: 10.1007/s00253-009-2278-z

McDaniel, L. D., Young, E., Delaney, J., Ruhnau, F., Ritchie, K. B., and Paul, J. H. (2010). High frequency of horizontal gene transfer in the oceans. *Science* 330:50. doi: 10.1126/science.1192243

McIlroy, S. J., and Nielsen, P. H. (2014). *The Family Saprospiraceae*. Berlin: Springer, 863–889. doi: 10.1007/978-3-642-38954-2_138

McKee, J. W. A., Kavalieris, L., Brasch, D. J., Brown, M. T., and Melton, L. D. (1992). Alginate content and composition of *Macrocystis pyrifera* from New Zealand. *J. Appl. Phycol.* 4, 357–369. doi: 10.1007/BF02185794

Meddeb-Mouelhi, F., Moisan, J. K., and Beauregard, M. (2014). A comparison of plate assay methods for detecting extracellular cellulase and xylanase activity. *Enzyme Microb. Technol.* 66, 16–19. doi: 10.1016/j.enzmictec.2014.07.004

Michel, G., Nyval-Collen, P., Barbeyron, T., Czjzek, M., and Helbert, W. (2006). Bioconversion of red seaweed galactans: a focus on bacterial agarases and carrageenases. *Appl. Microbiol. Biotechnol.* 71, 23–33. doi: 10.1007/s00253-006-0377-7

Michel, G., Tonon, T., Scornet, D., Cock, J. M., and Kloareg, B. (2010). The cell wall polysaccharide metabolism of the brown alga *Ectocarpus siliculosus*. Insights into the evolution of extracellular matrix polysaccharides in Eukaryotes. *New Phytol.* 188, 82–97. doi: 10.1111/j.1469-8137.2010.03374.x

Michelou, V. K., Caporaso, J. G., Knight, R., and Palumbi, S. R. (2013). The ecology of microbial communities associated with *Macrocystis pyrifera*. *PLoS One* 8:e67480. doi: 10.1371/journal.pone.0067480

Nedashkovskaya, O. I., Kim, S. B., Han, S. K., Lysenko, A. M., Rohde, M., Rhee, M. S., et al. (2004). *Maribacter* gen. nov., a new member of the family Flavobacteriaceae, isolated from marine habitats, containing the species *Maribacter sedimenticola* sp. nov., *Maribacter aquivivus* sp. nov., *Maribacter orientalis* sp. nov. and *Maribacter ulvicola* sp. nov. *Int. J. Syst. Evol. Microbiol.* 54, 1017–1023. doi: 10.1099/ijs.0.02849-0

Op den Camp, H. J., Islam, T., Stott, M. B., Harhangi, H. R., Hynes, A., Schouten, S., et al. (2009). Environmental, genomic and taxonomic perspectives on methanotrophic Verrucomicrobia. *Environ. Microbiol. Rep.* 1, 293–306. doi: 10.1111/j.1758-2229.2009.00022.x

Price, M. N., Dehal, P. S., and Arkin, A. P. (2010). FastTree 2–approximately maximum-likelihood trees for large alignments. *PLoS One* 5:e9490. doi: 10.1371/journal.pone.0009490

Pruesse, E., Peplies, J., and Glöckner, F. O. (2012). SINA: accurate high-throughput multiple sequence alignment of ribosomal RNA genes. *Bioinformatics* 28, 1823–1829. doi: 10.1093/bioinformatics/bts252

Quast, C., Pruesse, E., Yilmaz, P., Gerken, J., Schweer, T., Yarza, P., et al. (2012). The SILVA ribosomal RNA gene database project: improved data processing and web-based tools. *Nucleic Acids Res.* 41, D590–D596. doi: 10.1093/nar/gks1219

R Core Team (2017). *R: A Language and Environment for Statistical Computing*. Vienna: R Foundation for Statistical Computing.

Ravanal, M. C., Pezoa-Conte, R., von Schoultz, S., Hemming, J., Salazar, O., Anugwom, I., et al. (2016). Comparison of different types of pretreatment and enzymatic saccharification of *Macrocystis pyrifera* for the production of biofuel. *Algal Res.* 13, 141–147. doi: 10.1016/j.algal.2015.11.023

Ravanal, M. C., Sharma, S., Gimpel, J., Reveco-Urzua, F. E., Øverland, M., Horn, S. J., et al. (2017). The role of alginate lyases in the enzymatic saccharification of brown macroalgae, *Macrocystis pyrifera* and *Saccharina latissima*. *Algal Res.* 26, 287–293. doi: 10.1016/j.algal.2017.08.012

Reed, D. C., Carlson, C. A., Halewood, E. R., Nelson, J. C., Harrer, S. L., Rassweiler, A., et al. (2015). Patterns and controls of reef-scale production of dissolved organic carbon by giant kelp *Macrocystis pyrifera*. *Limnol. Oceanogr.* 60, 1996–2008. doi: 10.1002/lno.10154

Reed, D. C., Rassweiler, A., and Arkema, K. K. (2008). Biomass rather than growth rate determines variation in net primary production by giant kelp. *Ecology* 89, 2493–2505. doi: 10.1890/07-1106.1

Rognes, T., Flouri, T., Nichols, B., Quince, C., and Mahé, F. (2016). VSEARCH: a versatile open source tool for metagenomics. *PeerJ* 4:e2584. doi: 10.7717/peerj.2584

Roth-Schulze, A. J., Zozaya-Valdés, E., Steinberg, P. D., and Thomas, T. (2016). Partitioning of functional and taxonomic diversity in surface-associated microbial communities. *Environ. Microbiol.* 18, 4391–4402. doi: 10.1111/1462-2920.13325

Sawabe, T., Oda, Y., Shiomi, Y., and Ezura, Y. (1995). Alginate degradation by bacteria isolated from the gut of sea urchins and abalones. *Microb. Ecol.* 30, 193–202. doi: 10.1007/BF00172574

Säwström, C., Hyndes, G. A., Eyre, B. D., Huggett, M. J., Fraser, M. W., Lavery, P. S., et al. (2016). Coastal connectivity and spatial subsidy from a microbial perspective. *Ecol. Evol.* 6, 6662–6671. doi: 10.1002/ece3.2408

Schultz-Johansen, M., Glaring, M. A., Bech, P. K., and Stougaard, P. (2016). Draft genome sequence of a novel marine bacterium, *Paraglaciecola* sp. strain S66, with hydrolytic activity against seaweed polysaccharides. *Genome Announc.* 4, e304–e316. doi: 10.1128/genomeA.00304-16

Sim, P. F., Furusawa, G., and Teh, A. H. (2017). Functional and structural studies of a multidomain alginate lyase from *Persicobacter* sp. CCB-QB2. *Sci. Rep.* 7:13656. doi: 10.1038/s41598-017-13288-1

Singh, R. P., and Reddy, C. R. K. (2014). Seaweed–microbial interactions: key functions of seaweed-associated bacteria. *FEMS Microbiol. Ecol.* 88, 213–230. doi: 10.1111/1574-6941.12297

Stamatakis, A. (2014). RAxML version 8: a tool for phylogenetic analysis and post-analysis of large phylogenies. *Bioinformatics* 30, 1312–1313. doi: 10.1093/bioinformatics/btu033

Staufenberger, T., Thiel, V., Wiese, J., and Imhoff, J. F. (2008). Phylogenetic analysis of bacteria associated with Laminaria saccharina. *FEMS Microbiol. Ecol.* 64, 65–77. doi: 10.1111/j.1574-6941.2008.00445.x

Steneck, R. S., Graham, M. H., Bourque, B. J., Corbett, D., Erlandson, J. M., Estes, J. A., et al. (2002). Kelp forest ecosystems: biodiversity, stability, resilience and future. *Environ. Conserv.* 29, 436–459. doi: 10.1017/S0376892902000322

Tanaka, R., Shibata, T., Miyake, H., Mori, T., Tamaru, Y., Ueda, M., et al. (2015). Temporal fluctuation in the abundance of alginate-degrading bacteria in the gut of abalone *Haliotis gigantea* over 1 year. *Aquac. Res.* 47, 2899–2908. doi: 10.1111/are.12740

Teeling, H., Fuchs, B. M., Bennke, C. M., Krueger, K., Chafee, M., Kappelmann, L., et al. (2016). Recurring patterns in bacterioplankton dynamics during coastal spring algae blooms. *eLife* 5:e11888. doi: 10.7554/eLife.11888

Thomas, F., Barbeyron, T., Tonon, T., Génicot, S., Czjzek, M., and Michel, G. (2012). Characterization of the first alginolytic operons in a marine bacterium: from their emergence in marine Flavobacteriia to their independent transfers to marine *Proteobacteria* and human gut *Bacteroides*. *Environ. Microbiol.* 14, 2379–2394. doi: 10.1111/j.1462-2920.2012.02751.x

Van Tussenbroek, B. I. (1989). The life-span and survival of fronds of *Macrocystis pyrifera* (Laminariales, Phaeophyta) in the Falkland Islands. *Br. Phycol. J.* 24, 137–141. doi: 10.1080/00071618900650131

Vollmers, J., Frentrup, M., Rast, P., Jogler, C., and Kaster, A. K. (2017). Untangling genomes of novel Planctomycetal and Verrucomicrobial species from Monterey bay kelp forest metagenomes by refined binning. *Front. Microbiol.* 8:472. doi: 10.3389/fmicb.2017.00472

Wahl, M., Goecke, F., Labes, A., Dobretsov, S., and Weinberger, F. (2012). The second skin: ecological role of epibiotic biofilms on marine organisms. *Front. Microbiol.* 3:292. doi: 10.3389/fmicb.2012.00292

Wang, Y., Song, Q., and Zhang, X. H. (2016). Marine microbiological enzymes: studies with multiple strategies and prospects. *Mar. Drugs* 14:171. doi: 10.3390/md14100171

Wargacki, A. J., Leonard, E., Win, M. N., Regitsky, D. D., Santos, C. N. S., Kim, P. B., et al. (2012). An engineered microbial platform for direct biofuel production from brown macroalgae. *Science* 335, 308–313. doi: 10.1126/science.1214547

Wheeler, P. A., and North, W. J. (1981). Nitrogen supply, tissue composition and frond growth rates for *Macrocystis pyrifera* off the coast of southern California. *Mar. Biol.* 64, 59–69. doi: 10.1007/BF00394081

Whyte, J. N. C., and Englar, J. R. (1978). *Primary Organic Chemical Composition of the Marine Alga Macrocystis Integrifolia Over the Growing Season*. Technical Report, No. 787. Vancouver: Fisheries and Oceans Canada.

Wong, T. Y., Preston, L. A., and Schiller, N. L. (2000). Alginate lyase: review of major sources and enzyme characteristics, structure-function analysis, biological roles, and applications. *Annu. Rev. Microbiol.* 54, 289–340. doi: 10.1146/annurev.micro.54.1.289

Xu, F., Dong, F., Wang, P., Cao, H. Y., Li, C. Y., Li, P. Y., et al. (2017). Novel molecular insights into the catalytic mechanism of marine bacterial alginate lyase AlyGC from polysaccharide lyase family 6. *J. Biol. Chem.* 292, 4457–4468. doi: 10.1074/jbc.M116.766030

Yu, G., Smith, D. K., Zhu, H., Guan, Y., and Lam, T. T. Y. (2017). ggtree: an R package for visualization and annotation of phylogenetic trees with their covariates and other associated data. *Methods in Ecol. Evol.* 8, 28–36. doi: 10.1111/2041-210X.12628

Zhan, P., Tang, K., Chen, X., and Yu, L. (2017). Complete genome sequence of *Maribacter* sp. T28, a polysaccharide-degrading marine flavobacteria. *J. Biotechnol.* 259, 1–5. doi: 10.1016/j.jbiotec.2017.08.009

Zhu, B., Chen, M., Yin, H., Du, Y., and Ning, L. (2016). Enzymatic hydrolysis of alginate to produce oligosaccharides by a new purified endo-type alginate lyase. *Mar. Drugs* 14:E108. doi: 10.3390/md14060108

Zhu, Y., Thomas, F., Larocque, R., Li, N., Duffieux, D., Cladière, L., et al. (2017). Genetic analyses unravel the crucial role of a horizontally acquired alginate lyase for brown algal biomass degradation by *Zobellia galactanivorans*. *Environ. Microbiol.* 19, 2164–2181. doi: 10.1111/1462-2920.13699

Conflict of Interest Statement: The authors declare that the research was conducted in the absence of any commercial or financial relationships that could be construed as a potential conflict of interest.

Copyright © 2018 Lin, Lemay and Parfrey. This is an open-access article distributed under the terms of the Creative Commons Attribution License (CC BY). The use, distribution or reproduction in other forums is permitted, provided the original author(s) and the copyright owner(s) are credited and that the original publication in this journal is cited, in accordance with accepted academic practice. No use, distribution or reproduction is permitted which does not comply with these terms.

frontiers in Marine Science

ORIGINAL RESEARCH
published: 06 September 2018
doi: 10.3389/fmars.2018.00307

Enrichment of Bacterioplankton Able to Utilize One-Carbon and Methylated Compounds in the Coastal Pacific Ocean

Julie Dinasquet[1,2], Marja Tiirola[3] and Farooq Azam[1]*

[1] Marine Biology Research Division, Scripps Institution of Oceanography, University of California, San Diego, La Jolla, CA, United States, [2] Laboratoire d'Océanographie Microbienne, Observatoire Océanologique de Banyuls s/mer, Sorbonne Universités, UPMC, Banyuls-sur-Mer, France, [3] Department of Biological and Environmental Sciences, Nanoscience Center, University of Jyväskylä, Jyväskylä, Finland

OPEN ACCESS

Edited by:
Veronica Molina, Universidad de Playa Ancha, Chile

Reviewed by:
Héctor A. Levipan, Centro de Investigación Marina Quintay (CIMARQ), Chile
Camila Fernandez, UMR7621 Laboratoire d'Océanographie Microbienne (LOMIC), France

***Correspondence:**
Julie Dinasquet
jdinasquet@ucsd.edu

Specialty section:
This article was submitted to Aquatic Microbiology, a section of the journal Frontiers in Marine Science

Received: *12 April 2018*
Accepted: *10 August 2018*
Published: *06 September 2018*

Citation:
Dinasquet J, Tiirola M and Azam F (2018) Enrichment of Bacterioplankton Able to Utilize One-Carbon and Methylated Compounds in the Coastal Pacific Ocean. Front. Mar. Sci. 5:307. doi: 10.3389/fmars.2018.00307

Understanding the temporal variations and succession of bacterial communities involved in the turnover of one-carbon and methylated compounds is necessary to better predict bacterial impacts on the marine carbon cycle and air-sea carbon fluxes. The ability of the local bacterioplankton community to exploit one-carbon and methylated compounds as main source of bioavailable carbon during a productive and less productive period was assessed through enrichment experiments. Surface seawater was amended with methanol and trimethylamine-*N*-oxide (TMAO), and bacterial abundance, production, oxygen consumption, as well as methanol turnover and growth rates of putative methylotrophs were followed. Bacterial community structure and functional diversity was examined through amplicon sequencing of 16S rRNA and methanol dehydrogenase (*mxaF*) marker genes. 2-fold increase in oxygen consumption and bacterial growth rates, and up to 4-fold higher methanol assimilation were observed in the amended seawater samples. Capacity to drawdown the substrates was similar between both experiments. In less productive conditions, methanol enriched obligate methylotrophs, especially *Methylophaga* spp., accounted for ∼70% of bacterial cells analyzed by fluorescence *in situ* hybridization and 16S rRNA gene sequencing, while TMAO enriched taxa belonged to *Oceanospirillales* and putative β- and γ-Proteobacterial methylotrophs. In the experiment performed during the more productive period, bacterial communities were structurally resistant, suggesting that facultative organisms may have dominated the observed methylotrophic activity. Moreover, enrichment of distinct methylotrophic taxa but similar activity rates observed in response to different substrate additions suggests a functional redundancy of substrate specific marine methylotrophic populations. Marine bacterioplankton cycling of one-carbon and methylated compounds appears to depend on the system productivity, and hence may have predictable temporal impacts on air-sea fluxes of volatile organic compounds.

Keywords: C1, methanol, TMAO, bacterial community composition, mxaF, coastal ecosystem

INTRODUCTION

Marine bacteria play key roles in food webs and biogeochemical cycles of coastal surface waters (e.g., Ducklow et al., 1986). Bacterial community abundance, composition and function are tightly coupled with spatiotemporal gradients of dissolved organic carbon composition and concentration (Azam and Malfatti, 2007) and depend on the metabolic capacities of bacterial taxa (Mou et al., 2008; Poretsky et al., 2010). For instance, methylotrophic bacteria that use one carbon and methylated (hereafter C1) compounds as their sole source of carbon and energy are widespread in the ocean (Chistoserdova et al., 2009; Chistoserdova, 2015). C1 compounds are ubiquitous in the ocean (Beale et al., 2011; Carpenter et al., 2012; Beale and Airs, 2016) and therefore a potential carbon source for marine bacteria. Most of the C1 compounds are volatile and have the potential to influence atmospheric chemistry and climate (Williams et al., 2004). Hence, it is important to understand how marine bacteria interact with these compounds to better assess air-sea fluxes for climatic predictions.

Indeed, the directions of net air-sea fluxes of C1 compounds may vary depending on utilization by marine methylotrophs. Methanol is among the most abundant oxygenated volatile organic compounds in the atmosphere, where it can influence atmospheric chemistry through oxidation and ozone formation (Singh et al., 2000). Methanol is a source of carbon and energy for diverse marine bacteria (Murrell et al., 1993), and surface methylotrophs may act as oceanic sink of methanol (Dixon et al., 2011a,b, 2012). However, it is unclear if the ocean acts as a net source or sink of atmospheric methanol (Singh et al., 2000, 2003; Dixon et al., 2013). Measurements in some oceanic regions found them to be net sink of methanol (Yang et al., 2013, 2014a,b). On the other hand, methylamine (MA), can form aerosols and act as cloud condensation nuclei, are constantly emitted from the ocean (Facchini et al., 2008; Müller et al., 2009; Sorooshian et al., 2009). MA are products of the methylotrophic degradation of precursors trimethylamine-*N*-oxide (TMAO) and glycine betaine. Methylotrophs may thus act as a source of atmospheric aerosols derived from MA production through, for instance, TMAO demethylation (Lidbury et al., 2017).

Methanol and TMAO are ubiquitous in the ocean (Beale et al., 2011), as are bacteria able to use them. Bacteria use methanol and TMAO either only as energy source, such as the abundant surface α-Proteobacteria of the SAR11clade (Sun et al., 2011), or as both carbon and energy source (Chen et al., 2011; Lidbury et al., 2014a,b). In the ocean, these two C1 compounds are produced by phytoplankton (Nieder et al., 2014; Mincer and Aicher, 2016) and other organisms. Their concentrations in the ocean vary temporally (Beale et al., 2015) depending on sources, e.g., phytoplankton bloom, atmospheric wet and dry deposition, and photooxidation. Methylotrophic metabolism in the coastal ocean is also expected to follow a similar seasonal dynamic (Sargeant et al., 2016), with different feedbacks on the biogeochemical cycles and air-sea fluxes.

Here, we investigated the capacity of bacterioplankton community experimentally enriched with methanol and TMAO to assimilate and grow on C1 compounds during less productive winter and the following more productive summer. We measured carbon drawdown through bacterial production and respiration, as well as followed changes in the microbial community structure using 16S rRNA gene sequencing. The methylotrophic capacities of the bacterioplankton was assessed in terms of methanol assimilation and respiration, FISH enumeration of potential methylotrophs and composition of the methylotrophic population through sequencing of methanol dehydrogenase gene *mxaF*.

MATERIALS AND METHODS

Experimental Setup

Enrichment experiments were performed to examine the activity and structure of enriched coastal bacterial communities able to utilize C1 compounds during low productivity winter (February 2015) and higher productivity summer (July 2015). Aged (3 months) GF/F filtered seawater, kept in the dark at near *in situ* temperature (16 ± 0.5°C) was gently filtered through rinsed 0.2 μm filters (Supor 200; Pall Laboratory) and distributed randomly into 1 L bottles. This 0.2 μm filtered water was then inoculated (20% v/v) with freshly collected seawater gently filtered through 0.65 μm Isopore (Millipore) filters. The seawater was sampled on the day of the experiment from coastal surface (∼1 m below the surface) off the Pier of Scripps Institution of Oceanography, La Jolla, CA, United States (32°53′N, 117°15′W). Experimental setup consisted of triplicate 1 L bottles divided into five treatments: (1) control (no addition; hereafter called Control); (2) Control plus inorganic nutrients (10 μM $NaNO_3$; 10 μM NH_4Cl; 3 μM NaH_2PO_4; 20 pM vitamin B12), hereafter called Control + Nutrients; (3) methanol plus inorganic nutrients (20 μM methanol), MetOH; (4) Trimethylamine *N*-oxide (20 μM TMAO plus inorganic nutrients), TMAO; and (5) mixture of methanol and TMAO (10 μM each plus inorganic nutrients), hereafter called MetOH + TMAO. The bottles were incubated for 7 days in the dark at near *in situ* temperature (ca. 17°C in winter and ca. 21°C in summer). All materials in contact with the samples were acid washed in 10% HCl and repeatedly rinsed with Q-grade water (Millipore) prior to use.

Samples for bacterial abundance, fluorescence *in situ* hybridization (winter samples), bacterial production, methanol assimilation and respiration (summer samples) were taken at T_0, 24, 72, 120 h and at the end of the incubation (168 h). Dissolved oxygen concentration was measured daily and samples for bacterial community composition were filtered at the start and at the end of the experiment.

Bacterial Abundance

Samples (1.5 ml) for bacterial enumeration were fixed with EM grade glutaraldehyde (EMS; 1% v/v), flash frozen and stored at −80°C. The samples were stored for less than 2 months before further analyses. Thawed samples were filtered onto 0.2 μm white polycarbonate filters (Isopore, Millipore), stained with DAPI (Porter and Feig, 1980) and enumerated by epifluorescence microscopy on an Olympus BX51 microscope at 1000x magnification. At least 20 fields were counted.

Cell biovolumes were measured with Fiji (Schindelin et al., 2012) and averaged over several time points and treatments. Bacterial carbon content was calculated according to Bratbak (1985) and Simon and Azam (1989).

Fluorescence *in situ* Hybridization (FISH)

Duplicate samples (12 ml) were fixed with formaldehyde (3% final) overnight at 4°C and filtered onto 0.2 μm white polycarbonate filters (Isopore, Millipore). Preparations were stored at −20°C until further processing. All hybridization were carried out under the conditions previously described by Glöckner et al. (1996). The samples were hybridized for 2 h at 46°C and washed at 48°C. No formamide was added to the hybridization buffer (Tsien et al., 1990; Janvier et al., 2003). Pieces of filters (1/4) were double hybridized with fluorescent 16S rRNA targeting probes, FAM-MPH-730 (5′-CAGTAATGGCCCAGT GAGTCGCC-3′) complementary to *Methylophaga* spp. specific 16S rRNA region (Janvier et al., 2003) and cy3-10-γ (5′-GGTCC GAAGATCCCCCGCTT-3′) complementary to the 16S rRNA region of the methylotrophic species of β- and γ-Proteobacteria with the RuMP pathway (Tsien et al., 1990). Another piece of each filter was hybridized with 16S rRNA targeting probes, FAM-9-α (5′-CCCTGAGTTATTCCGAAC-3′) complementary to the 16S rRNA region of methylotrophic α- Proteobacteria with the serine pathway (Tsien et al., 1990). Images were analyzed with Fiji (Schindelin et al., 2012). The effect of time was tested in different treatments using a two-way ANOVA.

Bacterial Production, Respiration and Growth Efficiency

Bacterial production was measured by [H^3]-leucine incorporation (Kirchman et al., 1985) modified for microcentrifugation (Smith and Azam, 1992). Triplicate 1.7 ml aliquots were incubated with [H^3]-leucine (20 nM final conc.) in sterile 2.0 ml polypropylene tubes for 1 h at *in situ* temperature. Samples with 5% trichloroacetic acid added prior to [H^3]-leucine addition served as blanks. Leucine incorporation was converted to carbon production assuming 3.1 kg C (mol leucine)$^{-1}$ (Simon and Azam, 1989).

Dissolved oxygen was measured according to Kragh et al. (2008) using a fiber-optic oxygen mini-sensor (Fibox 4, PreSens Precision Sensing GmbH), which utilizes fluorescence quenching of the sensor by oxygen. A sensor spot (Pst3; 5 mm) inside each bottles allowed for readings with a fiber-optic probe from outside the bottle. A "control" bottle with Milli-Q water was used to ensure no inherent O_2 consumption. No leaching or O_2 consumption was observed in the control incubator.

O_2 consumption (ΔO_2) and cumulative time-integrated bacterial production (BP_{cum}) were used to calculate bacterial carbon demand (BCD) and bacterial growth efficiency (BGE), with BCD = $-\Delta O_2 + BP_{cum}$ and BGE = BP_{cum}/BCD. ΔO_2 and BP_{cum} were calculated over 0–120 h for the winter and 0–72 h for the summer experiment following the ΔO_2 leveling off for all treatments. The percentage of bioavailable carbon from the added substrate (bDOC) was calculated as the average of ($BCD_{treatment}$-$BCD_{control}$)/DOC added.

Statistical differences between treatments were calculated with a Student's *t*-test (two samples, assuming unequal variances).

Methanol Assimilation and Respiration

Bacterial methanol assimilation was measured by [C^{14}]-methanol incorporation. Triplicate 1.7 ml aliquots were incubated with [C^{14}]-methanol (100 nM final conc.) in sterile 2.0 ml polypropylene tubes for 24 h, at *in situ* temperature. Samples with 5% trichloroacetic acid added prior to methanol addition served as blanks. Following the incubation samples were centrifuged for 10 min at 16000 × g. The pellets were dried, scintillation cocktail (Ultima Gold, Perkin Elmer) was added and the samples were radioassayed in a liquid scintillation counter (Beckman LS6000).

Bacterial methanol respiration was measured by [C^{14}]-methanol respiration. Triplicate 1.7 ml aliquots were incubated with [C^{14}]-methanol (100 nM final) in sterile closed culture tubes for 24 h at *in situ* temperature. Samples with 4% formaldehyde added prior to the radioisotope served as blanks. After 24 h the samples were acidified with concentrated H_2SO_4 and a center well with a 2 × 2 cm piece of fluted filter soaked with β-phenylethylamine was added to the tube (Karl et al., 1998). After 72 h the fluted filters were dried in a dessicator and trapped$^{14}CO_2$ was measured.

Bacterial Community Composition

For each incubation and T_0 samples, cells from 800 mL of water were collected by gentle filtration onto 0.2 μm, 47 mm Supor membrane filters (Pall). Filters were subsequently frozen at −80°C. DNA was extracted using ZR Fungal/Bacterial DNA MiniPrep kit (ZYMO research) following manufacturer guidelines after a proteinase K digestion (20 mg ml^{-1} final) at 55°C for 2 h. PCR amplification with bacterial 16S rRNA gene (V1-V3 region) specific primers 27F and 338R was followed by a nested PCR with barcoded adapter primers to identify different samples. The products were then purified with Agencourt AmPure XP magnetic beads (Beckman Coulter). Ion Torrent PGM sequencing was performed as described by Stark et al. (2015). Methanol dehydrogenase genes (*mxaF*) were amplified using primers 1003F (McDonald and Murrell, 1997) and 1555R (Neufeld et al., 2007). PCR products were gel purified using GenElute DNA Gel extraction kit (Sigman-Aldrich) and barcodes were added to the PCR products through the M13-linker using the protocol described by Mäki et al. (2016). 16S rRNA and *mxaF* raw datasets were deposited to NCBI Sequence Read Archive under Bioproject PRJNA447999.

16S rRNA and mxaF Gene Sequence Analysis

All reads were processed using the Quantitative Insight Into Microbial Ecology pipeline (QIIME v1.9; Caporaso et al., 2010a). For 16S rRNA gene sequences, all reads with mismatches in the primer or lengths below 200 bp and quality scores < 25 were discarded. Reads were quality controlled and chimeras were removed using UPARSE (Edgar, 2013). Reads were clustered into operational taxonomic units (OTUs) at 99% pairwise identity

using the UPARSE and representative sequences from each bacterial OTU aligned to SILVA 128 reference alignment (Quast et al., 2013) using PyNAST (Caporaso et al., 2010b). Taxonomy assignments were made using UCLUST algorithm (Edgar, 2010) against the database SILVA 128.

For mxaF sequences, all reads with mismatches in the primer or lengths below 250 bp and quality score < 25 were discarded. Reads were quality controlled and chimeras were removed using UPARSE (Edgar, 2013). Reads were clustered into OTUs at 77% pairwise identity using UPARSE. This cutoff for mxaF corresponds to a 97% pairwise identity for 16S rRNA genes, based on pairwise comparison of both genes from different isolates described by Stacheter et al. (2012).

Alpha and beta-diversity indices were estimated for all samples after randomized subsampling to 1047 reads for 16S rRNA gene and to 1212 reads for *mxaF* sequences. Alpha diversity analyses (Richness: observed OTUs and diversity: Shannon index) were run in QIIME. Beta-diversity was investigated with Primer V.6 software package (Clarke and Warwick, 2001) on Bray Curtis dissimilarity. Differences between communities were tested with PERMANOVA (Permutational Multivariate Analysis of Variance) with pairwise test and 9999 permutations in Primer V.6 (Clarke et al., 2014). The *mxaF* OTUs contributing most to the dissimilarity between samples were identified using SIMPER (similarity percentage) on normalized samples, with Primer V.6. The sequences of OTUs contributing to 90% of the dissimilarity between samples were aligned with references sequences on their amino acid sequences, and maximum likelihood tree with bootstrap test was constructed using MEGA7: Molecular Evolutionary Genetics Analysis version 7.0 (Kumar et al., 2016).

RESULTS

In situ Parameters and System Productivity

The productivity of the system between winter and summer sampling was determined as the biological productivity differences between the two sampling points. The colder winter water was characterized by lower productivity compared to the more productive summer waters with higher Chl *a*, POC and bacterial production (**Table 1**). Moreover, the summer sample followed the spring phytoplankton bloom observed in May – June[1]. Overall, bacterial production and methanol assimilation were higher during the whole summer period compared to winter (J. Dinasquet, unpublished time series). At the time points sampled for this experiment bacterial production and methanol assimilation were 2.3-fold and 5.6-fold higher in summer compared to winter while bacterial abundances were similar for the two seasons (**Table 1**).

Bacterial Utilization of Added Substrates

Enhanced bacterial growth and oxygen consumption showed that coastal bacteria responded to substrates additions both in the winter and summer experiment (**Figure 1**). Increase in the bacterial production was higher in the winter than in the summer, but started later. The active parts of the experiment were determined as 0–120 h in the winter and 0–72 h in the summer incubations before oxygen consumption leveled off and bacterial abundance decreased (**Figures 1A–D**). Although samples were originally filtered, grazing affected the bacterial abundance during the later time points. At the time of sampling, the concentration of heterotrophic nanoflagellates *in situ* was also higher in summer (5300 cells ml^{-1}) compared to winter (2500 cells ml^{-1}), which may explain the highest mortality in the summer experiment. Substrate additions doubled the O_2 consumption in both the winter and summer experiments (**Figures 1A,B** and **Table 2**). The bacterial growth efficiency with the substrate additions was ∼1.6-fold higher in the winter experiment (**Table 2**). Of the studied C1 compounds, carbon drawdown was greater in winter in the methanol treatment, while in summer it was greater in the TMAO treatment. The drawdown of carbon in the substrate mixture fitted the combined carbon drawdown in the separate carbon source treatments.

In the winter experiment, bacterial growth efficiency (BGE) was significantly lower in the TMAO treatments (11–12%) than in the controls or methanol treatment alone (15–18%). There was no differences in the BGE in the summer experiment (**Table 2**).

At the end of the experiments, C1 treatments had increased methanol assimilation 2- to 4-fold, when compared to winter and summer controls, respectively (**Figures 2A,B**). Methanol respiration was also about 4-fold higher in all C1 treatments at the end of the summer experiment (**Figure 2C**). The BGE based on added [C^{14}]-methanol (BGE_M) was higher in the controls compared to the C1 treatments in summer. Growth efficiency on methanol (34.4 ± 2.3%) was not significantly different between different substrate addition treatments (**Table 2**).

Bacterial Community Composition in Response to Substrates Addition

A total of 300,618 16S rRNA gene sequences remained after quality control, and were clustered to 5995 OTUs (99% identity). Original bacterial community composition displayed higher

[1]http://www.sccoos.org/data/habs/history.php?location=Scripps%20Pier

TABLE 1 | *In situ* conditions off Scripps Pier at the time of sampling (mean ± standard deviation for $n = 3$).

	Temp.[1] (°C)	Chl *a* (μg L^{-1})	DOC (μM)	POC (μM)	BP[2] (μgC L^{-1} d^{-1})	MA[3] (ngC L^{-1} d^{-1})	BA[4] (cells mL^{-1})
Winter	17.1 ± *0.02*	0.76 ± *0.01*	71.4 ± *2.8*	14.2	3.9 ± *0.07*	2.36 ± *1.4*	1.94×10^6 ± *9.23 x* 10^5
Summer	21 ± *0.02*	1.29 ± *0.02*	71.2 ± *1.8*	31.1	8.8 ± *0.5*	13.5 ± *1.3*	1.98×10^6 ± *7.03 x* 10^5

[1]Temperature. [2]Bacterial production. [3]Methanol assimilation. [4]Bacterial abundance.

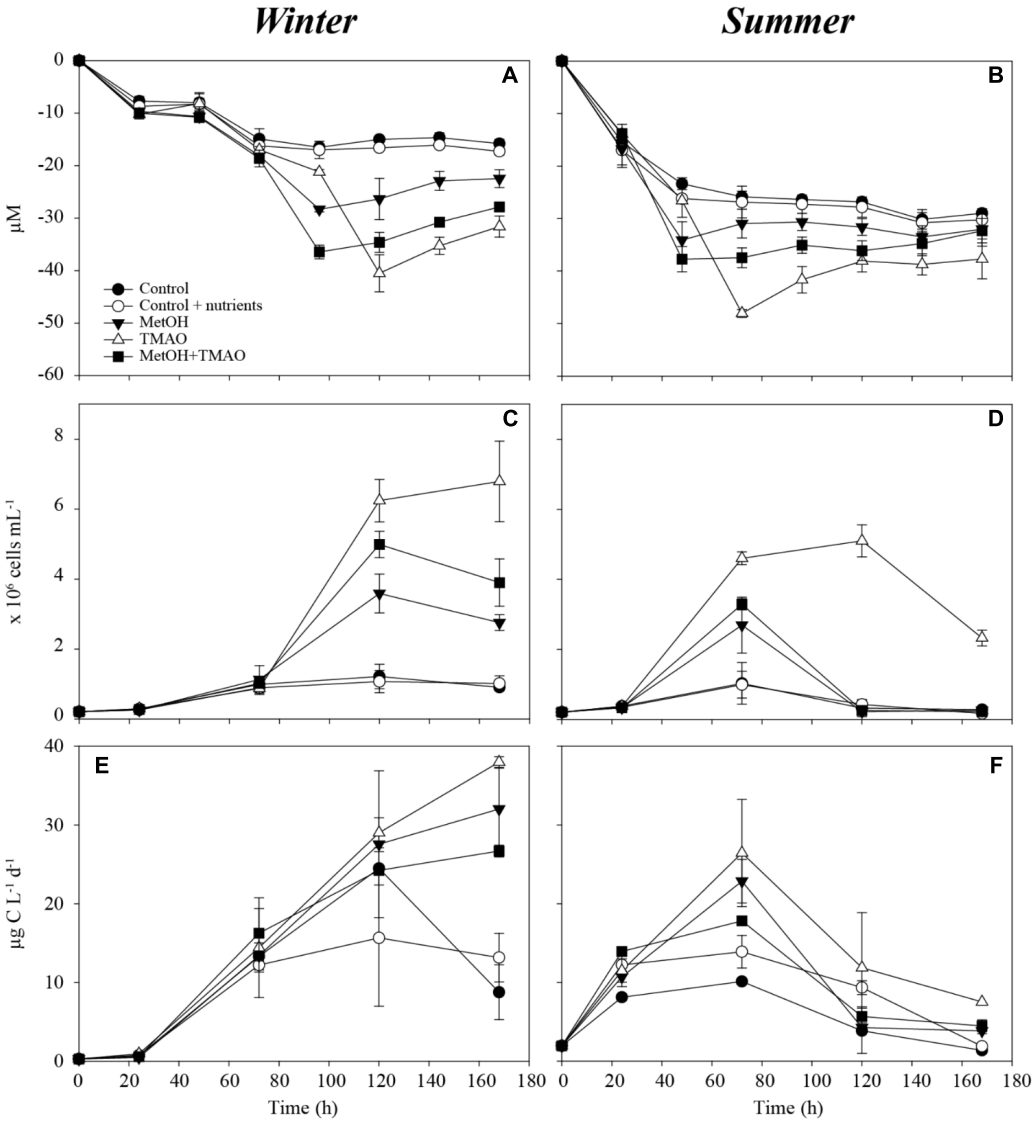

FIGURE 1 | Oxygen consumption over the course of the experiment in winter **(A)** and summer **(B)**, bacterial abundance over the course of the experiment in winter **(C)** and summer **(D)** and bacterial production over the course of the experiment in winter **(E)** and summer **(F)**. Mean ± standard deviation, $n = 3$.

TABLE 2 | Summary of data during the active phases of the enrichment experiments, 0–120 h and 0–72 h of incubation in winter and summer, respectively (mean ± standard deviation for $n = 3$ for enrichments and $n = 6$ for controls).

		BCD[2] (µM)		% bDOC[3]		BGE[4] (%)		BGE_M[5] (%)	
Winter (0–120 h)	Controls[1]	19.4	*±0.9*			18.4	±1.3	n.a	
	MetOH	30.9***	*±3.9*	57.2	*±19.6*	15.1	±2.1	n.a	
	TMAO	45.5***	*±3.5*	43.3	*±5.9*	10.9***	±0.9	n.a	
	MetOH+TMAO	39.4***	*±1.9*	49.8	*±4.8*	12.2***	±0.6	n.a	
Summer (0-72h)	Controls[1]	28.7	*±2.3*			8.2	±1.5	44.0	*±2.0*
	MetOH	34.3	*±2.7*	27.8	*±14.4*	9.7	±0.7	36.5	*±4.7*
	TMAO	51.8***	*±0.8*	38.4	*±1.5*	7.2	±0.1	32.0**	*±3.2*
	MetOH+TMAO	40.8***	*±1.9*	30.1	*±5.1*	8.1	±0.4	34.4*	*±3.4*

*[1]Control and Control + nutrients. [2]Bacterial carbon demand. [3]Bioavailability of DOC added. [4]Bacterial growth efficiency. [5]Bacterial growth efficiency on methanol. n.a, not available. Significantly different from controls with *$p < 0.05$, **$p < 0.01$, and ***$p < 0.001$ (t-test).*

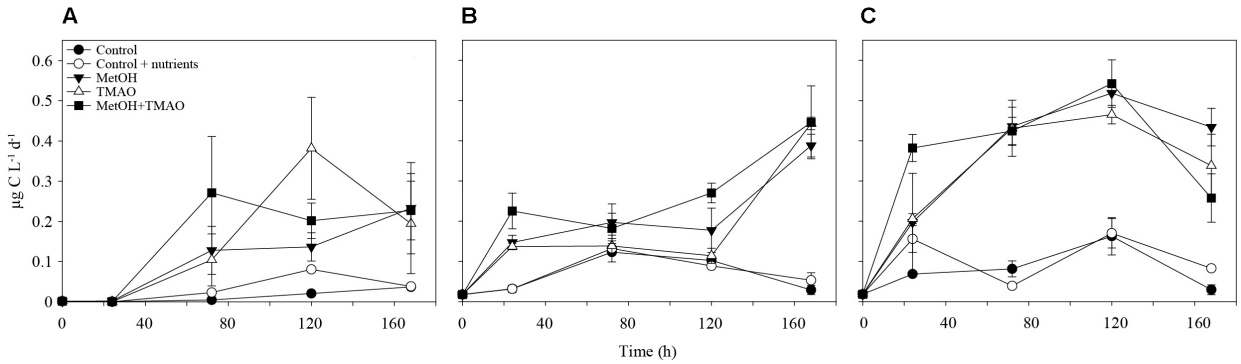

FIGURE 2 | Methanol assimilation over the course of the experiment in winter **(A)** and summer **(B)** and methanol respiration in summer **(C)**. Mean ± standard deviation, $n = 3$.

richness and diversity in summer than in winter (**Supplementary Table S1**). In winter, richness (as measured by observed OTUs and Chao1 index) and diversity (Shannon Index) decreased further in all C1 treatments when compared to the initial water, while diversity remained constant in the control samples. The richness and diversity indexes were significantly lower (∼0.5-fold) in the methanol treatments compared to the controls, and slightly lower in the TMAO treatments (**Supplementary Table S1**). In summer, richness and diversity did not significantly change between experiment start and end communities and between treatments, with the exception of TMAO treatments where it was slightly lower (**Supplementary Table S1**). The bacterial community composition in the 32 samples was compared with non-metric multidimensional scaling (nMDS) based on Bray-Curtis dissimilarity of rarefied data (**Figure 3**). The nMDS plot showed that winter and summer communities independent of time and treatment were significantly different. Incubation without carbon addition did not change the winter communities (PERMANOVA, $p = 0.53$ T0 to C and $p = 0.37$ T0 to CN), while control and C1 treatments communities were significantly different at the end of the experiment (PERMANOVA, control to methanol, $p = 0.012$, to TMAO $p = 0.01$ and to MetOH + TMAO $p = 0.013$). Furthermore, methanol communities were distinct from the two other C1 treatments (PERMANOVA, methanol to TMAO $p = 0.004$ and to MetOH + TMAO $p = 0.03$), while TMAO and MetOH + TMAO communities were similar ($p = 0.18$). On the other hand, neither time nor carbon addition affected the overall bacterial community structure in summer (**Figure 3**).

The winter inoculation consisted of significantly (*t-test* $p < 0.05$) higher abundance of α- and γ-Proteobacteria and lower abundance of Bacteroidetes than summer inoculation, as well as different OTUs of the clade SAR11. In winter the difference between controls and C1 treatments was mainly driven by a significant decrease (*t-test* $p < 0.05$) in relative abundance of α-Proteobacteria (especially SAR11 related OTUs) and a significant increase (*t-test* $p < 0.05$) of γ-Proteobacteria (especially *Methylophaga sp.* related OTUs in the methanol treatment, and *Oceanospirillales*, *Pseudomonadales* and *Methylophaga* sp. in the TMAO and MetOH + TMAO

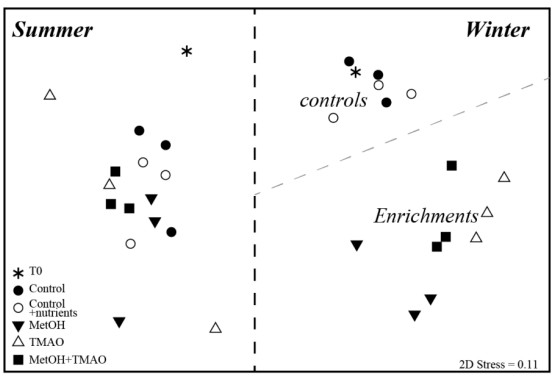

FIGURE 3 | nMDS clustering of bacterial community composition in winter and summer.

treatments). In summer, minor differences were observed such as an increase in δ- and γ-Proteobacteria and decrease in α-Proteobacteria at the end of the incubations compared to the start water. There was a small enrichment in *Methylophaga* sp. in the enrichment treatments compared to the control (**Figures 4A–C**).

Functional Community of Methanol Users in Response to Substrate Addition

A total of 40,000 sequences shared between 41 OTUs (at 77% identity) were recovered from sequencing of the methanol dehydrogenase gene *mxaF*. Richness and diversity of the methanol users (as defined by *mxaF*- methanol dehydrogenase sequences) were slightly lower in summer when compared to winter, and in the C1 treatments compared to the controls (**Supplementary Table S2**). Based on the nMDS plot (**Supplementary Figure S1**), the functional diversity was slightly different between winter and summer and between winter C1 treatments and controls, and MetOH+TMAO treatment and controls in summer. Nevertheless, these differences were not significant (PERMANOVA, $p > 0.05$, community was 78.4% similar in winter between all treatments and 83.2% similar in

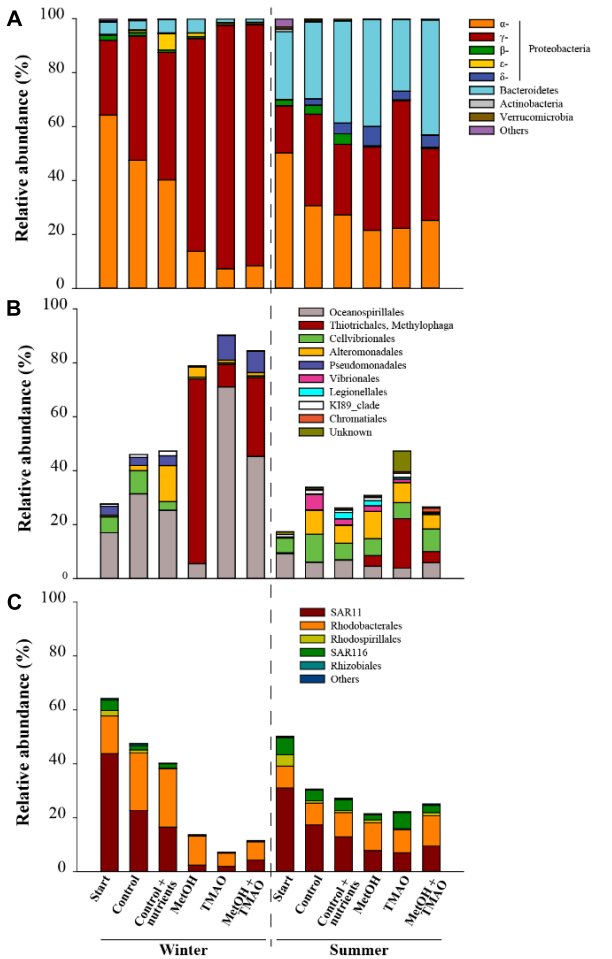

FIGURE 4 | Relative abundance of the main bacterial phyla and subclasses **(A)**, γ-Proteobacteria **(B)** and α-Proteobacteria **(C)** in winter and summer experiments. Relative abundances are expressed as % of total 16S rRNA gene sequences in the original assemblage or as a mean of the treatment triplicates at the end of the experiment.

summer). Few main *mxaF*-OTUs were driving over 70% of the dissimilarity of the functional community between treatment and controls in winter and summer (**Figure 5**). Some of the *mxaF*-OTUs were related to known *mxaF* sequences from β-, α- and γ-Proteobacteria (closely related to *Methylophilales*, *Methylobacterium* and *Methylophaga* respectively) but also from unknown putatively new methanol dehydrogenases from *Rhodobacterales* (*Confluentimicrobium* sp. and *Ruegiria* sp.) and *Oceanospirillales* (*Halomonas* sp., **Figure 6**).

Putative Methylotroph Abundance and Growth Rate in Winter

The abundance of the obligate methylotroph *Methylophaga* spp. increased significantly over the course of the experiment in all treatments (ANOVA $p < 0.001$), especially in the MetOH and MetOH + TMAO treatments, which had 28-fold higher growth rates than the controls and 1.8-fold higher growth rates than TMAO treatment (**Table 3** and **Figure 7**). Abundance of methylotrophic β- and γ-Proteobacteria with RumP pathway (except *Methylophaga* spp., Janvier et al., 2003) increased significantly in all treatments (ANOVA, $p < 0.001$). While growth rates were similar in the control and MetOH treatments, rates were 2-fold higher in the TMAO and MetOH + TMAO treatment compared to controls (**Table 3** and **Figure 7**). The total growth rates of methylotrophic bacteria in winter was similar in all enrichments despite being driven by different methylotrophs. No methylotrophic α-Proteobacteria with serine pathways were observed in any of the samples.

DISCUSSION

Marine bacterial communities exhibit strong temporal variations (Fuhrman et al., 2015; Bunse and Pinhassi, 2017) that are partly driven by the productivity of the system and variability in bioavailable carbon sources (Alonso-Saez and Gasol, 2007; Lønborg et al., 2009; Osterholz et al., 2016). Here, we show that the coastal bacterioplankton is rapidly responding to an addition of methylated compounds and that enrichment of coastal bacterioplankton with methylotrophic capacity varies with the productivity of the system. This also implies that methylotrophy may have seasonally varying effects on carbon cycling and air-sea fluxes in coastal waters.

Bacterial Carbon Drawdown in Response to Methanol and Trimethylamine-*N*-oxide Additions

Marine bacteria can use methanol and TMAO as a source of carbon for biomass and/or energy (e.g., Sun et al., 2011; Dixon et al., 2012; Lidbury et al., 2014b). In marine waters, methanol and TMAO may be produced by phytoplankton (Nieder et al., 2014; Mincer and Aicher, 2016) among others. Thus, their concentration may change depending on the productivity of the system. We hypothesized that marine bacteria would respond differently to C1 compounds during periods of different biological productivity. The colder less productive (lower Chl *a*, POC and bacterial production) winter water was characterized by lower bacterial activities compared to the warmer water that followed the spring bloom. Bacteria responded to the input of carbon in both experiments, but the lag phase was slightly longer in winter, which is typical for slower metabolism in colder waters (Degerman et al., 2012). The added compounds were more labile to the winter bacteria, probably due to the lower biological productivity during the winter season and subsequent lower concentration of fresh bioavailable carbon (Lønborg et al., 2009).

In summer, the minor differences observed between the controls and treatments, as well as lower bacterial growth efficiencies when compared to winter, suggest that added substrates were mainly shunted toward respiration and used as a source of energy. This may be explained by the presence of more bioavailable ambient substrates subsequent to the higher spring and summer biological productivity of the coastal system. As suggested in other studies, one-carbon and methylated

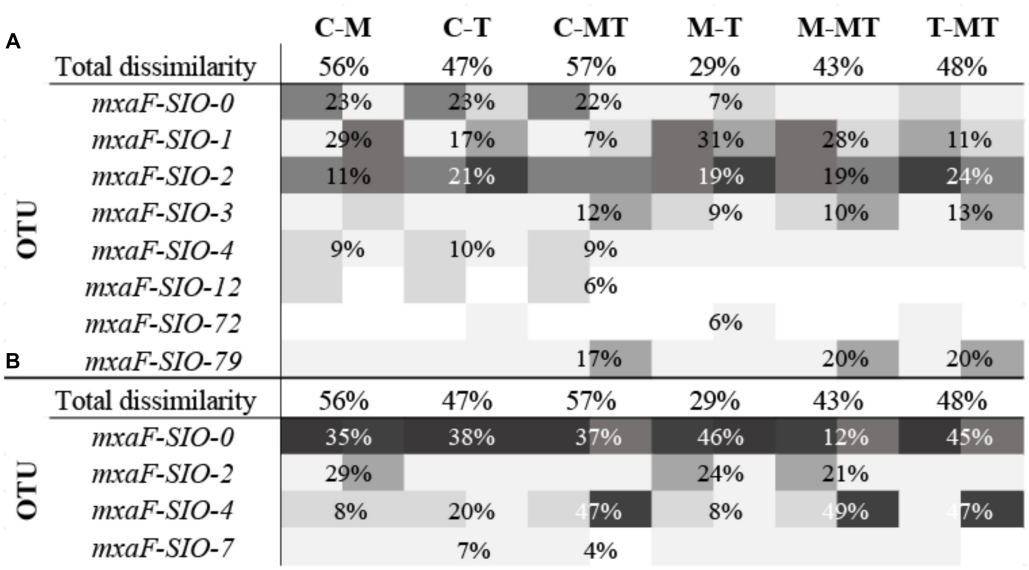

FIGURE 5 | Heatmap of percent relative abundance of bacterial OTUs responsible for more than 70% of the dissimilarity between two samples (calculated by Bray Curtis, SIMPER analysis), in winter **(A)** and in summer **(B)**. The percentages represent the average contribution of an OTU to the dissimilarity between the samples. Total dissimilarity includes the whole communities of the sample duplicates. C-M, controls to MetOH; C-T, controls to TMAO; C-MT, controls to metOH + TMAO; M-T, MetOH to TMAO; M-MT, MetOH to MetOH + TMAO; T-MT, TMAO to MetOH + TMAO.

compounds may sustain energy demand, while other compounds are used for biomass production (Sun et al., 2011; Halsey et al., 2012), nevertheless, the addition of C1 compounds did not elicit enhanced utilization of ambient DOC compared to the carbon used in the control treatments, suggesting that energy sources were not limiting at this time of the year.

Trimethylamine-*N*-oxide may be used as an energy source when methanol is available for growth (Halsey et al., 2012), but the mix of both substrates did not trigger enhanced utilization of carbon compared to the methanol-alone treatment. TMAO may also be used as a source of nitrogen by nutrient limited bacteria (Lidbury et al., 2014a; Taubert et al., 2017), but here nutrients were added to all treatments, which enabled unbiased testing of utilization of carbon. No major differences were observed between the controls with and without nutrients either in winter or summer, suggesting that *in situ* communities were not nutrient limited and that TMAO was probably mainly used, as intended, as a source of carbon.

Bacterial Taxa Enriched During Methanol and TMAO Incubations

In winter, the initial bacterial community composition was typical of assemblages usually observed in coastal waters at this time of the year (e.g., Fuhrman et al., 2006; Gilbert et al., 2010). The main differences between the controls and the initial water was the slight increase in γ-Proteobacteria, mainly related to *Oceanospirillales* and *Alteromonadales*, which are often observed in incubation experiments responding to bottle effect (Dinasquet et al., 2013). No major community changes were observed with the addition of nutrients. The main responses observed with the C1 additions was an increase in γ- and a decrease in α-Proteobacteria. The major group enriched in the methanol treatment was related to *Methylophaga* spp. which is an obligate marine methylotroph (Janvier et al., 1985; Neufeld et al., 2007, 2008). *Oceanospirillales* also increased in the treatments with TMAO and they are known to be capable of using this substrate (Kube et al., 2013). Therefore, it appears that in winter the lag phase observed in bacterial activity in response to the addition of C1 carbon sources may be due to an adaptation of the community to the input of C1.

The lack of obvious bottle effect in summer as well as very similar bacterial community between start and end incubations in all treatments, points toward the *in situ* presence of many generalists taxa capable of using different carbon substrates. The main difference was a decrease in β-Proteobacteria in the C1 treatments compared to the controls. This is unexpected considering that one of the most abundant coastal methylotrophs, the β-Proteobacteria OM43 (Giovannoni et al., 2008; Halsey et al., 2012; Gifford et al., 2016) is usually observed in summer and during incubation experiments (Sosa et al., 2015). Nevertheless, it appears that this oligotrophic methylotroph might have been outcompeted here. The observed low abundance of OM43 may also be the results of primer bias (Parada et al., 2016). Nevertheless, a moderate response to the added carbon compounds was observed at lower taxonomic resolutions as previously observed during incubation experiments (Dinasquet et al., 2013). *Methylophaga* spp. related OTUs increased in all C1 treatments, especially in the TMAO-only treatment, which was different from the pattern observed in winter. This might be due to the simultaneous utilization of TMAO between N users and C1 users (McCarren et al., 2010; Lidbury et al., 2014a) in

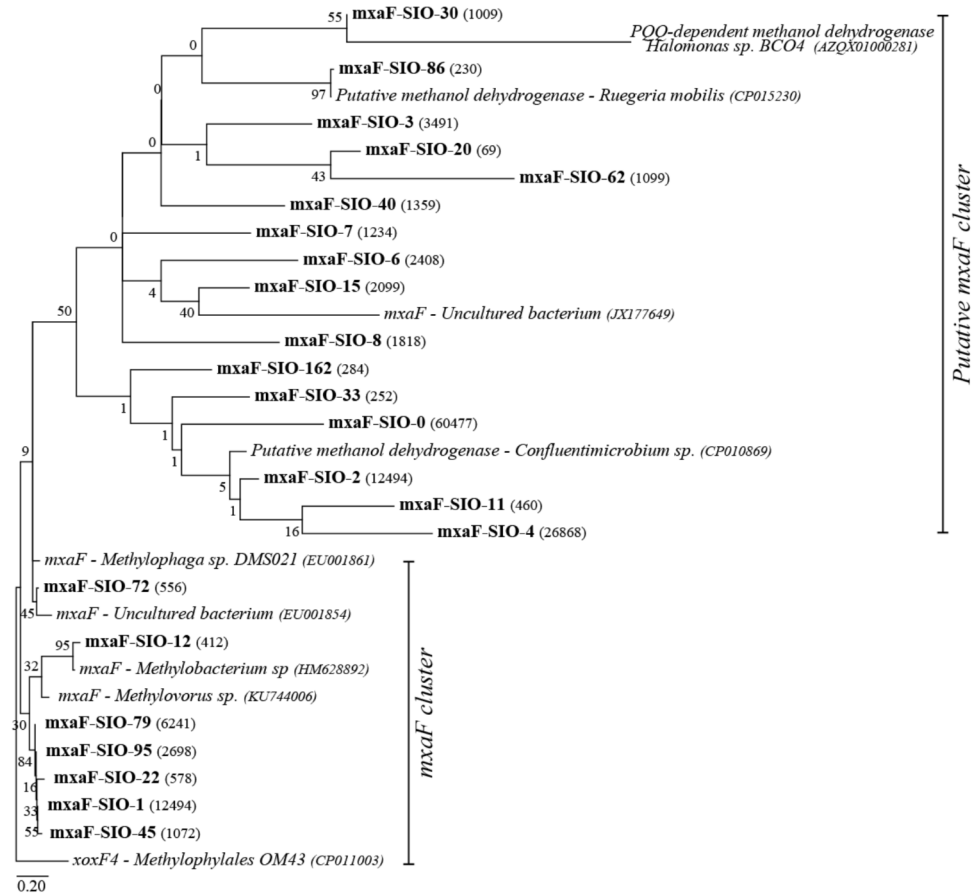

FIGURE 6 | Maximum likelihood tree of the main *mxaF* sequences ($OTU_{0.77}$), number of reads per OTUs are represented in parenthesis. Reference sequences are indicated in italics. Bootstrap values (n = 1000) are indicated at nodes; the scale bar represents changes per positions.

TABLE 3 | Winter contribution of methylotrophs (as a % of hybridized cells to DAPI cells at 120 h, standard deviation for n = 10 fields of view) to total bacterial abundance, and total bacterial growth rates during the active phase of the winter and summer experiments.

	Start	Control	MetOH	TMAO	MetOH + TMAO
Methylophaga spp.					
% of DAPI	0.2 ± *0.5*	25 ± *15*	72 ± *11*	3 ± *3*	23 ± *20*
Growth rate (d^{-1})		0.06 ± *0.1*	1.7 ± *0.03*	0.9 ± *0.6*	1.6 ± *0.3*
RumP β- and γ-Proteobacteria					
%	8.2 ± *4.3*	14 ± *4.5*	8 ± *5*	47 ± *6*	48 ± *14*
Growth rate		0.5 ± *0.13*	0.52 ± *0.14*	1.11 ± *0.03*	1.09 ± *0.07*
Total Methylotrophs					
%	8.4 ± *4.7*	25 ± *15*	80 ± *12*	50 ± *7*	70 ± *11*
Growth rate (d^{-1})		0.52 ± *0.14*	1.03 ± *0.43*	1.04 ± *0.01*	1.06 ± *0.05*
Winter bacterial growth rates (d^{-1})		0.33 ± *0.06*	0.56 ± *0.03*	0.68 ± *0.02*	0.63 ± *0.01*
Summer bacterial growth rates (d^{-1})		0.50 ± *0.14*	0.85 ± *0.09*	1.07 ± *0.07*	0.92 ± *0.02*

Mean ± standard deviation n = 4 for controls, for the treatment values are shown for each replicate. SD for the bacterial growth rates are based on n = 3 for the enrichment and n = 6 for the controls.

the TMAO-only treatment where *Methylophaga* did not have to compete with other C1 users, which may have been the case in the mixed treatment. The relative abundance of SAR11, the most abundant bacterial clade observed in marine ecosystems (Morris et al., 2002), decreased in all treatments and seasons. Despite its capacity to use C1 compounds as a source of energy (Sun et al., 2011) SAR11 is an oligotrophic clade, which is easily outcompeted in incubation experiments (Giovannoni, 2017).

Overall, it seems that while the winter bacterial community became enriched in specialist methylotrophs in response to the addition of methanol and TMAO, the already diverse and potentially generalist community was resistant

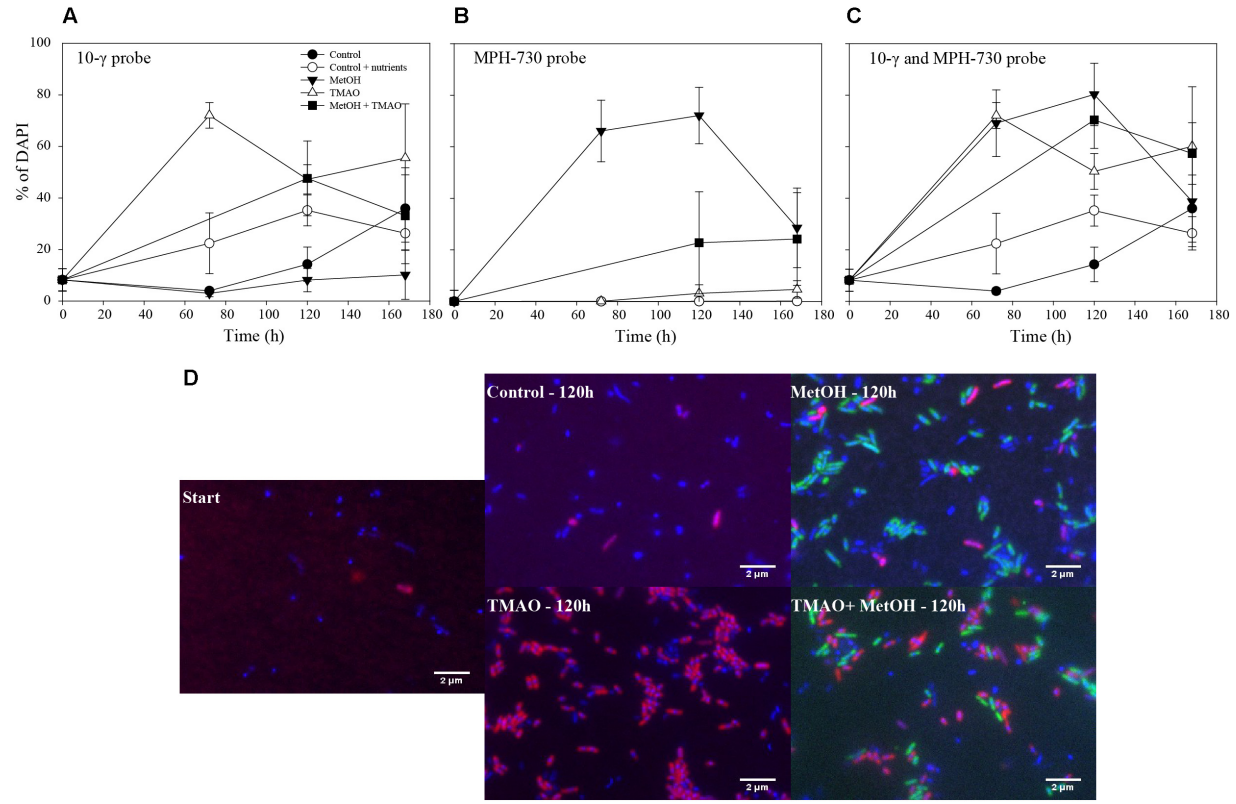

FIGURE 7 | Percentage of hybridization over time for the 10-γ probe **(A)**, MPH-730 probe **(B)** and the sum of both probes **(C)**. Merged epifluorescence images of fluorescence *in situ* hybridization for the 10-γ probe (red) accounting for γ- and β-Proteobacterial methylotrophs with the RumP pathway, MPH-730 probes (green) accounting for *Methylophaga* spp. bacteria and DAPI-stained organisms (blue) **(D)**.

to these perturbations during the productive period (summer).

Methylotrophic Tracers During Methanol and TMAO Incubations

Methanol incorporation measurements have been used as indicators of methylotrophic activities (Dixon et al., 2011b) and the marker gene for the methanol dehydrogenase large subunit *mxaF* has been used as a tracer for enrichment of methylotrophic taxa (McDonald and Murrell, 1997; Neufeld et al., 2007). However, *mxaF* may not be the most common gene marker for methylotrophy in marine environments, where *xoxF* is sometimes the most abundant methanol dehydrogenase (Ramachandran and Walsh, 2015; Taubert et al., 2015). Moreover, TMAO methylotrophic users do not all possess the *mxaF* gene and the capacity to assimilate methanol. Therefore, the tracers used in this study are probably underestimating the methylotrophic activity in the TMAO and mixed treatments (Chen, 2012). Sequencing the genes related to TMAO demethylation (Neufeld et al., 2007; Chen, 2012) and using radiolabeled TMAO marker could help better resolve the diversity and activities of TMAO users.

Methanol assimilation increased in both experiments, suggesting that both winter and summer enriched bacterial assemblages had the capacity to use methanol for biomass production. The measured assimilation rates were lower than in some coastal areas (Dixon et al., 2012; Halsey et al., 2012) but higher than in the English Channel (Sargeant et al., 2016) and overall in the range of methanol utilization (BGE_M) observed in the coastal areas (Dixon et al., 2012). Increase in methanol utilization was more remarkable in winter when compared to summer. In winter, methanol represented up to 1.2% of the carbon used for biomass production by bacteria, while it was only up to 0.01% of bacterial production in summer (average ratio of the methanol assimilation:bacterial production in the treatments with carbon addition integrated over the active phase of the experiment). In summer, the high methanol respiration observed in the treatments with carbon enrichment concords with the utilization of C1 compounds as energy source, as was suggested above.

The observed change in bacterial community composition in winter in response to the addition of carbon source was reflected in the change in functional community. While *Methylophilaceae* are known methylotrophs found in surface waters (Giovannoni et al., 2008; Halsey et al., 2012), 16S rRNA gene sequence related to β-Proteobacteria were low. However, the contribution of *mxaF*-OTUs related to *Methylophilaceae* increased especially in the treatments with methanol, suggesting that despite low overall abundance based on 16S rRNA genes,

they may have an important functional role in the system. In summer, the functional community appeared to be especially related to unknown/uncultured putative methylotrophs related to α- and γ-Proteobacteria. For instance, no *Oceanospirillales* representative have been previously shown to grow on methanol as their sole source of carbon, but they can use TMAO (Kube et al., 2013); the presence of *mxaF*-OTU related to *Oceanospirillales* in our treatment suggest that some may also be able to use methanol as a carbon source. This new capacities could have been acquired through horizontal gene transfer of *mxaF* between bacterial groups (Vuilleumier et al., 2009).

The growth of the specific winter methylotrophic population was further assessed through FISH over the course of the experiment. The enrichment of *Methylophaga* spp. observed at the end of the experiment through 16S rRNA gene sequencing was confirmed with FISH, showing a higher growth rate of *Methylophaga* spp. in the treatments with methanol. Other γ- and β-Proteobacteria methylotrophs grew faster in the treatments with TMAO. This is also consistent with the sequencing results. Overall, it appears that the change in the functional community observed in winter, but not in summer, was related to the enrichment of substrate specific methylotrophs. Nevertheless, the final growth and production rates of these different TMAO or methanol enriched populations were similar, suggesting a functional redundancy of the substrate specific methylotrophic populations.

Our results suggest that bacterial response to a pulse of C1 may be more important in less productive coastal waters. For instance a pulse of methanol could occur during methanol rich rainfalls (Felix et al., 2014; Mullaugh et al., 2015) more frequently in winter. And similar response could be observed at the onset of the spring bloom when waters are still carbon limited. But despite the subsequent enrichment of substrate specific methylotrophic populations their feedback on the marine carbon budget may be similar due to their functional redundancy. Nevertheless, it will be important to further study the effect of bacterial C1 drawdown and transformation, on air-sea fluxes as these will be substrate-dependent and unrelated to functional redundancy.

AUTHOR CONTRIBUTIONS

JD designed and carried out the study and data analysis. JD and MT prepared the samples for sequencing. JD wrote the manuscript. All authors contributed to the revisions, edited the manuscript, and approved the submitted version.

FUNDING

This work was supported by a Marie Curie Actions-International Outgoing Fellowship (PIOF-GA-2013-629378 to JD), the European Research Council (Consolidator Grant 615146 to MT) and the Gordon and Betty Moore Foundation (Grant GBMF4827 to FA).

ACKNOWLEDGMENTS

We would like to thank M. Sc. Anita Mäki and Lionel Le Toux for helping with the sequencing and bioinformatics. We would also like to acknowledge the SCOOS program for sharing their monitoring data for Chl *a* off SIO Pier, as well as B. Stephens and L. Aluwihare for sharing the *in situ* POC and DOC values.

SUPPLEMENTARY MATERIAL

The Supplementary Material for this article can be found online at: https://www.frontiersin.org/articles/10.3389/fmars.2018.00307/full#supplementary-material

REFERENCES

Alonso-Saez, L., and Gasol, J. M. (2007). Seasonal variations in the contributions of different bacterial groups to the uptake of low-molecular-weight compounds in northwestern Mediterranean coastal waters. *Appl. Environ. Microbiol.* 73, 3528–3535. doi: 10.1128/AEM.02627-06

Azam, F., and Malfatti, F. (2007). Microbial structuring of marine ecosystems. *Nat. Rev. Microbiol.* 5, 782–791. doi: 10.1038/nrmicro1747

Beale, R., and Airs, R. (2016). Quantification of glycine betaine, choline and trimethylamine N-oxide in seawater particulates: minimisation of seawater associated ion suppression. *Anal. Chim. Acta* 938, 114–122. doi: 10.1016/j.aca.2016.07.016

Beale, R., Dixon, J. L., Smyth, T. J., and Nightingale, P. D. (2015). Annual study of oxygenated volatile organic compounds in UK shelf waters. *Mar. Chem.* 171, 96–106. doi: 10.1016/j.marchem.2015.02.013

Beale, R., Liss, P. S., Dixon, J. L., and Nightingale, P. D. (2011). Quantification of oxygenated volatile organic compounds in seawater by membrane inlet-proton transfer reaction/mass spectrometry. *Anal. Chim. Acta* 706, 128–134. doi: 10.1016/j.aca.2011.08.023

Bratbak, G. (1985). Bacterial biovolume and biomass estimations. *Appl. Environ. Microbiol.* 49, 1488–1493.

Bunse, C., and Pinhassi, J. (2017). Marine bacterioplankton seasonal succession dynamics. *Trends Microbiol.* 6, 494–505. doi: 10.1016/j.tim.2016.12.013

Caporaso, J. G., Bittinger, K., Bushman, F. D., DeSantis, T. Z., Andersen, G. L., and Knight, R. (2010b). PyNAST: a flexible tool for aligning sequences to a template alignment. *Bioinformatics* 26, 266–267. doi: 10.1093/bioinformatics/btp636

Caporaso, J. G., Kuczynski, J., Stombaugh, J., Bittinger, K., Bushman, F. D., Costello, E. K., et al. (2010a). QIIME allows analysis of high-throughput community sequencing data. *Nat. Methods* 7, 335–336. doi: 10.1038/nmeth.f.303

Carpenter, L. J., Archer, S. D., and Beale, R. (2012). Ocean-atmosphere trace gas exchange. *Chem. Soc. Rev.* 41, 6473–6506. doi: 10.1039/c2cs35121h

Chen, Y. (2012). Comparative genomics of methylated amine utilization by marine *Roseobacter* clade bacteria and development of functional gene markers (*tmm, gmaS*). *Environ. Microbiol.* 14, 2308–2322. doi: 10.1111/j.1462-2920.2012.02765.x

Chen, Y., Patel, N. A., Crombie, A., Scrivens, J. H., and Murrell, J. C. (2011). Bacterial flavin-containing monooxygenase is trimethylamine monooxygenase. *Proc. Natl. Acad. Sci. U.S.A.* 108, 17791–17796. doi: 10.1073/pnas.1112928108

Chistoserdova, L. (2015). Methylotrophs in natural habitats: current insights through metagenomics. *Appl. Microbiol. Biotechnol.* 99, 5763–5779. doi: 10.1007/s00253-015-6713-z

Chistoserdova, L., Kalyuzhnaya, M. G., and Lidstrom, M. E. (2009). The expanding world of methylotrophic metabolism. *Annu. Rev. Microbiol.* 63, 477–499. doi: 10.1146/annurev.micro.091208.073600

Clarke, K. R., Gorley, R. N., Somerfield, P. J., and Warwick, R. M. (2014) *Change in Marine Communities: An Approach to Statistical Analysis and Interpretation*, 3rd Edn. Plymouth: PRIMER-E, 260.

Clarke, K. R., and Warwick, R. M. (2001). *Change in Marine Communities: an Approach to Statistical Analysis and Interpretation*, 2nd Edn. Plymouth: PRIMER-E, 172.

Degerman, R., Dinasquet, J., Riemann, L., De Luna, S. S., and Andersson, A. (2012). Effect of resource availability on bacterial community responses to increased temperature. *Aquat. Microb. Ecol.* 68, 131–142. doi: 10.3354/ame01609

Dinasquet, J., Kragh, T., Schroter, M. L., Sondergaard, M., and Riemann, L. (2013). Functional and compositional succession of bacterioplankton in response to a gradient in bioavailable dissolved organic carbon. *Environ. Microbiol.* 15, 2616–2628. doi: 10.1111/1462-2920.12178

Dixon, J. L., Beale, R., and Nightingale, P. D. (2011a). Microbial methanol uptake in northeast Atlantic waters. *ISME J.* 5, 704–716. doi: 10.1038/ismej.2010.169

Dixon, J. L., Beale, R., and Nightingale, P. D. (2011b). Rapid biological oxidation of methanol in the tropical Atlantic: significance as a microbial carbon source. *Biogeosciences* 8, 2707–2716. doi: 10.5194/bg-8-2707-2011

Dixon, J. L., Beale, R., and Nightingale, P. D. (2013). Production of methanol, acetaldehyde, and acetone in the Atlantic Ocean. *Geophys. Res. Lett.* 40, 4700–4705. doi: 10.1002/grl.50922

Dixon, J. L., Sargeant, S., Nightingale, P. D., and Murrell, J. C. (2012). Gradients in microbial methanol uptake: productive coastal upwelling waters to oligotrophic gyres in the Atlantic Ocean. *ISME J.* 7, 568–580. doi: 10.1038/ismej.2012.130

Ducklow, H. W., Purdie, D. A., Williams, P. J. L., and Davies, J. M. (1986). Bacterioplankton: a sink for carbon in a coastal marine plankton community. *Science* 232, 865–867. doi: 10.1126/science.232.4752.865

Edgar, R. C. (2010). Search and clustering orders of magnitude faster than BLAST. *Bioinformatics* 26, 2460–2461. doi: 10.1093/bioinformatics/btq461

Edgar, R. C. (2013). UPARSE: highly accurate OTU sequences from microbial amplicon reads. *Nat. Methods* 10, 996–998. doi: 10.1038/nmeth.2604

Facchini, M. C., Decesari, S., Rinaldi, M., Carbone, C., Finessi, E., Mircea, M., et al. (2008). Important source of marine secondary organic aerosol from biogenic amines. *Environ. Sci. Technol.* 42, 9116–9121. doi: 10.1021/es8018385

Felix, J., Jones, S., Avery, G., Willey, J., Mead, R., and Kieber, R. (2014). Temporal and spatial variations in rainwater methanol. *Atmos. Chem. Phys. Discuss.* 14, 1375–1398. doi: 10.5194/acpd-14-1375-2014

Fuhrman, J. A., Cram, J. A., and Needham, D. M. (2015). Marine microbial community dynamics and their ecological interpretation. *Nat. Rev. Microbiol.* 13, 133–146. doi: 10.1038/nrmicro3417

Fuhrman, J. A., Hewson, I., Schwalbach, M. S., Steele, J. A., Brown, M. V., and Naeem, S. (2006). Annually reoccurring bacterial communities are predictable from ocean conditions. *Proc. Natl. Acad. Sci. USA* 103, 13104–13109. doi: 10.1073/pnas.0602399103

Gifford, S. M., Becker, J. W., Sosa, O. A., Repeta, D. J., and Delong, E. F. (2016). Quantitative transcriptomics reveals the growth- and nutrient-dependent response of a streamlined marine methylotroph to methanol and naturally occurring dissolved organic matter. *mBio* 7:e01279-16. doi: 10.1128/mBio.01279-16

Gilbert, J. A., Field, D., Swift, P., Thomas, S., Cummings, D., Temperton, B., et al. (2010). The taxonomic and functional diversity of microbes at a temperate coastal site: a 'multi-Omic' study of seasonal and diel temporal variation. *PLoS One* 5:e15545. doi: 10.1371/journal.pone.0015545

Giovannoni, S. J. (2017). SAR11 bacteria: the most abundant plankton in the oceans. *Ann. Rev. Mar. Sci.* 9, 231–255. doi: 10.1146/annurev-marine-010814-015934

Giovannoni, S. J., Hayakawa, D. H., Tripp, H. J., Stingl, U., Givan, S. A., Cho, J.-C., et al. (2008). The small genome of an abundant coastal ocean methylotroph. *Environ. Microbiol.* 10, 1771–1782. doi: 10.1111/j.1462-2920.2008.01598.x

Glöckner, F. O., Amann, R., Alfreider, A., Pernthaler, J., Psenner, R., Trebesius, K., et al. (1996). An in situ hybridization protocol for detection and identification of planktonic bacteria. *Syst. Appl. Microbiol.* 19, 403–406. doi: 10.1016/S0723-2020(96)80069-5

Halsey, K. H., Carter, A. E., and Giovannoni, S. J. (2012). Synergistic metabolism of a broad range of C1 compounds in the marine methylotrophic bacterium HTCC2181. *Environ. Microbiol.* 14, 630–640. doi: 10.1111/j.1462-2920.2011.02605.x

Janvier, M., Frehel, C., Grimont, F., and Gasser, F. (1985). Methylophaga marina gen. nov., sp. nov. and *Methylophaga thalassica* sp. nov., marine methylotrophs. *Int. J. Syst. Evol. Microbiol.* 35, 131–139. doi: 10.1099/00207713-35-2-131

Janvier, M., Regnault, B., and Grimont, P. (2003). Development and use of fluorescent 16S rRNA-targeted probes for the specific detection of Methylophaga species by in situ hybridization in marine sediments. *Res. Microbiol.* 154, 483–490. doi: 10.1016/S0923-2508(03)00146-3

Karl, D. M., Hebel, D. V., Bjorkman, K., and Letelier, R. M. (1998). The role of dissolved organic matter release in the productivity of the oligotrophic North Pacific Ocean. *Limnol. Oceanogr.* 43, 1270–1286. doi: 10.4319/lo.1998.43.6.1270

Kirchman, D. L., Knees, E., and Hodson, R. (1985). Leucine incorporation and its potential as a measure of protein-synthesis by bacteria in natural aquatic systems. *Appl. Environ. Microbiol.* 49, 599–607.

Kragh, T., Søndergaard, M., and Tranvik, L. (2008). Effect of exposure to sunlight and phosphorus-limitation on bacterial degradation of coloured dissolved organic matter (CDOM) in freshwater. *FEMS Microbiol. Ecol.* 64, 230–239. doi: 10.1111/j.1574-6941.2008.00449.x

Kube, M., Chernikova, T. N., Al-Ramahi, Y., Beloqui, A., Lopez-Cortez, N., Guazzaroni, M.-E., et al. (2013). Genome sequence and functional genomic analysis of the oil-degrading bacterium *Oleispira antarctica*. *Nat. Commun.* 4:2156. doi: 10.1038/ncomms3156

Kumar, S., Stecher, G., and Tamura, K. (2016). MEGA7: molecular evolutionary genetics analysis version 7.0 for bigger datasets. *Mol. Biol. Evol.* 33, 1870–1874. doi: 10.1093/molbev/msw054

Lidbury, I., Mausz, M. A., Scanlan, D. J., and Chen, Y. (2017). Identification of dimethylamine monooxygenase in marine bacteria reveals a metabolic bottleneck in the methylated amine degradation pathway. *ISME J.* 11, 1592–1601. doi: 10.1038/ismej.2017.31

Lidbury, I., Murrell, J. C., and Chen, Y. (2014b). Trimethylamine N-oxide metabolism by abundant marine heterotrophic bacteria. *Proc. Natl. Acad. Sci. U.S.A.* 111, 2710–2715. doi: 10.1073/pnas.1317834111

Lidbury, I. D., Murrell, J. C., and Chen, Y. (2014a). Trimethylamine and trimethylamine N-oxide are supplementary energy sources for a marine heterotrophic bacterium: implications for marine carbon and nitrogen cycling. *ISME J.* 9, 760–769. doi: 10.1038/ismej.2014.149

Lønborg, C., Davidson, K., Álvarez–Salgado, X. A., and Miller, A. E. J. (2009). Bioavailability and bacterial degradation rates of dissolved organic matter in a temperate coastal area during an annual cycle. *Mar. Chem.* 113, 219–226. doi: 10.1016/j.marchem.2009.02.003

Mäki, A., Rissanen, A., and Tiirola, M. (2016). A practical method for barcoding and size-trimming PCR templates for amplicon sequencing. *Biotechniques* 60, 88–90. doi: 10.2144/000114380

McCarren, J., Becker, J. W., Repeta, D. J., Shi, Y. M., Young, C. R., Malmstrom, R. R., et al. (2010). Microbial community transcriptomes reveal microbes and metabolic pathways associated with dissolved organic matter turnover in the sea. *Proc. Natl. Acad. Sci. U.S.A.* 107, 16420–16427. doi: 10.1073/pnas.1010732107

McDonald, I. R., and Murrell, J. C. (1997). The methanol dehydrogenase structural gene mxaF and its use as a functional gene probe for methanotrophs and methylotrophs. *Appl. Environ. Microbiol.* 63, 3218–3224.

Mincer, T. J., and Aicher, A. C. (2016). Methanol production by a broad phylogenetic array of marine phytoplankton. *PLoS One* 11:e0150820. doi: 10.1371/journal.pone.0150820

Morris, R. M., Rappe, M. S., Connon, S. A., Vergin, K. L., Siebold, W. A., Carlson, C. A., et al. (2002). SAR11 clade dominates ocean surface bacterioplankton communities. *Nature* 420, 806–810. doi: 10.1038/nature01240

Mou, X. Z., Sun, S. L., Edwards, R. A., Hodson, R. E., and Moran, M. A. (2008). Bacterial carbon processing by generalist species in the coastal ocean. *Nature* 451, 708–711. doi: 10.1038/nature06513

Mullaugh, K. M., Hamilton, J. M., Avery, G. B., Felix, J. D., Mead, R. N., Willey, J. D., et al. (2015). Temporal and spatial variability of trace volatile organic compounds in rainwater. *Chemosphere* 134, 203–209. doi: 10.1016/j.chemosphere.2015.04.027

Müller, C., Iinuma, Y., Karstensen, J., Pinxteren, D. V., Lehmann, S., Gnauk, T., et al. (2009). Seasonal variation of aliphatic amines in marine sub-micrometer particles at the Cape Verde islands. *Atmos. Chem. Phys.* 9, 9587–9597. doi: 10.5194/acp-9-9587-2009

Murrell, J. C., Mcgowan, V., and Cardy, D. L. N. (1993). Detection of methylotrophic bacteria in natural samples by molecular probing techniques. *Chemosphere* 26, 1–11. doi: 10.1016/0045-6535(93)90408-W

Neufeld, J. D., Boden, R., Moussard, H., Schafer, H., and Murrell, J. C. (2008). Substrate-specific clades of active marine methylotrophs associated with a phytoplankton bloom in a temperate coastal environment. *Appl. Environ. Microbiol.* 74, 7321–7328. doi: 10.1128/AEM.01266-08

Neufeld, J. D., Schafer, H., Cox, M. J., Boden, R., Mcdonald, I. R., and Murrell, J. C. (2007). Stable-isotope probing implicates Methylophaga spp and novel Gammaproteobacteria in marine methanol and methylamine metabolism. *ISME J.* 1, 480–491. doi: 10.1038/ismej.2007.65

Nieder, J. B., Hussels, M., Bittl, R., and Brecht, M. (2014). Effect of TMAO and betaine on the energy landscape of photosystem I. *Biochim. Biophys. Acta Bioenerg.*1837, 849–856. doi: 10.1016/j.bbabio.2014.01.005

Osterholz, H., Singer, G., Wemheuer, B., Daniel, R., Simon, M., Niggemann, J., et al. (2016). Deciphering associations between dissolved organic molecules and bacterial communities in a pelagic marine system. *ISME J.* 10, 1717–1730. doi: 10.1038/ismej.2015.231

Parada, A. E., Needham, D. M., and Fuhrman, J. A. (2016). Every base matters: assessing small subunit rRNA primers for marine microbiomes with mock communities, time series and global field samples. *Environ. Microbiol.* 18, 1403–1414. doi: 10.1111/1462-2920.13023

Poretsky, R. S., Sun, S. L., Mou, X. Z., and Moran, M. A. (2010). Transporter genes expressed by coastal bacterioplankton in response to dissolved organic carbon. *Environ. Microbiol.* 12, 616–627. doi: 10.1111/j.1462-2920.2009.02102.x

Porter, K. G., and Feig, Y. S. (1980). The use of dapi for identifying and counting aquatic microflora. *Limnol. Oceanogr.* 25, 943–948. doi: 10.4319/lo.1980.25.5.0943

Quast, C., Pruesse, E., Yilmaz, P., Gerken, J., Schweer, T., Yarza, P., et al. (2013). The SILVA ribosomal RNA gene database project: improved data processing and web-based tools. *Nucleic Acids Res.* 41, 590–596. doi: 10.1093/nar/gks1219

Ramachandran, A., and Walsh, D. A. (2015). Investigation of XoxF methanol dehydrogenases reveals new methylotrophic bacteria in pelagic marine and freshwater ecosystems. *FEMS Microbiol. Ecol.* 91:fiv105. doi: 10.1093/femsec/fiv105

Sargeant, S. L., Murrell, J. C., Nightingale, P. D., and Dixon, J. L. (2016). Seasonal variability in microbial methanol utilisation in coastal waters of the western English Channel. *Mar. Ecol. Prog. Ser.* 550, 53–64. doi: 10.3354/meps11705

Schindelin, J., Arganda-Carreras, I., Frise, E., Kaynig, V., Longair, M., Pietzsch, T., et al. (2012). Fiji: an open-source platform for biological-image analysis. *Nat. Methods* 9, 676–682. doi: 10.1038/nmeth.2019

Simon, M., and Azam, F. (1989). Protein-content and protein-synthesis rates of planktonic marine-bacteria. *Mar. Ecol. Prog. Ser.* 51, 201–213. doi: 10.3354/meps051201

Singh, H., Chen, Y., Tabazadeh, A., Fukui, Y., Bey, I., Yantosca, R., et al. (2000). Distribution and fate of selected oxygenated organic species in the troposphere and lower stratosphere over the Atlantic. *J. Geophys. Res. Atmos.* 105, 3795–3805. doi: 10.1029/1999JD900779

Singh, H. B., Tabazadeh, A., Evans, M. J., Field, B. D., Jacob, D. J., Sachse, G., et al. (2003). Oxygenated volatile organic chemicals in the oceans: inferences and implications based on atmospheric observations and air-sea exchange models. *Geophys. Res. Lett.* 30, 1862–1866. doi: 10.1029/2003GL017933

Smith, D. C., and Azam, F. (1992). A simple, economical method for measuring bacterial protein synthesis rates in seawater using ^{3}H-leucine. *Mar. Microb. Food Webs* 6, 107–114.

Sorooshian, A., Padró, L. T., Nenes, A., Feingold, G., Mccomiskey, A., Hersey, S. P., et al. (2009). On the link between ocean biota emissions, aerosol, and maritime clouds: airborne, ground, and satellite measurements off the coast of California. *Global Biogeochem. Cycles* 23:GB4007. doi: 10.1029/2009GB003464

Sosa, O. A., Gifford, S. M., Repeta, D. J., and Delong, E. F. (2015). High molecular weight dissolved organic matter enrichment selects for methylotrophs in dilution to extinction cultures. *ISME J.* 9, 2725–2739. doi: 10.1038/ismej.2015.68

Stacheter, A., Noll, M., Lee, C. K., Selzer, M., Glowik, B., Ebertsch, L., et al. (2012). Methanol oxidation by temperate soils and environmental determinants of associated methylotrophs. *ISME J.* 7, 1051–1064. doi: 10.1038/ismej.2012.167

Stark, S., Mannisto, M. K., Ganzert, L., Tiirola, M., and Haggblom, M. M. (2015). Grazing intensity in subarctic tundra affects the temperature adaptation of soil microbial communities. *Soil Biol. Biochem.* 84, 147–157. doi: 10.1016/j.soilbio.2015.02.023

Sun, J., Steindler, L., Thrash, J. C., Halsey, K. H., Smith, D. P., Carter, A. E., et al. (2011). One carbon metabolism in SAR11 pelagic marine bacteria. *PLoS One* 6:e23973. doi: 10.1371/journal.pone.0023973

Taubert, M., Grob, C., Howat, A., Burns, O. J., Dixon, J. L., Chen, Y., et al. (2015). xoxF encoding an alternative methanol dehydrogenase is widespread in coastal marine environments. *Environ. Microbiol.* 17, 3937–3948. doi: 10.1111/1462-2920.12896

Taubert, M., Grob, C., Howat, A. M., Burns, O. J., Pratscher, J., Jehmlich, N., et al. (2017). Methylamine as a nitrogen source for microorganisms from a coastal marine environment. *Environ. Microbiol.* 19, 2246–2257. doi: 10.1111/1462-2920.13709

Tsien, H. C., Bratina, B. J., Tsuji, K., and Hanson, R. S. (1990). Use of oligodeoxynucleotide signature probes for identification of physiological groups of methylotrophic bacteria. *Appl. Environ. Microbiol.* 56, 2858–2865.

Vuilleumier, S., Chistoserdova, L., Lee, M.-C., Bringel, F., Lajus, A., Zhou, Y., et al. (2009). Methylobacterium genome sequences: a reference blueprint to investigate microbial metabolism of C1 compounds from natural and industrial sources. *PLoS One* 4:e5584. doi: 10.1371/journal.pone.0005584

Williams, J., Holzinger, R., Gros, V., Xu, X., Atlas, E., and Wallace, D. W. (2004). Measurements of organic species in air and seawater from the tropical Atlantic. *Geophys. Res. Lett.* 31:L23S06. doi: 10.1029/2004GL020012

Yang, M., Beale, R., Liss, P., Johnson, M., Blomquist, B., and Nightingale, P. (2014a). Air–sea fluxes of oxygenated volatile organic compounds across the Atlantic Ocean. *Atmos. Chem. Phys.* 14, 7499–7517. doi: 10.5194/acp-14-7499-2014

Yang, M., Blomquist, B. W., and Nightingale, P. D. (2014b). Air-sea exchange of methanol and acetone during HiWinGS: estimation of air phase, water phase gas transfer velocities. *J. Geophys. Res. Oceans* 119, 7308–7323. doi: 10.1002/2014JC010227

Yang, M., Nightingale, P. D., Beale, R., Liss, P. S., Blomquist, B., and Fairall, C. (2013). Atmospheric deposition of methanol over the Atlantic Ocean. *Proc. Natl. Acad. Sci. U.S.A.* 110, 20034–20039. doi: 10.1073/pnas.1317840110

Conflict of Interest Statement: The authors declare that the research was conducted in the absence of any commercial or financial relationships that could be construed as a potential conflict of interest.

Copyright © 2018 Dinasquet, Tiirola and Azam. This is an open-access article distributed under the terms of the Creative Commons Attribution License (CC BY). The use, distribution or reproduction in other forums is permitted, provided the original author(s) and the copyright owner(s) are credited and that the original publication in this journal is cited, in accordance with accepted academic practice. No use, distribution or reproduction is permitted which does not comply with these terms.

frontiers in Microbiology

ORIGINAL RESEARCH
published: 04 October 2018
doi: 10.3389/fmicb.2018.02203

Metagenomics of Coral Reefs Under Phase Shift and High Hydrodynamics

Pedro Milet Meirelles[1†‡], Ana Carolina Soares[1†‡], Louisi Oliveira[1], Luciana Leomil[1], Luciana Reis Appolinario[1], Ronaldo Bastos Francini-Filho[2], Rodrigo Leão de Moura[1], Renato Tenan de Barros Almeida[1], Paulo S. Salomon[1], Gilberto Menezes Amado-Filho[3], Ricardo Kruger[4], Eduardo Siegle[5], Diogo A. Tschoeke[1], Isao Kudo[6], Sayaka Mino[7], Tomoo Sawabe[7], Cristiane C. Thompson[1] and Fabiano L. Thompson[1]*

[1] Institute of Biology and SAGE-COPPE, Federal University of Rio de Janeiro, Rio de Janeiro, Brazil, [2] Department of Environment and Engineering, Federal University of Paraíba, Rio Tinto, Brazil, [3] Rio de Janeiro Botanical Garden Research Institute (IP-JBRJ), Rio de Janeiro, Brazil, [4] Department of Cellular Biology, University of Brasília, Brasília, Brazil, [5] Oceanographic Institute, University of São Paulo, São Paulo, Brazil, [6] Graduate School of Environmental Science, Hokkaido University, Sapporo, Japan, [7] Laboratory of Microbiology, Faculty of Fisheries Sciences, Hokkaido University, Hakodate, Japan

OPEN ACCESS

Edited by:
Alejandro A. Murillo,
EMBL Heidelberg, Germany

Reviewed by:
Swings Jean,
Ghent University, Belgium
Virginia Helena Albarracín,
Center for Electron Microscopy (CIME), Argentina

***Correspondence:**
Pedro Milet Meirelles
pedrommeirelles@gmail.com

[†] These authors have contributed equally to this work

‡Present address:
Pedro Milet Meirelles, Institute of Biology, Federal University of Bahia, Salvador, Brazil
Ana Carolina Soares, Laboratory of Bioinformatics, Institute of Chemistry, University of São Paulo, São Paulo, Brazil

Specialty section:
This article was submitted to Aquatic Microbiology, a section of the journal Frontiers in Microbiology

Received: 02 March 2018
Accepted: 29 August 2018
Published: 04 October 2018

Citation:
Meirelles PM, Soares AC, Oliveira L, Leomil L, Appolinario LR, Francini-Filho RB, de Moura RL, de Barros Almeida RT, Salomon PS, Amado-Filho GM, Kruger R, Siegle E, Tschoeke DA, Kudo I, Mino S, Sawabe T, Thompson CC and Thompson FL (2018) Metagenomics of Coral Reefs Under Phase Shift and High Hydrodynamics. Front. Microbiol. 9:2203. doi: 10.3389/fmicb.2018.02203

Local and global stressors have affected coral reef ecosystems worldwide. Switches from coral to algal dominance states and microbialization are the major processes underlying the global decline of coral reefs. However, most of the knowledge concerning microbialization has not considered physical disturbances (e.g., typhoons, waves, and currents). Southern Japan reef systems have developed under extreme physical disturbances. Here, we present analyses of a three-year investigation on the coral reefs of Ishigaki Island that comprised benthic and fish surveys, water quality analyses, metagenomics and microbial abundance data. At the four studied sites, inorganic nutrient concentrations were high and exceeded eutrophication thresholds. The dissolved organic carbon (DOC) concentration (up to 233.3 μM) and microbial abundance (up to 2.5×10^5 cell/mL) values were relatively high. The highest vibrio counts coincided with the highest turf cover (~55–85%) and the lowest coral cover (~4.4–10.2%) and fish biomass (0.06 individuals/m^2). Microbiome compositions were similar among all sites and were dominated by heterotrophs. Our data suggest that a synergic effect among several regional stressors are driving coral decline. In a high hydrodynamics reef environment, high algal/turf cover, stimulated by eutrophication and low fish abundance due to overfishing, promote microbialization. Together with crown-of-thorns starfish (COTS) outbreaks and possible of climate changes impacts, theses coral reefs are likely to collapse.

Keywords: coral reefs, microbialization, local stressors, early warning signals, metagenomics, resistence, hydrodynamics

INTRODUCTION

Coral reefs are subjected to cyclic and episodic natural disturbances (e.g., storms), but their recovery potential is affected by interacting factors that vary regionally and at ocean basin scales (Roff and Mumby, 2012). For instance, in contrast with Pacific Ocean reefs, the lower resilience of Caribbean reefs is attributed to: (i) higher macroalgae recruitment and growth rates; (ii) basin-wide iron-enrichment from aeolian dust; (iii) the low diversity and abundance of fast-growing

branching corals (e.g., Acroporidae) and herbivores; (iv) missing groups of herbivores (Roff and Mumby, 2012). The role of microbes in reef health is still under-acknowledged and represents an emerging frontier to a full understanding of coral reef resilience (Knowlton and Jackson, 2008; Garren and Azam, 2012). It is also not well understood how high hydrodynamics may affect reef microbial diversity.

The process by which a given marine ecosystem trophic structure shifts toward a higher microbial biomass and energy use is called "Microbialization" (Jackson et al., 2001). In coral reefs, the main possible causes of this process are overfishing and eutrophication, which act together in a positive feedback loop, increasing DOC concentrations, coral disease incidence, algal cover, and microbial abundance [DDAM model, see (Haas et al., 2016)]. Microbialization is positively correlated with human impacts across subregional (Bruce et al., 2012), ocean basin (McDole et al., 2012) and global spatial scales (Haas et al., 2016). Human influences also drive microbial energy use in the water column at Pacific coral reefs. The autotrophic activity alters energy fluxes at less impacted sites, increasing resistance mechanisms (McDoleSomera et al., 2016). However, the microbial abundance and metagenomic diversity are not well known in high hydrodynamic reefs, such as those in Ishigaki (Okinawa). These reefs experienced intense and chronic coral stress due to frequent typhoons which can became catastrophic with global warming (Hongo et al., 2012; Harii et al., 2014).

Japanese coral reefs are marine biodiversity hotspots with elevated endemism levels conditioned by non-reversing currents flowing from tropical to temperate latitudes (Roberts et al., 2002). Strong storms and typhoons are the foremost natural disturbance agents in the Okinawa region, where Japanese reefs are concentrated (Japanese Coral Reef Society, 2004). However, mass coral mortalities following thermal anomalies (Nishihira and Yamazato, 1974; Stone et al., 1999; Loya et al., 2001; Kayanne et al., 2002; Goto et al., 2010; Dadhich et al., 2012), crown-of-thorns starfish (COTS) outbreaks (Nishihira and Yamazato, 1974), and pollutant and nutrient runoffs (West and van Woesik, 2001; Kitada et al., 2008) are also escalating. Overfishing is a major feature of Southern Japan reefs (Liu et al., 2009). However, the microbial diversity in these reefs is not well documented.

Here, we investigated the metagenomic microbial diversity of the Ishigaki reefs, Okinawa, through a holistic approach. We incorporated data from benthic and fish assemblage assessments, water quality measurements (physical, chemical, biological, and microbiological parameters) and seawater metagenomics over three consecutive years (2012–2014) to investigate the following hypotheses: (I) eutrophication is leading coral to algal dominance states and (II) microbialization is an ongoing process and is more prevalent at high hydrodynamic reefs. Increased turf-algae dominance, low fish abundance, high nutrients, and DOC concentration, as well as heterotrophic microbial abundance, suggests a possible microbialization of Ishigaki reefs.

RESULTS

Wave Modeling

Based on the global wave generation model WaveWatch III (NOAA/NCEP), easterly waves dominate the study region (53% of occurrence), with heights ranging from 0.5 to 2.0 m (45% of occurrence). Waves reach the studied sites with varying power, and the exposed site is Miyara, followed by Osaki, Sekisei, and Taketomi (**Supplementary Table S13** and **Figure 1**). In a simulation of typhoon conditions, with an offshore wave height of 12 m combined with winds of up to 200 km/h (similar to the conditions observed during Super Typhoon Soulik, 2013) wave power increases by approx. 11,000 to 13,000% at Sekisei, Osaki, and Miyara. Typhoon conditions at Taketomi result in a lower increase in wave power, with an increase of approx. 4,000% (**Figure 1** and **Supplementary Table S13**).

Due to their positions, which protect them from incoming easterly waves, Taketomi and Sekisei present the lowest wave power levels for the tested conditions. Although protected from direct wave incidences, Sekisei still presents a high increase in wave power during typhoons, since the incoming swell and local wind action result in higher waves in Sekisei than in Taketomi. The high hydrodynamics also appear to contribute to the dispersion of microbes and coral disease among reefs. The high hydrodynamics may be considered an extra level of complexity while addressing coral reef microbialization and coral disease, not accounted for in previous studies.

Benthic Cover

Benthic cover differed significantly among sites and sampling years, and the interaction between sites and years was also significant (PERMANOVA, $P < 0.05$) (**Figure 2A** and **Supplementary Table S4**). The nMDS ordination diagram revealed three distinct groups of sites: (i) Miyara, (ii) Osaki, (iii) Taketomi and Sekisei (**Figure 2B**). This grouping supported our first hypothesis that Miyara is the site most affected by land runoff (and nutrient inputs). Turf algae (55.8% $\pm$ 2.5; mean $\pm$ SE), soft corals (10.8% $\pm$ 2.7), and sponges (2.07% $\pm$ 0.64) dominated Miyara reef (**Supplementary Figure S2**). Turf algae (85.8% $\pm$ 1.2) dominated Osaki reef, the only site where COTS (*Acanthaster planci*) were recorded (**Supplementary Figure S2**). *Acropora* was the dominant coral genus at Sekisei and Taketomi; *Pectinia* and *Porites* were dominant at Miyara and Osaki, respectively (**Figure 3A**). Corals were more abundant at Taketomi (mean 2012–2014: 62.4% $\pm$ 2.93) and Sekisei (44.07% $\pm$ 2.39) (**Figure 2A**) than at the other reefs, coinciding with the lower wave energy of these two areas. Miyara and Osaki presented a consistently lower coral cover (10.25 $\pm$ 1.69 and 4.4 $\pm$ 0.74, respectively) (hypothesis 1 confirmed) than the other reefs, and the proportions of corals and turf algae at these two areas were remarkably stable over the study period (**Figure 2A**). Recently, in 2013, dead coral cover increased at Sekisei and Taketomi (17.24% $\pm$ 0.9 and 7.75% $\pm$ 0.51, respectively) (**Supplementary Figure S3**). The dominance of turf in Miyara reinforces our hypothesis that nutrient inputs from the Miyara River may influence the status of the surrounding reefs. We proceeded

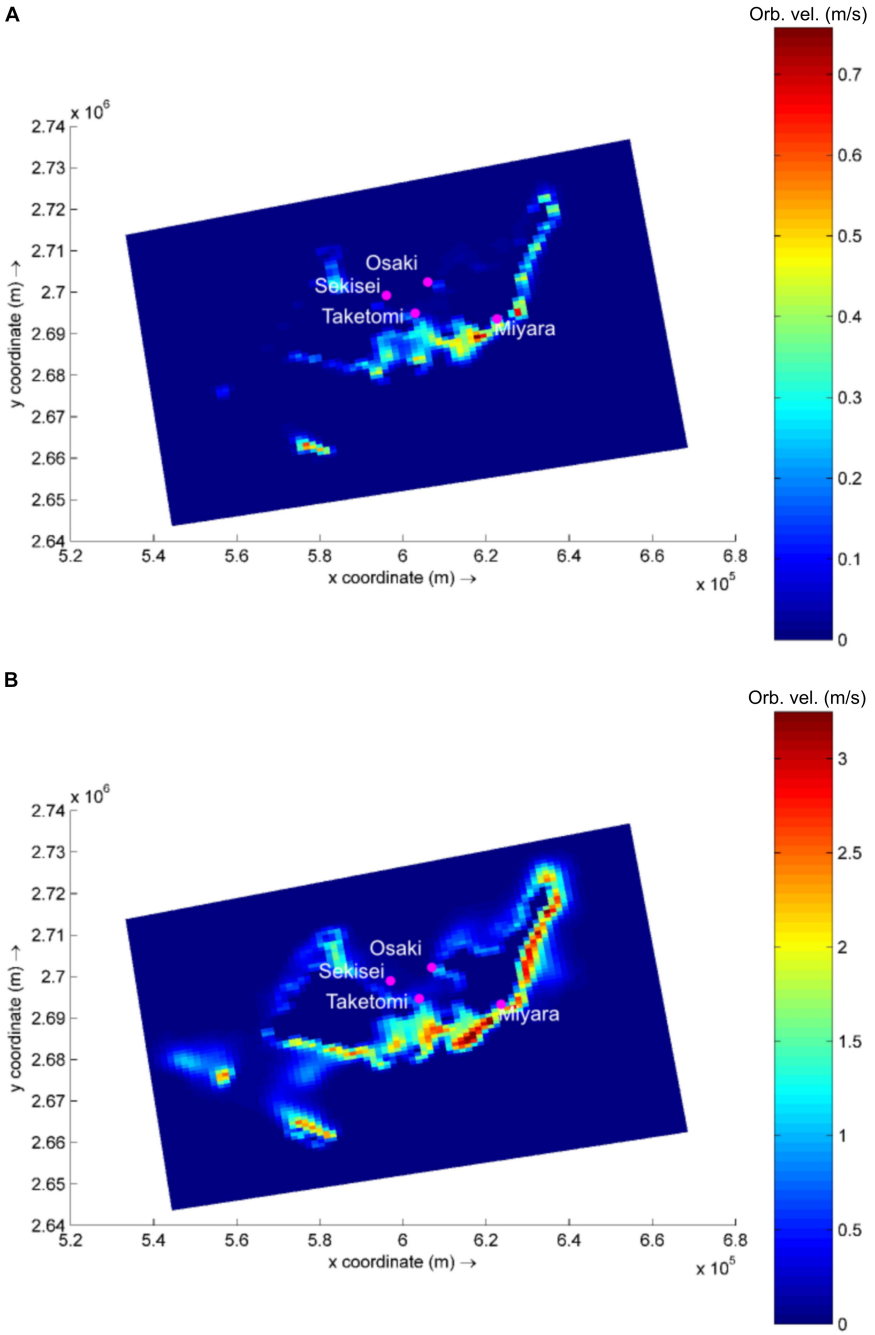

FIGURE 1 | Modeled wave generated near bottom orbital velocity (m/s) in the area of interest. Example for calm **(A)** and typhoon **(B)** wave conditions. Note difference in color bar scales.

to estimate the abundance of fish in an attempt to support hypothesis II. Reduced herbivorous fish assemblages may also contribute to the proliferation of turfs.

Fish Assemblages

A total of 81 fish species (25 families) were recorded. Fish abundance was overall low, with assemblages dominated by small-sized species (**Figure 2C** and **Supplementary Figures S4**, **S5**). The total fish abundance was significantly different among sites but not among years (ANOVA, $P < 0.005$; **Supplementary Table S5**). Sekisei and Taketomi had the highest fish abundances (average 0.17 individuals/m^2), while Osaki and Miyara had the lowest fish abundances (0.12 and 0.06 individuals/m^2, respectively). Clearly, the overall fish abundance was extremely low in all locations. Pomacentridae (damselfishes) were the most abundant fish at all reefs, with abundances up to 63%

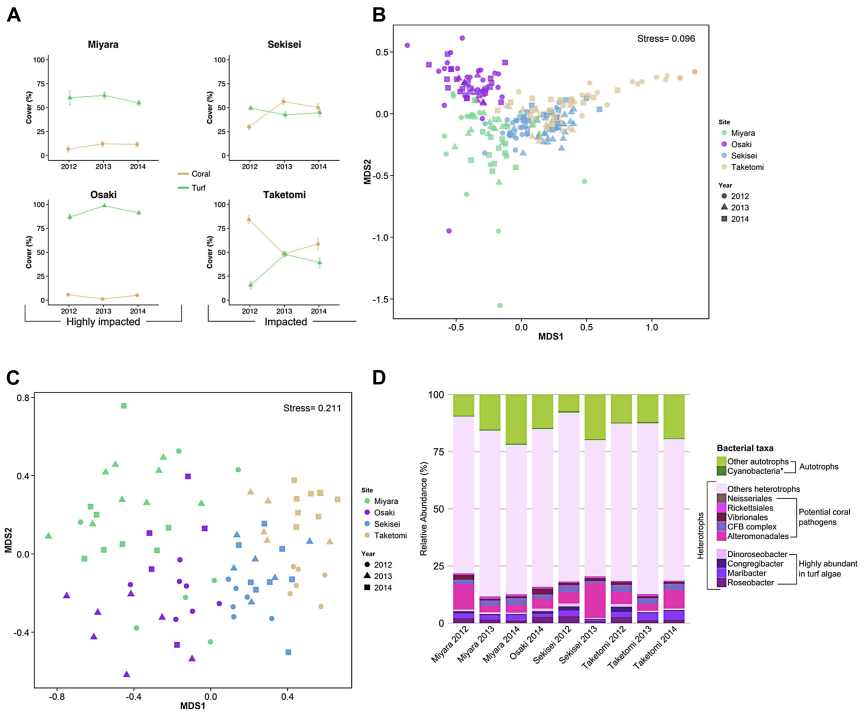

FIGURE 2 | Coral reefs from Ishigaki Island are impacted at different levels. Yellow and green lines represent coral and algal cover in percentages for the reef sites and years, respectively **(A)**. The first two axes of non-metric multidimensional scaling (nMDS) based on benthic cover **(B)** and fish abundance **(C)** show each benthic sample replicate using different colors for sites and different shapes for years. The taxonomic compositions of water metagenomes, heterotrophic bacteria, potential coral pathogenic bacteria, and highly abundant bacteria in turf algae are represented by different colors **(D)**. The asterisk in Cyanobacteria represents the bacterial genera *Anabaena*, *Nostoc*, and *Trichodesmium* (cyanobacteria genera commonly found in turf algae). CFB complex, Cytophaga–Flavobacterium–Bacteroides complex.

of the total number of individuals (**Figure 3B**). At Sekisei and Taketomi, planktivorous damselfishes (e.g., *Pomacentrus lepidogenys*, *Chromis* spp.) were remarkably more abundant than territorial herbivorous damselfishes (e.g., *Chrysiptera rex*, *Stegastes* spp.) (**Supplementary Figure S5**). Fish assemblages differed among sites and years, and the interaction between sites and years was also significant (PERMANOVA, $P < 0.005$; **Supplementary Table S6** and **Figures 2C**, 3B). The first two axes of the CCA explained 76.2% of the relationship between habitat characteristics and fish assemblage structure. The main predictor of fish assemblage structure was coral cover, followed by soft coral, turf algae and crustose coralline algae (**Figure 2C**). This pattern of high metagenomic similarity among the studied sites supports hypothesis II and may be related to an ongoing process of microbialization due to the loss of fish biomass and increase in microbial biomass. We proceeded to demonstrate that all studied reefs are under intense hydrodynamic stress that could function as an extra stress factor under these conditions.

Physical Chemical Water Analysis

The DOC concentration varied between 92 μM at Osaki, 2014, and 233 μM at Miyara, 2013. The highest value of chlorophyll a was observed at Miyara in 2014 (3 μg/L), and the lowest value of chlorophyll a was observed at Sekisei in 2013 (0.2 μg/L). There was no significant difference in DOC among years and sites. Concentrations of total dissolved inorganic nitrogen (TDIN) decreased sharply from 2012 to 2014 at all reefs. The highest values were recorded in 2012 at Miyara (5.4 μM), Osaki (4.3 μM), and Sekisei (3.9 μM), and the lowest values were recorded in 2014 at Osaki (0.6 μM), Sekisei (0.75 μM), Taketomi (0.8 μM), and Miyara (1.2 μM). Over the study period, ammonium decreased significantly (ANOVA $P < 0.05$; **Supplementary Table S9**) at all sites. Nitrate varied significantly only among sites (ANOVA $P < 0.05$; **Supplementary Table S9**), with Miyara presenting the highest concentrations (1.8 μM in 2012) and Osaki presenting the lowest concentrations (0.4 μM in 2014). Nitrite significantly differed among sites but not among years, with Osaki presenting the highest values (0.2 μM in 2013) and Miyara presenting the lowest values (0.2 μM in 2014) (ANOVA, $P < 0.05$; **Supplementary Table S9**). Phosphate concentrations were similar among sites and varied between 0.11 and 0.08 μM (ANOVA, $P < 0.05$; **Supplementary Table S9**). The highest silicate values were observed at Sekisei (1.7 μM in 2013), and the lowest silicate values were observed at Miyara (1.3 μM in 2012).

Microbial Abundance

The total microbial abundance varied from 1.0×10^5 cells/mL (Taketomi, 2014) to 3.1×10^5 cells/mL (Taketomi, 2012) (**Supplementary Table S1**). Microbial counts were significantly different among sites and years (ANOVA, $P < 0.05$;

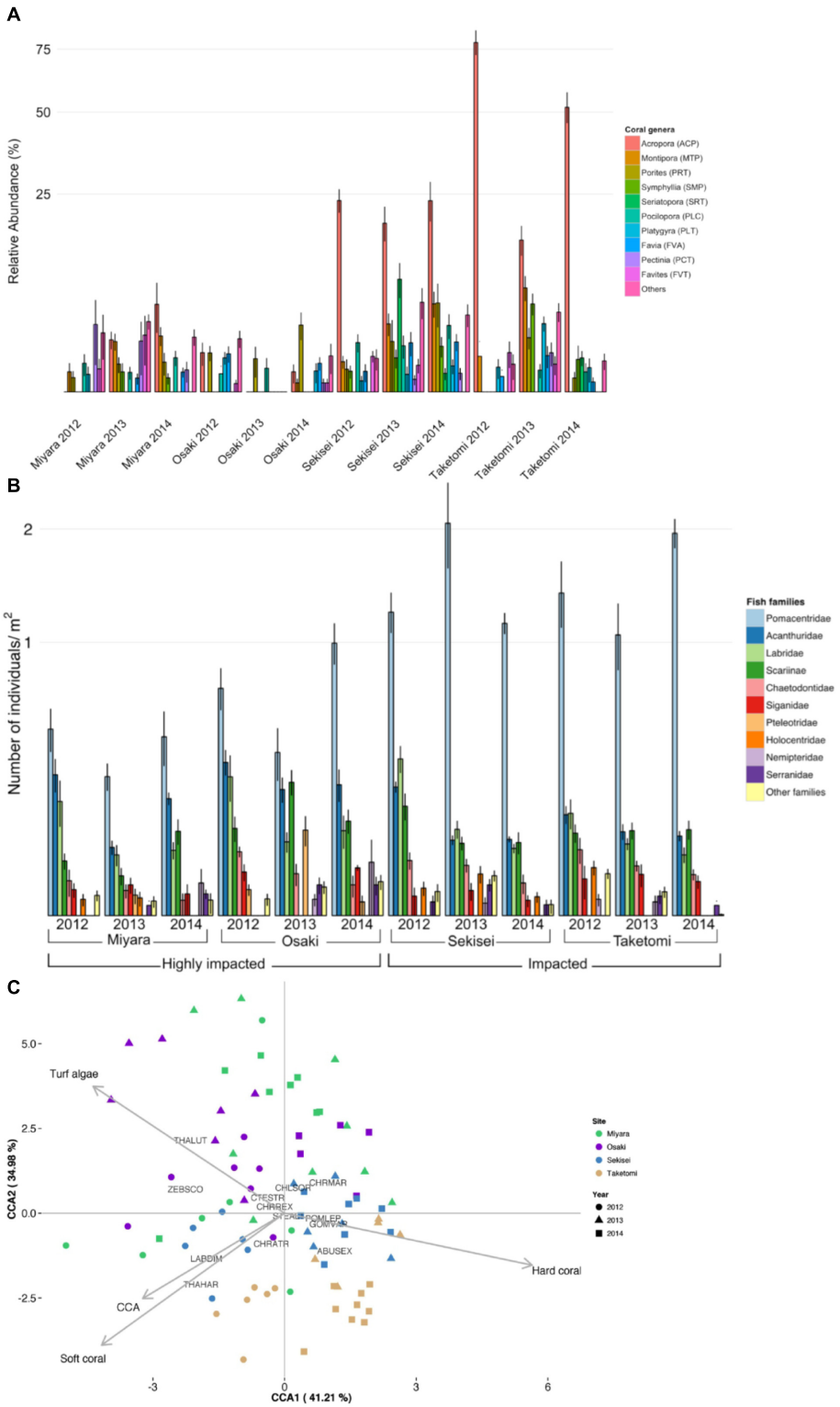

FIGURE 3 | Ishigaki coral reef and fish community composition structure. **(A)** Relative coral cover. **(B)** Relative abundance of fish families. **(C)** Canonical correspondence analysis (CCA) biplot of benthic cover and fish assemblages of Ishigaki coral reefs. Each replicate is represented by dots in different colors (for sites) and different shapes (for years). Species abbreviations are: CTESTR, *Ctenochaetus striatus*; STEALT, *Stegastes altus*; CHLSOR, *Chlorurus sordidus*; POMLEP, *Pomacentrus lepidogenys*; CHRMAR, *Chromis margaritifer*; CHRREX, *Chrysiptera rex*; CHRATR, *Chromis atripectoralis*; ABUSEX, *Abudefduf sexfasciatus*; THALUT, *Thalassoma lutescens*; THAHAR, *Thalassoma hardwicke*; GOMVAR, *Gomphosus varius*; LABDIM, *Labroides dimidiatus*; ZEBSCO, *Zebrasoma scopas*.

Supplementary Table S7). Vibrio counts were significantly different among sites, and the interaction between sites and years was also significant (ANOVA, $P < 0.05$; **Supplementary Table S8**). The lowest vibrio counts were recorded at Sekisei, 2014 [(24.3 ± 1.0 CFU/ml (N = 7)], and Taketomi, 2013 [37.1 ± 0.8 CFU/ml (N = 7)], while the highest vibrio counts were observed at Osaki, 2013 [137.1 ± 4.6 CFU/ml (N = 7)], and Miyara, 2014 [130.6 ± 3.4 CFU/ml (N = 8)] (**Supplementary Table S1** and **Supplementary Figure S6**). These two sites had the highest nutrient values and the lowest coral cover values (**Figure 3A**). The higher abundances of fast-growing vibrio bacteria in these sites is a relevant finding that supports hypothesis II.

Microbial Community Structure

A total of 19,146,788 high-quality metagenomic reads from 9 seawater samples were generated (**Supplementary Tables S2, S3**). The median values of taxonomically and functionally identified reads were 41.35% (varying from 19.21%, N = 437,356, to 60.85%, N = 720,291), and 27.89% (13.88%, N = 315,932, to 33.86%, N = 18,076), respectively (**Supplementary Tables S2, S3**). Most sequences were annotated as *Bacteria* (>87%). *Proteobacteria* reads were the most abundant at all sites (at least 48.53%, N = 291,028, at Miyara, 2014), followed by *Cyanobacteria* (at least 7.12%, N = 14,993, at Taketomi, 2013) and *Bacteroidetes* (at least 6.05%, N = 40,828, at Sekisei, 2013) reads (**Supplementary Figure S7**). Most reads corresponded to heterotrophic bacteria, ranging from 78.1% (N = 468,376) at Miyara in 2014 to 92.1% (N = 178,943) at Taketomi in 2013 (**Figure 2D**).

The percent of reads identified as potential coral pathogens [*Vibrionales*, *Cytophaga–Flavobacterium–Bacteroides* complex (CFB complex), *Rickettsiales*, *Neisseriales*, and *Alteromonadales*] varied from 6.9% (Miyara, 2013) to 18.2% (Sekisei, 2013) (**Figure 1D**). The percent of reads related to highly abundant bacterial groups in turf algae [*Roseobacter*, *Maribacter*, *Congregibacter*, *Dinoroseobacter*, and *Cyanobacteria* (*Anabaena*, *Nostoc*, and *Trichodesmium*)] varied from 2.55% (Sekisei, 2013) to 9.16% (Sekisei, 2012) (**Figure 2D**). Unlike for the abundance of the fish and benthic assemblages (**Figure 3**), we did not find strong grouping patterns for the metagenomes of the microbial communities based on the taxonomic (class level; **Supplementary Table S10**) and functional annotations (SEED subsystem level 1; **Supplementary Table S11**), dinucleotide composition (**Supplementary Table S12**) and cross-contigs (i.e., shared contigs containing reads from two or more metagenomes) after cross-assembling (**Figure 4**).

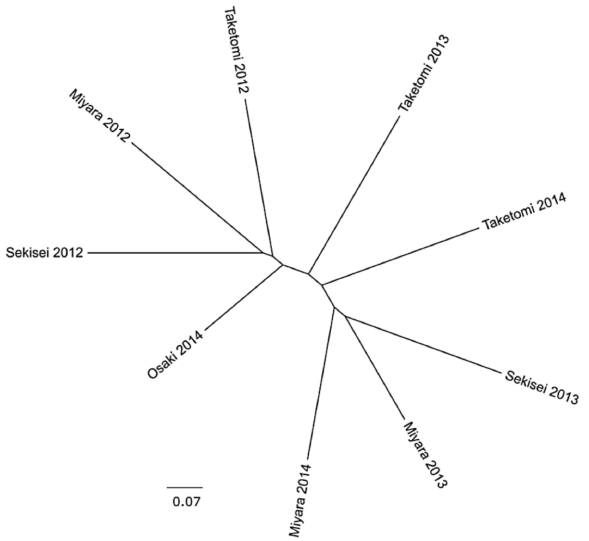

FIGURE 4 | The microbial communities of Ishigaki coral reef seawater have similar genetic compositions. Cladograms representing the fraction of cross-contigs (i.e., shared contigs that contain reads from two or more metagenomes) after cross-assembly.

DISCUSSION

The Ishigaki Island reefs have a 10-fold lower abundance of fish and other important herbivores (e.g., sea urchins) than other reef sites (**Table 1**). In addition, the nutrient levels measured in these reefs are higher than the previously reported eutrophication thresholds for Pacific reefs (Bell et al., 2007). Agriculture runoff is the major source of these high nutrient concentrations in the Ishigaki Islands (Tanaka et al., 2011). Nutrification, coupled with a low abundance of herbivores, is a well-known trigger of the transition from coral to algal dominance stages (Hughes, 1994; Birrell et al., 2008). Even under high nutrient concentrations, herbivory can control algal growth and impede algal dominance (Jessen et al., 2013). In Okinawa, an herbivore-exclusion experiment resulted in increased turf algae abundance and prevented coral growth (Tamai and Sakai, 2013), reinforcing the algal dominance mechanism.

Abundance of Small-Bodied Damselfishes (Pomacentridae)

Overfishing deeply alters the structures of reef fish assemblages via direct (e.g., removal of large predators) and cascading (e.g., increase in prey species) effects. For instance, reefs that are fully open to intense fisheries tend to have a low abundance of large-sized carnivores and herbivores and a higher abundance of small-bodied damselfishes (Pomacentridae) (Edwards et al., 2014). Damselfishes dominated the Ishigaki reef fish communities. However, the proportion of territorial herbivorous species was the highest in Miyara and Osaki, the sites with the lowest coral cover. In Osaki, the site where we recorded the greatest decline in coral cover, the proportions of territorial herbivorous and planktivorous damselfishes also varied significantly, with a marked increase in the abundance of territorial herbivorous species (**Supplementary Figure S5**). Territorial herbivorous damselfish species may positively influence turf algae growth by farming and the aggressive protection of their territories against other herbivorous fish (Arnold et al., 2010; Doropoulos et al., 2013). In addition, the territories of damselfishes may harbor coral pathogenic bacteria (Casey et al., 2014, 2015). Therefore, territorial damselfish may negatively influence coral recovery

after mass coral mortality events caused by typhoons and COTS outbreaks.

Insights on Microbialization

In coral reefs, an increased dominance of fleshy non-calcifying reef builder (e.g., turf and macroalgae) over calcifying reef builder (e.g., corals and coralline algae) organisms is often accompanied by major changes in the microbial community composition and abundance (McDole et al., 2012; Meirelles et al., 2015a; Roach et al., 2017). Nutrification, together with DOC addition from increased benthic algae exudation, further promotes the proliferation of microorganisms (Barott and Rohwer, 2012). Accordingly, we recorded increased abundances of heterotrophic and potentially pathogenic bacteria across the study region, and the DOC concentrations were overall high and comparable to those of other impacted tropical reefs (Dinsdale et al., 2008; Tanaka et al., 2011; Bruce et al., 2012). While DOC may be terrestrially sourced (Tanaka et al., 2011), its high levels and low spatial heterogeneity indicate major autochthonous sourcing. The combined effects of high nutrient concentrations, increased turf algae cover and low fish abundances are pivotal for the establishment of a microbialization process (McDole et al., 2012), as evidenced in our microbial counts and metagenomes, which supports our study hypotheses. The heterotrophic microbial community recorded in Ishigaki included cultured vibrios that have been implicated in coral diseases and mortality, as well as other microbial groups that are typically increased in multifactorial coral diseases (e.g., Bacteroidetes, Fusobacteria, Gammaproteobacteria, Nostocales) (Dinsdale et al., 2008; Bruce et al., 2012; Garcia et al., 2013). In a previous study at the same sampling sites, we found high abundances of globally recognized potential coral-pathogenic vibrio species using a culture-dependent approach (Amin et al., 2016). Indeed, the vibrio counts were significantly higher at Osaki and Miyara, the two reefs with a relatively high turf cover and low fish counts, than at the other reefs. Compared with healthy and impacted reefs from other locations, the benthic community structure of the Ishigaki reefs appears to be in an ongoing coral-to-algal shift in dominance regimes. We observed sites under different coral-turf algae dominance stages, coupled with extremely low fish abundances. In the Line Islands, the highest microbialization levels were observed in the reefs with the lowest fish biomasses (Kelly et al., 2014). Nevertheless, the lowest fish biomass in the Line Island study was at least 10-fold higher than the average fish biomass of the Ishigaki reefs (**Table 1**).

Extreme Environmental Conditions and Reef Resilience

According to Project Monitoring-Site 1000 reports[1], coral reefs from Ishigaki have experienced recent coral mass mortality events caused by both coral disease and COT outbreaks and typhoons. From 2007 to 2013, coral cover has generally decreased (to approx. 30%), with only few sites (e.g., Sekisei Lagoon) showing signs of coral cover recovery. Coral transplantation methods have been proposed to restore coral reefs from Okinawa (Omori, 2011); however, the microbialized environment dominated by turf algae and territorial damselfishes coral propagules may not favor coral propagule fixation and growth. In a large data set from more than fifty Central Pacific Islands, no evidence of phase shifts was found; however, fleshy non-calcifying organisms dominated benthic communities of human-populated islands (Smith et al., 2016). According to new definitions of reef health based on reef-building capacity (Smith et al., 2016), Ishigaki coral reefs can be classified as degraded. The new water quality, microbial abundance and diversity evidence provided in the present study reinforces this classification.

Extreme hydrodynamics (e.g., typhoons) may enhance microbialization via different processes, including (i) microbial dispersion and homogenization, as observed in the present study, (ii) loss of coral cover and the opening of benthic habitats for rapid colonization by turfs, and (iii) feedback processes that further alter benthic cover [phase shifts promoting increases in dissolved organic carbon (DOC) and allelopathic compounds

[1]http://www.biodic.go.jp/moni1000/findings/reports/index.html#2464

TABLE 1 | Ishigaki Island reef sites compared with other reefs.

	Ishigaki				Abrolhos		Line Islands	
	Miyara	**Osaki**	**Sekisei**	**Taketomi**	**Sebastião Gomes**	**Parcel dos Abrolhos**	**Kiritimati**	**Kingman**
Coral cover (ind./m^2)	10.19	4.03	45.42	63.72	0.33	33.33	21*	71*
Turf algae cover (ind./m^2)	59.29	92.17	45.55	34.28	93.23	29.94	68*	36*
Fish abundance (ind./m^3)	0.74	1.35	1.93	1.84	17.2	69.3	4	12
Microbial abund. (cells/ml)	1.40E+05	1.52E+05	1.78E+05	2.02E+05	6.62E+05	4.88E+05	8.4E+5	7.2E+04
Heterotrophs (%)	81	85	83.83	90.01	91	71	50	16
Vibrio (CFU/ml)	71.68	90.34	46.51	50.37	68000	0	940	0
DOC (μM)	166.67	95.84	170.84	164.17	67.4	41.8	51.2	32.3

*Ishigaki fish, benthic, and microbial data are given as the average of the three sampling years for each site. Benthic cover values are shown as percentages; fish abundances are shown as individuals/m^2; microbial abundances are shown as cells/mL; heterotroph abundances are shown as percentages; Vibrios values are shown as CFU/mL; DOC values are shown as μM. Data from other studies are presented as the minimum and maximum values observed in all studied reefs. Benthic cover and microbial data for Abrolhos were retrieved from (Francini-Filho et al., 2013) and (Bruce et al., 2012), respectively. Data for the Line Islands were retrieved from (Sandin et al., 2008) and (Dinsdale et al., 2008). *(Sandin et al., 2008) presented coral cover as CCA and stony coral cover together and fleshy algae cover as macro-algae and turf algae cover together.*

produced by turf/algae]. The negative feedback of nutrification and herbivore overfishing has driven several coral reefs to an algae-dominated state (Hoegh-Guldberg et al., 2007). Algae, in turn, are responsible for the production of allelopathic toxic compounds (Nelson et al., 2013), as well as the massive exudation of labile organic matter, which increases microbial abundance and activity (Haas et al., 2011). DOC produced by algae, especially turf algae, promotes the rapid growth of heterotrophic microbial communities and pathogenic bacteria (Smith et al., 2006). In coral-algal interfaces, heterotrophic bacteria may also cause hypoxia, promoting further tissue loss and coral death (Gregg et al., 2013; Jorissen et al., 2016). Overfished reefs that interact with agricultural and urban landscapes tend to lose their resilience and are dominated by heterotrophic microbial communities with high abundances of opportunistic and potential pathogens (Dinsdale et al., 2008; Bruce et al., 2012).

The two reefs with an increased algal dominance (Miyara and Osaki) are under consistently higher wave energy and episodic typhoons than the other reefs. The microbiomes of all the studied sites were relatively similar, reinforcing the possible role of hydrodynamics in the dispersion of microbes across the entire study area. Tropical cyclones have accounted for most of the coral decline recorded in Australia's Great Barrier Reef (GBR) (De'ath et al., 2012), and the importance of storms may be even higher in the high-latitude reefs of Southern Japan, where the frequency and intensity of cyclones are increasing (Tu and Chou, 2013). A recent study showed that typhoons can cause shifts in coral morphology dominance (i.e., from foliose to bushy) in the upper mesophotic coral reefs from Okinawa (White et al., 2017). Storms and typhoons have been reported to be associated with increases and shifts in phytoplankton compositions and to influence the calcification of corals in Ishigaki reefs (Blanco et al., 2008; Sowa et al., 2014). In the Caribbean, strong wave swells have increased diseases and snail predation in coral (Bright et al., 2016). In addition, COTS outbreaks seem to play a major role in reef resilience across the Pacific Ocean, including Japan (Nishihira and Yamazato, 1974; Sano, 1987) and the GBR, where COTS is the second most important stressor to coral communities (De'ath et al., 2012). During our study, we recorded a COTS outbreak in Osaki, and the coral cover of Miyara was drastically reduced due an outbreak in 2011 (T. Sawabe unpub. obs.). After a COTS outbreak, coral cover recovery may take years. For instance, coral cover recovery in Guam, Micronesia, was much faster (from 0.9 to 65% in 3 years) (Colgan, 1987) than that reported in the present study. Remarkably, COTS outbreaks are related to the increasing survival of plankton-feeding larvae in nutrient-enriched flood waters (Fabricius et al., 2010). After mass coral mortality events, coral community compositions can change. In our study, we found that, after COTS outbreaks, massive colonies (*Porites* and *Pectinia*) were dominant over branching colonies (*Acropora* and *Montipora*). Similar results were obtained in another study at the Ishigaki Island reefs (Harii et al., 2014). Increasing coverage of massive coral colonies rather branching coral colonies is associated with a loss in reef structural complexity and a decrease, based on the number of scales, coral recovery by reducing both the delivery of coral larvae to the substratum and larval settlement (Hata et al., 2017).

CONCLUSION

Our analysis has provided new insights into the microbial diversity of Ishigaki reefs. Here, we suggest that microbialization may be an important mechanism (via the DDAM model) influencing the coral community and can be used as an early warning signal for coral reef phase shifts in the Ishigaki reefs. The high latitude and high hydrodynamics in the Ishigaki coral reefs mean these reefs suffer periodic acute declines in coral cover due to, e.g., typhoons. The system's capacity to return to coral-dominated states after periodic typhoons is being increasingly compromised, possibly by an ongoing microbialization process. Hydrodynamics may play fundamental roles in coral reef microbialization. We suggest the inclusion of hydrodynamic analyses for future studies regarding coral reef microbialization. The proliferation of rapidly growing heterotrophic microbes (e.g., vibrios and other potential coral pathogens) demonstrated in the present study hints to important features of these Ishigaki reefs. Overfishing has nearly extinguished fish from these reefs, while turf and nutrification have promoted microbialization. Increased DOC from turf algae and runoff contribute to benthic assemblages under different coral-algal dominance stages. These stressors interact in positive feedback loops that enhance microbialization and reduce reef resilience.

MATERIALS AND METHODS

Study Area

Located in the southwestern part of the Ryukyu Islands, Ishigaki Island (approx. area 229 km^2 with approx. 49,075 habitants) is surrounded by fringing reefs exposed to high levels of anthropogenic and terrestrial influences (e.g., river, ground, and beach water) (Kawahata et al., 2000). Miyara River, the longest river of the island, has a catchment area of 35.4 km^2 and total length of approx. 12 km; considerable amounts of red soil and nutrient from the fields, which are emitted by animal wastes and chemical fertilizers from agricultural activities, outflow from this river (Banzai et al., 2003; Banzai and Nakamura, 2006; Abe, 2010).

We selected four sites exposed to different local stressors in Ishigaki Island, Okinawa, Japan (**Supplementary Figure S1** and **Supplementary Table S1**). We classified the reef sites as "impacted" based on previous coral declines due to mass mortality and/or COTS outbreaks (Program Monitoring Sites 1000 2007–2013 reports[2]) and "highly impacted" based on previous coral cover data and previous and ongoing COTS outbreaks (T. Sawabe unpub. obs.). The Taketomi (24°20.5260′N, 124°05.6443′E) and Sekisei reefs (24°21.7557′N, 124°02.7190′E, inside Iriomote Ishigaki National Park) were classified as "impacted," and the Miyara (24°20.5489′N, 124°13.0408′E) and Osaki reefs (24°25.4171′N, 124°04.4956′E) were classified as "highly impacted." Sampling occurred after the rainy season and before the typhoon season, in June 2012, 2013, and 2014. No specific permissions were required. All sampling efforts were conducted at the reef front.

[2]http://www.biodic.go.jp/moni1000/

Benthic Cover

Benthic cover was estimated following previously described procedures (Francini-Filho and de Moura, 2008; Francini-Filho et al., 2013). At each site, 15 photoquadrats with 0.7 m^2 were randomly placed in similar reef sections of approx. 100 m^2. In the subsequent sampling years, samples were obtained at the same positions, using GPS markings. Percent cover was estimated using Coral Point Count with Excel Extension software (CPCe) (Kohler and Gill, 2006), with 100 randomly distributed points per photoquadrat. Organisms below each point were identified and grouped in the following major benthic functional categories (Steneck and Dethier, 1994): turf algae, fleshy algae, sponges, echinoderms, tunicates, mollusks, sand, and corals (at the genus level). The health of each coral colony was classified into one of three categories: healthy, diseased (e.g., signs of tissue necrosis and bleaching), and recently dead (exposed skeleton).

Fish Assemblages

Fish assemblages were assessed from video records by SCUBA divers using a Sony HDR-XR550 V camera. Samples were obtained at the same sites where water samples and benthic cover estimates were obtained, at approx. 5 m depth. Recordings ($N = 7$ per site in each year) were made under slow movement near the bottom (approx. 1 m). Fish counts in the video footage were standardized by space and time (10′ video stretches, $N = 83$). Trophic guild assignments were based on literature data (Randall, 1967). The results are presented as number of individuals and relative abundance.

Physical, Chemical, and Biological Inventories

Divers collected water samples at the benthic boundary layer (up to 10 cm from the bottom) using a Beckson Thirsty-Mate® hand pump and clean 10 L water gallons. Temperature, Dissolved Oxygen (DO) and salinity were measured *in situ* using a U-50 Multiparameter Water Quality Checker (Horiba, Tokyo). Chlorophyll *a*, DOC, inorganic nutrients and microbial abundances were determined following previously described methods (Andrade et al., 2003; Grasshoff et al., 2009; Rezende et al., 2010). Chlorophyll *a* samples were collected using negative pressure filtration with 1–2 L of water. Filters (GF/C, Whatman®, GE Healthcare) were extracted in dimethylformamide at −20°C and analyzed by a Turner Design fluorometer. For the DOC analysis, 50 mL of seawater filtered using a calcinated and weighted Whatman GF/F glass microfibre filter was collected in a HCl-washed amber bottle and fixed with 100 μL of 85% phosphoric acid. Fixed samples were tightly sealed and refrigerated at 4°C to avoid microbial degradation until DOC quantification procedures could be conducted (Sharp et al., 2002; Shimada et al., 2010). The detection limits for DOC and nutrient analyses were 0.83 μmol/L (0.01 mg C/L) and 0.01 μmol/L, respectively, based on three times the standard deviation of the lowest concentration of the samples. The analytical precision (coefficient of variation, CV) was 2–3% by replicate measurements of each sample. For inorganic nutrient analyses, 10 mL of water was frozen and analyzed in the laboratory using an auto-analyser (Bran+Luebbe, Autoanalyzer II) (Shimada et al., 2010). Microbial abundance was determined by DAPI staining (Kepner and Pratt, 1994) under an Axioo Photo epifluorescence microscope (Zeiss, Germany) (Porter and Feig, 1980; Martinussen and Thingstad, 1991). Colony forming units (CFUs) of vibrios were estimated using 0.2 mL aliquots of seawater plated on TCBS selective medium (10 replicates) incubated at room temperature. Counts were performed up to 48 h after plating.

Coral Reef Seawater Metagenomic DNA Extraction

Water samples from each site were collected near the bottom (<10 cm) and filtered in four Sterivex (0.22 μm) filters. Four independent replicates of seawater were prefiltered through nets of 100 μm and 20 μm by gravity. Two liters of water per replicate were filtered. Microbial cells retained in the filter received SET buffer and were stored at 30°C until DNA extraction. DNA extraction was performed using modified column purification protocol (Nucleospin Tissue, Macherey-Nagel, Dueren, Germany), as previously described (Bruce et al., 2012). A pool of DNA extracted from the filters was used for sequencing. Quality control was performed with Nanodrop absorbance and quantification by using the 2100 Bioanalyzer and Qubit High Sensitivity DNA Kit (Agilent, Santa Clara, CA, United States).

Metagenome Sequencing and Sequence Analysis

Metagenomic DNA samples were sequenced by Illumina MiSeq (paired-end sequencing, 2 × 300 base pairs). Metagenomic libraries were prepared using the Nextera and Nextera XT Sample Preparation Kits (Illumina, San Diego, CA, United States). The size distribution of reads was accessed with the 2100 Bioanalyzer and the High Sensitivity DNA Kit (Agilent, Santa Clara, CA, United States). Quantification of libraries was performed with the 7500 Real Time PCR system (Applied Biosystems, Foster City, CA, United States) and the KAPA Library Quantification Kit (Kapa Biosystems, Wilmington, MA, United States).

Quality Control and Metagenomic Data Analysis

Low quality (quality score <30) and duplicate sequences were removed using PRINSEQ (Schmieder and Edwards, 2011). Metagenomic sequence annotation was conducted using MG-RAST v3.5 (Meyer et al., 2008) with a maximum *e*-value cut-off of 1×10^{-5}. Taxonomic and functional annotation was performed using the SEED database. To standardize the annotated metagenome sizes, we presented data as relative abundances (number of sequences of a given taxa or subsystem divided by the total number of identified sequences of the metagenome). Reads from all nine metagenomes were combined into a single fasta file and were cross-assembled using Mira (Chevreux et al., 2004). The results were visualized using the metagenome cross-assembly tool crAss (Dutilh et al., 2012). Briefly, crAss calculates a distance matrix between all pairs of

metagenomes and corrects for sample size using the SHOT formula, which has previously been used to correct for genome size when calculating phylogenetic distances (Korbel et al., 2002; Dutilh et al., 2004, 2007). This distance matrix was converted into a cladogram using BioNJ (Gascuel, 1997) and was visualized using FigTree[3]. All data are available at BaMBa (Meirelles et al., 2015b) (pmeirelles.19), and the metagenomes are also available in MG-RAST servers. The unique metagenome identifiers are listed in **Supplementary Tables S2, S3**.

Statistical Analysis

Analyses were performed with R (R Development Core Team, 2011), except where indicated. Abundance and multivariate figures were plotted with the packages ggplot2 and reshape. Non-metric multidimensional scaling (nMDS) ordination was used to summarize spatial and temporal similarities (Bray-Curtis) of benthic, fish, and microbial community structures using the metaMDS in the vegan package (Oksanen et al., 2005). To test if benthic, fish, and microbial assemblages (both taxonomically and functionally) differed among sampling sites and years, permutational multivariate analysis of variance (PERMANOVA) was performed using the function adonis (Oksanen et al., 2005) (Bray-Curtis distances and 999 permutations). To investigate the relationship between: (i) fish and benthic assemblages; (ii) microbial and benthic assemblages, and (ii) microbial assemblages and environmental variables (e.g., nutrients, dissolved oxygen, depth), we performed a canonical correspondence analysis (CCA) using the cca function (Oksanen et al., 2005). Only the most abundant species (>90% of individuals) were used in the CCA. The Monte Carlo permutation test was used to test for the statistical significance ($P < 0.05$) of the contribution of each variable in the CCA axes. Bacterial diversity indices [Shannon entropy and Shannon evenness (i.e., Hill's Ratio)] and richness were determined with data at the species level (Oksanen et al., 2005). To assess the genetic similarity of seawater microbiomes among reef sites and years, the dinucleotide compositions of seawater metagenomes were compared. Frequency tabulation of sequence data was performed according to (Willner et al., 2009) with a homemade Python script. A principal component analysis (PCA) was performed using the rda function (Oksanen et al., 2005) in order to visualize sample grouping. To test the hypothesis that the seawater microbiomes are genetic similar, the dinucleotide composition was analyzed among sites and years. PERMANOVA was performed using the adonis function (Oksanen et al., 2005). For all analysis *P*-values <0.05 were considered statistically significant. For multivariate analysis, percentages data were transformed to arcsin ($\sqrt{x}$). The results are presented as mean ± standard error.

Numerical Modeling

To assess the extreme wave conditions around the area of interest, simulated typhoon-generated waves were propagated nearshore with the Delft 3D (Deltares) numerical model. Simulations included offshore wave information extracted from the global wave generation model WaveWatch III (NCEP/NOAA) and typical wind conditions observed during typhoons (e.g., the 2013 SOULIK and the 2014 NEOGURI typhoons). The model domain covered the continental shelf of Ishigaki, Iriomote and adjacent islands, with a grid of 120 by 80 km, keeping the sites of interest well inside the domain. Bathymetry was based on the ETOPO1 Global Relief Model (NOAA). After running the model for the defined conditions, wave data were extracted close to the sites of interest. Based on wave characteristics, wave power was estimated in order to assess its relative impact among sites.

[3] http://tree.bio.ed.ac.uk/software/figtree/

AUTHOR CONTRIBUTIONS

PM, TS, CT, and FT conceived and designed the experiments. PM, AS, LO, LL, IK, SM, TS, and FT performed the experiments. PM, RF-F, IK, CT, TS, and FT contributed reagents, materials, and analysis tools. All authors analyzed the data. All authors wrote the paper.

FUNDING

We thank CNPq, CAPES, FAPERJ, UFBA, JST, and JSPS for funding. PM thanks CNPq, CAPES and FAPERJ for the Ph.D. scholarships (140869/2012-3 and 4848-14-9) and FAPERJ for postdoctoral scholarship (E-26/202.830/2016).

ACKNOWLEDGMENTS

We thank Dr. Takanori Kuribayashi, Hokkaido Central Fisheries Institute, for the seawater chemistry.

SUPPLEMENTARY MATERIAL

The Supplementary Material for this article can be found online at: https://www.frontiersin.org/articles/10.3389/fmicb.2018.02203/full#supplementary-material

FIGURE S1 | Study sites in Ishigaki Island, Okinawa, Japan. The maps were generated using Qgis software [1].

FIGURE S2 | Other benthic categories (complement of manuscript **Figure 2A**). Values are Mean ± Standard error (*N* = 15).

FIGURE S3 | Recent coral mortality and disease. Values are Mean ± Standard error (*N* = 15).

FIGURE S4 | Total fish abundance. Values are Mean ± Standard error (*N* = 7).

FIGURE S5 | Damselfishes (Pomacentridae) trophic guild composition. Values are Mean ± Standard error (*N* = 15).

FIGURE S6 | Vibrio counts. Values are Mean ± Standard error (*N* = 3) of colony forming unities.

FIGURE S7 | Major microbial phyla. The microbial composition was similar among the reef sites based on bacterial phyla composition **(A)** and other taxonomic and functional levels.

TABLE S1 | Information on the sampling sites and chemical and biological inventories of seawater samples.

TABLE S2 | General features of the metagenomes.

TABLE S3 | Metagenomes taxonomic annotation at Domain level and bacterial family diversity.

TABLE S4 | Adonis (Permanova) results of benthic cover based on Bray-Curtis distances with 999 permutations. MS, mean sum of squares; SS, sum of squares.

TABLE S5 | ANOVA results of total fish abundance. DF, degrees of freedom; SS, sum of squares; MS, mean sum of squares.

TABLE S6 | Adonis (Permanova) results of fish community abundance based on Bray-Curtis distances with 999 permutations. DF, degrees of freedom; SS, sum of squares; MS, mean sum of squares.

TABLE S7 | ANOVA results of total bacterial abundance. DF, degrees of freedom; SS, sum of squares; MS, mean sum of squares.

TABLE S8 | ANOVA results of Vibrio counts. DF, degrees of freedom; SS, sum of squares; MS, mean sum of squares.

TABLE S9 | ANOVA results of nutrients and chlorophyll a concentrations. DF, degrees of freedom; SS, sum of squares; MS, mean sum of squares.

TABLE S10 | Adonis (Permanova) results of metagenomic class composition (arcsin transformed) abundance based on Bray-Curtis distances with 999 permutations. MS, mean sum of squares; SS, sum of squares.

TABLE S11 | Adonis (Permanova) results of metagenomic level 1 subsystem composition (arcsin transformed) abundance based on Bray-Curtis distances with 999 permutations. MS, mean sum of squares; SS, sum of squares.

TABLE S12 | Adonis (Permanova) results of metagenomic dinucleotides composition abundance based on Bray-Curtis distances with 999 permutations. MS, mean sum of squares; SS, sum of squares.

TABLE S13 | Wave characteristics extracted based on typhoon wave conditions. Hs: significant wave height (m); Dir: direction in degrees North; P: wave power (W/m).

REFERENCES

Abe, K. (2010). Desorptive behavior of phosphate in the subtropical Miyara river, Ishigaki Island, Japan. *Limnology* 11, 179–183. doi: 10.1007/s10201-009-0294-4

Amin, A. K., Feng, G., Al-saari, N., Meirelles, P. M., Yamazaki, Y., Mino, S., et al. (2016). The first temporal and spatial assessment of vibrio diversity of the surrounding seawater of coral reefs in Ishigaki, Japan. *Front. Microbiol.* 7:1185. doi: 10.3389/fmicb.2016.01185

Andrade, L., Gonzalez, A. M., Araujo, F. V., and Paranhos, R. (2003). Flow cytometry assessment of bacterioplankton in tropical marine environments. *J. Microbiol. Methods* 55, 841–850. doi: 10.1016/.j.mimet.2003.08.002

Arnold, S. N., Steneck, R. S., and Mumby, P. J. (2010). Running the gauntlet: inhibitory effects of algal turfs on the processes of coral recruitment. *Mar. Ecol. Ser.* 414, 91–105. doi: 10.3354/meps08724

Banzai, K., and Nakamura, K. (2006). "Red soil runoff from the Miyarariver, and an environmental problem on Ishigaki island [Japan]," in *JIRCAS International Symposium Series Proceedings (Japan)*, Ishigaki.

Banzai, K., Nakamura, K., Khondaker, A., and Nagumo, F. (2003). Runoff of Suspended Solids, Nitrogen and Phosphorus Estimated From Catchment Basins of Miyara River on Ishigaki Island. Ishigaki: JIRCAS.

Barott, K. L., and Rohwer, F. L. (2012). Unseen players shape benthic competition on coral reefs. *Trends Microbiol.* 20, 621–628. doi: 10.1016/j.tim.2012.08.004

Bell, P. R. F., Lapointe, B. E., and Elmetri, I. (2007). Reevaluation of ENCORE: support for the eutrophication threshold model for coral reefs. *Ambio* 36, 416–424. doi: 10.1016/j.tim.2012.08.004

Birrell, C. L., Mccook, L. J., Willis, B. L., and Diaz-pulido, G. A. (2008). Effects of benthic algae on the replenishment of corals and the implications for the resilience of coral reefs. *Oceanogr. Mar. Biol.* 46, 25–63. doi: 10.1201/9781420065756.ch2

Blanco, A. C., Nadaoka, K., and Yamamoto, T. (2008). Planktonic and benthic microalgal community composition as indicators of terrestrial influence on a fringing reef in Ishigaki Island, Southwest Japan. *Mar. Environ. Res.* 66, 520–535. doi: 10.1016/j.marenvres.2008.08.005

Bright, A. J., Rogers, C. S., Brandt, M. E., Muller, E., and Smith, T. B. (2016). Disease prevalence and snail predation associated with swell-generated damage on the threatened coral, Acroporapalmata (Lamarck). *Front. Mar. Sci.* 3:77. doi: 10.3389/fmars.2016.00077

Bruce, T., Meirelles, P. M., Garcia, G., Paranhos, R., Rezende, C. E., de Moura, R. L., et al. (2012). Abrolhos bank reef health evaluated by means of water quality, microbial diversity, benthic cover, and fish biomass data. *PLoS One* 7:e36687. doi: 10.1371/journal.pone.0036687

Casey, J. M., Ainsworth, T. D., Choat, J. H., and Connolly, S. R. (2014). Farming behaviour of reef fishes increases the prevalence of coral disease associated microbes and black band disease. *Proc. R. Soc. B Biol. Sci. U.S.A.* 281: 20141032. doi: 10.1098/rspb.2014.1032

Casey, J. M., Connolly, S. R., and Ainsworth, T. D. (2015). Coral transplantation triggers shift in microbiome and promotion of coral disease associated potential pathogens. *Sci. Rep.* 5:11903. doi: 10.1038/srep11903

Chevreux, B., Pfisterer, T., Drescher, B., Driesel, A. J., Müller, W. E. G., Wetter, T., et al. (2004). Using the miraEST assembler for reliable and automated mRNA transcript assembly and SNP detection in sequenced ESTs. *Genome Res.* 14, 1147–1159. doi: 10.1101/gr.1917404

Colgan, M. W. (1987). Coral reef recovery on guam (Micronesia) after catastrophic predation by *Acanthasterplanci*. *Ecology* 68, 1592–1605. doi: 10.1016/0198-0254(88)92637-4

Dadhich, A. P., Nadaoka, K., Yamamoto, T., and Kayanne, H. (2012). Detecting coral bleaching using high-resolution satellite data analysis and 2-dimensional thermal model simulation in the Ishigaki fringing reef, Japan. *Coral Reefs* 31, 425–439. doi: 10.1016/0198-0254(88)92637-4

De'ath, G., Fabricius, K. E., Sweatman, H., and Puotinen, M. (2012). The 27–year decline of coral cover on the great barrier reef and its causes. *Proc. Natl. Acad. Sci. U.S.A.* 109, 17995–17999. doi: 10.1073/pnas.1208909109

Dinsdale, E. A., Pantos, O., Smriga, S., Edwards, R. A., Angly, F., Wegley, L., et al. (2008). Microbial ecology of four coral atolls in the northern line Islands. *PLoS One* 3:e1584. doi: 10.1371/journal.pone.0001584

Doropoulos, C., Hyndes, G. A., Abecasis, D., and Vergés, A. (2013). Herbivores strongly influence algal recruitment in both coral- and algal-dominated coral reef habitats. *Mar. Ecol. Prog. Ser.* 486, 153–164. doi: 10.3354/meps10325

Dutilh, B. E., Huynen, M. A., Bruno, W. J., and Snel, B. (2004). The consistent phylogenetic signal in genome trees revealed by reducing the impact of noise. *J. Mol. Evol.* 58, 527–539. doi: 10.1007/s00239-003-2575-6

Dutilh, B. E., Schmieder, R., Nulton, J., Felts, B., Salamon, P., Edwards, R. A., et al. (2012). Reference-independent comparative metagenomics using cross-assembly: crAss. *Bioinformatics* 28, 3225–3231. doi: 10.1093/bioinformatics/bts613

Dutilh, B. E., van Noort, V., van der Heijden, R. T. J. M., Boekhout, T., Snel, B., and Huynen, M. A. (2007). Assessment of phylogenomic and orthology approaches for phylogenetic inference. *Bioinformatics* 23, 815–824. doi: 10.1093/bioinformatics/btm015

Edwards, C. B., Friedlander, A. M., Green, A. G., Hardt, M. J., Sala, E., Sweatman, H. P., et al. (2014). Global assessment of the status of coral reef herbivorous fishes: evidence for fishing effects. *Proc. Biol. Sci.* 281:20131835. doi: 10.1098/rspb.2013.1835

Fabricius, K. E., Okaji, K., and De'ath, G. (2010). Three lines of evidence to link outbreaks of the crown-of-thorns seastar *Acanthasterplanci* to the release of larval food limitation. *Coral Reefs* 29, 593–605. doi: 10.1098/rspb.2013.1835

Francini-Filho, R. B., Coni, E. O. C., Meirelles, P. M., Amado-Filho, G. M., Thompson, F. L., Pereira-Filho, G. H., et al. (2013). Dynamics of coral reef benthic assemblages of the abrolhos bank, eastern brazil: inferences on natural

and anthropogenic drivers. *PLoS One* 8:e54260. doi: 10.1371/journal.pone.0054260

Francini-Filho, R. B., and de Moura, R. L. (2008). Dynamics of fish assemblages on coral reefs subjected to different management regimes in the Abrolhos Bank, eastern Brazil. *Aquat. Conserv. Freshw. Ecosyst.* 18, 1166–1179. doi: 10.1002/aqc.966

Garcia, G. D., Gregoracci, G. B., Santos Ede, O., Meirelles, P. M., Silva, G. G., Edwards, R., et al. (2013). Metagenomic analysis of healthy and white plague-affected Mussismiliabraziliensis corals. *Microb. Ecol.* 65, 1076–1086. doi: 10.1007/s00248-012-0161-4

Garren, M., and Azam, F. (2012). New directions in coral reef microbial ecology. *Environ. Microbiol.* 14, 833–844. doi: 10.1111/j.1462-2920.2011.02597.x

Gascuel, O. (1997). BIONJ: an improved version of the NJ algorithm based on a simple model of sequence data. *Mol. Biol. Evol.* 14, 685–695. doi: 10.1111/j.1462-2920.2011.02597.x

Goto, K., Miyagi, K., Kawamata, H., and Imamura, F. (2010). Discrimination of boulders deposited by tsunamis and storm waves at Ishigaki Island, Japan. *Mar. Geol.* 269, 34–45. doi: 10.1016/j.margeo.2009.12.004

Grasshoff, K., Kremling, K., and Ehrhardt, M. (2009). *Methods of Seawater Analysis*. Hoboken, NJ: John Wiley & Sons, doi: 10.1002/9783527613984

Gregg, A., Hatay, M., Haas, A., Robinett, N., Barott, K., Vermeij, M., et al. (2013). Biological oxygen demand optode analysis of coral reef-associated microbial communities exposed to algal exudates. *PeerJ* 1:e107. doi: 10.7717/peerj.107

Haas, A. F., Fairoz, M. F. M., Kelly, L. W., Nelson, C. E., Dinsdale, E. A., Edwards, R. A., et al. (2016). Global microbialization of coral reefs. *Nat. Microbiol.* 1:16042. doi: 10.1038/nmicrobiol.2016.42

Haas, A. F., Nelson, C. E., Kelly, L. W., Carlson, C. A., Rohwer, F., Leichter, J. J., et al. (2011). Effects of coral reef benthic primary producers on dissolved organic carbon and microbial activity. *PLoS One* 6:e27973. doi: 10.1371/journal.pone.0027973

Harii, S., Hongo, C., Ishihara, M., Ide, Y., and Kayanne, H. (2014). Impacts of multiple disturbances on coral communities at Ishigaki Island, Okinawa, Japan, during a 15 year survey. *Mar. Ecol. Prog. Ser.* 509, 171–180. doi: 10.1371/journal.pone.0027973

Hata, T., Madin, J. S., Cumbo, V. R., Denny, M., Figueiredo, J., Harii, S., et al. (2017). Coral larvae are poor swimmers and require fine-scale reef structure to settle. *Sci. Rep.* 7:2249. doi: 10.1038/s41598-017-02402-y

Hoegh-Guldberg, O., Mumby, P. J., Hooten, A. J., Steneck, R. S., Greenfield, P., Gomez, E., et al. (2007). Coral reefs under rapid climate change and ocean acidification. *Science* 318, 1737–1742. doi: 10.1126/science.1152509

Hongo, C., Kawamata, H., and Goto, K. (2012). Catastrophic impact of typhoon waves on coral communities in the Ryukyu islands under global warming. *J. Geophys. Res.* 117:G02029. doi: 10.1029/2011JG001902

Hughes, T. P. (1994). Catastrophes, phase-shifts, and large scale degradation of a caribbean coral-reef. *Science* 265, 1547–1551. doi: 10.1126/science.1152509

Jackson, J. B. C., Kirby, M. X., Berger, W. H., Bjorndal, K. A., Botsford, L. W., Bourque, B. J., et al. (2001). Historical overfishing and the recent collapse of coastal ecosystems. *Science* 293, 629–638. doi: 10.1126/science.1059199

Japanese Coral Reef Society. (2004). "*Coral Reefs of Japan*, eds M. Omori, K. Takahashi, N. Moriwake, K. Osada, T. Kimura, F. Kinoshita, et al. Okinawa: Japanese Coral Reef Society. doi: 10.1126/science.1059199

Jessen, C., Roder, C., Villa Lizcano, J. F., Voolstra, C. R., and Wild, C. (2013). In-situ effects of simulated overfishing and eutrophication on benthic coral reef algae growth, succession, and composition in the central red sea. *PLoS One* 8:e66992. doi: 10.1371/journal.pone.0066992

Jorissen, H., Skinner, C., Osinga, R., de Beer, D., and Nugues, M. M. (2016). Evidence for water-mediated mechanisms in coral–algal interactions. *Proc. Biol. Sci.* 283:20161137. doi: 10.1098/rspb.2016.1137

Kawahata, H., Yukino, I., and Suzuki, A. (2000). Terrestrial influences on the Shiraho fringing reef, Ishigaki Island, Japan: high carbon input relative to phosphate. *Coral Reefs* 19, 172–178. doi: 10.1007/s003380000093

Kayanne, H., Harii, S., Ide, Y., and Akimoto, F. (2002). Recovery of coral populations after the 1998 bleaching on Shiraho reef, in the southern Ryukyus, NW Pacific. *Mar. Ecol. Prog. Ser.* 239, 93–103. doi: 10.3354/meps239093

Kelly, L. W., Williams, G. J., Barott, K. L., Carlson, C. A., Dinsdale, E. A., Edwards, R. A., et al. (2014). Local genomic adaptation of coral reef-associated microbiomes to gradients of natural variability and anthropogenic stressors. *Proc. Natl. Acad. Sci. U.S.A* 111, 10227–10232. doi: 10.1073/pnas.1403319111

Kepner, R. L., and Pratt, J. R. (1994). Use of fluorochromes for direct enumeration of total bacteria in environmental samples: past and present. *Microbiol. Rev.* 58, 603–615.

Kitada, Y., Kawahata, H., Suzuki, A., and Oomori, T. (2008). Distribution of pesticides and bisphenola in sediments collected from rivers adjacent to coral reefs. *Appl. Catal. B Environ.* 82, 163–168. doi: 10.1016/j.apcatb.2008.01.023

Knowlton, N., and Jackson, J. B. C. (2008). Shifting baselines, local impacts, and global change on coral reefs. *PLoS Biol.* 6:e54. doi: 10.1371/journal.pbio.0060054

Kohler, K. E., and Gill, S. M. (2006). Coral point count with excel extensions (CPCe): a visual basic program for the determination of coral and substrate coverage using random point count methodology. *Comput. Geosci.* 32, 1259–1269. doi: 10.1016/j.cageo.2005.11.009

Korbel, J. O., Snel, B., Huynen, M. A., and Bork, P. (2002). SHOT: a web server for the construction of genome phylogenies. *Trends Genet.* 18, 158–162. doi: 10.1016/S0168-9525(01)02597-5

Liu, P. J., Shao, K. T., Jan, R. Q., Fan, T. Y., Wong, S. L., Hwang, J. S., et al. (2009). A trophic model of fringing coral reefs in Nanwan Bay, southern Taiwan suggests overfishing. *Mar. Environ. Res.* 68, 106–117. doi: 10.1016/j.marenvres.2009.04.009

Loya, Y., Sakai, K., Yamazato, K., Nakano, Y., Sambali, H., and van Woesik, R. (2001). Coral bleaching: the winners and the losers. *Ecol. Lett.* 4, 122–131. doi: 10.1046/j.1461-0248.2001.00203.x

Martinussen, I., and Thingstad, T. F. (1991). A simple double staining technique for simultaneous quantification of auto-and heterotrophic nano-and picoplankton. *Mar. Microb. Food Webs* 5, 5–11.

McDole, T., Nulton, J., Barott, K. L., Felts, B., Hand, C., Hatay, M., et al. (2012). Assessing coral reefs on a Pacific-wide scale using the microbialization score. *PLoS One* 7:e43233. doi: 10.1371/journal.pone.0043233

McDoleSomera, T., Bailey, B., Barott, K., Grasis, J., Hatay, M., Hilton, B. J., et al. (2016). Energetic differences between bacterioplankton trophic groups and coral reef resistance. *Proc. R. Soc. Lond. B Biol. Sci.* 283:20160467. doi: 10.1098/rspb.2016.0467

Meirelles, P. M., Amado-Filho, G. M., Pereira-Filho, G. H., Pinheiro, H. T., de Moura, R. L., Joyeux, J.-C., et al. (2015a). Baseline assessment of mesophotic reefs of the vitória-trindade seamount chain based on water quality, microbial diversity, benthic cover and fish biomass data. *PLoS One* 10:e0130084. doi: 10.1371/journal.pone.0130084

Meirelles, P. M., Gadelha, L. M. R., Francini-Filho, R. B., de Moura, R. L., Amado-Filho, G. M., Bastos, A. C., et al. (2015b). BaMBa: towards the integrated management of Brazilian marine environmental data. *Database* 2015: bav088. doi: 10.1093/database/bav088

Meyer, F., Paarmann, D., D'Souza, M., Olson, R., Glass, E. M., Kubal, M., et al. (2008). The metagenomics RAST server - a public resource for the automatic phylogenetic and functional analysis of metagenomes. *BMC Bioinformatics* 9:386. doi: 10.1186/1471-2105-9-386

Nelson, C. E., Goldberg, S. J., Wegley Kelly, L., Haas, A. F., Smith, J. E., Rohwer, F., et al. (2013). Coral and macroalgal exudates vary in neutral sugar composition and differentially enrich reef bacterioplankton lineages. *ISME J.* 7, 962–979. doi: 10.1038/ismej.2012.161

Nishihira, M., and Yamazato, K. (1974). "Human interference with the coral reef community and Acanthaster infestation of Okinawa," in *Proceedings of the Second International Symposium on Coral Reefs*, Harrisburg, PA.

Oksanen, J., Kindt, R., and O'Hara, B. (2005). *Vegan: R Functions for Vegetation Ecologists*. Available at: http://cc.oulu.fi/~jarioksa/softhelp/vegan.html

Omori, M. (2011). Degradation and restoration of coral reefs: experience in Okinawa. *Jan. Mar. Biol. Res.* 7, 3–12. doi: 10.1080/17451001003642317

Porter, K. G., and Feig, Y. S. (1980). The use of DAPI for identifying aquatic microfloral. *Limnol. Oceanogr.* 25, 943–948. doi: 10.4319/lo.1980.25.5.0943

R Development Core Team (2011). *R: A Language and Environment for Statistical Computing*. Available at: http://www.r-project.org/

Randall, J. E. (1967). *Food Habits of Reef Fishes of the West Indies*. Coral Gables, FL: Institute of Marine Sciences, University of Miami.

Rezende, C. E., Pfeiffer, W. C., Martinelli, L. A., Tsamakis, E., Hedges, J. I., and Keil, R. G. (2010). Lignin phenols used to infer organic matter sources to Sepetiba Bay - RJ, Brasil. *Estuar. Coast. Shelf Sci.* 87, 479–486. doi: 10.1016/j.ecss.2010.02.008

Roach, T. N. F., Abieri, M. L., George, E. E., Knowles, B., Naliboff, D. S., Smurthwaite, C. A., et al. (2017). Microbial bioenergetics of coral-algal interactions. *PeerJ* 5:e3423. doi: 10.7717/peerj.3423

Roberts, C. M., McClean, C. J., Veron, J. E. N., Hawkins, J. P., Allen, G. R., McAllister, D. E., et al. (2002). Marine biodiversity hotspots and conservation priorities for tropical reefs. *Science* 295, 1280–1284. doi: 10.1126/science.1067728

Roff, G., and Mumby, P. J. (2012). Global disparity in the resilience of coral reefs. *Trends Ecol. Evol.* 27, 404–413. doi: 10.1016/j.tree.2012.04.007

Sandin, S. A., Smith, J. E., DeMartini, E. E., Dinsdale, E. A., Donner, S. D., Friedlander, A. M., et al. (2008). Baselines and degradation of coral reefs in the Northern line Islands. *PLoS One* 3:e1548. doi: 10.1371/journal.pone.0001548

Sano, M. (1987). Long-term effects of destruction of hermatypic corals by *Acanthasterplanci* infestation on reef fish communities at Iriomote Island, Japan. *Mar. Ecol. Prog. Ser.* 37, 191–199. doi: 10.3354/meps037191

Schmieder, R., and Edwards, R. (2011). Quality control and preprocessing of metagenomic datasets. *Bioinformatics* 27, 863–864. doi: 10.1093/bioinformatics/btr026

Sharp, J. H., Carlson, C. A., Peltzer, E. T., Castle-Ward, D. M., Savidge, K. B., and Rinker, K. R. (2002). Final dissolved organic carbon broad community intercalibration and preliminary use of DOC reference materials. *Mar. Chem.* 77, 239–253. doi: 10.1016/S0304-4203(02)00002-6

Shimada, H., Sawada, M., Kuribayashi, T., Nakata, A., Miyazono, A., and Asami, H. (2010). Spatial distribution of the toxic dinoflagellateAlexandriumtamarense in summer in the Okhotsk Sea off Hokkaido, Japan. *Plankt. Benthos Res.* 5, 1–10. doi: 10.3800/pbr.5.1

Smith, J. E., Brainard, R., Carter, A., Dugas, S., Edwards, C., Harris, J., et al. (2016). Re-evaluating the health of coral reef communities?: baselines and evidence for human impacts across the central Pacific. *Proc. R. Soc. B Biol. Sci. U.S.A.* 283:20151985. doi: 10.1098/rspb.2015.1985

Smith, J. E., Shaw, M., Edwards, R. A., Obura, D., Pantos, O., Sala, E., et al. (2006). Indirect effects of algae on coral: algae-mediated, microbe-induced coral mortality. *Ecol. Lett.* 9, 835–845. doi: 10.1111/j.1461-0248.2006.00937.x

Sowa, K., Watanabe, T., Kan, H., and Yamano, H. (2014). Influence of land development on holoceneporites coral calcification at Nagura bay, Ishigaki island, Japan. *PLoS One* 9:e88790. doi: 10.1371/journal.pone.0088790

Steneck, R. S., and Dethier, M. N. (1994). A functional-group approach to the structure of algal-dominated communities. *Oikos* 69, 476–498. doi: 10.2307/3545860

Stone, L., Huppert, A., Rajagopalan, B., Bhasin, H., and Loya, Y. (1999). Mass coral reef bleaching: a recent outcome of increased El nino activity? *Ecol. Lett.* 2, 325–330. doi: 10.1046/j.1461-0248.1999.00092.x

Tamai, R. N., and Sakai, K. (2013). Space competition between coral and algae — effect of two functional groups of algae on juvenile *Acropora corals*. *Galaxea J. Coral Reef Stud.* 15, 115–122. doi: 10.3755/galaxea.15.115

Tanaka, Y., Miyajima, T., Watanabe, A., Nadaoka, K., Yamamoto, T., and Ogawa, H. (2011). Distribution of dissolved organic carbon and nitrogen in a coral reef. *Coral Reefs* 30, 533–541. doi: 10.1007/s00338-011-0735-5

Tu, J.-Y., and Chou, C. (2013). Changes in precipitation frequency and intensity in the vicinity of Taiwan: typhoon versus non-typhoon events. *Environ. Res. Lett.* 8:014023. doi: 10.1088/1748-9326/8/1/014023

West, K., and van Woesik, R. (2001). Spatial and temporal variance of river discharge on Okinawa (Japan): inferring the temporal impact on adjacent coral reefs. *Mar. Pollut. Bull.* 42, 864–872. doi: 10.1016/S0025-326X(01)00040-6

White, K. N., Weinstein, D. K., Ohara, T., Denis, V., Montenegro, J., and Reimer, J. D. (2017). Shifting communities after–typhoon damage on an upper mesophotic reef in okinawa, Japan. *PeerJ* 5:e3573. doi: 10.7717/peerj.3573

Willner, D., Thurber, R. V., and Rohwer, F. (2009). Metagenomic signatures of 86 microbial and viral metagenomes. *Environ. Microbiol.* 11, 1752–1766. doi: 10.1111/j.1462-2920.2009.01901.x

Conflict of Interest Statement: The authors declare that the research was conducted in the absence of any commercial or financial relationships that could be construed as a potential conflict of interest.

Copyright © 2018 Meirelles, Soares, Oliveira, Leomil, Appolinario, Francini-Filho, de Moura, de Barros Almeida, Salomon, Amado-Filho, Kruger, Siegle, Tschoeke, Kudo, Mino, Sawabe, Thompson and Thompson. This is an open-access article distributed under the terms of the Creative Commons Attribution License (CC BY). The use, distribution or reproduction in other forums is permitted, provided the original author(s) and the copyright owner(s) are credited and that the original publication in this journal is cited, in accordance with accepted academic practice. No use, distribution or reproduction is permitted which does not comply with these terms.

frontiers in Marine Science

ORIGINAL RESEARCH
published: 20 November 2018
doi: 10.3389/fmars.2018.00423

The Influence of River Discharge on Nutrient Export and Phytoplankton Biomass Off the Central Chile Coast (33°–37°S): Seasonal Cycle and Interannual Variability

Italo Masotti[1,2], Pilar Aparicio-Rizzo[1,2], Mariela A. Yevenes[2,3], René Garreaud[2,4], Lucy Belmar[2] and Laura Farías[2,3]*

[1] Facultad de Ciencias del Mar y de Recursos Naturales, Universidad de Valparaíso, Viña del Mar, Chile, [2] Center for Climate and Resilience Research, University of Chile, Santiago, Chile, [3] Department of Oceanography, Faculty of Natural and Oceanographic Sciences, University of Concepción, Concepción, Chile, [4] Department of Geophysics, Faculty of Physics and Mathematics Sciences, University of Chile, Santiago, Chile

Using *in situ* hydro-chemical data and MODIS-SeaWiFS ocean color images as a proxy of river plumes and phytoplankton biomass from 2000 to 2014, this study documents the temporal co-variability of river discharge, plume area, nitrate and phosphate export and phytoplankton biomass in the coastal waters off Central Chile (33°–37°S). Five major rivers (Maipo, Mataquito, Maule, Itata, and Biobío) drain into this region with annual mean discharge ranging from 120 to 1000 m^3 s^{-1}. River discharge and coastal plume area present a marked seasonal cycle, reaching maximum values during the winter rainy season (June-September). Export of riverine nutrients also peaks in winter, leading to an increase in phytoplankton biomass within the plumes that can be twice larger than the background values in coastal areas away from the river mouths. Wintertime river discharge, plume area and nutrient export are also correlated at interannual time scales. During a recent extended dry period (2010–2014), river discharges, plume areas and nutrient export clearly decreased by about 50% compared to historical values, reducing significantly the size of the chlorophyll pool within plumes off Central Chile during winter. The potential impacts of droughts are discussed in terms of coastal ecology and primary production, a highly relevant issue considering the projections of a dry climate over Central Chile in the future. Systematic evidence of mega-drought effects upon coastal productivity still does not exist, but it remains a priority to further investigate and quantify these impacts.

Keywords: drought, river discharge, nutrient export, phytoplankton biomass, satellite remote sensing, central Chile

OPEN ACCESS

Edited by:
Alejandro A. Murillo, EMBL Heidelberg, Germany

Reviewed by:
José Pinho, University of Minho, Portugal
Riccardo Briganti, University of Nottingham, United Kingdom

****Correspondence:***
Italo Masotti
italo.masotti@uv.cl

Specialty section:
This article was submitted to Coastal Ocean Processes, a section of the journal Frontiers in Marine Science

Received: *22 June 2018*
Accepted: *23 October 2018*
Published: *20 November 2018*

Citation:
Masotti I, Aparicio-Rizzo P, Yevenes MA, Garreaud R, Belmar L and Farías L (2018) The Influence of River Discharge on Nutrient Export and Phytoplankton Biomass Off the Central Chile Coast (33°–37°S): Seasonal Cycle and Interannual Variability. Front. Mar. Sci. 5:423. doi: 10.3389/fmars.2018.00423

INTRODUCTION

Phytoplankton biomass (PB) and primary production (PP) in coastal areas are highly variable over temporal and spatial scales, primarily regulated by nutrient supply, light availability and physical processes driving stratification/mixing and advection (e.g., Hickey and Banas, 2003). Organic matter, nutrients and particles from terrestrial sources are partially delivered into coastal areas

through rivers, which can support both PB and PP, as well as regulate coastal biogeochemical cycles of Nitrate (NO_3^-), Phosphate (PO_4^{-3}), and Silicate [$Si(OH)_4$] (Hopkinson and Vallino, 2005; Cotrim et al., 2007). Through their impact on precipitation, both natural variability (e.g., El Niño Southern Oscillation, ENSO) and anthropogenic climate change may alter river discharge into coastal areas over interannual and longer time scales, leading to considerable impacts on coastal PB and PP.

Several studies have reported a positive relationship between increased river discharge, nutrient input, and high PB in adjacent coastal areas to river mouths. For example, in coastal waters off Japan, chlorophyll (Chl-a) concentration from ocean color satellite estimates was two times higher during periods of high river discharge compared to periods of low discharge (Lihan et al., 2011). Similarly, high Chl-a levels were observed in winter and early spring, coinciding with an abrupt precipitation increase in the Apalachicola River in northwestern Florida (Morey et al., 2009). A similar trend of high Chl-a concentrations and productive plume waters, enriched by the Mississippi River nutrients, was observed across the shelf and along the coast of Louisiana (Wysocki et al., 2006). On the other hand, a reduction of freshwater input into coastal areas during droughts led to a marked decrease in Chl-a biomass over various shelf-coastal and estuarine environments, as observed in the North Atlantic and Pacific oceans (Cloern et al., 1983; Nichols, 1985; Wetz et al., 2011). Furthermore, ecological studies have indicated a deterioration of the planktonic food web during a period of drought in the coastal waters of the North Pacific, with negative consequences on fish populations due to cascading effects on higher trophic levels (Cloern et al., 1983; Nichols, 1985; Wetz et al., 2011).

Along eastern boundary systems, such as California, Humboldt and Benguela, the effects of the river discharge on coastal PB/PP are less apparent. This is due to the considerable influence of coastal upwelling, the process by which cold, nutrient-rich subsurface water ascends to the ocean's surface, creating the most biologically productive areas of the global ocean (Pauly and Christensen, 1995). The importance of nutrient and particle supply from river discharge with respect to coastal upwelling is seasonally variable, and depends on physical processes (such as thermal and haline stratification, wind stress, and rainfall), as well as the geographical and topographical features of the coastal area. For example, the Columbia River has been characterized as a major nutrient source to the adjacent coastal area, promoting positive effects on PB and PP during extended periods of reduced coastal upwelling (Hickey et al., 2010). A similar situation occurred in the Canadian Beaufort shelf where the Mackenzie River re-injects nutrients into the surface with a high N:P or N:Si ratio, influencing the phytoplankton physiology (Tremblay et al., 2014).

Central Chile, along the subtropical west coast of South America (33°–38°S), is characterized by an archetypical Mediterranean climate with an annual mean precipitation ranging from 100 to 1000 mm, predominantly occurring during the austral winter. Because part of the winter precipitation is stored as snow in the Andes cordillera most of the rivers in this region exhibit a seasonal mixed pluvio-nival regime (e.g., Garreaud et al., 2017). On interannual scales, variations in river discharges are correlated with ENSO, since an increase in precipitation over Central Chile during El Niño years leads to high river flows (Aceituno and Vidal, 1990; Waylen et al., 1993; Pellicciotti et al., 2007). Conversely, La Niña is often associated with a decrease in precipitation and low rivers discharge (Aceituno and Vidal, 1990). The ENSO fluctuations, however, only account for about 50% of the total precipitation variation in Central Chile (Montecinos et al., 2011), and many dry years do not coincide with La Niña events. Of particular relevance, the recent "mega-drought" in Central Chile (Garreaud et al., 2017), an uninterrupted sequence of dry years beginning in 2010, coincides with mostly ENSO-neutral conditions. The mega-drought has produced rainfall deficits of about 30% across much of Central Chile, a relatively small decrease compared with other droughts in the past (e.g., >60% in 1924, 1968, and 1988) but its duration is unprecedented in the historical record and millennial reconstruction (Garreaud et al., 2017). Furthermore, approximately one third of the dry signal has been associated with climate change (Boisier et al., 2016).

In the coastal waters off Central Chile both river discharge and coastal upwelling occur, but their seasonal cycles are out of phase. Strong southerly upwelling favorable winds prevail during spring-summer (e.g., Rahn and Garreaud, 2014), leading to an intense increase in PB and PP (Montecino et al., 2006; Thiel et al., 2007). During fall and winter the southerly winds relax, whereas rainfall and river discharge simultaneously reaches a maximum. Thus, the seasonal signal of river plumes extension in the region detected using satellite ocean color images showed persistent and large river plumes during fall-winter period (Saldías et al., 2012). Indeed, major plume events are associated with the warm phases of ENSO and PDO when precipitation tends to be above normal (Saldías et al., 2016).

In this region, recent studies have shown evidences of the impact of the nutrient export in these river plumes on the carbon biogeochemistry and phytoplankton community of coastal waters off Central Chile in winter (Iriarte et al., 2012; Léniz et al., 2012; Pérez et al., 2015; Yevenes et al., 2016) and its possible contribution in maintaining high primary productivity rates in coastal waters (Testa et al., 2018). Nonetheless, there is a lack of a systematic analysis into the regional scale influence of the river discharges variability on nutrient loading and phytoplankton biomass in coastal waters. The present work investigates the impact of discharge of the five major rivers in Central Chile on river plumes, nutrient export, and phytoplankton biomass in coastal waters, based on datasets from 2000 to 2014, and discerns the effect of the extended mega-drought in theses coastal processes. We also discuss the representativeness of the satellite based PB estimates in coastal areas by contrasting those values against *in situ* data, the effects of the present mega-drought on the ecology and trophic dynamics of adjacent areas. A full assessment of the consequences of regional climate change on coastal hydrobiology is beyond the scope of this work, but this key issue is discussed on the basis of the observed impacts of the recent mega-drought that is relevant considering the prospect of a drier,

warmer climate in central Chile (Fuenzalida et al., 2007; Bozkurt et al., 2017).

MATERIALS AND METHODS

Hydrological River Survey

The study area spans from 33° to 37°S along the west coast of South America, including the outlets from the Maipo, Mataquito, Maule, Itata, and Biobío Rivers (**Figure 1**). The main features of these basins are presented in **Table 1**. Daily mean discharge in these rivers is recorded at fluviometric stations located about 20 km from the river mouth. Data from January 2000 to December 2014 is provided by the Department of Water at the Ministry of Public Works, Chile (Dirección General de Aguas, DGA[1]). Monthly mean discharge values are calculated for months when more than 70% of the daily values were available. The annual mean discharge varies from ∼120 m^3 s^{-1} for the Maipo River to ∼1000 m^3 s^{-1} for the Biobío River, reflecting the north-to-south precipitation increase as well as differences between catchment areas (**Table 1**).

Nutrient (Nitrate-NO_3^- and Phosphate-PO_4^{-3}) concentrations in the rivers are measured on a quarterly basis at the same fluviometric stations. Thus, each year four simultaneous nutrient values are obtained for each river. Nutrient exportation (load) is estimated as a product of river discharge Q (m^3 s^{-1}) and nutrient concentration C (mg L^{-1}). Estimates of the daily nutrient load (Q × C, kg day^{-1}) are obtained using a load estimator (LOADEST, Runkel et al., 2004) as follow:

$$log\,(\text{Load}) = a_n + a_1 log\,(Q) \quad (1)$$

Where, Load is the pollutant burden, $a_{n\sim1}$ are the regression coefficients and Q is the streamflow in a specific period. The regression coefficients are obtained using multiple predictors (flow, time, and other variables) and a maximum likelihood estimation method (Cohn, 2005). The daily loads are then aggregated to obtain the NO_3^- and PO_4^{-3} river export over a monthly basis (expressed in Ton $month^{-1}$).

[1]www.dga.cl

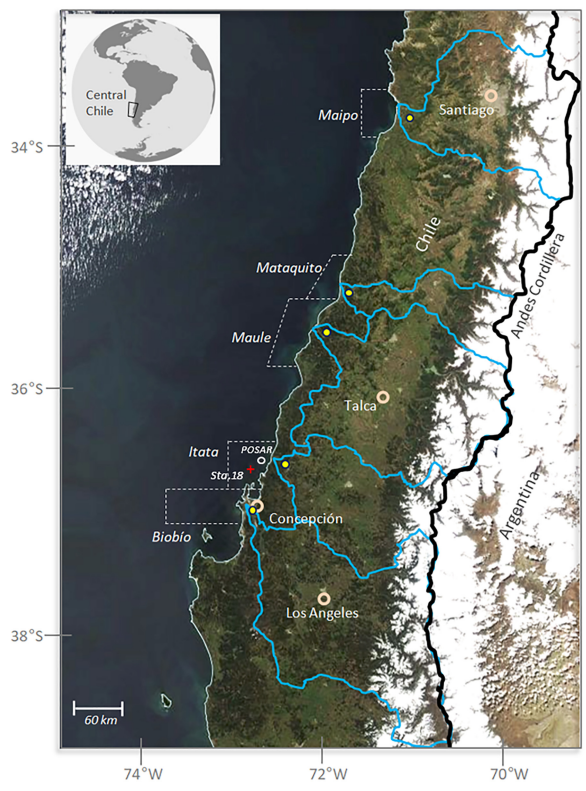

FIGURE 1 | General map of the study area. The background picture is a TERRA-MODIS visible image (September 22, 2013) upon, which we have mapped the main river basin boundaries (blue lines) and the Chile-Argentina border (black line following the Andes crest level). Off Itata River we have mapped the position of the Oceanographic Station 18 and the coastal buoy POSAR. Also shown are coastal adjacent areas at the mouth of each river (dashed polygons) and major cities.

Ocean Color Data: Plume Signal Detection and Phytoplankton Biomass

To study the seasonal and interannual variability of plumes extension and phytoplankton biomass in coastal waters we used ocean color (OC) datasets (4 km × 4 km pixels and 8-day composition) between January 2000 to December 2014, including chlorophyll and normalized water-leaving radiance at 555 nm (nLw555) from SeaWiFS (2000–2002) and MODIS-Aqua (Moderate Resolution Imaging Spectroradiometer, 2002–2014). Satellite images are obtained from the NASA Ocean Color web server[2] and the GlobColour core dataset[3]. Ocean color, 8-day composition datasets (3 or 4 scenes per month) are used to reduce the loss of information due to cloud effects, with cloud-free data available for over 90% of the region (Saldías et al., 2012, 2016).

The phytoplankton biomass (PB) is derived from chlorophyll-a (Chl-a) based on standard NASA's algorithms using OC datasets (O'Reilly et al., 2000; Hu et al., 2012), which are known to overestimate Chl-a concentrations in coastal waters (e.g., Lohrenz et al., 2008). Our study, however, focuses on the seasonal and interannual variability of PB rather than absolute values, for which the satellite timeseries estimates are a viable tool to represent the surface pigment dynamics in coastal waters as suggested before by other studies (Lohrenz et al., 2008; Hopkins et al., 2013). To further evaluate the satellite derived 8-day Chl-a concentrations we contrasted those valued against *in situ* surface measurements collected from 2006 to 2014 at Oceanographic Station 18 (77 match-up data points). Station 18 is under the influence of the Itata river plume and is located 18 nautical miles (30 km) from the coast (36°30′S–73°07′W; **Figure 1**). The correlation coefficient between both measurements on the logarithmic scale shows that both Chl-a series are well correlated (rs = 0.65, SD = 0.33, $p < 0.001$) supporting that satellite Chl-a retrieval can be useful to track and characterize the plume rivers.

[2]https://oceancolor.gsfc.nasa.gov
[3]http://hermes.acri.fr

TABLE 1 | Regional characterization of rivers in Central Chile, from 33° to 37°S.

River (station)	Location (°)	Rise (masl)	Watershed (km^2)	Coastal distance (km)	Discharge* ($m^3\ s^{-1}$)	Rainfall* (mm)	Soil type**	Land use (%)***			
								Non-arable land	Non-native forest	Forest	Cultivable land
Maipo (Cabimbao)	−33.72 −71.55	35	1516	±20.5	123.47	199	Entisols	29	21	11	42
Mataquito (Licantén)	−34.98 −72.01	20	619	±21	116.66	664	Mollisols	54	>15	<14	17
Maule (Forel)	−35.41 −72.21	30	2029	±27.5	511.65	827	Mollisols	48	>17	<12	22.9
Itata (Coelemu)	−36.47 −72.75	27	1110	±21.5	338.20	875	Alfisols	42	37	9	12
Biobío (Desembocadura)	−36.84 −73.09	16	2403	±8.5	1015.88	868	Mollisols/Ultisols	45	29	11	15

*Mean values computed from 15 years of recorded data (2000–2014). **Extracted by Luzio et al. (2010). ***Extracted by Lara et al. (2012), and CIREN (Centro de Información de Recursos Naturales, http://www.ciren.cl).

The nLw555 band is analyzed to detect the river plume signal in the coastal zone. Previous studies have confirmed the use of this band to detect the river plume signal associated with discharge variability (Otero and Siegel, 2004; Nezlin et al., 2005; Thomas and Weatherbee, 2006). The river plume is identified as the area close to the river mouth where nLw555 values are higher than 1.50 mW cm^{-2} μm^{-1} sr^{-1}, following criteria from Saldías et al. (2012).

Whenever the plume is present, area (expressed in km^2) and mean Chl-a are calculated to produce monthly mean values. The plume areas ranged between 120 and 500 km^2 (**Supplementary Table 1**) so that at least 10 pixels are used to define the previous statistics. Granted, higher spatial resolution will result in more accurate plume definitions but, once again, our focus is on the large month-to-month and year-to-year changes in plume's features. In addition to the monthly values, river plume frequency is calculated on a yearly basis (number of 8-days scenes with plume signal by year). In order to provide context for the potential PB enhancement generated by the rivers, the mean Chl-a concentration is calculated over a larger coastal area adjacent to each river mouth. For each river, the adjacent area is outlined by the maximal plume extent on record (**Figure 1**) and remains fixed in time.

RESULTS

Mean Seasonal Cycle

The coastal waters off Central Chile are characterized by marked seasonal differences in PB as shown in **Figure 2**. This figure shows satellite-derived maps of Chl-a during one week in winter (13–20 August 2008) and late spring (16–23 November 2008). In winter, Chl-a presents low values ($\leq$2.50 mg m^{-3}) along the coast with some patches of higher values surrounding the mouths of major rivers. The river plumes are clearly detected in coastal water by their large nLw555 values. In late spring, Chl-a values in excess of 5 mg m^{-3} are found along the coast, up to 100 km offshore. These high values in spring are due to coastal upwelling, whereas river plumes are undetected or considerably reduced compared to wintertime.

The seasonal cycles of river discharge and plume area are shown in **Figure 3**, using 15 years of hydrological records and satellite derived SeaWiFS-MODIS ocean color data. All rivers exhibit a clear seasonal cycle with higher discharge during winter (rainy season) compared to summer-fall (dry season). The areal extent of the river plumes follows a similar seasonal cycle, with a prominent maximum in all rivers during winter (**Figure 3B**). In general, mean wintertime plume areas are 3–12 times larger than in summer. During the fall-winter period (May-September) river plumes tend to be both larger and more frequent, detected during 85, 71, 99, 79, and 71% of the time in the Maipo, Mataquito, Maule, Itata, and Biobío Rivers, respectively.

The Maipo and Mataquito Rivers, located in the northern sector of the study area, exhibit water discharge with a secondary maximum in December due to snowmelt contribution. The secondary maxima do not cause a substantial increase in plume area, probably due to the plume signal being dissipated offshore through upwelling activity. Conversely, the Biobío River does not produce a detectable river plume from December to March, during minimum discharge (but still remains >500 $m^3\ s^{-1}$). This is due to wind-driven dynamics that seasonally maintain the plume within a close reach of the river mouth, and therefore undetectable by the satellite (Saldías et al., 2012). It is also noted that in Central Chile the mean river plume area during winter is not proportional to the average discharge. For instance, both the Maipo and Biobío River plumes reach about 180 km^2 in winter; however, the Biobío River flow is ∼10 times larger than the Maipo. Likewise, the largest wintertime plume is produced by the Maule River (>900 km^2), that has an intermediate values of discharge. This inter-river variability in plume areas may reflect differences in lithology and land-use of

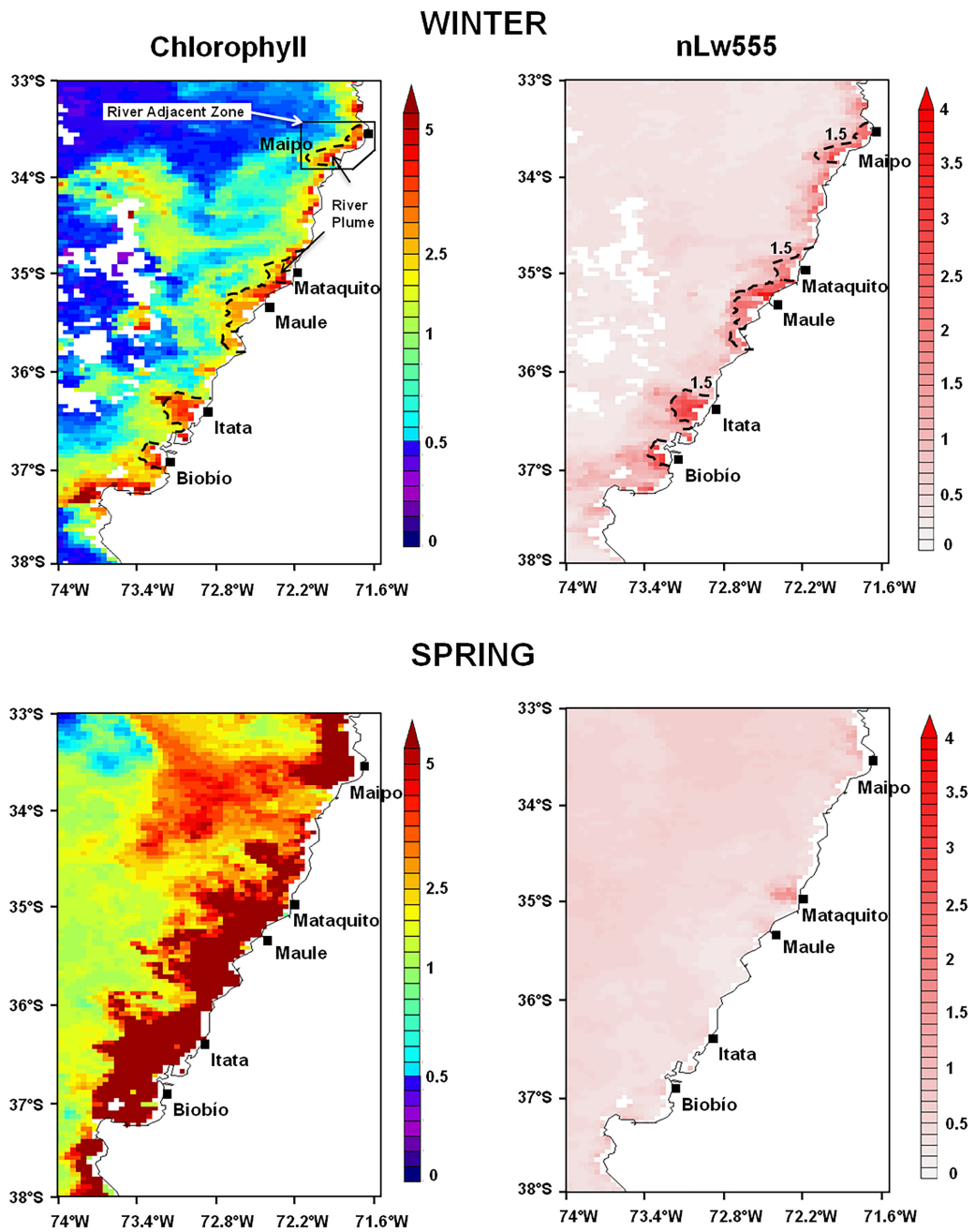

FIGURE 2 | Satellite-derived Chlorophyll (mg m^{-3}) and nLw555 (mW cm^{-2} μm^{-1} sr^{-1}) conditions observed during winter (13–20 August 2008) and spring (16–23 November 2008) along the coastal area off Central Chile. Black dashed line indicates the winter river plume boundaries (nLw555 > 1.5 mW cm^{-2} μm^{-1} sr^{-1}) detected in the adjacent coastal waters.

the draining basins (and hence river loads). The offshore and alongshore extent of these plumes are also controlled by the interplay of different processes like coriolis effect and surface wind stress, as well as by the mixing of the plume waters with the coastal ocean waters. Here the satellite-derived plume areas provide a broad but reasonably characterization of the seasonal variability of the whole plume under these complex dynamic processes.

Nutrient concentrations measured near the mouth of each river are extremely variable and have a very weak seasonal cycle (Pizarro et al., 2010). NO_3^- concentrations range from 0.01 to 10.50 mg L^{-1}, while mean PO_4^{-3} concentration ranges from <0.005 to 0.98 mg L^{-1}. In both cases, maximum NO_3^- and PO_4^{-3} concentrations were found in the Maipo River. However, nutrient exportations into coastal areas show a seasonal cycle certainly controlled by river discharge, reaching

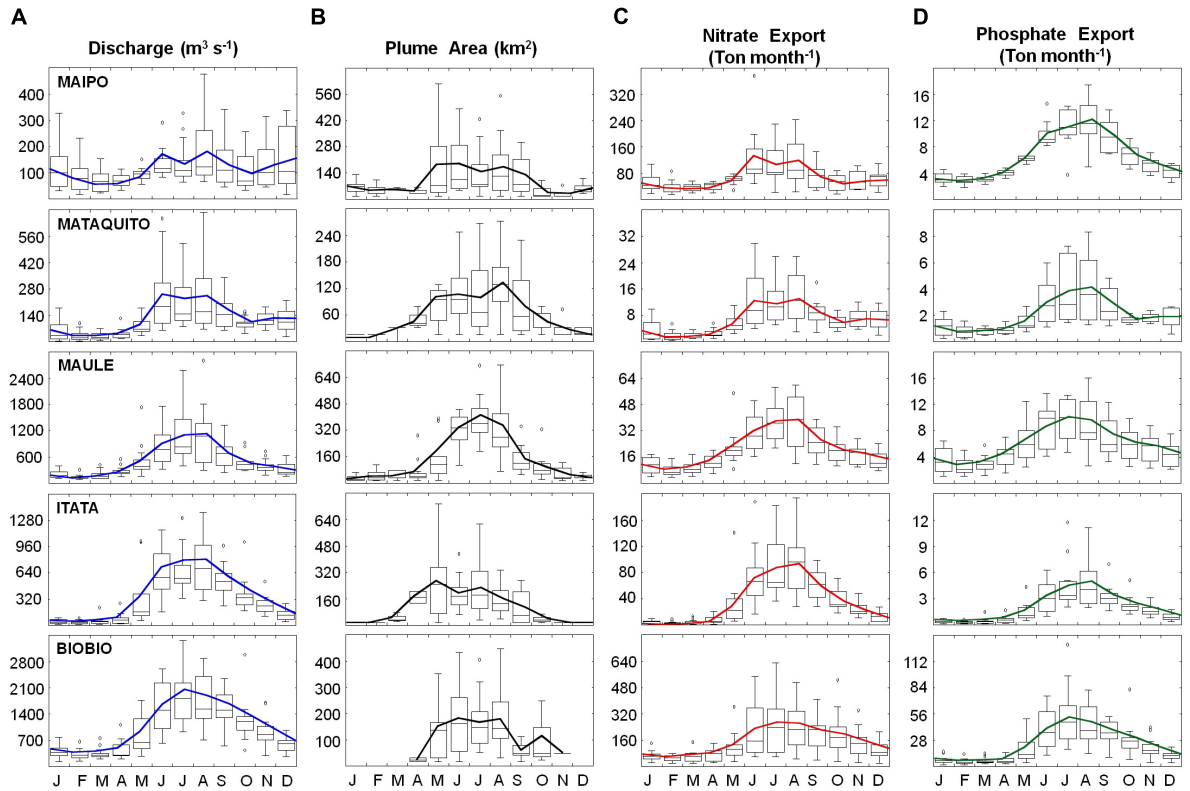

FIGURE 3 | Seasonal cycles of **(A)** river discharge ($m^3\ s^{-1}$), **(B)** satellite-derived river plume area (km^2), **(C)** nitrate- NO_3^- and **(D)** phosphate-PO_4^{-3} export (Ton $month^{-1}$) for the Maipo, Mataquito, Maule, Itata, and Biobío rivers. Solid colored lines correspond to the monthly mean value.

a marked maximum during winter (**Figures 3C,D**). Maximum mean values of NO_3^- and PO_4^{-3} export are observed in the Biobío River, with 245 and 45 Ton $month^{-1}$ in winter, respectively, whereas minimum mean values are found in summertime for the Mataquito and Itata Rivers with 3.95 NO_3^- Ton $month^{-1}$ and 0.56 PO_4^{-3} Ton $month^{-1}$ exported, respectively.

The phytoplankton biomass within river plumes (area mean Chl-a) remains fairly constant throughout the year, and similar between the rivers, with typical values about 4 mg m^{-3} (red lines in **Figure 4**). Thus, when the mean biomass is scaled by the plume area, a clear seasonal cycle of Chl-a pool size is observed, with higher values in winter (ca. June to August, 1.50 to 5.40 Chl-a Ton for the Mataquito and Maule Rivers, respectively). On the other hand, PB in coastal areas adjacent to the river mouth exhibit a marked seasonal cycle (displayed by the discontinuous lines in **Figure 4**), with summertime values being 2–4 times higher than in winter, following the wind-driven upwelling regime of the region. Notably, for all rivers in the study area, wintertime PB within the plume is 1.5–2 times larger than in the surrounding area (**Figure 4**). As discussed in section 4.2, locally increased PB near the river mouth, coupled with a large plume area and frequency, reinforces the crucial role of land-sourced nutrient inputs in winter when upwelling activity is at a minimum.

Inter-Annual Variability

Yearly variability of selected variables, averaged over fall-winter (May–September), is shown in **Figure 5**. Mean river discharge and plume area show a strong interannual variability, with a standard deviation of approximately half of the amplitude of the mean annual cycle. Not surprisingly, the year-to-year variability of river discharge is strongly correlated with the plume area for all rivers, except for the Biobío River (Spearman correlation coefficients larger than 0.50, **Table 2**).

Interannual variations in NO_3^- and PO_4^{-3} concentrations is generally not correlated with discharge, whereas total nutrient export only shows a significant positive correlation with discharge in the Maipo, Itata, and Biobío Rivers (**Figure 5** and **Table 2**). Likewise, year-to-year variability of PB is not significantly correlated with river discharge and nutrient exportation, except in the Maipo River (**Table 2**).

The Impact of the Mega-Drought

Two periods can be clearly distinguished in the timeseries of the discharge in all the rivers considered: a normal period between 2000 and 2009, and the mega-drought period between 2010 and 2014. The mean river discharge in winter during the mega-drought (2010–2014) is reduced to around half of the average of the previous decade (2000–2009) (**Table 3** and **Figure 6**), as the drought propagates from rainfall to stream

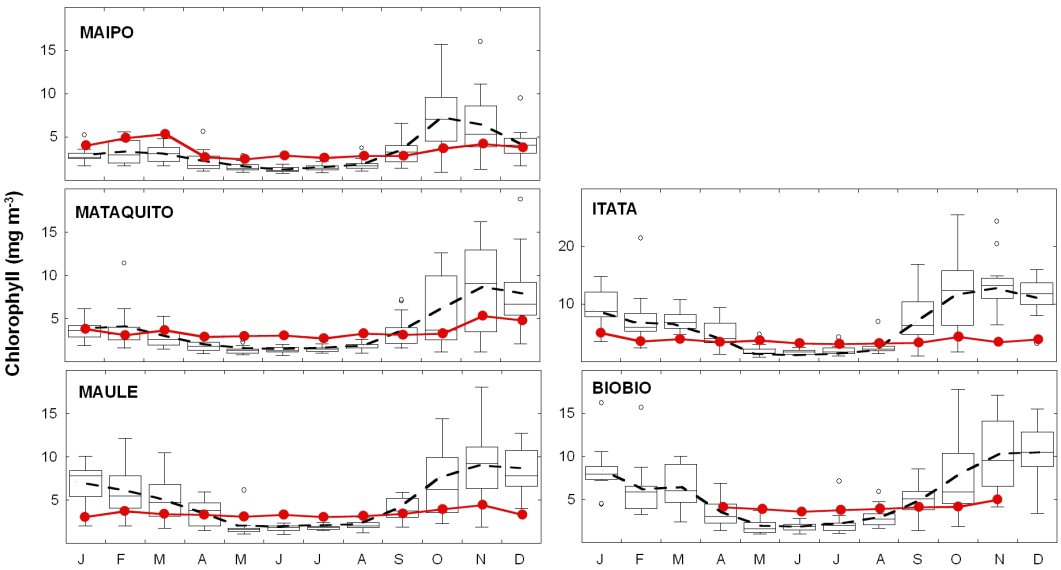

FIGURE 4 | Seasonal cycle of phytoplankton biomass (Chlorophyll; mg m^{-3}) in the river plume and coastal waters area adjacent to each river mouth. Solid red lines with circles and dashed black line indicate PB monthly mean for the river plume and coastal area adjacent to the river, respectively.

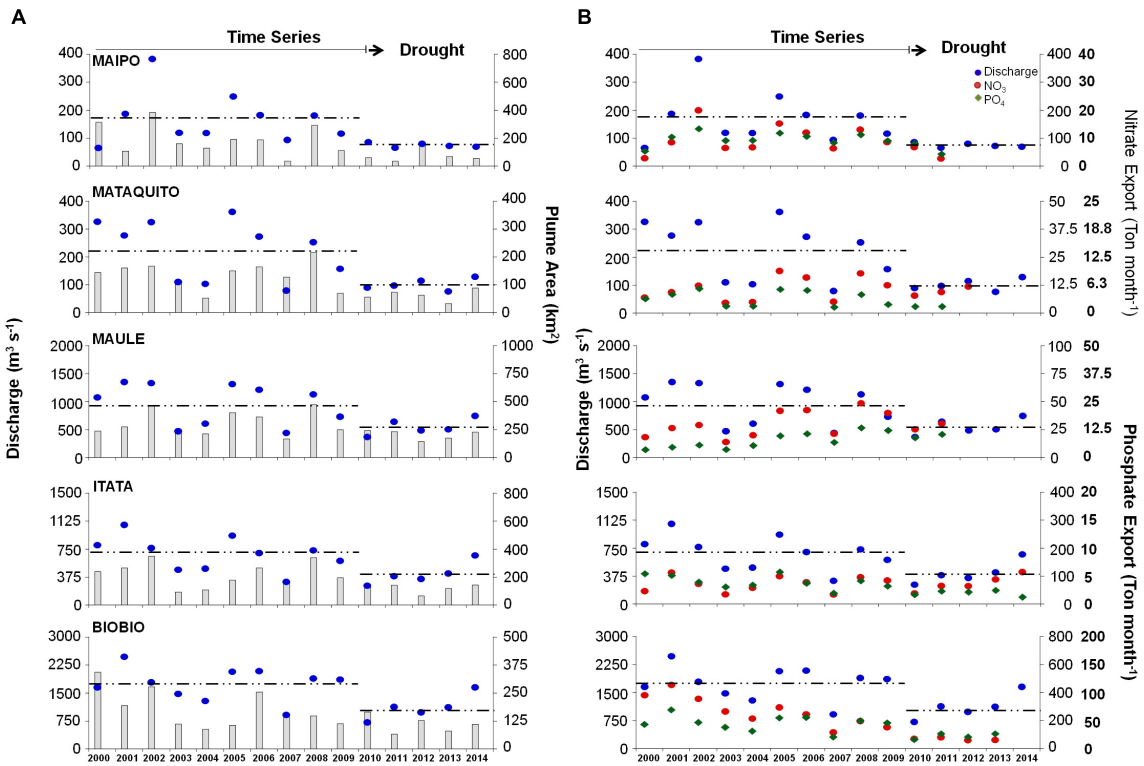

FIGURE 5 | Inter-annual variability of **(A)** river discharge (m^3 s^{-1}; blue circles), river plume area (km^2; gray bars) and **(B)** nitrate- NO_3^- (Ton $month^{-1}$; red circle) and phosphate-PO_4^{-3} export (Ton $month^{-1}$; green diamond). Dashed lines indicate river discharge mean value during normal (2000–09) and drought (2010–14) periods, respectively.

flow (Garreaud et al., 2017). Likewise, the mean plume area and nutrient loads during the mega-drought are only 40–60% of their corresponding "normal" values (2000–2009). On the contrary, the frequency of plume detection declines less markedly, and remains unchanged in the Maule River. However, the mega-drought period significantly affects the nutrients loads, its

TABLE 2 | Spearman correlation coefficients (rs) for the Maipo, Mataquito, Maule, Itata, and Biobío Rivers using 15 years of mean annual values of river discharge ($m^3\ s^{-1}$), river plume area (km^2), Nitrate- NO_3^-, and Phosphate-PO_4^{-3} export (Ton $month^{-1}$) and phytoplankton biomass plume (Chlorophyll; mg m^{-3}).

River discharge	Maipo	Mataquito	Maule	Itata	Biobío
Plume Area	0.771*	0.725*	0.689*	0.682*	0.293
NO_3^-	0.745*	0.544	0.510	0.607*	0.741*
PO_4^{-3}	0.939*	0.895*	0.063	0.854*	0.991*
PB plume					
River discharge	0.600*	0.246	0.386	0.129	−0.021
NO_3^-	0.697*	0.071	0.657*	0.404	−0.077
PO_4^{-3}	0.782*	0.259	0.531	−0.014	0.007

*Statistical significance, $p < 0.05$.

TABLE 3 | Comparison between the "normal" 2000–2009 (N) and the "mega-drought" 2010–2014 (MD) periods using mean values of the river discharge ($m^3\ s^{-1}$), river plume area (km^2), Nitrate- NO_3^-, and Phosphate-PO_4^{-3} export (Ton $month^{-1}$) and phytoplankton biomass (Chlorophyll; mg m^{-3}) in the river plume.

	Periods	Maipo	Mataquito	Maule	Itata	Biobío
River discharge	N	177.33	225.28	983.04	684.09	1744.70
	MD	75.68*	100.51*	544.98*	417.04*	1070.19*
Plume area	N	187.74	131.06	311.29	216.52	172.56
	MD	77.41*	66.38*	203.63*	120.37*	107.38
PB plume	N	2.76	2.98	3.13	3.49	4.02
	MD	2.44*	2.56*	3.07	3.57	4.12
NO_3^-	N	105	10.81	31.48	70.59	265.39
	MD	51.95*	9.60	27.34	67.91	64.75*
PO_4^{-3}	N	10.21	3.36	7.95	3.97	44.42
	MD	7.01*	1.45*	9.53	2.05*	21.72*

*Statistical significance, $p < 0.05$ by U Man-Whitney test.

exportation and PB within the Maipo and Mataquito river plumes (**Table 3**). In all rivers, large plume events (area $>2\times$ annual mean for each river) are observed from May to September during the period between 2000 and 2009, but these events were reduced by nearly 80% during the mega-drought.

DISCUSSION

Rivers and Enhanced Phytoplankton Biomass

Off Central Chile, over seasonal and interannual time scales there is a strong correlation between river discharge and the size and frequency of river plumes (derived from ocean color satellite data) as well as nutrient export (estimated from *in situ* measurements). The high input of land-sourced nutrients (mainly NO_3^- and PO_4^{-3}) appears to enhance biological activity near river mouths in Central Chile, as the mean Chl-a concentrations within the river plumes are approximately twice the background PB values in coastal areas during winter, when discharge is at a maximum but upwelling is at a minimum. This result agrees with observations from the north Pacific and Atlantic oceans (Cloern et al., 1983; Mallin et al., 1993;

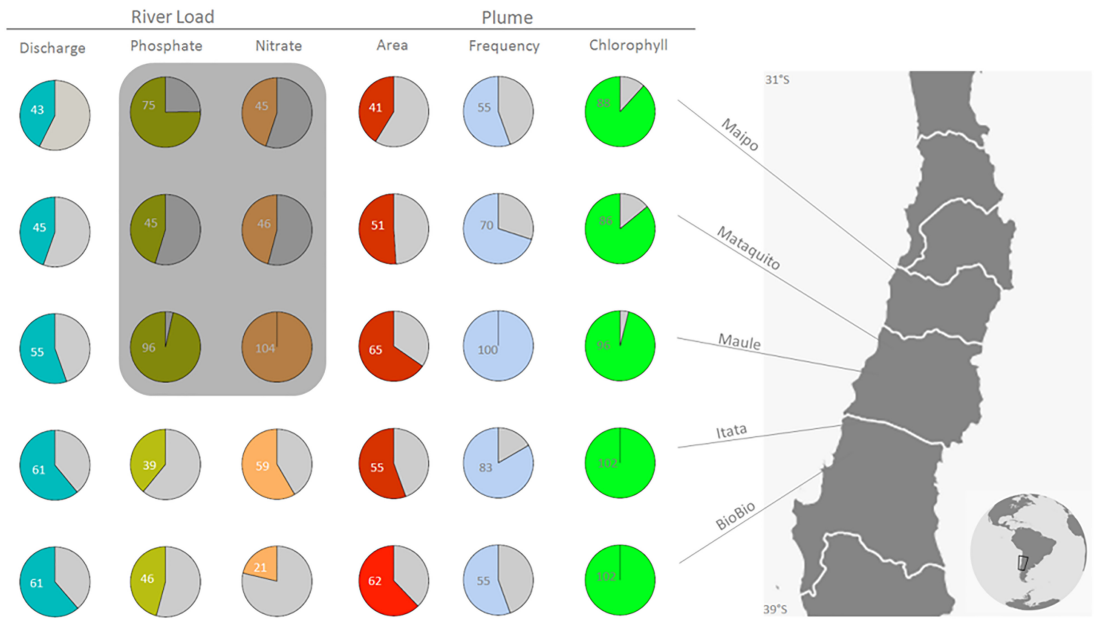

FIGURE 6 | Impact of mega-drought in coastal areas off Central Chile in terms of river load (Discharge; $m^3\ s^{-1}$, Phosphate-PO_4^{-3} and Nitrate- NO_3^- export; Ton $month^{-1}$), river plume area (km^2), frequency, and phytoplankton biomass (Chlorophyll; mg m^{-3}). Numbers and colored areas indicate the mega-drought (2010–2014), mean values as a percentage of the averages over the past decade (2000–2009) for five rivers in Central Chile. Shadow box indicates that Maipo, Mataquito, and Maule Rivers only have Phosphate-PO_4^{-3} and Nitrate- NO_3^- export data until 2011.

Wysocki et al., 2006; Morey et al., 2009; Hickey et al., 2010).

In situ measurements of phytoplankton biomass verify the results obtained from satellite-based data. Previous studies in the Maipo River suggest that river discharge has a positive influence on phytoplankton biomass during upwelling-relaxed conditions (Wieters et al., 2003). Off the Itata River, evidence suggests that nutrient inputs have a positive influence on the pico-nanophytoplankton community (Iriarte et al., 2012). Furthermore, Itata River discharge during austral winter may partially support basal productivity around the river mouth, as a result of nutrient input and the influence of the fresh water plume on water column stratification (Testa et al., 2018). Recently, salinity (measured by a SBE 37 MicroCAT) and chlorophyll data (measured by a C3^{TM} Submersible Fluorometer) was collected at approximately 1 m depth, taken from a coastal buoy located about 10 km off the mouth of the Itata River (Belmar et al., 2017). In late fall, when the river discharge was at a minimum and wind-driven upwelling has subsided, Chl-a was low (less than 200 RFU) and salinity was high (>33) (**Figure 7**). Winter storms caused an increase in river flow and episodes of low salinity in surface waters. Three weeks following the increase in base flow, the Chl-a exhibited a marked increase (>1000 RFU), indicating a delayed response of the phytoplankton population to nutrients availability. We also note that the maximum values of Chl-a during winter are of the same order of those observed in summer (**Figure 7**), when the region is exposed to strong upwelling, emphasizing the crucial role of the river in providing nutrients, thus increasing PB close to the river mouth.

Potential Impact of the River Plume on Coastal Ecological Processes

As showed by our results, these rivers can contribute to enhance biological activity in the coastal water off Central Chile. Although this contribution is small in comparison to that supplied by regional upwelling, they are probably sufficient to sustain the local ecosystem (e.g., larval survival and recruitment) during periods of minimum or delayed seasonal upwelling (winter and early spring). Significant levels of nutrient export from rivers over Central Chile is highly relevant to several larval fish taxa, as they present cross-shelf distribution, with an inner-shelf pattern concentrated mainly within >2 km offshore. For example, *Helcogrammoides chilensis* and *Hypsoblennius sordidus* larvae is observed in low abundances in slope waters (>10 km offshore) off the Chilean coast during winter and spring (Landaeta et al., 2008). Furthermore, river plumes have a direct influence on the

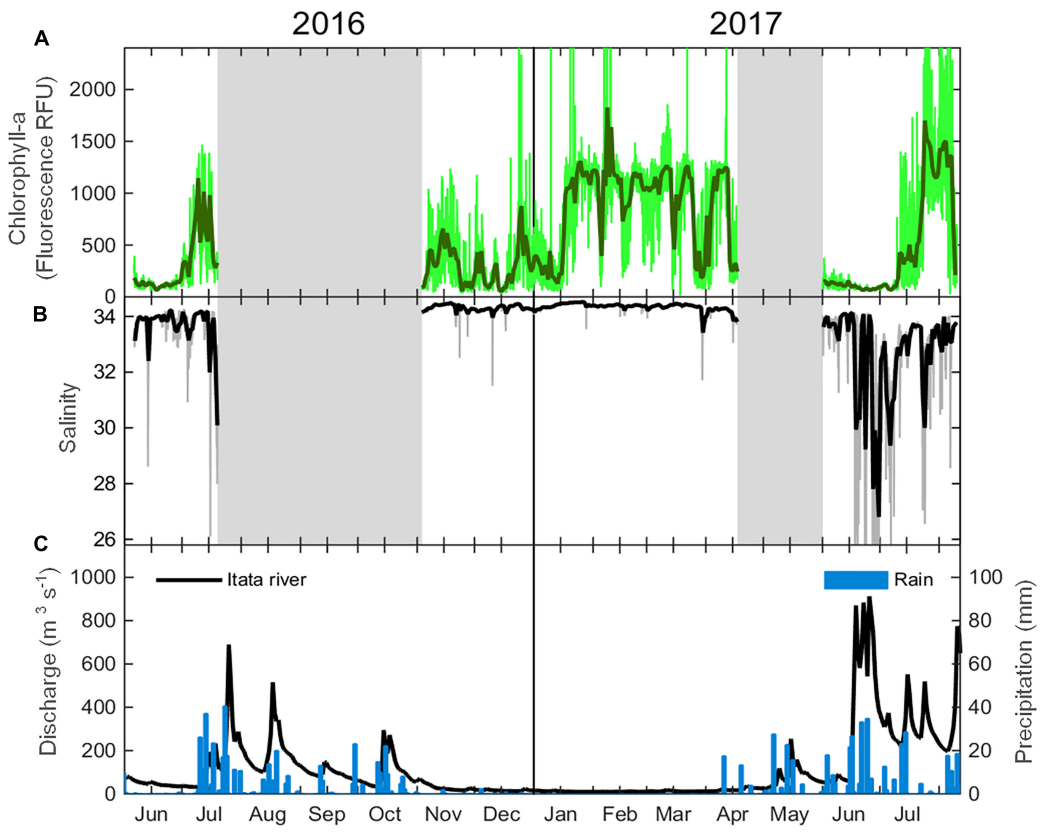

FIGURE 7 | Daily mean (thick lines) and hourly (thin lines) variability of **(A)** phytoplankton biomass (as fluorescence of chlorophyll in RFU) and **(B)** salinity captured by POSAR, an automated monitoring buoy located at ~10 km off the mouth of Itata River (see **Figure 1**), compared to **(C)** daily Itata river discharge (m^3 s^{-1}) and precipitation (mm) during 2016 to 2017 period (01 June 2016 to 10 August 2017).

development of rock and inter-tidal community (Vargas et al., 2006).

River influence is further appreciated when considering seasonal time scales, as the Chl-a pool (mean PB × plume area) in coastal areas near river mouths reach maximum levels during late winter and early spring (while wind-driven upwelling is low), coinciding with the larval recruitment of several fish (Castro et al., 2000; Landaeta et al., 2015). Previous studies in the Itata River have shown that high concentrations of Chl-a are accompanied by increased primary production in coastal waters (Salamanca and Pantoja, 2009). Moreover, it has been demonstrated that input from the Itata River, in particular during years of increased precipitation, can promote favorable environmental conditions for fish larvae and forage fish species (sardines and anchovies; Soto-Mendoza et al., 2010), as well as optimum conditions for growth and fish recruitment due to nutrient enriched waters (Grimes, 2001). Studies carried out in the Itata and Biobío Rivers suggest that river runoff and rainfall strongly influence local fish survival (e.g., Robalo, *Eleginops maclovinus*) during early life stages (Quiñones and Montes, 2001).

Future Projections

Model-based climate projections, under scenarios of high greenhouse gas emissions, consistently indicate a reduction in mean annual precipitation (up to 30% relative to current values) and an increase in surface air temperature (up to 2°C along the coast) over Central Chile for the 2070–2100 period (Fuenzalida et al., 2007; Bozkurt et al., 2017). It is expected that the rainfall decline will be most marked in winter due to the projected reduction in extratropical storms crossing this region. Given the small size of the Andean basins in central Chile and the previously found association between precipitation and river discharge (Vicuña et al., 2010; Bozkurt et al., 2017) and well correlated with nutrient exportation is probably expected to consistently decline over the 21st century, potentially causing detrimental impacts upon these river influenced coastal areas.

Studies elsewhere show that drought conditions are able to degrade coastal ecological processes. A decrease in diatoms and Chl-a biomass was associated with extremely low river flow during droughts in the Suisun Bay – San Francisco estuary and in the Neuse River estuary (Nichols, 1985; Lehman, 1996; Thompson et al., 2015). In the Neuse River estuary, droughts also caused significant shifts in the phytoplankton community, promoting cyanobacteria species (Paerl et al., 2010), as well as a decrease in phytoplankton productivity, directly associated with a decrease in nutrients (Wetz et al., 2011). Ecological studies in the San Francisco Bay demonstrate important changes in trophic webs under low river discharge, with the benthic community becoming more important with respect to the planktonic community, leading to negative consequences on fish populations in the estuary (Cloern et al., 1983; Nichols, 1985). The worst ever recorded red-tide event in the coastal waters of western Patagonia took place in summer/fall 2016, caused by an extensive bloom of *Pseudochattonella* sp. and *Alexandrium catenella*, was also connected with a very intense drought in southern Chile mediated by the marked reduction in fresh water input and subsequent alteration of the coastal hydrobiology (León-Muñoz et al., 2018).

This study shows that the recent mega-drought (2010–2014) has produced a consistent decrease in discharge (30–60% relative to historical values) and plume area (35 to 60%) for all the rivers considered within the study area (**Figure 6**). Furthermore, a reduction in phytoplankton biomass was observed in the coastal areas influenced by the Maipo and Mataquito rivers, situated in the northern (arid) sector of Central Chile (**Figure 6**). Given the intensity and duration of the mega-drought, it is considered to be an analog to future climate scenarios for this region (Fuenzalida et al., 2007; Bozkurt et al., 2017). Systematic evidence of mega-drought impacts upon coastal fish productivity still does not exist, however, it remains a priority to further investigate and quantify these impacts, considering the ongoing trend toward dry conditions (Boisier et al., 2016) and the persistence of this trend projected for the near future.

AUTHOR CONTRIBUTIONS

IM, PA-R, LF, and RG designed the study. MY and LF carried out data analysis of *in situ* hydro-chemical data. IM, PA-R, and RG acquired and processed the remote-sensed MODIS-SeaWiFS ocean color images. LB contributed to data analysis of the coastal buoy POSAR. All authors provided contributions for writing and correcting the paper.

FUNDING

This research was funded by the Center of Excellence FONDAP-CONYCIT N° 15110009 and PA-R was supported by beca FIP UV/Doctorado. Coastal buoy POSAR was funded by FONDEQUIP-CONICYT project EQM140134.

ACKNOWLEDGMENTS

PA-R acknowledges for support by the CID UV Centro de Observación Marino para Estudios de Riesgos del Ambiente Costero (COSTA-R). MY also acknowledges for support by the Fondecyt project 3150162. The authors thank NASA/GSFC Ocean Biology Processing Group and GlobColour – The European Service for Ocean Color for providing access to weekly L3 SeaWiFS and MODIS binned products. The authors also thank the Dirección General de Aguas (DGA) for nutrient and discharge data from fluviometric stations.

SUPPLEMENTARY MATERIAL

The Supplementary Material for this article can be found online at: https://www.frontiersin.org/articles/10.3389/fmars.2018.00423/full#supplementary-material

REFERENCES

Aceituno, P., and Vidal, F. (1990). Variabilidad interanual en el caudal de ríos andinos en Chile central en relación con la temperatura de la superficie del mar en el Pacífico central. *Revista de la Sociedad Chilena de Ingeniería Hidráulica* 5, 7–19.

Belmar, L., Garreaud, R., and Farías, L. (2017). "Plataforma de Observación del Sistema Acoplado Océano Atmósfera (POSAR): un sistema de observación de alta frecuencia en la zona costera de Chile central," in *Proceedings of the XXXVII Congreso de Ciencias del Mar 2017*, Valparaíso, CL.

Boisier, J. P., Rondanelli, R., Garreaud, R. D., and Muñoz, F. (2016). Anthropogenic and natural contributions to the Southeast Pacific precipitation decline and recent megadrought in central Chile. *Geophys. Res. Lett.* 43, 413–421. doi: 10.1002/2015GL067265

Bozkurt, D., Rojas, M., Boisier, J. P., and Valdivieso, J. (2017). Climate change impacts on hydroclimatic regimes and extremes over Andean basins in central Chile. *Hydrol. Earth Syst. Sci. Discuss* doi: 10.5194/hess-2016-690

Castro, L. R., Salinas, G. R., and Hernàndez, E. H. (2000). Environmental influences on winter spawning of the anchoveta *Engraulis ringens* off central Chile. *Mar. Ecol. Prog. Ser.* 197, 247–258. doi: 10.3354/meps197247

Cloern, J. E., Alpine, A. E., Cole, B. E., Wong, R. L. J., Arthur, J. F., and Ball, M. D. (1983). River discharge controls phytoplankton dynamics in northern San Francisco Bay estuary. *Estuar. Coast. Shelf Sci.* 16, 415–429. doi: 10.1016/0272-7714(83)90103-8

Cohn, T. A. (2005). Estimating contaminant loads in rivers: an application of adjusted maximum likelihood to type 1 censored data. *Water Resour. Res.* 41:W07003. doi: 10.1029/2004WR003833

Cotrim, da Cunha, L., Buitenhuis, E. T., Le Quéré, C., Giraud, X., and Ludwig, W. (2007). Potential impact of changes in river nutrient supply on global ocean biogeochemistry. *Global Biogeochem. Cycles* 21:GB4007. doi: 10.1029/2006GB002718

Fuenzalida, H., Aceituno, P., Falvey, M., Garreaud, R., Rojas, M., and Sánchez, R. (2007). "Study on Climate Variability for Chile during the 21st century," in *Proceedings of the Technical Report of the National Environmental Committee,* Santiago, CL.

Garreaud, R., Alvarez-Garreton, C., Barichivich, J., Boisier, J. P., Christie, D., Galleguillos, M., et al. (2017). The 2010-2015 mega drought in Central Chile: Impacts on regional hydroclimate and vegetation. *Hydrol. Earth Syst. Sci.* 2017, 1–37. doi: 10.5194/hess-2017-191

Grimes, C. B. (2001). Fishery production and the Mississippi River discharge. *Fisheries* 26, 17–26.

Hickey, B. M., and Banas, N. S. (2003). Oceanography of the U.S. Pacific Northwest coastal ocean and estuaries with application to coastal ecology. *Estuaries* 26, 1010–1031. doi: 10.1007/BF02803360

Hickey, B. M., Kudela, R. M., Nash, J. D., Bruland, K. W., Peterson, W. T., MacCready, P., et al. (2010). River influences on shelf ecosystems: introduction and synthesis. *J. Geophys. Res.* 115:C00B17. doi: 10.1029/2009JC005452

Hopkins, J., Lucas, M., Dufau, C., Sutton, M., Stum, J., Lauret, O., et al. (2013). Detection and variability of the Congo River plume from satellite derived sea surface temperature, salinity, ocean colour and sea level. *Remote Sens. Environ.* 139, 365–385. doi: 10.1016/j.rse.2013.08.015

Hopkinson, C. S., and Vallino, J. J. (2005). Efficient export of carbon to the deep ocean through dissolved organic carbon. *Nature* 433, 142–145. doi: 10.1038/nature03191

Hu, C., Lee, Z., and Franz, B. (2012). Chlorophyll a algorithms for oligotrophic oceans: a novel approach based on three-band reflectance difference. *J. Geophys. Res.* 117, 1–25. doi: 10.1029/2011jc007395

Iriarte, J. L., Vargas, C. A., Tapia, F. J., Bermúdez, R., and Urrutia, R. E. (2012). Primary production and plankton carbon biomass in a river-influenced upwelling area off Concepción. *Chile. Prog. Oceanogr.* 92–95, 97–109. doi: 10.1016/j.pocean.2011.07.009

Landaeta, M. F., Contreras, J. E., Bustos, C. A., and Muñoz, G. (2015). Larval growth of two lanternfishes at nearshore waters from an upwelling zone based in the otolith microstructure analysis. *J. Appl. Ichthyol.* 31, 106–113. doi: 10.1111/jai.12639

Landaeta, M. F., Veas, R., Letelier, J., and Castro, L. R. (2008). Larval fish assemblages off central Chile upwelling ecosystem. *Rev. Biol. Mar. Oceanogr.* 43, 569–584. doi: 10.4067/S0718-19572008000300016

Lara, A., Solari, M. E., Prieto, M. R., and Peña, M. P. (2012). Reconstrucción de la cobertura de la vegetación y uso de suelo hacia 1550 y sus cambios a 2007 en la ecorregióın de los bosques valdivianos lluviosos de Chile (35° - 43° 30' S). *Bosque* 33, 13–23. doi: 10.4067/S0717-92002012000100002

Lehman, P. W. (1996). "Changes in chlorophyll a concentration and phytoplankton community composition with water-year type in the upper San Francisco Bay estuary," in *San Francisco Bay: The Ecosystem. Pacific Division, American Association for the Advancement of Science*, ed. J. T. Hollibaugh (San Francisco, CA: Bay), 351–374.

Léniz, B., Vargas, C. A., and Ahumada, R. (2012). Characterization and comparison of microphytoplankton biomass in the lower reaches of the Biobío River and the adjacent coastal area off Central Chile during autumn-winter conditions. *Lat. Am. J. Aquat. Res.* 40, 847–857. doi: 10.3856/vol40-issue4-fulltext-3

León-Muñoz, J., Urbina, M., Garreaud, R., and Iriarte, J. L. (2018). Hydroclimatic conditions trigger record harmful algal bloom in western Patagonia (summer 2016). *Sci. Rep.* 8:1330. doi: 10.1038/s41598-018-19461-4

Lihan, T., Mustapha, M. A., Rahim, S. A., Saitoh, S., and Iida, K. (2011). Influence of River plume on variability of chlorophyll a concentration using satellite images. *J. Appl. Sci.* 11, 484–493. doi: 10.3923/jas.2011.484.493

Lohrenz, S. E., Redalje, D. G., Cai, W.-J., Acker, J., and Dagg, M. (2008). A retrospective analysis of nutrients and phytoplankton productivity in the Mississippi River plume. *Cont. Shelf Res.* 28, 1466–1475. doi: 10.1016/j.csr.2007.06.019

Luzio, W., Casanova, M., and Seguel, O. (2010). *Suelos de Chile*. Santiago de Chile, CL: Universidad de Chile.

Mallin, M. A., Paerl, H. W., Rudek, J., and Bates, P. W. (1993). Regulation of estuarine primary production by watershed rainfall and river flow. *Mar. Ecol. Prog. Ser.* 93, 199–203. doi: 10.3354/meps093199

Montecino, V., Strub, P. T., Chavez, F., Thomas, A., Tarazona, J., Baumgartner, T., et al. (2006). "Chapter 10, Bio-physical interactions off western South America," in *The Coastal Ocean: Interdisciplinary Regional Studies and Synthesis*, Vol. 14A, ed. A. R. Robinson (Cambridge: Harvard University Press), 329–390.

Montecinos, A., Kurgansky, M. V., Muñoz, C., and Takahashi, K. (2011). Non-ENSO interannual rainfall variability in central Chile during austral winter. *Theor. Appl. Climatol.* 106, 557–568. doi: 10.1007/s00704-011-0457-1

Morey, S. L., Dukhovskoy, D. S., and Bourassa, M. A. (2009). Connectivity of the Apalachicola River flow variability and the physical and bio-optical oceanic properties of the northern West Florida Shelf. *Cont. Shelf Res.* 29, 1264–1275. doi: 10.1016/j.csr.2009.02.003

Nezlin, N. P., DiGiacomo, P. M., Stein, E. D., and Ackerman, D. (2005). Stormwater runoff plumes observed by SeaWifs radiometer in the Southern California Bight. *Remote Sens. Environ.* 98, 494–510. doi: 10.1016/j.rse.2005.08.008

Nichols, F. H. (1985). Increased benthic grazing: an alternative explanation for low phytoplankton biomass in northern San Francisco Bay during the 1967-1977 drought. *Estuar. Coast. Shelf Sci.* 21, 379–388. doi: 10.1016/0272-7714(85)90018-6

O'Reilly, J. E., Maritorena, S., Siegel, D., O'Brien, M. C., Toole, D., Mitchell, B. G., et al. (2000). "SeaWiFS Postlaunch Calibration and Validation Analyses, Part 3," in *NASA Tech. Memo, TM-2000-206892*, Vol. 11, eds S. B. Hooker and E. R. Firestone (Greenbelt, MD: NASA Goddard Space Flight Center), 49.

Otero, M. P., and Siegel, D. A. (2004). Spatial and temporal characteristics of sediment plumes and phytoplankton blooms in the Santa Barbara Channel. *Deep Sea Res. II* 51, 1129–1149. doi: 10.1016/j.dsr2.2004.04.004

Paerl, H. W., Rossignol, K. L., Hall, S. N., Peierls, B. L., and Wetz, M. S. (2010). Phytoplankton Community Indicators of Short- and Long-term Ecological Change in the Anthropogenically and Climatically Impacted Neuse River Estuary, North Caroline, USA. *Estuaries Coast.* 33, 485–497. doi: 10.1007/s12237-009-9137-0

Pauly, D., and Christensen, V. (1995). Primary production required to sustain global fisheries. *Nature* 374, 255–257. doi: 10.1038/374255a0

Pellicciotti, F., Burlando, P., and Van Vliet, K. (2007). "Recent trends in precipitation and streamflow in the Aconcagua River Basin, central Chile", in Glacier Mass Balance Changes and Meltwater Discharge. *Centre Ecol. Hydrol.* 318, 17–38.

Pérez, C. A., DeGrandpre, M. D., Lagos, N. A., Saldías, G. S., Cascales, E.-K., and Vargas, C. A. (2015). Influence of climate and land use in carbon biogeochemistry in lower reaches of rivers in Central-Southern Chile: implications for the carbonate system in river-influenced rockyshore

environments. *J. Geophys. Res. Biogeosci.* 120, 673–692. doi: 10.1002/2014JG002699

Pizarro, J., Vergara, P. M., Sanhueza, P. A., Rodríguez, J. A., and Castro, S. A. (2010). Nutrients dynamics in the main river basins of the centre-southern region of Chile. *J. Hazard. Mater.* 175, 608–613. doi: 10.1016/j.jhazmat.2009.10.048

Quiñones, R. A., and Montes, R. M. (2001). Relationship between freshwater input to the coastal zone and the historical landings of the benthic/demersal fish Eliginops maclovinus in central-south Chile. *Fish. Oceanogr.* 10, 311–328. doi: 10.1046/j.1365-2419.2001.00177.x

Rahn, D. A., and Garreaud, R. D. (2014). A synoptic climatology of the near-surface wind along the west coast of South America. *Int. J. Climatol.* 34, 780–792. doi: 10.1002/joc.3724

Runkel, R. L., Crawford, C. G., and Cohn, T. A. (2004). "Load estimator (LOADEST): a fortran program for estimating constituent loads in streams and rivers," in *Proceedings of the Techniques and Methods Book 4, Chapter A5*, ed. U.S. Geological Survey (Reston, VA: Geological Survey), 75.

Salamanca, M. A., and Pantoja, S. (2009). ""Caracterización química en la zona marina adyacente a la desembocadura del río Itata"," in *La cuenca hidrográfica del río Itata. Aportes Científicos para su gestión sustentable*, eds O. Parra, J. C. Castilla, H. Romero, R. Quiñones, and A. Camaño (Concepción, CL: Editorial Universidad de Concepción), 177–191.

Saldías, G. S., Largier, J. L., Mendes, R., Pérez-Santos, I., Vargas, C. A., and Sobarzo, M. (2016). Satellite-measured interannual variability of turbid river plumes off central- southern Chile: spatial patterns and the influence of climate variability. *Prog. Oceanogr.* 146, 212–222. doi: 10.1016/j.pocean.2016.07.007

Saldías, G. S., Sobarzo, M., Largier, J., Moffat, C., and Letelier, R. M. (2012). Seasonal variability of turbid river plumes off central Chile based on high-resolution MODIS imagery. *Remote Sens. Environ.* 123, 220–233. doi: 10.1016/j.rse.2012.03.010

Soto-Mendoza, S., Castro, L. R., and Llanos-Rivera, A. (2010). Variabilidad espacial y temporal de huevos y larvas de Strangomera bentincki y Engraulis ringens, asociados a la desembocadura del río Itata. *Chile Rev. Biol. Mar. Oceanogr.* 45, 471–487. doi: 10.4067/S0718-19572010000300012

Testa, G., Masotti, I., and Farias, L. (2018). Temporal variability in net primary production in an upwelling area off central Chile (36°S). *Front. Mar. Sci.* 5:179. doi: 10.3389/fmars.2018.00179

Thiel, M., Macaya, E. C., Acuña, E., Arntz, W. E., Bastias, H., Brokordt, K., et al. (2007). The humboldt current system of northern and central Chile. *Oceanogr. Mar. Biol. Annu. Rev.* 45, 195–344. doi: 10.1201/9781420050943.ch6

Thomas, A. C., and Weatherbee, R. A. (2006). Satellite-measured temporal variability of the Columbia River plume. *Remote Sens. Environ.* 100, 167–178. doi: 10.1016/j.rse.2005.10.018

Thompson, P. A., O'Brien, T. D., Paerl, H. W., Peierls, B. L., Harrison, P. J., and Robb, M. (2015). Precipitation as a driver of phytoplankton ecology in coastal waters: a climatic perspective. *Estuar. Coast. Shelf Sci.* 162, 119–129. doi: 10.1016/j.ecss.2015.04.004

Tremblay, J. -È, Raimbault, P., Garcia, N., Lansard, B., Babin, M., and Gagnon, J. (2014). Impact of river discharge, upwelling and vertical mixing on the nutrient loading and productivity of the Canadian Beaufort Shelf. *Biogeosciences* 11, 4853–4868. doi: 10.5194/bg-11-4853-2014

Vargas, C. A., Narváez, D. A., Piñones, A., Navarrete, S. A., and Lagos, N. A. (2006). River plume dynamics influences transport of barnacle larvae in the inner shelf off central Chile. *J. Mar. Biol. Ass.* 86, 1057–1065. doi: 10.1017/S0025315406014032

Vicuña, S., Garreaud, R., and McPhee, J. (2010). Climate change impacts on the hydrology of a snow-melt driven basin in semiarid Chile. *Clim. Change* 105, 3–4.

Waylen, P. R., Caviedes, C. N., and Juricic, C. (1993). El Niño-Southern Oscillation and the surface hydrology of Chile: a window on the future? *Can. Water Resour. J.* 18, 425–441. doi: 10.4296/cwrj1804425

Wetz, M. S., Hutchinson, E. A., Lunetta, R. S., Paerl, H. W., and Taylor, J. C. (2011). Severe droughts reduce estuarine primary productivity with cascading effects on higher trophic levels. *Limnol. Oceanogr.* 56, 627–638. doi: 10.4319/lo.2011.56.2.0627

Wieters, E. A., Kaplan, D. M., Navarrete, S. A., Sotomayor, A., Largier, J., Nielsen, K. J., et al. (2003). Alongshore and temporal variability in chlorophyll a concentration in Chilean nearshore waters. *Mar. Ecol. Prog. Ser.* 249, 93–105. doi: 10.3354/meps249093

Wysocki, L. A., Bianchi, T. S., Powell, R. T., and Reuss, N. (2006). Spatial variability in the coupling of organic carbon, nutrients, and phytoplankton pigments in surface waters and sediments of the Mississippi River plume. *Estuar. Coast. Shelf Sci.* 69, 47–63. doi: 10.1016/j.ecss.2006.03.022

Yevenes, M. A., Arumí, J. L., and Farías, L. (2016). Unravel biophysical factors on river water quality response in Chilean Central-Southern watersheds. *Environ. Monit. Assess.* 188, 1–17. doi: 10.1007/s10661-016-5235-1

Conflict of Interest Statement: The authors declare that the research was conducted in the absence of any commercial or financial relationships that could be construed as a potential conflict of interest.

Copyright © 2018 Masotti, Aparicio-Rizzo, Yevenes, Garreaud, Belmar and Farías. This is an open-access article distributed under the terms of the Creative Commons Attribution License (CC BY). The use, distribution or reproduction in other forums is permitted, provided the original author(s) and the copyright owner(s) are credited and that the original publication in this journal is cited, in accordance with accepted academic practice. No use, distribution or reproduction is permitted which does not comply with these terms.

frontiers in Marine Science

ORIGINAL RESEARCH
published: 05 December 2018
doi: 10.3389/fmars.2018.00463

Controls on the Fate of Dissolved Organic Carbon Under Contrasting Upwelling Conditions

Mariana B. Bif, Dennis A. Hansell and Kimberly J. Popendorf*

Department of Ocean Sciences, Rosenstiel School of Marine and Atmospheric Sciences, University of Miami, Miami, FL, United States

To understand controls on the production and remineralization of recalcitrant dissolved organic carbon (DOC) produced in association with positive net community production (NCP), we simulated upwelling systems of different intensities by combining and incubating whole seawater collected from different depths in the Florida Strait (27°N, ∼79°W). The natural microbial communities in the treatments grew under controlled light and temperature for 15 days (i.e., the autotrophic phase); they were subsequently incubated for 35 days in the dark heterotrophic phase. We analyzed the phytoplankton composition and pigment fluorescence intensity during the light phase, and dissolved organic and inorganic variables during both phases. Initial high or low availability of inorganic nutrients controlled phytoplankton growth and the magnitude of NCP. In the strong upwelling treatment with higher initial inorganic nutrients, 25% of NCP accumulated as DOC after 15 days, however, this material was in turn fully remineralized during the dark phase. In contrast, low nutrients in the weak upwelling treatment limited the magnitude of NCP and accumulated DOC, which represented 11% of NCP. Surprisingly, most of this fraction resisted microbial remineralization in the dark phase, suggesting that upwellings of different intensities affect the quality of dissolved organic matter produced, thereby affecting the timing and location of its remineralization and, hence, its prospects for export to the deep ocean.

Keywords: carbon cycle, dissolved organic carbon, dissolved organic matter, net community production, remineralization, upwelling

OPEN ACCESS

Edited by:
Veronica Molina, Universidad de Playa Ancha, Chile

Reviewed by:
Elvira Pulido-Villena, UMR7294 Institut Méditerranéen d'océanographie (MIO), France
Marcelo H. Gutiérrez, Universidad de Concepción, Chile

****Correspondence:***
Mariana B. Bif
marianabif@gmail.com;
mbb78@miami.edu

Specialty section:
This article was submitted to Marine Biogeochemistry, a section of the journal Frontiers in Marine Science

Received: *17 May 2018*
Accepted: *19 November 2018*
Published: *05 December 2018*

Citation:
Bif MB, Hansell DA and Popendorf KJ (2018) Controls on the Fate of Dissolved Organic Carbon Under Contrasting Upwelling Conditions. Front. Mar. Sci. 5:463. doi: 10.3389/fmars.2018.00463

INTRODUCTION

Imbalance between primary production (PP) and respiration in the ocean's euphotic zone results in net community production (NCP) when integrated through time. When PP is stimulated by external inputs of inorganic nutrients, such as NO_3^-, new production (Dugdale and Goering, 1967) exceeds community respiration and NCP is positive, with a fraction accumulating as dissolved organic carbon (DOC) (Hansell and Carlson, 1998; Raimbault and Garcia, 2008; Guidi et al., 2016). The freshly-produced DOC that resists immediate degradation may survive long enough to be exported through vertical mixing and overturning circulation, thus contributing to the biological carbon pump (Copin-Montégut and Avril, 1993; Carlson et al., 1994; Ducklow et al., 2001; Hansell et al., 2009). The amount of DOC that escapes rapid remineralization varies across environments and seasons (Carlson et al., 1998; Hansell and Carlson, 1998; Hansell and Peltzer, 1998; Romera-Castillo et al., 2016), however, controls on the production of a resistant fraction that not only

accumulates in the system, but also retains a residence time allowing subsequent export, is unresolved.

The net production of DOC depends on the local microbial community composition and growth (Conan et al., 2007; Passow et al., 2007). For example, initial concentrations of inorganic nutrients impact the magnitude and quality of organic matter produced. Diatom cultures under nitrogen and phosphorus limitation release less dissolved organic matter (DOM) and of different composition, with a considerable fraction that is inaccessible to heterotrophic bacteria (Wear et al., 2015; Saad et al., 2016). Indeed, variations in NCP and DOC are often observed in environments experiencing periodic change in nutrient inputs, such as temperate systems during different seasons (Lønborg et al., 2009).

Upwelling systems, especially, are controlled by variations in wind that regulate uplift of nutrient-enriched subsurface waters, thereby stimulating NCP. Nutrient supply to the euphotic zone depends on the upwelling intensity, which impacts the autotroph growth and succession, and thereby reshapes the community structure (Abbott and Zion, 1985; Hanson et al., 2005; Loureiro et al., 2011). As a consequence, local accumulation of DOC should vary under different upwelling conditions, with an estimated ∼40% of the ocean's net production of DOC occurring in upwelling systems (Hansell and Carlson, 1998). A study from Wetz and Wheeler (2004) during an upwelling event off the Oregon coast identified a small portion of plankton-derived DOC that accumulated after nitrate depletion, and with potential to be transported offshore, however, the efficiency in the subsequent export of this material was not assessed.

Here we seek to understand controls on net DOC production under upwelling conditions of varying intensities and the potential for subsequent export to the deep ocean. We conducted laboratory experiments to recreate upwelling systems of different intensities by mixing waters collected from various depths in the Florida Strait; such a design simulates upwelling in this western boundary current system (Czeschel et al., 2012; Zhang et al., 2017). Laboratory experiments cannot mimic the complexity of nature, but they are useful to understand how controlled variables modify trends and processes on a small scale.

MATERIALS AND METHODS

Seawater for incubations was collected during a cruise across the Florida Strait aboard RV *Walton Smith* on July 17, 2016 (27∘N, 79.5∘W), using a rosette coupled with a CTD (conductivity + temperature + depth), from the surface layer (5 m depth), 300 and 600 m. The water was transferred to acid-cleaned 8 L polycarbonate carboys using a silicon tube, then brought to a shore-based laboratory for further processing on the same day as collection. Samples from the various depths were combined at various proportions to a final volume of 8 L each replicate, and prepared in triplicates to simulate three upwelling systems with varying deep source waters: 100% surface water to simulate a non-upwelling system (control); 80% surface + 20% 300 m water to simulate a weak upwelling; and 80% surface + 10% 300 m + 10% 600 m water to simulate a strong upwelling system.

Light Incubations

The carboys were maintained under controlled temperature (∼22°C) and light/dark cycles (16/8 h) for 15 days, with daily manual stirring in order to keep O_2 concentrations near supersaturation (∼6.5 mg l^{-1}). During this period, the biological community grew without interference, and samples were taken at fixed time points for the following parameters:

Fluorescence Intensity

Approximately 20 mL of the sample water was collected using test tubes, assessed for phytoplankton fluorescence intensity at 488 nm of excitation and 680 nm emission (10-AU Fluorometer, Turner Designs), and reported as relative fluorescence units (RFU).

Microscopy

Biological samples were fixed with Lugol's solution to 1% of preservative concentration and refrigerated in 10 mL amber glass vials prior to analysis. The samples where fluorescence intensity increased were stored in 5 mL vials and scanned by fluorescence microscopy (Olympus BX51) in order to identify the main groups of phytoplankton growing in the treatments.

Dissolved Organic Carbon (DOC) and Total Dissolved Nitrogen (TDN)

DOC + TDN were analyzed using a Shimadzu TOC-L system equipped with TNM-L for N detection, located at the University of Miami, following the method described by Dickson et al. (2007). The reference material used for equipment calibration and water comparison was provided by the Hansell CRM program (Hansell, 2005). Briefly, using acid-washed polycarbonate filter holders (Pall Corp.) and silicon tubing, 20 mL of sample passed through pre-combusted (450°F overnight) GF/F filters 0.7 μm nominal poresize and were collected into pre-combusted glass vials. The samples were acidified with 40 μL of 4 N hydrochloric acid (HCl) and stored at 4°C until all samples had been taken through the course of the incubation experiment. DOC concentrations are expressed as μmol kg^{-1} C, with an analytical precision of 1.4 μmol kg^{-1}. TDN results (μmol kg^{-1} N) were used to calculate dissolved organic nitrogen (DON) concentrations (μmol kg^{-1} N) by subtracting the inorganic components of TDN: [DON] = [TDN] – ([NO_3 + NO_2] + [NH_4]), with a detection limit of 0.01 μmol kg^{-1} for TDN.

Nitrate + Nitrite (NO_3^- + NO_2^-) Concentrations

Samples from the incubation were filtered by gravity through Whatman GF/F filters (nominal pore size of 0.7 μmol kg^{-1}) into 50 mL Falcon™ tubes and stored frozen until analysis. Nitrate (NO_3 + NO_2) was reduced to NO using an acidic solution of V^{3+} (Braman and Hendrix, 1989) and measured by chemoluminescence (Teledyne T200U). Each sample was injected in triplicate and alternated with KNO_3 standards in order to minimize analytical error. The detection limit for the method was 0.05 μmol kg^{-1}.

Ammonium (NH_4^+) Concentrations

Samples (4 mL) were filtered using GF/F into 10 mL Falcon™ tubes and immediately analyzed. Samples and NH_4^+ standard

replicates were reacted with 1 mL of orthophthaldialdehyde (OPA) solution for 2 h in the dark and quantified using a fluorometer (Turner Designs) at 350 nm/410–600 nm of excitation and emission wavelength, respectively, with a detection limit of 0.01 μmol kg^{-1}. The method was modified from Holmes et al. (1999) and Letscher et al. (2013).

Phosphate (PO_4^{3-}) Concentrations

Samples were filtered using GF/F into 50 mL Falcon™ tubes and frozen until analysis. Concentrations were determined colorimetrically following Strickland and Parsons (1968) using a Shimadzu UV-1800 spectrophotometer. Samples and KH_2PO_4 standards were reacted with 1 mL of ascorbic acid + 1 mL of mixed reagent for 30 min and read at 880 nm abs, at a detection limit of 0.05 μmol kg^{-1}.

Silicic Acid (SiO_4^{2-}) Concentrations

Samples from the light incubations were collected into 50 mL Falcon™ tubes, frozen upright and analyzed at the end of light experiment (15 days). Samples and standards (25 mL) were mixed with 10 mL of molybdate solution in pre-cleaned Falcon™ tubes. After 10 min, 15 mL of reducing reagent was added to the solution and results were quantified by spectrophotometry after 1 h at 810 nm wavelength, with a detection limit of 0.1 μM (Strickland and Parsons, 1968).

Dark Incubations

After 15 days under light conditions, the waters were prepared for dark incubations in order to measure heterotroph production/consumption processes. For each replicate in each treatment, 80% of the whole water was passed through pre-combusted GF/F filters; the filtrate was then recombined with the remaining 20% of unfiltered water. This filtration aimed to remove the majority of autotrophs and particulate organic matter (POM), relieved grazing pressure and allowed bacteria to grow primarily on DOM. The strong upwelling simulation was subdivided into subsequent treatments (**Figure 1**), i.e., dark incubations with and without inorganic nutrient additions. All chemical parameters were measured immediately before and after filtration for each replicate, and are shown as averaged values since the differences were not significant.

Dark Incubations Without Nutrient Additions

The simulations were grown in polycarbonate carboys in the dark under controlled temperature (∼22°C) for a 35 days period. The parameters collected at different time points were the same as for light treatments absent phytoplankton fluorescence intensity and silicic acid, and are detailed in section Light Incubations.

Dark Incubations With Nutrient and Metal Additions

In order to determine if inorganic nutrients and trace metals influence dissolved organic production/consumption, a fraction of the strong upwelling incubation received inorganic nutrient additions of 5 μmol kg^{-1} NO_3 + 1 μmol kg^{-1} PO_4 at the beginning of the dark incubation. Another fraction received the same concentration of inorganic nutrients and a cocktail of trace metals (Fe.EDTA, Zn, Mn, Co, and Cu) to final concentrations of 0.1 μmol kg^{-1} for each metal. These last incubations were named $Strong_{+nuts}$ and *TRACE*, respectively, and were carried out in duplicate for 35 days, following the same procedures as dark incubations from section Dark Incubations Without Nutrient Additions.

Statistical Analyses

We conducted several statistical tests in order to examine the significance of differences between specific treatments depending

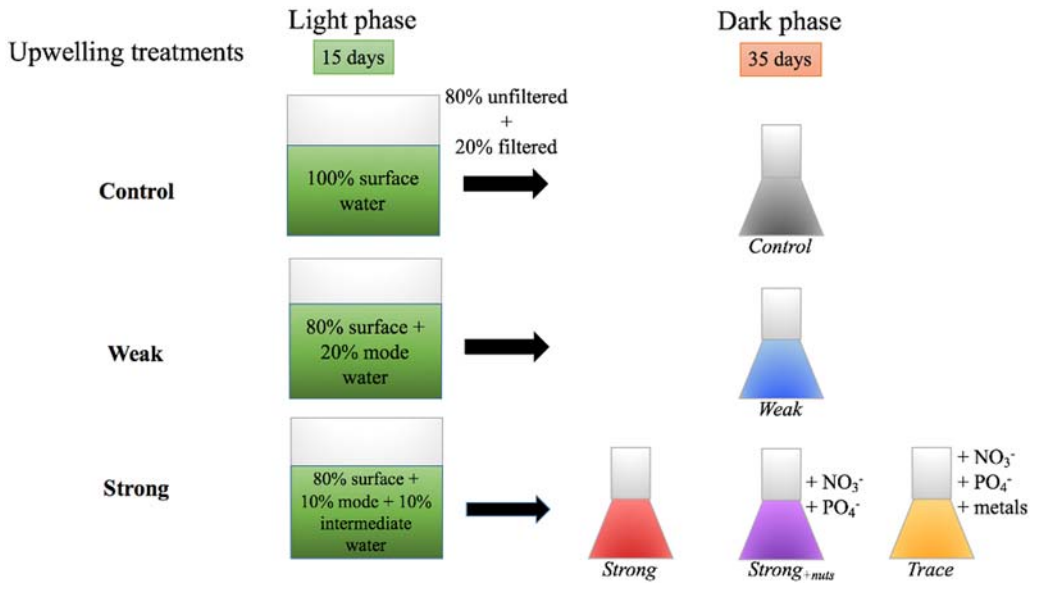

FIGURE 1 | Incubation scheme for the upwelling simulations. The experiments involved a 15 days light treatment followed by 35 days dark incubations, the latter with and without inorganic nutrient additions (red and purple vials), and trace metals (yellow vial).

on the data's normal distribution through Shapiro–Wilk test (Shapiro and Wilk, 1965). For normally-distributed data, analysis of variance (ANOVA) coupled with Tukey's *post hoc* test was performed for each parameter. For non-parametric data, Kruskal–Wallis test coupled with Dunn's *post hoc* with uncorrected significance was the most suitable analysis based on our data distribution. The statistical tests were performed using the freeware Past3 (v. 3.14) (Hammer et al., 2001) with an alpha level $\alpha = 0.05$; the results are shown throughout the text.

RESULTS

Characterization of the Waters for Incubations

Data from a section across Florida Strait at 27°N and between 79° and 80∘W are shown in **Figure 2**. The Florida Current, which passes northward through the strait, receives contributions from the North and South Atlantic Oceans via the Gulf of Mexico (Schmitz and McCartney, 1993; Schmitz, 1996; Talley et al., 2011). This region is directly influenced by both wind-driven and bathymetric-driven upwellings during the summer months that last 1–3 weeks. The events increase nutrient concentrations at surface up to 19 μM for NO_3^-, as previously documented, and are an important local source of nutrients (Pitts and Smith, 1997; Zhang et al., 2017). The waters collected for the experiments were from three depths (5, 300, and 600 m), each with distinctive nutrient properties. The surface water (control) had initial DOC and NO_3^- concentrations of ∼90 and ∼2 μmol kg^{-1}, respectively. At 300 m, Subtropical Mode Water (MW) ($26.5 < \sigma_\theta < 26.6$ kg m^{-3}; ∼18°C) originating in the western North Atlantic was present with low DOC (∼47 μmol kg^{-1}) and NO_3^- concentrations of ∼15 μmol kg^{-1}. The 600 m water was classified as upper Antarctic Intermediate Water (AAIW) ($27.0 < \sigma_\theta < 27.3$ kg m^{-3}; $7° < T < 12°$), characterized by high silicic acid concentrations ∼16 μmol kg^{-1}, low DOC ∼44 μmol kg^{-1} and high nitrate and phosphate ∼30 and 2 μmol kg^{-1}, respectively (**Figure 2**).

Given the variable DOC and nutrient concentrations across the water masses, mixing generated a range of initial conditions for the incubations. In comparison to the control, prepared with unmodified surface whole water, the weak upwelling treatment, enriched with 20% MW, had higher initial inorganic nutrient and lower DOC and DON concentrations. For the strong upwelling treatment, enriched with 10% AAIW and 10% MW, inorganic nutrients were the highest while initial DOC and DON were the lowest across the treatments (**Figure 3**).

Phytoplankton Response in the Light Experiments

Figure 3A shows changes in phytoplankton fluorescence intensity for each upwelling simulation during the light treatment. Intensity remained very low in the control through the 15 days, while a smaller peak was observed in the weak upwelling at day 12 (∼100 RFU) and a larger peak in the strong upwelling at day 9 (∼250 RFU). Samples from these

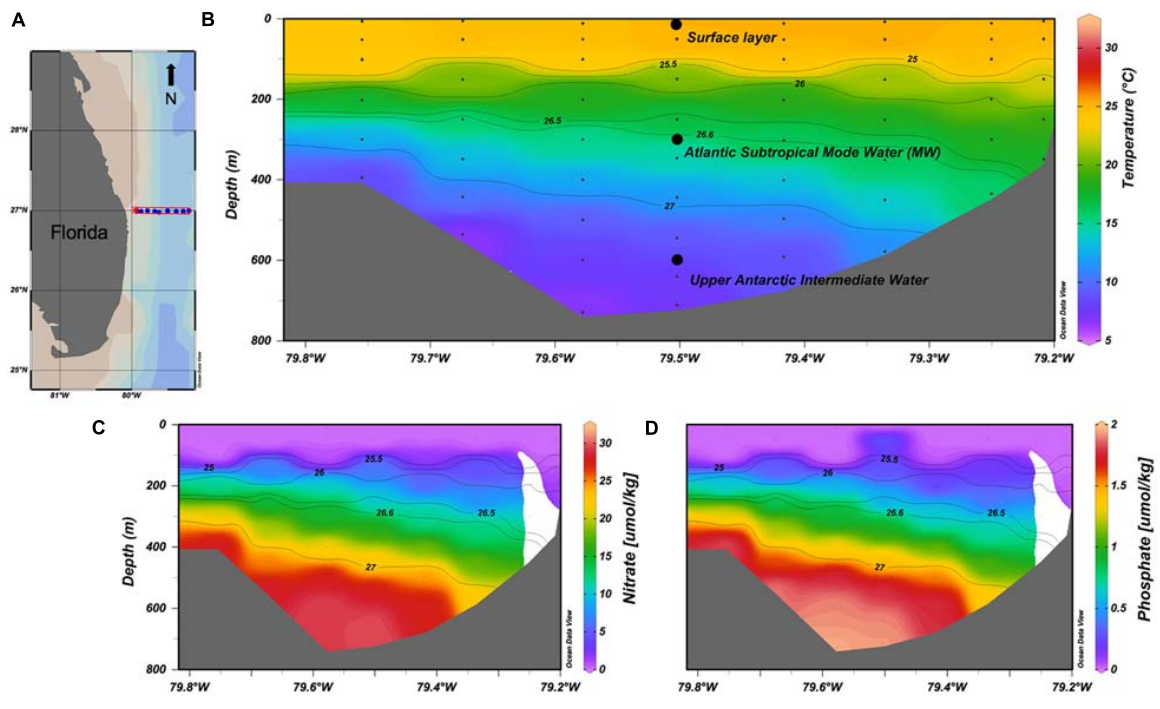

FIGURE 2 | In color, temperature **(B)**, nitrate concentrations **(C)**, and phosphate concentrations **(D)** in the Florida Strait **(A)** at the time of the cruise. All section plots are overlain with distributions of potential density (σ_θ). The sampling location and depths are shown in relation to water masses sampled **(B)**. Plotted using Ocean Data View software (Schlitzer, 2018).

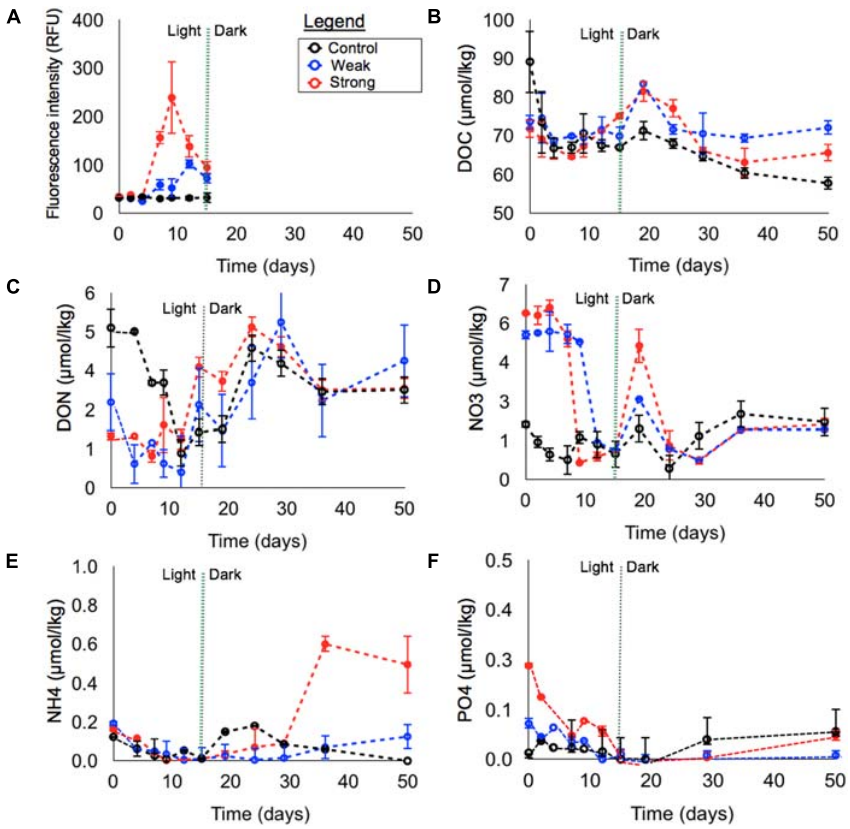

FIGURE 3 | Variation in concentrations versus time in light and subsequent dark incubations, separated by vertical dashed lines. Fluorescence intensity (RFU) **(A)**, DOC **(B)**, DON **(C)**, NO_3^- **(D)**, NH_4^+ **(E)**, and PO_4^{-3} **(F)**. Error bars are ± 1 S.D. from triplicates.

time points were analyzed qualitatively by microscopy to identify groups of phytoplankton that were growing; biomass concentrations (i.e., cell density) were not determined due to the limited volume of samples. The control showed an absence of phytoplankton cells, likely due to their low abundance. Both weak and strong upwelling conditions contained groups, during the RFU maximum, that are typical from the open ocean, such as diatoms from the Coscinodiscaceae family; dinoflagellates such as *Protoperidinium* sp. and *Neoceratium* sp. were present as well.

The concentrations of silicic acid (data not shown) in the light treatments at day 0 were undetectable in the control and weak upwelling treatments ($SiO_4^{2-} < 0.1$ µmol kg^{-1}), and was 4.1 µmol kg^{-1} in the strong upwelling; the nutrient was depleted by day 7 ($SiO_4^{2-} < 0.1$ µmol kg^{-1}). Full SiO_4^{2-} consumption in the strong upwelling resulted in accumulation of *Dactyliosolen* sp. chains at day 9, which corresponded to the maximum fluorescence intensity (**Figure 3A**).

Biogeochemical Variability Through Light and Dark Conditions

In the first 4 days, all treatments experienced net heterotrophy, as evidenced by net DOC loss (**Table 1**), and the absence of autotroph growth, as shown by unchanged fluorescence intensity (**Figure 3A**). Thus, we considered these initial days as the lag phase for photoautotroph acclimation in the incubations.

At the beginning of the light experiments, DOC concentrations were ∼89, 74, and 72 µmol kg^{-1} in control, weak and strong simulations, respectively. After 4 days, DOC changed by -22.3 µmol kg^{-1} in the control, -4.9 µmol kg^{-1} in the weak upwelling and -5.2 µmol kg^{-1} in the strong (**Figure 3B** and **Table 1**), to relatively uniform values of ∼67, 69, and 67 µmol kg^{-1}, respectively. During the lag phase, there was little to no change in DON in both control and strong treatments, and a change of -1.9 µmol kg^{-1} in the weak upwelling (**Figure 3C** and **Table 1**). For DIN (sum of NO_3^- and NH_4^+), 1.24 µmol kg^{-1} was consumed in the control; NH_4^+ was nitrified in the weak treatment according to mass balance (0.13 µmol kg^{-1} loss of NH_4^+ versus 0.1 µmol kg^{-1} gain of NO_3^-), while there was low net production of 0.16 µmol kg^{-1} in the strong upwelling treatment (**Figures 3D,E** and **Table 1**). During the same period, PO_4^{3-} had minor changes in all treatments (**Figure 3F** and **Table 1**).

Control Treatment

By the end of 15 days, the control experienced a decrease of 22.5 µmol kg^{-1} DOC, 3.2 µmol kg^{-1} DON and 1.2 µmol kg^{-1} DIN, with NH_4^+ falling to below detection limits (**Figure 3**

TABLE 1 | Net change of variables for the given periods and fractional shift in relation to initial concentrations.

		Net production/consumption (μmol kg^{-1})						Fractional shift from initial concentration				
Upwelling treatment	**Days**	**ΔDOC**	**ΔDON**	**ΔNO_3**	**ΔNH_4**	**ΔDIN (NO_3+NH_4)**	**ΔPO_4**	**DOC**	**DON**	**NO_3**	**NH_4**	**PO_4**
LIGHT PHASE												
Control	0–15	−22.5	−3.2	−1.05	−0.11	−1.16	BLD	−0.249	−0.652	−0.526	−0.889	BLD
Weak upwelling	0–4	−4.9	−1.9	0.13	−0.10	0.03	0	−0.066	−0.719	0.025	−0.684	NCH
	4–12	2.8	−0.3	−3.98	−0.05	−4.03	−0.08	0.028	−0.817	−0.743	−0.974	−1.000
Strong upwelling	0–4	−5.2	0	0.20	−0.04	0.16	−0.16	−0.072	NCH	0.030	−0.271	−0.667
	4–15	8.5	2.7	−5.12	−0.11	−5.22	−0.07	0.046	1.320	−0.824	−0.938	−0.958
DARK PHASE												
Control	15–50	−9.3	1.3	1.16	−0.01	1.15	0.07	−0.352	0.389	0.048	−1.000	2.500
Weak upwelling	12–50	0.5	3.4	0.46	0.12	0.58	0.05	−0.021	0.485	0.654	−0.342	−0.889
Strong upwelling	15–50	−9.5	−0.7	0.92	0.48	1.40	0.06	−0.087	0.908	0.670	2.094	−0.750
$Strong_{+nuts}$	15–50	−8.2	−1.4	−2.12	2.19	0.07	0.85	−0.065	0.428	−0.355	1.278	3.500
Trace	15–50	−7.8	0.5	−4.79	1.78	−3.01	0.15	−0.098	1.306	−0.729	1.019	0.333

Negative values mean drawdown and positive values mean net production. BLD, concentration fall below method's limit of detection; NCH, No net change in concentration.

and **Table 1**); PO_4^{-3} remained < 0.1 μmol kg^{-1} (**Figure 3F**). During the dark phase (from days 15 to 50), ΔDOC was -9.3 μmol kg^{-1}, indicating further net consumption, while there was an accumulation of DON (+1.3 μmol kg^{-1}) and DIN (+1.2 μmol kg^{-1}), with consistently < 0.1 μmol kg^{-1} PO_4^{-3} (**Figure 3F**). Overall, the control experienced a total DOC decrease of ∼31 μmol kg^{-1} after 50 days (**Figure 3B**), with statistically significant changes between light and dark phases ($p < 0.05$).

Weak Upwelling Treatment

Between days 4 and 12, there was a significant increase in autotroph fluorescence and DOC net production of ∼3 μmol kg^{-1}, with essentially unchanged DON (−0.3 μmol kg^{-1}). During this period, PO_4^{3-} and NH_4^+ were brought below detection limits, while ∼4 μmol kg^{-1} of NO_3^- was consumed (**Figure 3** and **Table 1**). After 12 days of light incubation, both DOC and DON had dropped ∼2 μmol kg^{-1}. From days 12 to 15 the system appears net heterotrophic, with chlorophyll decreasing along with the consumption of DOC = ∼2 μmol kg^{-1} (**Figures 3B,C**); as such, this 3 day period will be discussed together with the subsequent dark phase. DOC concentration was ∼74 μmol kg^{-1} at the beginning of the light incubation, and ∼71 and 70 μmol kg^{-1} at days 12 and 15, respectively. After 50 days of experiment, DOC experienced a net decrease of ∼2 μmol kg^{-1} C down to ∼72 μmol kg^{-1} (**Figure 3B**), a net change that was not statistically significant between light and dark phases ($p > 0.05$).

Strong Upwelling Treatment

The treatment experienced net autotroph growth between days 4 and 15 as evidenced by net DOC and DON production (+8.5 and +2.7 μmol kg^{-1}, respectively); significant removal of NO_3^- (-5.12 μmol kg^{-1}) and PO_4^{-3} (-0.07 μmol kg^{-1}) occurred, while NH_4^+ was drawn down to below detection limit (**Figure 3** and **Table 1**). The subsequent dark phase showed net consumption of DOC and DON (-9.5and -0.7 μmol kg^{-1}, respectively) (**Figures 3B,C**), similar to DOC remineralization in the control during the dark phase (-9.3 μmol kg^{-1}) and contrasting with unchanged DOC in the weak upwelling. DIN was produced at +1.4 μmol kg^{-1} while PO_4^{-3} experienced production, although remained < 0.1 μmol kg^{-1} (**Table 1** and **Figure 3F**). DOC was ∼72 μmol kg^{-1} at the beginning of the strong upwelling simulation and increased to ∼75 μmol kg^{-1} after 15 days, at the beginning of dark experiment. After 50 days, DOC was drawn down to ∼66 μmol kg^{-1} (**Figure 3B**), a net consumption of ∼6 μmol kg^{-1} C ($p < 0.05$ between light and dark phases). Changes in net DOC and DON concentrations through the incubations were statistically significant between control, weak and strong upwelling treatments ($p < 0.01$) for both light and dark phases, and when evaluated as a single continuous incubation.

After the addition of inorganic nutrients and trace metals (**Figure 4**), DOC did not show a significant difference between treatments by the end of the incubation ($p > > 0.05$ among strong upwelling, $Strong_{+nuts}$ and *TRACE*), with averaged DOC consumption of 8.5 ± 0.7 μmol kg^{-1} C by day 50. For nitrogen pools, strong and $Strong_{+nuts}$ upwelling treatments showed similar DON consumption of ∼1 μmol kg^{-1} ($p > > 0.05$), while *TRACE* showed slight production of 0.5 μmol kg^{-1} (**Figure 4B**). NO_3^- was consumed in $Strong_{+nuts}$ (2.1 μmol kg^{-1}) and at higher levels in *TRACE* (4.8 μmol kg^{-1}) (**Figure 4D**), as opposed to the strong upwelling treatment with no additions, that showed net production of 0.92 μmol kg^{-1} NO_3^-. NH_4^+ production was higher in treatments with additions: 2.19 μmol kg^{-1} in $Strong_{+nuts}$ and 1.78 μmol kg^{-1} in *TRACE* versus 0.48 μmol kg^{-1} in strong (**Figure 4C**). For the same period, PO_4^{-3} was produced in $Strong_{+nuts}$ (0.85 μmol kg^{-1}) and *TRACE* (0.15 μmol kg^{-1}), as opposed to the strong upwelling treatment, that did not show significant changes after 50 days (**Figure 4E** and **Table 1**).

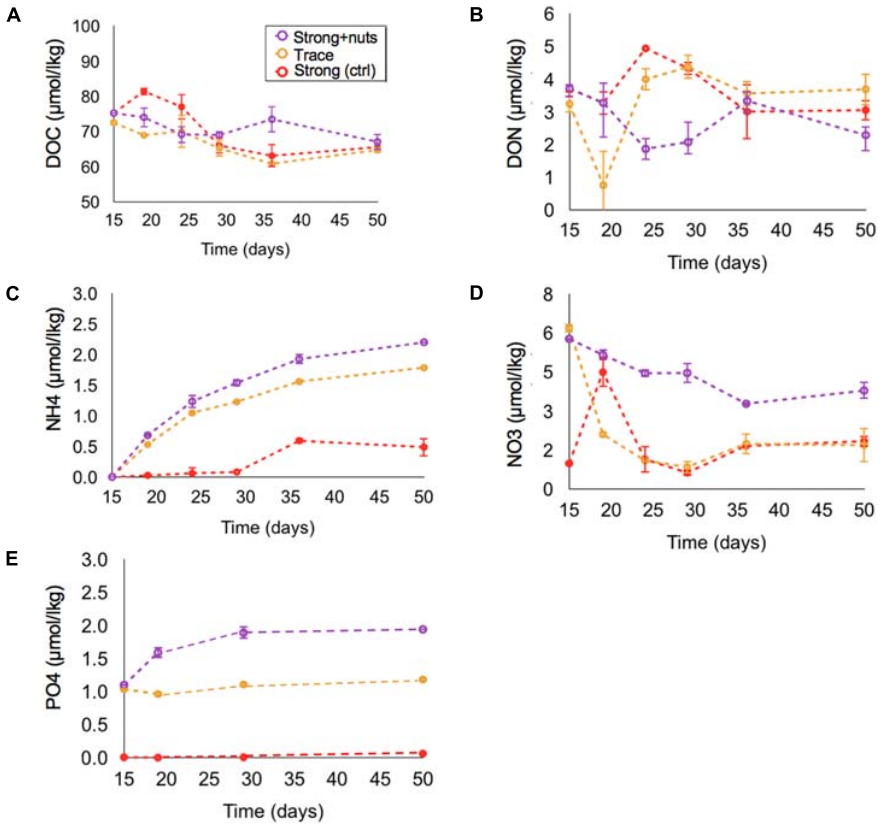

FIGURE 4 | Variation in concentrations versus time in the strong upwelling treatments following inorganic nutrient additions and/or trace metals: DOC **(A)**, DON **(B)**, NH_4^+ **(C)**, NO_3^- **(D)**, PO_4^- **(E)**. Error bars are ± 1 S.D. from triplicates.

DIN:DIP

Initial DIN:DIP ratios in all treatments suggest they were P-depleted at the time of collection, with values of 126:1 for control, 60:1 for the weak upwelling and 26:1 for the strong upwelling (**Table 2**). During the light phase with phytoplankton growth from day 4 to 12 in the weak treatment, and from day 4 to 15 in the strong treatment, DIN and PO_4^{-3} were consumed at different proportions until PO_4^{-3} fell below detection limits (**Figures 3D–F**). During this period of positive NCP, DIN:DIP increased in the weak upwelling, reaching 107:1 by day 9. In contrast, the ratio for the strong upwelling was reduced to 12:1 by day 12. Subsequent PO_4^{3-} concentrations were below detection limits in both treatments so ratios were not calculated.

Net Community Production (NCP), Net Dissolved Production Ratio (NDPr), and DOM Quality

In order to compare DOC produced during the weak versus strong upwelling simulations, we estimated net community production (NCP), net dissolved production ratios (NDPr; Romera-Castillo et al., 2016) and DOC:DON ratios, with the last parameter used as a proxy for DOM quality.

We estimated NCP in units of carbon during the light phase from DIN drawdown (ΔDIN *6.6) to the point where PO_4^{3-} was below the limit of detection in both weak and strong upwellings (**Table 1**). Days 0–4 were net heterotrophic for both experiments as confirmed by low fluorescence intensity, net DOC consumption and NO_3^- remineralization (**Figures 3A,B,D**), thus, were not considered in the calculations. In the weak upwelling, NCP was estimated as 26.6 µmol kg^{-1} C for the period

TABLE 2 | Derived variables for light and dark incubations in the given periods.

Upwelling treatment	Days	DOC:DON	NCP (µM C)	NDPr (ΔDOC/NCP)
Control	0	18		
	15	39		
Weak upwelling	0	28		
	4	93		
	12	149	26.6	0.11
	50	26		0.12
Strong upwelling	0	45		
	4	42		
	15	20	34.5	0.25
	50	20		-0.03

*DOC:DON, dissolved organic carbon and nitrogen ratios at a given day of light incubation; NCP, net community production converted to carbon units as ΔDIN * 6.6; NDPr, net DOC production ratio for periods where net production is positive and by the end of incubations at day 50.*

between days 4 and 12, while in the strong it was estimated as 34.5 μmol kg^{-1} C between days 4 to 15, as summarized in **Table 2** ($p < 0.01$). We then calculated the Net DOC Production ratio (NDPr), or the fraction of NCP that accumulated as DOC in the incubations, from ΔDOC/NCP for the same period. The ratio was 0.11 for the weak upwelling and 0.25 for the strong (**Table 2**). The values indicate that a smaller fraction of NCP accumulates as DOC in the weak upwelling, while in the strong upwelling twice as much of the NCP accumulated as DOC. The outcome suggests that under light (autotrophic) conditions, higher initial nutrient conditions resulted in a higher fraction of the NCP present as DOC.

The variation in the DOC:DON ratio during the light incubations was used as a proxy for the quality of DOM accumulated, as well as for the quality of DOM remaining during the dark phase. **Table 2** shows calculated ratios for initial conditions, as well as the average for periods of net autotrophy and heterotrophy. DOM produced in the weak upwelling was DON-poor relative to the strong upwelling. In the beginning of the experiment, DOC:DON for the weak upwelling was 28:1, and increased to 149:1 by day 12. In contrast, the ratio for the strong upwelling was 45:1 initially, decreasing to 20:1 by day 15. On average, DOC:DON during positive NCP phases remained unchanged in the strong upwelling, but increased significantly along the weak upwelling treatment ($p << 0.01$).

DISCUSSION

Net Production of DOC

Coastal upwelling events typically last from a few days to 1–2 weeks (Pitts and Smith, 1997; Wetz and Wheeler, 2004), resulting in phytoplankton blooms until the depletion of one or more essential nutrients such as N, P, and Fe (Arrigo, 2005; Hutchins and Fu, 2008; Burson et al., 2016). In this study, lower initial concentrations of inorganic nutrients in the weak upwelling treatment, especially PO_4^- (**Figure 3**), resulted in NCP = ∼27 μmol kg^{-1} C, with a smaller fraction accumulating as DOC (NDPr = 11%; **Table 2**). The accumulated DOM was carbon-enriched, with a C:N molar ratio of 149:1. In contrast, the strong upwelling treatment resulted in higher NCP (∼35 μmol kg^{-1} C), with a higher fraction accumulating as DOC (NDPr = 25%) and with a lower C:N molar ratio of 20:1 (**Figure 5A**). Phytoplankton composition was also different between the two treatments, as we observed chains of the diatom *Dactyliosolen* sp. during the high relative fluorescence peak in the strong upwelling treatment. These results suggest that different nutrient availability promotes the growth of distinct microbial communities that release DOM of different composition and reactivity, in agreement with previous studies (Conan et al., 2007; Wear et al., 2015; Saad et al., 2016).

Wetz and Wheeler (2004), who similarly simulated upwelling systems, showed that NO_3^--depletion ceased phytoplankton growth and this was followed by DOC accumulation. For comparison with the work done here, we estimate NCP and NDPr ratios using their results. Their NCP ranged between 198 and 290 μmol kg^{-1} C and NDPr from 0.25 to 0.39, with a diatom (*Leptocylindrus minimus*) dominating the community exhibiting lower NDPr values and *Chaetoceros* sp. dominating the higher. Variations in NCP and NDPr did not correlate with bacterial physiological state (high versus low nucleic acid content in bacteria) or grazers, suggesting that the autotroph composition exerted a more direct control on NDPr. NDPr from both Wetz and Wheeler (2004) and our results fall within ratios of 0.10–0.40, as observed across a variety of ecosystems experiencing different ecological states and NCP magnitudes (Hansell and Carlson, 1998; Conan et al., 2007; Mathis et al., 2007; Romera-Castillo et al., 2016). These results reinforce the

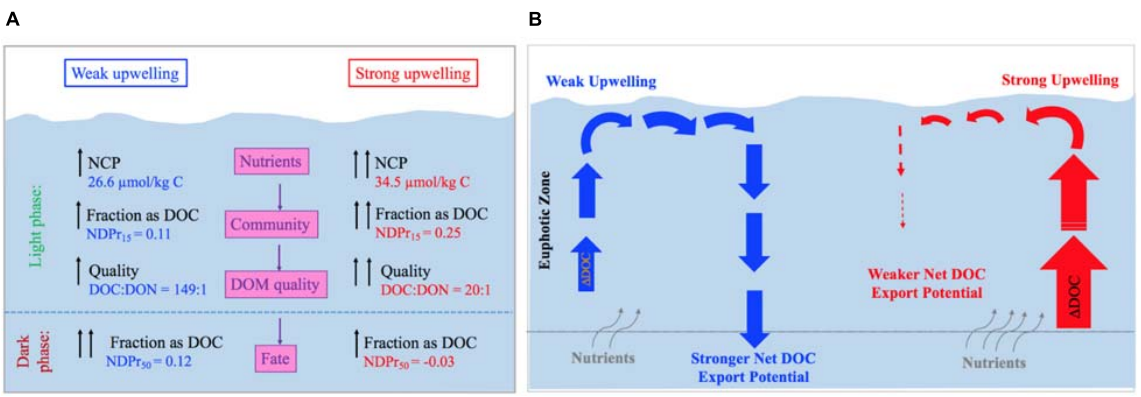

FIGURE 5 | (A) Chart comparing net community production (NCP) and organic matter dynamics in the weak (left side) and strong (right side) upwelling simulations during light and dark phases. Weak upwelling resulted in the production of a DOC fraction that was resistant to heterotrophic consumption, while higher nutrients in the strong upwelling favored net community production of a more labile DOC that was fully consumed over the course of the incubation. Fraction accumulated as DOC = $NDPr_{15}$ for light incubation and $NDPr_{50}$ for dark incubation; DOM Quality is as indicated by the DOC:DON ratios at day 15 (i.e., last day of light incubation). **(B)** From ∼27 μmol kg^{-1} C produced during positive NCP in the weak upwelling simulation, 3 μmol kg^{-1} (11%) accumulated as DOC. This fraction fully resisted microbial remineralization along >1 month of dark incubation and, thus, has potential to be exported out of the euphotic zone. In contrast, the stronger upwelling simulation produced 35 μmol kg^{-1} C, by which 9 μmol kg^{-1} (25%) accumulated as DOC. This fraction was subsequently and fully consumed, demonstrating this initial upwelling condition unlikely contributes for DOC export to the deep ocean.

importance of microbial community composition in controlling the net production of DOC.

The Fate of the Accumulated DOC

Although several previous works have addressed the impact of microbial communities on NCP and net DOC production, what happens after this DOC is released to the environment is unclear. The dark phase of our incubations indicate that DOC produced in the different upwelling treatments had different fates. In the weak upwelling, the fraction of DOC resulting from positive NCP (0.11) was not further remineralized in the dark, giving a relatively unchanged NDPr = 0.12 at 50 days (**Table 2**). In contrast, the strong upwelling treatment showed net DOC consumption in the dark phase, indicating further removal in the dark and a final NDPr = −0.03 (i.e., total consumption of accumulated DOC at 50 days). The strong upwelling incubation received microbes from deep waters that could have stimulated DOM consumption. Indeed, dark incubations using surface waters from the South Pacific showed higher DOC consumption when exposed to microbes from the mesopelagic zone than from the mixing layer (Letscher et al., 2015). When comparing DOC consumption between mesopelagic microbes exposed to oligotrophic versus mesotrophic waters, those from the mesotrophic region consumed more DOC. The two mesotrophic microbial communities, however, were only exposed to their locally accumulated DOM, that was dependent on the magnitude NCP and had different composition. The link between accumulated DOM and its potential to be exported, thus, still seems to be the production side. Hence, results from our dark incubations suggest that DOC accumulated from upwellings of different intensities experience different fates, where reactivity is dependent on the quality of accumulated DOM (as evidenced by DOC:DON ratios), itself dependent on the autotroph composition (**Figure 5A**).

A study comparing the Ross and Sargasso Seas, similarly, suggested a link between net DOM production and the ultimate fate of the accumulated fraction (Carlson et al., 1998). The authors assessed differences in DOC-POC partitioning, as well as production and consumption between the two systems, which are very distinctive in terms of PP, community composition and availability of nutrients. Although PP in the Ross Sea was much higher than in the nutrient-depleted Sargasso Sea, DOC represented a smaller fraction (11%) of the total accumulated organic carbon pool (DOC plus POC) in the Ross Sea compared to the Sargasso Sea (∼15–20%). As found in the study reported here, accumulated DOC in the productive Ross Sea was consumed more completely late in the season than that produced in the less productive Sargasso Sea, with the latter DOM typically surviving until export with convective overturn (Hansell and Carlson, 2001).

Sensitivity of DOC Consumption to Inorganic Nutrients and Trace Metals Additions

Our results for the inorganic nutrient and trace metals amendments indicate no change in DOC concentrations relative to non-amended conditions (**Figure 4A**, $p > > 0.05$). The amended treatments did experience higher NO_3^- consumption and PO_4^{3-} production in comparison to the strong upwelling without additions (the control treatment for this addendum experiment), and enhanced NH_4^+ production (**Figure 4** and **Table 1**), but none of these had consequence for DOC or DON concentrations.

Limitation by inorganic nutrients and trace metals has been well documented for autotrophs (Arrigo, 2005; Schoffman et al., 2016), but its role in heterotroph metabolism requires attention. Heterotrophic bacteria are able to assimilate NO_3^-, as observed in the North Pacific and Atlantic Oceans (Kirchman, 1994; Kirchman and Wheeler, 1998), thus competing with phytoplankton for the nutrient. The availability of NO_3^- promotes changes in bacterial community structure and may favor the assimilation of less labile DOM fractions (Carlson et al., 2004), however, the role of PO_4^{3-} in bacterial catabolism of DOM is uncertain. Some experiments with PO_4^{3-} amendments show that its addition enhances bacterial growth in oligotrophic waters (Rivkin and Anderson, 1997; Obernosterer et al., 2003) and that P limitation results in less DOM consumption (Kragh and Søndergaard, 2009). In contrast, other studies showed no relationship between bacterial production and PO_4^{3-} (Thingstad et al., 2005; Tanaka et al., 2011) or heterotrophic growth and DOM consumption (Carlson and Ducklow, 1996; Zweifel, 1999). Interestingly, amendment by 1 μmol kg^{-1} PO_4^{3-} here resulted in a further production of ∼0.85 μmol kg^{-1} PO_4^{3-} (**Figure 4E**), suggesting that the amendment may overcome phosphorus limitation of dissolved organic phosphorus (DOP) mineralization by microbes; unfortunately, DOP was not measured directly in this work.

Heterotrophic bacteria also compete with phytoplankton for trace elements, especially Fe, as their requirement for the element is high (Tortell et al., 1996). Lower concentrations of Fe decrease bacterial growth efficiency and increase their carbon demand due to its critical role in respiratory activity (Tortell et al., 1999). More recently, *in situ* experiments involving iron fertilization in the Southern Ocean observed the indirect effect of the element to bacterial communities. Although bacterial diversity increased with increasing Fe (West et al., 2008), other environmental conditions control their growth since a less dramatic shift is observed in comparison to phytoplankton (Hutchins et al., 2001; Arrieta et al., 2004). A study conducted by Kirchman et al. (2003) suggested low growth rate and efficiency in *Vibrio harveyi* due to Fe and NO_3^- co-limitation, and perhaps explaining low activities in bacterial communities from high-nutrient low-chlorophyll (HNLC) regions. Although our experiments did not assess bacterial growth efficiency or rates, they support Kirchman's findings that trace metal additions stimulated NO_3^- uptake by more than 2× in comparison to the strong and $Strong_{+nut}$ treatments (**Figure 4** and **Table 1**).

OVERVIEW

The initial availability of inorganic nutrients not only dictates the magnitude of NCP, but also the quantity and quality of freshly-accumulated DOM (**Figure 5A**). In the weak upwelling simulation, early depletion of PO_4^{3-} resulted in

a relatively low NCP, with a small fraction accumulating as DOC. However, net DOC remained unchanged by the end of experiment, suggesting that a transition from nutrient-replete to -deplete conditions produces a fraction of DOC that resists remineralization (rather than DOC consumption being controlled by nutrients, as that scenario was assessed with amendments), allowing its survival for export to greater depths through mixing processes (**Figure 5B**). In contrast, availability of nutrients in the strong upwelling treatment stimulated NCP, with ∼25% of net fixed carbon accumulating as DOC. This fraction was subsequently and fully remineralized within ∼1 month in the dark. This contrasting outcome suggests that, even though more DOC accumulates as a result of high NCP, it may not survive for export when quality, as indicated by low C:N, is higher; thus, it is less likely to contribute to long-term DOC storage and export in the ocean (**Figure 5B**).

AUTHOR CONTRIBUTIONS

MB conducted the experiments, analyzed the data, wrote the manuscript. DH contributed to the experiment design, quality of figures, provided valuable insights in the discussion, as well as edited the manuscript. KP contributed to the interpretation of results and edited the manuscript.

FUNDING

MB has a Ph.D. Fellowship supported by Cnpq (Conselho Nacional de Desenvolvimento Científico e Tecnológico), Process No. 205233/2014-7. DH was supported by NSF award OCE-1436748.

ACKNOWLEDGMENTS

We thank 27°N NOAA cruise Chief Scientist Ryan Smith for the opportunity to join the cruise and collect water samples for the experiments, Research Associate Lillian Custals for support in DOC and DON analyses, and Dr. Larry Brand for use of his incubation facilities at RSMAS.

REFERENCES

Abbott, M. R., and Zion, P. M. (1985). Satellite observations of phytoplankton variability during an upwelling event. *Cont. Shelf Res.* 4, 661–680. doi: 10.1016/0278-4343(85)90035-4

Arrieta, J. M., Weinbauer, M. G., Lute, C., and Herndl, G. J. (2004). Response of bacterioplankton to iron fertilization in the Southern Ocean. *Limnol. Oceanogr.* 49, 799–808. doi: 10.3389/fmicb.2015.00863

Arrigo, K. R. (2005). Marine microorganisms and global nutrient cycles. *Nature* 437, 349–355. doi: 10.1038/nature04159

Braman, R. S., and Hendrix, S. A. (1989). Nanogram nitrite and nitrate determination in environmental and biological materials by vanadium (III) reduction with chemoluminescence detection. *Anal. Chem.* 61, 2715–2718. doi: 10.1021/ac00199a007

Burson, A., Stomp, M., Akil, L., Brussaard, C. P., and Huisman, J. (2016). Unbalanced reduction of nutrient loads has created an offshore gradient from phosphorus to nitrogen limitation in the North Sea. *Limnol. Oceanogr.* 61, 869–888. doi: 10.1002/lno.10257

Carlson, C. A., and Ducklow, H. W. (1996). Growth of bacterioplankton and consumption of dissolved organic carbon in the Sargasso Sea. *Aquat. Microb. Ecol.* 10, 69–85. doi: 10.3354/ame010069

Carlson, C. A., Ducklow, H. W., Hansell, D. A., and Smith, W. O. Jr. (1998). Organic carbon partitioning during spring phytoplankton blooms in the Ross Sea polynya and the Sargasso Sea. *Limnol. Oceanogr.* 43, 375–386. doi: 10.4319/lo.1998.43.3.0375

Carlson, C. A., Ducklow, H. W., and Michaels, A. F. (1994). Annual flux of dissolved organic carbon from the euphotic zone in the northwestern Sargasso Sea. *Nature* 371, 405–408. doi: 10.1038/371405a0

Carlson, C. A., Giovannoni, S. J., Hansell, D. A., Goldberg, S. J., Parsons, R., and Vergin, K. (2004). Interactions among dissolved organic carbon, microbial processes, and community structure in the mesopelagic zone of the northwestern Sargasso Sea. *Limnol. Oceanogr.* 49, 1073–1083. doi: 10.4319/lo.2004.49.4.1073

Conan, P., Søndergaard, M., Kragh, T., Thingstad, F., Pujo-Pay, M., Williams, P. J. L. B., et al. (2007). Partitioning of organic production in marine plankton communities: the effects of inorganic nutrient ratios and community composition on new dissolved organic matter. *Limnol. Oceanogr.* 52, 753–765. doi: 10.4319/lo.2007.52.2.0753

Copin-Montégut, G., and Avril, B. (1993). Vertical distribution and temporal variation of dissolved organic carbon in the North-Western Mediterranean Sea. *Deep Sea Res. Part 1 Oceanogr. Res. Pap.* 40, 1963–1972. doi: 10.1016/0967-0637(93)90041-Z

Czeschel, L., Eden, C., and Greatbatch, R. J. (2012). On the driving mechanism of the annual cycle of the florida current transport. *J. Phys. Oceanogr.* 42, 824–839. doi: 10.1175/JPO-D-11-0109.1

Dickson, A. G., Sabine, C. L., and Christian, J. R. (2007). *Guide to Best Practices for Ocean CO2 Measurements*. Sidney, BC: North Pacific Marine Science Organization, 191.

Ducklow, H. W., Steinberg, D. K., and Buesseler, K. O. (2001). Upper ocean carbon export and the biological pump. *Oceanography* 14, 50–58. doi: 10.5670/oceanog.2001.06

Dugdale, R. C., and Goering, J. J. (1967). Uptake of new and regenerated forms of nitrogen in primary productivity. *Limnol. Oceanogr.* 12, 196–206. doi: 10.4319/lo.1967.12.2.0196

Guidi, L., Chaffron, S., Bittner, L., Eveillard, D., Larhlimi, A., Roux, S., et al. (2016). Plankton networks driving carbon export in the oligotrophic ocean. *Nature* 532, 465–470. doi: 10.1038/nature16942

Hammer, Ø, Harper, D. A. T., and Ryan, P. D. (2001). PAST: paleontological statistics software package for education and data analysis. *Palaeontol. Electron.* 4:9.

Hansell, D. A. (2005). Dissolved organic carbon reference material program. *EOS Trans. Am. Geophys. Union* 86, 318–318. doi: 10.1029/2005EO350003

Hansell, D. A., and Carlson, C. A. (2001). Biogeochemistry of total organic carbon and nitrogen in the Sargasso Sea: control by convective overturn. *Deep Sea Res. Part 2 Top. Stud. Oceanogr.* 48, 1649–1667. doi: 10.1016/S0967-0645(00)00153-3

Hansell, D. A., and Carlson, C. A. (1998). Net community production of dissolved organic carbon. *Global Biogeochem. Cycles* 12, 443–453. doi: 10.1029/98GB01928

Hansell, D. A., Carlson, C. A., Repeta, D. J., and Schlitzer, R. (2009). Dissolved organic matter in the ocean: new insights stimulated by a controversy. *Oceanography* 22, 202–211. doi: 10.5670/oceanog.2009.109

Hansell, D. A., and Peltzer, E. T. (1998). Spatial and temporal variations of total organic carbon in the Arabian Sea. *Deep Sea Res. II* 45, 2171–2193. doi: 10.1016/S0967-0645(98)00067-8

Hanson, C. E., Pattiaratchi, C. B., and Waite, A. M. (2005). Sporadic upwelling on a downwelling coast: phytoplankton responses to spatially variable nutrient dynamics off the Gascoyne region of Western Australia. *Cont. Shelf Res.* 25, 1561–1582. doi: 10.1016/j.csr.2005.04.003

Holmes, R. M., Aminot, A., Kérouel, R., Hooker, B. A., and Peterson, B. J. (1999). A simple and precise method for measuring ammonium in marine and freshwater ecosystems. *Can. J. Fish. Aquat. Sci.* 56, 1801–1808. doi: 10.1139/f99-128

Hutchins, D. A., Campbell, B. J., Cottrell, M. T., and Takeda, S. (2001). Response of marine bacterial community composition to iron additions in three iron-limited regimes. *Limnol. Oceanogr.* 46, 1535–1545. doi: 10.4319/lo.2001.46.6.1535

Hutchins, D. A., and Fu, F. X. (2008). "Linking the oceanic biogeochemistry of iron and phosphorus with the marine nitrogen cycle," in *Nitrogen in the Marine Environment*, 2nd Edn, eds D. G. Capone, D. A. Bronk, M. R. Mulholland, and E. J. Carpenter (Boston, MA: Academic Press), 1627–1666.

Kirchman, D. L. (1994). The uptake of inorganic nutrients by heterotrophic bacteria. *Microb. Ecol.* 28, 255–271. doi: 10.1007/BF00166816

Kirchman, D. L., Hoffman, K. A., Weaver, R., and Hutchins, D. A. (2003). Regulation of growth and energetics of a marine bacterium by nitrogen source and iron availability. *Mar. Ecol. Progr. Ser.* 250, 291–296. doi: 10.3354/meps250291

Kirchman, D. L., and Wheeler, P. A. (1998). Uptake of ammonium and nitrate by heterotrophic bacteria and phytoplankton in the sub-Arctic Pacific. *Deep Sea Res. Part I Oceanogr. Res. Pap.* 45, 347–365. doi: 10.1016/S0967-0637(97)00075-7

Kragh, T., and Søndergaard, M. (2009). Production and decomposition of new DOC by marine plankton communities: carbohydrates, refractory components and nutrient limitation. *Biogeochemistry* 96, 177–187. doi: 10.1007/s10533-009-9357-1

Letscher, R. T., Hansell, D. A., Kadko, D., and Bates, N. R. (2013). Dissolved organic nitrogen dynamics in the Arctic Ocean. *Mar. Chem.* 148, 1–9. doi: 10.1016/j.marchem.2012.10.002

Letscher, R. T., Knapp, A. N., James, A. K., Carlson, C. A., Santoro, A. E., and Hansell, D. A. (2015). Microbial community composition and nitrogen availability influence DOC remineralization in the South Pacific Gyre. *Mar. Chem.* 177, 325–334. doi: 10.1016/j.marchem.2015.06.024

Lønborg, C., Davidson, K., Álvarez–Salgado, X. A., and Miller, A. E. (2009). Bioavailability and bacterial degradation rates of dissolved organic matter in a temperate coastal area during an annual cycle. *Mar. Chem.* 113, 219–226. doi: 10.1016/j.marchem.2009.02.003

Loureiro, S., Reñé, A., Garcés, E., Camp, J., and Vaqué, D. (2011). Harmful algal blooms (HABs), dissolved organic matter (DOM), and planktonic microbial community dynamics at a near-shore and a harbour station influenced by upwelling (SW Iberian Peninsula). *J. Sea Res.* 65, 401–413. doi: 10.1016/j.seares.2011.03.004

Mathis, J. T., Hansell, D. A., Kadko, D., Bates, N. R., and Cooper, L. W. (2007). Determining net dissolved organic carbon production in the hydrographically complex western Arctic Ocean. *Limnol. Oceanogr.* 52, 1789–1799. doi: 10.4319/lo.2007.52.5.1789

Obernosterer, I., Kawasaki, N., and Benner, R. (2003). P-limitation of respiration in the Sargasso Sea and uncoupling of bacteria from P-regeneration in size-fractionation experiments. *Aquat. Microb. Ecol.* 32, 229–237. doi: 10.3354/ame032229

Passow, U., Christina, L., Arnosti, C., Grossart, H. P., Murray, A. E., and Engel, A. (2007). Microbial dynamics in autotrophic and heterotrophic seawater mesocosms. I. Effect of phytoplankton on the microbial loop. *Aquat. Microb. Ecol.* 49, 109–121. doi: 10.3354/ame01138

Pitts, P., and Smith, N. (1997). An investigation of summer upwelling across central florida's atlantic coast: the case for wind stress forcing. *J. Coast. Res.* 13, 105–110.

Raimbault, P., and Garcia, N. (2008). Evidence for efficient regenerated production and dinitrogen fixation in nitrogen-deficient waters of the South Pacific Ocean: impact on new and export production estimates. *Biogeosciences* 5, 323–338. doi: 10.5194/bg-5-323-2008

Rivkin, R. B., and Anderson, M. R. (1997). Inorganic nutrient limitation of oceanic bacterioplankton. *Limnol. Oceanogr.* 42, 730–740. doi: 10.1038/nature07236

Romera-Castillo, C., Letscher, R. T., and Hansell, D. A. (2016). New nutrients exert fundamental control on dissolved organic carbon accumulation in the surface Atlantic Ocean. *Proc. Natl. Acad. Sci. U.S.A.* 113, 10497–10502. doi: 10.1073/pnas.1605344113

Saad, E. M., Longo, A. F., Chambers, L. R., Huang, R., Benitez-Nelson, C., Dyhrman, S. T., et al. (2016). Understanding marine dissolved organic matter production: compositional insights from axenic cultures of *Thalassiosira pseudonana*. *Limnol. Oceanogr.* 61, 2222–2233. doi: 10.1002/lno.10367

Schlitzer, R. (2018). *Ocean Data View*. Available at: https://odv.awi.de.

Schmitz, W. J. (1996). *On the World Ocean Circulation. The Pacific and Indian Oceans/a Global Update*, Vol. 2, Woods Hole, MA: Woods Hole Oceanographic Institution. doi: 10.21236/ADA323804

Schmitz, W. J., and McCartney, M. S. (1993). On the north Atlantic circulation. *Rev. Geophys.* 31, 29–49. doi: 10.1029/92RG02583

Schoffman, H., Lis, H., Shaked, Y., and Keren, N. (2016). Iron–nutrient interactions within phytoplankton. *Front. Plant Sci.* 7:1223. doi: 10.3389/fpls.2016.01223

Shapiro, S. S., and Wilk, M. B. (1965). An analysis of variance test for normality (complete samples). *Biometrika* 52, 591–611. doi: 10.1093/biomet/52.3-4.591

Strickland, J. D. H., and Parsons, T. R. (1968). A practical handbook of seawater analysis. *Fish. Res. Board Can. Bull.* 167, 49–56.

Talley, L. D., Pickard, G. L., Emery, W. J., and Swift, J. H. (2011). *Descriptive Physical Oceanography: An Introduction*, 6th Edn. Boston, MA: Academic press, 560.

Tanaka, T., Thingstad, T. F., Christaki, U., Colombet, J., Cornet-Barthaux, V., Courties, C., et al. (2011). Lack of P-limitation of phytoplankton and heterotrophic prokaryotes in surface waters of three anticyclonic eddies in the stratified Mediterranean Sea. *Biogeosciences* 8, 525–538. doi: 10.5194/bg-8-525-2011

Thingstad, T. F., Krom, M. D., Mantoura, R. F. C., Flaten, G. F., Groom, S., Herut, B., et al. (2005). Nature of phosphorus limitation in the ultraoligotrophic eastern Mediterranean. *Science* 309, 1068–1071. doi: 10.1126/science.1112632

Tortell, P. D., Maldonado, M. T., Granger, J., and Price, N. M. (1999). Marine bacteria and biogeochemical cycling of iron in the oceans. *FEMS Microbiol. Ecol.* 29, 1–11. doi: 10.1111/j.1574-6941.1999.tb00593.x

Tortell, P. D., Maldonado, M. T., and Price, N. M. (1996). The role of heterotrophic bacteria in iron-limited ocean ecosystems. *Nature* 383, 330–332.

Wear, E. K., Carlson, C. A., Windecker, L. A., and Brzezinski, M. A. (2015). Roles of diatom nutrient stress and species identity in determining the short-and long-term bioavailability of diatom exudates to bacterioplankton. *Mar. Chem.* 177, 335–348. doi: 10.1016/j.marchem.2015.09.001

West, N. J., Obernosterer, I., Zemb, O., and Lebaron, P. (2008). Major differences of bacterial diversity and activity inside and outside of a natural iron-fertilized phytoplankton bloom in the Southern Ocean. *Environ. Microbiol.* 10, 738–756. doi: 10.1111/j.1462-2920.2007.01497.x

Wetz, M. S., and Wheeler, P. A. (2004). Production and partitioning of organic matter during simulated phytoplankton blooms. *Limnol. Oceanogr.* 48, 1808–1817. doi: 10.4319/lo.2003.48.5.1808

Zhang, J. Z., Baringer, M. O., and Fischer, C. J. (2017). An estimate of diapycnal nutrient fluxes to the euphotic zone in the Florida Straits. *Sci. Rep.* 7:16098. doi: 10.1038/s41598-017-15853-0

Zweifel, U. L. (1999). Factors controlling accumulation of labile dissolved organic carbon in the Gulf of Riga. *Estuar. Coast. Shelf Sci.* 48, 357–370. doi: 10.1006/ecss.1998.0428

Conflict of Interest Statement: The authors declare that the research was conducted in the absence of any commercial or financial relationships that could be construed as a potential conflict of interest.

Copyright © 2018 Bif, Hansell and Popendorf. This is an open-access article distributed under the terms of the Creative Commons Attribution License (CC BY). The use, distribution or reproduction in other forums is permitted, provided the original author(s) and the copyright owner(s) are credited and that the original publication in this journal is cited, in accordance with accepted academic practice. No use, distribution or reproduction is permitted which does not comply with these terms.

frontiers in Microbiology

ORIGINAL RESEARCH
published: 09 January 2019
doi: 10.3389/fmicb.2018.03259

Picoeukaryotic Diversity And Activity in the Northwestern Pacific Ocean Based on rDNA and rRNA High-Throughput Sequencing

*Feipeng Wang[1], Yuyuan Xie[1], Wenxue Wu[2], Ping Sun[1], Lei Wang[3] and Bangqin Huang[1]**

[1] Fujian Provincial Key Laboratory of Coastal Ecology and Environmental Studies, State Key Laboratory of Marine Environmental Science, Xiamen University, Xiamen, China, [2] School of Marine Sciences, Sun Yat-sen University, Zhuhai, China, [3] Third Institute of Oceanography, State Oceanic Administration, Xiamen, China

Picoeukaryotes play an important role in the biogenic element cycle and energy flow in oligotrophic ecosystems. However, their biodiversity and activity are poorly studied in open ocean systems, such as the northwestern Pacific Ocean, which is characterized by a complex hydrological setting. Here, we investigated the diversity and activity of picoeukaryotes in the northwestern Pacific Ocean using high-throughput sequencing targeting the V9 region of 18S rDNA and rRNA. Our results showed that the DNA picoeukaryotic communities were mainly represented by Mamiellophyceae, MAST, MALV-II, Spirotrichea, Prymnesiophyceae, and MALV-I (69.33% of the total DNA reads), and the RNA communities were dominated by Spirotrichea, Mamiellophyceae, MAST, Pelagophyceae, and MALV-II (67.46% of the total RNA reads). The number of operational taxonomic units (OTUs) was significantly affected by temperature and salinity, and was decreased with the increasing nutrient concentration both in the DNA and RNA surveys. Significant differences were observed in the community composition between DNA-based and RNA-based molecular approaches, and these differences were mainly attributed to Mamiellophyceae, Spirotrichea, and Pelagophyceae. The RNA: DNA ratio was used as a proxy for relative metabolic activity of the individual OTUs. We found that the relative metabolic activities of Mamiellophyceae, Spirotrichea, and Pelagophyceae species in the northwestern Pacific Ocean were highly affected by the nutrient concentration, i.e., the NO_3 + NO_2 and SiO_3 concentration. Overall, our study shed light on picoeukaryotic diversity and distribution in the northwestern Pacific Ocean and revealed the correlation between the diversity, relative metabolic activities of marine picoeukaryotes, and the environmental factors.

Keywords: picoeukaryotic diversity, Illumina sequencing, 18S rRNA gene and cDNA sequencing, RNA/DNA comparison, metabolic activity, northwestern Pacific Ocean

OPEN ACCESS

Edited by:
Veronica Molina, Universidad de Playa Ancha, Chile

Reviewed by:
Adriana Lopes Dos Santos, Nanyang Technological University, Singapore
Ludwig Jardillier, Université Paris-Sud, France

***Correspondence:**
Bangqin Huang
bqhuang@xmu.edu.cn

Specialty section:
This article was submitted to Aquatic Microbiology, a section of the journal Frontiers in Microbiology

Received: *10 July 2018*
Accepted: *14 December 2018*
Published: *09 January 2019*

Citation:
Wang F, Xie Y, Wu W, Sun P, Wang L and Huang B (2019) Picoeukaryotic Diversity And Activity in the Northwestern Pacific Ocean Based on rDNA and rRNA High-Throughput Sequencing. Front. Microbiol. 9:3259. doi: 10.3389/fmicb.2018.03259

INTRODUCTION

Picoeukaryotes (cell sizes at 0.2–3 μm) are key components of marine ecosystems and microbial food webs (Pomeroy et al., 2007; Vaulot et al., 2008; Caron et al., 2012). Picoeukaryotes are widely distributed and consist of multiple metabolic types, including phototrophs, heterotrophs, and mixotrophs (Zubkov and Tarran, 2008; de Vargas et al., 2015). Photosynthetic picoeukaryotes

(PPEs) are vital contributors of marine plankton biomass and primary production in coastal and oceanic environments (Worden et al., 2004; Grob et al., 2007; Jardillier et al., 2010). Heterotrophic picoeukaryotes within Stramenopiles and Alveolates can feed on bacteria and therefore play an important role in nutrient recycling (from prokaryotic fractions to higher trophic levels, Sherr and Sherr, 1994; Massana et al., 2009), as well as bacterial community composition and abundance (Jardillier et al., 2005). Recent studies have expanded our knowledge of the ecological roles of mixotrophic picoeukaryotes, showing that they are important consumers of prokaryotes and have the potential to dominate the primary production and bacterivory in marine ecosystems (Hartmann et al., 2012; Sanders and Gast, 2012; Unrein et al., 2014).

Using the sequencing of environmental DNA (eDNA) based on the 18S rRNA gene, previous studies reveled an astonishing picoeukaryotic diversity in aquatic environments (Díez et al., 2001; Moon-van der Staay et al., 2001; Berney et al., 2004; Massana et al., 2004; Richards et al., 2005; Not et al., 2007). With the development of sequencing technologies, high throughput sequencing (HTS) highlights the phylogenetic diversity of protist communities with high-resolution exploration (Zinger et al., 2011; Massana et al., 2015; Hu et al., 2016; Xu et al., 2017; Bellaaj Zouari et al., 2018). rRNA gene sequencing (hereafter, referred to as DNA) has been commonly used for the investigation of microbial diversity in environmental samples (Moon-van der Staay et al., 2001; Shi et al., 2009). However, microbial community structures inferred from DNA sequencing can be distorted by extracellular free DNA (Karl and Bailiff, 1989; Massana et al., 2015), dormant cells or fragments of dead materials (Stoeck et al., 2007; Not et al., 2009). In contrast, rRNA (hereafter, referred to as RNA) is much more unstable in extracellular conditions, and sequence information derived from RNA can imply ribosomal activity and the potential of protein synthesis (Not et al., 2009; Blazewicz et al., 2013; Egge et al., 2015). RNA molecular approach is nowadays generally accepted to identify the active protist community (Massana et al., 2015), although several critical limitations should be carefully considered (Blazewicz et al., 2013). Thus, RNA sequencing can act as a supplement to DNA sequencing to achieve a better understanding of picoeukaryotic communities in the natural environment (Not et al., 2009; Terrado et al., 2011). The RNA: DNA ratio (based on relative abundances) have been used as a proxy for the relative metabolic activity in protist (Massana et al., 2015; Hu et al., 2016; Xu et al., 2017), while this strategy needed to be applied with caution (Blazewicz et al., 2013; Hu et al., 2016). Significant changes of the RNA: DNA ratio may indicate ecological season events. A recent study have found that the changes of RNA: DNA ratio of *Phaeocystis globose*, collected at a coastal station of the eastern English Channel, unveiled well to the *Phaeocystis* bloom dynamic (Rachik et al., 2018).

The northwestern Pacific Ocean is a complex system of multiple ocean currents, including the Kuroshio Current (KC), Kuroshio Extension Current (KEC), and Oyashio Current (OC). The KC and its extension (KEC) are characterized by warm and saline waters (salinity above 34.2) from the southern subtropical area, and they flow in a northeastern direction. The OC transports cold waters of lower salinities (below 33.5; Qiu, 2001) from the north subarctic area and flows to the southwest. The Kuroshio-Oyashio mixing region is the location where the warm subtropical KEC waters encounter the cold subarctic OC waters, roughly ranging from 36 to 44°N (Chen, 2008). Hydrographical characteristics in this area exhibit complicated frontal structures, tongues, and eddies (Yasuda, 2003). Several previous studies have revealed the response of picoplankton diversity to changing environmental factors, e.g., temperature, nutrient content, and oxygen concentration (Doney et al., 2012; Grossmann et al., 2016). However, only a few studies have focused on picoeukaryotic community structures in the northwestern Pacific Ocean, and the correlation between varied environmental factors and picoeukaryotic diversity in this area has rarely been examined (Liu et al., 2002; Choi et al., 2016). Nishibe et al. (2015, 2017) revealed that phytoplankton communities across the KEC during spring mainly comprised chlorophytes, cryptophytes, and prasinophytes (based on pigment analysis). The small phytoplankton groups ($<10\,\mu m$) were the main contributors for the phytoplankton biomass and primary production (Nishibe et al., 2015). To the best of our knowledge, this was the first study of the investigation of picoeukaryotic diversity and activity in the northwestern Pacific Ocean based on HTS (DNA and RNA). The aim of this study was to: (1) reveal picoeukaryotic assemblages in the northwestern Pacific Ocean based on rDNA and rRNA sequencing, and (2) examine the extent to which environmental factors influenced picoeukaryotic diversity and relative metabolic activity.

MATERIALS AND METHODS

Cruise, Sampling, and Measurement of Environmental Parameters

HTS samples were taken from 8 stations in the northwestern Pacific Ocean, from 134 to 152°E and 25 to 38°N from March 29th to May 4th, 2015 (**Figure 1**). For each station, 20–30 L seawater was collected from both the surface (Sur, 5 m) and deep chlorophyll maximum (DCM) layers using Niskin bottles mounted on a CTD (conductivity, temperature, and depth) rosette (Sea-Bird Electronics, USA). The seawater was sequentially filtered using a peristaltic pump through 3 and 0.2 μm pore size polycarbonate membranes (142 mm diameter, Millipore, USA) at a rate of 0.5–1 L/min. The filters (samples collected between 0.2 and 3 μm) were transferred into a 5 mL cryo tube containing 4.6 mL of RNA*later* (Thermo Fisher, Lithuania). The tubes were immediately frozen in liquid nitrogen on board. In this study, HTS samples were named by the combination of sampling station and depth, e.g., K2Sur indicates that the sample was collected at the surface layer of Stn. K2. Environmental parameters (i.e., temperature, salinity, and depth) were recorded with SBE-911 CTD (Sea-Bird Electronics, USA) in each sampling site including the B transect (**Figure 1**). The samples for pigment analyses were also collected in the Sur and DCM layers of the 8 HTS stations. For the pigment measurements, 4–6 L of seawater without pre-filtration were directly filtered onto 25 mm GF/F

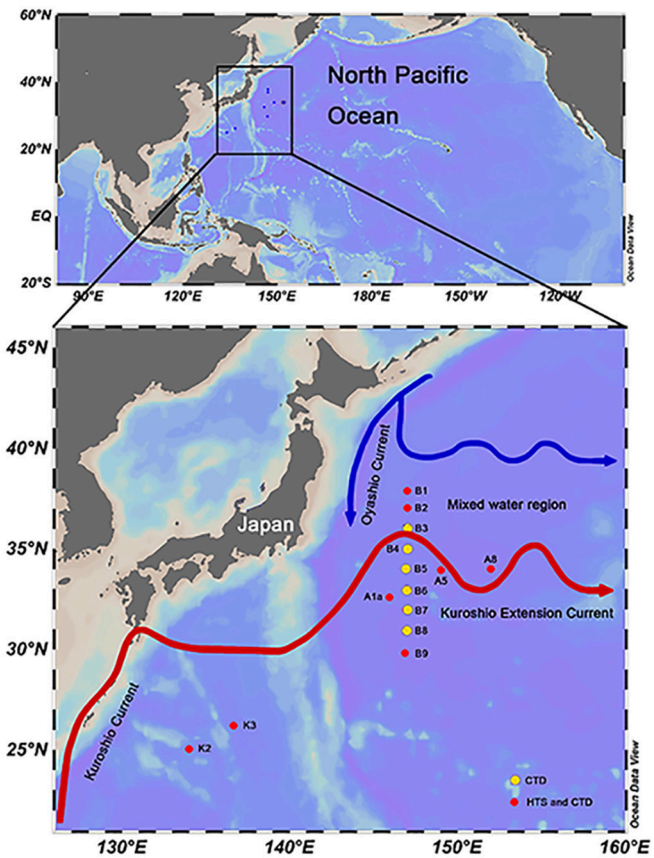

FIGURE 1 | Sampling sites in the northwestern Pacific Ocean during the spring cruise conducted in 2015. Flow paths of Kuroshio and its Extension Current and the Oyashio Current were modified according to the study of Qiu (2001). The red dots on the map indicate the high-throughput sequencing stations. The yellow dots on the map indicate stations within the B transect for which only physical and chemical parameters were recorded by CTD. The map was produced using the Ocean Data View 4 software.

glass microfiber filters (Whatman, USA) under 200 mm Hg pressure. These filters were then protected from the light and immediately stored in liquid nitrogen on board, kept at −80°C in the laboratory until analysis. Photosynthetic pigment concentrations were measured by high-performance liquid chromatography (HPLC) (Zapata et al., 2000). The chlorophyll *a* (Chl *a*) concentrations were derived from the pigment analysis. The CHEMical TAXonomy (CHEMTAX, Mackey et al., 1996) was applied to acquire the relative contributions of different phytoplankton groups to the total Chl *a*. Samples for flow cytometry analysis were also collected in the HTS sampling sites. 1.8 ml seawater was transferred into a 2 ml cryo tube, and then fixed with paraformaldehyde (1% final concentrations). The tubes were incubated at room temperature for 15 min and then frozen in liquid nitrogen on board. Estimation of the cell abundance of picoeukaryotes was performed by a Becton Dickinson FACSCalibur flow cytometer.

DNA and RNA Co-extraction, PCR Amplification, and Sequencing

The total DNA and RNA were extracted simultaneously from each sample using the AllPrep DNA/RNA Mini Kit (Qiagen, #80204, Germany). For the RNA extraction, gDNA wipeout buffer (Qiagen, #205311, Germany) was used to remove the genomic DNA. The purified RNA was reverse transcribed into cDNA using the QuantiTect Reverse Transcription Kit (Qiagen, #205311, Germany). The resulting DNA and cDNA were amplified using the eukaryotic-specific V9 forward primer 1380F 5′-CCCTGCCHTTTGTACACAC-3′ and reverse primer 1510R 5′-CCTTCYGCAGGTTCACCTAC-3′ (Amaral-Zettler et al., 2009). The polymerase chain reaction (PCR) mixtures contained 12.5 μL 2 × *Taq* PCR mix (Takara, China), ≤1 μg templates, 1 μL forward primer (10 μM), and 1 μL reverse primer (10 μM). RNase-free water was added to a final volume of 25 μL. The PCR thermal cycle was performed under the following conditions: a denaturation step at 95°C for 5 min, 34 cycles of 94°C for 1 min, 57°C for 45 s, 72°C for 1 min, and a final extension at 72°C for 10 min. The duplicate PCR products were pooled and purified using a 2% agarose gel using QIAquick Gel Extraction Kit (Qiagen, #28704, Germany). All purified hypervariable V9 region amplicons were paired-end sequenced (2 × 250 bp) on the Illumina HiSeq 2500 platform at Novogene sequencing company (Beijing, China). Sequence data have been deposited in the NCBI SRA database under accession number SRP 151579.

Sequence Processing and Statistical Analysis

Barcodes and primers were trimmed from paired-end sequences and then merged using FLASH (v. 1.2.7, http://ccb.jhu.edu/software/FLASH/; Magoč and Salzberg, 2011). A sequence quality check was performed using the Quantitative Insights Into Microbial Ecology (QIIME v. 1.7.0) pipeline (Caporaso et al., 2010). Chimeras were identified and removed with the chimera search module (USEARCH, version 4.2; Edgar et al., 2011) using the Silva 123 release (Quast et al., 2013) as a reference. The remaining high quality sequences were clustered into operational taxonomic units (OTUs) using a 95% similarity threshold with UPARSE (v. 7.0.100; Edgar, 2013). The representative sequence of each OTU (most abundant) was assigned using BLAST (Altschul et al., 1990) against the *V9_PR2* database (de Vargas et al., 2015). For further analysis, OTUs with only one read (singleton) as well as OTUs only represented in a single sample were discarded. operational taxonomic units (OTUs) only represented in DNA or RNA surveys were also removed from the downstream analyses, as biases in the rDNA copy number and chimeras resulted from the cDNA synthesis (Egge et al., 2013). operational taxonomic units (OTUs) assigned to Metazoan, Archaea, Bacteria, Organelle, and those that were unclassified were also excluded. To reduce the biases of sequencing coverage, the sequencing depth of the DNA and RNA results was separately rarefied to an equal sequence number based on their minimums.

Alpha diversity estimations (Shannon and Chao1) were calculated using QIIME. For the beta diversity, Bray-Curtis dissimilarity matrices were constructed based on the log-transformed relative abundance of each OTU using the "hclust" function in R (R Core Team., 2014). PERMANOVA was applied to establish the significant differences between dendrogram nodes resulting from the cluster analysis. Principal component analysis (PCA) was conducted to assess the difference in assemblage of picoeukaryotic communities among samples using the Vegan package in R (Oksanen et al., 2015). The RNA: DNA ratio of individual OTUs was calculated based on its proportions in the RNA and DNA results. Redundancy analysis (RDA) was performed using the Vegan package in R to identify the relationship between environmental parameters and the relative metabolic activities of invidious OTUs.

RESULTS

Environmental Conditions of Sampling Stations

Stn. K2 and K3, located in the KC east area, were characterized by higher temperature and salinity (**Table S1**). The temperature ranged from 23.13 to 24.70°C and 19.78 to 20.24°C at the surface and DCM, respectively, while salinity ranged from 34.98 to 35.03 and 34.86 to 34.98 at the surface and DCM, respectively (**Table S1**). Stn. B1 and B2, located at the mixed area between KEC and OC (**Figure 1**), were characterized by lower temperature and salinity levels, with uniform distributions due to the vertical mixing of the water column (**Table S1**). The temperature ranged from 13.8 to 14.7°C and 13.74 to 14.33°C at the surface and DCM, respectively, while salinity ranged from 34.44 to 34.48 and 34.44 to 34.46 at the surface and DCM, respectively (**Table S1**). The Kuroshio front is defined by 15°C isotherms at a depth of 100 m (Kawamura et al., 1986). The vertical profile of the temperature and salinity across the B transect revealed that the KEC water and OC water were encountered near Stn. B3 (**Figure S1**). Maximum values of nutrient and Chl *a* concentrations were observed at the KEC and OC mixed water (Stn. B1 and B2, **Table S1**). At the DCM layer of Stn. B2, lower values of Chl *a* concentration were detected. Stn. A1a, A5, A8, and B9 were located around the KEC area and the nutrient concentrations at Stn. A1a (both at surface and DCM layers) and Stn. A5 (both at surface and DCM layers) as well as at the surface layer of Stn. A8 were all below detection (**Table S1**).

Alpha Diversity of Picoeukaryotes

A total of 661,340 DNA and 752,333 RNA sequences with an average length of 134 bp were generated and were clustered into 2,779 phylogenetically different OTUs both in the DNA and RNA datasets (95% similarity). The OTUs identified were affiliated to ten super-groups, including Archaeplastida, Alveolata, Stramenopiles, Hacrobia, Rhizaria, Opisthokonta, Picozoa, Amoebozoa, Excavata, and Apusozoa (**Figure 2**). Alveolata was the most diverse group, encompassing 1,486 OTUs. Most of them were affiliated to Dinophyta (1,117 OTUs) and Ciliophora (336 OTUs) (**Figure 2**). Within Dinophyta, marine alveolates (MALV)- II had the highest numbers of OTUs (734 OTUs), followed by Dinophyceae (187 OTUs) and MALV- I (147 OTUs). Within Ciliophora, Spirotrichea (172 OTUs), and Oligohymenophorea (64 OTUs) contributed largely followed by Litostomatea (34 OTUs) and Phyllopharyngea (15 OTUs). Stramenopiles was the second most diverse super-group, encompassing 505 OTUs, including members of the marine stramenopiles (MAST, 183 OTUs), Bacillariophyta (97 OTUs), Labyrinthulea (65 OTUs), Chrysophyceae-Synurophyceae (28 OTUs), Dictyochophyceae (25 OTUs), MOCH (18 OTUs), Bicoecea (12 OTUs), and Pelagophyceae (10 OTUs) (**Figure 2**). OTUs in Rhizaria (301 OTUs) were mainly affiliated to Radiolaria (201 OTUs) and Cercozoa (99 OTUs). The super-group Hacrobia (182 OTUs) was mainly composed of Prymnesiophyceae (112 OTUs), Cryptophyceae (31 OTUs) and Telonemia (25 OTUs) (**Figure 2**). One hundred and thirty two OTUs were affiliated to Archaeplastida, including members of Mamiellophyceae (32 OTUs), Trebouxiophyceae (18 OTUs), Prasino-Clade-5, −7, −9 (22 OTUs), and Chlorophyceae (13 OTUs). Members in Opisthokonta (87 OTUs), Picozoa (9 OTUs), Amoebozoa (26 OTUs), Excavata (38 OTUs), and Apusozoa (12 OTUs) made only minor contribution of the diversity of picoeukaryotes (**Figure 2**).

Correlations Between Alpha Diversity and Environmental Factors

The number of OTUs was varied substantially among samples (**Figures 3A,B** and **Table S2**). Higher number of OTUs was found

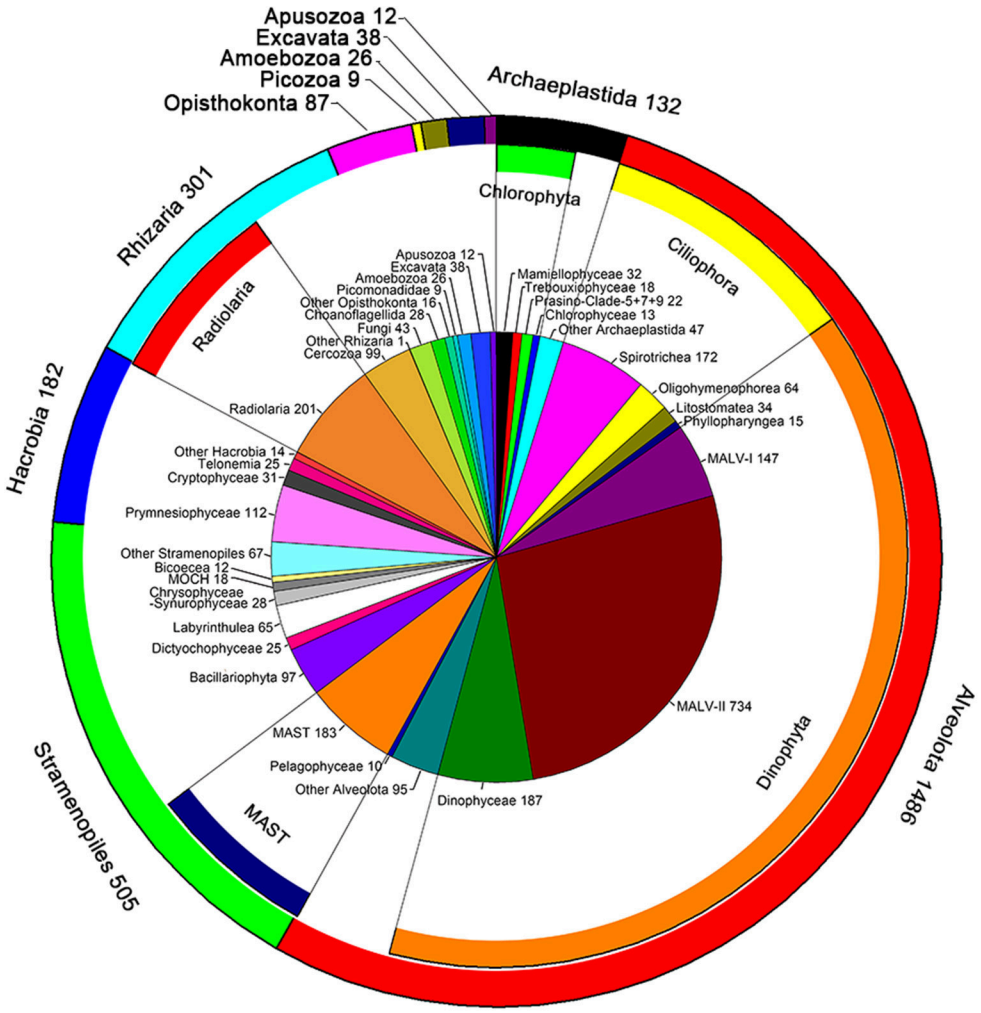

FIGURE 2 | Number of OTUs unveiled by DNA and RNA surveys. The pie chart indicated the OTU numbers mainly at class level; the inner ring represented these classes belong to the phylum; the outer ring indicated the number of OTUs at super-group level.

in Stn. K2, K3, and B9 both in the DNA and RNA surveys (DNA: from 1,387 OTUs in B9Sur to 1,657 OTUs in K3DCM; RNA: from 1,342 in K3Sur to 1,571 in B9Sur), while lower values was found in the KEC and OC mixed water (Stn. B1 and B2) both in the DNA and RNA surveys (DNA: from 722 OTUs in the B2Sur to 1,028 OTUs in the B1DCM; RNA: from 692 OTUs in B2Sur to 1,044 OTUs in B1DCM), except for at the DCM layer of Stn. B2 (DNA: 1,270 OTUs; RNA: 1,260 OTUs) (**Figures 3A,B** and **Table S2**). The diversity indices, i.e., the Shannon and Chao 1 indices also showed the same trend in the DNA and RNA surveys (**Table S2**). MALV- II was always the most diverse group, varied from 18 to 31.22% in the individual DNA samples and from 15.95 to 25.25% in the individual RNA samples, respectively (**Figures 3A,B**). Statistical analysis revealed the number of OTUs in each sample inferred from the DNA and RNA approaches exhibited similar trends against the selected environmental factors (**Figure 3C**). The number of OTUs had a significantly negative relationship with latitude (DNA, $P < 0.001$, $r = -0.742$; RNA, $P = 0.008$, $r = -0.635$) and a significantly positive relationship with temperature (DNA, $P = 0.019$, $r = 0.579$; RNA, $P = 0.012$, $r = 0.611$) and salinity (DNA, $P = 0.018$, $r = 0.584$; RNA, $P = 0.004$, $r = 0.674$). The number of OTUs had no significant correlation with the nutrient concentrations, although the RNA-based OTU numbers in each sample was negatively correlated with SiO_3 (**Figure 3C**).

Community Composition of Picoeukaryotes

The number of the DNA and RNA reads ranged from 28,169 to 57,097 and from 36,483 to 57,507 per sample, respectively. To minimize the bias of the sequencing depth and allow for the comparison of sequencing results among samples, the DNA/RNA sequences were normalized to 28,169 (DNA) and 36,483 (RNA) in each sample, respectively (**Table S2**). The community captured by our DNA/RNA approaches were dominated by three super-groups, the Archaeplastida (33.54% of

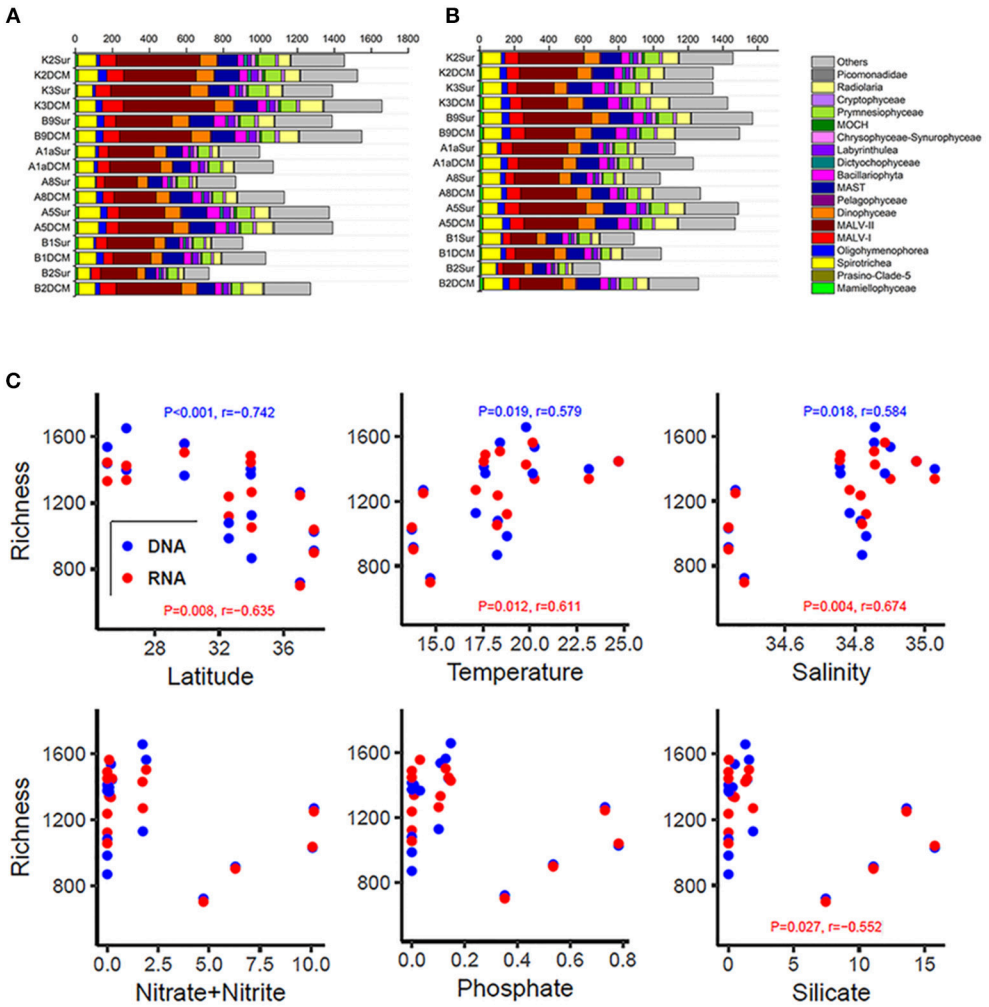

FIGURE 3 | Number of OTUs of higher taxonomic groups (sequences proportion over 1% of the total DNA or RNA abundance) based on the DNA-derived **(A)** and RNA-derived **(B)** approaches for each sample. Others refer to groups with relatively lower abundance (sequences proportion <1% of the total DNA and RNA abundance). **(C)** Pearson correlations between the number of OTUs and the latitude, temperature, salinity, nitrate + nitrite, phosphate, and silicate based on the DNA and RNA datasets at each sampling site.

the total DNA reads; 20.05% of the total RNA reads), Alveolata (28.98% of the total DNA reads; 32.65% of the total RNA reads) and Stramenopiles (21.21% of the total DNA reads; 33.82% of the total RNA reads) (**Figures S2A,B**). **Figures 4A,B** showed the relative abundance of 18 dominant higher taxonomic groups (sequences proportion over 1% of the total DNA or RNA abundance) at each sample. Statistical analyses showed that the community composition inferred from the DNA and RNA approaches was significantly different from that of samples K2Sur, K3Sur, K3DCM, B9DCM, B1Sur, B1DCM, B2Sur, and B2DCM, with $P < 0.05$ (**Figures 4A,B**).

In the DNA survey, Mamiellophyceae, although little diverse (32 OTUs), was the most abundant group, representing 31.5% reads per sample on average (ranged from 8.46% reads in K3DCM to 68.63% reads in B2Sur) (**Figures 2**, **4A** and **Table 1**). The most abundant OTU (24.22% of the total DNA reads) during our DNA survey was affiliated to *Ostreococcus lucimarinus* (OTU1, **Table S4**), which was observed with a peak of relative abundance in B2Sur (53.91%). MAST, mainly represented by MAST-4 (3.84%, on average) and MAST-3 (3.23%, on average), was the second abundant group, representing 11.13% reads per sample on average (**Table 1**). This group was less represented in the KEC and OC mixed water (Stn. B1 and B2, from 6.33% reads in B2Sur to 10.61% reads in B1DCM) and with higher relative abundance in A8DCM (16.89%) (**Figure 4A**). MALV-II was the most diverse group, representing 9.59% reads per sample on average (**Figure 2** and **Table 1**). However, the relative abundance of its OTUs was detected always in low proportion. The most abundant OTU within MALV-II was affiliated to MALV-II-Clade-8_X sp. (OTU71, **Table S4**), which was only represented 0.35% reads per sample on average. Spirotrichea, the most diverse and abundant group in Ciliophora, was less represented in Stn. K2 and K3 (from 2.38% reads in K3Sur to 4.83% reads in K2Sur), and higher relative abundance was detected

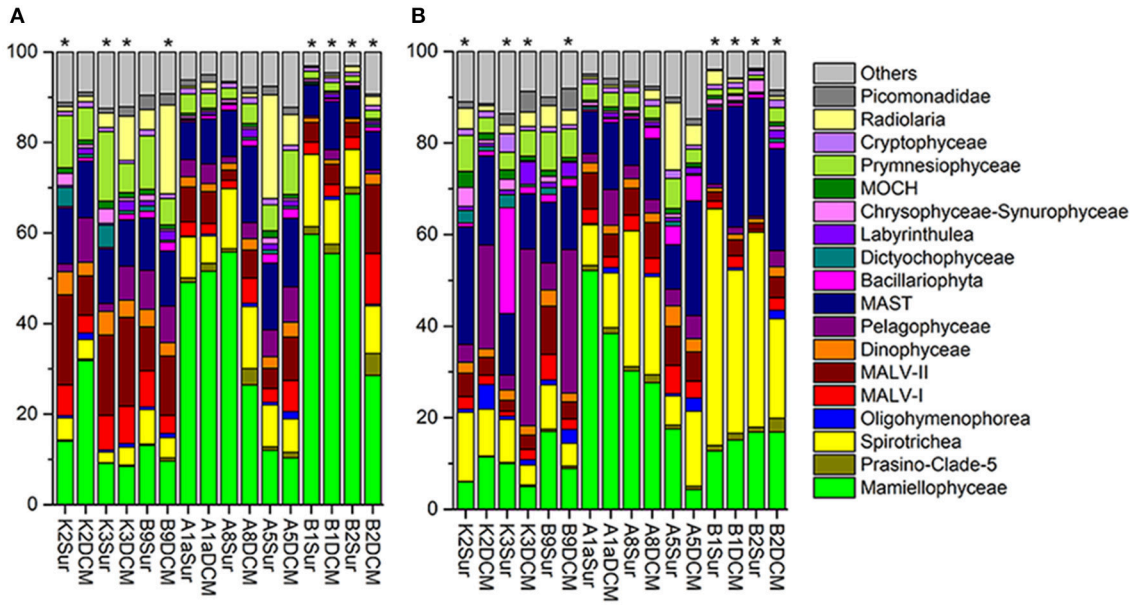

FIGURE 4 | Relative abundance of higher taxonomic groups (sequences proportion over 1% of the total DNA or RNA abundance) based on the DNA-derived **(A)** and RNA-derived **(B)** approaches for each sample. Others refer to groups with relatively lower abundance (sequences proportion <1% of the total DNA and RNA abundance). Asterisks indicate that the community composition was significantly different (*Chi-square test*, $P < 0.05$) between the DNA and RNA approaches for the same sample.

in Stn. A8 (13.34% reads in A8Sur and 13.73% in A8DCM) (**Figures 2**, **4A**). Prymnesiophyceae, MALV-I and Radiolaria were detected in low proportion (<6% reads per sample on average, **Table 1**), but occasionally reached higher proportions, for example, Prymnesiophyceae (11.81% reads in K3Sur), MALV-I (11.21% reads in B2DCM), and Radiolaria (22.92% reads in A5Sur) (**Figure 4A**). Only 10 OTUs in our survey was affiliated to Pelagophyceae, representing 3.94% reads per sample on average (**Table 1**). The most abundant OTU within this group was affiliated to *Pelagomonas calceolate* (OTU2, **Table S4**), which was detected with highest relative abundance in K2DCM (9.37%) (**Figure 4A**).

In the RNA survey, Spirotrichea was the most abundant group, representing 18.75% reads per sample on average (**Figure 4B** and **Table 1**). This group was highly abundant in the KEC and OC mixed water (Stn. B1 and B2), reaching up to 51.64% of the reads in B1Sur (**Figure 4B**). Within Spirotrichea, the most abundant OTU was affiliated to *strobilidiidae_X* sp. (OTU3, **Table S4**), was also highly represented in B1Sur (31.14%). In general, the relative abundance of Mamiellophyceae in the RNA samples (18.15%, on average) was lower than in the DNA samples (**Figures 4A,B** and **Table 1**). OTU1 (*O. lucimarinus*) was also the most abundant OTU during the RNA survey (**Table S4**), with the highest relative abundance reaching up to 41.37% of the reads in A1aSur. MAST represented 16.91% of the reads per sample on average (**Table 1**), and was mainly dominated by MAST-4 (10.18%, on average). High contributions of MAST-4 reads were detected in the KEC and OC mixed water (Stn. B1 and B2), ranging from 6.75% reads in B1Sur to 10.23% reads to B2DCM. MAST-3 represented 5.66% reads per sample on average, and was occasionally highly abundant, reaching 21.43% of the reads in A5DCM. Pelagophyceae (8.53%, on average, **Table 1**) was dominant by *P. calceolate* (OTU2, **Table S4**), which was highly abundant at the DCM layers of Stn. K2, K3, and B9 (**Figure 4B**). MALV-II represented 5.12% reads per sample on average (**Table 1**). The most abundant OTU (MALV-II_XX sp., OTU58, **Table S4**) within this group was detected in rather low proportion (0.18%, on average). Bacillariophyta (2.95%, on average) and Radiolaria (2.9%, on average) were less abundant, but occasionally detected with higher proportions, for example, Bacillariophyta (29.92% reads in K3Sur), Radiolaria (14.73% reads in A5Sur) (**Figure 4B** and **Table 1**).

Based on the HPLC method, phytoplankton communities were characterized by a relatively high dominance of Prasinophytes and Haptophytes_8 (**Figure S3A**). The contribution of *Prochlorococcus* and *Synechococcus* was decreased with the increasing latitude, and the contribution of diatoms was highest in samples collected at Stn. A5 (**Figure S3A**). Cell abundance of Picoeukaryotes estimated by flow cytometry was generally increased with the increasing latitude, while low values were detected in samples A8DCM, A5Sur, A5DCM, and B2DCM (**Figure S3B**).

Beta Diversity of Picoeukaryotic Assemblages in the Northwestern Pacific Ocean

The Bray-Curtis dissimilarity results from the DNA and RNA sequences were both clustered the samples into two groups (**Figures 5A,B**). In the DNA survey, the community composition of Stn. A1a, A8, B1, and B2, where Mamiellophyceae was the dominant group, was significantly different from Stn. K2, K3,

TABLE 1 | The number of DNA and RNA sequences, and percentage of the total number of sequences by higher taxonomic groups (sequences proportion over 1% of the total DNA or RNA abundance).

Higher taxonomic groups	DNA		RNA	
	Sequences	Percent	Sequences	Percent
Mamiellophyceae	141,960	31.50	105,950	18.15
Prasino-Clade-5	5,937	1.32	5,497	0.94
Spirotrichea	36,862	8.18	109,432	18.75
Oligohymenophorea	2,678	0.59	7,385	1.27
MALV-I	22,679	5.03	16,588	2.84
MALV-II	43,244	9.59	29,892	5.12
Dinophyceae	12,099	2.68	12,648	2.17
Pelagophyceae	19,258	4.27	49,807	8.53
MAST	50,177	11.13	98,701	16.91
Bacillariophyta	4,555	1.01	17,243	2.95
Dictyochophyceae	4,649	1.03	5,042	0.86
Labyrinthulea	4,077	0.90	6,790	1.16
Chrysophyceae-Synurophyceae	4,245	0.94	6,726	1.15
MOCH	3,541	0.79	6,041	1.03
Prymnesiophyceae	26,623	5.91	23,326	4.00
Cryptophyceae	4,780	1.06	8,114	1.39
Radiolaria	21,433	4.76	16,903	2.90
Picomonadidae	5,615	1.25	8,590	1.47
Others	36,292	8.05	49,053	8.40

The other category refers to groups with relatively lower abundance (sequences proportion <1% of the total DNA and RNA abundance).

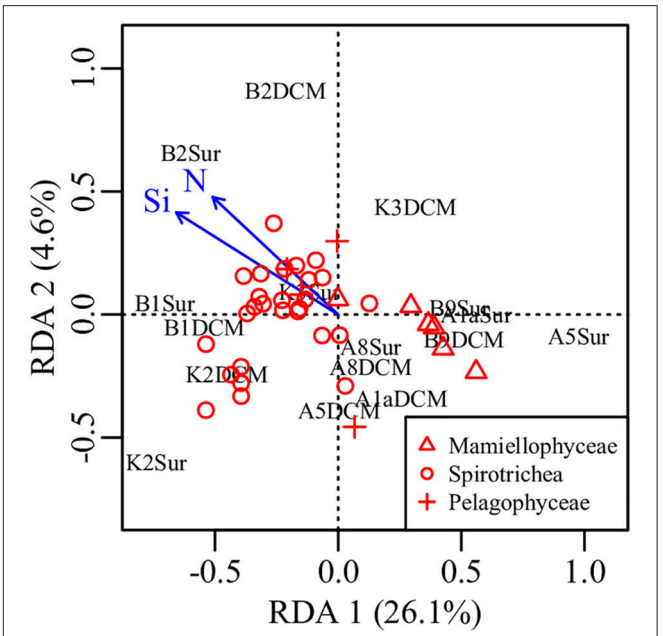

FIGURE 7 | Plot of the RDA integrating environmental factors and the relative metabolic activities of Mamiellophyceae, Pelagophyceae, and Spirotrichea species. N, nitrate + nitrite, Si, silicate.

and B9 according to the statistical analyses (PERMANOVA, $r^2 = 0.31718$, $P = 0.001$) (**Figure 5A**). The samples collected in the KEC and OC mixed water (Stn. B1 and B2) were grouped together, except for the sample B2DCM, which was grouped as a sister cluster with A8DCM (**Figure 5A**). In Stn. A1a and A5, the samples collected at the surface and DCM layers were grouped as sister clusters (**Figure 5A**), indicating the minor composition difference in the two depths at these two stations. In the RNA survey, the samples were clustered with a similar pattern as the results of the DNA analysis, and the community composition of the two clusters was also significantly different (PERMANOVA, $r^2 = 0.27023$, $P = 0.001$) (**Figure 5B**). The sample collected at the DCM layer of Stn. B2 was grouped separately as a single cluster (**Figure 5B**). Minor differences in the community composition at the surface and DCM layers were observed in Stn. B1 and A1a (**Figure 5B**).

Comparison Between DNA- and RNA-Based Picoeukaryotic Communities

PCA was conducted on the variabilities of the higher taxonomic groups among samples (**Figure 6A**). The top variables contributed to the total variabilities were Mamiellophyceae DNA and RNA sequences, Spirotrichea RNA sequences, and Pelagophyceae RNA sequences (**Figure 6A**). According to the scatter plot of first two axes, these four variables illustrated several sampling stations and depths with distinct picoeukaryotic composition: B1Sur, B2Sur, and B1DCM were associated with relative high abundance of Spirotrichea RNA sequences and Mamiellophyceae DNA sequences, but lesser Mamiellophyceae RNA sequences; by contrast, A8Sur, A1aSur, and A1aDCM were related with relative high abundance of both DNA and RNA sequences of Mamiellophyceae, but lesser Spirotrichea RNA sequences; meanwhile, K3DCM and B9DCM showed relative high Pelagophyceae RNA sequences (**Figure 6A**). The **Figures 4A,B** displayed these features as well. Taking all samples together, the RNA: DNA ratio (as a proxy of cell relative metabolic activity) for Mamiellophyceae (average RNA: DNA ratio = 1.38) was slightly above 1. Varied ratios was observed in individual samples, with higher values was found in the samples A8Sur, A1aSur, and A1aDCM and lower values was found in samples B1Sur, B1DCM, and B2Sur (**Figure 6B**). High relative metabolic activity of Pelagophyceae (average RNA: DNA ratio = 1.64) was recorded in the sample B9CM (**Figure 6C**). High relative metabolic activity of Spirotrichea (average RNA: DNA ratio = 2.79) was recorded in the samples B1Sur, B1DCM, B2Sur, and A8Sur (**Figure 6D**). At the OTU level, the species within these three groups presented varied DNA: RNA ratio across samples (**Figure S4** and **Table S3**), indicating their changing relative cell activity in different environmental conditions in the northwestern Pacific Ocean. Redundancy analysis (RDA) showed this varied cell activities was significantly affected by the $NO_3 + NO_2$ and SiO_3 concentration (**Figure 7**).

DISCUSSION

Previously, most studies of picoeukaryotic diversity were mainly based on the rDNA analysis (Vaulot et al., 2008; Lepère

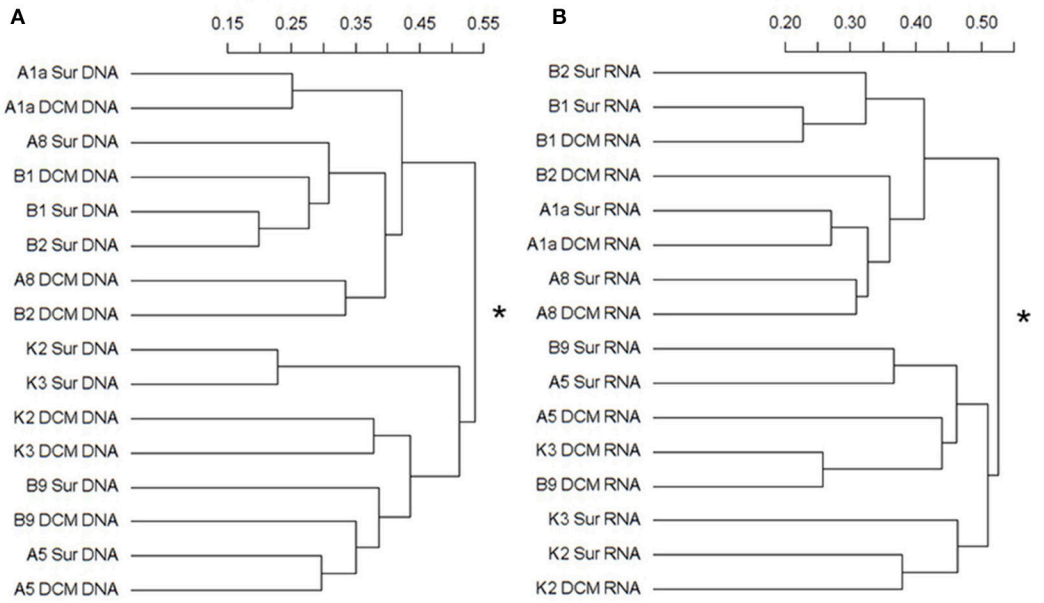

FIGURE 5 | Cluster diagram of the Bray-Curtis dissimilarities based on the log-transformed relative OTU abundance for each sample. The separated DNA **(A)** and RNA **(B)** community groups (with asterisks at the node) exist with significant compositional differences (DNA: $r^2 = 0.31718$, $P = 0.001$; RNA: $r^2 = 0.27023$, $P = 0.001$) as determined by PERMANOVA. The percent dissimilarity among samples is shown along the horizontal axes.

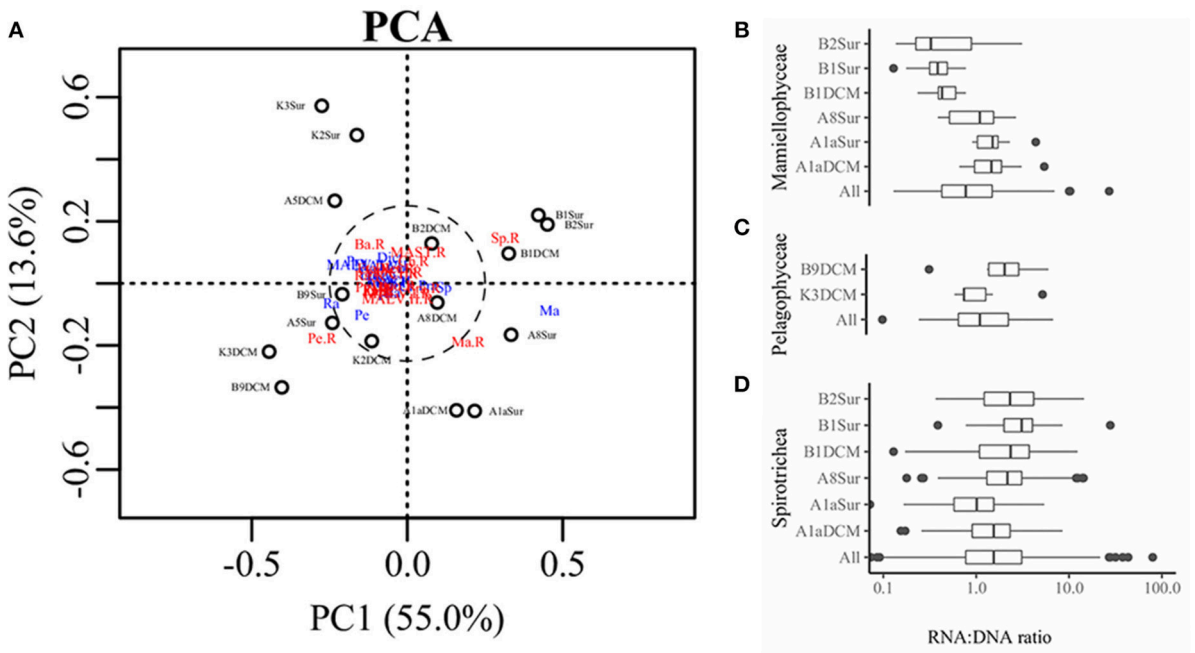

FIGURE 6 | (A) Scatter diagram of PC_1 and PC_2 derived from the relative abundance of higher taxonomic groups in the DNA and RNA databases detected in each sample, blue color indicated the sequences was derived from the DNA survey and red color indicated the sequences was derived from the RNA survey. Ma, Mamiellophyceae; Sp, Spirotrichea; Pe, Pelagophyceae; Ba, Bacillariophyta; Dict, Dictyochophyceae; Prym, Prymnesiophyceae. Boxplot representing the RNA: DNA ratios for Mamiellophyceae **(B)**, Pelagophyceae **(C)**, and Spirotrichea **(D)** in all and individual samples.

et al., 2009; Shi et al., 2009; Wu et al., 2014). Though, DNA-based survey allows for the investigation of all present picoeukaryotic species, this method could lead several biases by including DNA from the dissolved extracellular pools or dormant/dead cells (Karl and Bailiff, 1989). The RNA-based molecular survey better depict picoeukaryotic diversity and indicate the active fractions in natural sample, although this approach faced a numbers of limitations (Blazewicz et al., 2013). Overall, combined the DNA with RNA molecular surveys provide complementary information for picoeukaryotic diversity in a natural environment. First, picoeukaryotic diversity was less studied in the northwestern Pacific Ocean. The current study used HTS based on the DNA and RNA sequences to access the picoeukaryotic diversity and assemblages. Second, the northwestern Pacific Ocean is characterized by intricate oceanic currents and complex oceanographic conditions. Information on how picoeukaryotic diversity and relative metabolic activities impacted by environmental factors in this area is rare. In the present study, the correlation between picoeukaryotic diversity, relative metabolic activities and environmental factors were conducted.

Correlations Between Picoeukaryotic Diversity and Environmental Factors in the Northwestern Pacific Ocean

Previous studies that investigated the relationships between picoeukaryotic assemblages and environmental factors have shown that these micro-organisms respond to many factors (Not et al., 2005; Hamilton et al., 2008; Kirkham et al., 2013; Bellaaj Zouari et al., 2018). In the Gulf of Gabès, picoeukaryotic diversity was known to be affected by both physical and chemical factors (Bellaaj Zouari et al., 2018). In the Atlantic-Arctic confluence region, picoeukaryotic assemblages was affected by geographic proximity, abiotic, and biotic factors and water mass origin (Hamilton et al., 2008). Nutrient concentration was also an important environmental factor affecting the picoeukaryotic assemblages, e.g., the distribution pattern of Prymnesiophyceae and Chrysophyceae was possibly associated with the nitrogen: phosphorus (N: P) ratio (Kirkham et al., 2013) and *micromonas pusilla* was more likely abundant in nutrient rich environments (Not et al., 2005). In the present study, picoeukaryotic diversity was positively correlated with temperature and salinity (**Figure 3C**), indicating that the two environmental factors played an important role in affecting the diversity of picoeukaryotes in the northwestern Pacific Ocean. Picoeukaryotic diversity appears not to be correlated with the nutrient concentrations; however, the number of OTUs was decreased with the increasing nutrient concentrations. High values of the numbers of OTUs were occurred at the stations with low nutrient concentrations, while lower values were detected in the converse environmental conditions (**Figure 3C**).

Picoeukaryotic Assemblages in the Northwestern Pacific Ocean

Picoeukaryotes in the northwestern Pacific Ocean were mainly represented by Mamiellophyceae, MAST, MALV-II, Spirotrichea, Prymnesiophyceae, and MALV-I (69.33% of the total DNA reads) in the DNA survey, and by Spirotrichea, Mamiellophyceae, MAST, Pelagophyceae, and MALV-II (67.46% of the total RNA reads) in the RNA survey (**Table 1** and **Figures 4A**,**B**). The large proportion of Mamiellophyceae was contributed by *O. lucimarinus* (OTU1, **Table S4**) both in the DNA and RNA surveys. This species is surface and high-light-adapted ecotype, and have been found in coastal and marine environments (Palenik et al., 2007; Demir-Hilton et al., 2011). The decreased proportion of Mamiellophyceae in the RNA survey compared to its DNA counterpart, particularly in the KEC and OC mixed water samples (Stn. B1 and B2) (**Figures 4A,B**), suggested that part of Mamiellophyceae DNA molecular during our survey may obtained from dormant or dead cells. The contribution of prasinophytes based on our HPLC method showed comparable pattern of Mamiellophyceae assemblages based on the DNA survey across samples (**Figure S3A** and **Figure 4A**). The calculation of pigment-based composition was largely influenced by the increasing accessory pigment to chl *a* ratios from lower latitude to higher latitude by photo-acclimation. The CHEMTAX calculation might overestimate the percentage of Prasinophytes at Stn. B1 and B2, however the mechanism was different from that of more relative abundance of DNA than RNA. The high proportion of prasinophytes in the KE and adjacent regions was consistent with a recent study reporting prasinophytes became a major group of phytoplankton during the spring bloom (Nishibe et al., 2017). MALV-I and MALV-II, most of which were characterized as parasites on a range of hosts (Skovgaard et al., 2005; Bachvaroff et al., 2012), have been shown to be abundant groups of picoeukaryotes based on the DNA survey in different marine ecosystems (Guillou et al., 2008; Massana, 2011), while were less represented in the RNA survey (Massana et al., 2015). The higher genomic rDNA copy numbers than other picoeukaryotes is the most reasonable explanation for this discrepancy (Massana et al., 2015). During our survey, the overrepresented of the DNA sequences of MALV-I, -II than their RNA counterparts was also observed (**Figures 4A,B** and **Table 1**). *P. calceolate*, the dominant OTU in Pelagophyceae (**Table S4**), is a low-light-adapted species with the ability to adapt well to environmental conditions in the DCM layer (Timmermans et al., 2005; Shi et al., 2009). In our survey, higher proportion of *P. calceolate* sequences in the DCM layer than the surface layer was also observed both in the DNA and RNA datasets (**Table S4**).

In the Bray-Curtis dissimilarity analysis, samples were clustered into two groups both in the DNA and RNA surveys (**Figures 5A,B**). Samples collected at Stn. B1, B2, A1a, A8 were grouped separate from samples collected at Stn. B9, A5, K3, K2, suggesting the presence of a significant compositional differences in these two clusters. Notably, the samples (DNA/RNA) collected at the DCM layer of Stn. B2 were always clustered separately from the other samples collected in the Stn. B1 and B2 (**Figures 5A,B**), and the number of OTUs, Chl *a* concentration and FCM data were also very different from the other samples in Stn. B1 and B2 (**Figures 3A,B**, **Table S1**, and **Figure S3B**). These differences appear to cause by the complex horizontal

and vertical motion of seawater in the KEC and OC mixed water.

Relative Metabolic Activities of Picoeukaryotes in the Northwestern Pacific Ocean

Nowadays, it is generally accepted that protist assemblages inferred from DNA survey represented the whole species, whereas its RNA counterparts specifically represented the active fraction (Massana et al., 2015), in spite of several limitations should be carefully considered in this approach, e.g., the dormant or dead cells (Stoeck et al., 2007; Not et al., 2009), the varied gene copy numbers (Godhe et al., 2008; Gong et al., 2013) and cell size (Zhu et al., 2005). In the present study, picoeukaryotic community composition inferred from DNA and RNA approaches was significantly different (**Figures 4A,B**), and the top variables contributed to the total variabilities were the sequences (DNA or RNA) affiliated to Mamiellophyceae, Pelagophyceae, and Spirotrichea (**Figure 6A**). Previous studies have used the RNA: DNA ratio as a proxy for the relative metabolic activity of taxonomic groups of protist (Hu et al., 2016; Xu et al., 2017). However, the varied RNA: DNA ratios of taxonomic groups among samples should be interpreted cautiously, because the presence of rRNA indicates the possible ribosomal activity and the potential of protein synthesis, instead of providing an indicator of cell activity (Blazewicz et al., 2013). Confined to a specific group, Wu and Liu (2018) found the relative metabolic activities of Bacillariophyceae species in Pearl River-South China Sea Continuum were significantly affected by the PO_4 concentration and salinity. In order to obtain continuous relationship of the relative metabolic activities of individual OTUs in our samples, we selected OTUs only occurred in both DNA and RNA surveys (Hu et al., 2016) and appeared in all samples within Mamiellophyceae, Pelagophyceae, and Spirotrichea for the further metabolic activities analyses. The varied RNA: DNA ratios of individual OTUs across samples suggested the changing metabolic activities of these species in varied environmental conditions (**Figure S4** and **Table S3**), and the relative metabolic activities of these species was mainly affected by the nutrient concentration, i.e., the NO_3 + NO_2 and SiO_3 concentration (**Figure 7**).

In the KEC and OC mixed water samples (Stn. B1 and B2), the relative activities of Mamiellophyceae species were stayed at a low level, while the Spirotrichea species were highly active (**Figure S4** and **Table S3**). Spirotrichea was found to be an active predator of picoeukaryotes and bacteria in the euphotic zone (Calbet and Landry, 2004; McKie-Krisberg and Sanders, 2014). Moreover, MAST-4, which was potential predator of picoeukaryotes (Lin et al., 2012), was also found very active in the KEC and OC mixed water (Stn. B1 and B2) in our RNA survey (**Figure 4B**). Dilution experiments in the same cruise revealed that there was no significant difference in the food selection for microzooplankton in the KEC and OC mixed water. Thus, the abundant picoplankton were more likely to be grazed (unpublished data). So, we suggested that Mamiellophyceae species probably be grazed during our survey, and the overrepresented DNA sequences in the KEC and OC mixed water samples (Stn. B1 and B2) may partially contributed by the dead materials.

CONCLUDING REMARKS

This study represents the first contribution regarding the diversity and activity of picoeukaryotes in the northwestern Pacific Ocean based on the HTS (DNA/RNA). Our finding showed that picoeukaryotes exists high and variable diversity in the study area with different hydrologic conditions. Temperature and salinity were the two important environmental factors affecting the picoeukaryotic diversity. The relative metabolic activities of Mamiellophyceae, Spirotrichea, and Pelagophyceae species were highly affected by the nutrient concentration, i.e., the NO_3 + NO_2 and SiO_3 concentration. Due to the lack of sufficient samples in our survey and the complex oceanographic conditions in the northwestern Pacific Ocean, further investigations are needed to accumulate sufficient data during seasons and years. Overall, these findings contributed to the understanding of picoeukaryotic assemblages and activity in the open ocean system.

AUTHOR CONTRIBUTIONS

FW, BH, and LW designed the experiments and onboarded the processing. FW carried out the experiment and wrote the paper. FW, YX, WW, and PS analyzed the data and improved the manuscript.

FUNDING

This work was supported by grants from the National Natural Science Foundation of China (NSFC, No. U1606404), the National Key R&D Program of China (No. 2016YFA0601201), and another NSFC project (No. 417 76146).

ACKNOWLEDGMENTS

We thank Profs. Huiwang Gao for sampling support and Shuh-Ji Kao for nutrient data. We also thank captains and crew of R/V Dongfanghong II for their cooperation during the cruises.

SUPPLEMENTARY MATERIAL

The Supplementary Material for this article can be found online at: https://www.frontiersin.org/articles/10.3389/fmicb.2018.03259/full#supplementary-material

REFERENCES

Altschul, S. F., Gish, W., Miller, W., Myers, E. W., and Lipman, D. J. (1990). Basic local alignment search tool. *J. Mol. Biol.* 215, 403–410. doi: 10.1016/S0022-2836(05)80360-2

Amaral-Zettler, L. A., Mccliment, E. A., Ducklow, H. W., and Huse, S. M. (2009). A method for studying protistan diversity using massively parallel sequencing of v9 hypervariable regions of small-subunit ribosomal rna genes. *PLoS ONE* 4:e6372. doi: 10.1371/journal.pone.0006372

Bachvaroff, T. R., Kim, S., Guillou, L., Delwiche, C. F., and Coats, D. W. (2012). Molecular diversity of the syndinean genus *Euduboscquella* based on single-cell PCR analysis. *Appl. Environ. Microbiol.* 78, 334–345. doi: 10.1128/AEM.06678-11

Bellaaj Zouari, A., Bel Hassen, M., Balagué, V., Sahli, E., Ben Kacem, M., Akrout, F., et al. (2018). Picoeukaryotic diversity in the Gulf of Gabès: variability patterns and relationships to nutrients and water masses. *Aquat. Microb. Ecol.* 81, 37–53. doi: 10.3354/ame01857

Berney, C., Fahrni, J., and Pawlowski, J. (2004). How many novel eukaryotic 'kingdoms'? Pitfalls and limitations of environmental dna surveys. *BMC Biol.* 2:13. doi: 10.1186/1741-7007-2-13

Blazewicz, S. J., Barnard, R. L., Daly, R. A., and Firestone, M. K. (2013). Evaluating rRNA as an indicator of microbial activity in environmental communities: limitations and uses. *ISME J.* 7, 2061–2068. doi: 10.1038/ismej.2013.102

Calbet, A., and Landry, M. R. (2004). Phytoplankton growth, microzooplankton grazing, and carbon cycling in marine systems. *Limnol. Oceanogr.* 49, 51–57. doi: 10.4319/lo.2004.49.1.0051

Caporaso, J. G., Kuczynski, J., Stombaugh, J., Bittinger, K., Bushman, F. D., Costello, E. K., et al. (2010). QIIME allows analysis of highthroughput community sequencing data. *Nat. Methods* 7, 335–336. doi: 10.1038/nmeth.f.303

Caron, D. A., Countway, P. D., Jones, A. C., Kim, D. Y., and Schnetzer, A. (2012). Marine protistan diversity. *Annu. Rev. Mar. Sci.* 4, 467–493. doi: 10.1146/annurev-marine-120709-142802

Chen, S. (2008). The Kuroshio Extension Front from satellite sea surface temperature measurements. *J. Oceanogr.* 64, 891–897. doi: 10.1007/s10872-008-0073-6

Choi, D. H., An, S. M., Chun, S., Yang, E. C., Selph, K. E., Lee, C. M., et al. (2016). Dynamic changes in the composition of photosynthetic picoeukaryotes in the northwestern Pacific Ocean revealed by high-throughput tag sequencing of plastid 16S rRNA genes. *FEMS. Microbiol. Ecol.* 92:fiv170. doi: 10.1093/femsec/fiv170

de Vargas, C., Audic, S., Henry, N., Decelle, J., Mahé, F., Logares, R., et al. (2015). Eukaryotic plankton diversity in the sunlit ocean. *Science* 348:1261605. doi: 10.1126/science.1261605

Demir-Hilton, E., Sudek, S., Cuvelier, M. L., Gentemann, C. L., Zehr, J. P., and Worden, A. Z. (2011). Global distribution patterns of distinct clades of the photosynthetic picoeukaryote Ostreococcus. *ISME J.* 5, 1095–1107. doi: 10.1038/ismej.2010.209

Díez, B., Pedrós-Alió, C., and Massana, R. (2001). Study of genetic diversity of eukaryotic picoplankton in different oceanic regions by small-subunit rRNA gene cloning and sequencing. *Appl. Environ. Microbiol.* 67, 2932–2941. doi: 10.1128/AEM.67.7.2932-2941.2001

Doney, S. C., Ruckelshaus, M., Duffy, J. E., Barry, J. P., Chan, F., and English, C. A., et al. (2012). Climate change impacts on marine ecosystems. *Ann. Rev. Mar. Sci.* 4, 11–37. doi: 10.1146/annurev-marine-041911-111611

Edgar, R. C. (2013). UPARSE: highly accurate OTU sequences from microbial amplicon reads. *Nat. Methods* 10, 996–998. doi: 10.1038/nmeth.2604

Edgar, R. C., Haas, B. J., Clemente, J. C., Quince, C., and Knight, R. (2011). UCHIME improves sensitivity and speed of chimera detection. *Bioinformatics* 27, 2194–2200. doi: 10.1093/bioinformatics/btr381

Egge, E. S., Bittner, L., Andersen, T., Audic, S., de Vargas, C., and Edvardsen, B. (2013). 454 Pyrosequencing to describe microbial eukaryotic community composition, diversity and relative abundance: a test for marine Haptophytes. *PLoS ONE* 8:e74371. doi: 10.1371/journal.pone.0074371

Egge, E. S., Johannessen, T. V., Andersen, T., Eikrem, W., Bittner, L., Larsen, A., et al. (2015). Seasonal diversity and dynamics of haptophytes in the Skagerrak, Norway, explored by high-throughput sequencing. *Mol. Ecol.* 24, 3026–3042. doi: 10.1111/mec.13160

Godhe, A., Asplund, M. E., Harnstrom, K., Saravanan, V., Tyagi, A., and Karunasagar, I. (2008). Quantification of Diatom and Dinoflagellate biomasses in coastal marine seawater samples by real-time PCR. *Appl. Environ. Microbiol.* 74, 7174–7182. doi: 10.1128/AEM.01298-08

Gong, J., Dong, J., Liu, X., and Massana, R. (2013). Extremely high copy numbers and polymorphisms of the rDNA operon estimated from single cell analysis of oligotrich and peritrich Ciliates. *Protist* 164, 369–379. doi: 10.1016/j.protis.2012.11.006

Grob, C., Ulloa, O., Li, W., Alarcón, G., Fukasawa, M., and Watanabe, S. (2007). Picoplankton abundance and biomass across the eastern South Pacific Ocean along latitude 32.5°S. *Mar. Ecol. Prog. Ser.* 332, 53–62. doi: 10.3354/meps332053

Grossmann, L., Jensen, M., Pandey, R., Jost, S., Bass, D., Psenner, R., et al. (2016). Molecular investigation of protistan diversity along an elevation transect of alpine lakes. *Aquat. Microb. Ecol.* 78, 25–37. doi: 10.3354/ame01798

Guillou, L., Viprey, M., Chambouvet, A., Welsh, R. M., Kirkham, A. R., Massana, R., et al. (2008). Widespread occurrence and genetic diversity of marine parasitoids belonging toSyndiniales (*Alveolata*). *Environ. Microbiol.* 10, 3349–3365. doi: 10.1111/j.1462-2920.2008.01731.x

Hamilton, A. K., Lovejoy, C., Galand, P. E., and Ingram, R. G. (2008). Water masses and biogeography of picoeukaryote assemblages in a cold hydrographically complex system. *Limnol. Oceanogr.* 53, 922–935. doi: 10.4319/lo.2008.53.3.0922

Hartmann, M., Grob, C., Tarran, G. A., Martin, A. P., Burkill, P. H., Scanlan, D. J., et al. (2012). Mixotrophic basis of Atlantic oligotrophic ecosystems. *Proc. Natl. Acad. Sci. U. S. A.* 109, 5756–5760. doi: 10.1073/pnas.1118179109

Hu, S. K., Campbell, V., Connell, P., Gellene, A. G., Liu, Z., Terrado, R., et al. (2016). Protistan diversity and activity inferred from RNA and DNA at a coastal site in the eastern North Pacific. *FEMS Microbiol. Ecol.* 92:fiw050. doi: 10.1093/femsec/fiw050

Jardillier, L., Bettarel, Y., Richardot, M., Bardot, C., Amblard, C., Sime-Ngando, T., et al. (2005). Effects of viruses and predators on prokaryotic community composition. *Microb. Ecol.* 50, 557–569. doi: 10.1007/s00248-005-5030-y

Jardillier, L., Zubkov, M. V., Pearman, J., and Scanlan, D. J. (2010). Significant CO2 fixation by small prymnesiophytes in the subtropical and tropical northeast Atlantic Ocean. *ISME J.* 4, 1180–1192. doi: 10.1038/ismej.2010.36

Karl, D. M., and Bailiff, M. D. (1989). The measurement and distribution of dissolved nucleic acids in aquatic environments. *Limnol. Oceanogr.* 34, 543–558. doi: 10.4319/lo.1989.34.3.0543

Kawamura, H., Mizuno, K., and Toba, Y. (1986). Formation process of a warm-core ring in the Kuroshio-Oyashio frontal zone—December 1981–October 1982. *Deep Sea Res.* 33, 1617–1640. doi: 10.1016/0198-0149(86)90070-1

Kirkham, A. R., Lepère, C., Jardillier, L. E., Not, F., Bouman, H., Mead, A., and Scanlan, D. J. (2013). A global perspective on marine photosynthetic picoeukaryote community structure. *ISME J.* 7, 922–936. doi: 10.1038/ismej.2012.166

Lepère, C., Vaulot, D., and Scanlan, D. J. (2009). Photosynthetic picoeukaryote community structure in the South East Pacific Ocean encompassing the most oligotrophic waters on Earth. *Environ. Microbiol.* 11, 3105–3117. doi: 10.1111/j.1462-2920.2009.02015.x

Lin, Y. C., Campbell, T., Chung, C. C., Gong, G. C., Chiang, K. P., and Worden, A. Z. (2012). Distribution patterns and phylogeny of marine Stramenopiles in the North Pacific Ocean. *Appl. Environ. Microbiol.* 78, 3387–3399. doi: 10.1128/AEM.06952-11

Liu, H., Imai, K., Suzuki, K., Nojiri, Y., Tsurushima, N., and Saino, T. (2002). Seasonal variability of picophytoplankton and bacteria in the western subarctic Pacific Ocean at station KNOT. *Deep Sea Res. II Top. Stud. Oceanogr.* 49, 5409–5420. doi: 10.1016/S0967-0645(02)00199-6

Mackey, M., Mackey, D., Higgins, H., and Wright, S. (1996). CHEMTAX - a program for estimating class abundances from chemical markers:application to HPLC measurements of phytoplankton. *Mar. Ecol. Prog. Ser.* 144, 265–283. doi: 10.3354/meps144265

Magoč, T., and Salzberg, S. L. (2011). FLASH: fast length adjustment of short reads to improve genome assemblies. *Bioinformatics* 27, 2957–2963. doi: 10.1093/bioinformatics/btr507

Massana, R. (2011). Eukaryotic picoplankton in surface oceans. *Annu. Rev. Microbiol.* 65, 91–110. doi: 10.1146/annurev-micro-090110-102903

Massana, R., Castresana, J., Balague, V., Guillou, L., Romari, K., Groisillier, A., et al. (2004). Phylogenetic and ecological analysis of

novel marine Stramenopiles. *Appl. Environ. Microbiol.* 70, 3528–3534. doi: 10.1128/AEM.70.6.3528-3534.2004

Massana, R., Gobet, A., Audic, S., Bass, D., Bittner, L., Boutte, C., et al. (2015). Marine protist diversity in European coastal waters and sediments as revealed by high-throughput sequencing. *Environ. Microbiol.* 17, 4035–4049. doi: 10.1111/1462-2920.12955

Massana, R., Unrein, F., Rodriguez-Martinez, R., Forn, I., Lefort, T., Pinhassi, J., et al. (2009). Grazing rates and functional diversity of uncultured heterotrophic flagellates. *ISME J.* 3,588–596. doi: 10.1038/ismej.2008.130

McKie-Krisberg, Z. M., and Sanders, R. W. (2014). Phagotrophy by the picoeukaryotic green alga *Micromonas*: implications for Arctic Oceans. *ISME J.* 8, 1953–1961. doi: 10.1038/ismej.2014.16

Moon-van der Staay, S. Y., De Wachter, R., and Vaulot, D. (2001). Oceanic 18S rDNA sequences from picoplankton reveal unsuspected eukaryotic diversity. *Nature* 409, 607–610. doi: 10.1038/35054541

Nishibe, Y., Takahashi, K., Sato, M., Kodama, T., Kakehi, S., Saito, H., et al. (2017). Phytoplankton community structure, as derived from pigment signatures, in the Kuroshio extension and adjacent regions in winter and spring. *J. Oceanogr.* 73, 463–478. doi: 10.1007/s10872-017-0415-3

Nishibe, Y., Takahashi, K., Shiozaki, T., Kakehi, S., Saito, H., and Furuya, K. (2015). Size-fractionated primary production in the Kuroshio Extension and adjacent regions in spring. *J. Oceanogr.* 71, 27–40. doi: 10.1007/s10872-014-0258-0

Not, F., del Campo, J., Balagué, V., de Vargas, C., and Massana, R. (2009). New insights into the diversity of marine picoeukaryotes. *PLoS ONE* 4:e7143. doi: 10.1371/journal.pone.0007143

Not, F., Massana, R., Latasa, M., Marie, D., Colson, C., Eikrem, W., et al. (2005). Late summer community composition and abundance of photosynthetic picoeukaryotes in Norwegian and Barents Seas. *Limnol. Oceanogr.* 50, 1677–1686. doi: 10.4319/lo.2005.50.5.1677

Not, F., Valentin, K., Romari, K., Lovejoy, C., Massana, R., Tobe, K., et al. (2007). Picobiliphytes: a marine picoplanktonic algal group with unknown affinities to other eukaryotes. *Science* 315, 253–255. doi: 10.1126/science.1136264

Oksanen,. J., Blanchet, F. G., Kindt, R., Legendre, P., Minchin, P. R., O'Hara, R. B., et al. (2015) *Vegan: Community Ecology Package. R Package Version 2.2-0*. Available online at: http://CRAN.R-project.org/package5vegan/

Palenik, B., Grimwood, J., Aerts, A., Rouze, P., Salamov, A., Putnam, N., et al. (2007). The tiny eukaryote *Ostreococcus* provides genomic insights into the paradox of plankton speciation. *Proc. Natl. Acad. Sci. U. S. A.* 104, 7705–7710. doi: 10.1073/pnas.0611046104

Pomeroy, L. R., , leB Williams, P. J., Azam, F., and Hobbie, J. (2007). The microbial loop. *Oceanography* 20, 28–33. doi: 10.5670/oceanog.2007.45

Qiu, B. (2001). "Kuroshio and Oyashio currents," in *Encyclopedia of Ocean Sciences,* eds J. Steele, S. Thorpe, and K. Turekian (New York, NY: Academic Press), 1413–1425.

Quast, C., Pruesse, E., Yilmaz, P., Gerken, J., Schweer, T., Yarza, P., et al. (2013). The SILVA ribosomal RNA gene database project: improved data processing and web-based tools. *Nucleic Acids Res.* 41, D590–D596. doi: 10.1093/nar/gks,1219

R Core Team. (2014). *R: A Language and Environment for Statistical Computing*. Vienna: R. Foundation for Statistical Computing.

Rachik, S., Christaki, U., Li, L. L., Genitsaris, S., Breton, E., and Monchy, S. (2018). Diversity and potential activity patterns of planktonic eukaryotic microbes in a mesoeutrophic coastal area (eastern English Channel). *PLoS ONE* 13:e0196987. doi: 10.1371/journal.pone.0196987

Richards, T. A., Vepritskiy, A. A., Gouliamova, D. E., and Nierzwicki-Bauer, S. A. (2005). The molecular diversity of freshwater picoeukaryotes from an oligotrophic lake reveals diverse, distinctive and globally dispersed lineages. *Environ. Microbiol.* 7, 1413–1425. doi: 10.1111/j.1462-2920.2005.00828.x

Sanders, R. W., and Gast, R. J. (2012). Bacterivory by phototrophic picoplankton and nanoplankton in Arctic waters. *FEMS Microbiol. Ecol.* 82, 242–253. doi: 10.1111/j.1574-6941.2011.01253.x

Sherr, E. B., and Sherr, B. F. (1994). Bacterivory and herbivory: key roles of phagotrophic protists in pelagic food webs. *Microb. Ecol.* 28, 223–235. doi: 10.1007/BF00166812

Shi, X. L., Marie, D., Jardillier, L., Scanlan, D. J., and Vaulot, D. (2009). Groups without cultured representatives dominate eukaryotic picophytoplankton in the oligotrophic south east Pacific Ocean. *PLoS ONE* 4:e7657. doi: 10.1371/journal.pone.0007657

Skovgaard, A., Massana, R., Balagué, V., and Saiz, E. (2005). Phylogenetic position of the copepod-infesting parasite syndinium turbo (*Dinoflagellata*, *Syndinea*). *Protist* 156, 413–423. doi: 10.1016/j.protis.2005.08.002

Stoeck, T., Zuendorf, A., Breiner, H.-W., and Behnke, A. (2007). A Molecular approach to identify active microbes in environmental eukaryote clone libraries. *Microb. Ecol.* 53, 328–339. doi: 10.1007/s00248-006-9166-1

Terrado, R., Medrinal, E., Dasilva, C., Thaler, M., Vincent, W. F., and Lovejoy, C. (2011). Protist community composition during spring in an Arctic flaw lead polynya. *Polar. Biol.* 34, 1901–1914. doi: 10.1007/s00300-011-1039-5

Timmermans, K. R., van der Wagt, B., Veldhuis, M. J. W., Maatman, A., and de Baar, H. J. W. (2005). Physiological responses of three species of marine pico-phytoplankton to ammonium, phosphate, iron and light limitation. *J. Sea. Res.* 53, 109–120. doi: 10.1016/j.seares.2004.05.003

Unrein, F., Gasol, J. M., Not, F., Forn, I., and Massana, R. (2014). Mixotrophic haptophytes are key bacterial grazers in oligotrophic coastal waters. *ISME J.* 8, 164–176. doi: 10.1038/ismej.2013.132

Vaulot, D., Eikrem, W., Viprey, M., and Moreau, H. (2008). The diversity of small eukaryotic phytoplankton ($\leq$3 μm) in marine ecosystems. *FEMS Microbiol. Rev.* 32, 795–820. doi: 10.1111/j.1574-6976.2008.00121.x

Worden, A. Z., Nolan, J. K., and Palenik, B. (2004). Assessing the dynamics and ecology of marine picophytoplankton: the importance of the eukaryotic component. *Limnol. Oceanogr.* 49, 168–179. doi: 10.4319/lo.2004.49.1.0168

Wu, W., Huang, B., Liao, Y., and Sun, P. (2014). Picoeukaryotic diversity and distribution in the subtropical-tropical South China Sea. *FEMS Microbiol. Ecol.* 89, 563–579. doi: 10.1111/1574-6941.12357

Wu, W., and Liu, H. (2018). Disentangling protist communities identified from DNA and RNA surveys in the Pearl River-South China Sea Continuum during the wet and dry seasons. *Mol. Ecol.* 27, 4627–4640. doi: 10.1111/mec.14867

Xu, D., Li, R., Hu, C., Sun, P., Jiao, N., and Warren, A. (2017). Microbial eukaryote diversity and activity in the water column of the south china sea based on DNA and RNA high throughput sequencing. *Front. Microbiol.* 8:1121. doi: 10.3389/fmicb.2017.01121

Yasuda, I. (2003). Hydrographic structure and variability in the kuroshio-oyashio transition area. *J. Oceanogr.* 59, 389–402. doi: 10.1023/A:1025580313836

Zapata, M., Rodríguez, F., and Garrido, J. (2000). Separation of chlorophylls and carotenoids from marine phytoplankton:a new HPLC method using a reversed phase C8 column and pyridine-containing mobile phases. *Mar. Ecol. Prog. Ser.* 195, 29–45. doi: 10.3354/meps195029

Zhu, F., Massana, R., Not, F., Marie, D., and Vaulot, D. (2005). Mapping of picoeucaryotes in marine ecosystems with quantitative PCR of the 18S rRNA gene. *FEMS Microbiol. Ecol.* 52, 79–92. doi: 10.1016/j.femsec.2004.10.006

Zinger, L., Gobet, A., and Pommier, T. (2011). Two decades of describing the unseen majority of aquatic microbial diversity. *Mol. Ecol.* 21, 1878–1896. doi:10.1111/j.1365-294x.2011.05362.x

Zubkov, M. V., and Tarran, G. A. (2008). High bacterivory by the smallest phytoplankton in the North Atlantic Ocean. *Nature* 455, 224–226. doi: 10.1038/nature07236

Conflict of Interest Statement: The authors declare that the research was conducted in the absence of any commercial or financial relationships that could be construed as a potential conflict of interest.

Copyright © 2019 Wang, Xie, Wu, Sun, Wang and Huang. This is an open-access article distributed under the terms of the Creative Commons Attribution License (CC BY). The use, distribution or reproduction in other forums is permitted, provided the original author(s) and the copyright owner(s) are credited and that the original publication in this journal is cited, in accordance with accepted academic practice. No use, distribution or reproduction is permitted which does not comply with these terms.

frontiers in Marine Science

ORIGINAL RESEARCH
published: 14 January 2019
doi: 10.3389/fmars.2018.00512

Microbial Communities in Coastal Glaciers and Tidewater Tongues of Svalbard Archipelago, Norway

*Eva Garcia-Lopez, Irene Rodriguez-Lorente, Paula Alcazar and Cristina Cid**

Microbial Evolution Laboratory, Centro de Astrobiologia (CSIC-INTA), Madrid, Spain

Global warming is having a great impact on the Arctic region, due to the change of air temperature and precipitation. As a consequence, the glacial ice melts and englacial materials are being transported into the ocean. These substances can constitute a source of nutrients in food webs or, on the contrary, a source of contaminants. In this research seven marine Svalbard glaciers and their tidewater tongues were focused. This survey provides a first attempt comparing microbial communities from coastal and tidewater glaciers that reveal a hitherto unknown microbial diversity. A wider diversity was found in glaciers than in seawater samples. Glacier microorganisms mainly corresponded to the phylum Proteobacteria (48.8%), Bacteroidetes (29.1%) and Cyanobacteria (16.3%) (**Figure 3A**). Seawater microorganisms belonged to Bacteroidetes (40.3%), Actinobacteria (31.7%) and Proteobacteria (25.4%). Other phyla found such as Firmicutes, Thermi, Gemmatimonadetes, Verrucomicrobia, Nitrospirae, Chloroflexi, Planctomycetes, and Chlamydiae were less abundant. The distribution of microbial communities was affected in different extent by the concentration of nutrients (nitrogen nutrients, dissolved organic carbon and soluble reactive phosphorus) and by environmental parameters such as salinity. Nevertheless, the environmental variables did not influence in the distribution of the microbial communities as much as the concentration of nutrients did. Our results demonstrate an interchange between glacier and coastal microbial populations as well as the presence of some indicator species (i.e., *Hymenobacter*) as possible sentinels for bacterial transport between glaciers and their downstream seawaters. The consequence of this process could be the alteration of the water composition of the fiords producing serious consequences throughout the marine ecosystem and in the cycling of globally important elements.

Keywords: coastal glaciers, next-generation sequencing, food web, Svalbard archipelago, Arctic

OPEN ACCESS

Edited by:
Alejandro A. Murillo, EMBL Heidelberg, Germany

Reviewed by:
Raghab Ray, University of Tokyo, Japan
Tatiana A. Vishnivetskaya, University of Tennessee, Knoxville, United States

***Correspondence:**
Cristina Cid
cidsc@inta.es;
cidsc@cab.inta-csic.es

Specialty section:
This article was submitted to Coastal Ocean Processes, a section of the journal Frontiers in Marine Science

Received: *26 June 2018*
Accepted: *21 December 2018*
Published: *14 January 2019*

Citation:
Garcia-Lopez E, Rodriguez-Lorente I, Alcazar P and Cid C (2019) Microbial Communities in Coastal Glaciers and Tidewater Tongues of Svalbard Archipelago, Norway. Front. Mar. Sci. 5:512. doi: 10.3389/fmars.2018.00512

Abbreviations: BGN, Brøggerbreen glacier; CCA, Canonical Correspondence Analysis; CG, samples from coastal glaciers; CT, samples from the tidewater area closest to a coastal glacier; DCA, Detrended Correspondence Analysis; DOC, Dissolved organic matter; ICP-MS, Inductively coupled plasma-mass spectrometry; IG, samples from inland glaciers; IT, samples from the tidewater area closest to an inland glacier; KGV, Kongsvegen glacier; KNB, Kronebreen glacier; LBE, Lovénbreen Austre glacier; LVM, Lovénbreen Midtre glacier; OTU, operational taxonomic units; PCA, principal components analysis; POOL, Poolepynten; SRP, soluble reactive phosphorus; TDN, total dissolved nitrogen; YTRE, Ytre Norskøya.

INTRODUCTION

Glaciers have been considered authentic biomes (Anesio and Laybourn-Parry, 2012), in which microbial life goes by enduring a hostile environment. Microbial communities associated with glaciers found all over the world, are being increasingly studied. Specifically, these microorganisms have been reported in Polar Arctic (Amato et al., 2007; Hell et al., 2013; Larose et al., 2013) and Antarctic Regions (Foreman et al., 2007) and in high mountains (Garcia-Descalzo et al., 2013; Hotaling et al., 2017). However, glaciers are very different from each other, which influence the life of their inhabitants. The effect of environmental variables, of chemical composition (Møller et al., 2011) and nutrient concentration on microbial communities have been extensively researched (Mindl et al., 2007).

The Svalbard archipelago (74° to 81° N) (**Figure 1**) comprise an area of 62,248 km^2, with more than 2,000 glaciers; and ice covers 60% of its surface (Lang, 2011). Svalbard glaciers are of various kinds (Hagen et al., 1993; Hagen et al., 2003), although most of them are sub-polar or polythermal, sharing the characteristics of the cold and temperate glaciers (Hagen et al., 1993). Some of them have a coastal margin and terminate in a calving front, what establishes important differences with respect to glaciers with inland margin. Coastal glaciers calve icebergs into the ocean (McNabb et al., 2016). These glaciers greatly affect the physical and chemical characteristics of the sea to which they discharge (Garcia-Lopez et al., 2016). In glaciers ending on land, there is continuous permafrost at ice front; while calving glaciers present partly or completely temperate tidewater tongues (Hagen et al., 2003).

Global warming is nowadays one of the most worrying problems. It is having a great impact on the Arctic region, because of the change of air temperature and precipitation (Solomon et al., 2007; Førland et al., 2009). As a consequence, the glacial ice melts and disappears, and microbial communities are being seriously affected (Hallbeck, 2009; Zeng et al., 2013). One of the effects of global warming is the change in the basal temperature of the ice, moving from cold to polythermal; this causes the growth of new microorganisms that are not psychrophiles, thus leading to changes in the diversity (Hell et al., 2013; Nowak and Hodson, 2014). It is essential to know how climate change is shaping the distribution and diversity of microbial communities, as microorganisms participate particularly in the ecology of the Arctic ecosystems. They constitute the basis of trophic networks and they are an essential element in carbon and nutrient cycling (Hoham and Duval, 2001; Garcia-Descalzo et al., 2013).

In the last few decades, recently deglaciated areas present in different glacial zones in the world, are available for colonization and primary succession, especially initiated by pioneer microorganisms (Kastovska et al., 2005; Deiglmayr et al., 2006). It has been researched that in glacier forelands, soil microorganisms are essential for plant growth as they play a key role in the nutrient cycling. In this phase, nitrogen, phosphorus, and other nutrients accumulate and facilitate

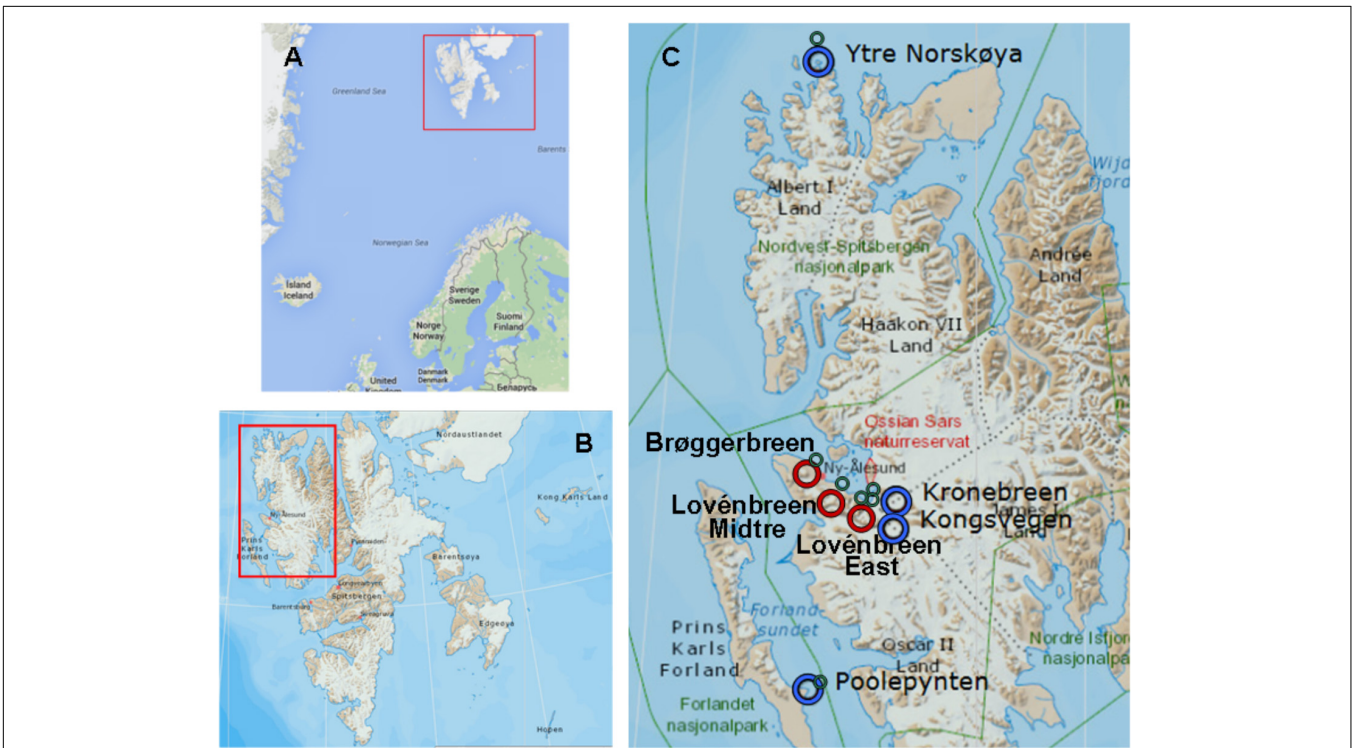

FIGURE 1 | Geographic maps the Arctic Svalbard archipelago. **(A)** Svalbard archipelago. **(B)** Spitsbergen and Prins Karls Forland. **(C)** Map showing the distribution of ice samples collected at marine glaciers (blue rings), inland glaciers (red rings) and tidewaters tongues (green rings). Image sources: Google maps **(A)** and TopoSvalbard (Copyright Norwegian Polar Institute) **(B,C)**.

succeeding plant growth (Garcia-Lopez and Cid, 2017; Kim M. et al., 2017). Similarly, in seawater, these microorganisms could also contribute to the development and evolution of marine trophic webs.

The role of microorganisms in polar environments is essential (Kirchman et al., 2009). They are responsible for carrying out key functions in the ecosystems. For instance, phosphorus is a major growth-limiting nutrient, which can be made biologically available by a group of heterotrophic microorganisms (Khan et al., 2009). Other important nutrients such as natural polysaccharides from plants and algae (cellulose, and laminarin) are degraded by some bacteria such as Cytophaga and a few *Clostridium* species (Lopez-Ramirez et al., 2015). The denitrification or reduction of NO_3^- to N_2, NO, or N_2O, is the main means by which N_2 and N_2O are biologically formed. Nitrification (the oxidation of NH_3 to NO_3^-) is a main process in oxic environments, and it is carried out by the nitrifying bacteria (Madigan et al., 2012). Sulfate-reducing bacteria are also a highly diverse group. Many reduced sulfur compounds are used as electron donors by sulfur bacteria. The most common sulfur compounds used as electron donors are H_2S, S^0, SO_3^{2-}. Hydrogen sulfide H_2S is oxidized by chemolithotrophic microorganisms to sulfur S^0 and sulfate SO_4^{2-}. SO_4^{2-} can then be reduced to H_2S by activities of the sulfate-reducing bacteria (organisms that consume organic carbon) and this reduction closes the biogeochemical sulfur cycle while regenerating CO_2 (Madigan et al., 2012).

With the aim of studying whether a process of colonization analogous to what happens in soils can be initiated in the coastal glaciers, the microbial populations of seven glaciers and their corresponding discharge seawaters were studied. The studied glaciers were: Lovénbreen Midtre (LVM), Lovénbreen Austre (LBE), Kongsvegen (KGV), Kronebreen (KNB), Brøggerbreen (BGN), Ytre Norskøya (YTRE) (Hamiltonbukta), and Poolepynten (POOL) (Archibald Geikiebreen) (**Figure 2**). Of these seven glaciers, two are more distant (YTRE and POOL) and the other five form a glacial circus. One of them (BGN) is close to a populated area, which can also condition the microbial communities. In addition, some are marine and others are terrestrial, and each has its particular physico-chemical characteristics. The study of such microorganisms involved the sequencing of the 16S rRNA genes to identify bacteria. The chemical composition of ice and seawater was also one of the main goals of study. Once the microorganisms in the samples were identified, their distribution and relationship with the chemical composition of glacial ice and seawater were determined.

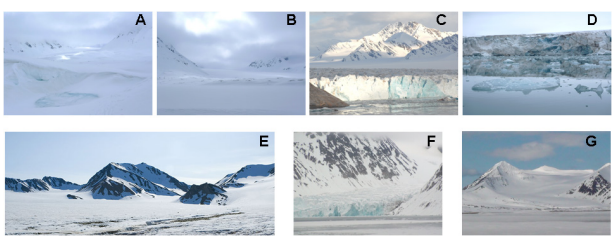

FIGURE 2 | Images of the seven Svalbard glaciers. **(A)** Lovénbreen Midtre, Sherdahlfjellet (LVM); **(B)** Lovénbreen Austre, Slatlofjellet (LBE); **(C)** Kongsvegen (KGV); **(D)** Kronebreen (KNB); **(E)** Brøggerbreen (BGN); **(F)** Ytre Norskøya, Hamiltonbukta (YTRE); **(G)** Poolepynten, Archibald Geikiebreen (POOL). GPS Coordinates: Kongsvegen: 78°51′44″N 12°32′29″E; Kronebreen 78°52′23″N 12°39′14″E; Ytre Norskøya: 79°47′11″N 11°44′14″E; Poolepynten: 78°27′29″N 11°32′55″E; Lovénbreen Midtre: 78°53′12″N 12°2′57″E; Lovénbreen Austre: 78°53′51″N 11°49′15″E; Brøggerbreen: 78°54′49″N 11°43′42″ E.

MATERIALS AND METHODS

Sample Collection and Processing

Two types of samples were obtained, during summer 2014, from seven Svalbard glaciers and their corresponding nearest tidewater (**Figures 1**, **2**). The glaciers considered in the study were: Lovénbreen Midtre, Sherdahlfjellet (LVM); Lovénbreen Austre, Slatlofjellet (LBE); Kongsvegen (KGV); Kronebreen (KNB); Brøggerbreen (BGN); Ytre Norskøya, Hamiltonbukta (YTRE); Poolepynten, Archibald Geikiebreen (POOL). Four glaciers, KGV, KNB, YTRE and POOL, present all or part of the glacier front in the sea, and are termed "coastal glaciers"; the rest are termed "inland glaciers." Samples were named as: CG, glacial ice samples from coastal glaciers (KGV, KNB, YTRE, and POOL); IG, glacial ice samples from inland glaciers (LVM, LBE, and BGN); CT, seawater samples from the tidewater area closest to a coastal glacier; and IT, seawater samples from the tidewater area closest to an inland glacier. GPS coordinates of the sampling areas are detailed in **Table 1**.

Glacial ice samples were obtained, by removing 20–30 cm of thick debris and by drilling with a Mark II Kovacs Core System. Each ice core of 9 cm × 3 m was cut into three parts to obtain three sampling replicates. Glacial ice samples (a total of 21) were wrapped in sterile plastic bags, transported in ice and stored at −20°C until analyzing in the laboratory at the Kings Bay Research Station (Ny Ålesund, Svalbard). Then, ice samples were decontaminated following a surface decontamination and melting procedure described in previous studies (Garcia-Descalzo et al., 2013). In a UV-irradiated laminar flow hood, each section of block ice was removed from −20°C and soaked in ice-cold 95% ethanol for 1 min, followed by extensive rinsing with 0.22 μm-filtered MilliQ water, effectively ablating the exterior 2-cm shell of ice samples. The decontaminated interior ice was thawed in a sterile plastic bag at 4°C and used for analyses.

Tidewater samples (3 sampling replicates, a total of 21) were obtained at the seaside, in the nearest point from each glacier. They were collected in Niskin bottles at a depth of 2 m as in Zaikova et al. (2009), transported and immediately filtered in the laboratory.

Both, the meltwater and tidewater samples were individually filtered through filters with pores of 0.22 μm attached to a vacuum pump in a flow hood, previously sterilized with ethanol. Both filters and water were stored at −20°C until use in the laboratory at the Centro de Astrobiología (Madrid, Spain). To control for laboratory contamination, 500 ml of MilliQ water were subjected to identical analytical procedures.

TABLE 1 | Glacier coordinates and geochemical properties.

	Kongsvegen KGV		Kronebreen KNB		Ytre Norskøya YTRE		Poolepynten POOL		Lovénbreen Midtre LVM		Lovénbreen Austre LBE		Brøggerbreen BGN	
	Glacier	Tidewater	Glacier	Tidewater	Glacier	Tidewater	Glacier	Tidewater	Glacier	Tidewater	Glacier	Tidewater	Glacier	Tidewater
GPS Coordinates*	78°51′44′′N 12°32′29′′E		78°52′23′′N 12°39′14′′E		79°47′11′′N 11°44′14′′E		78°27′29′′N 11°32′55′′E		78°53′12′′N 12°2′57′′E		78°53′51′′N 11°49′15′′E		78°54′49′′N 11°43′42′′E	
Altitude(m)	10	−2	25	−2	100	− 2	25	−2	59	−2	49	−2	100	−2
Temperature (°C)	0.3	0.8	0.3	0.7	0.1	0.9	0.8	2.2	0.6	2.1	0.6	2.5	0.1	2.1
pH	4.5	4.5	4.5	4.5	4.5	5.1	4.5	4.0	5	5.5	5	4.5	4.5	5.2
Salinity (ppt)	30.11 (2.98)	224.45 (7.32)	30.11 (2.98)	234.65 (3.82)	100.13 (6.23)	31.25 (2.36)	120.01 (4.45)	29.21 (1.32)	0.24 (0.03)	25.33 (2.04)	0.35 (0.06)	29.52 (1.99)	0.22 (0.02)	26.12 (2.14)
Type of samples	CG	CT	CG	CT	CG	CT	CG	CT	IG	IT	IG	IT	IG	IT
Glacier margin	Coastal		Coastal		Coastal		Coastal		Inland		Inland		Inland	

**According to http://toposvalbard@npolar.no/ (Norwegian Polar Institute).*

Chemical Analysis of Meltwater

Basic measurements of physical and chemical parameters of meltwater from sampling sites were made with a temperature-calibrated pH, conductivity, and salinity meter (WTW, Weilheim, Germany). Assays for dissolved nitrogen and phosphorus (NH_4^+, NO^{2-}, NO^{3-}, TDN, SRP, and DOC) were performed by ion chromatographic method using suppressed conductivity detection (Garcia-Descalzo et al., 2013) and by HPLC-Size Exclusion Chromatography with UV and On-Line DOC Detection (Her et al., 2002) in a 861 Advance Compact IC system (Metrohm AG, Herisau, Switzerland). Chromatograms were recorded using the Metrohm IC Net 2.3 SR6 software.

Extraction, Quantification and Sequencing of Genomic DNA

Genomic DNA from each sampling replicate (500 ml) was extracted by using the DNA Isolation PowerWater kit (MO BIO Laboratory, Inc.). Extraction procedures were identical for all samples. DNA concentration was determined using a Nanodrop 2000p.

Then, Illumina sequencing was applied to each sampling replicate. Purified DNA was quantified and 1ng of input DNA was used in a first PCR of 20 cycles with Q5® Hot Start High-Fidelity DNA Polymerase (New England Biolabs) in the presence of 100 nM primers of the regions V3 and V4 of the 16S rRNA gene. Primers sequences were: (V3-V4) 341F, 5′-AC ACTGACGACATGGTTCTACACCTACGGGNGGCWGCAG-3′ and (V3-V4) 805R, 5′-TACGGTAGCAGAGACTTG GTCTGACTACHVGGGTATCTAATCC-3′ (Herlemann et al., 2011). After the first PCR, a second PCR of 15 cycles was carried out with Q5® Hot Start High-Fidelity DNA Polymerase (New England Biolabs) in the presence of 400 nM of primers 5′-AATGATACGGCGACCACCGAGATCTACACTGACGACATG GTTCTACA-3′ and 5′-CAAGCAGAAGACGGCATACGAGAT-[10 nucleotides barcode]-TACGGTAGCAGAGACTTGGTCT-3′ of the Access Array Barcode Library for Illumina Sequencers (Fluidigm). Amplicons were validated and quantified by Bioanalyzer and an equimolecular pool was purified using AMPure beads and titrated by quantitative PCR using the Kapa-SYBR FAST qPCR kit for LightCycler 480 and a reference standard for quantification. The pool of amplicons were denatured prior to be seeded on a flowcell at a density of 10 pM, where clusters were formed and sequenced using a MiSeq Reagent Kit v3, in a 2 × 300 pair-end sequencing run on a MiSeq sequencer to obtain 100000 reads per sample approximately.

Sequencing data were analyzed with the Base Space platform. All DNA sequences obtained have been deposited in NCBI Short Read Archive (SRA).

Statistical Analysis

A rarefaction analysis was performed using Analytic Rarefaction 1.3 software[1] (Tipper, 1979).

Statistical differences on the number of sequences and number of OTUs were studied by ANOVA test. Data of sequences and

[1]https://strata.uga.edu/software

OTUs are media values of three sampling replicates. Significant differences between two types of samples were identified using Student's *t*-test. All of the statistical analyses were performed using GraphPad Prism version 7.00 (GraphPad Software, La Jolla, CA, United States)[2].

Effects of the type of sample, nutrient concentrations and environmental variables on the bacterial community composition were investigated by a combination of multivariate statistical analysis developed with CANOCO version 5 software (Microcomputer Power, Ithaca, NY, United States) (Jongman et al., 1995; Ter Braak, 1995). For statistical analysis, Monte Carlo permutation tests with 500 permutations were used.

RESULTS AND DISCUSSION

General Characteristics and Chemical Properties of the Glacial Ice and Seawater Samples

Most of the physico-chemical characteristics of glacier samples were very analogous to each other (**Tables 1**, **2**). These samples differed mainly on their salinity, since the samples from coastal glaciers had a much higher salinity than those from inland glaciers.

Nevertheless, it was observed that seawater samples corresponding to the two types of glaciers were very different in terms of their physico-chemical characteristics. IT samples are combined with the runoff waters dragged from glaciers located inland. These waters transport inorganic and organic matter from the snow or soil they pass through in their way to the sea. However, as coastal glaciers emit icebergs directly into the sea, waters of these tidewater tongues (CT samples) contain less organic matter and less inorganic salts in solution. Their different physico-chemical characteristics can affect the microbial populations these samples contain.

Soluble nitrogen nutrients were analyzed in the forms of NH_4^+, NO_2^-, NO_3^-, and TDN. The occurrence of the different forms of ammonia depends on pH.

In an aqueous medium, ammonia (NH_3) and ammonium (NH_4^+) ions take part in an equilibrium reaction. Ammonia reacts as a base, raising the pH by generating OH^- ions. This equilibrium depends on pH and temperature. At a lower pH, the concentration of NH_3 is lower (Weiner, 2008). At the observed pH of between 4 and 5, about 95% of ammonia is in the cationic form ammonium (NH_4^+). Highly variable contents were obtained for each glacier (**Table 2**). Samples from KNB showed the highest amounts of NH_4^+, NO_2^-, and NO_3^- while the highest TDN values were found in LVM, LBE and KNB. The soluble reactive phosphorous (SRP) ranged between 0.51 μM in Brøggerbreen Vestre and 1.55 μM in LBE. No differences with respect to these parameters could be established between samples from coastal or land margin neither between ice or seawater samples.

In glaciers, the movement of carbon from the atmosphere to the rocks and moraines begins with snow precipitation.

TABLE 2 | Chemical analysis of soluble nutrients in melt water.

	Kongsvegen KGV		Kronebreen KNB		Ytre Norskøya YTRE		Poolepynten POOL		Lovénbreen Midtre LVM		Lovénbreen Austre LBE		Brøggerbreen BGN	
	Glacier	Tidewater	Glacier	Tidewater	Glacier	Tidewater	Glacier	Tidewater	Glacier	Tidewater	Glacier	Tidewater	Glacier	Tidewater
NH_4^+	2.22 (0.04)	0.81 (0.87)	61.04 (5.36)	0.56 (0.03)	1.81 (0.18)	0.81 (0.04)	2.01 (0.09)	0.59 (0.61)	1.91 (0.26)	0.66 (0.56)	6.32 (0.51)	0.57 (0.02)	2.10 (0.26)	0.68 (0.03)
NO_2^-	4.54 (0.33)	5.32 (0.48)	69. 87 (6.66)	1.21 (0.09)	5.36 (0.55)	3.21 (0.21)	6.87 (0.44)	1.02 (0.09)	3.02 (0.30)	3.02 (0.31)	70.21 (5.51)	1.25 (0.11)	4.21 (0.03)	1.08 (0.06)
NO_3^-	6.38 (0.97)	8.52 (0.75)	100.87 (8.33)	2.35 (0.11)	6.33 (0.35)	6.95 (0.74)	7.22 (0.58)	2.48 (0.22)	5.21 (0.44)	4.32 (0.21)	100.01 (7.21)	3.41 (0.33)	5.62 (0.14)	3.97 (0.21)
TDN[a]	90.58 (9.54)	29.98 (3.87)	136.11 (7.55)	21.38 (0.22)	88.78 (5.47)	20.54 (0.19)	99.11 (6.33)	22.14 (0.14)	190.25 (9.33)	25.14 (3.21)	150.33 (6.22)	34.66 (4.21)	96.35 (6.47)	35.01 (0.29)
SRP[b]	0.86 (0.11)	0.79 (0.21)	1.33 (0.01)	1.22 (0.09)	0.51 (0.01)	0.98 (0.09)	BD	BD	0.42 (0.11)	0.45 (0.09)	1.55 (0.12)	1.14 (0.12)	BD[d]	BD
DOC[c]	41.28 (7.23)	39.22 (4.21)	121.22 (5.98)	147.11 (15.27)	54.37 (7.95)	56.88 (6.32)	111.04 (4.54)	125.54 (16.22)	75.21 (9.23)	153.24 (20.11)	81.18 (24.01)	193.54 (11.54)	95.24 (14.17)	167.98 (12.54)

Concentrations are expressed in μM (±SEM) of three replicates. [a]TDN, total dissolved nitrogen. [b]SRP, soluble reactive phosphorus. [c]DOC, dissolved organic carbon. [d]BD, below detection or < 0.3 μM.

[2]www.graphpad.com

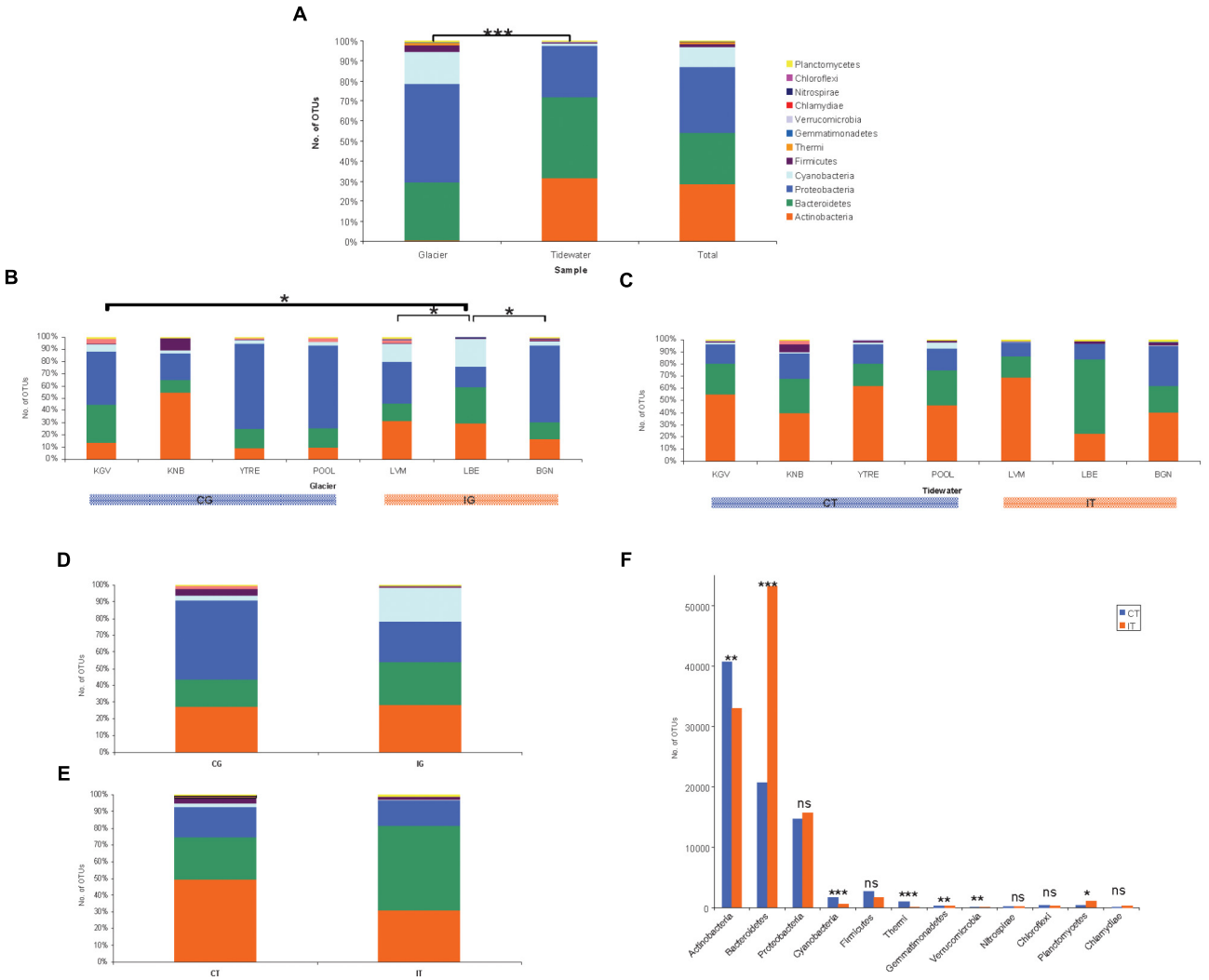

FIGURE 3 | Microbial communities composition. Number of counts aggregates at OTU level of three sampling replicates from glacial ice and tidewater samples. The values represent means of three replicates from each glacier. **(A)** Comparison of bacterial abundance between samples from glacier ice and tidewater. Significant differences were observed by Student's *t*-test for Cyanobacteria, Proteobacteria, and Actinobacteria (***$p < 0.0001$). **(B)** Comparison of bacterial abundance among samples from glaciers was analyzed by ANOVA and Newman–Keuls Multiple Comparison Test. The number of OTUs was significantly different to between LBE and BGN, LVM and KGV (*$p < 0.05$). **(C)** Comparison of bacterial abundance among seawater samples by ANOVA demonstrated significant differences (***$p < 0.0001$). The Newman–Keuls Multiple Comparison Test revealed that the number of OTUs in LBE was significantly different to the rest seawater samples in almost all pairs (*$p < 0.001$). **(D)** Comparison of bacterial total abundance between samples from coastal glaciers (CG) and inland glaciers (IG). Differences determined by Student's *t*-test were not significant. **(E)** Comparison of bacterial total abundance between samples from the tidewater area closest to a coastal glacier (CT) and samples from the tidewater area closest to an inland glacier (IT). Differences determined by Student's *t*-test were not significant. **(F)** Comparison of bacterial abundance at the phylum level between samples from the tidewater area closest to a coastal glacier (CT) and samples from the tidewater area closest to an inland glacier (IT) by Student's *t*-test. Differences in the number of OTUs of were very significant for Bacteroidetes, Cyanobacteria and Thermi (***$p < 0.0001$), moderately significant for actinobacteria, Gemmatimonadetes and Verrucomicrobia (**$p < 0.001$), and little significant for and (*$p < 0.01$) Planctomycetes.

Atmospheric carbon combines with water to form carbonic acid that falls to the glacier surface. The acid dissolves rocks and releases several ions such as calcium, magnesium, potassium, or sodium. Calving glaciers transport these ions (Zeebe and Caldeira, 2008), carbon particles and organic matter contained in ice to their downstreaming tidewater (Sipler et al., 2017). Storage and release of organic carbon from glaciers have been extensively studied (Hood et al., 2015); and it has been calculated that climate change contributes to this release approximately 13% of the annual flux of glacier dissolved organic carbon as a result of glacier mass loss. In coastal glacier samples, DOC concentrations were very similar to DOC values in their downstreaming seawater samples. But DOC concentrations were significantly higher in seawater samples than they were in inland glacier samples. These amounts are comparable to previously described DOC concentrations for glaciers and ice sheets (Hood et al., 2015), and for Arctic seawater (Benner et al., 2005). All results about the chemical composition of ice and seawater will be discussed

in relationship to the structure of microbial communities in glaciers.

Microbial Community Composition

In order to identify the microbial communities that inhabit the glacial and seawater samples, 16S rRNA gene sequencing was performed by Illumina MiSeq. A total of 695307 sequences were obtained (**Supplementary Table S1**). The correspondence of sequences to OTUs was assessed considering a 97% identity threshold. According to **Supplementary Figure S1**, corresponding to the seven glacier samples and seven tidewater samples, graphs tended to an asymptotic behavior. At 3% sequence divergence rarefaction curves reached saturation, indicating that the surveying attempt covered almost the full extent of taxonomic diversity at this genetic distance.

Statistical analyses of microbial abundance were only run on OTUs that were present in two or more sampling point. Glacier microorganisms mainly corresponded to the phylum Proteobacteria (48.8%), Bacteroidetes (29.1%) and Cyanobacteria (16.3%) (**Figure 3A**). Seawater microorganisms belonged to Bacteroidetes (40.3%), Actinobacteria (31.7%), and Proteobacteria (25.4%). Other phyla found such as Firmicutes, Thermi, Gemmatimonadetes, Verrucomicrobia, Nitrospirae, Chloroflexi, Planctomycetes, and Chlamydiae were less abundant. The total number of sequences found in glaciers and seawater was significantly different ($^{***}p < 0.0001$) (**Figure 1A**). When abundances were compared at the phylum level, significant differences were also observed for Cyanobacteria, Proteobacteria, and Actinobacteria ($^{***}p < 0.0001$). It has been published that these bacterial phylum constitute some of the typically most well-represented bacterial groups in glaciers (Lutz et al., 2015) and marine habitats (Michaud et al., 2014) respectively.

Several researches (Michaud et al., 2014) have described the input of marine microorganisms and organic particles which could be transported to glaciers by atmospheric deposition. We observe that, even in the inland glaciers, an important influence from marine environment seems to exist in both directions, from the glaciers to the sea and vice versa. The presence of bacterial genus characteristic of a given glacier could be sentinels for tracking this transport.

The best example of sentinel microorganism in this study would be the OTUs identified as *Hymenobacter*. *Hymenobacter* is the most abundant genus found in this study due to its great presence in the inland glacier LBE. In spite of being the glacier farthest from the coast of all considered in this study, a great influence in its tidewater is observed, because it is also the most abundant OTU in its corresponding tidewater. Currently, about 50 species of the genus *Hymenobacter* are known (Sun et al., 2018). Some of them are psychotrophs from Arctic and Antarctic environments and high altitudes at Qinghai-Tibet Plateau (Zhang et al., 2008), but they have also been isolated from deep sea water samples (Sun et al., 2018) and from Arctic marine sediments (Kim M.C. et al., 2017).

Other sentinel microorganisms from the exchange of materials from the glaciers to the seawaters could be numerous OTUs common to the sampling points. Among them, the most abundant OTUs belong to the genus *Aquaspirillum*, *Streptomyces*, *Polaromonas*, *Candidatus Pelagibacter*, *Pseudonocardia*, *Polaribacter*, *Salinibacterium*, *Paracoccus*, and *Streptosporangium*.

When of the number of OTUs among all glaciers was analyzed by ANOVA it was little significant. The Newman–Keuls Multiple Comparison Test demonstrated that the most different glacier in terms of the number of OTUs, was LBE, which is significantly different to BGN, LVM, and KGV ($^{*}p < 0.05$) (**Figure 3B**). The number of sequences found in LBE-CG samples was more abundant than the number of sequences in any of the rest glaciers.

In the seawater samples, the number of OTUs was also significantly different by ANOVA ($^{***}p < 0.0001$) (**Figure 3C**). When comparing the number of OTUs using the Newman–Keuls Multiple Comparison Test, LBE samples were significantly different to the rest seawater samples in almost all pairs ($^{*}p < 0.001$), except for Proteobacteria and Firmicutes. The number of sequences found in LBE-CT samples also was more abundant than the number of sequences in any of the other seawater samples.

Regarding the number of sequences corresponding to the most abundant genus (**Supplementary Table S2**), the highest abundance of sequences belonged to *Hymenobacter*, both in glaciers and seawater. The abundance of the genus *Hymenobacter* could be a consequence of its broad presence in the LBE glacier. LBE is an inner glacier but its flux of water can transport this bacterium that is also the most abundant in the seawater samples (LBE-CT). However, in the other glaciers, the highest number of sequences corresponded to *Pseudomonas*, *Polaromonas* and *Aquaspirillum* (**Supplementary Table S2**). In seawater samples, in addition to *Hymenobacter*, the most

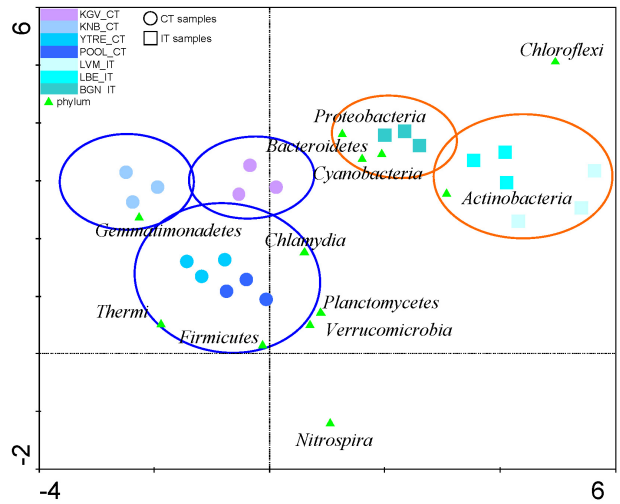

FIGURE 4 | Detrended Correspondence Analysis. The relative abundances of the microbial phyla from tidewater samples were compared to find their gradient. The diagram displays triangles that represent phyla. Sampling sites are represented by different shapes (○: CT samples and □: IT samples). Venn diagrams cluster and discriminate sampling points in different groups (glacier orange diagrams and tidewater blue diagrams). The axes are scaled in standard deviation units. CT, samples from the tidewater area closest to a coastal glacier; IT, samples from the tidewater area closest to an inland glacier.

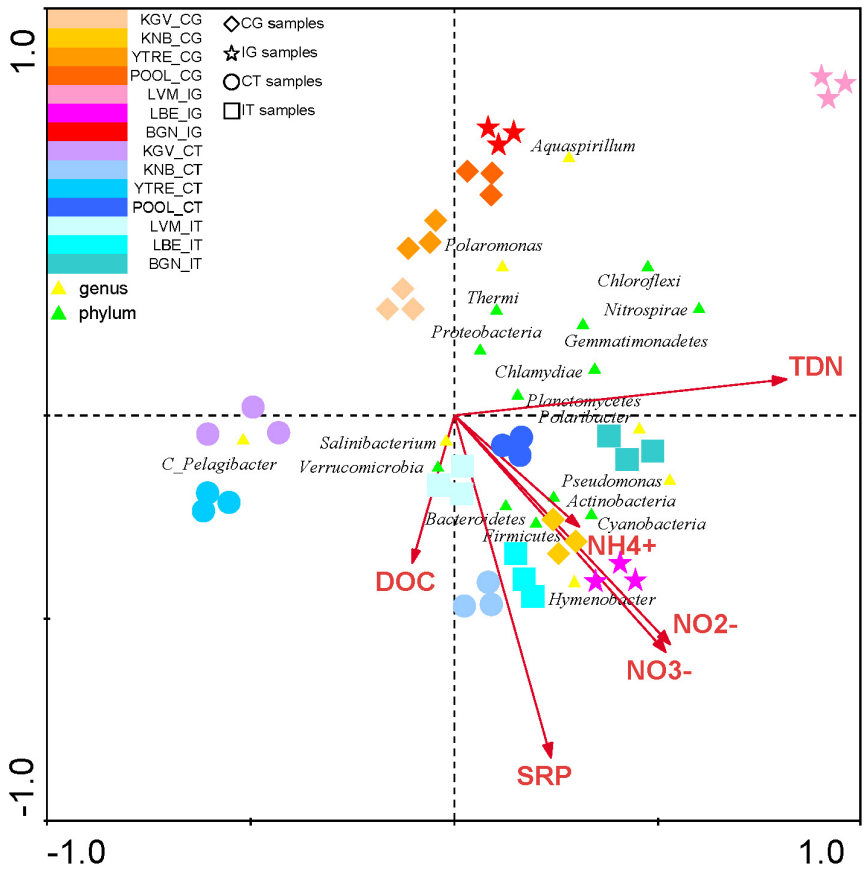

FIGURE 5 | Canonical Correspondence Analysis of the microbial phyla and of the main genus in each sampling site with respect to the concentration of nutrients. The analysis of the bacterial communities with respect to concentration of NH_4^+, NO^{2-}, NO^{3-}, TDN, SRP, and DOC. The diagram displays triangles that represent taxonomic groups. Sampling sites are represented by different shapes (◇: CG samples, ∗: IG samples, ○: CT samples, and □: IT samples). Arrows symbolize dissolved nitrogen and phosphorus concentrations. The axes are scaled in standard deviation units. CT, samples from the tidewater area closest to a coastal glacier; CG, samples from coastal glaciers; IG, samples from inland glaciers; IT, samples from the tidewater area closest to an inland glacier.

abundant OTUs belonged to *Pelagibacter*, *Salinibacterium* and *Polaribacter* (**Supplementary Table S2**).

When comparing by Student's *t*-test the number of OTUs found in the CG samples with the number of OTUs in the IG samples, the differences were not significant (**Figure 3D**). Neither were they when comparing the number of OTUs between the CT and IT samples (**Figure 3E**).

Microbial diversity in glaciers was very similar (**Figure 3B**). The most significant difference was a greater abundance of Actinobacteria in KNB as well as of Cyanobacteria in LVM and LBE.

Microbial diversity among seawater samples (**Figure 3C**) was only higher for Cyanobacteria at POOL, Bacteroidetes at LBE and Firmicutes at KNB. The higher and specific abundance of Firmicutes at KNB glacier and its downstreaming tidewater could be also a consequence of the microbial interchange between both populations.

In addition, OTUs have been found in glaciers that corresponded with typical marine microorganisms such as *Pelagibacter* (Giovannoni, 2017), *Polaribacter* (Staley and Gosink, 1999), and *Roseospira* (Kalyan Chakravarthy et al., 2007) or vice versa, OTUs of terrestrial microorganisms as *Acidisoma* (Belova et al., 2009) or *Propionibacterium* (Koussémon et al., 2001) were found in seawater samples.

A relevant result was the significant difference found between microbial populations inhabiting CT and IT by Student's *t*-test (**Figure 3F**). The difference in the number of OTUs was very significant for Bacteroidetes, Cyanobacteria, and Thermi ($^{***}p < 0.0001$), moderately significant for Actinobacteria, Gemmatimonadetes, and Verrucomicrobia ($^{**}p < 0.001$), and little significant for ($^{*}p < 0.01$) Planctomycetes.

In order to determine the distribution of microbial communities and how they are affected by environmental variables and by the concentration of nutrients in the environment, several multivariate statistical analysis of community data were carried out with.

Detrended Correspondence Analysis with the relative abundances of the microbial phyla from tidewater samples was performed. This analysis clustered tidewater samples into two groups (**Figure 4** and **Supplementary Table S3**): seawater samples corresponding to inland glaciers (samples IT) and seawater samples corresponding to coastal glaciers

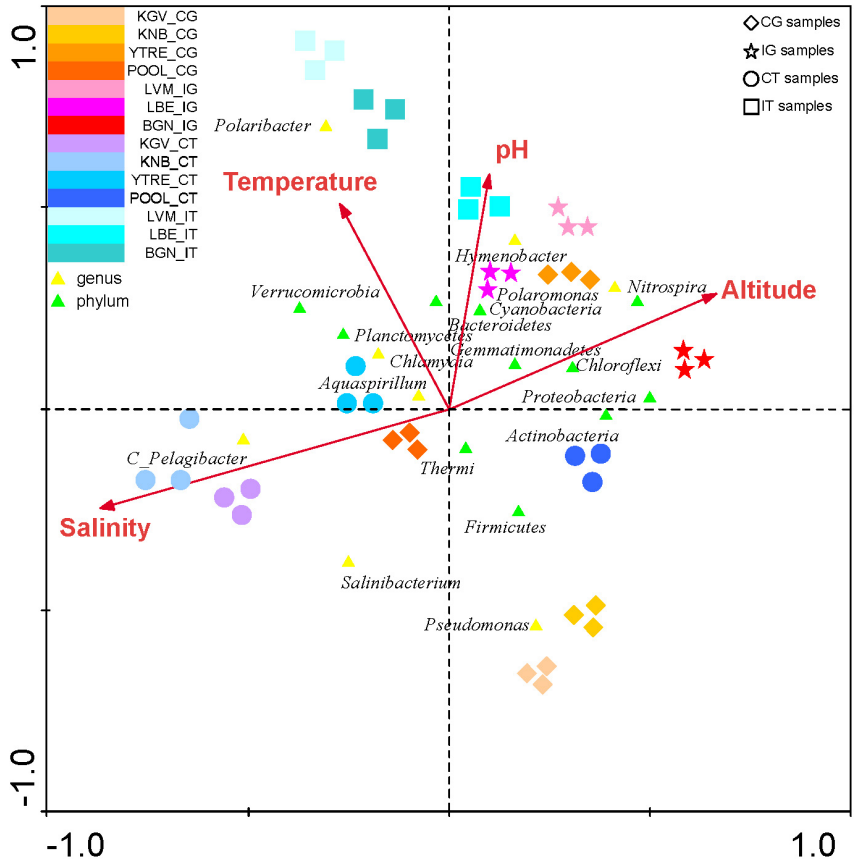

FIGURE 6 | Canonical Correspondence Analysis of the microbial phyla and of the main genus in each sampling site with respect to environmental variables. The analysis of the bacterial communities with respect to both environmental variables (temperature, pH, salinity and altitude) was represented. The diagram displays triangles that represent taxonomic groups. Sampling sites are represented by different shapes (◇: CG samples, ∗: IG samples, ○: CT samples and □: IT samples). Arrows symbolize environmental variables. The axes are scaled in standard deviation units.

(CT). These two microbial populations presented an equivalent number of species (**Figure 3C**), but their microbial composition in the tidewater region were different, although they are very close geographically and their seawaters can be mixed easily and quickly by wave effect.

The CCA of all phyla and of the most abundant OTUs in each sampling site demonstrated a significant correlation of the genus *Hymenobacter* with NO_2^-, NO_3^- and NH_4^+ (**Figure 5** and **Supplementary Table S3**). Other abundant genus such as *Pseudomonas* and *Polaribacter* were correlated with levels of all nitrogen species (NO_2^-, NO_3^-, NH_4^+ and TDN). OTUs identified as *Salibacterium* were correlated to DOC, on the contrary other OTUs such as *Polaromonas* presented a negative correlation with these compounds.

The CCA of was also applied to study the influence of environmental variables such as altitude, temperature, pH and salinity in all phyla and in the most abundant OTUs in each sampling site (Analyses 1–4) (**Figure 6** and **Supplementary Table S3**). The presence of some genus such as *Pelagibacter* was correlated to salinity, and the presence of the genus *Polaromonas* and the phylum Thermi were correlated to low temperatures. However, according to the eigenvalues obtained in the analysis 5 (**Supplementary Table S3**), which are less significant than in the previous analysis, the environmental variables do not influence in the distribution of the microbial communities as much as the nutrients do.

Metabolism and Element Cycling Inferred From Taxonomy

Carbon Cycle

In glaciers, organic compounds CH_2O (**Figure 7**) are scarce. In a dark environment such as the englacial area these compounds must be biologically synthesized by CO_2 fixation by chemolithotrophs. Even though in most environments the contributions of these organisms to the accumulation of organic matter are trivial compared to that of oxygenic phototrophs, in the englacial ecosystem their small inputs are important. They are degraded biologically to CH_4 and CO_2.

Some aerobes and facultative anaerobes oxidize CO to produce CO_2. The aerobic CO oxidizers described in the scientific literature include members of Proteobacteria, Firmicutes, and Actinobacteria (Park et al., 2003). These organisms can grow chemolithotrophically on CO as the sole

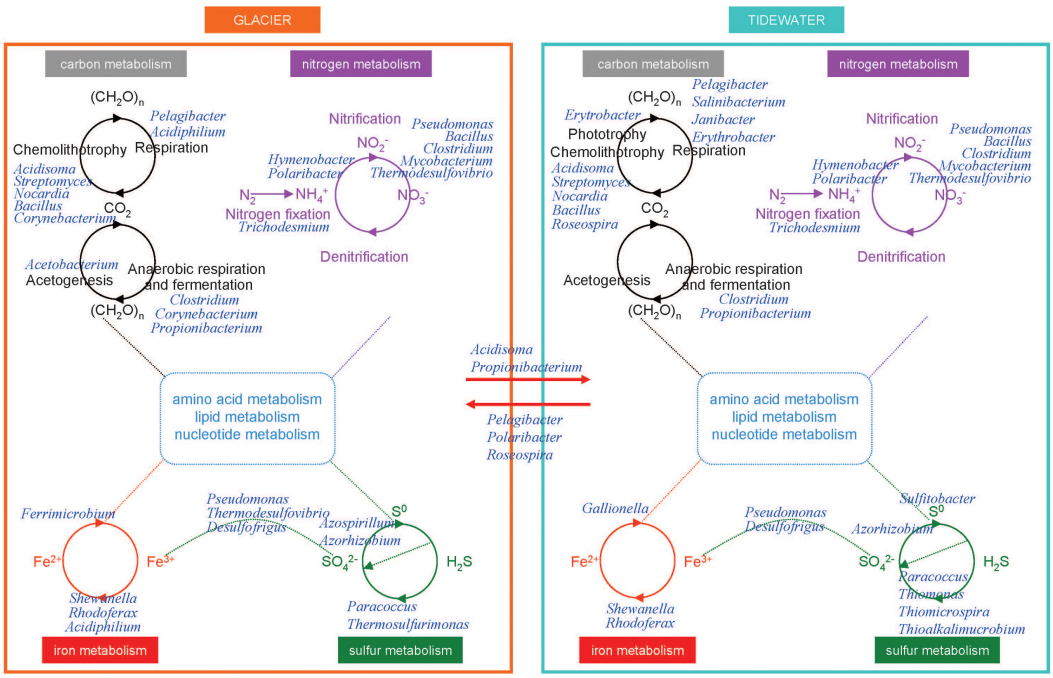

FIGURE 7 | Overview of the tentative interactions with the biogeochemical cycles in microorganisms from glaciers and tidewater samples. Microorganisms were identified by Illumina sequencing. Some key members of carbon, nitrogen, iron, and sulfur cycles in glacier **(left)** and tidewater samples **(right)**. They are represented at the genus level.

carbon and energy source under aerobic conditions and play important roles in global CO biogeochemistry; and it has been assessed that they contribute to CO uptake in soils, plant roots, seas and other natural systems (King, 2006), among which glaciers should be included. In our research we have found the Actinobacteria *Streptomyces* as well as other aerobic CO oxidizers like *Bacillus*, *Nocardia,* and *Corynebacterium* (Park et al., 2003).

In tidewater samples, much of the primary productivity comes from photosynthesis by Cyanobacteria. Phototrophs and chemolithotrophs, produce new organic carbon from CO2. Besides oxygenic phototrophs (which are the majority), anoxygenic phototrophs are also present. Aerobic anoxygenic phototrophs include bacteria such as *Erythrobacter*.

Some marine bacteria such as *Pelagibacter* are ecologically important in the so called "secondary production" because they consume high amounts of organic carbon produced from photosynthesis and are responsible for nutrient regeneration. Thus, these marine bacteria return organic matter to the marine food web that would otherwise be lost because of the inability of larger organisms to use such organic nutrients.

Nitrogen Cycle

On glacier surface, phototrophs such as cyanobacteria (i.e. *Trichodesmium*) are important nitrogen-fixing bacteria. In tidewater samples, nitrogen-fixing cyanobacteria were also identified (**Figure 7**).

The nitrogen cycle is driven by both chemolithotrophic and chemoorganotrophic microorganisms. In the biological utilization of N_2, it is reduced to NH_3, and then assimilated into organic forms, such as amino acids and nucleotides. Nitrification results from the sequential activities of two physiological groups of organisms: the ammonia-oxidizing bacteria (which oxidize NH_3 to nitrite, NO_2^-), and the nitrite-oxidizing bacteria, which oxidize NO_2^- to NO_3^-. Many species of bacteria are nitrifiers. The majority of them belonged to Proteobacteria and Nitrospirae (i.e., *Thermodesulfovibrio*). The first step is performed both in glacier and tidewater samples by very abundant bacteria such as *Hymenobacter* and *Polaribacter*.

Iron Cycle

The biological redox reactions in the iron cycle include both oxidations and reductions. Some bacteria can use Fe^{3+} as an electron acceptor in anaerobic respiration, and Fe^{2+} is oxidized in the chemolithotrophic metabolism. Important Fe^{3+} reducers as *Shewanella*, *Rhodoferax*, and *Acidiphilium* were identified in glacier samples (**Figure 7**). Among Fe^{2+} oxidizers we found *Ferrimicrobium*. The electron donors that are coupled to iron reduction could be inorganic (sulfur or hydrogen), as in the case of chemolithotrophic acidophiles; or it could be organic (glucose, glycerol), as in the case of heterotrophic acidophiles (e.g., *Acidiphilium*). In tidewater samples, *Shewanella*, *Rhodoferax*, were also identified, as well as some Fe^{2+} oxidezers such as *Gallionella*.

Sulfur Cycle

In glaciers, several Epsilonproteobacteria (*Sulfurospirillum* and *Sulfurimonas*) were identified. These bacteria oxidize sulfide and sulfur as electron donors with either O_2 or nitrate as

electron acceptors. Some Deltaproteobacteria are specialized in anaerobic metabolisms using oxidized sulfur compounds as electron acceptors. These include organisms such as *Desulfovibrio* and *Desulfuromusa*, a group of sulfate-reducing bacteria that reduces sulfate to sulfide, with lactate, pyruvate, or H_2 as electron donors. However, in anoxic environments acetate-oxidizing sulfate-reducing bacteria dominate. Acetate-oxidizing sulfate reducers include genera such as *Desulfofrigus* identified in glacier samples.

Other bacteria, *Paracoccus*, found both in glacier and tidewater samples (**Figure 7**), contains a sulfide and thiosulfate oxidation system, named Sox, that is also present in and many other sulfur bacteria both chemolithotrophic and phototrophic. This system oxidizes reduced sulfur compounds.

In tidewater samples, hydrogen sulfide (H_2S) is oxidized by phototrophic and chemolithotrophic microorganisms (*Thiomonas*, *Thiomicrospira,* and *Thioalkalimucrobium*) to sulfur (S_0) and sulfate (SO_4^{2-}), the latter being a key nutrient for algae and marine plants.

However, SO_4^{2-} can be reduced to H_2S by activities of the sulfate-reducing bacteria. These organisms consume organic carbon, and this reduction closes the biogeochemical sulfur cycle while regenerating CO_2.

Phosphorous Cycle

Among the phosphorous solubilizing bacterial communities, strains from *Pseudomonas*, *Bacilli*, *Rhizobium* and *Enterobacter* have been described as phosphate solubilizers (Khan et al., 2009). In glacier samples the presence of microorganisms involved in phosphorus acquisition include strains from bacterial genera *Pseudomonas*, *Mesorhizobium*, *Azorhizobium*, *Bradyrhizobium, Bacillus* and *Azospirillum*. In tidewater samples, these same genera except *Azospirillum* were found.

Possible Consequences of Differences in Microbial Composition

Glaciers constitute a key link between coasts and their downstreaming tidewaters and are of increasing importance in land-to-ocean fluxes. In published reports about other coastal glaciers such as the Antarctic Wanda Glacier (Pessi et al., 2015), it has been observed that marine microorganisms could colonize glaciers. In our study we have also observed that some marine bacterial OTUs were present in the glaciers. Additionally, we did also observe that OTUs corresponding to specific seawater bacteria were identified in the glacier samples. That is to say, it is possible that part of the microbial diversity found in the seawater samples comes partially from the upstream glaciers. When the glaciers thaw, the inland runoff waters transport more materials than the coastal glaciers do. This progression would alter the seawater composition, by increasing both nutrients and contaminants, or by changing the physicochemical characteristics of water. Over time, microbial populations from CT samples would become more similar to populations from IT samples.

CONCLUSION

The glaciers on the Northwest coast of Svalbard are undergoing a rapid change due to climate change. This effect is important in the coastal glaciers, but it is even more so in the interior glaciers. If the glaciers inland continue to melt, they will increasingly drag a greater amount of materials and sediments in their runoff waters. The consequence of this process will be the possible alteration of the water composition of the fiords. If this effect is maintained over time, the microbial populations of the coasts (CT) could be modified and they would be more similar to the current populations of the IT samples. This process can have serious consequences throughout the marine ecosystem and in the cycling of globally important elements.

AUTHOR CONTRIBUTIONS

All authors listed have made a substantial, direct and intellectual contribution to the work, and approved it for publication.

FUNDING

This work was supported by the Spanish Ministerio de Economía y Competitividad (MINECO) (CTM2011-16003-E) and by the Institute of Health Carlos III (PI14/00705). EG-L is recipient of a MINECO Fellowship (PTAT2010-03424).

ACKNOWLEDGMENTS

We are indebted to Maria Paz Martín Redondo from the Geology Laboratory of the Centro de Astrobiologia. We thank Christiane Hübner and Christian Zoelly from the Norwegian Sverdrup Station (Ny Ålesund, Svalbard) for their skillful assistance. We also thank the staff of the Norwegian Kings Bay Research Station (Ny Ålesund, Svalbard) for their logistic support (RiS-ID 6845).

SUPPLEMENTARY MATERIAL

The Supplementary Material for this article can be found online at: https://www.frontiersin.org/articles/10.3389/fmars.2018.00512/full#supplementary-material

REFERENCES

Amato, P., Hennebelle, R., Magand, O., Sancelme, M., Delort, A. M., Barbante, C., et al. (2007). Bacterial characterization of the snow cover at Spitzberg, Svalbard. *FEMS Microbiol. Ecol.* 59, 255–264. doi: 10.1111/j.1574-6941.2006.00198.x

Anesio, A. M., and Laybourn-Parry, J. (2012). Glaciers and ice sheets as a biome. *Trends Ecol. Evol.* 27, 219–225. doi: 10.1016/j.tree.2011.09.012

Belova, S. E., Pankratov, T. A., Detkova, E. N., Kaparullina, E. N., and Dedysh, S. N. (2009). *Acidisoma tundrae* gen. nov., sp. nov. and *Acidisoma sibiricum* sp. nov., two acidophilic, psychrotolerant members of the *Alphaproteobacteria*

from acidic northern wetlands. *Int. J. Syst. Evol. Microbiol.* 59, 2283–2290. doi: 10.1099/ijs.0.009209-0

Benner, R., Louchouarn, P., and Amon, R. M. W. (2005). Terrigenous dissolved organic matter in the arctic ocean and its transport to surface and deep waters of the north atlantic. *Global Biogeochem. Cycles* 19:GB2025. doi: 10.1029/2004GB002398

Deiglmayr, K., Philippot, L., Tscherko, D., and Kandeler, E. (2006). Microbial succession of nitrate-reducing bacteria in the rhizosphere of *Poa alpina* across a glacier foreland in the central alps. *Environ. Microbiol.* 8, 1600–1612. doi: 10.1111/j.1462-2920.2006.01051.x

Foreman, C. M., Sattler, B., Mikucki, J. A., Porazinska, D. L., and Priscu, J. C. (2007). Metabolic activity and diversity of cryoconites in the taylor valley, Antarctica. *J. Geophys. Res.* 112:G04S32. doi: 10.1029/2006JG000358

Førland, E. J., Benestad, R. E., Flatøy, F., Hanssen-Bauer, I., Haugen, J. E., Isaksen, K., et al. (2009). *Climate Development in North Norway and the Svalbard Region During 1900-2100*. Norwegian Polar Institute Report Series No. 128. Tromsø: Norwegian Polar Institute.

Garcia-Descalzo, L., Garcia-Lopez, E., Postigo, M., Baquero, F., Alcazar, A., and Cid, C. (2013). Eukariotic microorganisms in cold enviroments: examples from *Pyrenean* glaciers. *Front. Microbiol.* 4:55. doi: 10.3389/fmicb.2013.00055

Garcia-Lopez, E., Alcazar, P., Postigo, M., and Cid, C. (2016). "The effect of climate change on microbial communities from glaciers," in *Glaciers: Formation, Climate Change and Their Effects*, ed. N. Doyle (New York, NY: Nova Science Publishers, Inc.), 71–88.

Garcia-Lopez, E., and Cid, C. (2017). "The role of microbial ecology in glacier retreat analysis," in *Glaciers*, ed. W. V. Tangborn (Rijeka: InTech).

Giovannoni, S. J. (2017). SAR11 Bacteria: the most abundant plankton in the oceans. *Annu. Rev. Mar. Sci.* 9, 231–255. doi: 10.1146/annurev-marine-010814-015934

Hagen, J. O., Kohler, J., Melvold, K., and Winther, J. G. (2003). Glaciers in Svalbard: mass balance, runoff and freshwater flux. *Polar Res.* 22, 145–159. doi: 10.3402/polar.v22i2.6452

Hagen, J. O., Liestøl, O., Roland, E., and Jørgensen, T. (1993). *Glacier Atlas of Svalbard and Jan Mayen*. Oslo: Norwegian Polar Institute.

Hallbeck, L. (2009). *Microbial Processes in Glaciers and Permafrost. A Literature Study on Microbiology Affecting Groundwater at Ice Sheet Melting. SKB R-09-37*. Stockholm: Svensk Kärnbränslehantering AB.

Hell, K., Edwards, A., Zarsky, J., Podmirseg, S. M., Girdwood, S., Pachebat, J. A., et al. (2013). The dynamic bacterial communities of a melting High Arctic glacier snowpack. *ISME J.* 7, 1814–1826. doi: 10.1038/ismej.2013.51

Her, N., Amy, G., Foss, D., Cho, J., Yoon, Y., and Kosenka, P. (2002). Optimization of method for detecting and characterizing nom by HPLC-size exclusion chromatography with UV and on-line DOC detection. *Environ. Sci. Technol.* 36, 1069–1076. doi: 10.1021/es015505j

Herlemann, D. P., Labrenz, M., Jurgens, K., Bertilsson, S., Waniek, J. J., and Andersson, A. F. (2011). Transitions in bacterial communities along the 2000 km salinity gradient of the Baltic Sea. *ISME J.* 5, 1571–1579. doi: 10.1038/ismej.2011.41

Hoham, R. W., and Duval, B. (2001). "Microbial ecology of snow and freshwater ice with emphasis on snow algae," in *Snow Ecology: An Interdisciplinary Examination of Snow-Covered Ecosystems*, eds H. G. Jones, J. W. Pomeroy, D. A. Walker, and R. W. Hoham (Cambridge: Cambridge University Press), 168–228.

Hood, E., Battin, T. J., Fellman, J., O'Neel, S., and Spencer, R. G. (2015). Storage and release of organic carbon from glaciers and ice sheets. *Nat. Geosci.* 8, 91–96. doi: 10.1038/NGEO2331

Hotaling, S., Hood, E., and Hamilton, T. L. (2017). Microbial ecology of mountain glacier ecosystems: biodiversity, ecological connections and implications of a warming climate. *Environ. Microbiol.* 19, 2935–2948. doi: 10.1111/1462-2920.13766

Jongman, R. H. G., Ter Braak, C. J. F., and Van Tongeren, O. F. R. (1995). *Data Analysis in Community and Landscape Ecology*. Cambridge: Cambridge University Press. doi: 10.1017/CBO9780511525575

Kalyan Chakravarthy, S., Srinivas, T. N., Anil Kumar, P., Sasikala, C. H., and Ramana, C. H. V. (2007). *Roseospira visakhapatnamensis* sp. nov. and *Roseospira goensis* sp. nov. *Int. J. Syst. Evol. Microbiol.* 57, 2453–2457. doi: 10.1099/ijs.0.65105-0

Kastovska, K., Elster, J., Stibal, M., and Santruckova, H. (2005). Microbial assemblages in soil microbial succession after glacial retreat in Svalbard (high Arctic). *Microb. Ecol.* 50, 396–407. doi: 10.1007/s00248-005-0246-4

Khan, A., Jilani, G., Akhtar, M. S., Naqvi, S. M. S., and Rasheed, M. (2009). Phosphorus solubilizing bacteria: occurrence, mechanisms and their role in crop production. *J. Agric. Biol. Sci.* 1, 48–58.

Kim, M., Jung, J. Y., Laffly, D., Kwon, H. Y., and Lee, Y. K. (2017). Shifts in bacterial community structure during succession in a glacier foreland of the High Arctic. *FEMS Microbiol. Ecol.* 93:fiw213. doi: 10.1093/femsec/fiw213

Kim, M. C., Kim, C. M., Kang, O. C., Zhang, Y., Liu, Z., Wangmu, D., et al. (2017). *Hymenobacter rutilus* sp. nov., isolated from marine sediment in the Arctic. *Int. J. Syst. Evol. Microbiol.* 67, 856–861. doi: 10.1099/ijsem.0.001685

King, G. M. (2006). Nitrate-dependent anaerobic carbon monoxide oxidation by aerobic CO-oxidizing bacteria. *FEMS Microbiol. Ecol.* 56, 1–7. doi: 10.1111/j.1574-6941.2006.00065.x

Kirchman, D. L., Morán, X. A., and Ducklow, H. (2009). Microbial growth in the polar oceans - role of temperature and potential impact of climate change. *Nat. Rev. Microbiol.* 7, 451–459. doi: 10.1038/nrmicro2115

Koussémon, M., Combet-Blanc, Y., Patel, B. K., Cayol, J. L., Thomas, P., Garcia, J. L., et al. (2001). *Propionibacterium* microaerophilum sp. nov., a microaerophilic bacterium isolated from olive mill wastewater. *Int. J. Syst. Evol. Microbiol.* 51, 1373–1382. doi: 10.1099/00207713-51-4-1373

Lang, C. (2011). *Modeling of the Surface Mass Balance in Svalbard With the Regional Climate Model Mar Over 1958-2010*. Ph.D. thesis, Université de Liège, Liège.

Larose, C., Dommergue, A., and Vogel, T. M. (2013). The dynamic arctic snow pack: an unexplored environment for microbial diversity and activity. *Biology* 2, 317–330. doi: 10.3390/biology2010317

Lopez-Ramirez, M. P., Sanchez-Lopez, K. B., Sarria-Guzman, Y., Bello-Lopez, J. M., Cano-Garcia, V. L., Ruiz-Valdiviezo, V. M., et al. (2015). Haloalkalophilic cellulose-degrading bacteria isolated from an alkaline saline soil. *J. Pure Appl. Microbiol.* 9, 2879–2886.

Lutz, S., Anesio, A. M., Edwards, A., and Benning, L. G. (2015). Microbial diversity on icelandic glaciers and ice caps. *Front. Microbiol.* 6:307. doi: 10.3389/fmicb.2015.00307

Madigan, M. T., Martinko, J. M., Stahl, D. A., and Clark, D. P. (2012). *Brock Biology of Microorganisms*, 13th Edn. San Francisco, CA: Pearson Education, Inc.

McNabb, R. W., Womble, J. N., Prakash, A., Gens, R., and Haselwimmer, C. E. (2016). Quantification and analysis of icebergs in a tidewater glacier fjord using an object-based approach. *PLoS One* 11:e0164444. doi: 10.1371/journal.pone.0164444

Michaud, L., Lo Giudice, A., Mysara, M., Monsieurs, P., Raffa, C., Leys, N., et al. (2014). Snow surface microbiome on the high antarctic plateau (DOME C). *PLoS One* 9:e104505. doi: 10.1371/journal.pone.0104505

Mindl, B., Anesio, A. M., Meirer, K., Hodson, A. J., Laybourn-Parry, J., Sommaruga, R., et al. (2007). Factors influencing bacterial dynamics along a transect from supraglacial runoff to proglacial lakes of a high Arctic glacier. *FEMS Microbiol. Ecol.* 59, 307–317. doi: 10.1111/j.1574-6941.2006.00262.x

Møller, A. K., Barkay, T., Al-Soud, W. A., Sørensen, S. J., Skov, H., and Kroer, N. (2011). Diversity and characterization of mercury-resistant bacteria in snow, freshwater and sea-ice brine from the high arctic. *FEMS Microbiol. Ecol.* 75, 390–401. doi: 10.1111/j.1574-6941.2010.01016.x

Nowak, A., and Hodson, A. (2014). Changes in meltwater chemistry over a 20-year period following a termal regime switch from polythermal to cold-based glaciation at austre broggerbreen, Svalbard. *Polar Res.* 33:22779. doi: 10.3402/polar.v33.22779

Park, S. W., Hwang, E. H., Park, H., Kim, J. A., Heo, J., Lee, K. H., et al. (2003). Growth of mycobacteria on carbon monoxide and methanol. *J. Bacteriol.* 185, 142–147. doi: 10.1128/JB.185.1.142-147.2003

Pessi, I. S., Osorio-Forero, C., Gálvez, E. J. C., Simões, F. L., Simões, J. C., Junca, H., et al. (2015). Distinct composition signatures of archaeal and bacterial phylotypes in the wanda glacier forefield, Antarctic Peninsula. *FEMS Microbiol. Ecol.* 91, 1–10. doi: 10.1093/femsec/fiu005

Sipler, R. E., Kellogg, C. T. E., Connelly, T. L., Roberts, Q. N., Yager, P. L., and Bronk, D. A. (2017). Microbial community response to terrestrially

derived dissolved organic matter in the coastal Arctic. *Front. Microbiol.* 8:1018. doi: 10.3389/fmicb.2017.01018

Solomon, S., Qin, D., Manning, M., Chen, M., Marquis, K., Averyt, B., et al. (2007). *The Physical Science Basis: Contribution of Working Group I to the Fourth Assessment Report of the Intergovernmental Panel on Climate Change, in Climate Change 2007*. Cambridge: Cambridge University Press.

Staley, J. T., and Gosink, J. J. (1999). Poles apart: biodiversity and biogeography of sea ice bacteria. *Annu. Rev. Microbiol.* 53, 189–215. doi: 10.1146/annurev.micro.53.1.189

Sun, J., Xing, M., Wang, W., Dai, F., Liu, J., and Hao, J. (2018). *Hymenobacter* profundi sp. nov., isolated from deep-sea water. *Int. J. Syst. Evol. Microbiol.* 68, 947–950. doi: 10.1099/ijsem.0.002621

Ter Braak, C. J. F. (1995). *Data Analysis in Community and Landscape Ecology*, eds R. H. G. Jongman, C. J. F. Ter Braak, and O. F. R. Van Tongeren. Cambridge: Cambridge University Press.

Tipper, J. C. (1979). Rarefaction and rarefaction -the use and abuse of a method in paleontology. *Paleobiology* 5:423434. doi: 10.1017/S0094837300016924

Weiner, E. R. (2008). *Applications of Environmental Aquatic Chemistry: A Practical Guide*, 3rd Edn. Boca Raton, FL: CRC Press. doi: 10.1201/9781420008371

Zaikova, E., Hawley, A., Walsh, D. A., and Hallam, S. J. (2009). Seawater sampling and collection. *J. Vis. Exp.* 28:e1159. doi: 10.3791/1159

Zeebe, R. E., and Caldeira, K. (2008). Close mass balance of long-term carbon fluxes from ice-core CO2 and ocean chemistry records. *Nat. Geosci.* 1, 312–315. doi: 10.1038/ngeo185

Zeng, Y. X., Yan, M., Yu, Y., Li, H. R., He, J. F., Sun, K., et al. (2013). Diversity of bacteria in surface ice of austre lovénbreen glacier, Svalbard. *Arch. Microbiol.* 195, 313–322. doi: 10.1007/s00203-013-0880-z

Zhang, G., Niu, F., Busse, H. J., Ma, X., Liu, W., Dong, M., et al. (2008). *Hymenobacter psychrotolerans* sp. nov., isolated from the Qinghai-Tibet Plateau permafrost region. *Int. J. Syst. Evol. Microbiol.* 58, 1215–1220. doi: 10.1099/ijs.0.65588-0

Conflict of Interest Statement: The authors declare that the research was conducted in the absence of any commercial or financial relationships that could be construed as a potential conflict of interest.

Copyright © 2019 Garcia-Lopez, Rodriguez-Lorente, Alcazar and Cid. This is an open-access article distributed under the terms of the Creative Commons Attribution License (CC BY). The use, distribution or reproduction in other forums is permitted, provided the original author(s) and the copyright owner(s) are credited and that the original publication in this journal is cited, in accordance with accepted academic practice. No use, distribution or reproduction is permitted which does not comply with these terms.

frontiers in Marine Science

ORIGINAL RESEARCH
published: 19 March 2019
doi: 10.3389/fmars.2019.00108

Microbial Community Structure and Functionality in the Deep Sea Floor: Evaluating the Causes of Spatial Heterogeneity in a Submarine Canyon System (NW Mediterranean, Spain)

Sara Román[1†], Rüdiger Ortiz-Álvarez[2†], Chiara Romano[1,3], Emilio O. Casamayor[2] and Daniel Martin[1]*

[1] *Molecular Ecology of the Marine Benthos Group, Centre d'Estudis Avançats de Blanes, Consejo Superior de Investigaciones Científicas, Blanes, Spain,* [2] *Integrative Freshwater Ecology Group, Centre d'Estudis Avançats de Blanes, Consejo Superior de Investigaciones Científicas, Blanes, Spain,* [3] *Marine Invertebrate Phylogenetics Laboratory, Scripps Institution of Oceanography, La Jolla, CA, United States*

OPEN ACCESS

Edited by:
Ramiro Logares, Institute of Marine Sciences (ICM), Spain

Reviewed by:
Rohit Ghai, Biology Centre (ASCR), Czechia
Anders Lanzen, Centro Tecnológico Experto en Innovación Marina y Alimentaria (AZTI), Spain

***Correspondence:**
Rüdiger Ortiz-Álvarez
rudigerortiz@gmail.com

† These authors have contributed equally to this work

Specialty section:
This article was submitted to Aquatic Microbiology, a section of the journal Frontiers in Marine Science

Received: *04 September 2018*
Accepted: *21 February 2019*
Published: *19 March 2019*

Citation:
Román S, Ortiz-Álvarez R, Romano C, Casamayor EO and Martin D (2019) Microbial Community Structure and Functionality in the Deep Sea Floor: Evaluating the Causes of Spatial Heterogeneity in a Submarine Canyon System (NW Mediterranean, Spain). Front. Mar. Sci. 6:108. doi: 10.3389/fmars.2019.00108

Understanding community assembly and processes driving diversity in deep-sea environments is a major challenge in marine microbial ecology. The deep sea represents the largest ecosystem on Earth, but its remoteness makes the microbial community composition and functionality largely unknown. Moreover, microbial-focused studies comparing different deep-sea habitats like dynamic submarine canyons and slope ecosystems altogether are rare. The present work aims to study the deep-sea seafloor microbial communities (Bacteria and Archaea) of Blanes Canyon and its adjacent western open slope (NW Mediterranean) at ca. 1500 m deep, in autumn and spring, and along the vertical sediment profile. Microbial assemblages were studied in terms of abundance, diversity (α and β), community structure and functional potential through 16S rRNA tag-sequencing to assess their adaptations to the canyon's idiosyncrasy. Furthermore, the relationships of microbes with environmental variables and a potential predator (nematodes) were also assessed. We observed the microbial assemblages and their predicted functional profiles to be more heterogeneous and with higher temporal variability in the canyon than in the open slope. Although their phyla composition was similar, both the dominant and richest phyla showed significant differences in proportion between canyon and slope. Bacterial diversities were higher in the canyon than in the open slope, together with nematode abundances. Along the vertical sediment profile, microbial abundances consistently decreased with depth in the open slope, while we found more variability within the canyon, linked to an enhancement of aerobic metabolisms in the most superficial sediment layer. Grain size was correlated with microbial abundances and explained part of the variability in the community structure. Nematode and microbial abundances were correlated in slope environments, while in the canyon phytodetritics inputs (Chl *a* and Chl *a*: phaeo) and organic carbon seemed

to play a role in controlling microbial diversity and abundance. These results suggest that the deep-sea seafloor is strongly connected to coastal and pelagic productive areas through the canyon system in a stronger manner than to the open slope, thus modulating resource availability while driving changes in the microbial biosphere and the higher trophic levels of the deep-sea food web.

Keywords: submarine canyon, open slope, deep-sea, microbial communities, bacteria, archaea, biogeochemistry, sediments

INTRODUCTION

The deep seafloor comprises a variety of dynamic habitats that highly contribute to the heterogeneity and diversity of biota and ecosystems on Earth (Stuart et al., 2003; Ramirez-Llodra et al., 2010). These habitats are generally characterized by low organic matter (OM) supply, with the food web depending ultimately on the photosynthetic production supply from the photic zone (Gage, 2003). Bacteria dominate these deep-sea environments in terms of abundance and biomass, playing a key role in the food web (Deming and Baross, 1993; Pfannkuche, 1993) and mobilizing buried nutrients through biogeochemical cycles (Berner, 1982). Indeed, deep-sea benthic microbial communities are generally more diverse than pelagic or open ocean surface waters (Zinger et al., 2011; Lindh et al., 2017). Still, studies in the marine realm mainly focused on pelagic ecosystems (e.g., Galand et al., 2010; Sunagawa et al., 2015; Sebastián et al., 2018). Large-scale patterns of deep-sea microbes seem to indicate that communities are vulnerable to temperature shifts, and very susceptible to changes in trophic characteristics and 'food' inputs (Danovaro et al., 2016). At the regional scale, submarine canyons are among the most pervasive and dynamic deep-sea habitats (Ramirez-Llodra et al., 2010) that play the role of preferential particle-transport conduits and therefore act as drivers of trophic characteristics. However, because of the difficulties in accessing the deep seafloor, there is a fragmented available knowledge regarding the processes ruling the microbial community composition in these systems (Barone et al., 2018; Rzeznik-Orignac et al., 2018).

Canyons drive shelf-slope exchange as they accelerate the particle transit from both productive coastal zones and inner shelf environments toward the deep seafloor (Allen and Durrieu de Madron, 2009; Puig et al., 2014). They can also enhance seasonal processes such as the upwelling of cold, nutrient-rich waters (Allen et al., 2001) or increase primary productions during spring and summer (Granata et al., 2004; Harris and Whiteway, 2011; Chauvet et al., 2018) and are also subject to seasonally variable disturbances caused by bottom currents, benthic storms, dense shelf water cascading events (Canals et al., 2006) and mass wasting events (De Stigter et al., 2007). Furthermore, particle fluxes, often enriched in OM, are funneled and sediment accumulation rates may even be of one order of magnitude higher than those in adjacent non-dissected margins at comparable depths in the north-western Mediterranean Sea, thus altering sediment vertical composition (Zúñiga et al., 2009; Pasqual et al., 2010; López-Fernández et al., 2013). Furthermore, anthropogenic activities like intensive bottom trawling along canyon flanks proved to impact canyon sedimentary regimes (Puig et al., 2014; Pusceddu et al., 2014). In the NW Mediterranean and, more specifically in Blanes Canyon, sediment rates substantially increased since the 1970s in parallel with the expansion of the trawling fleet (Paradis et al., 2018). Submarine canyons thus offer heterogeneous habitats that are proved to host highly diverse fauna at different spatial scales, which are subjected to complex natural and anthropogenic processes (Sardà et al., 2009; De Leo et al., 2014; Ismail et al., 2018). Despite the increasing research focusing over the last decades on canyon ecosystems and the associated environmental functioning, the microbial assemblages thriving under these circumstances are still being unveiled (Barone et al., 2018; Celussi et al., 2018; Rzeznik-Orignac et al., 2018), and their response to both canyons' natural and anthropogenic processes remains poorly known. Remarkably, very few studies have aimed at evaluating how different sedimentation conditions (e.g., OM accumulation) may alter the microbial communities, the first compartment of benthic food web, along submarine canyons (Danovaro et al., 2000; Goffredi and Orphan, 2010). Nevertheless, higher bacterial (Danovaro et al., 1999) and fungal (Barone et al., 2018) biomasses have been reported along canyon axes in response to OM increases in sediments, while parallel information on associated changes in community composition remains scarce (Goffredi and Orphan, 2010; Barone et al., 2018).

Microbial-focused studies taking into account canyon and adjacent open slope ecosystems altogether are very rare (but see Polymenakou et al., 2009). Since microbial community idiosyncrasies in canyons and in their adjacent slopes may associate to differential seafloor dynamics, comparative studies may reveal effects along the whole food web. Specifically, patterns of association between individual canyon bacteria and nematodes have been reported (Rzeznik-Orignac et al., 2018) through predation (Moens and Vincx, 1997) or microbial commensalism (Moens et al., 2005). Indeed, organically enriched sediments in canyons support higher nematode densities, biomasses (Ingels et al., 2009; Leduc et al., 2014) and diversities (Bianchelli et al., 2013; Román, 2017; Bianchelli and Danovaro, 2019) than at the adjacent open slope. Moreover, seafloor surface and subsurface sediments also have distinct microbial (Bienhold et al., 2016; Lindh et al., 2017) and nematode distributions (Román et al., 2016), likely performing different processes with particular nutrient or oxygenation requirements. Therefore, since the functional and structural attributes of the benthic communities may result from the interaction of the multiple parts of the trophic food web (Leduc et al., 2014; Romano et al.,

2016), a deeper understanding of the higher trophic levels should be contextualized within the particularities of the microbial communities at different scales (Zinger et al., 2011; Sevastou et al., 2013).

Accordingly, the main objective of the present study was to investigate the microbial community (Bacteria and Archaea) of Blanes Canyon (NW Mediterranean Sea) and its adjacent open slope in terms of abundance, diversity, composition, and potential functionality. In particular, we compared two locations at similar depths (1500 m) along the canyon axis and on its western open slope. We studied the microbial responses at three different levels: ecosystem (canyon vs. slope), vertical sediment profile (three progressively deeper layers) and season (autumn vs. spring). We also tested whether the environmental/trophic variables (mainly sediment characteristics) and biotic conditions (meiofaunal nematode abundances as potential predators) inside the canyon do affect the microbial communities differently to those on the adjacent open slope.

MATERIALS AND METHODS

Study Area

The head of Blanes Canyon (North Catalan Margin, Iberian Peninsula, NW Mediterranean, **Figures 1A,B**) deeply cuts the continental shelf slope at 60 m depth, 4 km off the Tordera Delta (**Figures 1B,C**). The canyon (184 km long, 20 km of maximum width at about 2000 m depth) has a complex topography strongly influencing the near bottom currents resulting in highly variable (eastern wall) and prevailing offshore-directed (western wall) flows (Zúñiga et al., 2009; Lastras et al., 2011). Major particle transport responds to flooding from Tordera River and the numerous coastal creeks of its catchment and to major coastal storms (autumn–winter), as well as to phytoplankton blooms (spring–summer) (Flexas et al., 2008; Zúñiga et al., 2009; López-Fernández et al., 2013).

Sampling Strategy and Data Collection

Sediment samples were obtained on board of the R/V García del Cid in autumn 2012 and spring 2013 in two stations 35 km apart (Blanes Canyon axis, western open slope) at ca. 1500 m depth (**Figure 1C** and **Supplementary Table S1**, Román et al., 2016). Sediment was collected by means of 6-tube multiple-corer (KC Denmark A/S, inner diameter 9.4 cm; length 60 cm), yielding intact sediment profiles. Multicore deployments (three replicates per sampling station) yielded large sediment corers that were sub-sampled on board for microbial and sediment analyses with a sub-corer (3.6 cm diameter, 5 cm thickness), and sliced down to 5 cm into three sediment layers (0–1 cm: surface; 1–2 cm: sub-surface; 2–5 cm: deep) thus giving rise to 36 individual sediment samples. Samples for microbial and environmental sediment analyses were preserved in absolute ethanol and stored frozen at −20°C, respectively. Among the full set of sediment variables described by Román et al. (2016), we are here using grain size (clay, silt, and sand fractions), organic carbon (OC, %), total nitrogen (TN, %), chlorophyll *a* (Chl *a*, μg/g) and the chloroplastic pigments equivalents (CPEs: sum of Chl *a* and its degradation products as phaeopigments, mg/g), as a proxy of surface-produced OM (Thiel, 1978), and the Chl *a*: phaeopigments ratio (Chl *a*: phaeo), as a proxy of the freshness of photosynthetically derived OM (Plante-Cuny and Bodoy, 1987). High phaeopigments vs. Chl *a* ratios are generally associated with detrital and degraded autotrophic matter inputs.

Total microbial community DNA was extracted from 10 g of sediment per sample and processed with the PowerMax®Soil DNA Isolation Kit from MO BIO Laboratories, Inc. (Guardiola et al., 2016). Meiofaunal nematode samples, methods and data (i.e., abundance) come from Román et al. (2016, 2018).

Sequencing and Data Filtering

High-speed multiplexed 16S rRNA gene microbial sequencing with the Illumina MiSeq System (2 × 250 bp) was carried out in the V4 region using 515f and 806r primers (Caporaso et al., 2011), the earth microbiome project protocols (EMP), and the genomics core facilities of the Research Technology Support Facility, Michigan State University (RTSF-MSU, United States). The selected primers are widely used to amplify both Bacteria and Archaea with few known biases (Apprill et al., 2015; Parada et al., 2016). A total of 5398793 raw sequences were filtered and further clustered with UPARSE (Edgar, 2013) by read length (above or equal to 250 pb) with an expected error of 0.25. After singleton and chimera removal, sequences were further clustered into 22059 97%-identity OTUs. The 3530733 filtered sequences were mapped back into these OTUs and classified with the SILVA 119 database (Quast et al., 2013) through the SILVA-ngs pipeline[1]. Raw files are available in the National Center for Biotechnology (NCBI) repository under the project code PRJNA489177.

Functional Prediction

Functional predictions based on representative genomes are useful for the estimation of metabolic potential when metagenomes are not available (Langille et al., 2013; Nemergut et al., 2015). Although some strains within the same taxonomic rank may have distinct functional signatures or environmental distributions, functional predictions provide an approximation to functional patterns at the community level (Ortiz-Álvarez et al., 2018). We applied an adaptation of the Tax4Fun2 routine (Wemheuer et al., 2018) using gene presence/absence weighted by the relative abundance of each taxa in each sample. The numeric results represent a fraction of the community that matched with the functional database, and indicate the community proportions containing each specific function. We filtered a total of 106 KEGGs (functional orthologs) within 30 metabolic pathways (Llorens-Marès et al., 2015), including five additional phosphorous cycle pathways (G-3-P transport, phosphate transport -high and low efficiency-, phosphonate transport, and phosphonate metabolism) (Vila-Costa et al., 2013), and four complex OM

[1]https://www.arb-silva.de/ngs/

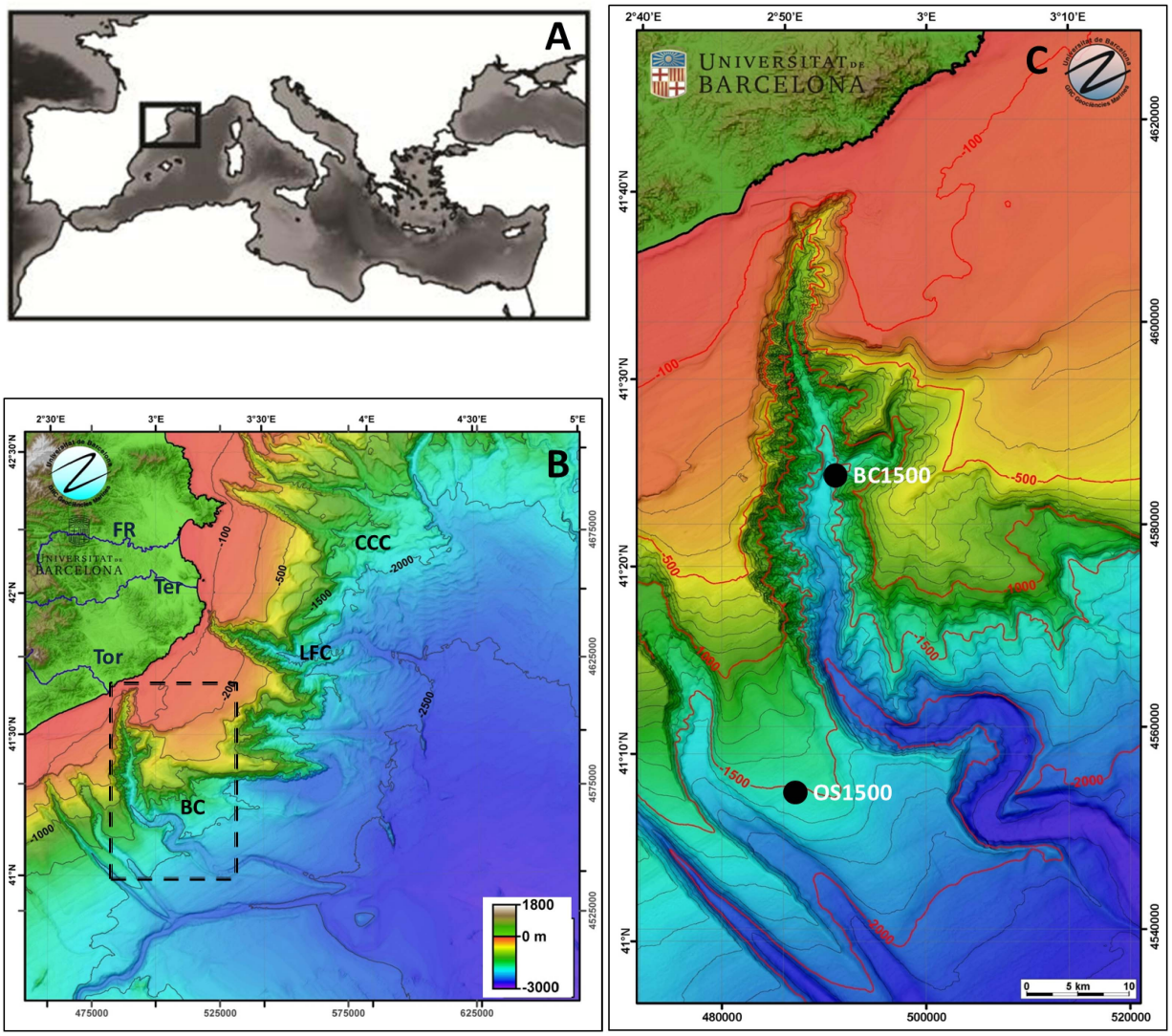

FIGURE 1 | (A) Location of the study area in the Mediterranean Sea. **(B)** Color bathymetric map of the study area in the North-Catalan margin. **(C)** Color bathymetric map and the sampling stations (white and black dots) in the Blanes Canyon region (marked with an arrow in **B**). ToR, Tordera River; TeR, Ter River; FR, Fluvià River; BC, Blanes canyon; LFC, La Fonera Canyon; CCC, Cap de Creus Canyon; OS, Open slope. Color maps are redrawn from the bathymetric map of GRC of Marine Geosciences of University of Barcelona.

decomposition pathways (chitin, cellulose, hemicellulose, and lignin) (Lüneberg et al., 2018).

Quantification of 16S rRNA Gene (qPCR Analyses) and Microbial Abundance Estimation

The determination of 16S rRNA gene copies was carried out per sample through quantitative PCR amplification using the bacterial universal primers 341F-534R (Muyzer et al., 1996; Watanabe et al., 2001). Q-PCR assays were run on 96-well white qPCR plates (Bio-Rad, Hercules, CA, United States) in a DNA engine thermal cycler (Bio-Rad) equipped with a Chromo 4 real-time detector (Bio-Rad) (López-Gutiérrez et al., 2004). The reaction mixture (20 μl) contained 10 μl of SsoFast EvaGreen supermix (Bio-Rad), 5 μl of template DNA (1 ng), 10 μM primers and molecular biology-grade water (Sigma, St. Louis, MO, United States). Standard curves were obtained from clones containing *E. coli* 16S rRNA using 10-fold serial dilutions. All reactions were run in triplicate with standard curves spanning from 10^2 to 10^7 DNA copies. Since each bacterial taxon has different 16S gene copies in their genomes, qPCR results required a 16S copy number correction by bacterial OTU. We used the curated database rrnDB version 5.4 (Stoddard et al., 2014) to calculate an estimated 16S rRNA copy number for each OTU based on the lower taxonomic rank available with a 0.85 cut-off. The conversion factor was the average number of copies per OTU weighted by their relative abundances

per sample. The final abundance estimate was corrected by the % of archaea per sample, since the qPCR primers were bacteria-specific.

Statistical Analyses

Alpha diversity, as OTU Richness and Shannon index (Shannon, 1948), were estimated after rarefaction to the minimum sampling size of 35000 sequences per sample, and separately for archaea (2000 sequences) and bacteria (35000 sequences). One canyon sample was removed due to a low number of sequences after rarefaction. Shannon index was calculated with the function *diversity* in package 'vegan' (Oksanen et al., 2017). The community structure based on OTUs was standardized through Hellinger transformation, fitted under a non-metric multidimensional scaling (nMDS) based on Bray–Curtis dissimilarities calculated with function *vegdist* in package 'vegan,' and plotted with *ggplot2* function in package 'ggplot2' (Wickham, 2009). We quantified beta diversity (i.e., variability in species composition between sampling units for a given area, per habitat and per sediment layer) using the function *betadisper* in package 'vegan.' Indicative OTUs were detected with function IndVal in package 'labdsv' (Roberts, 2013). Microbial community descriptors (estimated abundance, alpha diversity, community structure, and functional prediction structure) were analyzed by means of non-parametric permutational analyses of variance (PERMANOVA) using PRIMER v6 (Anderson, 2005; Anderson et al., 2008). Similarity matrices for univariate descriptors (i.e., standing stocks and structural diversity) were built based on Euclidean similarity. Differences in microbial communities were analyzed using a three-way fixed model, with a fully crossed design by habitat (Ha: canyon and slope), season (Se: autumn and spring) and sediment layer (SL: surface, sub-surface and deep) in PERMANOVA + for Primer (Anderson et al., 2008). The same three-way design was used to analyze differences in sediment environmental variables by univariate PERMANOVAs, except for the grain size, where clay, silt, and sand percentages were considered as multivariate variables. Sediment variable matrices were based on Euclidean similarities. Additionally, principal component analysis (PCA) was performed on the environmental data matrix to show the ordination pattern of the samples. Significant differences were indicated as $p < 0.05$, $p < 0.01$, or $p < 0.001$.

The strength of the relationships between the selected environmental and biological variables (clay, silt, sand, OC, TN, Chl *a*, CPE, and Chl *a*: phaeo, nematode densities) and univariate community descriptors (i.e., abundance and structural diversity), for both canyon and slope habitats separately, were assessed by Spearman Rank correlations by means of the XLSTAT (Addinsoft) software, with a *fdr* p-adjustment. RELATE and DISTLM (distance-based linear model) PRIMER routines based on the normalized environmental data (Anderson et al., 2008) allowed to analyze and model the relationship between microbial community structure and environmental variables, following the same design as for univariate metrics. Metabolism differences by factors were explored through Kruskal–Wallis test (Ha and SL) and Spearman correlations with univariate descriptors (% Archaea, microbial abundances, and nematode densities). The same PERMANOVA design described for microbial assemblages was used to analyze metabolism differences, based on a Bray–Curtis dissimilarity matrix.

RESULTS

Sediment Physical and Chemical Variability

Both canyon and slope sediments were predominantly muddy (2–63 μm in grain diameter) with high silt content (64 to 77%, respectively) (**Figure 2**). However, canyon and slope samples were differentiated according to the environmental variables in the PCA plot (**Figure 3**). The first two PCA axes explained a total of 66.5% of the variation (**Figure 3**). The main contributors were clay (−0.392), sand (0.449) and Chl *a* (0.398) for PC1, and OC (−0.517), TN (−0.444), silt (−0.444), and CPE (−0.423) for PC2 (numbers in parenthesis represent eigenvectors). Sediment grain size showed significant differences for the interactions Ha × Se and Ha × SL (**Table 1**: PERMANOVA, $p < 0.01$). Differences between seasons indicated that sediments were coarser in spring than in autumn (pair-wise test, Ha × Se, $p < 0.05$, see **Figure 2**), and particularly, canyon sediments had up to 20% more sand in spring. Slope sediments became progressively finer along the vertical sediment profile (pair-wise test, Ha × SL, $p < 0.05$, see **Supplementary Figure S1**).

OC and TN differed significantly between habitats and seasons, as well as in the interaction Ha × Se (PERMANOVA, $p < 0.05$, **Table 1**). In autumn, they were significantly higher in the canyon (0.76 and 0.11%, respectively) than on the slope (0.60 and 0.09%, respectively) ($p < 0.05$, see **Figure 2**). On the slope, they differed in autumn and spring, while in the canyon only TN differed (pair-wise, $p < 0.05$, see **Figure 2**).

Chl *a* and CPE also differed significantly between habitats, being higher in the canyon (0.03 and 0.7 μg/g on average, respectively) than on the slope (0.01 and 0.3 μg/g on average, respectively) (**Figure 2** and **Table 1**), but also the interaction Se × SL differed significantly (**Table 1**). Chl *a* at the surface sediment layer was higher in spring (pair-wise test, Se × SL, $p < 0.05$, **Supplementary Figure S1**), while CPE was progressively lower along the vertical sediment profile (pair-wise test, Se × SL, $p < 0.05$, **Supplementary Figure S1**). The Chl *a*: phaeo ratio was significantly higher in spring (PERMANOVA, $p < 0.05$, **Table 1**).

Taxonomic Groups of Bacteria and Archaea

The dataset comprised 16694 OTUs in the canyon and 13318 in the slope, sharing 37% of the total (8161). Sequences were classified into 10 archaeal and 45 bacterial phyla, out of which 10 were candidate divisions. Classified sequences (98.7%) were assigned to members of bacteria (87% canyon, 85% slope), with Proteobacteria (including Alpha-, Beta-, Gamma-, Delta- and Epsilon- proteobacteria) being dominant (45% canyon, 36% slope) (**Figure 4A**). Gammaproteobacteria (1679 OTUs)

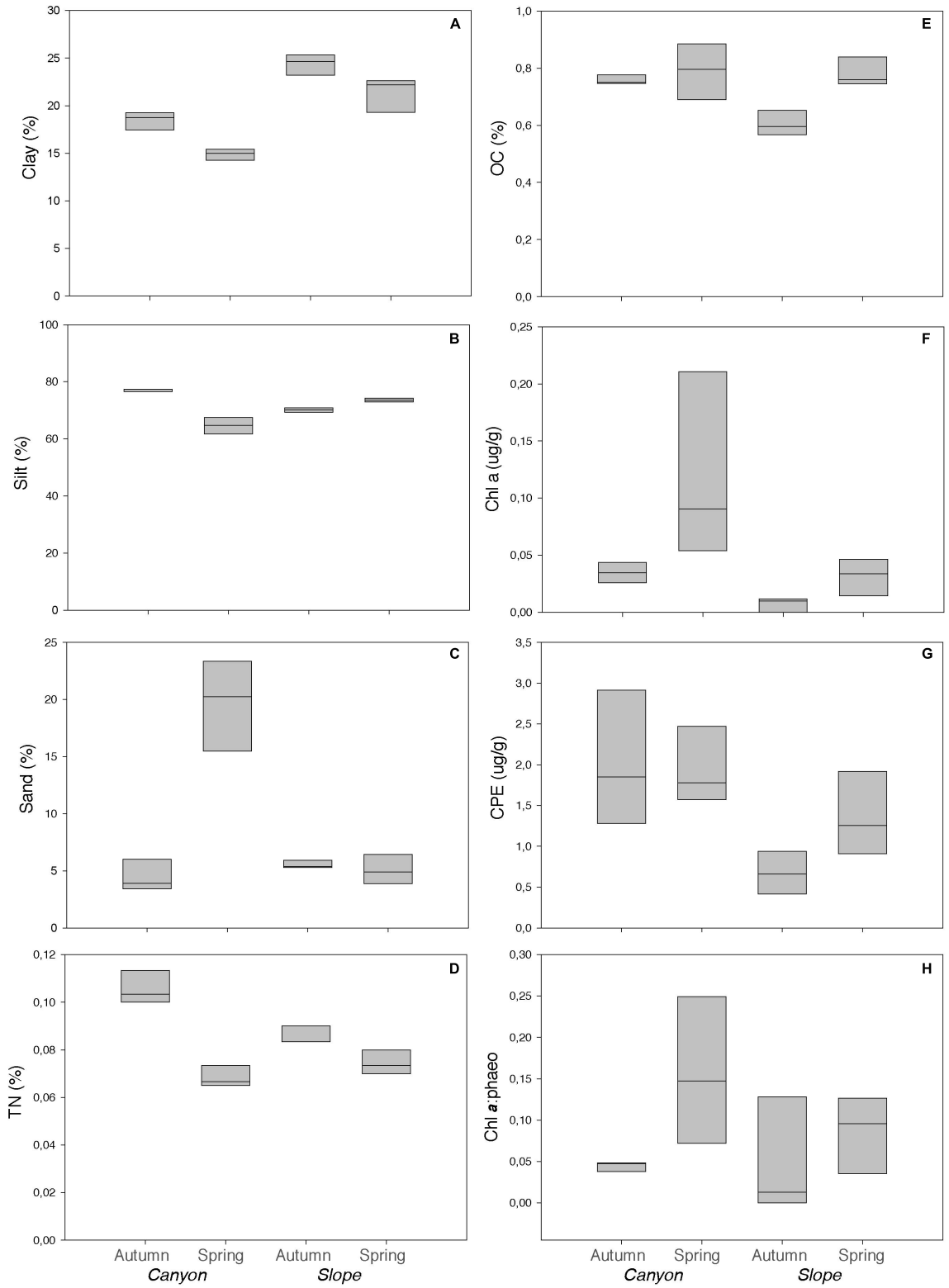

FIGURE 2 | Environmental variables used in this study for canyon (BC) and slope (OS) stations: **(A–C)** Granulometry (%Clay, %Silt, and %Sand), **(D)** TN (total nitrogen), **(E)** OC (organic carbon), **(F)** Chl *a* (Chlorophyll a), **(G)** CPEs (chloroplastic pigment equivalents) and **(H)** Chl *a*: phaeo (Chlorophyll *a*: phaeopigments). Black lines represent the median, and lower box indicates the first quartile and upper box the third quartile. Upper line on the boxes shows the maximum value and lower line the minimum value.

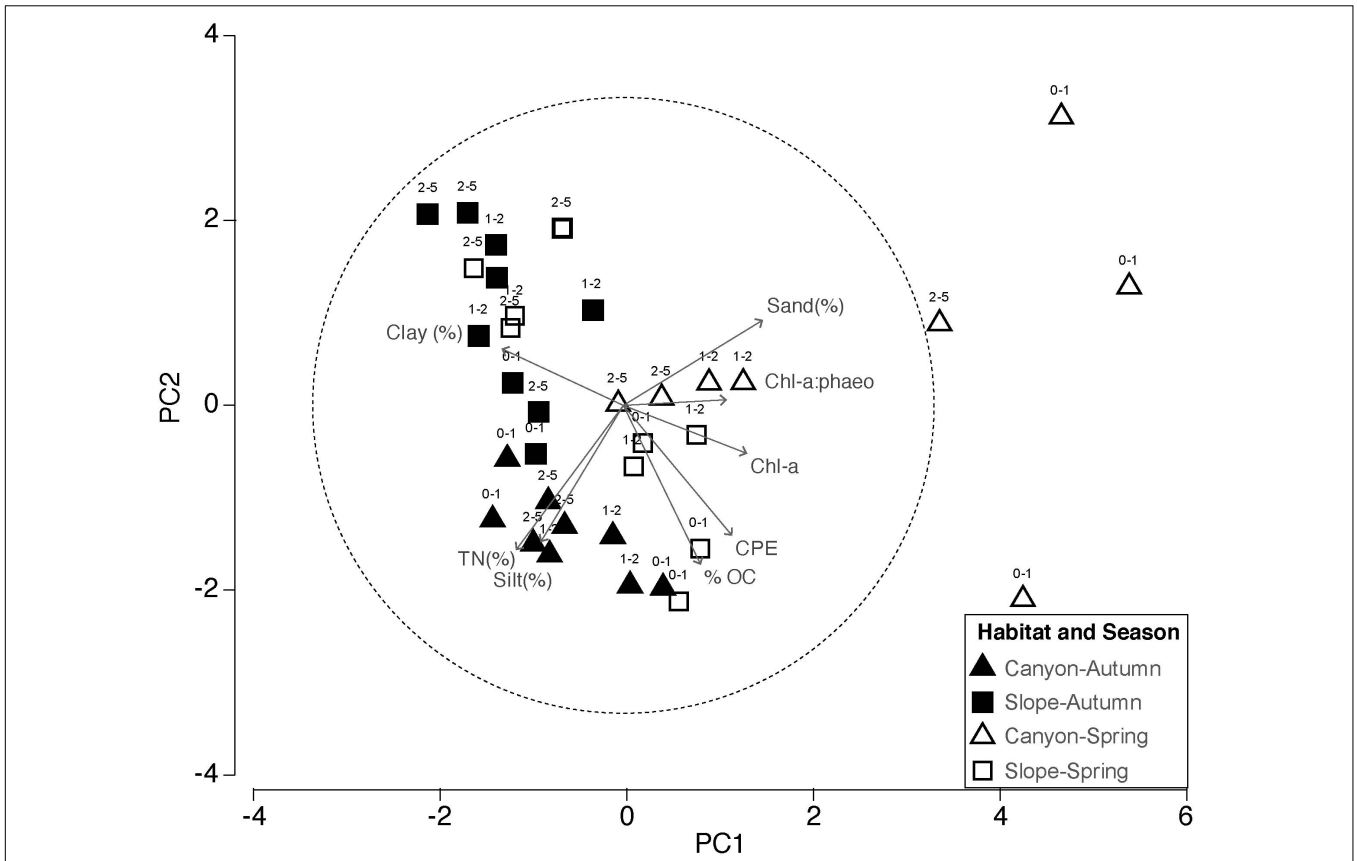

FIGURE 3 | Principal component analysis (PCA) ordination based on selected environmental variables at the studied stations. Parameters included in the analyses were: clay (%), silt (%); sand (%), organic carbon (OC), total nitrogen (TN), chlorophyll a (chl *a*), chloroplast pigments equivalents (CPE), chlorophyll a: phaeopigment ratio (chl *a*: phaeo).

TABLE 1 | Results from univariate and multivariate PERMANOVA three-way analyses for differences in environmental sediment variables, using Habitat (Ha), Season (Se), and Sediment Layer (SL) as factors.

Source	df	Mean grain size (%)	TN (%)	OC (%)	Chl *a* (μg/g)	CPE (μg/g)	Chl *a*: phaeo
Ha	1	***0.0001***	**0.0252**	**0.0240**	***0.0084***	***0.0053***	0.3084
Se	1	***0.0019***	***0.0001***	***0.0096***	**0.0135**	0.2467	**0.0473**
SL	2	***0.0073***	0.7918	0.3037	0.1156	**0.0131**	0.9209
Ha × Se	1	***0.0005***	***0.0008***	**0.0248**	0.1949	0.3891	0.2806
Ha × SL	2	**0.0424**	0.1656	0.1836	0.3699	0.5765	0.3950
Se × SL	2	0.1976	0.3054	0.4381	**0.0339**	**0.0170**	0.4151
Ha × Se × SL	2	0.3255	0.8139	0.4232	0.1466	0.3020	0.6479
Res	23						
Total	34						

TN, total nitrogen concentration; OC, organic carbon concentration; Chl a, chlorophyll a; CPE, chloroplastic pigment equivalents; Chl a:phaeo, chlorophyll a: phaeopigments ratio. Data was normalized; resemblance was calculated using Euclidean Distance. Bold: $p < 0.05$; bold italic: $p < 0.01$.

were dominant among them, showing a higher proportion in the canyon than in the slope (25.2% canyon vs. 18.4% slope). The Deltaproteobacteria (3343 OTUs) were also enhanced in the canyon (12.7% canyon vs. 9.8% slope), being surpassed by Planctomycetes (4055 OTUs) on the open slope (10.6% canyon, 12.9% slope). Within this phylum, we found genera such as *Scalindua* and *Kuenenia*, involved in the annamox pathway. Also relevant in proportion and richness were Acidobacteria (1379 OTUs; 9% canyon, 13% slope) and Alphaproteobacteria (1049 OTUs; both 5.7%). Interestingly, the ratio richness:abundance consistently differed by bacterial phyla in the canyon and on the slope (**Figure 4**). Particularly Gammaproteobacteria (mostly Oceanospirillales and Xanthomonadales) and Alphaproteobacteria were more abundant than rich. Conversely, Planctomycetes or Deltaproteobacteria showed a higher OTU richness:abundance ratio (**Figure 4**). Regarding the sediment

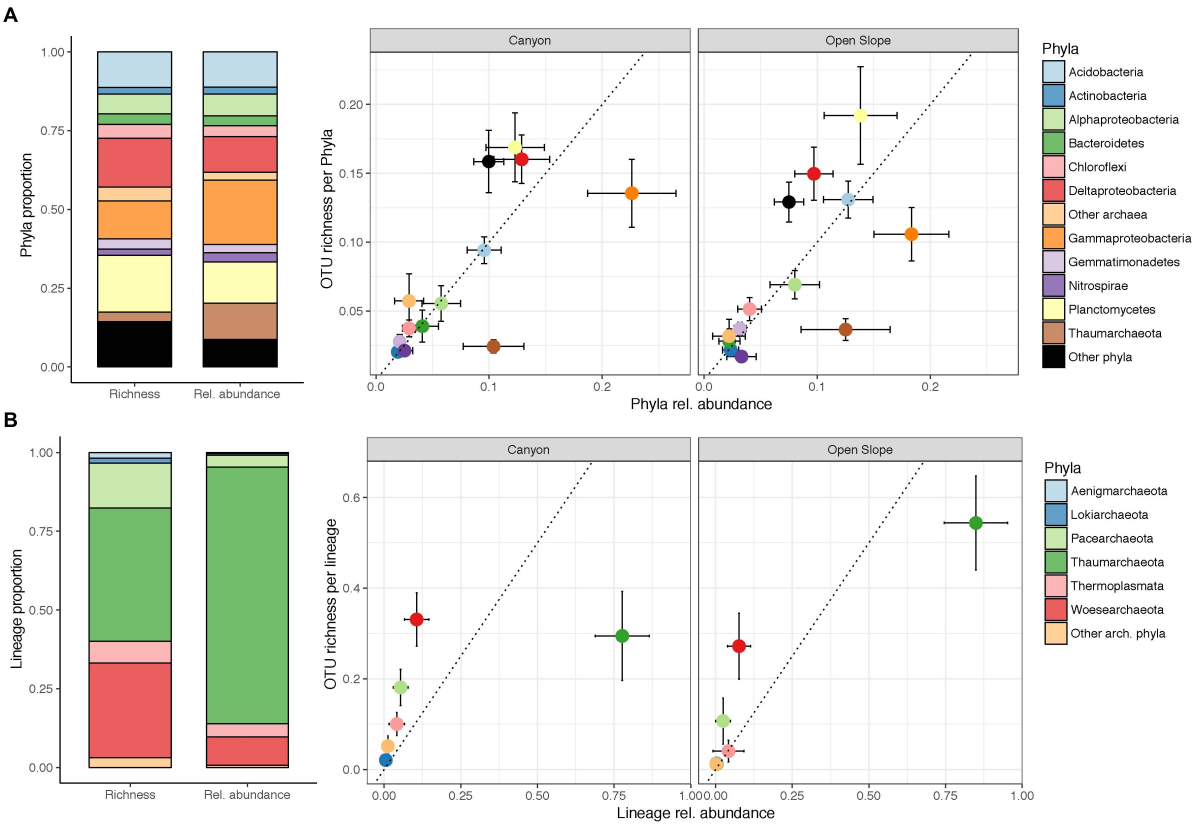

FIGURE 4 | Average microbial community profile per sample (richness and relative abundance), and phyla ratios between the proportion of richness and relative abundances per habitat (canyon and slope) based on the average number of reads per sample. Error bars indicate the standard deviation (SD). Panels indicate: **(A)** overall taxonomic profile and ratios and **(B)** archaea specific profile and ratios.

layers, there were not evident differences in taxonomic profile nor at the phylum nor at the class level and only Verrucomicrobia (236 OTUs) significantly ($p < 0.001$) decreased in abundance along the vertical sediment profile. At lower taxonomic ranks, there were many OTUs that exhibited differences between the three sediment layers according to their indicative values (IndVal > 0.5). These indicative OTUs showed differences at the phyla level: Planctomycetes and Nitrospirae had more indicators in the deeper layer, while Gammaproteobacteria, Alphaproteobacteria, and Bacteroidetes were more characteristic of the surface and subsurface layers (**Supplementary Figure S2**).

Archaea were highly abundant in most samples, accounting for a 14% on average (ranging from 4.2 to 23.4%). Archaeal sequences were classified within the lineages Euryarchaeota, Aenigmarchaeota, Woesearchaeota, Pacearchaeota, Diapherotrites, Lokiarchaeota, Crenarchaeota, and Thaumarchaeota. However, most OTUs belonged to the Woesearchaeota (1250), followed by Pacearchaeota (651), Euryarchaeota (187), and Thaumarchaeota (181). Thaumarchaeota showed the highest abundance, which was not linked to a high proportion of OTUs (**Figure 4B**). Moreover, OTU proportions of Woesearchaeota and Thaumarchaeota greatly differed between canyon and slope, inverting their ranks. Some of the most abundant (14) and widespread (100%) OTUs were assigned to *Candidatus Nitrosopumilus*. The thaumarchaeotal groups AK31 and Marine Benthic group 'A' were significantly more abundant on the slope.

Patterns of Microbial Abundances and Diversity

The estimated cell abundances in the canyon and on the slope ranged from 1.56×10^6 to 3.57×10^{10} and 3.81×10^9 to 4.39×10^{10} cells per sediment gram, respectively (**Figure 5**). Both habitats showed significant higher abundances in autumn than in spring in the surface and subsurface layers (Se × SL PERMANOVA, **Table 2** and **Supplementary Table S2**). The abundances decreased along the vertical sediment profile on the slope, particularly in autumn, while were evenly distributed in the canyon (**Figure 5**). Furthermore, abundances were significantly higher in the canyon than on the slope only for the deep sediment layer (Ha × SL PERMANOVA, **Table 2** and **Supplementary Table S2**). Alpha diversity differed significantly between habitats ($\rho < 0.05$, **Table 2**). The richness of Archaea and Bacteria was higher in the canyon than on the slope, being strongly correlated with microbial abundances ($\rho = 0.42$, $p < 0.01$). Shannon index was higher in the canyon than on the slope for Bacteria, contrary

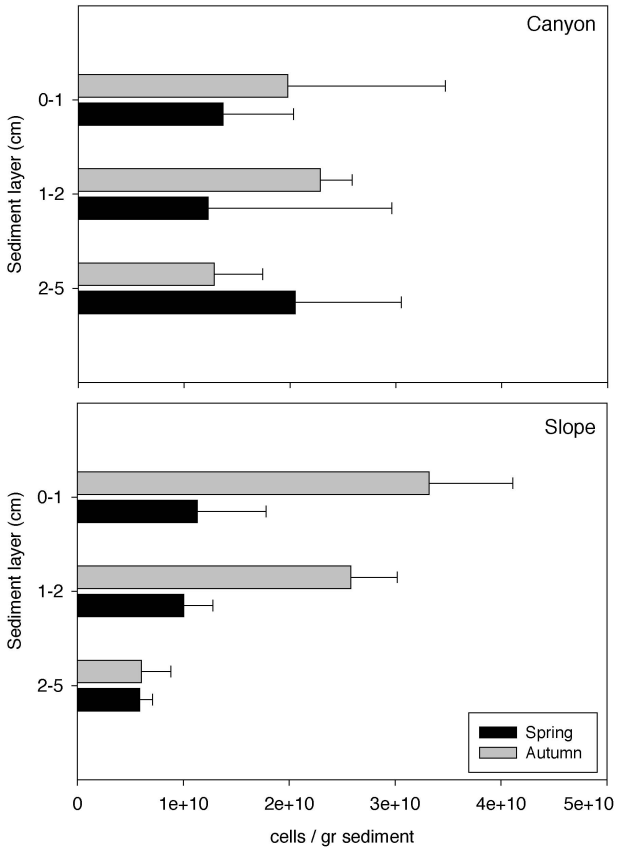

FIGURE 5 | Estimated microbial abundances (number of cells/gram of sediment) along the vertical sediment profile in the canyon and on the slope during autumn and spring. Errors bars are standard deviations.

to Archaea (**Figure 6**). Beta diversity was higher in the canyon along the whole vertical sediment profile (**Figure 7**).

On the slope, abundance and Shannon Index were negatively correlated with clay and positively with silt, and positively with nematode densities (**Table 3**). In the canyon, there was a negative correlation between abundance and OC, while alpha diversity was positively correlated with Chl *a* only in autumn (**Table 3**). Additionally, only archaeal richness was negatively correlated with nematode abundance ($\rho = -0.43$, $p < 0.01$) on the slope.

TABLE 2 | Results of three-way PERMANOVA analyses for differences in microbial descriptors using Habitat (Ha), Season (Se), and Sediment Layer (SL) as factors.

Source	df	Microbial abundance	OTU richness	Shannon diversity	Community structure	Microbial functions
Ha	1	0.6418	**0.02**	***0.005***	***0.0001***	**0.0001**
Se	1	***0.0091***	0.1942	0.6063	***0.0008***	0.0955
SL	2	0.0997	0.8914	0.8018	***0.0001***	0.0807
Ha × Se	1	0.3058	0.5898	0.3588	***0.0033***	0.1008
Ha × SL	2	**0.0428**	0.9627	0.211	**0.0033**	**0.0487**
Se × SL	2	**0.0279**	0.5597	0.4099	0.1424	**0.0219**
Ha × Se × SL	2	0.5123	0.0821	0.2437	0.2448	0.2774
Residuals	23					
Total	34					

Bold: $p < 0.05$; bold italic: $p < 0.01$.

Patterns of Community Structure

Community structure based on OTU-derived Bray–Curtis dissimilarities, clearly differed between canyon and slope (**Figure 8** and **Table 2**), showing significant differences in terms of Habitat, Season and Sediment Layer, but also for the interactions Ha × Se and Ha × SL (PERMANOVA, **Table 2**). Canyon and slope significantly differed in both seasons, but seasonal variations were only significant in the canyon (pair-wise tests, **Figure 8A** and **Supplementary Table S3**). Additionally, all sediment layers showed strongly differentiated OTU communities both in the canyon and on the slope (Ha × SL, **Figure 8B** and **Supplementary Table S3**). Within habitats, significant differences among all sediment layers were found on the slope, while in the canyon these were mainly observed between surface and deep layers (**Figure 8B** and **Supplementary Table S3**).

We only found significant explanatory environmental variables in the canyon, explaining 24.4% of the community variability (according to RELATE analysis-PRIMER). The responses were TN, clay, sand, and silt (marginal -individual variables- test, DISTLM, $p < 0.05$; 12.9, 11.7, 11.1, and 10.7% of variation explained, respectively, **Supplementary Table S5**). The combination TN and silt constituted the best explanatory model for the community patterns (sequential test, ca. 58% of total variability explained), which imply that grain size explains a large part of the observed variability (**Supplementary Table S5**). Samples showed separation between seasons, with the most influencing environmental variables being Chl *a* and Chl *a*: phaeo in spring (**Supplementary Figure S3**). The first two dbRDA axes explained 42.2% of the community variation (**Supplementary Figure S3**).

Relationships of Functional Predictions With Spatial Factors and Densities

The functional predictions correspond, on average, to 30% of reads/sample (minimum 24.4%, maximum 40.5%), according to the matches with the Tax4Fun2 reference functional dataset. Without considering the spatial factors, the community proportion of pathways of the different biogeochemical cycles (**Figure 9**) had significant correlations with independently measured variables such as nematode density, which was positively correlated with aerobic respiration, and negatively with the NO_3 reduction/NO_2 oxidation two-way pathway. Also, microbial abundance was positively correlated to the carbon cycle, specifically with arnon C fixation and fermentative processes. Furthermore, the relative abundance of Archaea was positively correlated with N mineralization and nitrification.

In addition, spatial factors and seasons significantly separated the functional profiles according to PERMANOVA (**Figure 9**, **Table 2** and **Supplementary Table S4**). Habitat alone statistically differentiated the profiles, but there were *post hoc* differences

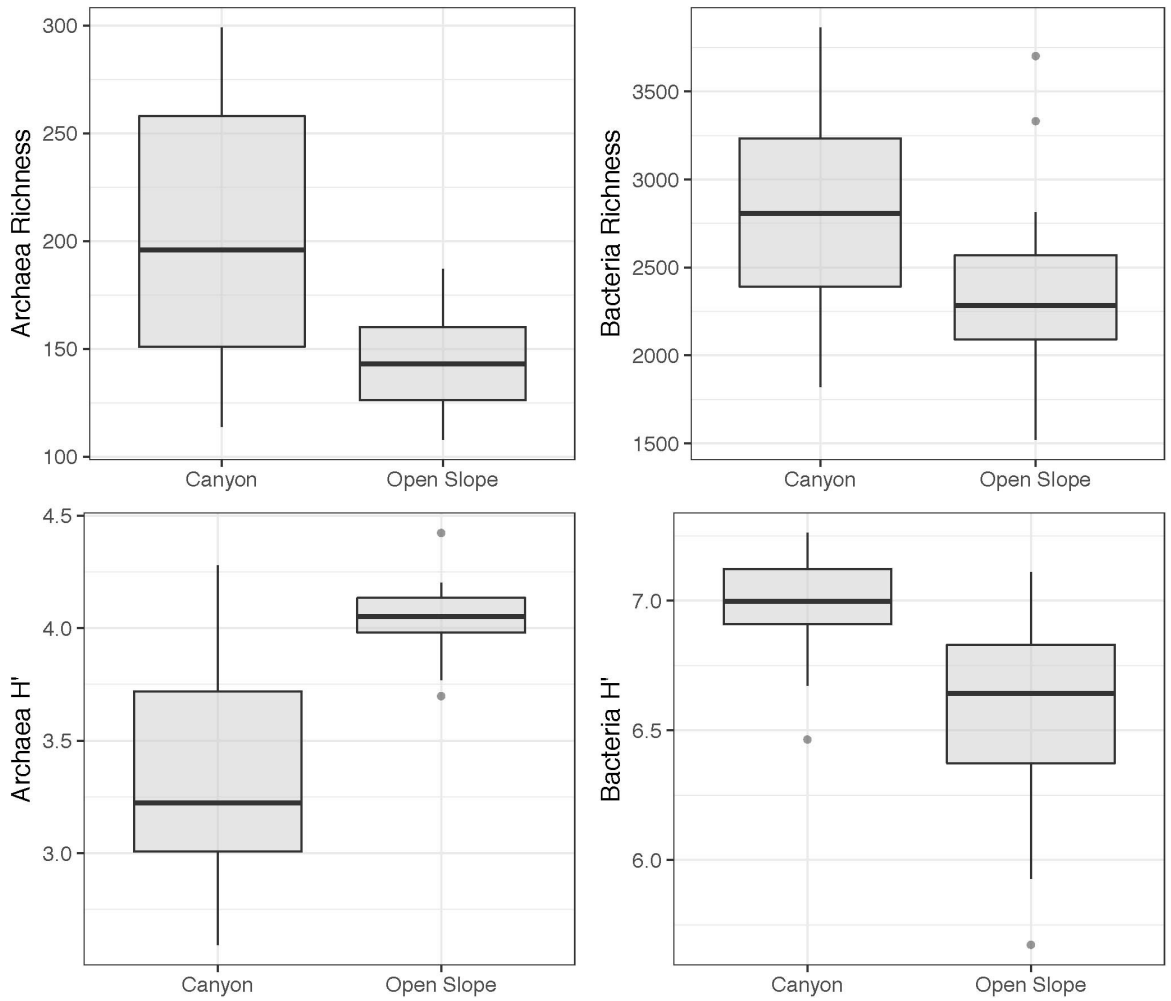

FIGURE 6 | Alpha diversity of Archaea and Bacteria measured as Richness (OTU number) and Shannon index (H').

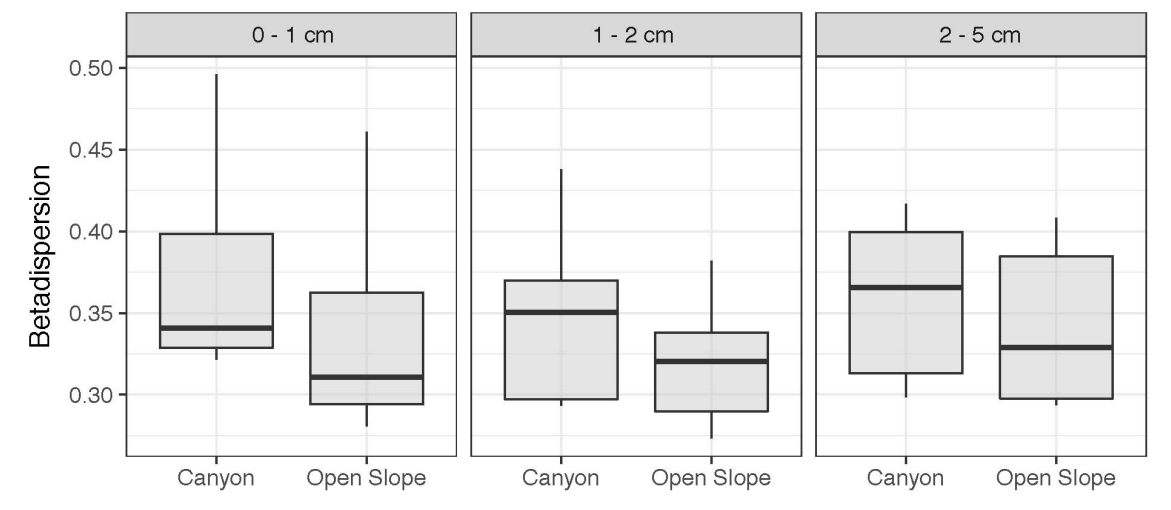

FIGURE 7 | Beta-diversity (as Betadispersion) of samples (with both Archaea and Bacteria) grouped by habitat and sediment layer.

between habitats in the three sediment layers (Ha × SL). Specifically, aerobic respiration, Arnon C fixation, chitin and cellulose break, or N assimilation/fixation were significantly higher in the canyon; while nitrification, annamox or P transport were significantly higher on the open slope. Furthermore, there were differences between the three sediment layers but only during autumn (Se × SL), and regardless of the season solely on the open slope (Ha × SL). The upper layer had significantly higher aerobic respiration (both habitats), and assimilatory sulfate reduction (canyon only). The deeper layer showed higher potential for the sulfate reduction and sulfide oxidation pathway (both habitats) (**Figure 9**).

DISCUSSION

Differences Between Canyon and Open Slope

We expected that the differential environmental dynamics affecting canyon and slope habitats would lead the respective microbial communities to assemble differently, thus giving place to particular patterns. Indeed, Blanes Canyon's higher dynamism promotes diversity (both for bacterial and archaeal taxa pools) and community heterogeneity. The complex topography and strong, variable currents characterising submarine canyons enhance marine landscape diversity at regional scales, providing singular habitats to a highly diverse fauna (Huvenne and Davies, 2014; Fernandez-Arcaya et al., 2017; Ismail et al., 2018). In Blanes Canyon, high-rank taxa showed similar profiles to the open slope, but only 37% of the OTUs were shared. Accordingly, the two habitats at the same depth (ca. 1,500 m) showed clearly different sediment communities. Deep-sea microbial communities often have shown a high degree of specificity in terms of taxa and ecological specializations as a response to characteristic nutrient and particle fluxes (Dang et al., 2009; Li et al., 2009; Jacob et al., 2013; Sevastou et al., 2013; Ristova et al., 2015). Blanes Canyon shows a high TN level through its whole vertical sediment profile, suggesting sedimentation rates higher than those on the slope leading to major environmental differences. OM indicators (OC, Chl *a*, CPE) were also higher in the canyon (Román et al., 2016), which may contribute to the environmental idiosyncrasy influencing microbial community assembly. Downward particle fluxes are higher in the canyon axis than those in the eastern and western adjacent open slopes due to external forcing such as storm and/or dense shelf water cascading events (Canals et al., 2006; Zúñiga et al., 2009; López-Fernández et al., 2013). In particular, sedimentation rates at 1500 m depth inside the canyon were twice as high than in the slope (Paradis et al., 2018). These environmental differences among habitats may certainly contribute to explain the canyon's singularity as a habitat for microbial communities. Differences also occur in meiofaunal communities between Blanes Canyon and their adjacent slopes (Romano et al., 2013a; Román et al., 2016). Consequently, ecological interactions may also contribute to the observed differences in microbial communities. For instance, specific associations between nematodes and bacteria have been detected in a nearby canyon system (Rzeznik-Orignac et al., 2018). As a more general trend, we have observed that nematode densities lacked seasonal changes and showed positive relationships with bacterial diversity and abundance only on the slope, whereas nematode densities increased in the canyon during spring (Román et al., 2016). This suspected association between meiofaunal and microbial communities might reflect different trophic interactions in the benthic sediments at the two contrasting habitats. Predatory/scavenger nematodes (such as *Sphaerolaimus* and *Pomponema*) dominate the Blanes Canyon communities, while non-selective deposit feeders were less numerous compared to the adjacent slope (Román et al., 2018), which appear to be related to their different roles in the trophic web (Ingels et al., 2009). These differences in nematode community composition may thus enhance the differential environmental trends discussed above, joining them in explaining the observed between-habitat differences concerning the microbial assemblages' establishment and growth.

Interestingly, when comparing bacterial and archaeal phyla by habitat, we observed that Planctomycetes and Thaumarchaeota, both containing taxa with roles in the N cycle (Sintes et al., 2013; Restrepo-Ortiz et al., 2014; Kuypers et al., 2018), had higher richness in the open slope than in the canyon. Part of the microbial richness observed may also act as seed microbes or opportunists, actively changing their abundances as a response to environmental situations matching their functional requirements (Sebastián et al., 2018). These functional requirements displayed differences along habitats and sediment layers. The pathway with the highest proportion, aerobic respiration, is more abundant in the canyon, particularly in surface sediments. In parallel, nematode abundance is also higher in the canyon (**Supplementary Figure S4**), contributing to sediment oxygenation through bioturbation (Sturdivant et al.,

TABLE 3 | Spearman correlations between independent variables (environmental factors and nematode abundance) with microbial metrics (abundance and Shannon index) for both habitats.

Habitat	Season	Metric	Variables	*r*	*p*	*n*
Slope	All	Abundance	Nematodes	0.67	**0.027***	18
	Autumn	Abundance	Nematodes	0.817	**0.042***	9
	Autumn	Abundance	Clay (%)	−0.8	**0.042***	9
	Autumn	Abundance	Silt (%)	0.8	**0.042***	9
	Autumn	Shannon-Index	Nematodes	0.933	**0.009****	9
	Autumn	Shannon-Index	Clay (%)	−0.883	**0.014***	9
	Autumn	Shannon-Index	Silt (%)	0.867	**0.015***	9
Canyon	Autumn	Abundance	% OC	−0.877	**0.027***	9
	Autumn	Shannon-Index	Chl *a*	0.854	*0.054.*	9
	Autumn	Shannon-Index	Chl *a*:phaeo	0.753	*0.108.*	9
	Spring	Shannon-Index	% OC	−0.719	*0.113.*	9

*Significance levels (fdr adjusted): p < 0.01 (**bold), p < 0.05 (*bold), p < 0.1 (.italics).*

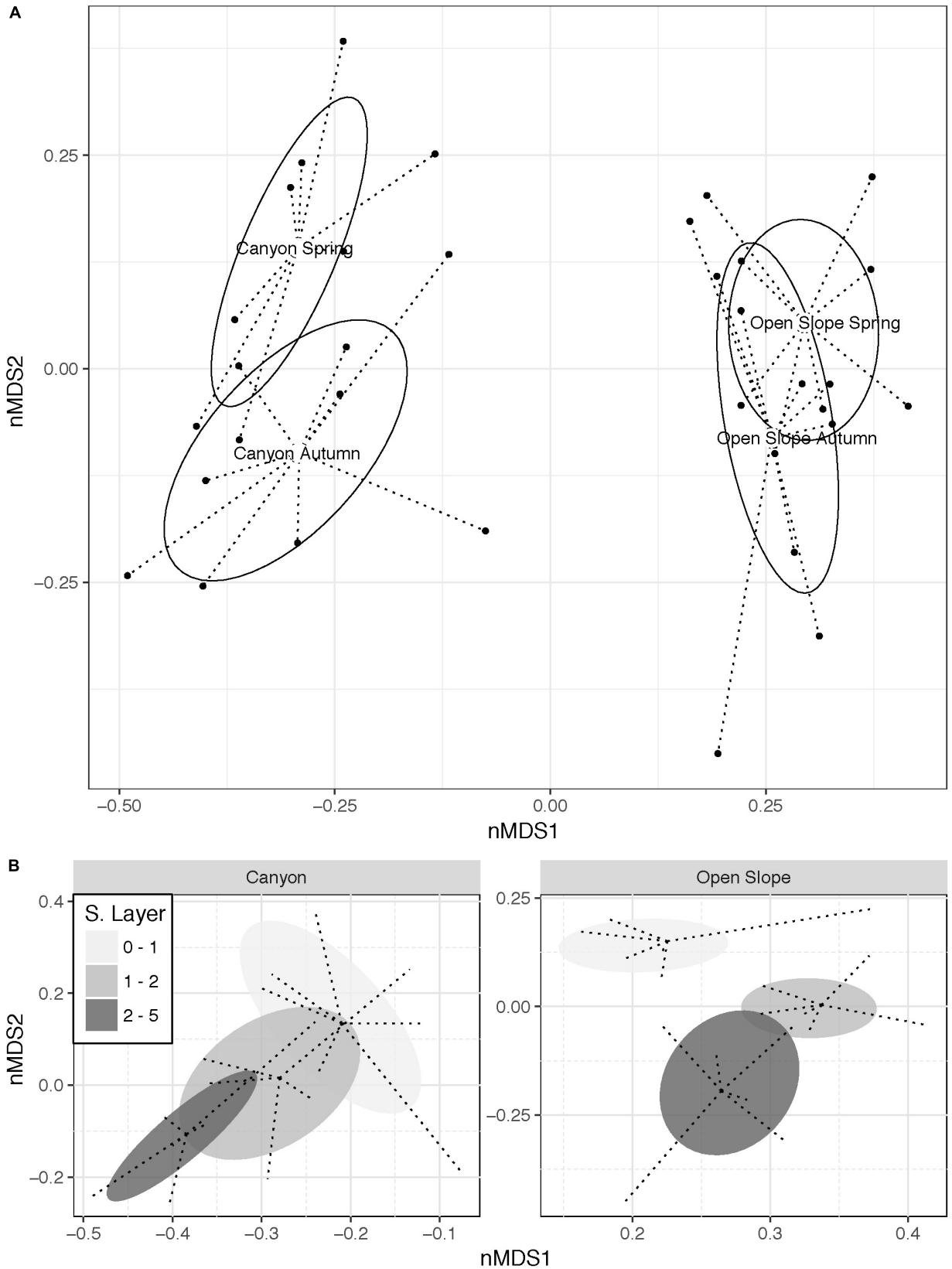

FIGURE 8 | Non-metric MDS plots (Bray–Curtis similarity) based on Hellinger transformed microbial community data (OTUs) illustrating the significant interactions: **(A)** Habitat × Season and **(B)** Habitat × Sediment Layer.

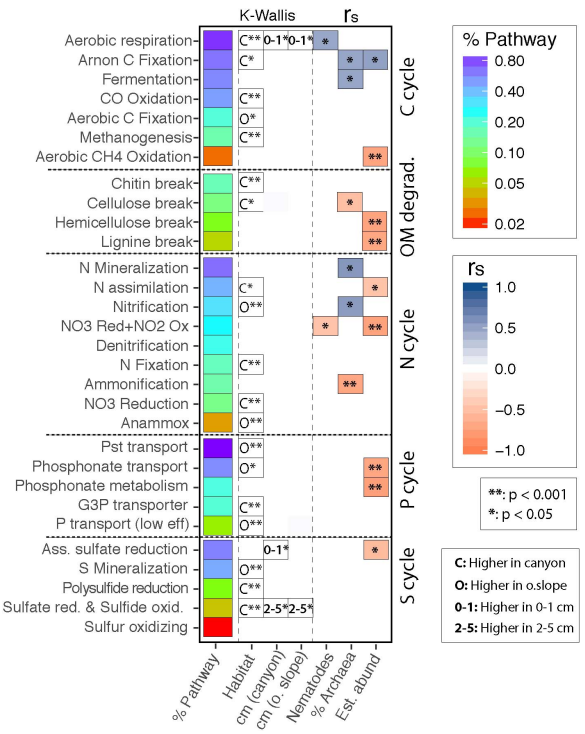

FIGURE 9 | Predicted functional pathways sorted by mean dataset abundance and element. Significant differences for each pathway are shown for spatial factors (Habitat and Sediment Layer in the Canyon and on the Slope separately), nematodes and microbial abundances, and the % of archaea/sample. The heatmap displays statistically significant relationships after *fdr* adjustment (**$p < 0.001$, *$p < 0.05$), according to Kruskal–Wallis test (spatial factors) and spearman correlations (univariate metrics). C/O 0-1/2-5 indicate the factor level harboring a significantly increased value, and the color scale the Spearman's r magnitude.

2012). Also, vegetal debris occurred more often in Blanes Canyon than on the open slope (C. Romano, unpublished data), together with the associated wood-degrading macrofauna (Romano et al., 2013b, 2014). Therefore, we also expected to encounter enhanced predicted chitin and cellulose pathways in the canyon sediments.

Differences Between Seasons

The marked between-season differences in microbial communities observed in Blanes Canyon was associated to increases in available phytodetritus in spring. These may probably be explained by the winter 2012 unusual atmospheric conditions, which led to the formation of dense shelf water cascading in the whole NW Mediterranean (Durrieu de Madron et al., 2013). These increases in available phytodetritus in spring (Román et al., 2016) may have led to increased nematode densities (**Supplementary Figure S4**), and surprisingly lower microbial densities. Despite microbial community structure lacked relationships with environmental variables on the open slope, we found positive relationships between microbial abundance and diversity with nematode densities and silt content solely during autumn. This may be explained by multiple heterogeneous processes, including anthropogenic activities, affecting the Blanes submarine canyon and its sedimentation characteristics (López-Fernández et al., 2013; Román et al., 2016; Paradis et al., 2018) with distinct intensities over time. Food availability may certainly be a key driver (Goffredi and Orphan, 2010; Sevastou et al., 2013; Bienhold et al., 2016), but also others may play a role in shaping these communities that may explain the often non-consistent relationships with food sources. Therefore, the consistency of these observations require further checking over time before allowing us to derive accurate seasonal predictions in microbial assemblage trends.

Adaptations Along the Vertical Sediment Profile

Substrate heterogeneity has often been considered a possible cause of spatial variability in deep-sea environments and their biodiversity (Rex and Etter, 2010). In our study, the differentiation of microbial community structure and abundance along the vertical sediment profile has been the second most important pattern observed. Differences between microbial communities from upper to deeper layers have been reported for both habitats, being in agreement with the down-core stratification reported in previous studies (e.g., Fry et al., 2006; Jorgensen et al., 2012; Bienhold et al., 2016). Surface and subsurface communities in the canyon seemed to harbor homogeneous communities, which may be supported by mixing and depositional processes (Harrison et al., 2018), consistent with its sedimentation characteristics (Lastras et al., 2009; Zúñiga et al., 2009; Pusceddu et al., 2010). Microbial abundances decreased particularly on the open slope, suggesting a more stable sediment stratification responding to a higher environmental homogeneity and stability (e.g., in terms of particle fluxes or ocean currents) compared to Blanes Canyon (Zúñiga et al., 2009). In the canyon, clay content gradually increased with depth, as reported in other regions (Nunoura et al., 2018), while productivity variables were linked to seasonal events showing higher variability. Consequently, the high microbial abundances in canyon's subsurface and deeper layers may be explained by the higher seasonal production variability together with its higher sediment heterogeneity (Ingels et al., 2009; Zúñiga et al., 2009). Overall, the differences in sediment and OM deposition and accumulation rates appear to be mirrored by the microbial communities (likely due to their size), thus contributing to explain the more homogeneous distribution patterns observed on the slope. The relationship between sediment environmental variables and microbial abundances also differed between habitats, suggesting the existence of different drivers. Sediment OM content emerged as a key factor associated with changes in bacterial community structure in other locations (Sevastou et al., 2013; Bienhold et al., 2016). However, while we have found weak 'food-source' relationships with the microbial descriptors (abundance and community), these only occurred in the canyon, where the sediments were more organically enriched than on the slope (Román et al., 2016; Román, 2017). In turn, sediment granulometry arose as a

fundamental driver for microbial assemblages both in canyon and slope environments.

Ecological Roles and Potential Functionality of Deep-Sea Sediments

We found a noteworthy proportion of sequences assigned to archaeal lineages. In general, contrasting to their scarcity in the water column (Sunagawa et al., 2015), archaeal contribution to the total benthic microbial biomass in particular from Thaumarchaeota, has been pointed out to be greater than previously hypothesized (Danovaro et al., 2016). Some of these archaea are critical players in the N cycle in marine sediments (Kuypers et al., 2018), and the observed high relative abundances in our study probably benefit from the ammonia excretion coming from the nematodes (Barnes, 1980). However, despite the high proportion of Thaumarchaeota per sample, the richest groups were Pacearchaeota and Woesearchaeota, considering the whole sampling area but particularly in the canyon. These lineages have an unknown ecological role in the Blanes Canyon system but display an enormous environmental versatility and biome occurrence (Ortiz-Álvarez and Casamayor, 2016). Studies in inland environments support their anaerobic heterotrophic lifestyle and metabolic complementarity with other microbes (Liu et al., 2018). Given that archaeal richness was negatively correlated with nematode abundance, we suggest a niche differentiation of these lineages along the vertical sediment profile. Regarding N, both microbial abundances and nematode densities were negatively correlated to the predicted NO_3 reduction/NO_2 oxidation two-way pathway. Accordingly, nematodes likely play a strong role in the N cycle by supplying ammonia to the system (Ferris et al., 1998). And both nitrification and anammox processes, which require ammonia, are particularly enhanced on the open slope. Annamox is a process exclusive to a few genera (*Kuenenia* and *Scalindua*) from the phylum Planctomycetes (Kuenen, 2008; Sonthiphand et al., 2014), genera that were indeed detected in our dataset. Planctomycetes is also dominant in the deep-sea sediments from the Eastern Mediterranean Sea (Quaiser et al., 2011; Bienhold et al., 2016), and the South Atlantic Ocean (Schauer et al., 2010). In addition, in South China sediments, the deep-sea harbors a higher abundance of microbes involved in nitrification, anammox, and ammonification than the shallower sediments (Yu et al., 2018).

The deep ocean floor copes with all the debris deposited from the water column. In this environment, biogeochemical cycling is key in avoiding the particles to remain buried by transforming them into available nutrients that nurture the complex trophic chain. Microbes degrading sunken wood produce significant amounts of hydrogen sulfide through S mineralization, which is the base of the wood chemosynthetic ecosystem (Kalenitchenko et al., 2017), that also exist in Blanes Canyon (Fagervold et al., 2013, 2014; Romano et al., 2013b, 2014; Bessette et al., 2014). The high burial rates in the canyon (López-Fernández et al., 2013) lead oxygen levels to quickly drop a few centimeters below the sediment surface, while causing higher aerobic activity in the surface sediment layers (indicated by the increased aerobic respiration and aerobic sulfate reduction pathway). The occurrence of the chemosynthetic nematode *Astomonema* only in the canyon (Román, 2017), especially at deeper layers (Román et al., 2018), supports the presence of hydrogen sulfide by the lack of oxygen and sulfate respiration in the sediments (Ingels et al., 2011). The reduced conditions at the deep layers found both in the canyon and on the slope were supported by the dominance of *Sabatieria* (Román et al., 2018), indicating reduced oxygen availability (Soetaert et al., 1995; Vanreusel et al., 1997).

CONCLUSION

We report idiosyncratic microbial characteristics (in terms of abundance, diversity, composition, and predicted functions) in two closely related geographical regions, a canyon and its adjacent open slope. Our results suggest that the deep-sea seafloor is strongly connected to coastal and pelagic productive areas through the canyon system in a stronger manner than to the open slope, thus modulating resource availability while driving changes in the microbial biosphere and the deep-sea food web. Overall, the microbial communities were dominated by bacteria, in which Gammaproteobacteria were the most abundant, followed by Deltaproteobacteria (the richest group), Planctomycetes, Acidobacteria, and Alphaproteobacteria. Although not dominant, Archaeal contribution to diversity and abundance was significant. Most OTUs belonged to Woesearchaeota followed by Pacearchaeota, Euryarchaeota and Thaumarchaeota, which showed the higher proportion and occurrence. The gradually decreasing abundance along the vertical sediment profile on the slope was explained by environmental stability and correspondingly low food availability. Conversely, canyon sediments showed much more variable geomorphological and environmental conditions which, together with the greater amount of available food (as Chl *a*, CPE, and OC), lead this habitat to harbor distinctive microbial assemblages in terms of composition and structure. In addition, the observed differences in community structure between autumn and spring were only evident in the canyon, again tracing a higher dynamism than on the open slope. The high downward particle fluxes driven by bottom trawling activities along canyon flanks appear to be directly related with the high reported sedimentation rates inside the canyon. This supports the existence of a considerable anthropogenic influence on microbial assemblages at the studied depth, but long-term studies are required to confirm this hypothesis. Furthermore, the arrangement of communities along the 0–5 cm vertical sediment profile, and the differences in predicted metabolisms, indicates niche specialization with potential consequences in higher trophic levels. Correlations between sediment microbiota and nematodes were only observed on the slope, in the absence of seasonal variability, and corresponding with differences along the vertical sediment profile. However, only ecological studies targeting both fauna and microbiological composition, for example under a co-occurrence network approach, will reveal the different ecological

specificities of these two food web compartments. In light of our results, we conclude that Blanes Canyon notably contributes to the deep-sea microbial biodiversity, enlarging the idea of the 'canyon effect' shaping deep-sea microbial benthic communities.

AUTHOR CONTRIBUTIONS

SR and RO-A contributed equally to the manuscript, leading writing, and data analysis. SR, CR, and DM collected and processes samples. RO-A and EC contributed with sequence analysis, statistical analyses, and microbiological interpretations. SR, RO-A, and CR contextualized microbial data in the deep-sea realm. All authors contributed to manuscript revision, read and approved the submitted version.

FUNDING

This research has been supported by DOS MARES (Reference No. CTM2010-21810-C03-03) research project, funded by the Spanish "Agencia Estatal de Investigación" (AEI) and the European Funds for Regional Development (FEDER). CR received an International Outgoing Fellowship from the People Programme (Marie S. Curie Actions) of the European Union's Seventh Framework Programme (FP7/2007-2013) under REA Grant Agreement No. PIOF-GA-2013-628146. RO-A and SR were supported by the FPI fellowship programme from the Spanish Government. DM was supported by the Consolidated Research Group on Marine Benthic Ecology of the Generalitat de Catalunya (2017SGR378) and the Research Project PopCOmics (CTM2017-88080), funded by AEI and FEDER. RO-A and EC were supported by project DARKNESS CGL2012-32747.

ACKNOWLEDGMENTS

The authors would like to thank the crew of the R.V. García del Cid and colleagues from CSIC, UB, and other institutions for helping on board. Thanks to Dr. Galderic Lastras (UB) for GIS expertise. In addition, they thank M. Guardiola, G. Carreras, and X. Turon for laboratory assistance.

SUPPLEMENTARY MATERIAL

The Supplementary Material for this article can be found online at: https://www.frontiersin.org/articles/10.3389/fmars.2019.00108/full#supplementary-material

REFERENCES

Allen, S., and Durrieu de Madron, X. (2009). A review of the role of submarine canyons in deep-ocean exchange with the shelf. *Ocean Sci.* 5, 607–620. doi: 10.5194/os-5-607-2009

Allen, S., Vindeirinho, C., Thomson, R., Foreman, M. G., and Mackas, D. (2001). Physical and biological processes over a submarine canyon during an upwelling event. *Can. J. Fish. Aquat. Sci.* 58, 671–684. doi: 10.1139/f01-008

Anderson, M., Gorley, R. N., and Clarke, K. R. (2008). *PERMANOVA for PRIMER: Guide to Software and Statistical Methods*. Plymouth: PRIMER-E.

Anderson, M. J. (2005). Permutational multivariate analysis of variance. *Dep. Stat. Univ. Auckland* 26, 32–46.

Apprill, A., Mcnally, S., Parsons, R., and Weber, L. (2015). Minor revision to V4 region SSU rRNA 806R gene primer greatly increases detection of SAR11 bacterioplankton. *Aquat. Microb. Ecol.* 75, 129–137. doi: 10.3354/ame01753

Barnes, R. G. (1980). *Invertebrate Zoology*. Philadelphia, PA: Sanders College.

Barone, G., Rastelli, E., Corinaldesi, C., Tangherlini, M., Danovaro, R., and Dell'Anno, A. (2018). Benthic deep-sea fungi in submarine canyons of the Mediterranean Sea. *Prog. Oceanogr.* 168, 57–64. doi: 10.1016/j.pocean.2018.09.011

Berner, R. A. (1982). Burial of organic carbon and pyrite sulfur in the modern ocean: its geochemical and environmental significance. *Am. J. Sci.* 282, 451–473. doi: 10.2475/ajs.282.4.451

Bessette, S., Fagervold, S., Romano, C., Martin, D., Le Bris, N., and Galand, P. E. (2014). Diversity of bacterial communities on sunken woods in the Mediterranean Sea. *J. Mar. Sci. Technol.* 22, 60–66.

Bianchelli, S., and Danovaro, R. (2019). Meiofaunal biodiversity in submarine canyons of the Mediterranean Sea: a meta-analysis. *Prog. Oceanogr.* 170, 69–80. doi: 10.1016/j.pocean.2018.10.018

Bianchelli, S., Gambi, C., Mea, M., Pusceddu, A., and Danovaro, R. (2013). Nematode diversity patterns at different spatial scales in bathyal sediments of the Mediterranean Sea. *Biogeosciences* 10, 5465–5479. doi: 10.5194/bg-10-5465-2013

Bienhold, C., Zinger, L., Boetius, A., Ramette, A., and Kellogg, C. (2016). Diversity and biogeography of bathyal and abyssal seafloor bacteria. *PLoS One* 11:e0148016. doi: 10.1371/journal.pone.0148016

Canals, M., Puig, P., de Madrn, X., Heussner, S., Palanques, A., and Fabre, J. (2006). Flushing submarine canyons. *Nature* 444, 354–357. doi: 10.1038/nature05271

Caporaso, J. G., Lauber, C. L., Walters, W. A., Berg-Lyons, D., Lozupone, C. A., Turnbaugh, P. J., et al. (2011). Global patterns of 16S rRNA diversity at a depth of millions of sequences per sample. *Proc. Natl. Acad. Sci. U.S.A.* 108, 4516–4522. doi: 10.1073/pnas.1000080107

Celussi, M., Quero, G. M., Zoccarato, L., Franzo, A., Corinaldesi, C., Rastelli, E., et al. (2018). Planktonic prokaryote and protist communities in a submarine canyon system in the Ligurian Sea (NW Mediterranean). *Prog. Oceanogr.* 168, 210–221. doi: 10.1016/j.pocean.2018.10.002

Chauvet, P., Metaxas, A., Hey, A., and Matabos, M. (2018). Annual and seasonal variations in the deep-sea megafaunal epibenthic communities in Barkley Canyon (British Columbia, Canada): a response to surface and deep-sea environment. *Prog. Oceanogr.* 169, 89–105. doi: 10.1016/j.pocean.2018.04.002

Dang, H., Li, J., Chen, M., Li, T., Zeng, Z., and Yin, X. (2009). Fine-scale vertical distribution of bacteria in the East Pacific deep-sea sediments determined via 16S rRNA gene T-RFLP and clone library analyses. *World J. Microbiol. Biotechnol.* 25, 179–188.

Danovaro, R., Dinet, A., Duineveld, G., and Tselepides, A. (1999). Benthic response to particulate fluxes in different trophic environments: a comparison between the Gulf of Lions–Catalan Sea (western-Mediterranean) and the Cretan Sea (eastern-Mediterranean). *Prog. Oceanogr.* 44, 287–312. doi: 10.1016/S0079-6611(99)00030-0

Danovaro, R., Marrale, D., Dell'Anno, A., Della Croce, N., Tselepides, A., and Fabiano, M. (2000). Bacterial response to seasonal changes in labile organic matter composition on the continental shelf and bathyal sediments of the Cretan Sea. *Prog. Oceanogr.* 46, 345–366. doi: 10.1016/S0079-6611(99)00030-0

Danovaro, R., Molari, M., Corinaldesi, C., and Dell'Anno, A. (2016). Macroecological drivers of archaea and bacteria in benthic deep-sea ecosystems. *Sci. Adv.* 2:e1500961. doi: 10.1126/sciadv.1500961

De Leo, F. C., Vetter, E. W., Smith, C. R., Rowden, A. A., and Mcgranaghan, M. (2014). Spatial scale-dependent habitat heterogeneity influences submarine canyon macrofaunal abundance and diversity off the main and Northwest Hawaiian Islands. *Deep Sea Res. Part II* 104, 267–290. doi: 10.1016/j.dsr2.2013.06.015

De Stigter, H., Boer, W., Thomsen, L., and Jesus, C. (2007). Recent sediment transport and deposition in the Nazaré Canyon, Portuguese continental margin. *Mar. Geol.* 246, 144–164. doi: 10.1016/j.dsr2.2013.06.015

Deming, J. W., and Baross, J. A. (1993). *The Early Diagenesis of Organic Matter: Bacterial Activity. Organic Geochemistry*. Berlin: Springer. doi: 10.1016/j.margeo.2007.04.011

Durrieu de Madron, X., Houpert, L., Puig, P., Sanchez-Vidal, A., Testor, P., Bosse, A., et al. (2013). Interaction of dense shelf water cascading and open-sea convection in the northwestern Mediterranean during winter 2012. *Geophys. Res. Lett.* 40, 1379–1385. doi: 10.1002/grl.50331

Edgar, R. C. (2013). UPARSE: highly accurate OTU sequences from microbial amplicon reads. *Nat. Methods* 10:996. doi: 10.1038/nmeth.2604

Fagervold, S., Bessette, S., Romano, C., Martin, D., Plyuscheva, M., Le Bris, N., et al. (2013). Microbial communities associated with the degradation of oak wood in the Blanes submarine canyon and its adjacent open slope (NW Mediterranean). *Prog. Oceanogr.* 118, 137–143. doi: 10.1007/s00248-016-0923-5

Fagervold, S., Romano, C., Kalenitchenko, D., Martin, D., and Galand, P. E. (2014). Microbial communities in sunken wood are structured by wood-boring bivalves and location in a submarine canyon. *PLoS One* 9:e96248. doi: 10.1371/journal.pone.0096248

Fernandez-Arcaya, U., Ramirez-Llodra, E., AguzzI, J., Allcock, A. L., Davies, J. S., Dissanayake, A., et al. (2017). Ecological role of submarine canyons and need for canyon conservation: a review. *Front. Mar. Sci.* 4:5. doi: 10.3389/fmars.2017.00005

Ferris, H., Venette, R. C., Van Der Meulen, H. R., and Lau, S. S. (1998). Nitrogen mineralization by bacterial-feeding nematodes: verification and measurement. *Plant Soil* 203, 159–171. doi: 10.1023/A:1004318318307

Flexas, M. M., Boyer, D. L., Espino, M., Puig De Fabregas, J., and Rubio, A. (2008). Circulation over a submarine canyon in the NW Mediterranean. *J. Geophys. Res.* 113, 1–18. doi: 10.1029/2006JC003998

Fry, J. C., Webster, G., Cragg, B. A., Weightman, A. J., and Parkes, R. J. (2006). Analysis of DGGE profiles to explore the relationship between prokaryotic community composition and biogeochemical processes in deep subseafloor sediments from the Peru Margin. *FEMS Microbiol. Ecol.* 58, 86–98. doi: 10.1111/j.1574-6941.2006.00144.x

Gage, J. (2003). in *Food Inputs, Utilization, Carbon Flow and Energetics*, ed. P. A. Tyler (Amsterdam: Elsevier Science B.V).

Galand, P. E., Gutiérrez-Provecho, C., Massana, R., Gasol, J. M., and Casamayor, E. O. (2010). Interannual recurrence of archaeal assemblages in the coastal NW Mediterranean Sea (Blanes Bay Microbial Observatory). *Limnol. Oceanogr.* 55, 2117–2125. doi: 10.4319/lo.2010.55.5.2117

Goffredi, S. K., and Orphan, V. J. (2010). Bacterial community shifts in taxa and diversity in response to localized organic loading in the deep sea. *Environ. Microbiol.* 12, 344–363. doi: 10.1111/j.1462-2920.2009.02072.x

Granata, T. C., Estrada, M., Zika, U., and Merry, C. (2004). Evidence for enhanced primary production resulting from relative vorticity induced upwelling in the Catalan Current. *Cont. Shelf Res.* 19, 1249–1263. doi: 10.1016/S0278-4343(98)00118-6

Guardiola, M., Wangensteen, O. S., Taberlet, P., Coissac, E., Uriz, M. J., and Turon, X. (2016). Spatio-temporal monitoring of deep-sea communities using metabarcoding of sediment DNA and RNA. *PeerJ* 4:e2807. doi: 10.7717/peerj.2807

Harris, P., and Whiteway, T. (2011). Global distribution of large submarine canyons: geomorphic differences between active and passive continental margins. *Mar. Geol.* 285, 69–86. doi: 10.1016/j.margeo.2011.05.008

Harrison, B. K., Myrbo, A., Flood, B. E., and Bailey, J. V. (2018). Abrupt burial imparts persistent changes to the bacterial diversity of turbidite-associated sediment profiles. *Geobiology* 16, 190–202. doi: 10.1111/gbi.12271

Huvenne, V. A., and Davies, J. S. (2014). Towards a new and integrated approach to submarine canyon research. Introduction. *Deep Sea Res. Part II* 104, 1–5. doi: 10.1016/j.dsr2.2013.09.012

Ingels, J., Kiriakoulakis, K., Wolff, G., and Vanreusel, A. (2009). Nematode diversity and its relation to the quantity and quality of sedimentary organic matter in the deep Nazaré Canyon, Western Iberian Margin. *Deep Sea Res. Part 1 Oceanogr. Res. Papers* 56, 1521–1539. doi: 10.1016/j.dsr.2009.04.010

Ingels, J., Tchesunov, A. V., and Vanreusel, A. (2011). Meiofauna in the gollum channels and the Whittard Canyon, Celtic margin – how local environmental conditions shape nematode structure and function. *PLoS One* 9:e20094. doi: 10.1371/journal.pone.0020094

Ismail, K., Huvenne, V., and Robert, K. (2018). Quantifying spatial heterogeneity in submarine canyons. *Prog. Oceanogr.* 169, 181–198. doi: 10.1016/j.pocean.2018.03.006

Jacob, M., Soltwedel, T., Boetius, A., and Ramette, A. (2013). Biogeography of deep-sea benthic bacteria at regional scale (LTER HAUSGARTEN, Fram Strait, Arctic). *PLoS One* 8:e72779. doi: 10.1371/journal.pone.0072779

Jorgensen, S. L., Hannisdal, B., Lanzén, A., Baumberger, T., Flesland, K., Fonseca, R., et al. (2012). Correlating microbial community profiles with geochemical data in highly stratified sediments from the Arctic Mid-Ocean Ridge. *PNAS* 109, E2846–E2855. doi: 10.1073/pnas.1207574109

Kalenitchenko, D., Le Bris, N., Dadaglio, L., Peru, E., Besserer, A., and Galand, P. E. (2017). Bacteria alone establish the chemical basis of the wood-fall chemosynthetic ecosystem in the deep-sea. *ISME J.* 12:367. doi: 10.1038/ismej.2017.163

Kuenen, J. G. (2008). Anammox bacteria: from discovery to application. *Nat. Rev. Microbiol.* 6:320. doi: 10.1038/nrmicro1857

Kuypers, M. M., Marchant, H. K., and Kartal, B. (2018). The microbial nitrogen-cycling network. *Nat. Rev. Microbiol.* 16:263. doi: 10.1038/nrmicro.2018.9

Langille, M. G., Zaneveld, J., Caporaso, J. G., Mcdonald, D., Knights, D., Reyes, J. A., et al. (2013). Predictive functional profiling of microbial communities using 16S rRNA marker gene sequences. *Nat. Biotechnol.* 31:814. doi: 10.1038/nbt.2676

Lastras, G., Arzola, R. G., Masson, D. G., and Wynn, R. B. (2009). Geomorphology and sedimentary features in the central portuguese submarine canyons, Western Iberian margin. *Geomorphology* 103, 310–329. doi: 10.1016/j.geomorph.2008.06.013

Lastras, G., Canals, M., Amblas, D., Lavoie, C., and Church, I. (2011). Understanding sediment dynamics of two large submarine valleys from seafloor data: blanes and la fonera canyons, northwestern Mediterranean Sea. *Mar. Geol.* 280, 20–39. doi: 10.1016/j.margeo.2010.11.005

Leduc, D., Rowden, A. A., Nodder, S. D., Berkenbusch, K., Probert, P. K., and Hadfield, M. G. (2014). Unusually high food availability in Kaikoura Canyon linked to distinct deep-sea nematode community. *Deep Sea Res. Part II* 104, 310–318. doi: 10.1016/j.dsr2.2013.06.003

Li, H., Yu, Y., Luo, W., Zeng, Y., and Chen, B. (2009). Bacterial diversity in surface sediments from the Pacific Arctic Ocean. *Extremophiles* 13, 233–246. doi: 10.1007/s00792-009-0225-7

Lindh, M., Maillot, B., Shulse, C., Gooday, A., Amon, D., Smith, C., et al. (2017). From the surface to the deep-sea: bacterial distributions across polymetallic nodule fields in the clarion-clipperton zone of the Pacific Ocean. *Front. Microbiol.* 8:1696. doi: 10.3389/fmicb.2017.01696

Liu, X., Li, M., Castelle, C. J., Probst, A. J., Zhou, Z., Pan, J., et al. (2018). Insights into the ecology, evolution, and metabolism of the widespread Woesearchaeotal lineages. *Microbiome* 6:102. doi: 10.1186/s40168-018-0488-2

Llorens-Marès, T., Yooseph, S., Goll, J., Hoffman, J., Vila-Costa, M., Borrego, C. M., et al. (2015). Connecting biodiversity and potential functional role in modern euxinic environments by microbial metagenomics. *ISME J.* 9:1648. doi: 10.1038/ismej.2014.254

López-Fernández, P., Calafat, A., Sanchez-Vidal, A., Canals, M., Flexas, M. M., Cateura, J., et al. (2013). Multiple drivers of particle fluxes in the Blanes submarine canyon and southern open slope: results of a year round experiment. *Prog. Oceanogr.* 118, 95–107. doi: 10.1016/j.pocean.2013.07.029

López-Gutiérrez, J. C., Henry, S., Hallet, S., Martin-Laurent, F., Catroux, G., and Philippot, L. (2004). Quantification of a novel group of nitrate-reducing bacteria in the environment by real-time PCR. *J. Microbiol. Methods* 57, 399–407. doi: 10.1016/j.mimet.2004.02.009

Lüneberg, K., Schneider, D., Siebe, C., and Daniel, R. (2018). Drylands soil bacterial community is affected by land use change and different irrigation practices in the Mezquital Valley, México. *Sci. Rep.* 8:1413. doi: 10.1038/s41598-018-19743-x

Moens, T., Bouillon, S., and Gallucci, F. (2005). Dual stable isotope abundances unravel trophic position of estuarine nematodes. *J. Mar. Biol. Assoc. U.K.* 85, 1401–1407. doi: 10.1017/S0025315405012580

Moens, T., and Vincx, M. (1997). Observations on the feeding ecology of estuarine nematodes. *J. Mar. Biol. Assoc. U.K.* 77, 211–227. doi: 10.1017/S0025315400033889

Muyzer, G., Hottentrager, S., Teske, A., and Waver, C. (1996). "Denaturing gradient gel electrophoresis of PCR-amplified 16S rDNA. A new molecular approach to analyze the genetic diversity of mixed microbial communities," in *Molecular Microbial Ecology Manual*, eds A. D. L. Akkermans, J. D. van Elsas, and F. J. de Bruijn (Dordrecht: Kluwer Academic Publishing).

Nemergut, D. R., KnelmaN, J. E., Ferrenberg, S., Bilinski, T., Melbourne, B., Jiang, L., et al. (2015). Decreases in average bacterial community rRNA operon copy number during succession. *ISME J.* 10:1147. doi: 10.1038/ismej.2015.191

Nunoura, T., Nishizawa, M., Hirai, M., Shimamura, S., Harnvoravongchai, P., Koide, O., et al. (2018). Microbial diversity in sediments from the bottom of the challenger deep, the mariana trench. *Microbes Environ.* 33, 186–194. doi: 10.1264/jsme2.ME17194

Oksanen, J., Blanchet, F., Friendly, M., Kindt, R., Legendre, P., and Mcglinn, D. (2017). *vegan: Community Ecology Package. R Packag. Version 2.4–2*.

Ortiz-Álvarez, R., and Casamayor, E. O. (2016). High occurrence of Pacearchaeota and Woesearchaeota (A rchaea superphylum DPANN) in the surface waters of oligotrophic high altitude lakes. *Environ. Microbiol. Rep.* 8, 210–217. doi: 10.1111/1758-2229.12370

Ortiz-Álvarez, R., Fierer, N., De Los Ríos, A., Casamayor, E. O., and Barberán, A. (2018). Consistent changes in the taxonomic structure and functional attributes of bacterial communities during primary succession. *ISME J.* 12:1658. doi: 10.1038/s41396-018-0076-2

Parada, A. E., Needham, D. M., and Fuhrman, J. A. (2016). Every base matters: assessing small subunit rRNA primers for marine microbiomes with mock communities, time-series and global field samples. *Environ. Microbiol.* 18, 1403–1414. doi: 10.1111/1462-2920.13023

Paradis, S., Puig, P., Sánchez-Vidal, A., Masqué, P., García-Orellana, J., Calafat, A., et al. (2018). Spatial distribution of sedimentation-rate increases in Blanes Canyon caused by technification of bottom trawling fleet. *Prog. Oceanogr.* 169, 241–252. doi: 10.1016/j.pocean.2018.07.001

Pasqual, C., Sanchez Vidal, A., Zuniga, D., Calafat, A., and Canals, M. (2010). Flux and composition of settling particles across the continental margin of the gulf of lion: the role of dense shelf water cascading. *Biogeosciences* 7, 217–231. doi: 10.5194/bg-7-217-2010

Pfannkuche, O. (1993). Benthic response to the sedimentation of particulate organic matter at the BIOTRANS station, 47 N, 20 W. *Deep Sea Res. Part II Top. Stud. Oceanogr.* 40, 135–149. doi: 10.1016/0967-0645(93)90010-K

Plante-Cuny, M.-R., and Bodoy, A. (1987). Biomasse et production primaire du phytoplancton et du microphytobenthos de deux biotopes sableux (Golfe de Fos, France). *Oceanol. Acta* 10, 223–237.

Polymenakou, P. N., Lampadariou, N., Mandalakis, M., and Tselepides, A. (2009). Phylogenetic diversity of sediment bacteria from the southern Cretan margin, Eastern Mediterranean Sea. *Syst. Appl. Microbiol.* 32, 17–26. doi: 10.1016/j.syapm.2008.09.006

Puig, P., Palanques, A., and Martín, J. (2014). Contemporary sediment-transport processes in submarine canyons. *Ann. Rev. Mar. Sci.* 6, 53–77. doi: 10.1146/annurev-marine-010213-135037

Pusceddu, A., Bianchelli, S., Martín, J., Puig, P., Palanques, A., Martín, J., et al. (2014). Chronic and intensive bottom trawling impairs deep-sea biodiversity and ecosystem functioning. *Proc. Natl. Acad. Sci. U.S.A.* 111, 8861–8866. doi: 10.1073/pnas.1405454111

Pusceddu, A., Bianchellia, S., Canals, M., Sanchez-Vidal, A., De Madron, X. D., Heussner, S., et al. (2010). Organic matter in sediments of canyons and open slopes of the Portuguese, Catalan, Southern Adriatic and Cretan Sea margins. *Deep Sea Res. Part 1 Oceanogr. Res. Papers* 57, 441–457. doi: 10.1016/j.dsr.2009.11.008

Quaiser, A., Zivanovic, Y., Moreira, D., and López-García, P. (2011). Comparative metagenomics of bathypelagic plankton and bottom sediment from the Sea of Marmara. *ISME J.* 5, 285–304. doi: 10.1038/ismej.2010.113

Quast, C., Pruesse, E., Yilmaz, P., Gerken, J., Schweer, T., Yarza, P., et al. (2013). The SILVA ribosomal RNA gene database project: improved data processing and web-based tools. *Nucleic Acids Res.* 41, D590–D596. doi: 10.1093/nar/gks1219

Ramirez-Llodra, E., Brandt, A., Danovaro, R., De Mol, B., Escobar, E., German, C. R., et al. (2010). Deep, diverse and definitely different: unique attributes of the world's largest ecosystem. *Biogeosciences* 7, 2851–2899. doi: 10.5194/bg-7-2851-2010

Restrepo-Ortiz, C. X., Auguet, J. C., and Casamayor, E. O. (2014). Targeting spatiotemporal dynamics of planktonic SAGMGC-1 and segregation of ammonia-oxidizing thaumarchaeota ecotypes by newly designed primers and quantitative polymerase chain reaction. *Environ. Microbiol.* 16, 689–700. doi: 10.1111/1462-2920.12191

Rex, M. A., and Etter, R. J. (2010). *Deep-Sea Biodiversity: Pattern and Scale*. Cambridge, MA: Harvard University Press.

Ristova, P. P., Wenzhöfer, F., Ramette, A., Felden, J., and Boetius, A. (2015). Spatial scales of bacterial community diversity at cold seeps (Eastern Mediterranean Sea). *ISME J.* 9:1306. doi: 10.1038/ismej.2014.217

Roberts, D. W. (2013). *Package 'Labdsv'. R Package Version 1.6–1*.

Román, S. (2017). *Ecology and Biodiversity of the Deep-Sea Meiobenthos from the Blanes Canyon and its Adjacent Slope (NW Mediterranean)*. Ph.D. thesis, University of Barcelona, Barcelona.

Román, S., Vanreusel, A., Ingels, J., and Martin, D. (2018). Nematode community zonation in response to environmental drivers in Blanes Canyon (NW Mediterranean). *J. Exp. Mar. Biol. Ecol.* 502, 111–128. doi: 10.1016/j.jembe.2017.08.010

Román, S., Vanreusel, A., Romano, C., Ingels, J., Puig, P., Company, J. B., et al. (2016). High spatiotemporal variability in meiofaunal assemblages in Blanes Canyon (NW Mediterranean) subject to anthropogenic and natural disturbances. *Deep Sea Res. Part I Oceanogr. Res. Papers* 117, 70–83. doi: 10.1016/j.dsr.2016.10.004

Romano, C., Coenjaerts, J., Flexas, M. M., Zúñiga, D., Vanreusel, A., Company, J. B., et al. (2013a). Spatio-temporal variability of meiobenthic density in the Blanes submarine canyon (NW Mediterranean). *Prog. Oceanogr.* 118, 159–174.

Romano, C., Fanelli, E., D'Anna, G., Pipitone, C., Vizzini, S., Mazzola, A., et al. (2016). Spatial variability of soft-bottom macrobenthic communities in northern Sicily (Western Mediterranean): contrasting trawled vs. untrawled areas. *Mar. Environ. Res.* 122, 113–125. doi: 10.1016/j.marenvres.2016.10.002

Romano, C., Voight, J., Company, J. B., Plyuscheva, M., and Martin, D. (2013b). Submarine canyons as the preferred habitat for wood-boring species of *Xylophaga* (Mollusca, Bivalvia). *Prog. Oceanogr.* 118, 175–187. doi: 10.1016/j.pocean.2013.07.028

Romano, C., Voight, J. R., Pérez-Portela, R., and Martin, D. (2014). Morphological and genetic diversity of the wood-boring *Xylophaga* (Mollusca, Bivalvia): new species and records from deep-sea Iberian canyons. *PLoS One* 9:e102887. doi: 10.1371/journal.pone.0102887

Rzeznik-Orignac, J., Puisay, A., Derelle, E., Peru, E., Le Bris, N., and Galand, P. E. (2018). Co-occurring nematodes and bacteria in submarine canyon sediments. *PeerJ* 6:e5396. doi: 10.7717/peerj.5396

Sardà, F., Company, J. B., Bahamón, N., Rotllant, G., Flexas, M. M., Sánchez, J. D., et al. (2009). Relationship between environment and the occurrence of the deep-water rose shrimp *Aristeus antennatus* (Risso, 1816) in the Blanes submarine canyon (NW Mediterranean). *Prog. Oceanogr.* 82, 227–238. doi: 10.1016/j.pocean.2009.07.001

Schauer, R., Bienhold, C., Ramette, A., and Harder, J. (2010). Bacterial diversity and biogeography in deep-sea surface sediments of the South Atlantic Ocean. *ISME J.* 4, 159–170. doi: 10.1038/ismej.2009.106

Sebastián, M., Auguet, J. C., Restrepo-Ortiz, C. X., Sala, M. M., Marrasé, C., and Gasol, J. M. (2018). Deep ocean prokaryotic communities are remarkably malleable when facing long-term starvation. *Environ. Microbiol.* 20, 713–723. doi: 10.1111/1462-2920.14002

Sevastou, K., Lampadariou, N., Polymenakou, P. N., and Tselepides, A. (2013). Benthic communities in the deep Mediterranean Sea: exploring microbial and meiofaunal patterns in slope and basin ecosystems. *Biogeosciences* 10, 4861–4878. doi: 10.5194/bg-10-4861-2013

Shannon, C. (1948). A mathematical theory of communication. *Bell Syst. Tech. J.* 27, 379–423; 623–656. doi: 10.1002/j.1538-7305.1948.tb01338.x

Sintes, E., Bergauer, K., De Corte, D., Yokokawa, T., and Herndl, G. J. (2013). Archaeal amoA gene diversity points to distinct biogeography of ammonia-oxidizing Crenarchaeota in the ocean. *Environ. Microbiol.* 15, 1647–1658. doi: 10.1111/j.1462-2920.2012.02801.x

Soetaert, K., Vincx, M., and Heip, C. (1995). Nematode community structure along a Mediterranean shelf-slope gradient. *Mar. Ecol.* 16, 189–206. doi: 10.1111/j.1439-0485.1995.tb00405.x

Sonthiphand, P., Hall, M. W., and Neufeld, J. D. (2014). Biogeography of anaerobic ammonia-oxidizing (anammox) bacteria. *Front. Microbiol.* 5:399. doi: 10.3389/fmicb.2014.00399

Stoddard, S. F., Smith, B. J., Hein, R., Roller, B. R., and Schmidt, T. M. (2014). rrn DB: improved tools for interpreting rRNA gene abundance in bacteria and archaea and a new foundation for future development. *Nucleic Acids Res.* 43, D593–D598. doi: 10.1093/nar/gku1201

Stuart, C. T., Rex, M. A., and Etter, R. J. (2003). in *Large-Scale Spatial And Temporal Patterns of Deep-Sea Benthic Species Diversity*, ed. P. A. Tyler (Amsterdam: Elsevier), 295–312.

Sturdivant, S. K., Díaz, R. J., and Cutter, G. R. (2012). Bioturbation in a declining oxygen environment, in situ observations from Wormcam. *PLoS One* 7:e34539. doi: 10.1371/journal.pone.0034539

Sunagawa, S., Coelho, L. P., Chaffron, S., Kultima, J. R., Labadie, K., Salazar, G., et al. (2015). Structure and function of the global ocean microbiome. *Science* 348:1261359. doi: 10.1126/science.1261359

Thiel, H. (1978). *Benthos in Upwelling Regions. Upwelling Ecosystems*. Berlin: Springer, 124–138. doi: 10.1007/978-3-642-66985-9_11

Vanreusel, A., Vandenbossche, I., and Thiermann, F. (1997). Free-living marine nematodes from hydrothermal sediments: similarities with communities from diverse reduced habitats. *Mar. Ecol. Prog. Ser.* 157, 207–219. doi: 10.3354/meps157207

Vila-Costa, M., Sharma, S., Moran, M. A., and Casamayor, E. O. (2013). Diel gene expression profiles of a phosphorus limited mountain lake using metatranscriptomics. *Environ. Microbiol.* 15, 1190–1203. doi: 10.1111/1462-2920.12033

Watanabe, K., Kodama, Y., and Harayama, S. (2001). Design and evaluation of PCR primers to amplify bacterial 16S ribosomal DNA fragments used for community fingerprinting. *J. Microbiol. Methods* 44, 253–262. doi: 10.1016/S0167-7012(01)00220-2

Wemheuer, F., Taylor, J., Daniel, R., Johnston, E. L., Meinicke, P., Thomas, T., et al. (2018). Tax4Fun2: a R-based tool for the rapid prediction of habitat-specific functional profiles and functional redundancy based on 16S rRNA gene marker gene sequences. *bioRxiv* [Preprint]. doi: 10.1101/490037

Wickham, H. (2009). *ggplot2: Elegant Graphics For Data Analysis*. New York, NY: Springer. doi: 10.1007/978-0-387-98141-3

Yu, T., Li, M., Niu, M., Fan, X., Liang, W., and Wang, F. (2018). Difference of nitrogen-cycling microbes between shallow bay and deep-sea sediments in the South China Sea. *Appl. Microbiol. Biotechnol.* 102, 447–459. doi: 10.1007/s00253-017-8594-9

Zinger, L., Amaral Zettler, L., Fuhrman, J., Horner Devine, M. C., Huse, S., Sogin, M., et al. (2011). Global patterns of bacterial beta-diversity in seafloor and seawater ecosystems. *PLoS One* 6:e24570. doi: 10.1371/journal.pone.0024570

Zúñiga, D., Flexas, M. M., Sanchez-Vidal, A., Coenjaerts, J., Calafat, A. I., Jordà, G., et al. (2009). Particle fluxes dynamics in Blanes submarine canyon (Northwestern Mediterranean). *Prog. Oceanogr.* 82, 239–251. doi: 10.1016/j.pocean.2009.07.002

Conflict of Interest Statement: The authors declare that the research was conducted in the absence of any commercial or financial relationships that could be construed as a potential conflict of interest.

Copyright © 2019 Román, Ortiz-Álvarez, Romano, Casamayor and Martin. This is an open-access article distributed under the terms of the Creative Commons Attribution License (CC BY). The use, distribution or reproduction in other forums is permitted, provided the original author(s) and the copyright owner(s) are credited and that the original publication in this journal is cited, in accordance with accepted academic practice. No use, distribution or reproduction is permitted which does not comply with these terms.

Advantages of publishing in Frontiers

OPEN ACCESS
Articles are free to read for greatest visibility and readership

FAST PUBLICATION
Around 90 days from submission to decision

HIGH QUALITY PEER-REVIEW
Rigorous, collaborative, and constructive peer-review

TRANSPARENT PEER-REVIEW
Editors and reviewers acknowledged by name on published articles

Frontiers
Avenue du Tribunal-Fédéral 34
1005 Lausanne | Switzerland

Visit us: www.frontiersin.org
Contact us: info@frontiersin.org | +41 21 510 17 00

REPRODUCIBILITY OF RESEARCH
Support open data and methods to enhance research reproducibility

DIGITAL PUBLISHING
Articles designed for optimal readership across devices

FOLLOW US
@frontiersin

IMPACT METRICS
Advanced article metrics track visibility across digital media

EXTENSIVE PROMOTION
Marketing and promotion of impactful research

LOOP RESEARCH NETWORK
Our network increases your article's readership